

LATEST TRENDS on SYSTEMS - VOLUME II

**Proceedings of the 18th International Conference on Systems
(part of CSCC '14)**

**Santorini Island, Greece
July 17-21, 2014**

LATEST TRENDS on SYSTEMS - VOLUME II

**Proceedings of the 18th International Conference on Systems
(part of CSCC '14)**

**Santorini Island, Greece
July 17-21, 2014**

Copyright © 2014, by the editors

All the copyright of the present book belongs to the editors. All rights reserved. No part of this publication may be reproduced, stored in a retrieval system, or transmitted in any form or by any means, electronic, mechanical, photocopying, recording, or otherwise, without the prior written permission of the editors.

All papers of the present volume were peer reviewed by no less than two independent reviewers. Acceptance was granted when both reviewers' recommendations were positive.

Series: Recent Advances in Electrical Engineering Series | 38

ISSN: 1790-5117

ISBN: 978-1-61804-244-6

LATEST TRENDS on SYSTEMS - VOLUME II

**Proceedings of the 18th International Conference on Systems
(part of CSCC '14)**

**Santorini Island, Greece
July 17-21, 2014**

Organizing Committee

Editors:

Prof. Nikos Mastorakis, Technical University of Sofia, Bulgaria and HNA, Greece
Prof. Kleanthis Psarris, The City University of New York, USA
Prof. George Vachtsevanos, Georgia Institute of Technology, Atlanta, Georgia, USA
Prof. Philippe Dondon, École Nationale Supérieure d'Électronique, Talence, Cedex, France
Prof. Valeri Mladenov, Technical University of Sofia, Bulgaria
Prof. Aida Bulucea, University of Craiova, Craiova, Romania
Prof. Imre Rudas, Obuda University, Budapest, Hungary
Prof. Olga Martin, Politehnica University of Bucharest, Romania

Associate Editors:

Vladimír Vašek
Libor Pekař
Eduardo Mario Dias
Nikolaos Bardis

Steering Committee:

Prof. Theodore B. Trafalis, University of Oklahoma, USA
Prof. Charles A. Long, Professor Emeritus, University of Wisconsin, Stevens Point, Wisconsin, USA
Prof. Maria Isabel García-Planas, Universitat Politècnica de Catalunya, Spain
Prof. Reinhard Neck, Klagenfurt University, Klagenfurt, Austria
Prof. Myriam Lazard, Institut Supérieur d'Ingenierie de la Conception, Saint Die, France
Prof. Zoran Bojkovic, University of Belgrade, Serbia
Prof. Claudio Talarico, Gonzaga University, Spokane, USA

International Scientific Committee:

Prof. Lotfi Zadeh (IEEE Fellow, University of Berkeley, USA)
Prof. Leon Chua (IEEE Fellow, University of Berkeley, USA)
Prof. Michio Sugeno (RIKEN Brain Science Institute (RIKEN BSI), Japan)
Prof. Dimitri Bertsekas (IEEE Fellow, MIT, USA)
Prof. Demetri Terzopoulos (IEEE Fellow, ACM Fellow, UCLA, USA)
Prof. Georgios B. Giannakis (IEEE Fellow, University of Minnesota, USA)
Prof. George Vachtsevanos (Georgia Institute of Technology, USA)
Prof. Brian Barsky (IEEE Fellow, University of Berkeley, USA)
Prof. Aggelos Katsaggelos (IEEE Fellow, Northwestern University, USA)
Prof. Josef Sifakis (Turing Award 2007, CNRS/Verimag, France)
Prof. Hisashi Kobayashi (Princeton University, USA)
Prof. Kinshuk (Fellow IEEE, Massey Univ. New Zeland),
Prof. Leonid Kazovsky (Stanford University, USA)
Prof. Narsingh Deo (IEEE Fellow, ACM Fellow, University of Central Florida, USA)
Prof. Kamisetty Rao (Fellow IEEE, Univ. of Texas at Arlington, USA)
Prof. Anastassios Venetsanopoulos (Fellow IEEE, University of Toronto, Canada)
Prof. Steven Collicott (Purdue University, West Lafayette, IN, USA)
Prof. Nikolaos Paragios (Ecole Centrale Paris, France)
Prof. Nikolaos G. Bourbakis (IEEE Fellow, Wright State University, USA)
Prof. Stamatios Kartalopoulos (IEEE Fellow, University of Oklahoma, USA)
Prof. Irwin Sandberg (IEEE Fellow, University of Texas at Austin, USA),
Prof. Michael Sebek (IEEE Fellow, Czech Technical University in Prague, Czech Republic)
Prof. Hashem Akbari (University of California, Berkeley, USA)
Prof. Yuriy S. Shmaliy, (IEEE Fellow, The University of Guanajuato, Mexico)
Prof. Lei Xu (IEEE Fellow, Chinese University of Hong Kong, Hong Kong)
Prof. Paul E. Dimotakis (California Institute of Technology Pasadena, USA)

Prof. Martin Pelikan (UMSL, USA)
Prof. Patrick Wang (MIT, USA)
Prof. Wasfy B Mikhael (IEEE Fellow, University of Central Florida Orlando, USA)
Prof. Sunil Das (IEEE Fellow, University of Ottawa, Canada)
Prof. Panos Pardalos (University of Florida, USA)
Prof. Nikolaos D. Katopodes (University of Michigan, USA)
Prof. Bimal K. Bose (Life Fellow of IEEE, University of Tennessee, Knoxville, USA)
Prof. Janusz Kacprzyk (IEEE Fellow, Polish Academy of Sciences, Poland)
Prof. Sidney Burrus (IEEE Fellow, Rice University, USA)
Prof. Biswa N. Datta (IEEE Fellow, Northern Illinois University, USA)
Prof. Mihai Putinar (University of California at Santa Barbara, USA)
Prof. Wlodzislaw Duch (Nicolaus Copernicus University, Poland)
Prof. Tadeusz Kaczorek (IEEE Fellow, Warsaw University of Technology, Poland)
Prof. Michael N. Katehakis (Rutgers, The State University of New Jersey, USA)
Prof. Pan Agathoklis (Univ. of Victoria, Canada)
Dr. Subhas C. Misra (Harvard University, USA)
Prof. Martin van den Toorn (Delft University of Technology, The Netherlands)
Prof. Malcolm J. Crocker (Distinguished University Prof., Auburn University, USA)
Prof. Urszula Ledzewicz, Southern Illinois University, USA.
Prof. Dimitri Kazakos, Dean, (Texas Southern University, USA)
Prof. Ronald Yager (Iona College, USA)
Prof. Athanassios Manikas (Imperial College, London, UK)
Prof. Keith L. Clark (Imperial College, London, UK)
Prof. Argyris Varonides (Univ. of Scranton, USA)
Prof. S. Furfari (Direction Generale Energie et Transports, Brussels, EU)
Prof. Constantin Udriste, University Politehnica of Bucharest, ROMANIA
Dr. Michelle Luke (Univ. Berkeley, USA)
Prof. Patrice Brault (Univ. Paris-sud, France)
Prof. Jim Cunningham (Imperial College London, UK)
Prof. Philippe Ben-Abdallah (Ecole Polytechnique de l'Universite de Nantes, France)
Prof. Photios Anninos (Medical School of Thrace, Greece)
Prof. Ichiro Hagiwara, (Tokyo Institute of Technology, Japan)
Prof. Andris Buikis (Latvian Academy of Science, Latvia)
Prof. Akshai Aggarwal (University of Windsor, Canada)
Prof. George Vachtsevanos (Georgia Institute of Technology, USA)
Prof. Ulrich Albrecht (Auburn University, USA)
Prof. Imre J. Rudas (Obuda University, Hungary)
Prof. Alexey L Sadovskii (IEEE Fellow, Texas A&M University, USA)
Prof. Amedeo Andreotti (University of Naples, Italy)
Prof. Ryszard S. Choras (University of Technology and Life Sciences Bydgoszcz, Poland)
Prof. Remi Leandre (Universite de Bourgogne, Dijon, France)
Prof. Moustapha Diaby (University of Connecticut, USA)
Prof. Brian McCartin (New York University, USA)
Prof. Elias C. Aifantis (Aristotle Univ. of Thessaloniki, Greece)
Prof. Anastasios Lyrintzis (Purdue University, USA)
Prof. Charles Long (Prof. Emeritus University of Wisconsin, USA)
Prof. Marvin Goldstein (NASA Glenn Research Center, USA)
Prof. Costin Cepisca (University POLITEHNICA of Bucharest, Romania)
Prof. Kleanthis Psarris (University of Texas at San Antonio, USA)
Prof. Ron Goldman (Rice University, USA)
Prof. Ioannis A. Kakadiaris (University of Houston, USA)
Prof. Richard Tapia (Rice University, USA)
Prof. F.-K. Benra (University of Duisburg-Essen, Germany)
Prof. Milivoje M. Kostic (Northern Illinois University, USA)

Prof. Helmut Jaberg (University of Technology Graz, Austria)
Prof. Ardeshir Anjomani (The University of Texas at Arlington, USA)
Prof. Heinz Ulbrich (Technical University Munich, Germany)
Prof. Reinhard Leithner (Technical University Braunschweig, Germany)
Prof. Elbrous M. Jafarov (Istanbul Technical University, Turkey)
Prof. M. Ehsani (Texas A&M University, USA)
Prof. Sesh Commuri (University of Oklahoma, USA)
Prof. Nicolas Galanis (Universite de Sherbrooke, Canada)
Prof. S. H. Sohrab (Northwestern University, USA)
Prof. Rui J. P. de Figueiredo (University of California, USA)
Prof. Valeri Mladenov (Technical University of Sofia, Bulgaria)
Prof. Hiroshi Sakaki (Meisei University, Tokyo, Japan)
Prof. Zoran S. Bojkovic (Technical University of Belgrade, Serbia)
Prof. K. D. Klaes, (Head of the EPS Support Science Team in the MET Division at EUMETSAT, France)
Prof. Emira Maljevic (Technical University of Belgrade, Serbia)
Prof. Kazuhiko Tsuda (University of Tsukuba, Tokyo, Japan)
Prof. Milan Stork (University of West Bohemia , Czech Republic)
Prof. C. G. Helmis (University of Athens, Greece)
Prof. Lajos Barna (Budapest University of Technology and Economics, Hungary)
Prof. Nobuoki Mano (Meisei University, Tokyo, Japan)
Prof. Nobuo Nakajima (The University of Electro-Communications, Tokyo, Japan)
Prof. Victor-Emil Neagoe (Polytechnic University of Bucharest, Romania)
Prof. P. Vanderstraeten (Brussels Institute for Environmental Management, Belgium)
Prof. Annaliese Bischoff (University of Massachusetts, Amherst, USA)
Prof. Virgil Tiponut (Politehnica University of Timisoara, Romania)
Prof. Andrei Kolyshkin (Riga Technical University, Latvia)
Prof. Fumiaki Imado (Shinshu University, Japan)
Prof. Sotirios G. Ziavras (New Jersey Institute of Technology, USA)
Prof. Constantin Volosencu (Politehnica University of Timisoara, Romania)
Prof. Marc A. Rosen (University of Ontario Institute of Technology, Canada)
Prof. Thomas M. Gatton (National University, San Diego, USA)
Prof. Leonardo Pagnotta (University of Calabria, Italy)
Prof. Yan Wu (Georgia Southern University, USA)
Prof. Daniel N. Riahi (University of Texas-Pan American, USA)
Prof. Alexander Grebennikov (Autonomous University of Puebla, Mexico)
Prof. Bennie F. L. Ward (Baylor University, TX, USA)
Prof. Guennadi A. Kouzaev (Norwegian University of Science and Technology, Norway)
Prof. Eugene Kindler (University of Ostrava, Czech Republic)
Prof. Geoff Skinner (The University of Newcastle, Australia)
Prof. Hamido Fujita (Iwate Prefectural University(IPU), Japan)
Prof. Francesco Muzi (University of L'Aquila, Italy)
Prof. Claudio Rossi (University of Siena, Italy)
Prof. Sergey B. Leonov (Joint Institute for High Temperature Russian Academy of Science, Russia)
Prof. Arpad A. Fay (University of Miskolc, Hungary)
Prof. Lili He (San Jose State University, USA)
Prof. M. Nasseh Tabrizi (East Carolina University, USA)
Prof. Alaa Eldin Fahmy (University Of Calgary, Canada)
Prof. Paul Dan Cristea (University "Politehnica" of Bucharest, Romania)
Prof. Gh. Pascovici (University of Koeln, Germany)
Prof. Pier Paolo Delsanto (Politecnico of Torino, Italy)
Prof. Radu Munteanu (Rector of the Technical University of Cluj-Napoca, Romania)
Prof. Ioan Dumitrache (Politehnica University of Bucharest, Romania)
Prof. Miquel Salgot (University of Barcelona, Spain)
Prof. Amaury A. Caballero (Florida International University, USA)

Prof. Maria I. Garcia-Planas (Universitat Politecnica de Catalunya, Spain)
Prof. Petar Popivanov (Bulgarian Academy of Sciences, Bulgaria)
Prof. Alexander Gegov (University of Portsmouth, UK)
Prof. Lin Feng (Nanyang Technological University, Singapore)
Prof. Colin Fyfe (University of the West of Scotland, UK)
Prof. Zhaohui Luo (Univ of London, UK)
Prof. Wolfgang Wenzel (Institute for Nanotechnology, Germany)
Prof. Weilian Su (Naval Postgraduate School, USA)
Prof. Phillip G. Bradford (The University of Alabama, USA)
Prof. Ray Hefferlin (Southern Adventist University, TN, USA)
Prof. Gabriella Bognar (University of Miskolc, Hungary)
Prof. Hamid Abachi (Monash University, Australia)
Prof. Karlheinz Spindler (Fachhochschule Wiesbaden, Germany)
Prof. Josef Boercsoek (Universitat Kassel, Germany)
Prof. Eyad H. Abed (University of Maryland, Maryland, USA)
Prof. F. Castanie (TeSA, Toulouse, France)
Prof. Robert K. L. Gay (Nanyang Technological University, Singapore)
Prof. Andrzej Ordys (Kingston University, UK)
Prof. Harris Catrakis (Univ of California Irvine, USA)
Prof. T Bott (The University of Birmingham, UK)
Prof. T.-W. Lee (Arizona State University, AZ, USA)
Prof. Le Yi Wang (Wayne State University, Detroit, USA)
Prof. Oleksander Markovskyy (National Technical University of Ukraine, Ukraine)
Prof. Suresh P. Sethi (University of Texas at Dallas, USA)
Prof. Hartmut Hillmer (University of Kassel, Germany)
Prof. Bram Van Putten (Wageningen University, The Netherlands)
Prof. Alexander Iomin (Technion - Israel Institute of Technology, Israel)
Prof. Roberto San Jose (Technical University of Madrid, Spain)
Prof. Minvydas Ragulskis (Kaunas University of Technology, Lithuania)
Prof. Arun Kulkarni (The University of Texas at Tyler, USA)
Prof. Joydeep Mitra (New Mexico State University, USA)
Prof. Vincenzo Niola (University of Naples Federico II, Italy)
Prof. Ion Chrysosoverghi (National Technical University of Athens, Greece)
Prof. Dr. Aydin Akan (Istanbul University, Turkey)
Prof. Sarka Necasova (Academy of Sciences, Prague, Czech Republic)
Prof. C. D. Memos (National Technical University of Athens, Greece)
Prof. S. Y. Chen, (Zhejiang University of Technology, China and University of Hamburg, Germany)
Prof. Duc Nguyen (Old Dominion University, Norfolk, USA)
Prof. Tuan Pham (James Cook University, Townsville, Australia)
Prof. Rossella Cancelliere (University of Torino, Italy)
Prof. Dr-Eng. Christian Bouquegneau (Faculty Polytechnique de Mons, Belgium)
Prof. Wladyslaw Mielczarski (Technical University of Lodz, Poland)
Prof. Ibrahim Hassan (Concordia University, Montreal, Quebec, Canada)
Prof. Stavros J. Baloyannis (Medical School, Aristotle University of Thessaloniki, Greece)
Prof. Vilem Srovnal, (Technical University of Ostrava, Czech Republic)
Prof. J. M. Giron-Sierra (Universidad Complutense de Madrid, Spain)
Prof. Walter Dosch (University of Luebeck, Germany)
Prof. Rudolf Freund (Vienna University of Technology, Austria)
Prof. Erich Schmidt (Vienna University of Technology, Austria)
Prof. Alessandro Genco (University of Palermo, Italy)
Prof. Martin Lopez Morales (Technical University of Monterey, Mexico)
Prof. Ralph W. Oberste-Vorth (Marshall University, USA)
Prof. Vladimir Damgov (Bulgarian Academy of Sciences, Bulgaria)
Prof. P. Borne (Ecole Central de Lille, France)

Additional Reviewers

Santoso Wibowo	CQ University, Australia
Lesley Farmer	California State University Long Beach, CA, USA
Xiang Bai	Huazhong University of Science and Technology, China
Jon Burley	Michigan State University, MI, USA
Genqi Xu	Tianjin University, China
Zhong-Jie Han	Tianjin University, China
Kazuhiko Natori	Toho University, Japan
João Bastos	Instituto Superior de Engenharia do Porto, Portugal
José Carlos Metrôlho	Instituto Politecnico de Castelo Branco, Portugal
Hessam Ghasemnejad	Kingston University London, UK
Matthias Buyle	Artesis Hogeschool Antwerpen, Belgium
Minhui Yan	Shanghai Maritime University, China
Takuya Yamano	Kanagawa University, Japan
Yamagishi Hiromitsu	Ehime University, Japan
Francesco Zirilli	Sapienza Università di Roma, Italy
Sorinel Oprisan	College of Charleston, CA, USA
Ole Christian Boe	Norwegian Military Academy, Norway
Deolinda Rasteiro	Coimbra Institute of Engineering, Portugal
James Vance	The University of Virginia's College at Wise, VA, USA
Valeri Mladenov	Technical University of Sofia, Bulgaria
Angel F. Tenorio	Universidad Pablo de Olavide, Spain
Bazil Taha Ahmed	Universidad Autónoma de Madrid, Spain
Francesco Rotondo	Polytechnic of Bari University, Italy
Jose Flores	The University of South Dakota, SD, USA
Masaji Tanaka	Okayama University of Science, Japan
M. Javed Khan	Tuskegee University, AL, USA
Frederic Kuznik	National Institute of Applied Sciences, Lyon, France
Shinji Osada	Gifu University School of Medicine, Japan
Dmitrijs Serdjuks	Riga Technical University, Latvia
Philippe Dondon	Institut polytechnique de Bordeaux, France
Abelha Antonio	Universidade do Minho, Portugal
Konstantin Volkov	Kingston University London, UK
Manoj K. Jha	Morgan State University in Baltimore, USA
Eleazar Jimenez Serrano	Kyushu University, Japan
Imre Rudas	Obuda University, Budapest, Hungary
Andrey Dmitriev	Russian Academy of Sciences, Russia
Tetsuya Yoshida	Hokkaido University, Japan
Alejandro Fuentes-Penna	Universidad Autónoma del Estado de Hidalgo, Mexico
Stavros Ponis	National Technical University of Athens, Greece
Moran Wang	Tsinghua University, China
Kei Eguchi	Fukuoka Institute of Technology, Japan
Miguel Carriegos	Universidad de Leon, Spain
George Barreto	Pontificia Universidad Javeriana, Colombia
Tetsuya Shimamura	Saitama University, Japan

Table of Contents

Plenary Lecture 1: Floating Offshore Wind Turbines: The Technologies and the Economics <i>Paul D. Sclavounos</i>	22
Plenary Lecture 2: Detecting Critical Elements in Large Networks <i>Panos M. Pardalos</i>	24
Plenary Lecture 3: Overview of the Main Metaheuristics used for the Optimization of Complex Systems <i>Pierre Borne</i>	26
Plenary Lecture 4: Minimum Energy Control of Fractional Positive Electrical Circuits <i>Tadeusz Kaczorek</i>	28
Plenary Lecture 5: Unmanned Systems for Civilian Operations <i>George Vachtsevanos</i>	30
Plenary Lecture 6: Iterative Extended UFIR Filtering in Applications to Mobile Robot Indoor Localization <i>Yuriy S. Shmaliy</i>	32
PART I	33
Short Distance Earth Current Measurements Related to Atmospheric Electric Fields <i>Ernst D. Schmitter</i>	35
Implementation of Direction Cosine Matrix on a PSoC-5 Microcontroller for Robot Localization on Inclined Terrains <i>Garth Herman, Aleksander Milshteyn, Airs Lin, Manuel Garcia, Charles Liu, Khosrow Rad, Darrel Guillaume, Helen Boussalis</i>	39
Indirect Adaptive Control for Underwater Vehicles on Base of Nonlinear Estimator of Disturbances <i>V. Kh. Pshikhopov, M. Yu. Medvedev, B. V. Gurenko, A. M. Maevsky</i>	46
The Representativeness Reliability Importance Measure <i>Josep Freixas, Montserrat Pons</i>	52
CDM Controller Order and Disturbance Rejection Ability <i>Joao Paulo Coelho, Wojciech Giernacki, Jose Boaventura-Cunha</i>	57
The Influence of Variable Friction Coefficient on Spatial Stability of Slightly Curved Shallow Mixing Layers <i>Andrei Kolyshkin, Valentina Koliskina, Inta Volodko</i>	62

Equations of Motion and Physical Model of Quad-copter in Plain <i>Zdeněk Úředníček, Milan Opluštil</i>	66
OWA – Type Possibilistic Aggregations in a Decision Making Regarding Selection of Investments <i>Gia Sirbiladze, Gvantsa Tsulaia</i>	71
Identification of Dynamical Systems using Recurrent Complex-Valued Neural Networks <i>Víctor M. Arellano-Quintana, Ieroham S. Baruch</i>	74
Unitary Theory of Direct Electromechanical Transformers <i>Zdeněk Úředníček</i>	80
Anti-Synchronization of WINDMI Systems via Adaptive Backstepping Control Method and its FPGA Implementation <i>Sundarapandian Vaidyanathan, Christos K. Volos, Ionnis M. Kyprianidis, Ioannis N. Stouboulos, Karthikeyan Rajagopal, Prasina Alexander</i>	86
Analytical Modeling of Pneumatic Muscle Actuator Torque Characteristics <i>Mária Tóthová, Ján Pitel'</i>	92
Combined Effect of Small Curvature and Variable Friction on Temporal Instability of Shallow Mixing Layers <i>Ilmars Iltins, Marija Iltina, Andrei Kolyshkin</i>	96
Application of Self-Tuning Polynomial Controller <i>Stanislav Plšek, Vladimír Vašek</i>	100
Resistive Parameter Identification of a Li-ion Battery Using Sliding Mode Observer <i>Daehyun Kim, Taedong Goh, Seung Hun Kim, Sang Woo Kim</i>	104
Statistical Wound-Rotor IM Diagnosis Method Based on Standard Deviation using NVSA <i>Khalid Dahi, Soumia Elhani, Said Guedira</i>	109
A Seven-Term Novel 3-D Chaotic System with Three Quadratic Nonlinearities and its LABVIEW Implementation <i>Sundarapandian Vaidyanathan, Christos K. Volos, Ionnis M. Kyprianidis, Ioannis N. Stouboulos, Karthikeyan Rajagopal, Prasina Alexander</i>	117
The Surface Properties of Linear Low-Density Polyethylene After Radiation Cross-Linking <i>Martin Bednarik, David Manas, Miroslav Manas, Michal Stanek, Jan Navratil, Ales Mizera</i>	123
Pipe Measurement System Using a Laser Range Finder with KINECT <i>K. Yoshida, N. Hidaka, K. Kawasue</i>	127
Edible Oil Comparison by Terahertz Time Domain Spectroscopy System Tera OSCAT <i>Marie Tobolova, Vojtech Kresalek</i>	134

Application of the Static and Dynamic Models in Predicting the Future Strength of Pozzolanic Cements	138
<i>Dimitris C. Tsamatsoulis</i>	
Mobile Meteorological Radar Uses in Crisis Management	147
<i>David Šaur, Stanislav Plšek</i>	
Motion Detection in Thermal Images Sequence Using Wigner Distributions	153
<i>Sn. Pleshkova, Al.Bekyarski</i>	
Fuzzy Control of the Position Servo Motor Drives with Elasticity and Friction	157
<i>Dmitry V. Lukichev, Galina L. Demidova</i>	
Using Fuzzy Logic to Control an Innovative Active Vehicle Suspension System	161
<i>K. Hyniova, L. Smitkova-Janku</i>	
Using Neural Networks to Design Predictive Model of Creation of Aluminium Oxide Layer	168
<i>P. Michal, A. Vagaská, M. Gombár, J. Kmec, E. Spišák, D. Kučerka</i>	
Microwave Pulse Generator	174
<i>R. Krizan, L. Drazan</i>	
Synchronization Error Detection of Data Transmission Errors in Asynchronous Channels	179
<i>Olga Fedorechko, Oleksandr P. Markovskiy, Nikos Doukas, Nikos Bardis</i>	
Statistical Analysis of Surface Roughness in Grinding of Titanium	184
<i>Bílek Ondřej, Javořík Jakub, Sámek David</i>	
New Approach to Building Hierarchy for Patients Attendance in Intensive Care Unit with Use of Fuzzy Information and Dynamic Modeling	189
<i>Maria Milanova, Mikhail Matveev</i>	
3D Data Acquisition and CAD/CAM Systems for CNC Manufacturing of Artificial Limbs	193
<i>Bílek Ondřej, Javořík Jakub, Sámek David</i>	
Unidirectional Coupling Scheme of Nonlinear Circuits via a Memristor	198
<i>Christos K. Volos, Sundarapandian Vaidyanathan, Ioannis M. Kyprianidis, Nikos G. Bardis, Ioannis N. Stouboulos</i>	
Investigation of Thermal Degradation of Vegetable Oils During Frying using Terahertz Time-Domain Spectroscopy	202
<i>Marie Tobolova, Vojtech Kresalek</i>	
Architecture and Design of a Dynamic Real-Time Alarm System for Power Plants	206
<i>Ilse Leal Aulenbacher, Jose Maria Suarez Jurado, Efren R. Coronel Flores</i>	

Measuring and Identification of Oils	211
<i>Hana Vaskova, Martina Buckova</i>	
Tensional Psychological Mechanism and the Topological Invariants of the Tensional Configurations	216
<i>Alin Gilbert Sumedrea</i>	
A Thermoelectric Generator as an Electric Energy Source for the Building Sensors	226
<i>Michal Oplustil, Martin Zalesak, Stanislav Sehnalek, Pavel Chrobak</i>	
Diagnostics and Evaluation of Limit Strain States from Digital Image	230
<i>J. Kmec, E. Fechová, S. Hrehová</i>	
Device for Heat Transport Parameters Monitoring of Solids	234
<i>P. Košťal, I. Ružiak, R. Igaz, Z. Jančíková, V. Rusnák, R. Garzinová, P. Hlaváček</i>	
Oilmarks Detection Algorithm in Steel Plates	239
<i>Doo-Chul Choi, Yong-Ju Jeon, Sang Jun Lee, Jong Pil Yun, Sang Woo Kim</i>	
Temperature Stability of Construction Polymers After Radiation Cross-Linking	243
<i>Ales Mizera, Miroslav Manas, Zdenek Holik, David Manas, Michal Stanek, Jan Navratil, Martin Bednarik</i>	
Unsupervised Robot System using Computational Geometry and Neural Network	247
<i>Marios Poulos</i>	
Testing Thermal Images Characteristics for Thermal Images Quality Estimation	251
<i>Sn. Pleshkova, Al. Bekyarski, K.Peeva</i>	
Nano-Hardness of PA12 After Radiation	257
<i>Martin Ovsik, David Manas, Miroslav Manas, Michal Stanek, Petr Kratky, Vojtech Senkerik</i>	
Developing a Query Interface for Biomedical Questions Answering	262
<i>Ioana Branescu-Raspop, Victor Lorin Purcarea, Radu Dobrescu</i>	
Physical Properties' Determination of PA6/HDPEx Blends	268
<i>Jan Navratil, Miroslav Manas, Michal Stanek, David Manas, Martin Bednarik, Ales Mizera</i>	
Enhancing Images using the Forward-Backward UFIR Algorithm	273
<i>L. J. Morales-Mendoza, M. González-Lee, E. Morales-Mendoza, R. F Vázquez-Bautista, J. Huerta-Chua, S. Pérez-Cáceres, G. Triano-Carballo, O. G. Ibarra-Manzano, Y. S. Shmaliy</i>	
Impact of Irradiation Dose on Mechanical Properties of PA 11	279
<i>Petr Kratky, David Manas, Miroslav Manas, Michal Stanek, Martin Ovsik, Adam Skrobak, Martin Reznicek</i>	

Elearning Platform Assessment for Military Distance Education with Multicriteria Analysis	285
<i>George Rigopoulos, Nikolaos V. Karadimas</i>	
Impact of Irradiation Dose on Mechanical Properties of PMMA	290
<i>Petr Kratky, David Manas, Miroslav Manas, Michal Stanek, Martin Ovsik, Vojtech Senkerik, Jan Navratil</i>	
Visual Information Processing Routines for Intelligent Vehicles	296
<i>Jarnea Alexandru Daniel, Florea Gheorghe, Dobrescu Radu</i>	
The Behaviour of Recycled Material with Particles of Various Sizes at Increased Temperature and their Tensile Properties	302
<i>Vojtech Senkerik, Michal Stanek, Miroslav Manas, David Manas, Adam Skrobak, Jan Navratil</i>	
New Approach to Thresholding and Contour Detection for Object Surface Inspection in Machine Vision	306
<i>K. Židek, A. Hošovský, J. Dubják</i>	
Microcomputer I/O Converter and Control Unit for Heating Systems	310
<i>Libor Pekař, Petr Dostálek, Zdeněk Oborný</i>	
Defect Detection for Vertical Cracks in Hot-slabs using Dual Light Switching Lighting Method	315
<i>Yong-Ju Jeon, Doo-chul Choi, Sang Jun Lee, Jong Pil Yun, Sang Woo Kim</i>	
Two Suboptimal Controller Parameters Tuning Approaches for Systems with Delays: Selected Highlights of Preliminary Studies	321
<i>Libor Pekař, Roman Prokop</i>	
Belonging Probability Inverse Image Technique to Early Detection of Volcanic Eruption	326
<i>B. Yagoubi, S. Benkraouda, A. Bouziane</i>	
Optimization of a Batch Reactor Dimensions	330
<i>David Novosad, Lubomír Macků, Milan Navrátil</i>	
MAP and MMSE Estimation of HEV State of Charge	334
<i>Nazha Abed, Hatem Boujemaa, Sami Touati, Ramdane Hedjar</i>	
Scanning Probe Microscopy Method for Diagnostics of Ultra-Thin Tungsten Films on Silicon Substrate	338
<i>Milan Navrátil, Vojtěch Křesálek, František Hruška, Tomáš Martínek, Josef Kudělka, Jaroslav Sobota</i>	
Feature Level Compensation for Robust Speaker Identification in Mismatched Conditions	344
<i>Sharada V. Chougule, Mahesh S. Chavan</i>	

On Experimental Verification of Vehicle Active Suspension Robust Control	353
<i>K. Hyniova</i>	
A Study of Pressure Distribution Droplets Motion in Convergence-Divergence Shape Microchannel	359
<i>Maryam Ghelichkhani</i>	
Modeling and Optimization of Hydrolysate Yields in Leather Waste Processing	363
<i>Hana Vaskova, Karel Kolomaznik</i>	
Discrete-Time State Estimation Using Unbiased FIR Filters with Minimized Variance	367
<i>Shunyi Zhao, Fei Liu, Yuriy S. Shmaliy</i>	
Applying “ABCD Rule of Dermatoscopy” using Cognitive Systems	374
<i>Ionut Taranu, Iunia Iacovici</i>	
Obstacle Avoidance by Unmanned Aerial Vehicles using Image Recognition Techniques	378
<i>Priya Bajju Parappat, Anand Kumar, R. K. Mittal, Suhel Ahmad Khan</i>	
Pyramid Method for Reversible Discrete Wavelet Transformation of 3D Image	382
<i>Eustache Muteba Ayumba</i>	
Procedural Aspects of Data Seizure	385
<i>Jan Kolouch, Andrea Kropáčová</i>	
PART II	389
Robust Feature Matching for Aerial Visual Odometry	391
<i>Tarek Mouats, Nabil Aouf</i>	
The Cost Function for Extraction of Bound Component from Material	395
<i>D. Janáčková, V. Vašek, K. Kolomazník</i>	
Multiple Pattern-Dependent Controller Design for Markovian Jump Linear Systems	399
<i>Taesoo Kim, Sung Hyun Kim</i>	
Adaptive Continuous-Time Decoupling Control	402
<i>Marek Kubalčík, Vladimír Bobál</i>	
Comparing Accuracy and Solution Times in Coverage Models	408
<i>George P. Alexandris, Nikolaos G. Bardis</i>	
Determination of Thermal Steady State in the Wall with Semi Dirichlet Boundary Conditions	414
<i>Martin Zalesak</i>	

Performance Evaluation of Two Radial Basis Function Neural Network Models	419
<i>Nikolinka G. Christova, Gancho L. Vachkov, Agata H. Manolova, Georgi T. Tsenov</i>	
Graphical Analysis of Robust Stability for Fractional Order Time-Delay Systems Integer Order PID Controllers	424
<i>Radek Matušů, Roman Prokop</i>	
Building a Model of Family House Heating System using 1-Wire Sensor Network Protocol	430
<i>Dominik Kujawa</i>	
Multivariable Control of Unstable Systems – A Matrix Equation Approach	438
<i>Roman Prokop, Jiří Korbel</i>	
Comparison of Acoustic Barriers Noise Reductions Evaluated by Different Calculation Methods	443
<i>Claudio Guarnaccia, Joseph Quartieri, Nikos E. Mastorakis</i>	
Relay Feedback Identification of Dynamical SISO Systems – Analysis Settings	450
<i>Roman Prokop, Jiří Korbel, Radek Matušů</i>	
Control of Direct-Driven PMSG for Wind Energy System	455
<i>F. Khater, A. Shaltout, A. Omar</i>	
Signal Condition of Embedded Unit Inputs	462
<i>F. Hruska, M. Navratil, J. Otahal</i>	
An Operational Model of Bus Terminal Management based on Daily Passengers Demands	467
<i>José A. M. de Gouveia, Maurício L. Ferreira, Maria L. R. P. Dias, Melissa S. Porkorny, Eduardo M. Dias</i>	
Holonic Concept in the Heat Production Distribution Control Systems	474
<i>Lubomir Vasek, Viliam Dolinay, Tomas Sysala</i>	
Automatic Complexity Estimation based on Requirements	478
<i>Radek Silhavy, Petr Silhavy, Zdenka Prokopova</i>	
Dynamic Patients Scheduling in the Pediatric Emergency Department	482
<i>Sara Ben Othman, Nesrine Zoghalmi, Slim Hammadi, Alain Quillot, Alain Martinot, Jean-Marie Renard</i>	
Program Modules for Control Applications of Microcontrollers	488
<i>Jan Dolinay, Petr Dostálek, Vladimír Vašek</i>	
Evaluation of SolidWorks Flow Simulation by Ground-Coupled Heat Transfer Test Cases	492
<i>S. Sehnalek, M. Zalesak, J. Vincenec, M. Oplustil, P. Chrobak</i>	

Time Series Predictive Model Application to Air Pollution Assessment	499
<i>Claudio Guarnaccia, Julia Griselda Cerón Bretón, Joseph Quartieri, Carmine Tepedino, Rosa Maria Cerón Bretón</i>	
Educational Microprocessor Development Kit – Low-Cost Access System Application	506
<i>Tomas Sysala, Petr Neumann, Filip Zanka, Lubomir Vasek</i>	
Fuzzy Logic Controller in Servo Drive Control System with Speed Limitation	511
<i>Nikita Smirnov, Dmitry Lukichev</i>	
Chaos Enhanced Differential Evolution with the Dissipative Map for the PID Tuning Problem	516
<i>Roman Senkerik, Michal Pluhacek, Zuzana Kominkova Oplatkova</i>	
A VSC Approach for Wave Energy Converters	521
<i>Aitor J. Garrido, Izaskun Garrido, Mikel Alberdi, Modesto Amundarain, Edorta Carrascal</i>	
Control System for Chemical Thermal Processes	523
<i>Petr Chalupa, Martin Beneš, Jakub Novák, Michaela Bařinová</i>	
Galvanically Isolated Interface for an Oscilloscope	529
<i>Martin Pospisilik, Petr Neumann, Roman Honig, Peter Scheibenreiter</i>	
Identification Control of Oscillatory Dynamical Systems using Recurrent Complex-Valued Neural Networks	534
<i>Ieroham S. Baruch, Víctor M. Arellano-Quintana</i>	
Implementation of Fuzzy MPC on Embedded System	540
<i>Jakub Novak, Petr Chalupa</i>	
Analysis Web Structures Optimization	546
<i>Zdenka Prokopova, Radek Silhavy, Petr Silhavy</i>	
Artificial Intelligence Systems for Knowledge Management in e-Health: The Study of Intelligent Software Agents	551
<i>M. Furmankiewicz, A. Sořtysik-Piorunkiewicz, P. Ziuziański</i>	
Simulation of Time-Continuous Chaotic Systems for the Generating of Random Numbers	557
<i>Roman Senkerik, Michal Pluhacek, Zuzana Kominkova Oplatkova</i>	
Development of Control System for Rehabilitation Device Actuated by Pneumatic Artificial Muscles	562
<i>O. Liška, M. More</i>	
Analysis of Behavior of Car Stabilizer Bushing	566
<i>Jakub Javorik, David Samek, Ondrej Bilek</i>	

Traffic Management Solutions in Large Cities – the Integrated Centre of Urban Mobility (CIMU) in São Paulo	570
<i>Dariusz Swiatek, Melissa S. Pokorny, Jilmar A. Tatto, José E. Gonçalo, Vidal A. Z. C. Melo, Eduardo M. Dias</i>	
Treatment of Chromium Wastewater using Membrane Separation Processes	577
<i>Pavel Kocurek, Karel Kolomazník, Michaela Bařinová</i>	
Return on Investment in Photovoltaic Panels Verification their Effectiveness	581
<i>P. Chrobak, M. Zalesak, M. Oplustil, S. Sehnalek, J. Vincenec</i>	
Big Data Processing for E-Health Applications using a Decentralized Cloud M2M System	588
<i>George Suciu, Victor Suciu, Octavian Fratu</i>	
Modeling of Protein Sorption on Chromium Sludge as a Tool for Optimization of its Deproteination	594
<i>Michaela Bařinová, Jiří Pecha, Karel Kolomazník</i>	
Real Time Monitoring of Public Transit Passenger Flows through Radio Frequency Identification - RFID Technology Embedded in Fare Smart Cards	599
<i>Maurício L. Ferreira, José A. M. de Gouveia, Eduardo Facchini, Melissa S. Pokorny, Eduardo M. Dias</i>	
Families of Spherical Polynomials: Description and Robust Stability Analysis	606
<i>Radek Matušů</i>	
Mathematical Description of Magnesium Oxide Extraction from Chrome-Tanned Leather Waste	611
<i>Michaela Bařinová, Karel Kolomazník</i>	
The ITS Components in the Optimization Control of People Vehicles Circulation at the Brazilian Ports	616
<i>Vander S. de Abreu, Luiz N. Rossi, Eduardo M. Dias</i>	
Computer Application for Determination of Optimal Economic Costs of Biomaterial Waste Treatment by Enzymatic Hydrolysis	621
<i>H. Charvátová, D. Janáčová, V. Vašek, K. Kolomazník</i>	
Automatic Recognition and Synthesis System of Arabic Digit	625
<i>H. Tebbi, M. Hamadouche, H. Azzoune</i>	
On the Usage of Differential Evolution for Effort Estimation	632
<i>T. Urbanek, Z. Prokopova, R. Silhavy</i>	
Measurement and Simulation of Electromagnetic Interference in Low Frequencies Range	636
<i>Jiří Otáhal, František Hruška, Stanislav Sehnálek</i>	

Power Spectral Density in the RFID Systems its Impacts in Celular Systems	640
<i>Leandro R. Sergio, Maria L. R. P. Dias, Sergio L. Pereira, Eduardo M. Dias</i>	
Parameterization of Module for Testing of Thermal Stability in the Room	647
<i>H. Charvátová, M. Zálešák, S. Sehnálek</i>	
Modelling and Analysis of Neural Network and Perturb and Observe MPPT Algorithm for PV Array Using Boost Converter	651
<i>Naoufel Khaldi, Hassan Mahmoudi, Malika Zazi, Youssef Barradi</i>	
Computer Simulation of the Heating Sensor PIR Detector by Radiation	656
<i>R. Drga, D. Janáčová, H. Charvátová</i>	
Electromagnetic Field Distribution within a Semi Anechoic Chamber	662
<i>Martin Pospíšilik, Josef Soldan</i>	
The Role of Traceability in the Pharmaceutical Safety Supply Chain	668
<i>Jair Calixto, Maria L. R. P. Dias, Melissa S. Pokorny, Eduardo M. Dias</i>	
Testing the Properties of Materials used for the Measurement of the PIR Detector in the Infrared Range	674
<i>R. Drga, D. Janáčová, H. Charvátová</i>	
Vehicle Inspection & Maintenance Program in São Paulo - Results and Environmental Benefits	679
<i>Marcelo C. Branco, Fábio C. Branco, Gabriel M. Branco, Eduardo M. Dias, Alfred Szwarc</i>	
Communication Requirements of Laboratory Management System	686
<i>M. Krbeček, F. Schauer, K. Vlček</i>	
ITS to Monitor Small Vessels Movements within Port Area - A Study at Santos Estuary	692
<i>Aureo E. P. Figueiredo, Sérgio L. Hoeflich, Maria L. R. P. Dias, Sergio L. Pereira, Luiz N. Rossi, Eduardo M. Dias</i>	
Numerical Model of Behavior of Pneumatic Actuator	696
<i>Jakub Javorik</i>	
Plasticity of the Error Monitoring and Processing System	700
<i>Menizibeya O. Welcome, Nikos E. Mastorakis, Vladimir A. Pereverzev</i>	
Conversion of the METCM into the METEO-11	708
<i>Karel Šilinger, Ladislav Potužák, Jiří Šotnar</i>	
Criteria for Efficiency Determination of Inspection Maintenance Programs	714
<i>Gabriel M. Branco, Fábio C. Branco, Marcelo C. Branco, Eduardo M. Dias, José M. Napoleone, Alfred Szwarc</i>	

Electronic Switch for Accumulator Connection in a Backup Power Source	720
<i>Martin Pospisilik, Tomas Dulik</i>	
ITS Components in Risk Management in the Port of Santos	726
<i>Alexsandro S. de Lima, Melissa S. Pokorny, Eduardo M. Dias</i>	
Authors Index	731

Plenary Lecture 1

Floating Offshore Wind Turbines: The Technologies and the Economics



Prof. Paul D. Sclavounos

Professor of Mechanical Engineering and Naval Architecture
Massachusetts Institute of Technology (MIT)
77 Massachusetts Avenue
Cambridge MA 02139-4307
USA
E-mail: pauls@mit.edu

Abstract: Wind is a vast, renewable and clean energy source that stands to be a key contributor to the world energy mix in the coming decades. The horizontal axis three-bladed wind turbine is a mature technology and onshore wind farms are cost competitive with coal fired power plants equipped with carbon sequestration technologies and in many parts of the world with natural gas fired power plants.

Offshore wind energy is the next frontier. Vast sea areas with higher and steadier wind speeds are available for the development of offshore wind farms that offer several advantages. Visual, noise and flicker impacts are mitigated when the wind turbines are sited at a distance from the coastline. A new generation of 6-10MW wind turbines with diameters exceeding 160m have been developed for the offshore environment. They can be fully assembled at a coastal facility and installed by a low cost float-out operation. Floater technologies are being developed for the support of multi-megawatt turbines in waters of moderate to large depth, drawing upon developments by the offshore oil & gas industry.

The state of development of the offshore wind energy sector will be discussed. The floating offshore wind turbine technology will be reviewed drawing upon research carried out at MIT since the turn of the 21st century. Floating wind turbine installations worldwide and planned future developments will be presented. The economics of floating offshore wind farms will be addressed along with the investment metrics that must be met for the development of large scale floating offshore wind power plants.

Brief Biography of the Speaker: Paul D. Sclavounos is Professor of Mechanical Engineering and Naval Architecture at the Massachusetts Institute of Technology. His research interests focus upon the marine hydrodynamics of ships, offshore platforms and floating wind turbines. The state-of-the-art computer programs SWAN and SML developed from his research have been widely adopted by the maritime, offshore oil & gas, and wind energy industries. His research

activities also include studies of the economics, valuation and risk management of assets in the crude oil, natural gas, shipping and wind energy sectors. He was the Georg Weinblum Memorial Lecturer in 2010-2011 and the Keynote Lecturer at the Offshore Mechanics and Arctic Engineering Conference in 2013. He is a member of the Board of the North American Committee of Det Norske Veritas since 1997, a member of the Advisory Committee of the US Navy Tempest program since 2006 and a member of the Advisory Board of the Norwegian Center for Offshore Wind Energy Technology since 2009. He has consulted widely for the US Government, shipping, offshore, yachting and energy industries.

<http://meche.mit.edu/people/?id=76>

Keynote Lecture 2

Detecting Critical Elements in Large Networks



Professor Panos M. Pardalos

Center for Applied Optimization (CAO)
Department of Industrial and Systems Engineering,
University of Florida, Gainesville, FL, USA.

and

Laboratory of Algorithms and Technologies for Networks Analysis (LATNA)
National Research University, Higher School of Economics
Moscow, Russia

E-mail: p.m.pardalos@gmail.com

Abstract: In network analysis, the problem of detecting subsets of elements important to the connectivity of a network (i.e., critical elements) has become a fundamental task over the last few years. Identifying the nodes, arcs, paths, clusters, cliques, etc., that are responsible for network cohesion can be crucial for studying many fundamental properties of a network. Depending on the context, finding these elements can help to analyze structural characteristics such as, attack tolerance, robustness, and vulnerability. Furthermore we can classify critical elements based on their centrality, prestige, reputation and can determine dominant clusters and partitions.

From the point of view of robustness and vulnerability analysis, evaluating how well a network will perform under certain disruptive events plays a vital role in the design and operation of such a network. To detect vulnerability issues, it is of particular importance to analyze how well connected a network will remain after a disruptive event takes place, destroying or impairing a set of its elements. The main goal is to identify the set of critical elements that must be protected or reinforced in order to mitigate the negative impact that the absence of such elements may produce in the network. Applications are typically found in homeland security, energy grid, evacuation planning, immunization strategies, financial networks, biological networks, and transportation.

From the member-classification perspective, identifying members with a high reputation and influential power within a social network could be of great importance when designing a marketing strategy. Positioning a product, spreading a rumor, or developing a campaign against drugs and alcohol abuse may have a great impact over society if the strategy is properly targeted among the most influential and recognized members of a community. The recent emergence of social networks such as Facebook, Twitter, LinkedIn, etc. provide countless applications for problems of critical-element detection.

In addition, determining dominant cliques or clusters over different industries and markets via critical clique detection may be crucial in the analysis of market share concentrations and debt

concentrations, spotting possible collusive actions or even helping to prevent future economic crises.

This presentation surveys some of the recent advances for solving these kinds of problems including heuristics, mathematical programming, dynamic programming, approximation algorithms, and simulation approaches. We also summarize some applications that can be found in the literature and present further motivation for the use of these methodologies for network analysis in a broader context.

Brief Biography of the Speaker: Panos M. Pardalos serves as Distinguished Professor of Industrial and Systems Engineering at the University of Florida. He is also an affiliated faculty member of the Computer and Information Science Department, the Hellenic Studies Center, and the Biomedical Engineering Program. He is also the Director of the Center for Applied Optimization. Dr. Pardalos is a world leading expert in global and combinatorial optimization. His recent research interests include network design problems, optimization in telecommunications, e-commerce, data mining, biomedical applications, and massive computing.

Full CV: http://www.ise.ufl.edu/pardalos/files/2011/08/CV_Dec13.pdf

Recent Achievements: <http://www.eng.ufl.edu/news/first-engineering-chair-appointed-under-ufs-preeminence-initiative-goes-to-big-data-expert/>

Profile in Scholar Google: scholar.google.com/scholar?q=P+Pardalos&btnG=&hl=en&as_sdt=0,5

Plenary Lecture 3

Overview of the Main Metaheuristics used for the Optimization of Complex Systems



Professor Pierre Borne

Co-author: Mohamd Benrejeb

Ecole Centrale de Lille

France

E-mail: pierre.borne@ec-lille.fr

Abstract: For complex systems such as in planning and scheduling optimization, the complexity which corresponds usually to hard combinational optimization prevents the implementation of exact solving methodologies which could not give the optimal solution in finite time. It is the reason why engineers prefer to use metaheuristics which are able to produce good solutions in a reasonable computation time. Two types of metaheuristics are presented here:

* The local searches, such as: Tabu Search, Simulated Annealing, GRASP method, Hill Climbing, Tunnelling...

* The global methods which look for a family of solutions such as: Genetic or Evolutionary Algorithms, Ant Colony Optimization, Particle Swarm Optimization, Bees algorithm, Firefly algorithm, Bat algorithm, Harmony search....

Brief Biography of the Speaker: Pierre BORNE received the Master degree of Physics in 1967 and the Master of Electrical Engineering, the Master of Mechanics and the Master of Applied Mathematics in 1968. The same year he obtained the Diploma of "Ingénieur IDN" (French "Grande Ecole"). He obtained the PhD in Automatic Control of the University of Lille in 1970 and the DSc in physics of the same University in 1976. Dr BORNE is author or co-author of about 200 Publications and book chapters and of about 300 communications in international conferences. He is author of 18 books in Automatic Control, co-author of an english-french, french-english « Systems and Control » dictionary and co-editor of the "Concise Encyclopedia of Modelling and Simulation" published with Pergamon Press. He is Editor of two book series in French and co-editor of a book series in English. He has been invited speaker for 40 plenary lectures or tutorials in International Conferences. He has been supervisor of 76 PhD Thesis and member of the committee for about 300 doctoral thesis . He has participated to the editorial board of 20 International Journals including the IEEE, SMC Transactions, and of the Concise Subject Encyclopedia . Dr BORNE has organized 15 international conferences and symposia, among them the 12th and the 17 th IMACS World Congresses in 1988 and 2005, the IEEE/SMC Conferences of 1993 (Le Touquet – France) and of 2002 (Hammamet - Tunisia) , the CESA IMACS/IEEE-SMC multiconferences of 1996 (Lille – France) , of 1998 (Hammamet – Tunisia) , of 2003 (Lille-France) and of 2006 (Beijing, China) and the 12th IFAC LSS symposium (Lille France, 2010) He was chairman or co-chairman of the IPCs of 34 international conferences (IEEE, IMACS, IFAC) and member of the IPCs of more than 200 international conferences. He was the

editor of many volumes and CDROMs of proceedings of conferences. Dr BORNE has participated to the creation and development of two groups of research and two doctoral formations (in Casablanca, Morocco and in Tunis, Tunisia). twenty of his previous PhD students are now full Professors (in France, Morocco, Tunisia, and Poland). In the IEEE/SMC Society Dr BORNE has been AdCom member (1991-1993 ; 1996-1998), Vice President for membership (1992-1993) and Vice President for conferences and meetings (1994-1995, 1998-1999). He has been associate editor of the IEEE Transactions on Systems Man and Cybernetics (1992-2001). Founder of the SMC Technical committee « Mathematical Modelling » he has been president of this committee from 1993 to 1997 and has been president of the « System area » SMC committee from 1997 to 2000. He has been President of the SMC Society in 2000 and 2001, President of the SMC-nomination committee in 2002 and 2003 and President of the SMC-Awards and Fellows committee in 2004 and 2005. He is member of the Advisory Board of the "IEEE Systems Journal" . Dr. Borne received in 1994, 1998 and 2002 Outstanding Awards from the IEEE/SMC Society and has been nominated IEEE Fellow the first of January 1996. He received the Norbert Wiener Award from IEEE/SMC in 1998, the Third Millennium Medal of IEEE in 2000 and the IEEE/SMC Joseph G. Wohl Outstanding Career Award in 2003. He has been vice president of the "IEEE France Section" (2002-2010) and is president of this section since 2011. He has been appointed in 2007 representative of the Division 10 of IEEE for the Region 8 Chapter Coordination sub-committee (2007-2008) He has been member of the IEEE Fellows Committee (2008- 2010) Dr BORNE has been IMACS Vice President (1988-1994). He has been co-chairman of the IMACS Technical Committee on "Robotics and Control Systems" from 1988 to 2005 and in August 1997 he has been nominated Honorary Member of the IMACS Board of Directors. He is since 2008 vice-president of the IFAC technical committee on Large Scale Systems. Dr BORNE is Professor "de Classe Exceptionnelle" at the "Ecole Centrale de Lille" where he has been Head of Research from 1982 to 2005 and Head of the Automatic Control Department from 1982 to 2009. His activities concern automatic control and robust control including implementation of soft computing techniques and applications to large scale and manufacturing systems. He was the principal investigator of many contracts of research with industry and army (for more than three millions €) Dr BORNE is "Commandeur dans l'Ordre des Palmes Académiques" since 2007. He obtained in 1994 the french " Kulman Prize". Since 1996, he is Fellow of the Russian Academy of Non-Linear Sciences and Permanent Guest Professor of the Tianjin University (China). In July 1997, he has been nominated at the "Tunisian National Order of Merit in Education" by the Republic of Tunisia. In June 1999 he has been nominated « Professor Honoris Causa » of the National Institute of Electronics and Mathematics of Moscow (Russia) and Doctor Honoris Causa of the same Institute in October 1999. In 2006 he has been nominated Doctor Honoris Causa of the University of Waterloo (Canada) and in 2007 Doctor Honoris Causa of the Polytechnic University of Bucharest (Romania). He is "Honorary Member of the Senate" of the AGORA University of Romania since May 2008 He has been Vice President of the SEE (French Society of Electrical and Electronics Engineers) from 2000 to 2006 in charge of the technical committees. He his the director of publication of the SEE electronic Journal e-STA and chair the publication committee of the REE Dr BORNE has been Member of the CNU (French National Council of Universities, in charge of nominations and promotions of French Professors and Associate Professors) 1976-1979, 1992-1999, 2004-2007 He has been Director of the French Group of Research (GDR) of the CNRS in Automatic Control from 2002 to 2005 and of a "plan pluriformations" from 2006 to 2009. Dr BORNE has been member of the Multidisciplinary Assessment Committee of the "Canada Foundation for Innovation" in 2004 and 2009. He has been referee for the nominations of 24 professors in USA and Singapore. He is listed in the « Who is Who in the World » since 1999.

Plenary Lecture 4

Minimum Energy Control of Fractional Positive Electrical Circuits



Professor Tadeusz Kaczorek (Fellow IEEE)

Warsaw University of Technology
Poland

Abstract: The talk will consist of two parts. In the first part the minimum energy control of standard positive electrical circuits will be discussed and in the second part the similar problem for fractional positive electrical circuits. Necessary and sufficient conditions for the positivity and reachability of electrical circuits composed of resistors, coils and capacitors will be established. The minimum energy control problem for the standard and fractional positive electrical circuits will be formulated and solved. Procedures for computation of the optimal inputs and minimal values of the performance indices will be given and illustrated by examples of electrical circuits.

Brief Biography of the Speaker: Prof. Tadeusz Kaczorek graduated from the Faculty of Electrical Engineering Warsaw University of Technology in 1956, where in 1962 he defended his doctoral thesis. In 1964, he received a postdoctoral degree. In the years 1965-1970 he was head of the Department of Electronics and Automation, 1969-1970, and Dean of the Faculty of Electrical Engineering University of Warsaw. In the years 1970-1973 Vice-Rector of the Technical University of Warsaw in the years 1970-1981 the director of the Institute of Control and Industrial Electronics Warsaw University of Technology. He was also head of the Department of Control of the above Institute. In 1971 he received the title of Professor and Associate Professor of Warsaw University of Technology. In 1974 he received the title of professor of Warsaw University of Technology. In 1987-1988 he was chairman of the Committee for Automation and Robotics. Since 1986, corresponding member, and since 1998 member of the Polish Academy of Sciences. In 1988-1991 he was Head of the Scientific Academy in Rome. For many years a member of the Foundation for Polish Science. From June 1999 ordinary member of the Academy of Engineering. He is currently a professor at the Faculty of Electrical Engineering of Bialystok and Warsaw University of Technology. Since 1991 he is a member, and now chairman of the Central Commission for Academic Degrees and Titles (Vice-President in 2003-2006). In 2012 he was chairman of the Presidium of the Scientific Committee of the conference devoted to research crash of the Polish Tu-154 in Smolensk methods of science.

Scientific achievements

His research interests relate to automation, control theory and electrical engineering, including analysis and synthesis of circuits and systems with parameters determined and random polynomial methods for the synthesis of control systems and singular systems. Author of 20 books and monographs and over 700 articles and papers in major international journals such as

IEEE Transactions on Automatic Control, Multidimensional Systems and Signal Processing, International Journal of Control, Systems Science and Electrical Engineering Canadian Journal. He organized and presided over 60 scientific sessions at international conferences, and was a member of about 30 scientific committees. He has lectured at over 20 universities in the United States, Japan, Canada and Europe as a visiting professor. He supervised more than 60 doctoral dissertations completed and reviewed many doctoral theses and dissertations. His dozens of alumni received the title of professor in Poland or abroad.

He is a member of editorial boards of journals such as International Journal of Multidimensional Systems and Signal Processing, Foundations of Computing and Decision Sciences, Archives of Control Sciences. From 1 April 1997, is the editor of the Bulletin of the Academy of Technical Sciences.

Honours, awards and honorary doctorates.

Honours

Tadeusz Kaczorek has been honored with the following awards:

* Officer's Cross of the Order of Polonia Restituta Polish

* Meritorious Polish

* Medal of the National Education Commission

Honorary doctorates

He received honorary degrees from the following universities:

Silesian University of Technology (2014)

Rzeszow University of Technology (2012)

Poznan University of Technology (2011)

Opole University of Technology (2009)

Technical University of Lodz (3 December 2008)

Bialystok University of Technology (August 20, 2008)

Warsaw University of Technology (22 December 2004)

Szczecin University of Technology (November 8, 2004)

Lublin University of Technology (13 May 2004)

University of Zielona Gora (27 November 2002)

Honorary Member of the Hungarian Academy of Sciences and the Polish Society of Theoretical and Applied Electrical (1999). He received 12 awards of the Minister of National Education of all levels (including 2 team).

Plenary Lecture 5

Unmanned Systems for Civilian Operations



Professor George Vachtsevanos

Professor Emeritus

Georgia Institute of Technology

USA

E-mail: george.vachtsevanos@ece.gatech.edu

Abstract: In this plenary talk we will introduce fundamental concepts of unmanned systems (Unmanned Aerial Vehicles and Unmanned Ground Vehicles) and their emerging utility in civilian operations. We will discuss a framework for multiple UAVs tasked to perform forest fire detection and prevention operations. A ground station with appropriate equipment and personnel functions as the support and coordination center providing critical information to fire fighter as derived from the UAVs. The intent is to locate a swarm of vehicles over a designated area and report at the earliest the presence of such fire precursors as smoke, etc. the UAVs are equipped with appropriate sensors, computing and communications in order to execute these surveillance tasks accurately and robustly. Meteorological sensors monitor wind velocity, temperature and other relevant parameters. The UAV observations are augmented, when appropriate, with satellite data, observation towers and human information sources. Other application domains of both aerial and ground unmanned systems refer to rescue operations, damage surveillance and support for areas subjected to earthquakes and other natural disasters, border patrol, agricultural applications, traffic control, among others.

Brief Biography of the Speaker: Dr. George Vachtsevanos is currently serving as Professor Emeritus at the Georgia Institute of Technology. He served as Professor of Electrical and Computer Engineering at the Georgia Institute of Technology from 1984 until September, 2007. Dr Vachtsevanos directs at Georgia Tech the Intelligent Control Systems laboratory where faculty and students began research in diagnostics in 1985 with a series of projects in collaboration with Boeing Aerospace Company funded by NASA and aimed at the development of fuzzy logic based algorithms for fault diagnosis and control of major space station subsystems. His work in Unmanned Aerial Vehicles dates back to 1994 with major projects funded by the U.S. Army and DARPA. He has served as the Co-PI for DARPA's Software Enabled Control program over the past six years and directed the development and flight testing of novel fault-tolerant control algorithms for Unmanned Aerial Vehicles. He has represented Georgia Tech at DARPA's HURT program where multiple UAVs performed surveillance, reconnaissance and tracking missions in an urban environment. Under AFOSR sponsorship, the Impact/Georgia Team is developing a biologically-inspired micro aerial vehicle. His research work has been supported over the years by ONR, NSWC, the MURI Integrated Diagnostic program at Georgia Tech, the U.S. Army's Advanced Diagnostic program, General Dynamics,

General Motors Corporation, the Academic Consortium for Aging Aircraft program, the U.S. Air Force Space Command, Bell Helicopter, Fairchild Controls, among others. He has published over 300 technical papers and is the recipient of the 2002-2003 Georgia Tech School of ECE Distinguished Professor Award and the 2003-2004 Georgia Institute of Technology Outstanding Interdisciplinary Activities Award. He is the lead author of a book on Intelligent Fault Diagnosis and Prognosis for Engineering Systems published by Wiley in 2006.

Plenary Lecture 6

Iterative Extended UFIR Filtering in Applications to Mobile Robot Indoor Localization



Professor Yuriy S. Shmaliy
Department of Electronics
DICIS, Guanajuato University
Salamanca, 36855, Mexico
E-mail: shmaliy@ugto.mx

Abstract: A novel iterative extended unbiased FIR (EFIR) filtering algorithm is discussed to solve suboptimally the nonlinear estimation problem. Unlike the Kalman filter, the EFIR filtering algorithm completely ignores the noise statistics, but requires an optimal horizon of N points in order for the estimate to be suboptimal. The optimal horizon can be specialized via measurements with much smaller efforts and cost than for the noise statistics required by EKF. Overall, EFIR filtering is more successful in accuracy and more robust than EKF under the uncertain conditions. Extensive investigations of the approach are conducted in applications to localization of mobile robot via triangulation and in radio frequency identification tag grids. Better performance of the EFIR filter is demonstrated in a comparison with the EKF. It is also shown that divergence in EKF is not only due to large nonlinearities and large noise as stated by the Kalman filter theory, but also due to errors in the noise covariances ignored by EFIR filter.

Brief Biography of the Speaker: Dr. Yuriy S. Shmaliy is a full professor in Electrical Engineering of the Universidad de Guanajuato, Mexico, since 1999. He received the B.S., M.S., and Ph.D. degrees in 1974, 1976 and 1982, respectively, from the Kharkiv Aviation Institute, Ukraine. In 1992 he received the Dr.Sc. (technical) degree from the Soviet Union Government. In March 1985, he joined the Kharkiv Military University. He serves as full professor beginning in 1986 and has a Certificate of Professor from the Ukrainian Government in 1993. In 1993, he founded and, by 2001, had been a director of the Scientific Center “Sichron” (Kharkiv, Ukraine) working in the field of precise time and frequency. His books *Continuous-Time Signals* (2006) and *Continuous-Time Systems* (2007) were published by Springer, New York. His book *GPS-based Optimal FIR Filtering of Clock Models* (2009) was published by Nova Science Publ., New York. He also edited a book *Probability: Interpretation, Theory and Applications* (Nova Science Publ., New York, 2012) and contributed to several books with invited chapters. Dr. Shmaliy has authored more than 300 Journal and Conference papers and 80 patents. He is IEEE Fellow; was rewarded a title, Honorary Radio Engineer of the USSR, in 1991; and was listed in *Outstanding People of the 20th Century*, Cambridge, England in 1999. He is currently an Associate Editor for *Recent Patents on Space Technology*. He serves on the Editorial Boards of several International Journals and is a member of the Organizing and Program Committees of various Int. Symposia. His current interests include statistical signal processing, optimal estimation, and stochastic system theory.

PART II

Robust Feature Matching for Aerial Visual Odometry

Tarek Mouats¹, Nabil Aouf¹

¹ Cranfield University, Shrivenham Campus

Centre for Electronic Warfare

Shrivenham, SN6 8LA, UK

t.mouats@cranfield.ac.uk

Abstract—Interest points matching for aerial visual odometry using quadrotor MAV is tackled in this work. First, a set of sparse feature points are extracted using ORB detector. These are then grouped using Gradient Vector Flow (GVF) fields by finding points of high symmetry within the image. A robust matching strategy is introduced to improve the motion estimation. In order to validate ORB features matches, their grouping points are compared. Using the matched points, windowed bundle adjustment incorporating Gauss-Newton optimization is utilised for motion estimation. In order to deal with matching outliers, a Random sample consensus outlier rejection scheme is integrated. Lack of MAV stereo datasets in the literature motivated the generation of such vital data. Detailed results validating the proposed strategy are illustrated using these datasets. Also, a comparison with other approaches is also provided and shows the superiority of our approach.

Keywords—Visual odometry; feature grouping; feature matching; gradient vector flow; binary descriptors

I. INTRODUCTION

In recent years, the field of robotics witnessed a remarkable shift in researchers' interests towards unmanned air vehicles and more specifically small quadrotors. Self-localization is a key component for these systems during operations such as surveillance or search and rescue. This information is ordinarily provided by the Global Positioning System (GPS). However, it is known to suffer from a number of shortcomings (e.g. signal shortage). Visual odometry (VO) has emerged as a solution consisting in the process of estimating the egomotion of a moving platform using only visual information. In this context, cameras were found to be an interesting alternative to GPS due to their cost effectiveness and low power consumption. VO earliest attempts go back three decades ago [1] and its applications span ground vehicles [2], space missions [3], aerial vehicles [4] as well as underwater [5]. There are typically stereo [3] and monocular [4] approaches. While the captured visual information can overcome GPS issues, a large amount of data is produced. To alleviate this, interesting regions extractors are utilized where SIFT [6] and SURF [7] are the most established examples used in many computer vision applications. Recently, binary based feature detectors/descriptors have emerged (BRIEF [8], FREAK [9], ORB [10]). They are claimed to be as accurate as SIFT (SURF) while being orders of magnitude faster to compute. This is a true advantage for UAVs where payload (i.e. com-

putational power) is crucial. Aerial odometry has been investigated using both monocular [4] and stereo [11] algorithms as well as RGB-D sensors [12]. In general, approaches based on multiple cameras provide better performance. However, the ratio between the baseline and scene depth has to be relatively large for accurate triangulation. Indeed, as noted in [13], the stereo case can sometimes degenerate to monocular if this ratio is too small. Many efforts have been ongoing to enhance the performance of VO. Integrating other sensors (e.g. IMU, low-cost GPS) within the motion estimation framework represents one alternative [14], [15]. Another option is the improvement of feature matching that was shown to increase VO accuracy. For instance, a ten-fold improvement was achieved in [16]. Grouping interest points to enhance matching performance has also been investigated. The approach introduced in [17] led to reliable matches. It consists in forming local groups covering only small areas of the image. An initial group match is robustly computed and propagated to find all the matches. The main issue with this approach is that a wrong initial group matching yields all the matches to be wrong. In [18], features were grouped according to their spatial relations to tackle the problem of appearance-based localization. Here, we propose another grouping strategy based on the underlying gradient vector flow to cluster feature points. This will be shown to provide better matching results yielding accurate motion estimation. With regard to the latter, we opted for a windowed bundle adjustment framework incorporating Gauss-Newton optimization. In this scheme, the quadrotor's motion is estimated incrementally on a frame-to-frame basis using only acquired images without prior knowledge of the environment nor filtering techniques.

The paper is organised as follows: Section II describes the proposed feature extraction, grouping and matching strategy. The motion estimation scheme is explained in Section III and the experimental results are illustrated in Section IV. Conclusions are drawn in Section V where some insights into our future work are highlighted.

II. FEATURE EXTRACTION AND MATCHING

Feature extraction represents a prerequisite for most computer vision applications. This is especially true in the case of autonomous navigation applications where essential information contained within an image needs to be extracted.

A. Feature Extraction and Description

ORB detector/descriptor is used to extract highly localized interest points that can be easily re-detected in subsequent frames using FAST [19]. A pyramidal representation of the image is used to get features' scales information. In addition, first moments are computed to obtain a measure of their orientations. ORB descriptor is based on BRIEF which is a bit string constructed from a set of binary intensity tests. The previously computed orientations are used when the binary tests are performed. The output is the sought rBRIEF descriptor for each feature. The descriptor size implemented in this work is $n = 256$ bits.

B. Medial Keypoints

Medial keypoints extraction is based on Gradient Vector Flow (GVF) field introduced by Xu and Prince [20] and implemented in [21]. The GVF at a point $P(x, y)$ in the image is the vector field $V(P) = [u(P), v(P)]$ that minimizes the energy function ϵ given by

$$\epsilon = \int \int \underbrace{g(|\nabla f|) |V - \nabla f|^2}_{\text{data term}} + \underbrace{h(|\nabla f|) \nabla^2 V}_{\text{smoothing term}} dx dy \quad (1)$$

In (1), the two functions g and h define a trade-off between stability of orientation information at the gradients and smoothness across the image. A flux flow is then applied to the normalized GVF field (V_N) to extract the sought medial keypoints as follows

$$\mathcal{F}(V_N(p)) = \text{div } V_N = \frac{\oint \langle V_N, \mathcal{N} \rangle ds}{\text{Area}} \quad (2)$$

These keypoints are located at the maxima of the flux flow field \mathcal{F} and extracted using non-maxima suppression.

C. Feature Grouping and Matching

The grouping process follows a strategy inspired from [21]. The vectors in the GVF field are followed starting from ORB features. This needs to be done in all directions to investigate all possible medial keypoints linking. This process allows to iteratively determine 2D image positions linking ORB features to medial keypoints. In contrary to the original approach, our aim is to have each ORB feature linked to one medial keypoint at maximum. This is achieved by keeping only the strongest links and discarding the others. It allows us to add a layer in the matching process of ORB features where accepting more than one association would increase the ambiguity of matching. These keypoints help discarding solitary ORB features due to the nature of the underlying GVF fields near the keypoints. This approach might lead to less but more robust features. Computing similarity between binary descriptors is done using the Hamming distance. In our work, the multi-probe Local Sensitive Hashing (LSH) is used to match ORB descriptors. The matching is carried out in a loop fashion [22] ($im_{L_p} \rightarrow im_{R_p} \rightarrow im_{R_c} \rightarrow im_{L_c} \rightarrow im_{L_p}$) where $(im_{* \#}) : * \in \{L = \text{left}, R = \text{right}\}$ and $\# \in \{p = \text{previous}, c = \text{current}\}$. At this stage, if the starting feature is identical to the ending feature then the match is accepted. Otherwise it

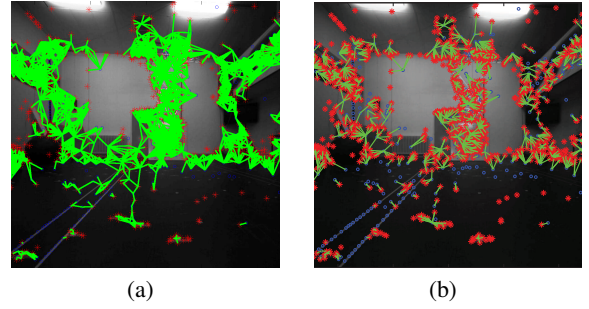


Fig. 1. (a) Original feature grouping (b) modified version (blue: medial keypoints; red: ORB features; green lines: associations). Images taken from our datasets.

is simply rejected. Furthermore, an additional matching layer is added for robustness. In order to validate ORB features matches, their associated medial features are compared. If their similarity is higher than a user defined threshold then the ORB matches are accepted. Otherwise, they are rejected.

III. MOTION ESTIMATION

A. Motion Parameters

The camera motion (i.e MAV motion) is a combination of rotations and translations embodied in a parameter vector $m = (\phi, \theta, \psi, t_x, t_y, t_z)$. The first 03 parameters form the rotation matrix R whereas the last parameters form the translation vector t . Writing the transformation matrix $M_p(m)$ gives

$$M_p(m) = T_{xyz}(t) \cdot R_x(\phi) \cdot R_y(\theta) \cdot R_z(\psi) \quad (3)$$

It represents the evolution of the motion of the MAV according to the 6DOF parameters m . In order to retrieve the vector m , the following bundle adjustment formulation of the reprojection error function is minimized:

$$S(m) = \frac{1}{2} \sum_{i=1}^n \sum_{j=1}^q r_j(m, X^{(i)})^2 \quad (4)$$

where r_j represent the residuals that are function of the motion vector m . $X^{(i)}$ correspond to the 3D coordinates obtained from the triangulation of matched features. According to [23], Gauss-Newton optimization postulate that the optimal solution m to equation (4) can be computed in an iterative manner by calculating an increment δm at each iteration using the Jacobian matrix $J \equiv \frac{dr}{dm}$ of the residuals vector with respect to the motion parameters m as:

$$(J^T \cdot J) \cdot \delta m = -J^T \cdot r \quad (5)$$

where $r \in \mathbb{R}^n$ is the residual vector and $(J^T \cdot J)$ represents an approximation of the Hessian matrix [23]. There are typically two reprojection strategies for motion estimation where either points from the previous pair are reprojected into the current frame or the other way round. However, as stated in [24], combining both reprojections yields better accuracy. A similar approach is adopted here. Finally, we assume that the camera parameters do not change with time allowing the bundle adjustment to not recompute them.

B. Outlier Rejection

Outliers are generally caused by matched features belonging to non-stationary objects or simply undetected false matches. We deal with them by constraining the reprojection error residuals by a user defined threshold μ as expressed here

$$\left(\sum_{j=1}^q r_j(m, X^{(i)})^2 \right) < \mu \quad (6)$$

To this end, the bundle adjustment estimation is wrapped in a RANSAC scheme. At each iteration, 03 matched points are randomly selected to estimate the motion parameters. The rest of the points are tested and classified as inliers or outliers according to (6). The winning solution with the largest number of inliers is then used to refine the motion parameters m in the final optimization step.

IV. EXPERIMENTS AND RESULTS

A. Experimental Setup

This section provides details about the system used in our experiments and shown in Fig. 2. The stereo head mounted on the MAV quadrotor consists of 02 mvBlueFOX-IGC cameras with ultra wide FOV lenses of 110x94 (HxV). The cameras are separated by a baseline of 30 cm and acquire images at 30fps with a resolution of 1280x960 pixels. They were calibrated using [25] and the captured images were rectified using the OpenCV library [26]. We used a motion capture system covering a flight arena of approximately $8m \times 7m \times 3m$. It provides a sub-millimetre accuracy tracking of the quadrotor that is used as ground truth (GT). Although the flight area does not correspond to a large volume, it allows the comparison to accurate ground truth while being representative of indoor environments. All the datasets are available for benchmarking purposes on request to the authors in 02 formats (gray and colour).

B. Results and Discussion

Fig. 2c illustrates a typical image from our datasets. One can notice that indoor images lack features as most of the

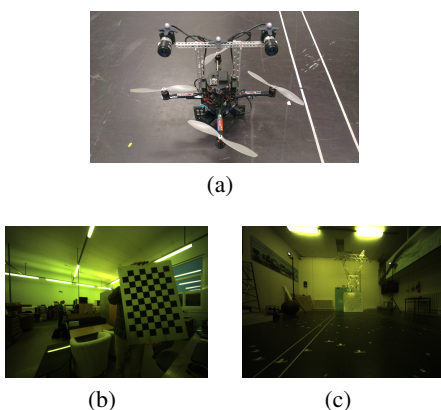


Fig. 2. Experimental setup; calibration and typical images (a) quadrotor with stereo head (b) calibration image (c) typical images

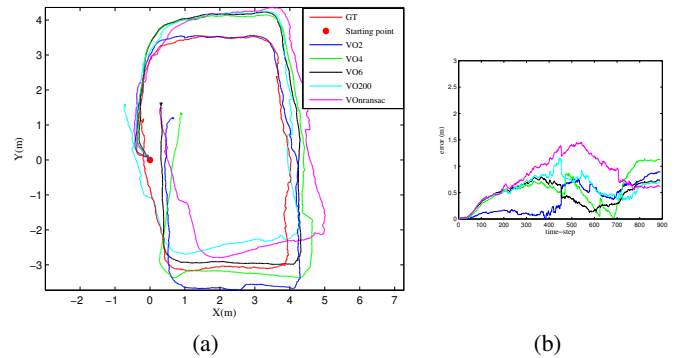


Fig. 3. VO trajectories and travelled errors using different thresholds: (a) VO trajectories (red dot: starting point; red line: GT; blue line: $\mu = 2$; green line: $\mu = 4$; black line: $\mu = 6$; cyan line: $\mu = 200$; magenta line: 1 iteration of RANSAC) (b) corresponding travelled errors

scene corresponds to flat walls with low texture. We recorded a set of sequences where substantial movement was carried out (especially in sequence 3) using the stereo head and the motion capture system (GT). However, only some results are illustrated due to shortage of space. We compared our approach to the technique developed in [22] who made their source code available. Their method also relies solely on visual clues for motion estimation (i.e. no external sensor is required).

1) *Outlier Rejection Analysis:* Here we show the influence of allowing more incorrect matches into the pose estimation step. This can be done through the manipulation of the rejection threshold μ implemented within the RANSAC scheme. Fig. 3 illustrates the estimated trajectories and errors for $\mu = \{2, 4, 6, 200\}$ and without outlier rejection where only 01 iteration of RANSAC was performed in the motion estimation. Regarding the latter, note that the outputted trajectory does not diverge dramatically from the others. This can be explained by the matching robustness where low numbers of outliers are passed on to the motion estimation step. Nevertheless, the accuracy of VO decreases with the increase of the outlier rejection threshold as more outliers are allowed.

2) *Visual odometry:* Based on IV-B1, a rejection threshold $\mu = 2$ was selected. Fig. 4 illustrates the estimated trajectories for sequences 2 and 3 respectively. It can be seen that adding a matching layer by grouping ORB features yields better egomotion estimates. We also compare our approach to [22] and illustrate it in Fig. 4 where it is shown to provide better localisation accuracy. Grouping features allowed the accuracy in terms of travelled error to reach 0.01% and 0.03% in sequences 2 and 3 respectively.

V. CONCLUSION

In this paper, we presented a feature grouping strategy based on gradient vector flows to improve matching robustness. A set of features are extracted and the underlying gradient flow is used to associate them to medial keypoints. Indoor datasets were generated for testing. Experiments showed that improving matching robustness increased the accuracy of VO. Although these results show interesting findings, we plan to

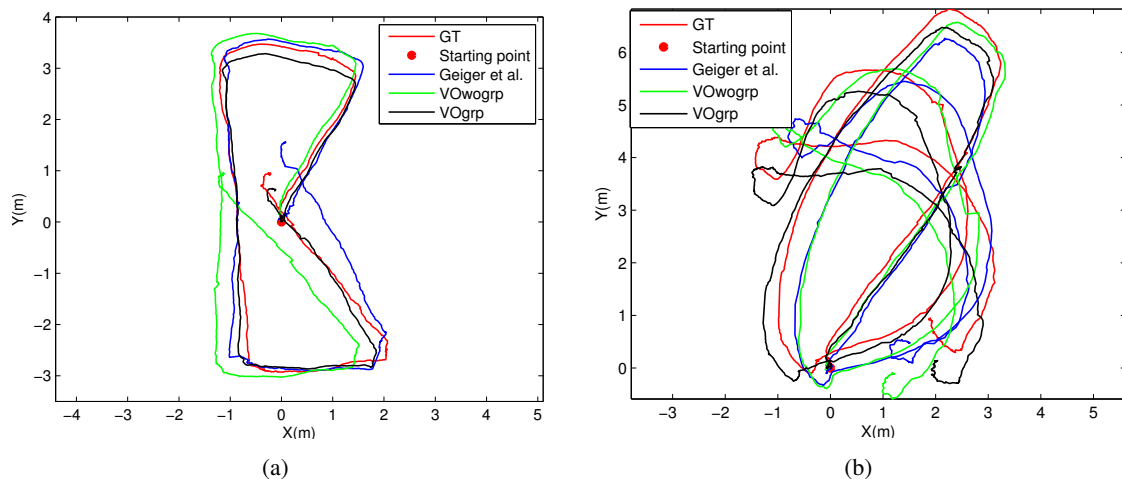


Fig. 4. Estimated VO trajectories (a) sequence 2 (red dot: starting point; red line: GT; blue line: Geiger et al.; green line: ORB features NOT grouped; black line: ORB features grouped) (b) sequence 3 (the same legend applies)

investigate further grouping methods. Another research path currently under work relates to the optimization techniques used for the motion estimation in order to improve the accuracy. Also, we intend to generate more challenging aerial stereo datasets to further test our system and make them available for researchers to test their stereo vision based algorithms. They include large scale outdoor sequences.

REFERENCES

- [1] H. P. Moravec, *Obstacle Avoidance and Navigation in the Real World by a Seeing Robot Rover*. PhD thesis, Stanford University, Stanford, CA, 1980.
- [2] K. Konolige, M. Agrawal, and J. Sola, "Large-scale visual odometry for rough terrain," in *International Symposium on Robotics Research*, pp. 201–212, 2007.
- [3] M. Maimone, Y. Cheng, and L. Matthies, "Two years of Visual Odometry on the Mars Exploration Rovers," *Journal of Field Robotics*, vol. 24, pp. 169–186, Mar. 2007.
- [4] V. Grabe, H. H. Bulthoff, and P. Robuffo Giordano, "Robust optical-flow based self-motion estimation for a quadrotor UAV," *IEEE/RSJ International Conference on Intelligent Robots and Systems*, pp. 2153–2159, Oct. 2012.
- [5] S. S. da Costa Botelho, P. Drews, G. L. Oliveira, and M. da Silva Figueiredo, "Visual odometry and mapping for Underwater Autonomous Vehicles," in *6th Latin American Robotics Symposium*, pp. 1–6, Oct. 2009.
- [6] D. Lowe, "Distinctive image features from scale-invariant keypoints," *International journal of computer vision*, vol. 60, pp. 91–110, Nov. 2004.
- [7] H. Bay, T. Tuytelaars, and L. V. Gool, "Surf: Speeded up robust features," in *European Conference on Computer Vision*, pp. 404–417, 2006.
- [8] M. Calonder, V. Lepetit, C. Strecha, and P. Fua, "Brief: Binary robust independent elementary features," *Computer Vision/ECCV*, 2010.
- [9] A. Alahi, R. Ortiz, and P. Vanderghenst, "FREAK: Fast Retina Keypoint," *IEEE Conference on Computer Vision and Pattern Recognition*, pp. 510–517, June 2012.
- [10] E. Rublee, V. Rabaud, K. Konolige, and G. Bradski, "ORB: An efficient alternative to SIFT or SURF," in *International Conference on Computer Vision*, pp. 2564–2571, Nov. 2011.
- [11] F. Fraundorfer, L. Heng, D. Honegger, G. H. Lee, L. Meier, P. Tanskanen, and M. Pollefeys, "Vision-based autonomous mapping and exploration using a quadrotor MAV," *IEEE/RSJ International Conference on Intelligent Robots and Systems*, pp. 4557–4564, Oct. 2012.
- [12] A. S. Huang, A. Bachrach, P. Henry, M. Krainin, F. Dieter, and N. Roy, "Visual odometry and mapping for autonomous flight using an RGB-D camera," in *Intl. Sym. of Robot. Research*, pp. 1–16, 2011.
- [13] F. Fraundorfer and D. Scaramuzza, "Visual Odometry : Part II: Matching, Robustness, Optimization, and Applications," *IEEE Robotics & Automation Magazine*, vol. 19, pp. 78–90, June 2012.
- [14] L. R. García Carrillo, A. E. Dzúl López, R. Lozano, and C. Pégard, "Combining Stereo Vision and Inertial Navigation System for a Quadrotor UAV," *Journal of Intelligent & Robotic Systems*, vol. 65, pp. 373–387, Aug. 2011.
- [15] M. Agrawal and K. Konolige, "Real-time Localization in Outdoor Environments using Stereo Vision and Inexpensive GPS," in *18th International Conference on Pattern Recognition (ICPR'06)*, pp. 1063–1068, 2006.
- [16] Z. Zhu, T. Oskiper, S. Samarasekera, R. Kumar, and H. S. Sawhney, "Ten-fold Improvement in Visual Odometry Using Landmark Matching," in *11th IEEE International Conference on Computer Vision*, pp. 1–8, 2007.
- [17] I.-K. Jung, *SLAM in 3D Environments with Stereovision*. Ph.d, Toulouse, 2004.
- [18] A. Ascani, E. Frontoni, A. Mancini, and P. Zingaretti, "Feature group matching for appearance-based localization," in *IEEE/RSJ International Conference on Intelligent Robots and Systems*, pp. 3933–3938, IEEE, Sept. 2008.
- [19] E. Rosten and T. Drummond, "Machine learning for high-speed corner detection," *European Conference on Computer Vision*, vol. 1, pp. 430–443, 2006.
- [20] C. Xu and J. L. Prince, "Snakes, shapes, and gradient vector flow," *IEEE transactions on image processing : a publication of the IEEE Signal Processing Society*, vol. 7, pp. 359–69, Jan. 1998.
- [21] D. Engel and C. Curio, "Shape centered interest points for feature grouping," in *IEEE Conference on Computer Vision and Pattern Recognition - Workshops*, pp. 9–16, June 2010.
- [22] A. Geiger, J. Ziegler, and C. Stiller, "StereoScan: Dense 3d reconstruction in real-time," in *IEEE Intelligent Vehicles Symposium*, pp. 963–968, IEEE, June 2011.
- [23] B. Triggs, P. F. McLauchlan, R. I. Hartley, and A. W. Fitzgibbon, "Bundle adjustment modern synthesis," in *In Proceedings of the International Workshop on Vision Algorithms: Theory and Practice, ICCV 99*, vol. LNCS 1883, (London), pp. 298–372, Springer-Verlag, 2000.
- [24] D. Rodriguez and N. Aouf, "Robust egomotion for large-scale trajectories," *2012 IEEE International Conference on Multisensor Fusion and Integration for Intelligent Systems (MFI)*, pp. 156–161, Sept. 2012.
- [25] J. Y. Bouguet, "Camera calibration toolbox for matlab," 2008.
- [26] G. Bradski, "The OpenCV Library," *Dr. Dobb's Journal of Software Tools*, July 2000.
- [27] J.-P. Tardif, M. George, M. Laverne, A. Kelly, and A. Stentz, "A new approach to vision-aided inertial navigation," in *IEEE/RSJ International Conference on Intelligent Robots and Systems*, no. 2008, pp. 4161–4168, Oct. 2010.

The cost function for extraction of bound component from material

D. Janáčová, V. Vašek, and K. Kolomazník

Abstract—The paper contents mathematic models describing variable cases of extraction processes with bound substance ordering which we suggested for their optimization. Without mathematical simulation and optimization are extraction processes of bound component connected with enormous consumption of extraction liquid.

Keywords—Diffusion process, extraction, mathematical modeling.

I. INTRODUCTION

FOR reason of often solved problem in For reason of often solved problem in extraction technology processes we worked out mathematic models describing extraction of bound component from material. On the base of them, we suggested goal cost functions for optimization of extraction processes. The main part of operating costs connected with the consumption of active aqueous solutions, eventually technological extraction liquid bath, depends on the operating time, which simultaneously determines the consumption of electrical energy necessary to the drum drive (move). The bigger liquid consumption, the bigger gradient of diffusive components concentration and the bigger decrease of operating time needed for the achievement of required level of the material. The result of mentioned consideration is the minimum main part of operating costs in their dependence on the liquid consumption. Our task is to estimate this minimum and to compare the result with real process.

II. THE GOAL COST FUNCTION

It is possible to find the optimum of consumption of liquid of process to be successful course of the process respectively, and that all from the corresponding the operating costs-

This work was supported by the European Regional Development Fund under the project CEBIA-Tech No. CZ.1.05/2.1.00/03.0089.

D. Janáčová, Tomas Bata University in Zlín, Faculty of Applied Informatics, Department of Automation and Control Engineering, nám. T. G. Masaryka 5555, 760 01 Zlín, Czech Republic; phone: +420 576 035 241; fax: +420 576 032 716; (e-mail: janacova@fai.utb.cz)

V. Vašek, Tomas Bata University in Zlín, Faculty of Applied Informatics, Department of Automation and Control Engineering, nám. T. G. Masaryka 5555, 760 01 Zlín, Czech Republic (e-mail: vasek@fai.utb.cz)

K. Kolomazník, Tomas Bata University in Zlín, Faculty of Applied Informatics, Department of Automation and Control Engineering, nám. T. G. Masaryka 5555, 760 01 Zlín, Czech Republic (e-mail: kolomaznik@fai.utb.cz)

function. To determine the operating costs-function for the material by liquid we assumed that we are able to eliminate component from the material by the liquid and that the main operating costs N_T of considered process are given by the sum of the consumed electric energy to the drive of machinery costs N_E and the consumed extraction liquid costs N_L . The following physico-chemical model serves for the determination of minimum operating costs:

$$N_T = N_L + N_E = K_L V_L + K_E P t. \quad (1)$$

III. EXTRACTION PROCESSES

It is possible to divide the extraction processes of bound component into several cases according to the way of adjustment:

One-stage extraction

The balance of extracted component we can write:

$$c_p V + c_{Ap} V = V_0 c_0 + c V + c_A V. \quad (2)$$

$$\text{In equilibrium } \varepsilon \cdot c_0 = c. \quad (3)$$

The constant of proportionality (an equilibrium constant of sorption) characterizes the strength of linkage to solid phase, i.e. largely it can determine how the extraction process is effective in this area.

In the simplest case it is possible to express this dependence by Langmuir sorption isotherm:

$$c_A = \frac{Kc}{Bc + 1} \quad (4)$$

For very low concentrations, when $Bc \ll 1$, it is possible to delimitate the area of linear dependence of sorption isotherm by relation:

$$c_A = K c. \quad (5)$$

For high concentrations, when $Bc \gg 1$, it is approximately

$$c_A = K / B, \tag{6}$$

which is the maximum value of absorbed component concentration, sometimes called the sorption capacity of solid phase.

After modification (2) we obtain:

$$c_0 = \frac{c_p(1+K)V}{V_0 + \varepsilon(1+K)V} = \frac{c_p(1+K)}{Na + \varepsilon(1+K)}. \tag{7}$$

Total degree of extraction is represented next equation

$$y = \frac{c_0 V_0}{V(c_p + Kc_p)} = \frac{c_0 Na}{c_p(1+K)}, \tag{8}$$

where $Na = \frac{V_0}{V}$ and means dimensionless consumption of liquid.

For next modification c_0 we can use previous equation (8):

$$y = \frac{Na}{Na + \varepsilon(1+K)}, \tag{9}$$

Fig. 1 shows the influence of degree of extraction on fixing power constant K .

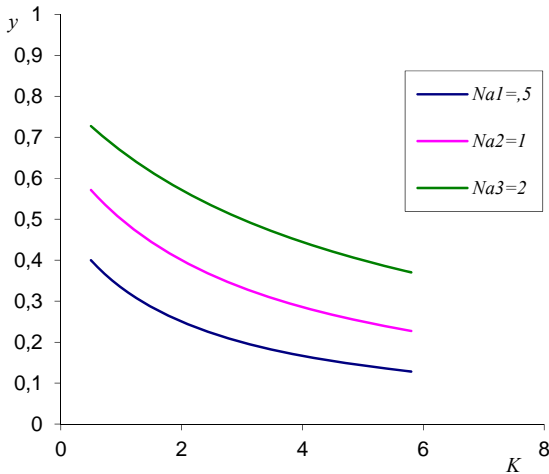


Fig. 1 Influence of degree of extraction on fixing power constant K .

One-stage extraction – diffusion model

In this process, the material is put into the extraction liquid. The extraction liquid flows neither in nor out of the bath. Under assumptions that bound component content in material is lower than its solubility in the same volume of extraction liquid at the given temperature and the influence of flanges on diffusion inside of the material sample is neglectable can formulate one-dimensional space-model of bath extraction of material sample by diffusion model of transport of extract out component.

$$\frac{D}{K+1} \cdot \frac{\partial^2 c(x,t)}{\partial x^2} = \frac{\partial c(x,t)}{\partial t}, t > 0, 0 \leq x \leq b \tag{10}$$

$$\frac{\partial c}{\partial x}(b,t) = - \frac{V_0}{D \cdot S} \cdot \frac{dc_0}{dt}(t) \tag{11}$$

$$c(x,0) = c_p \tag{12}$$

$$c_0(0) = 0 \tag{13}$$

$$\frac{\partial c}{\partial x}(0,t) = 0 \tag{14}$$

$$c(b,t) = \varepsilon \cdot c_0(t), \tag{15}$$

Equation (10) represents component ions diffusion from material in the direction of extraction liquid bath. The expression of the right hand side last term of equation depends on desorption mechanism of extraction component from solid phase. If we suppose that diffusion is determining for change rate of concentration then it is possible to express the dependence of bound component c_A on the bound component c by the relation of Langmuir's sorption isotherm [6]. Condition (12) shows the initial distribution of component concentration in solid phase-material. Relation (13) describes that we use pure water for material bath extraction. Relation (9) holds under condition of a perfectly mixed liquid phase. Boundary condition (14) denotes that field of concentration in solid phase is symmetric. Boundary balance condition (11) denotes the equality of the diffusion flux at the boundary between the solid and the liquid phases with the speed of accumulation of the diffusing element in the surrounding.

Dimensionless variables for the solution of equation (10) with additional conditions (11-15) are:

$$C = \frac{c}{c_p}, C_0 = \frac{c_0}{c_p}, Fo = \frac{Dt}{b^2(1+K)}, X = \frac{x}{b} \tag{16 a, b, c, d}$$

By means of Laplace transformation we obtain analytic solution. Final solution of extraction degree for this case is:

$$y = \frac{C_0 Na}{1+K} = \frac{Na}{\varepsilon(1+K) + Na} - 2 \frac{Na^2}{\varepsilon(1+K)} \sum_{n=1}^{\infty} \frac{\exp(-F_0 q_n^2)}{\varepsilon(1+K) + \frac{q_n^2 Na^2}{\varepsilon(1+K)} + Na}, \quad (17)$$

where q_n is the n -th positive root of the following transcendent equation

$$-\frac{Na \cdot q}{\varepsilon \cdot (1+K)} = \tan(q). \quad (18)$$

In the Fig. 2 we show detailed sketch of determination time to reaching demanded extraction degree.

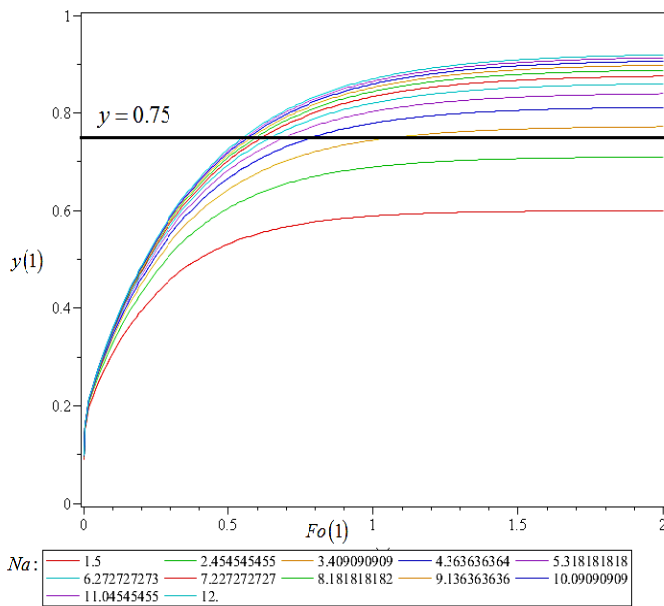


Fig. 2 Detail of determination time to reaching demanded extraction degree,
 $b = 0.0015 \text{ m}, D = 2 \cdot 10^{-8} \text{ m}^2 \cdot \text{s}^{-1}, V = 1 \text{ m}^3, \varepsilon = 0.5$

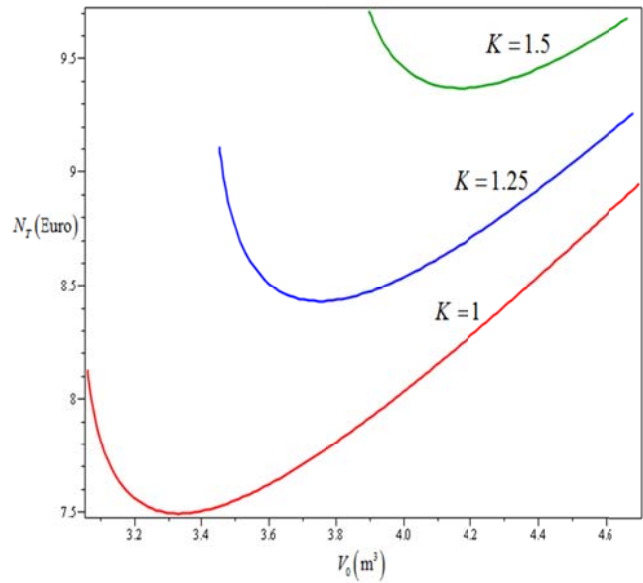


Fig. 3 Cost functions - determination of the optimal extraction number for variable K ,
 $b = 0.0015 \text{ m}, D = 2 \cdot 10^{-8} \text{ m}^2 \cdot \text{s}^{-1}, V = 1 \text{ m}^3, \varepsilon = 0.5,$
 $N_E = 0.3 \text{ €} \cdot \text{W}^{-1} \cdot \text{h}^{-1}, N_V = 1.6 \text{ €} \cdot \text{m}^{-3}, P = 10 \text{ kW}$

IV. CONCLUSION

The target function is dependent on the mathematical model of the real process and on the main purpose to be achieved by this operation.

For the design of the control of extraction we have chosen minimisation of operating costs. The volume of extraction and the time of operation should be chosen so as to minimize the costs of water and power necessary for drum. We can obtain the same quality of extraction by using a lower volume of water and prolonged extraction time. At the beginning the cost function, total extraction time is decreasing, because for short extraction times the water volume required is increasing of proportion and for longer times it is increasing because reduced water consumption cannot compensate the long operation time connected with power consumption.

Quantitative description for mentioned cases of extraction processes were verified and implemented. We created the program for calculation of the extraction process is to extract out the undesirable components from solid phase by solvent in which the extracted component is not very well soluble during extraction process.

LIST OF SYMBOLS

- A - sorption coefficient, [1]
 b - half thickness of the material, [m]
 B - sorption constant, [1]
 c - concentration of bound component in the material, [kg.m⁻³]
 c_A - concentration of bound component in the material, [kg.m⁻³]
 c_0 - concentration of component in the liquid phase, [kg.m⁻³]
 C_0 - dimensionless concentration of bound component in material, [1]
 c_p - initial concentration of component in the material, [kg.m⁻³]
 D - diffusion coefficient, [m².s⁻¹]
 Fo - Fourier number, [1]
 K - power of fixing, [1]
 K_L - price of liquid, [€·m³]
 K_E - price of electric energy, [€·W⁻¹·h⁻¹]
 Na - dimensionless volume of liquid bath, [1]
 N_T - total main operating costs, [€]
 N_L - extraction liquid costs, [€]
 N_E - electric energy costs, [€]
 V - volume of the material, [m³]
 V_L - volume of the liquid phase, [m³]
 x - space coordinate, [m]
 X - dimensionless space coordinate, [1]
 P - power of engine
 q_n - n -th roots of transcendent equation (18), [1]
 S - area of the material, [m²]
 t - time, [s]
 y - degree of extraction process, [1]
 ε - porosity of the material, [1]

REFERENCES

- [1] J. Crank, *The Mathematics of Diffusion*. Oxford: Clarendon Press, 1975.
- [2] H. Charvátová, "Modeling of Pelt Chemical Delimiting", (in Czech), Ph.D. dissertation, Tomas Bata University in Zlín, Zlín, 2007.
- [3] D. Janáčová, H. Charvátová, K. Kolomazník, and V. Vašek, *Creating software applications for solving diffusion problems in the MAPLE interface*. (in Czech), Zlín: Tomas Bata University in Zlín, 2012.
- [4] H. Charvátová, V. Vašek, R. Drga, and J. Křenek, "Software application for solving of non-stationary temperature fields," in *22nd International DAAAM Symposium*. Vienna: DAAAM International Vienna, 2011.
- [5] M. Feriančík, O. Liška, and M. More, "Navigation of industrial manipulator based on computer vision," *Transfer inovací*, vol. 28, 2013, pp. 140-142.
- [6] D. Janáčová, et al., "Washing Processes Optimization," in *Proceedings of International Union of Material Technologists and Chemists Societies*, London, 1997.
- [7] R. Drga, "Tepelné pozadí a PIR detektory," (in Czech), in *Bezpečnostní technologie, systémy a management 2013*, Zlín: Univerzita Tomáše Bati ve Zlíně, 2013, pp. 1-8.
- [8] R. Drga, "Nepřesnosti při měření teploty zdroje IR záření termovizní kamerou," (in Czech), in *ARTEP*, Košice: Technická univerzita v Košiciach, 19.1 - 19.8. 2012.
- [9] P. Mokrejš, F. Langmaier, and M. Mládek, "Acid treatment of chromed material waste from footwear and garment production," *Indian Chemical Engineer*, vol. 4, 2003, no. 4, pp. 259-263.
- [10] H. Charvátová, "Modeling of grinding process by printed circuit boards recycling," in *The 21st International DAAAM Symposium „Intelligent Manufacturing & Automation“*, 2010, pp. 475-476.
- [11] M. Staněk, D. Mañas, M. Mañas, and J. Javořík, "Simulation of injection molding process by cadmould rubber," *International Journal of Mathematics and Computers in Simulations*, vol. 5, 2011, p. 422-429.
- [12] L. Sýkorová, I. Lukovics, and O. Šuba, "Modelling and Prediction on the Laser Cutting of PMMA," in *13th International Conference on Tools*, Miskolc: University of Miskolc, pp. 417-422. 2012.
- [13] P. Mokrejš, F. Langmaier, M. Mládek, "Thermal properties of hydrolysates of chrome-tanned material waste", in *3rd Freiberg Collagen Symposium*, Freiberg, 2004, pp. 1-12.
- [14] M. Mañas, M. Staněk, Š. Šanda, and D. Mañas, "Rychlá příprava prototypů a reverzní inženýrství v konstrukci dílů a nástrojů", (in Czech), in *Proceedings of the 7th International Tools Conference ITC 2009*, Zlín, 2009, pp. 1-7.
- [15] O. Liška and J. Kováč, "Monitoring functions designing of assembling system with Petri networks utilization," *Acta Mechanica Slovaca*, vol. 3, pp. 81-84. 2003.
- [16] J. Piteř, M. Balara, and J. Boržiková, "Control of the Actuator with Pneumatic Artificial Muscles in Antagonistic Connection," *Collection of scientific works of the VŠB - Technical University of Ostrava*, vol. LIII, no. 2, pp. 101-106. 2007.
- [17] K. Židek and O. Liška, "Accelerometers usability for danger tilt off-highway vehicles and signal filtration with kalman filter", *Journal of Applied Science in the Thermodynamics and Fluid Mechanics*, vol. 4, no. 2, p. 1-6. 2010.
- [18] M. Veseliny, O. Liška, O., and K. Židek, "Využitie UI a moderných prvkov v rehabilitačnom procese," (in Slovak), *Strojárstvo extra*. [CD-ROM]. vol. 1. no. 5, pp. 45/1-45/4. 2011.
- [19] O. Liška, "Monitorizačné systémy pre automatizovanú výrobu," (in Slovak), *Transfer inovácií*, vol.12, pp. 121-123. 2008.

Dagmar Janáčová is a Professor in the Department of Automation and Control Engineering, Faculty of Applied Informatics, of Tomas Bata University in Zlín. Her research activities include: modeling of treatment processes of natural polymers, transport processes, recycling of tannery waste, and optimization and ecological approach of tannery processes. She has received the following honors: Diploma of England, XXIII IULTCS Congress, London, 11–14 September, 1997; Gold Medal - EUREKA EU Brussels 1997; Special Prize, Ministry of Agriculture, Belgium, 1997.

Vladimír Vašek is a Professor in the Department of Automation and Control Engineering, Faculty of Applied Informatics, of Tomas Bata University in Zlín. His research activities include: microcomputer applications in technology processes, computer monitoring and control systems, and discrete deterministic controllers approach of tannery processes. He has received the following honors: Diploma of England, XXIII IULTCS Congress, London, 11–14 September, 1997; Gold Medal - EUREKA EU Brussels 1997; Special Prize, Ministry of Agriculture, Belgium, 1997.

Karel Kolomazník is a Professor in the Department of Automation and Control Engineering, Faculty of Applied Informatics, of Tomas Bata University in Zlín. His research activities include: modeling of biopolymers treatment, chemical engineering transport processes, recycling of proteins, optimization and ecologization of tanning processes, and turning of vegetable and animal fats into biodiesel. He has received the following honors: Germany, American, England Leather Associations, XXIII IULTCS Congress, Friedrichshafen, May 15–20, 1995; England, XXIII IULTCS Congress, London, 11–14 September, 1997; USA, ALCA 1997, Annual Meeting, Regent Resort, NJ; Gold Medal - EUREKA EU Brussels 1997.

Multiple pattern-dependent controller design for Markovian jump linear systems

Taeso Kim and Sung Hyun Kim*

Abstract—This paper is concerned with deriving the stabilization condition for discrete-time Markovian jump linear systems (MJLSs) with multiple patterns of mode transition probabilities. In the derivation, a method of establishing the pattern-dependent transition probability matrices is proposed, which offers possibilities for extending our result to other issues of MJLSs.

Keywords—Markovian jump systems, control synthesis, networked control systems

I. INTRODUCTION

OVER the past decades, considerable efforts have been made in the study of Markovian jump linear systems (MJLSs) because a class of dynamic systems subject to random abrupt variations can be modeled by MJLSs (see [1], [2] and the references therein). Based on such efforts, the MJLS model has been applied in many practical applications [3], [4]. However, despite the numerous works available, most studies in the available literature regarding the control synthesis problem were found to have been carried out without consideration of the multiple patterns for mode transition probabilities.

Indeed, as reported in [5], the use of unified pattern-oriented transition probabilities may pose considerable uncertainties in the process of expressing the considered systems as MJLSs. For this reason, [5] proposed a method capable of stabilizing multiple pattern-dependent MJLSs in order to improve the convergence rate of the state response of networked control systems (NCSs). However, the drawback of [5] lies in the fact that the NCSs are designed irrespective of the utilization of the sequence that indicates the variation of patterns.

Motivated by the above concern, this paper focuses on deriving the stabilization condition for a class of discrete-time MJLSs with multiple patterns for mode transition probabilities. In contrast with existing results, this paper employs an additional discrete-time Markov process to incorporate information related to patterns into the derivation of the stabilization conditions. In addition, this paper proposes a method of establishing the pattern-dependent transition probability matrices, which offers possibilities for extending our result to other issues of MJLSs.

II. NOTATION

The notations $X \geq Y$ and $X > Y$ indicate that $X - Y$ is positive semi-definite and positive definite, respectively.

* The author is with the Department of Electrical Engineering, University of Ulsan (UOU), Ulsan, 680-749, Korea (e-mail: shnkim@ulsan.ac.kr)

In symmetric block matrices, (*) is used as an ellipsis for terms that are induced by symmetry. For any square matrix Q , $\mathbf{He}(Q) = Q + Q^T$ and $\mathbf{diag}(e_1, e_2, \dots, e_n)$ indicates a diagonal matrix with diagonal entries e_1, e_2, \dots, e_n . For $a_i \in \mathcal{N}^+ \triangleq \{1, 2, \dots\}$ such that $a_i < a_{i+1}$, $i \in \mathcal{N}_n^+ \triangleq \{1, 2, \dots, n\}$, the notation

$$\begin{aligned} [Q_i]_{i \in \{a_1, \dots, a_n\}} &= [Q_{a_1} \cdots Q_{a_n}] \\ [Q_{ij}]_{i, j \in \{a_1, \dots, a_n\}} &= \left[[Q_{a_1 j}]_{j \in \{a_1, \dots, a_n\}}^T \cdots [Q_{a_n j}]_{j \in \{a_1, \dots, a_n\}}^T \right]^T, \end{aligned}$$

where Q_i and Q_{ij} denote real submatrices with appropriate dimensions. $\mathbf{E}(\cdot)$ denotes the mathematical expectation.

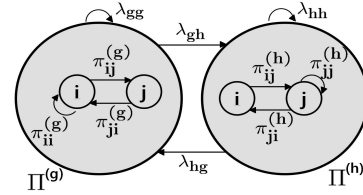


Fig. 1. Transition of multiple patterns for MTP matrices.

III. PRELIMINARIES

Consider the following discrete-time MJLSs:

$$x_{k+1} = A(r_k)x_k + B(r_k)u_k, \quad (1)$$

where $x_k \in \mathcal{R}^{n_x}$ and $u_k \in \mathcal{R}^{n_u}$ denote the state and the control input, respectively; and r_k denotes a discrete-time Markov process on the probability space that takes the values in a finite set \mathcal{N}_s^+ . Here, we employ an additional discrete-time Markov process $p_k \in \mathcal{N}_c^+$ to describe the multiple patterns for mode transition probabilities (MTPs) whose transition probabilities are given by $\Pr(p_{k+1} = h | p_k = g) = \lambda_{gh}$ (see Fig. 1). Then, the mode transition probabilities of r_k are taken to be $\Pr(r_{k+1} = j | p_k = g, r_k = i) = \pi_{ij}^{(g)}$, where p_0 and r_0 become the initial operation mode and pattern, respectively. In particular, we define the MTP matrix for any pattern g as $\Pi^{(g)} = [\pi_{ij}^{(g)}]_{i, j \in \mathcal{N}_s^+}$ (see Fig. 1).

Now, let us consider the following state-feedback control law: $u_k = F(p_k, r_k)x_k$, where $F(p_k, r_k)$ denotes the pattern-dependent control gain, to be designed later. For later convenience, we set $A_i = A(r_k = i)$, $B_i = B(r_k = i)$, and $F_{gi} = F(p_k = g, r_k = i)$. Then, the closed-loop system is described as follows:

$$x_{k+1} = \bar{A}_{gi}x_k, \quad (2)$$

where $\bar{A}_{gi} = A_i + B_i F_{gi}$. In addition, the following definition is adopted to address the stabilization problem under consideration.

Definition 3.1 ([2], [5]): System (2) is said to be mean square stable if its solution is such that $\lim_{k \rightarrow \infty} \mathbf{E}(\|x_k\|^2) = 0$ for any initial conditions x_0, p_0 , and r_0 .

Lemma 3.1: System (2) is said to be mean square stable if there exist matrices $F_{gi} \in \mathcal{R}^{n_u \times n_x}$ and symmetric matrices $P_{gi} \in \mathcal{R}^{n_x \times n_x}$ such that

$$0 > \mathcal{M}_{gi} = \left(\sum_{h=1}^c \sum_{j=1}^s \lambda_{gh} \pi_{ij}^{(h)} \bar{A}_{gi}^T P_{hj} \bar{A}_{gi} \right) - P_{gi}, \quad \forall g, i. \quad (3)$$

Proof: Consider the following Lyapunov function candidate dependent on both the pattern p_k and the mode r_k : $V_k = V(p_k, r_k) = x_k^T P(p_k, r_k) x_k$, where $P(p_k, r_k) > 0$ for all $p_k \in \mathcal{N}_c^+$ and $r_k \in \mathcal{N}_s^+$. Then, from the Rayleigh quotient, it follows that

$$\mathbf{E}(V_k) \geq \min_{g \in \mathcal{N}_c^+, i \in \mathcal{N}_s^+} \lambda_{\min}(P_{gi}) \cdot \mathbf{E}(\|x_k\|^2), \quad (4)$$

where $P_{gi} = P(p_k = g, r_k = i)$ and $\lambda_{\min}(P_{gi})$ denotes the minimum eigenvalue of P_{gi} . Note that there exists a scalar δ such that $0 < \delta I \leq \min_{g \in \mathcal{N}_c^+, i \in \mathcal{N}_s^+} \lambda_{\min}(P_{gi})$ in the sense that $P_{gi} > 0$ for all g, i . As a result, $\mathbf{E}(V_k) \geq \delta \mathbf{E}(\|x_k\|^2)$, which leads to

$$\mathbf{E}(\|x_k\|^2) \leq \delta^{-1} \mathbf{E}(V_k), \quad \delta > 0. \quad (5)$$

Next, we see that

$$\begin{aligned} & \mathbf{E}(V(p_{k+1}, r_{k+1} | p_k = g, r_k = i)) - V(p_k = g, r_k = i) \\ &= x_k^T \left(\sum_{h=1}^c \sum_{j=1}^s \lambda_{gh} \pi_{ij}^{(h)} \bar{A}_{gi}^T P_{hj} \bar{A}_{gi} - P_{gi} \right) x_k \\ &= x_k^T \mathcal{M}_{gi} x_k. \end{aligned} \quad (6)$$

In addition, for $x_k \neq 0$,

$$\begin{aligned} & \frac{\mathbf{E}(V(p_{k+1}, r_{k+1} | p_k = g, r_k = i)) - V(p_k = g, r_k = i)}{V(p_k = g, r_k = i)} \\ &= -\frac{x_k^T (-\mathcal{M}_{gi}) x_k}{x_k^T P_{gi} x_k} \leq -\min_{g,i} \frac{\lambda_{\min}(-\mathcal{M}_{gi})}{\lambda_{\max}(P_{gi})}. \end{aligned} \quad (7)$$

Let $\alpha - 1 = -\min_{g,i} \frac{\lambda_{\min}(-\mathcal{M}_{gi})}{\lambda_{\max}(P_{gi})}$. Then, (3) implies $\alpha < 1$, and (7) allows that

$$\begin{aligned} \mathbf{E}(V(p_{k+1}, r_{k+1} | p_k = g, r_k = i)) &\leq \alpha V(p_k = g, r_k = i), \\ 0 &< \alpha < 1, \end{aligned}$$

that is, $\mathbf{E}(V_k) \leq \alpha^k V(p_0, r_0)$ for any x_0, p_0 , and r_0 . As a result, (5) can be converted into $0 \leq \mathbf{E}(\|x_k\|^2) \leq \delta^{-1} \alpha^k V(p_0, r_0)$, where $0 < \alpha < 1$. Hence, we can see that $\lim_{k \rightarrow \infty} \mathbf{E}(\|x_k\|^2) = 0$ because $\lim_{k \rightarrow \infty} \alpha^k = 0$. Therefore, by Definition 1, the proof can be completed. ■

IV. MAIN RESULTS

For simplicity of the discussion, this paper assumes that the sequence of patterns, designated as PAT in Fig. 2, is generated by a proper pattern indicator. Based on PAT, we can then reconstruct the sequences SEQ 1, SEQ 2, ..., SEQ c from SEQ 0, which result in the MTP matrices $\Pi^{(1)}, \dots, \Pi^{(c)}$ required in Fig. 1.

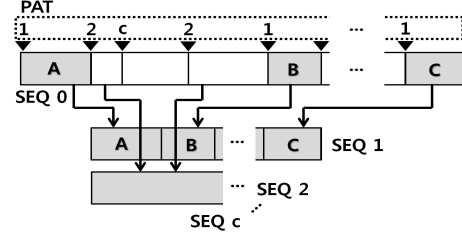


Fig. 2. Diagram for the construction of MTP matrices $\Pi^{(1)}, \dots, \Pi^{(c)}$.

The following theorem presents a set of conditions for the control synthesis of (2).

Theorem 4.1: Suppose that there exist matrices $\bar{F}_{gi} \in \mathcal{R}^{n_u \times n_x}$ and symmetric matrices $\bar{P}_{gi}, Q_{gi,hj} \in \mathcal{R}^{n_x \times n_x}$ such that, for all g, i ,

$$0 < \bar{P}_{gi} - \sum_{h=1}^c \sum_{j=1}^s \lambda_{gh} \pi_{ij}^{(g)} Q_{gi,hj}, \quad (8)$$

$$0 \leq \begin{bmatrix} \bar{P}_{hj} & A_i \bar{P}_{gi} + B_i \bar{F}_{gi} \\ (*) & Q_{gi,hj} \end{bmatrix}, \quad \forall h, j. \quad (9)$$

Then, the closed-loop control system (2) is stochastically stable and the mode-dependent control gains are given by $F_{gi} = \bar{F}_{gi} \bar{P}_{gi}^{-1}$ for all g, i .

Proof: By Lemma 1, the stability condition of (2) is given by $0 < P_{gi} - \sum_{h=1}^c \sum_{j=1}^s \lambda_{gh} \pi_{ij}^{(g)} \bar{A}_{gi}^T P_{hj} \bar{A}_{gi}$. Furthermore, performing a congruent transformation to the stability condition by $\bar{P}_{gi} = P_{gi}^{-1}$ yields

$$0 < \bar{P}_{gi} - \sum_{h=1}^c \sum_{j=1}^s \lambda_{gh} \pi_{ij}^{(g)} \bar{P}_{gi} \bar{A}_{gi}^T P_{hj} \bar{A}_{gi} \bar{P}_{gi}, \quad \forall g, i. \quad (10)$$

In the sense that $\lambda_{gh} \geq 0$ and $\pi_{ij}^{(g)} \geq 0$, (10) can be converted into (8),

$$0 \leq Q_{gi,hj} - \bar{P}_{gi} \bar{A}_{gi}^T P_{hj} \bar{A}_{gi} \bar{P}_{gi}. \quad (11)$$

Finally, after applying the Schur complement to (11), it becomes (9), where $\bar{F}_{gi} = F_{gi} \bar{P}_{gi}$. ■

V. NUMERICAL EXAMPLES

To verify the effectiveness of our result, we consider the following discrete-time MJLS with $s = 3$:

$$\begin{aligned} A_1 &= \begin{bmatrix} 0.25 & -0.83 \\ 2.50 & -3.50 \end{bmatrix}, A_2 = \begin{bmatrix} 1.0 & -0.25 \\ 2.5 & -3.00 \end{bmatrix}, B_1 = \begin{bmatrix} 1 \\ -1 \end{bmatrix}, \\ A_3 &= \begin{bmatrix} 1.5 & -0.56 \\ 2.5 & -2.75 \end{bmatrix}, B_2 = \begin{bmatrix} 1 \\ 1 \end{bmatrix}, B_3 = \begin{bmatrix} 0.8 \\ -1 \end{bmatrix}, \end{aligned}$$

$$\Pi^{(1)} = \begin{bmatrix} 0.0 & 0.5 & 0.5 \\ 0.3333 & 0.6667 & 0.0 \\ 0.5000 & 0.0 & 0.5 \end{bmatrix},$$

$$\Pi^{(2)} = \begin{bmatrix} 0.5 & 0.25 & 0.25 \\ 0.0 & 0.3333 & 0.6667 \\ 0.25 & 0.5 & 0.25 \end{bmatrix},$$

$\lambda_{11} = 0.9091, \lambda_{12} = 0.0909, \lambda_{21} = 0.0833, \lambda_{22} = 0.9167$. By the definition of $\Pi^{(g)}$, the MTP $\pi_{ij}^{(g)}$ can be obtained by the (i, j) th element of $\Pi^{(g)}$. In addition, the control gains F_{gi} for multiple patterns (i.e., $c = 2$) can be characterized in terms of the solution to a set of LMIs in Theorem 1, which are given as follows:

$$F_{11} = \begin{bmatrix} 1.4229 & -1.8047 \end{bmatrix},$$

$$F_{21} = \begin{bmatrix} 1.4539 & -1.8532 \end{bmatrix},$$

$$F_{12} = \begin{bmatrix} -4.0191 & 5.7839 \end{bmatrix},$$

$$F_{22} = \begin{bmatrix} -3.8518 & 5.4816 \end{bmatrix},$$

$$F_{13} = \begin{bmatrix} 0.8039 & -1.3743 \end{bmatrix},$$

$$F_{23} = \begin{bmatrix} 1.1040 & -1.6588 \end{bmatrix}.$$

Fig. 3 shows the behavior of the state response by Algorithm 1 based on the obtained control gains, and the mode evolution used therein, where $x_0 = [-0.3 \ 0.4]^T, p_0 = 1$, and $r_0 = 1$. Here, by letting the cost index $\mathcal{J}_m = \sum_{k=0}^m x_k^T x_k$, it follows that $\mathcal{J}_{20} = 21.0661$ for $c = 1$ and $\mathcal{J}_{20} = 14.9114$ for $c = 2$. In this sense, we can see that, in comparison with the case of $c = 1$, Theorem 1 is in a better position for improving system performance because it offers the multiple pattern-dependent stabilization condition.

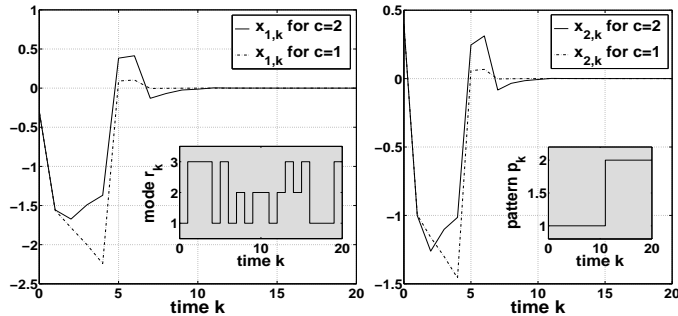


Fig. 3. Mode evolution and behavior of the state response $x_k = [x_{1,k} \ x_{2,k}]^T$.

VI. CONCLUDING REMARKS

In this paper, we have paid considerable attention to deriving the multiple pattern-dependent stabilization condition for a class of discrete-time MJLSs. Our future work is directed toward extending our result to other interesting problems associated with MJLSs.

ACKNOWLEDGMENT

This work was supported by the National Research Foundation of Korea Grant funded by the Korean Government (NRF-2012R1A1A1013687).

REFERENCES

- [1] Boukas, E.-K. and Liu, Z. K.: ‘Robust \mathcal{H}_∞ control of discrete-time Markovian jump linear systems with mode-dependent time-delays’, *IEEE Trans. Autom. Control*, 2001, **46**, p. 1918-1924.
- [2] Costa, O. L. V., Fragoso, M. D., and Marques, R. P.: *Discrete-time Markovian jump linear systems*, 2005, London: Springer-Verlag.
- [3] Xie., L. and Xie., L.: ‘Stability analysis of networked sampled-data linear systems with Markovian packet losses’, *IEEE Trans. Autom. Control*, 2009, **54**, p. 1375-1381.
- [4] Tao, F. and Zhao, Q.: ‘Synthesis of active fault-tolerant control based on Markovian jump system models’, *IET Contr. Theory Appl.*, 2007, **1**, p. 1160-1168.
- [5] Kim, S. H. and Park, P.: ‘Networked-based robust \mathcal{H}_∞ control design using multiple levels of network traffic’, *Automatica*, 2009, **45**, p. 764-770

Adaptive Continuous-Time Decoupling Control

Marek Kubalčík, Vladimír Bobál

I.

Abstract— The paper is focused on a design and implementation of a decoupling multivariable controller. The controller was designed in continuous-time version. The control algorithm is based on polynomial theory and pole – placement. A decoupling compensator is used to suppress interactions between control loops. The controller integrates an on – line identification of an ARX model of a controlled system and a control synthesis on the basis of the identified parameters. The model parameters are recursively estimated using the recursive least squares method. It is not possible to measure directly input and output derivatives of a system in case of continuous – time control loop. One of the possible approaches to this problem is establishing of filters and filtered variables to substitute the primary variables. The filtered variables are then used in the recursive identification procedure.

Keywords— multivariable control, control algorithms, adaptive control, polynomial methods, pole assignment, recursive identification

II. INTRODUCTION

TYPICAL technological processes require the simultaneous control of several variables related to one system. Each input may influence all system outputs. The design of a controller for such a system must be quite sophisticated if the system is to be controlled adequately. There are many different methods of controlling MIMO (multi input – multi output) systems. Several of these use decentralized PID controllers [1], others apply single input-single-output (SISO) methods extended to cover multiple inputs [2]. The classical approach to the control of multi-input–multi-output (MIMO) systems is based on the design of a matrix controller to control all system outputs at one time. The basic advantage of this approach is its ability to achieve optimal control performance because the controller can use all the available information about the controlled system. Controllers are based on various approaches and various mathematical models of controlled

processes. A standard technique for MIMO control systems uses polynomial methods [3], [4], [5] and is also used in this paper. Controller synthesis is reduced to the solution of linear Diophantine equations [6].

One controller, which enables decoupling control of TITO (two input-two output) systems, is presented. The proposed control algorithm applies a decoupling compensator [7], [8], [9] to suppress undesired interactions between control loops. The controller was realized in continuous-time version. It was realized as a self-tuning controller [10], [11] with recursive identification of a model of the controlled system. The recursive least squares method is used in the identification part. The reason why the controller was realized as a self-tuning controller is following: a model of the controlled TITO system is supposed in the form of the matrix fraction. The controller's synthesis is based on a model with a diagonal matrix in its matrix fraction description (the reason is described in further sections). A recursive identification used in the identification part of the self-tuning controller enables to describe a dynamics of a system with a full matrix by a model with the diagonal matrix. Self-tuning controllers are also suitable for control of nonlinear systems or systems with variable parameters.

III. MODEL OF THE CONTROLLED SYSTEM

A general transfer matrix of a two-input–two-output system with significant cross-coupling between the control loops is expressed as

$$\mathbf{G}(s) = \begin{bmatrix} G_{11}(s) & G_{12}(s) \\ G_{21}(s) & G_{22}(s) \end{bmatrix} \quad (1)$$

$$\mathbf{Y}(s) = \mathbf{G}(s)\mathbf{U}(s) \quad (2)$$

where $\mathbf{U}(s)$ and $\mathbf{Y}(s)$ are vectors of the manipulated variables and the controlled variables.

$$\mathbf{Y}(s) = [y_1(s), y_2(s)]^T \quad \mathbf{U}(s) = [u_1(s), u_2(s)]^T \quad (3)$$

It may be assumed that the transfer matrix can be transcribed to the following form of the matrix fraction:

$$\mathbf{G}(s) = \mathbf{A}^{-1}(s)\mathbf{B}(s) = \mathbf{B}_1(s)\mathbf{A}_1^{-1}(s) \quad (4)$$

where the polynomial matrices $\mathbf{A} \in R_{22}[s]$, $\mathbf{B} \in R_{22}[s]$ represent the left coprime factorization of matrix $\mathbf{G}(s)$ and the

Marek Kubalčík is with Tomas Bata University in Zlín, Faculty of Applied Informatics, Nám. T. G. Masaryka 5555, 760 05 Zlín (corresponding author to provide phone: +420 57-603-5198; e-mail: kubalcik@fai.utb.cz).

Vladimír Bobál is with Tomas Bata University in Zlín, Faculty of Applied Informatics, Nám. T. G. Masaryka 5555, 760 05 Zlín (e-mail: bobal@fai.utb.cz).

matrices $A_1 \in R_{22}[s]$, $B_1 \in R_{22}[s]$ represent the right coprime factorization of $G(s)$. The further described algorithm is based on a model with polynomials of second order. This model proved to be effective for control of several TITO laboratory processes [12], where controllers based on a model with polynomials of the first order failed. In case of decoupling control using a compensator it is useful to consider matrix $A(s)$ as diagonal. The reason is explained in the following section.

$$A(s) = \begin{bmatrix} s^2 + a_1s + a_2 & 0 \\ 0 & s^2 + a_7s + a_8 \end{bmatrix} \quad (5)$$

$$B(s) = \begin{bmatrix} b_1s + b_2 & b_3s + b_4 \\ b_5s + b_6 & b_7s + b_8 \end{bmatrix} = \begin{bmatrix} B_{11} & B_{12} \\ B_{21} & B_{22} \end{bmatrix} \quad (6)$$

Differential equations describing dynamical behavior of the system are as follows

$$y_1'' + a_1y_1' + a_2y_1 = b_1u_1' + b_2u_1 + b_3u_2' + b_4u_2 \quad (7)$$

$$y_2'' + a_3y_2' + a_4y_2 = b_5u_1' + b_6u_1 + b_7u_2' + b_8u_2 \quad (8)$$

IV. DESIGN OF THE DECOUPLING CONTROLLER

One of possible approaches to control of multivariable systems is the serial insertion of a compensator ahead of the system [7], [8], [9]. The compensator then becomes a part of the controller. The objective, in this case, is to suppress undesirable interactions between the input and output variables so that each input affects only one controlled variable. The block diagram for this kind of system is shown in Figure 1 (R is a transfer matrix of a controller and C is a decoupling compensator).

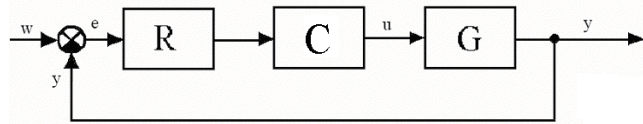


Fig. 1 Closed loop system with compensator

The resulting transfer function H (the operator s will be omitted from some operations for the purpose of simplification) is then determined by

$$H = GC = A^{-1}BC = A^{-1}H_1 \quad (9)$$

The decoupling conditions are fulfilled when matrix H is diagonal. As it was mentioned above the matrix A is supposed to be diagonal. The reason for this simplification is apparent from equation (9). When matrix A is assumed to be non-diagonal it has to be included into the compensator in order to obtain a diagonal matrix H . The order of the controller and consequently complexity of its design would increase.

The compensator is defined as

$$C = \frac{1}{\det(B)} \begin{bmatrix} B_{11}B_{22} & -B_{12}B_{22} \\ -B_{11}B_{21} & B_{11}B_{22} \end{bmatrix} \quad (10)$$

The matrix H_1 then takes following form

$$H_1 = BC = \begin{bmatrix} B_{11} & 0 \\ 0 & B_{22} \end{bmatrix} \quad (11)$$

Generally, the vector of input reference signals W is specified as

$$W(s) = F_w^{-1}(s)h(s) \quad (12)$$

Further the reference signals are considered as step functions. In this case h is a vector of constants and F_w is expressed as

$$F_w(s) = \begin{bmatrix} s & 0 \\ 0 & s \end{bmatrix} \quad (13)$$

The controller can be described both by left and right matrix fractions as well as the controlled system

$$G_R(s) = P^{-1}(s)Q(s) = Q_1(s)P_1^{-1}(s) \quad (14)$$

In order to achieve asymptotic tracking of the reference signal, an integrator must be incorporated into the controller. The controller including the integrator can be defined as

$$R = F^{-1}Q_1P_1^{-1} \quad (15)$$

The component F is the integrator. The resulting matrix of the controller can be then defined as follows

$$CR = CF^{-1}Q_1P_1^{-1} \quad (16)$$

It is possible to derive an equation for the system output, which can be modified by matrix operations to the form

$$Y = P_1(AFP_1 + H_1Q_1)^{-1}H_1Q_1P_1W \quad (17)$$

The determinant of the matrix in the denominator ($AFP_1 + H_1Q_1$) is the characteristic polynomial of the MIMO system. The roots of this polynomial matrix determine the behaviour of the closed loop system. They must be placed on the left side of the Gauss complex plane for the system to be stable. Conditions of BIBO stability can be defined by the following Diophantine matrix equation:

$$AFP_1 + HQ_1 = M \quad (18)$$

where $M \in R_{22}[s]$ is a stable diagonal polynomial matrix. If the system has the same number of inputs and outputs, matrix M can be chosen as diagonal, which allows easier computation of the controller parameters. Correct pole placement of the matrix M is very important for good control performance.

$$M(s) = \begin{bmatrix} s^4 + m_1s^3 + m_2s^2 + & 0 \\ +m_3s + m_4 & \\ 0 & s^4 + m_5s^3 + m_6s^2 + \\ & +m_7s + m_8 \end{bmatrix} \quad (19)$$

The degree of the controller polynomial matrices depends on the internal properness of the closed loop. The structures of matrices P_1 and Q_1 were chosen so that the number of unknown controller parameters equals the number of algebraic equations resulting from the solution of the Diophantine equation (18) using the method of uncertain coefficients:

$$P_1(s) = \begin{bmatrix} s + p_1 & 0 \\ 0 & s + p_2 \end{bmatrix} \quad (20)$$

$$Q_1(s) = \begin{bmatrix} q_1 s^2 + q_2 s + q_3 & 0 \\ 0 & q_4 s^2 + q_5 s + q_6 \end{bmatrix} \quad (21)$$

The solution of the Diophantine equation results in a set of 8 algebraic equations with unknown controller parameters. Using matrix notation, the algebraic equations are expressed in the following form.

$$\begin{bmatrix} 1 & b_1 & 0 & 0 \\ a_1 & b_2 & b_1 & 0 \\ a_2 & 0 & b_2 & b_1 \\ 0 & 0 & 0 & b_2 \end{bmatrix} \begin{bmatrix} p_1 \\ q_1 \\ q_2 \\ q_3 \end{bmatrix} = \begin{bmatrix} m_1 - a_1 \\ m_2 - a_2 \\ m_3 \\ m_4 \end{bmatrix} \quad (22)$$

$$\begin{bmatrix} 1 & b_7 & 0 & 0 \\ a_3 & b_8 & b_7 & 0 \\ a_4 & 0 & b_8 & b_7 \\ 0 & 0 & 0 & b_8 \end{bmatrix} \begin{bmatrix} p_2 \\ q_4 \\ q_5 \\ q_6 \end{bmatrix} = \begin{bmatrix} m_5 - a_3 \\ m_6 - a_4 \\ m_7 \\ m_8 \end{bmatrix} \quad (23)$$

The control law is defined as:

$$FU = CQ_1P_1^{-1}E \quad (24)$$

where E is a vector of control errors. This matrix equation can be transcribed to the differential equations of the controller

$$u_1^{(5)} + u_1^{(4)}K_1 + u_1^{(3)}K_2 + u_1^{(2)}K_3 + u_1'K_4 = e_1^{(5)}T_1 + e_1^{(4)}T_2 + e_1^{(3)}T_3 + e_1^{(2)}T_4 + e_1^{(1)}T_5 + e_1T_6 - e_2^{(5)}T_7 - e_2^{(4)}T_8 - e_2^{(3)}T_9 - e_2^{(2)}T_{10} - e_2^{(1)}T_{11} - e_2T_{12} \quad (25)$$

$$u_2^{(5)} + u_2^{(4)}K_1 + u_2^{(3)}K_2 + u_2^{(2)}K_3 + u_2'K_4 = -e_1^{(5)}T_{13} - e_1^{(4)}T_{14} - e_1^{(3)}T_{15} - e_1^{(2)}T_{16} - e_1^{(1)}T_{17} - e_1T_{18} + e_2^{(5)}T_{19} + e_2^{(4)}T_{20} + e_2^{(3)}T_{21} + e_2^{(2)}T_{22} + e_2^{(1)}T_{23} + e_2T_{24} \quad (26)$$

Where

$$X_1 = b_1b_7 - b_3b_5 \quad (27)$$

$$\begin{aligned} K_1 &= (b_1b_7p_2 - b_3b_5p_2 + b_1b_7p_1 - b_3b_5p_1 + b_1b_8 + b_2b_7 - b_4b_5 - b_3b_6)/X_1 \\ K_2 &= (b_1b_7p_1p_2 - b_3b_5p_1p_2 + b_1b_8p_2 + b_2b_7p_2 - b_4b_5p_2 - b_3b_6p_2 + b_1b_8p_1 + b_2b_7p_1 - b_4b_5p_1b_3b_6p_1 + b_2b_8 - b_4b_6)/X_1 \\ K_3 &= (b_1b_8p_1p_2 + b_2b_7p_1p_2 - b_4b_5p_1p_2 - b_3b_6p_1p_2 + b_2b_8p_2 - b_4b_6p_2 + b_2b_8p_1 - b_4b_6p_1)/X_1 \\ K_4 &= b_2b_8p_1p_2 - b_4b_6p_1p_2)/X_1 \end{aligned} \quad (28)$$

$$\begin{aligned} T_1 &= (b_1b_7q_1)/X_1 \\ T_2 &= (b_1b_8q_1 + b_2b_7q_1 + b_1b_7q_2 + b_1b_7q_1p_2)/X_1 \\ T_3 &= (b_2b_8q_1 + b_1b_8q_2 + b_2b_7q_2 + b_1b_7q_3 + b_1b_8q_1p_2 + b_2b_7q_1p_2 + b_1b_7q_2p_2)/X_1 \\ T_4 &= (b_2b_8q_2 + b_1b_8q_3 + b_2b_7q_3 + b_2b_8q_1p_2 + b_1b_8q_2p_2 + b_2b_7q_2p_2 + b_1b_7q_3p_2)/X_1 \\ T_5 &= (b_2b_8q_3 + b_2b_8q_2p_2 + b_1b_8q_3p_2 + b_2b_7q_3p_2)/X_1 \\ T_6 &= (b_2b_8q_3p_2)/X_1 \\ T_7 &= (b_3b_7q_4)/X_1 \\ T_8 &= (b_3b_8q_4 + b_4b_7q_4 + b_3b_7q_5 + b_3b_7q_4p_1)/X_1 \\ T_9 &= (b_4b_8q_4 + b_3b_8q_5 + b_4b_7q_5 + b_3b_7q_6 + b_3b_8q_4p_1 + b_4b_7q_4p_1 + b_3b_7q_5p_1)/X_1 \\ T_{10} &= (b_4b_8q_5 + b_3b_8q_6 + b_4b_7q_6 + b_4b_8q_4p_1 + b_3b_8q_5p_1 + b_4b_7q_5p_1 + b_3b_7q_6p_1)/X_1 \\ T_{11} &= (b_4b_8q_6 + b_4b_8q_5p_1 + b_3b_8q_6p_1 + b_4b_7q_6p_1)/X_1 \\ T_{12} &= (b_4b_8q_6p_1)/X_1 \\ T_{13} &= (b_1b_5q_1)/X_1 \\ T_{14} &= (b_1b_6q_1 + b_2b_5q_1 + b_1b_5q_2 + b_1b_5q_1p_2)/X_1 \\ T_{15} &= (b_2b_6q_1 + b_1b_6q_2 + b_2b_5q_2 + b_1b_5q_3 + b_1b_6q_1p_2 + b_2b_5q_1p_2 + b_1b_5q_2p_2)/X_1 \\ T_{16} &= (b_2b_6q_2 + b_1b_6q_3 + b_2b_5q_3 + b_2b_6q_1p_2 + b_1b_6q_2p_2 + b_1b_6q_3p_2)/X_1 \\ T_{17} &= (b_2b_6q_3 + b_2b_6q_2p_2 + b_1b_6q_3p_2 + b_2b_5q_3p_2)/X_1 \\ T_{18} &= (b_2b_6q_3p_2)/X_1 \\ T_{19} &= (b_1b_7q_4)/X_1 \\ T_{20} &= (b_1b_8q_4 + b_2b_7q_4 + b_1b_7q_5 + b_1b_7q_4p_1)/X_1 \\ T_{21} &= (b_2b_8q_4 + b_1b_8q_5 + b_2b_7q_5 + b_1b_7q_6 + b_1b_8q_4p_1 + b_2b_7q_4p_1 + b_1b_7q_5p_1)/X_1 \\ T_{22} &= (b_2b_8q_5 + b_1b_8q_6 + b_2b_7q_6 + b_2b_8q_4p_1 + b_1b_8q_5p_1 + b_2b_7q_5p_1 + b_1b_7q_6p_1)/X_1 \\ T_{23} &= (b_2b_8q_6 + b_2b_8q_5p_1 + b_1b_8q_6p_1 + b_2b_7q_6p_1)/X_1 \\ T_{24} &= (b_2b_8q_6p_1)/X_1 \end{aligned} \quad (29)$$

For purposes of simulation, the controller was realized in the Matlab/Simulink environment as an S-function. It was then necessary to obtain its state equations. Further there it is introduced a conversion of the first differential equation (25) to the state equations. The second differential equation (26) was conversed similarly. Equation (25) can be itemized as follows

$$\begin{aligned} u_{1A}^{(5)} + u_{1A}^{(4)}K_1 + u_{1A}^{(3)}K_2 + u_{1A}^{(2)}K_3 + u_{1A}'K_4 &= \\ = e_1^{(5)}T_1 + e_1^{(4)}T_2 + e_1^{(3)}T_3 + e_1^{(2)}T_4 + e_1^{(1)}T_5 + e_1T_6 \end{aligned} \quad (31)$$

$$\begin{aligned} u_{1B}^{(5)} + u_{1B}^{(4)}K_1 + u_{1B}^{(3)}K_2 + u_{1B}^{(2)}K_3 + u_{1B}'K_4 &= \\ = -e_2^{(5)}T_7 - e_2^{(4)}T_8 - e_2^{(3)}T_9 - e_2^{(2)}T_{10} - e_2^{(1)}T_{11} - e_2T_{12} \end{aligned} \quad (32)$$

Equation (31) can be transcribed to the transfer function. It is also possible to establish an auxiliary variable Z

$$G(s) = \frac{T_1 s^5 + T_2 s^4 + K_2 s^3 + K_3 s^2 + K_4 s}{s^5 + K_1 s^4 + T_3 s^3 + T_4 s^2 + T_5 s + T_6} = \frac{U_{1A}}{E_1} = \frac{U_{1A}}{Z} \frac{Z}{E_1} \quad (33)$$

By means of the variable Z it is possible to define following equations

$$T_1 z^{(5)} + T_2 z^{(4)} + T_3 z''' + T_4 z'' + T_5 z' + T_6 z = u_{1A} \quad (34)$$

$$z^{(5)} + K_1 z^{(4)} + K_2 z''' + K_3 z'' + K_4 z' = e_1 \quad (35)$$

Equation (35) can be converted to a set of differential equations of the first order (state equations). Choice of the state variables is as follows

$$x_1 = z \quad x_2 = z' \quad x_3 = z'' \quad x_4 = z''' \quad x_5 = z^{(4)} \quad (36)$$

And the state equations are

$$\begin{aligned} x_1' &= x_2 \\ x_2' &= x_3 \\ x_3' &= x_4 \\ x_4' &= x_5 \\ x_5' &= e_1 - K_1 x_5 - K_2 x_4 - K_3 x_3 - K_4 x_2 \end{aligned} \quad (37)$$

On the basis of the state variables, which are substituted to equation (34), it is possible to derive the first part of the manipulated variable u_{1A}

$$u_{1A} = T_1(e_1 - K_1 x_5 - K_2 x_4 - K_3 x_3 - K_4 x_2) + T_2 x_5 + T_3 x_4 + T_4 x_3 + T_5 x_2 + T_6 x_1 \quad (38)$$

Similarly it is possible to transcribe equation (32)

$$-T_7 z^{(5)} - T_8 z^{(4)} - T_9 z''' - T_{10} z'' - T_{11} z' - T_{12} z = u_{1B} \quad (39)$$

$$z^{(5)} + K_1 z^{(4)} + K_2 z''' + K_3 z'' + K_4 z' = e_2 \quad (40)$$

State variables were chosen similarly as in the previous case

$$x_6 = z \quad x_7 = z' \quad x_8 = z'' \quad x_9 = z''' \quad x_{10} = z^{(4)} \quad (41)$$

The state equations are then as follows

$$\begin{aligned} x_6' &= x_7 \\ x_7' &= x_8 \\ x_8' &= x_9 \\ x_9' &= x_{10} \\ x_{10}' &= e_2 - K_1 x_{10} - K_2 x_9 - K_3 x_8 - K_4 x_7 \end{aligned} \quad (42)$$

The second part of the manipulated variable u_{1B} can be computed similarly like the part u_{1A} by substitution of the state variables to equation (39)

$$u_{1B} = -T_7(e_2 - K_1 x_{10} - K_2 x_9 - K_3 x_8 - K_4 x_7) - T_8 x_{10} - T_9 x_9 - T_{10} x_8 - T_{11} x_7 - T_{12} x_6 \quad (43)$$

The manipulated variable u_1 is then defined by the following sum

$$u_1 = u_{1A} + u_{1B} \quad (44)$$

An expression for computation of the manipulated variable u_2 is obtained similarly on the basis of differential equation (26).

V. RECURSIVE IDENTIFICATION

The controller was realized as a self-tuning controller with recursive identification of a model of the controlled system. A recursive identification used in the identification part of the self-tuning controller enables to describe a dynamics of a system with a full matrix by a model with the diagonal matrix. Self-tuning controllers are also suitable for control of nonlinear systems or systems with variable parameters. The recursive least squares method [11] proved to be effective for self-tuning controllers and was used as the basis for our algorithm. For our two-variable example we considered the disintegration of the identification into two independent parts.

As the regression model we considered the ARX (AutoRegressive model with Exogenous input) [13]. Usually the ARX model is tested first and more complex model structures are only examined if it does not perform satisfactorily. Linear continuous time ARX model is

$$\begin{aligned} y_1''(t) + a_1 y_1'(t) + a_2 y_1(t) + a_3 y_2'(t) + a_4 y_2(t) &= \\ = b_1 u_1'(t) + b_2 u_1(t) + b_3 u_2'(t) + b_4 u_2(t) + n_1(t) & \\ y_2''(t) + a_5 y_1'(t) + a_6 y_1(t) + a_7 y_2'(t) + a_8 y_2(t) &= \\ = b_5 u_1'(t) + b_6 u_1(t) + b_7 u_2'(t) + b_8 u_2(t) + n_2(t) & \end{aligned} \quad (45)$$

where n_1 and n_2 are non - measurable random signals, which are assumed to have zero mean value and constant covariance.

It is not possible to measure directly input and output derivatives of a system in case of continuous - time control loop. One of the possible approaches to this problem is establishing of filters and filtered variables to substitute the primary variables. This approach is described in detail in [14], [15], [16]. The filtered variables are then used in the recursive identification procedure.

$$\begin{aligned} C(\sigma)u_{1f}(t) &= u_1(t) \\ C(\sigma)u_{2f}(t) &= u_2(t) \\ C(\sigma)y_{1f}(t) &= y_1(t) \\ C(\sigma)y_{1f}(t) &= y_1(t) \end{aligned} \quad (46)$$

where σ is the derivative operator and $C(\sigma)$ is a stable polynomial in σ . The degree of $C(\sigma)$ must be equal or greater than polynomials of the highest order in the matrix A . The time constants of the filters must be smaller than the time constants of the model. Since the latter are unknown at the beginning of the estimation procedure, it is necessary to make the filter time constants, selected a priori, sufficiently small.

It can be easily proved that the transfer behaviour between

the filtered and between the non – filtered variables is equivalent. This fact enables to employ the filtered variables for the model parameter estimation. If these are computed via filters (46) in discrete time intervals $t_k = kT_s$, $k = 0,1,2, \dots$, where T_s is the sampling period, then the parameters of the model can be recursively estimated from the equations

$$y_{1f}''(t_k) = -a_1 y_{1f}'(t_k) - a_2 y_{1f}(t_k) + b_1 u_{1f}'(t_k) + b_2 u_{1f}(t_k) + b_3 u_{2f}'(t_k) + b_4 u_{2f}(t_k) \quad (47)$$

$$y_{2f}''(t_k) = -a_3 y_{2f}'(t_k) - a_4 y_{2f}(t_k) + b_5 u_{1f}'(t_k) + b_6 u_{1f}(t_k) + b_7 u_{2f}'(t_k) + b_8 u_{2f}(t_k) \quad (48)$$

The regression vectors have the form

$$\phi_1^T(t_k) = [-y_{1f}'(t_k), -y_{1f}(t_k), -u_{1f}'(t_k), -u_{1f}(t_k), -u_{2f}'(t_k), -u_{2f}(t_k)] \quad (49)$$

$$\phi_2^T(t_k) = [-y_{2f}'(t_k), -y_{2f}(t_k), -u_{1f}'(t_k), -u_{1f}(t_k), -u_{2f}'(t_k), -u_{2f}(t_k)] \quad (50)$$

and the parameter vectors are

$$\theta_1^T(t_k) = [a_1, a_2, b_1, b_2, b_3, b_4] \quad (51)$$

$$\theta_2^T(t_k) = [a_3, a_4, b_5, b_6, b_7, b_8] \quad (52)$$

Considering the order of the system, the filters for all variables were chosen to have the second order. A right choice of the coefficients of the filter's polynomials and choice of the sampling period are the ruling factors for the speed of the parameter's convergence.

$$\begin{aligned} y_{1f}''(t) + c_1 y_{1f}'(t) + c_0 y_{1f}(t) &= y_1(t) \\ y_{2f}''(t) + c_1 y_{2f}'(t) + c_0 y_{2f}(t) &= y_2(t) \\ u_{1f}''(t) + c_1 u_{1f}'(t) + c_0 u_{1f}(t) &= u_1(t) \\ u_{2f}''(t) + c_1 u_{2f}'(t) + c_0 u_{2f}(t) &= u_2(t) \end{aligned} \quad (53)$$

The recursive least squares method was then used for the estimation of the parameters.

VI. SIMULATION VERIFICATION

Verification by simulation was carried out on a range of plants with various dynamics. The control of the model below is given here as an example. The controller's synthesis is based on the model with diagonal matrix A , which is obtained by recursive identification and which describes the dynamics of the system with full matrix A .

$$A(s) = \begin{bmatrix} s^2 + 2s + 0,7 & 0,2s + 0,4 \\ -0,5s - 0,1 & s^2 + 2s + 0,7 \end{bmatrix} \quad (54)$$

$$B(s) = \begin{bmatrix} 0,5s + 0,2 & 0,1s + 0,3 \\ 0,5s + 0,1 & 0,3s + 0,4 \end{bmatrix} \quad (55)$$

Figure 2 shows the plant's step response

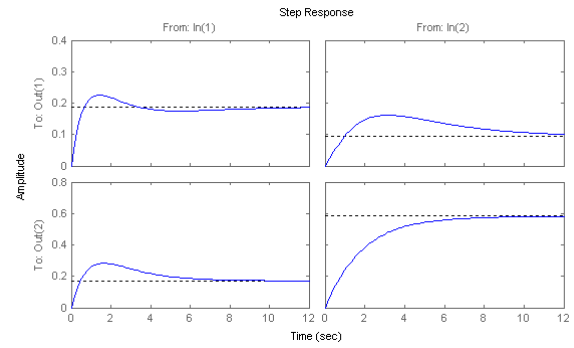


Fig. 2 Step response of the controlled system

The matrix $M(s)$ on the right side of the diophantine equation (18) obtained from experiments is

$$M(s) = \begin{bmatrix} s^4 + 4s^3 + 6s^2 + 4s + 1 & 0 \\ 0 & s^4 + 4s^3 + 6s^2 + 4s + 1 \end{bmatrix} \quad (56)$$

The time responses of the control are shown in Figure 2.

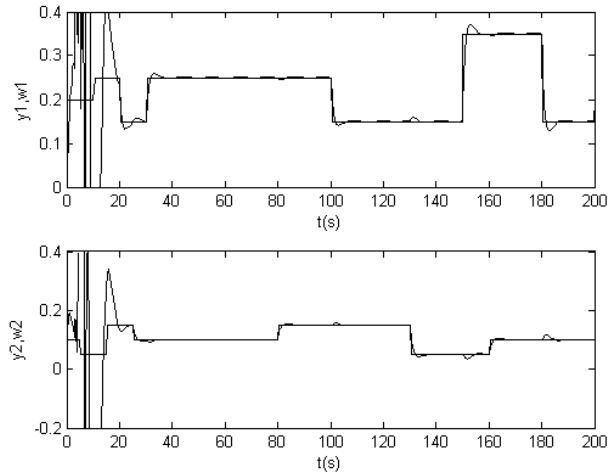


Fig. 3 Adaptive control with decoupling controller

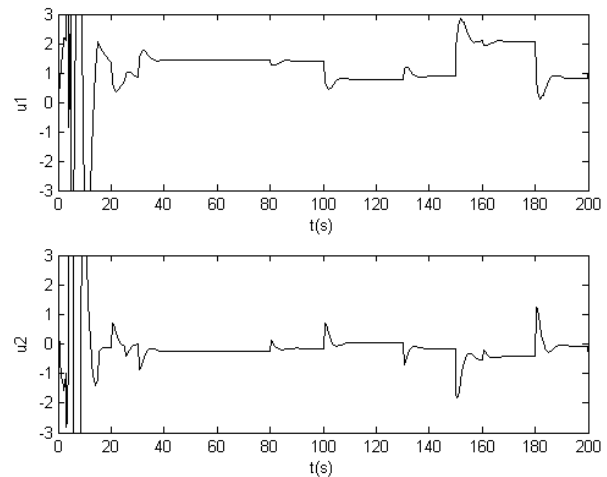


Fig. 4 Adaptive control with decoupling controller-manipulated variables

From the courses of the variables in Figure 3 it is obvious that the basic requirements on control were satisfied. The system was stabilized and the asymptotic tracking of the reference signals was achieved. With regards to decoupling, interactions between the control loops are negligible.

VII. CONCLUSION

A TITO controller with the decoupling compensator was designed and implemented. The simulation results proved that the method is suitable for control of linear systems. With regards to decoupling, it is clear that the compensator reduces interactions between the control loops. The described method of continuous – time models parameters estimation proved to be effective. A right choice of the filter's constants and the sampling period improves convergence of the parameters. The method is suitable for the identification part of continuous – time self – tuning controllers.

REFERENCES

- [1] W. L. Luyben, "Simple Method for Tuning SISO Controllers in Multivariable Systems", *Ing. Eng. Chem. Process Des. Dev.*, Vol. 25, pp. 654 – 660, 1986.
- [2] I.L. Chien, D.E. Seborg and D. A. Mellichamp, "Self-Tuning Control with Decoupling", *AIChE J.*, Vol. 33, No. 7, 1079 – 1088, 1987.
- [3] V. Kučera, "Stochastic multivariable control: a polynomial approach", *IEEE Trans. of Automatic Control*, 5, pp. 913–919, 1980.
- [4] V. Kučera, V., *Analysis and Design of Discrete Linear Control Systems*. Prentice Hall, Englewood Cliffs, New Jersey, 1991.
- [5] Vidyasagar, M., *Control System Synthesis: A Factorization Approach*. MIT Press, Cambridge MA, 1985.
- [6] V. Kučera, "Diophantine Equations in Control – a Survey". *Automatica*, 29, pp. 1361 – 1375, 1993.
- [7] P.R. Krishnawamy, et al., "Reference System Decoupling for Multivariable Control". *Ind. Eng. Chem. Res.*, 30, pp. 662-670, 1991.
- [8] Y. Peng, "A General Decoupling Precompensator for Linear Multivariable Systems with Application to Adaptive Control", *IEEE Trans. Aut. Control*, Vol. 35, No. 3, pp. 344-348, 1990.
- [9] M.O. Tade, M.M. Bayoumi, D.W. Bacon, "Adaptive Decoupling of a Class of Multivariable Dynamic Systems Using Output Feedback", *IEE Proc. Pt.D*, No. 6, pp. 265-275, 1986.
- [10] I. D. Landau, R. Lozano, M. M'Saad, *Adaptive Control*, Springer - Verlag, Berlin, 1998.
- [11] V. Bobal, J., Böhm, J., Fessl, J., Machacek, *Digital Self-Tuning Controllers*, Springer - Verlag, London, 2005.
- [12] Kubalčík, M. and V. Bobál, "Adaptive Control of Coupled Drives Apparatus Based on Polynomial Theory". In Proc. IMechE Vol. 220 Part I: *J. Systems and Control Engineering*, 220(I7), pp. 641-654, 2006.
- [13] Ljung, L., *System Identification: Theory for the User*, 2nd edn, Prentice Hall, Upper Saddle River, N.J., 1999.
- [14] Wahlberg, B., On the identification of continuous – time dynamical systems, *Report LiTH-ISY-I-0905*, Linköping, 1990.
- [15] Unbehauen, H., Rao, G.P., *Identification of Continuous Systems*, North Holland, Amsterdam, 1987.
- [16] Gawthrop, P. J., *Continuous – Time Self – Tuning Control*, John Wiley, Chichester, 1987.

Comparing accuracy and solution times in coverage models

GEORGE P. ALEXANDRIS, NIKOLAOS G. BARDIS
 Department of Mathematics and Science Engineering
 Hellenic Military University
 Vari-Koropi Ave, 16673, Vari
 GREECE
gpa@aub.gr, bardis@ilabsse.gr

Abstract— A common problem we face during our trials to discover new coverage models is the trade off we have to make between the accuracy of the results and the solution times. The more accurate results we produce the more time we need to discover the solution of the problem. In real life there are categories of problems where high accuracy of the results is not of a great importance and other categories where the minimization of the solution times means life or death. What we usually do is to select either to maximize the accuracy of the results or to minimize solution times, so as to solve a particular problem. But in some cases, problems are really complex and we need both high accuracy and very low solution times. For example in military decisions, where a simulation or a real scenarios is taking place, we need both to be accurate and fast, so as to deal with the problem effectively. In this paper we propose the addition of G.I.S tools in the formulation of the original mclp model and we measure the effect of these specific G.I.S tools in both the accuracy and the solution times of the problem.

Keywords—Geographic Information Systems, covering models, Solution times and accuracy

1 Introduction

Coverage problems constitute an extensive set of problems in location analysis. A wide set of applications have been solved using the above problems and many others will be solved in the near future. Their main objective is to locate a number of facilities, p , in such a way as the demand in the area is covered. Coverage is achieved when the service provided by a facility is available to any point within the demand area within some predetermined distance or time.

One can identify two main classes of demand covering problems, as proposed by Daskin [1]: (a) *mandatory covering problems*, where all the demand area must be covered using the minimum number of servers and (b) *maximal covering models*, where the largest possible part of the demand area must be covered using a given number of available servers.

In our paper we concentrate on the class of maximal covering problems, whose main representative is the Maximal Covering Location Problem (MCLP), first stated by Church and ReVelle [2].

Corresponding author: George P. Alexandris, Ph.D., Lecturer
 Department of Mathematics and Science Engineering
 Hellenic Military University.

Since then MCLP has been used extensively for solving problems in many different fields. Applications can be found in the design of congested service systems (Marianov and Serra [3], the location of emergency facilities (Current and O’Kelly [4], the design of hierarchical health care systems (Moore and ReVelle [5] and many others.

Murray [6] concluded that the main mandatory representative of covering models known as Location Set Covering Model suffers from the so-called modifiable areal unit problem (MAUP) which suggests that modeling results are susceptible to manipulation by altering spatial scale or by changing how spatial units are defined. For solving the above vulnerability Murray used the capabilities of Geographic Information Systems and developed a new set covering model which is less susceptible to MAUP and produces better results.

The use of GIS in the area of covering models had started. G Alexandris and I.Giannikos [7], used the capabilities of G.I.S and formulated a new type of MCLM, using spatial objects like polygons, partial coverage and introducing α parameter as the correlation between fully and partial coverage, so as to improve the accuracy of the results, and minimize the coverage gaps that could be observed by the use of the classical MCLP.

What we would examine in this paper is the behavior of the classical MCLM against MCLM with spatial objects and α parameter, focusing not only in coverage gaps but in addition we will examine the behavior of the models concerning solution times.

The rest of the paper is organized as follows. We review MCLP and MCLP-SO and demonstrate the classic discretization process for the municipality of Athens. We present the results of the municipality of Athens concerning real coverage and solution times. Finally, we draw some conclusions and discuss some future research directions.

2 Mathematical Models

The Maximal Covering Location Problem was first stated by Church and ReVelle [12]. It considers a discrete set of demand points, each associated with a weight reflecting its importance, and a discrete set of

candidate locations where servers may be located. The objective is to choose locations for a given number of servers such that a weighted sum of demand points is covered. The problem can be formally stated as follows:

Notation

Indices

i : index for candidate locations
 j : index for demand points

Parameters

d_{ij} : distance from j to i
 D_j : distance standard for demand point j
 w_j : coefficient reflecting the desirability of covering demand point j

Sets

I : set of all candidate locations
 J : set of demand points
 $N(j)$: set of locations that can cover demand point j :
 $N(j) = \{i \mid d_{ij} \leq D_j\}$,

Decision variables

$x_i = 1$ if a server is located in location i , 0 otherwise
 $y_j = 1$, if demand point j is covered by at least one server, 0 otherwise

The model

Using the above notation the objective function and the constraints take the following form:

(MCLP) Maximize $Z = \sum_{j \in J} w_j y_j$
 subject to $y_j - \sum_{i \in N(j)} x_i \leq 0$, for all $j \in J$

(MCLP1) $\sum_{i \in I} x_i = S$, (MCLP2)

$x_i \in \{0, 1\}$ for all $i \in I$
 $y_j \in \{0, 1\}$ for all $j \in J$

where S is the number of available servers. Constraints (MCLP1) ensure that a demand point j is covered only if there is at least one server located in a candidate location within distance D_j from that demand point whereas constraint (MCLP2) specifies the number of available servers to be located.

G.Alexandris and I. Giannikos [7] presented the MCLP-SO which we present below:

Notation

Indices

i : index for candidate locations
 j : index for demand areas

Parameters

b : minimum acceptable coverage percent in the range $[0,100]$
 θ : minimum number of partial coverage facilities needed for complete coverage
 $\alpha_{ij} = 1$ if a server located at i can fully cover demand area A_j and 0 otherwise
 D_j : distance standard for demand area j
 w_j : the benefit of fully covering area A_j
 w'_j : the benefit of partially covering area A_j at least θ times

Sets

I : set of all candidate locations
 J : set of demand areas
 $N(j)$: set of locations that can cover demand area A_j
 $W(j)$: set of candidate locations i partially covering demand area A_j at least b , but less than 100%

Note that the values α_{ij} as well as the sets $N(j)$ and $W(j)$ are now determined using the capabilities of GIS rather than by a single calculation. More simply, assuming that the service provided by a server can be described by a circle, $\alpha_{ij}=1$ if demand area A_j is fully contained within a circle whose centre is at i and its radius is equal to D_j . A similar GIS function can determine the percentage of containment in the case of partial coverage. Clearly, the same logic applies if the service area can be represented by a polygon or any other shape.

Decision variables

$x_i = 1$ if a server is located in location i , 0 otherwise
 $y_j = 1$, if demand area A_j is covered by at least one server, 0 otherwise
 $v_j = 1$, if demand area A_j is partially covered at least θ times, 0 otherwise

The complete model, called Maximal Covering Location Problem with Spatial Objects (MCLP-SOP), can now be formulated as follows:

(MCLP-SOP) Maximize $Z = \sum_{j \in J} w_j y_j + \sum_{j \in J} w'_j v_j$

subject to $\sum_{i \in I} a_{ij} x_i \geq y_j - v_j$ for all $j \in J$

(MCLP-SOP1)

$$\sum_{i \in I} x_i = S, \quad (\text{MCLP-SOP2})$$

$$\sum_{j \in W(j)} x_j \geq \theta \cdot v_j \quad \text{for all } j \in J \quad (\text{MCLP-SOP3})$$

$$y_j + v_j \leq 1 \quad \text{for all } j \in J \quad (\text{MCLP-SOP4})$$

$$x_i \in \{0, 1\} \quad \text{for all } i \in I$$

$$y_j, v_j \in \{0, 1\} \quad \text{for all } j \in J$$

Constraints (MCLP-SOP1) ensure that if $y_j=1$ and $v_j=0$ then demand area A_j is fully covered by at least one server. If $v_j=1$, no real restriction is imposed. Constraint (MCLP-SOP2) specifies the number of available servers whereas constraints (MCLP-SOP3) imply that if $v_j=1$ then demand area A_j is partially covered by at least θ servers. Finally, constraints (MCLP-SOP4) ensure that a demand area may either be fully covered or partially covered, but not both.

In many practical applications it makes sense to assume that the benefit of partially covering a demand area A_j is a proportion α of the benefit of fully covering A_j . In this case, the objective function of (MCLP-SOP) may be written as

$$\text{Maximize } z = \sum_{j \in J} w_j (y_j + \alpha v_j)$$

where $0 \leq \alpha \leq 1$.

3 Computational implementation and results.

As we know, the geographical information can be presented in two formats, vector or raster. In the case of continuous demand, using vector maps a common approach to the discretization process is to divide the demand area into sub-regions and select a single point out of each sub-region. For instance, this point could be the center of the sub-region, one of its vertices if the sub-region is represented by a polygon, a point selected randomly within the sub-region etc. In this way the continuous demand is transformed into a discrete set of demand points (discretization process) and models (MCLP) can be applied to determine the locations of the servers.

Below we can see the classic discretization process for the municipality of Athens. The municipality comprising the demand space is shown in Figure 1.



Figure 1: The demand space (Municipality of Athens)

This demand space can be broken up into a finite set of demand polygons by laying down a grid of square blocks of equal size. The centroid of each polygon is defined as a demand point representing the demand corresponding to that polygon. (see Figures 2 and 3).

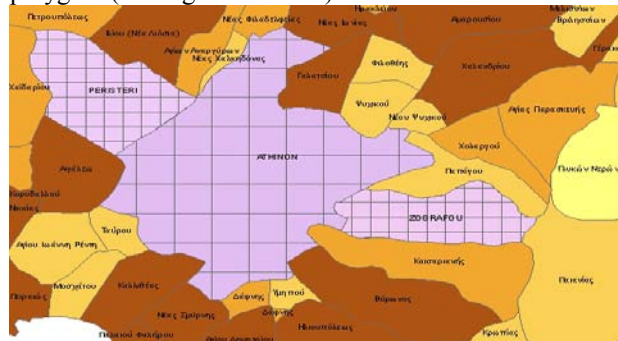


Figure 2: Partitioning the Demand Space into Blocks

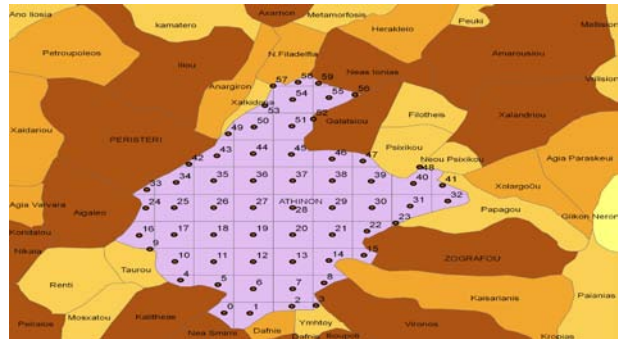


Figure 3: Demand Points and candidate service points

Although the total population of the municipality is known, detailed data concerning the exact location of demand within each sub-polygon was not available. Hence, we assumed that demand (population) is uniformly distributed within each sub-polygon.

The models were solved using Premium Solver 7.1 on a Pentium PC with a 3.2 Ghz processor and 2 Mbytes of RAM. The input files were prepared using ArcGIS of ESRI and the solutions were exported back into ArcGIS for visualization (see Figures 4).

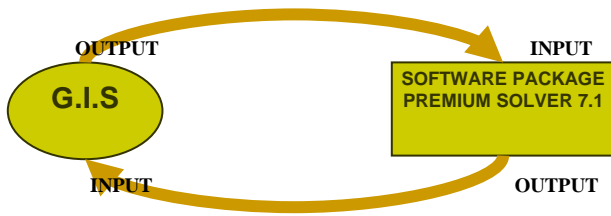


Figure 4: Loose coupling approach

Table 1 at the end of the paper presents the coverage solutions of the above models and the real coverage of each solution as can be verified using ARCGIS tools.

At first, it appears that the classical MCLP model produces better results than the MCLP-SO2 since it yields higher levels of coverage. However, this observation is misleading (see G.Alexandris and I.Giannikos, 2010). Real results using G.I.S functions indicate that classic MCLP always overestimates coverage and creates coverage gaps while MCLP-SO slightly underestimates coverage results. When a sufficient number of servers are used, MCLP-SO2 can exploit the increased possibilities for partial coverage and reduce the underestimation by considering partially covered blocks in the objective function. As far as solution times is concerning we can see that the classical MCLP solves the problem faster a bit faster. For example for a full coverage of the demand of the municipality of Athens classical MCLP uses 18 service points, needs 2,1 seconds to solve the problem and the real coverage is 77,36% of the total area, in other words creates coverage gaps of 22,64%. From the other hand the MCLP-SO2 which makes use of G.I.S capabilities uses 35 service points, covers the 100% of the area without leaving coverage gaps and needs 2,4 seconds for producing the solution. For locating 18 service points MCLP-SO2 needs 3,4 seconds and underestimates slightly the coverage of the area by 5,13%. So the trade – off between the extra time we needs to solve the problem and the accuracy of the results turns to be quite good. For solving the problem classical MCLP needs 0,3 seconds less than the MCLP-SO2 but the accuracy of the results is not quite good. Table 1 reveals that the location of 18 service points of the classical model creates huge coverage gaps which are measured be G.I.S functions to be the 22,64% of the total area. So what is the real factor for increased solution times, if the difference for solving the problem between the two models is not so big, while the accuracy of the results is so huge?

If we start to increase or decrease the grid size during the discretization process, from 1000 meters to 850 or 1200 what will happen? Table 2 presents the solution data for the above changes. For the classical MCLP and a grid size of 850, we have 80 demand points to cover and we need 16 service points so as to cover the whole area. The variables of the problem are 160, we need 2,5 seconds to solve the problem and the coverage gaps which are created are 22,01% of the total area. Changing the grid size to 1000 meters, we have 60 demand points to cover, and we need 18 servers to cover the whole area. The variables of the problem are 120, we need 2,1 seconds to solve the problem and as we mentioned earlier the coverage gaps are 22,64% of the whole area. Last but not

least, for a grid size of 1200 meters we have 43 demand points and we need 23 service points to cover the whole area. The variables of the problem are 86, we need less time to solve the problem (1,8 seconds) and coverage gaps are 23,27% of the whole area.

Table 3 presents the similar data concerning the MCLP-SO models. More specifically for a grid size of 850 meters, we have 80 demand points to cover and we need 35 service points to cover the whole area. The variables of the problem are 240 and we need 3,4 seconds to solve the problem without the presence of coverage gaps. For a grid size of 1000 meters, we have 60 demand points and we need again 35 service points to cover the whole area as the model which uses spatial objects presents a more robust behaviour in comparison with the classical MSCLP. The variables of the problem are 180 and we need 2,4 seconds to solve the problem without having coverage gaps too. Finally for a grid size of 1200, we have 43 demand points and we need 35 service points to cover the whole area. The variables of the problem are less (140) and we need 2,4 seconds to solve the problem. Again in this case, coverage gaps do not exist.

All the above numbers were calculated using the optimization package of premium solver and the ArcMap of ESRI.

The figure below presents a snapshot as a picture of the optimization software environment.

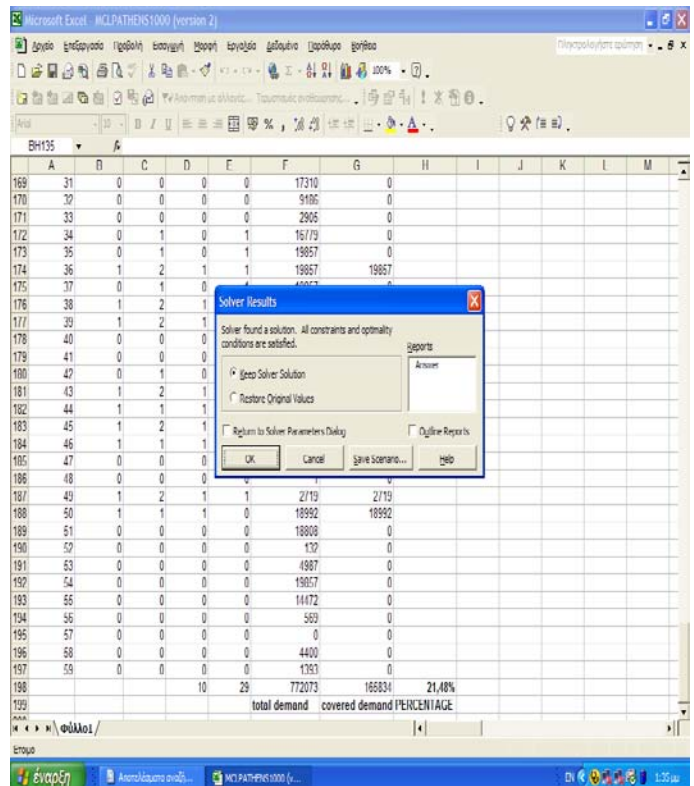


Figure 5: Optimization Software snapshot

Using G.I.S we can present any of the above solutions. Figure 6 presents the solution of the classical problem for the municipality of Athens. The grid size equals with 1000 meters, we have 60 demand points in total and we have 13 available servers to locate.

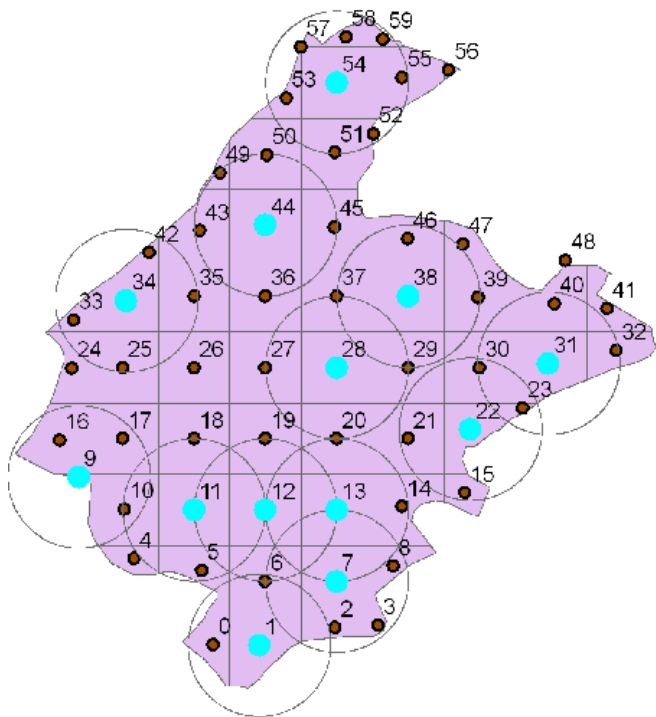


Figure 6:Gis solution for Athens with 13 available servers

Figure6 presents the solution of the same problem for the municipality of Athens using MSCLP-SO2. The grid size equals with 850 meters, we have 80 demand points in total and we have 24 available servers to locate.

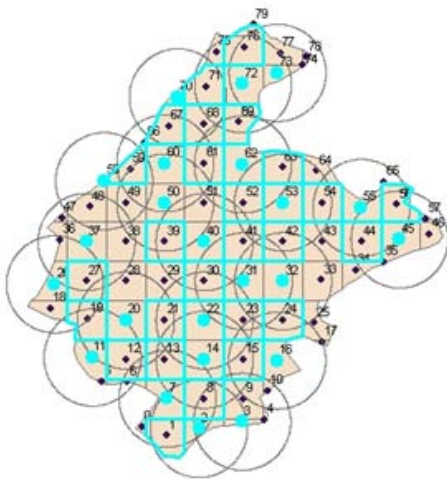


Figure 7:Gis solution for Athens with 24 available servers

4 Conclusions

In this paper we discuss the issue of the tradeoff between accuracy and solution times in location covering models. With the traditional models, most of the times, when we need to solve a problem fast, we cannot achieve accurate results and vice versa.

Using G.I.S capabilities, we presented a Maximal Coverage Location Model which was first presented by G.Alexandris and I.Giannikos. We used the above coverage models in the municipality of Athens and we run different scenarios concerning availability of servers, grid sizes and demand points so as to produce useful results. The above results indicate that while the classical model minimizes solution times, the results which produces are not accurate and coverage gaps are created. These coverage gaps indicate that using classical models in application where accuracy is very important (military operations, estimations etc) produces misleading and not effective results.

For applications of this type, exploiting G.I.S capabilities is very important. The MCLP-SO2 model, may increase solution times slightly, but from the other hand produces much more accurate results which is very important in many applications.

Furthermore the model which makes full use of G.I.S presents a much more robust behavior.

Through the change of the grid size, we found out that the decision variables of the problem varies, and that by increasing decision variables we also increase solution times, without improving accuracy significantly.

Furthermore we used the capabilities of Geographic Information Systems so as to measure the difference between the reported coverage, given by the solution of each integer problem and the real (actual) coverage that can be verified using appropriate ARCGIS tools.

Finally, from the implementation point of view, it would have been interesting to incorporate the GIS and optimization software so as to produce an integrated system that will not require significant intervention by the user.

References:

- [1] Daskin M.(1995) “*Network and discrete location*”, New York, Wiley.
- [2] Church, R. and ReVelle C. (1974), “The maximal covering location model,” *Papers of the Regional Science Association* 32, 101-118.
- [3] Serra D. and Marianov V. (2004), “New trends in public facility location modeling”, *Universitat Pompeu Fabra*

Economics and Business Working Paper 755, available at <http://www.econ.upf.edu/docs/papers/downloads/755.pdf>

[4] Current J. and O’Kelly M. (1992), “Locating emergency warning sirens”, *Decision Sciences* 23, 221-234.

[5] Moore G. and ReVelle C. (1982), “The hierarchical service location problem”, *Management Science* 28/7, 775-780.

[6] Murray A. (2005), “Geography in coverage modeling: exploiting spatial structure to address complementary partial service of areas”, *Annals of the Association of American Geographers* 95/4, 761-772.

[7] G. Alexandris and I. Giannikos, “A New Model for Maximal Coverage Exploiting GIS Capabilities”, *European Journal of Operational Research* 202/2, 328-338, 2010.

	Demand points	Service points	Number of variables	Solutin times (seconds)
g=1000	grid			
MCLP-SO2 $\alpha=1$	60	35	180	2.4
g=850	grid			
MCLP-SO2 $\alpha=1$	80	35	240	3.4
g=1200	grid			
MCLP-SO2 $\alpha=1$	43	34	140	2,2

TABLE 1

K	MCLP coverage	GIS coverage	Gaps	Solution times (seconds)	MCLP-SO1 $\alpha=1$	GIS coverage	Gaps	Solution times (seconds)
1	12,31%	8,08%	4,23%	1,1	3,43%	5,60%	-2,17%	1,1
2	21,48%	16,16%	5,32%	1,1	6,85%	10,47%	-3,62%	1,4
3	30,59%	20,16%	10,43%	1,2	13,56%	17,81%	-4,25%	1,4
4	39,34%	24,01%	15,33%	1,2	18,51%	24,31%	-5,80%	1,3
5	47,63%	28,03%	19,60%	1,1	21,03%	28,31%	-7,28%	1,4
6	55,70%	32,38%	23,32%	1,3	25,77%	33,04%	-7,27%	1,5
7	63,56%	35,01%	28,55%	1,2	30,92%	37,86%	-6,94%	1,4
8	68,99%	37,89%	31,10%	1,2	31,77%	38,58%	-6,81%	1,6
9	74,13%	42,07%	32,06%	1,3	36,77%	43,67%	-6,90%	2,0
10	79,27%	46,26%	33,01%	1,2	42,35%	49,05%	-6,70%	3,0
11	83,78%	50,72%	33,06%	1,2	44,15%	50,82%	-6,67%	3,1
12	87,41%	52,78%	34,63%	1,3	48,83%	54,90%	-6,07%	2,9
13	91,33%	55,87%	35,46%	1,4	49,99%	55,96%	-5,97%	3,1
14	94,96%	57,69%	37,27%	1,7	54,38%	59,77%	-5,39%	3,1
15	97,53%	60,60%	36,93%	1,7	55,40%	60,80%	-5,40%	3,2
16	98,13%	64,37%	33,76%	1,8	61,10%	66,37%	-5,27%	3,3
17	99,32%	68,40%	30,92%	2,0	62,85%	68,36%	-5,51%	3,3
18	100%	77,36%	22,64%	2,1	65,91%	71,04%	-5,13%	3,4
35					100%	100,00%	0,00%	2,4

TABLE 2

Grid size	Demand points	Service points	Coverage gaps	Solution times	Number of var
Athens850	80	16	22,01%	2,5	160
Athens1000	60	18	22,64%	2,1	120
Athens1200	43	23	23,27%	1,8	86

TABLE 3

Determination of thermal steady state in the wall with semi Dirichlet boundary conditions

Martin Zalesak

Abstract — An important task in the measurement in a calorimetric chamber is to determine the time in what the steady state thermal conditions in the walls are reached, in order to eliminate errors in measurement of the heat flow due to the thermal accumulative properties of the walls of the chamber. There are several ways to get boundary conditions in which the steady state conditions could be reached. In this article the process of getting the steady state conditions is studied with the semi Dirichlet boundary conditions. The aim is to determine the required time of the process in the relation with the possible measurement error.

Keywords— Heat transfer, transient thermal conditions, semi Dirichlet boundary conditions.

I. INTRODUCTION

THE common problems in measurements of thermal properties of materials and energy properties of equipment are to determine the time in which the thermal steady state of the measuring equipment is reached after the measurement process has been started. The same problem occurs in measurement in a calorimetric chamber, where the thermal accumulative properties of the chamber walls should be considered. The task is to determine the required time of the process in the relation with the possible measurement error. In this article the transient process with semi Dirichlet conditions is studied.

II. BASES

The principles of heat transfer in the solids are described by the well known Fourier's second order partial differential equation

$$\nabla^2 \theta = a \cdot \Delta \theta \quad (1)$$

where

θ - temperature, [°C],

a - thermal diffusivity, [m²/s].

One dimensional heat transfer in the wall, the equation (1) has the form as follows

$$\frac{\partial \theta}{\partial t} = a \cdot \frac{\partial^2 \theta}{\partial x^2} \quad (2)$$

where

θ, a - see (1),

x - dimension, [m],

t - time, [s, h]

The one dimensional case is described in the Fig .1.

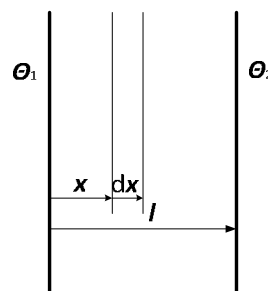


Fig. 1 One dimensional case in the heat transfer

The solution of (2) derives from both the initial and boundary conditions. In the relevant case, the semi Dirichlet boundary conditions were considered

$$Bi \rightarrow \infty$$

$$t = 0; \theta_1 = \theta_2 = konst = k$$

$$t > 0; x = 0, \theta = \theta_1; x = l, \theta = \theta_2$$

where

Bi - Biot number, [-],

$$Bi = \frac{h \cdot l}{\lambda} \quad (3)$$

where

h - heat transfer coefficient, [W/(m².s)],

l - dimension (thickness of the wall), [m],

λ - thermal conductivity of the wall material, [W/(m.K)].

This work was supported by the project CEBIA-TECH NO. CZ.1.05/2.1.00/03.00089

M. Zalesak is with the Tomas Bata University in Zlin, Faculty of Applied Informatics, Department of Automation and Control Technologies, Zlin, 76005 Czech Republic (e-mail: zalesak@fai.utb.cz).

III. THE SOLUTION

First the substitution was introduced

$$\vartheta = \theta - \theta_2 \tag{4}$$

Equation (2) now has the form

$$\frac{\partial \vartheta}{\partial t} = a \cdot \frac{\partial^2 \vartheta}{\partial x^2} \tag{5}$$

For the solution of (5) the Laplace transform was used

$$\mathcal{L} \left\{ \frac{\partial \vartheta}{\partial t} \right\} = \mathcal{L} \left\{ a \cdot \frac{\partial^2 \vartheta}{\partial x^2} \right\} \tag{6}$$

Equation (6) become second order linear differential equation with constant coefficients

$$s \cdot T - \vartheta(x, 0) = a \cdot T'' \tag{7}$$

The boundary conditions will then has the form as

$$\vartheta(0, t) = \vartheta_1; T(0, s) = \frac{T_1}{s} \tag{8}$$

$$\vartheta(l, t) = 0; T(l, s) = 0 \tag{9}$$

The general solution of (7) could be expressed as

$$T = A \cdot \cosh\left(\sqrt{\frac{s}{a}} \cdot x\right) + B \cdot \sinh\left(\sqrt{\frac{s}{a}} \cdot x\right) \tag{10}$$

When conditions (8) and (9) are considered, the constant A, B , are as follows

$$x = 0; A = \frac{T_1}{s} \tag{11}$$

and

$$x = l; 0 = \frac{T_1}{s} \cdot \cosh\left(\sqrt{\frac{s}{a}} \cdot l\right) + B \cdot \sinh\left(\sqrt{\frac{s}{a}} \cdot l\right) \tag{12}$$

$$B = - \frac{T_1}{s} \cdot \frac{\cosh\left(\sqrt{\frac{s}{a}} \cdot l\right)}{\sinh\left(\sqrt{\frac{s}{a}} \cdot l\right)} \tag{13}$$

Equation (10) will be

$$T = \frac{T_1}{s} \cdot \cosh\left(\sqrt{\frac{s}{a}} \cdot x\right) - \frac{T_1}{s} \cdot \frac{\cosh\left(\sqrt{\frac{s}{a}} \cdot l\right)}{\sinh\left(\sqrt{\frac{s}{a}} \cdot l\right)} = \frac{\cosh\left(\sqrt{\frac{s}{a}} \cdot x\right) \cdot \sinh\left(\sqrt{\frac{s}{a}} \cdot l\right) - s \cdot \sinh\left(\sqrt{\frac{s}{a}} \cdot l\right)}{s \cdot \sinh\left(\sqrt{\frac{s}{a}} \cdot l\right)} = T_1 \cdot \left(\frac{\cosh\left(\sqrt{\frac{s}{a}} \cdot x\right) \cdot \sinh\left(\sqrt{\frac{s}{a}} \cdot l\right) - s \cdot \sinh\left(\sqrt{\frac{s}{a}} \cdot l\right)}{s \cdot \sinh\left(\sqrt{\frac{s}{a}} \cdot l\right)} \right) \tag{14}$$

and (14) could be expressed as a division of the two functions $\Phi(s)$ and $\Psi(s)$

$$\frac{T}{T_1} = \frac{\sinh\left(\sqrt{\frac{s}{a}} \cdot (l-x)\right)}{s \cdot \sinh\left(\sqrt{\frac{s}{a}} \cdot l\right)} = \frac{\Phi(s)}{\Psi(s)} = F(s) \tag{15}$$

$F(s)$, in (15) could be expressed as

$$F(s) = \sum_{i=1}^n \frac{A_i}{s-s_i} \tag{16}$$

where

$$A_i = \frac{\Phi(s)}{\Psi'_s} \tag{17}$$

The function of $\sinh(x)$, could be expressed as the series

$$\sinh(x) = x + \frac{x^3}{3!} + \dots + \frac{x^{2n-1}}{(2n-1)!} \tag{18}$$

The functions $\Phi(s), \Psi'_s$, in (17) could be expressed as

$$\Phi(s) = \sinh\left(\sqrt{\frac{s}{a}} \cdot (l-x)\right) = \left(\sqrt{\frac{s}{a}} \cdot (l-x)\right) \cdot \left(1 + \frac{s}{a} \cdot \frac{(l-x)^2}{3!} + \dots\right) \tag{19}$$

and

$$\Psi'_s = \frac{1}{2} \cdot \frac{l}{\sqrt{a}} \cdot \frac{s}{\sqrt{s}} \cdot \cosh\left(\sqrt{\frac{s}{a}} \cdot l\right) + \sinh\left(\sqrt{\frac{s}{a}} \cdot l\right) = \frac{1}{2} \cdot \frac{l}{\sqrt{a}} \cdot \sqrt{s} \cdot \cosh\left(\sqrt{\frac{s}{a}} \cdot l\right) + \sinh\left(\sqrt{\frac{s}{a}} \cdot l\right) \quad (20)$$

Roots of (16) must be found to suit the boundary conditions. For $x = l$ results

$s_0 = 0$
and roots s_n , should suit the condition

$$\sinh\left(\sqrt{\frac{s}{a}} \cdot l\right) = 0 \quad (22)$$

It is possible to express

$$\sinh\left(\sqrt{\frac{s}{a}} \cdot l\right) = i \cdot \sin\left(\sqrt{\frac{s}{a}} \cdot l\right) \quad (23)$$

Condition (22) will be fulfilled if

$$\frac{1}{i} \cdot \sqrt{\frac{s}{a}} \cdot l = n \cdot \pi \quad (24)$$

This is valid for all s_n

$$s_n = -\frac{n^2 \cdot \pi^2}{l^2} \cdot a; n = \langle 1, \infty \rangle \quad (25)$$

Next task is to get the reverse transform. In order to make it, it is possible to use the rule

$$\mathcal{L} \left\{ \frac{t^{(k-1)} \cdot e^{s_i t}}{(k-1)!} \right\} = \frac{1}{(s-s_i)^k} \quad (26)$$

Inversion fiction may be expected as an addition of two functions

$$\frac{\vartheta}{\vartheta_1} = f_1 + f_2 \quad (27)$$

where

$$f_1 = \frac{\Phi_{(0)}}{\Psi_{(0)}} \cdot e^{s_0 t} \quad (28)$$

and

$$f_2 = \sum_{n=1}^{n=\infty} \frac{\Phi_{(s_n)}}{\Psi_{(s_n)}} \cdot e^{s_n t} \quad (29)$$

For $s_0 = 0$ will be

$$f_1 = \frac{\Phi_{(s_0)}}{\Psi_{(s_0)}} \cdot e^{s_0 t} = \frac{0}{0} \quad (30)$$

The L'Hopital rule could be applied for solution (30)

$$f_1 = \lim_{s \rightarrow 0} \frac{\Phi'(s)}{\Psi'(s)} = \left(1 - \frac{x}{l}\right) \quad (31)$$

for $s_n \neq 0$

Using condition (25) and by introducing Fourier number, Fo

$$\frac{a \cdot t}{l^2} = Fo \quad (32)$$

f_2 could be expressed as

$$f_2 = \sum_{n=1}^{n=\infty} \frac{\Phi_{(s_n)}}{\Psi_{(s_n)}} \cdot e^{s_n t} = \sum_{n=1}^{n=\infty} \frac{\sin(i \cdot n \cdot \pi \cdot (1 - \frac{x}{l}))}{\frac{1}{2} \cdot \frac{l}{\sqrt{a}} \cdot \frac{i \cdot n \cdot \pi}{l} \cdot \sqrt{a} \cdot \cosh(i \cdot n \cdot \pi)} \cdot e^{-n^2 \cdot \pi^2 \cdot Fo} = \sum_{n=1}^{n=\infty} -1^{n+1} \cdot \frac{1}{n} \cdot \frac{2}{\pi} \cdot \sin(n \cdot \pi \cdot (1 - \frac{x}{l})) \cdot e^{-n^2 \cdot \pi^2 \cdot Fo} = \frac{2}{\pi} \cdot \sum_{n=1}^{n=\infty} -1^{n+1} \cdot \frac{1}{n} \cdot \sin(n \cdot \pi \cdot (1 - \frac{x}{l})) \cdot e^{-n^2 \cdot \pi^2 \cdot Fo} \quad (33)$$

The final expression for the temperature in the distance x (Fig. 1) is then as follows

$$\vartheta = \vartheta_1 \cdot (f_1 + f_2) = \vartheta_1 \cdot \left[\left(1 - \frac{x}{l}\right) + \frac{2}{\pi} \cdot \sum_{n=1}^{n=\infty} -1^{n+1} \cdot \frac{1}{n} \cdot \sin(n \cdot \pi \cdot (1 - \frac{x}{l})) \cdot e^{-n^2 \cdot \pi^2 \cdot Fo} \right] \quad (34)$$

Deviation from the steady state condition is expressed in the part of (34) by

$$\Delta\vartheta = \vartheta_1 \cdot \left[\frac{2}{\pi} \cdot \sum_{n=1}^{\infty} -1^{n+1} \cdot \frac{1}{n} \cdot \sin(n \cdot \pi \cdot \left(1 - \frac{x}{l}\right)) \cdot e^{-n^2 \cdot \pi^2 \cdot Fo} \right] \quad (35)$$

Maximal value of the $\Delta\vartheta$, in (35) for the certain value of time t , is in the distance

$$x = \frac{l}{2}$$

IV. TIME LIMITS TO REACH THE STEADY STATE CONDITIONS

The task is to find minimal time necessary to reach acceptable steady state conditions – it means to evaluate the conditions of $\frac{\Delta\vartheta_{max}}{\vartheta_1}$, as a function of time. The limit can be found from the equation as follows

$$\frac{\Delta\vartheta_{max}}{\vartheta_1} = \frac{2}{\pi} \cdot \sum_{n=1}^{\infty} -1^{n+1} \cdot \frac{1}{n} \cdot \sin(n \cdot \pi \cdot \left(1 - \frac{x}{l}\right)) \cdot e^{-n^2 \cdot \pi^2 \cdot Fo} \leq \frac{2}{\pi} \cdot \ln 2 \cdot e^{-\pi^2 \cdot Fo} < \varepsilon \quad (36)$$

where

$$\sum_{n=1}^{\infty} -1^{n+1} \cdot \frac{1}{n} = \ln 2 \quad (37)$$

and

$$\sin(n \cdot \pi \cdot \left(1 - \frac{x}{l}\right)) \leq 1 \quad (38)$$

For any value of ε , is then valid the relation

$$\frac{\Delta\vartheta_{max}}{\vartheta_1} \leq \frac{2}{\pi} \cdot \ln 2 \cdot e^{-\pi^2 \cdot Fo} < \varepsilon \quad (39)$$

where

ε is an acceptable deviation from the steady state.

Now the task is to find the Fo , which will suit the above stated conditions

$$Fo > -\frac{1}{\pi^2} \cdot \ln\left(\frac{\varepsilon \cdot \pi}{2 \cdot \ln 2}\right) = -0,101 \cdot \ln(2,27 \cdot \varepsilon) \quad (40)$$

V. APPLICATION OF THE RESULTS

The utilization of the results was studied in some materials and conditions, which can occur in practical application.

Relation of Fo and ε shows the Fig. 1.

Physical parameters of studied materials are stated in the Table 1.

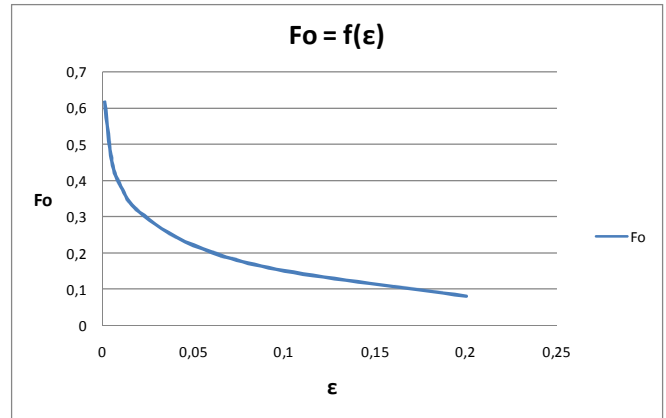


Fig 2 Relation $Fo - \varepsilon$

Table I Physical parameters of studied materials

Material	Thermal conductivity	Density	Thermal capacity	Thermal diffusivity
	λ	ρ	c	a
	[W/(m.K)]	[kg/m ³]	[J/(kg.K)]	[m ² /s]
Concrete	1,16	2100	1020	5,41E-07
Foam polystyrol	0,034	50	1270	5,35E-07
Foam polyurethan	0,03	35	1510	5,68E-07
Hard wood	0,4	600	2510	2,66E-07
Brick wall	0,75	1800	900	4,63E-07
Plywood	0,17	800	1500	1,42E-07
Stone	1,4	2400	840	6,94E-07
Clay	1,6	2000	920	8,69E-07

Necessary time t , left for stabilizing condition with the acceptable errors describe Fig. 3 ($\varepsilon = 0,005$) and Fig. 4 ($\varepsilon = 0,01$) for different dimensions of the wall l , thermal diffusivity of materials a . It results from the figures that for practical thickness of the wall the time in tens of hours should be left for thermal stabilizing process.

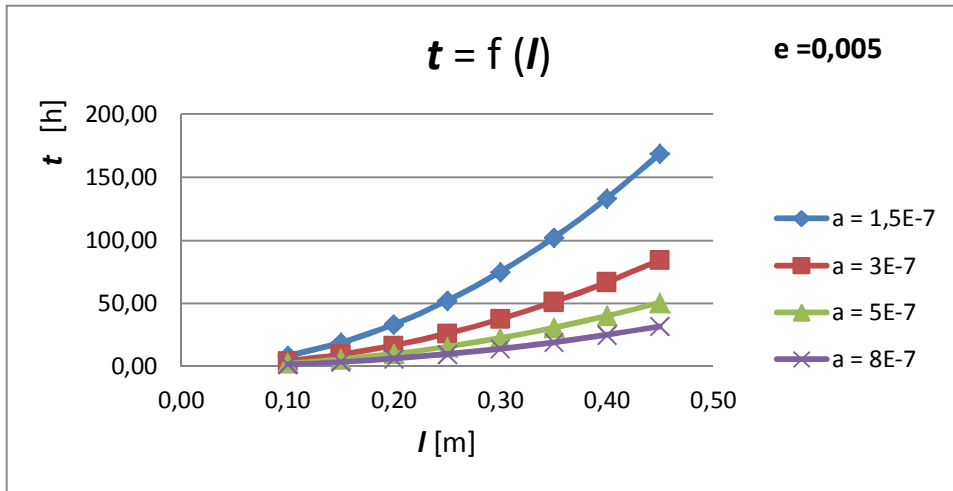


Fig. 3 Relation between stabilizing time t , the acceptable error $\varepsilon = 0,005$ for different dimensions of the wall l , thermal diffusivity of materials α .

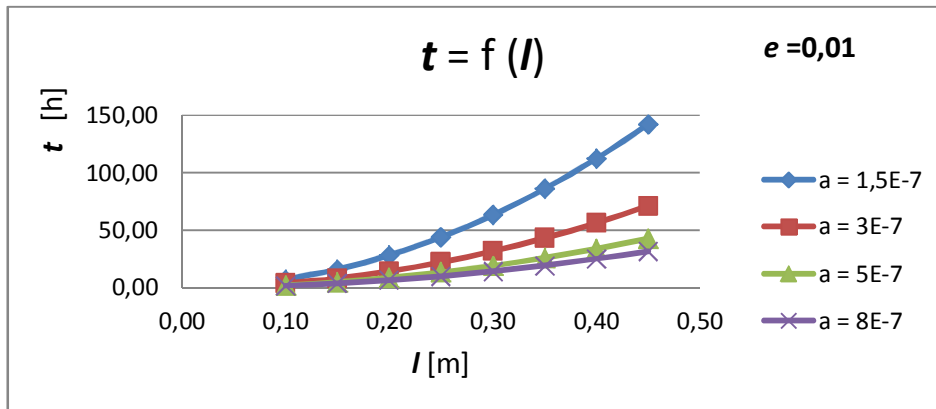


Fig. 4 relation between stabilizing time t , the acceptable error $\varepsilon = 0,01$ for different dimensions of the wall l , thermal diffusivity of materials α .

It results from the figures that r practical thickness of the wall the time in tens of hours should be left for the thermal stabilizing process.

REFERENCES

- [1] M. Zalesak, *Calorimeter Room Thermal Properties*. Report Unido. 45 pp. Chulalongkorn University Bangkok, 1991
- [2] W.M. Rohsenow, J.P.Harrett, Y.I.Cho, *Handbook of Heat Transfer*, ch. 3,7. 3rd ed. McGraw-Hill, 1997
- [3] M.F.Carslaw, J.C.Jaeger, *Conduction of Heat in Solids*. Oxf. Un. Press,
- [4] G.A. Korn,T.M. Korn, *Mathematical Handbook*. McGraw-Hill, 1968.
- [5] A.V.Luikov, *Analytical Heat Diffusion Theory*. Academic Press , New York, 1968
- [6] M.Zalesak, J.Postava, "Realization of the Non-steady State Measurement Method of Thermal Properties of Building Materials", *ZTV. Academia Prague*, 1990

Performance evaluation of two radial basis function neural network models

Nikolinka G. Christova, Gancho L. Vachkov, Agata H. Manolova and Georgi T. Tsenov

Abstract—In this paper performance evaluation of two modification of the classical Radial Basis Function Neural Network (RBFNN) model, called Reduced and Simplified RBFNN models is carried out. Different RBFNN models with different number of Radial Basis Functions (RBFs) are created and analyzed. Particle Swarm Optimization (PSO) algorithm with constraints for the parameter tuning of the models is applied. Simultaneous optimization of all three groups of parameters, namely the centers, widths and the weights of the RBFNN is performed. It is shown that the Simplified RBFNN models, which have smaller number of parameters, can achieve even better modeling accuracy than the Reduced RBFNN models.

Keywords—Particle Swarm Optimization, performance evaluation, Radial Basis Function Neural Networks, RBFNN models.

I. INTRODUCTION

ARTIFICIAL Neural Networks (ANNs) are essentially a nonlinear modeling approach that provides a fairly accurate universal approximation to any function [2]. Radial Basis Function Neural Networks (RBFNNs) [3] correspond to a particular class of function approximators which can be trained, using a set of samples. They have been receiving a growing amount of attention since their initial proposal, and now a great deal of theoretical and empirical results are available [5], [7].

The RBFNNs have proven to be useful and powerful neural network architecture for problem solving in classification, modeling, simulation, and others due to their rapid training, generality, and simplicity [2], [5], [10]. They are feed-forward networks and are typically configured with a single hidden layer of units whose activation function is selected from a class of functions called basis functions. While similar to back propagation in many respects, RBFNNs have several advantages [4], [8]. They usually train much faster than back propagation networks and are less susceptible to problems with non-stationary inputs because of the behavior of the radial basis function hidden units.

The most important difference is that the RBFNNs are not homogeneous in parameters. They have three different groups of parameters that need to be appropriately tuned, normally by

using different learning algorithms [3], [7]. This makes the total learning process of the RBFNNs more complex, because it is usually done as a sequence of several learning phases. This obviously affects the accuracy of the produced model.

In this paper, detailed investigation of two modifications of the classical (general) RBFNNs, called Reduced and Simplified RBFNNs is studied. These RBFNNs have less number of tuning parameters, which makes the learning faster. An universal optimization procedure to tune all three groups of parameters is used. Essentially this is a modified version of the classical Particle Swarm Optimization (PSO) [6], [9] that includes separate constraints for each group of parameters. Such constrained optimization strategy is able to produce more plausible solutions with parameters that have physical meaning.

Different RBFNN models with different RBFs are examined. The obtained result of the performance evaluation are analyzed and discussed.

II. CLASSICAL RADIAL BASIS FUNCTION NEURAL NETWORK (RBFNN) MODEL

Radial Basis Function Neural Network (RBFNN) [3] can be used for a wide range of application primarily because it can approximate any regular function and its training is faster than that of a multi-layer perceptron [4]. This faster learning speed comes from the fact that RBFNN has just two layers of weights and each layer can be determined sequentially.

Despite of these advantages RBFNNs are not as widely used as they should be. The main reason for this seems to be that it is not straight forward to design an optimal RBFNN to solve the given problem.

An RBFNN is a three layer feed-forward network that consists of one input layer, one middle layer and one output layer. The input layer corresponds to the input vector space. Each input neuron is fully connected to the middle layer neurons except the bias one. Each middle layer neuron uses a Gaussian or some other basis kernel function computes a kernel function (activation function) [5], [7]. The kernel function decreases rapidly if the width is small, and slowly if it is large. A typical hidden node in an RBFNN is characterized by its center, which is a vector with dimension equals to the number of inputs to the node. Each hidden unit acts as a locally tuned processor that computes a score for the match between the input vector and its connection weights or centers. The output layer is fully connected to the middle layer. Each output layer neuron computes a linear weighted sum of the outputs of the middle layer.

N. G. Christova is with the Department of Automation of Industry, University of Chemical Technology and Metallurgy, 1756 Sofia, Bulgaria (phone: +359 888 602070; e-mail: nchrist@uctm.edu).

G. L. Vachkov was with University of Chemical Technology and Metallurgy, 1756 Sofia, Bulgaria (e-mail: gancho.vachkov@gmail.com).

So the whole architecture is fixed only by determining the middle layer and the weights between the middle and the output layers. The weights between the input and the middle layer are fixed when the middle layer is determined.

In this study the aim is to create a model of a real process (system) with K inputs and one output by using a collection of M available experiments (*input-output* pairs) in the form:

$$\{(\mathbf{X}_1, y_1), \dots, (\mathbf{X}_i, y_i), \dots, (\mathbf{X}_M, y_M)\} \quad (1)$$

Here $\mathbf{X}=[x_1, x_2, \dots, x_K]$ is the vector of all K inputs and y is the respected measured output from the process.

The modeled output, calculated by the RBF neural network is as follows:

$$y_m = f(\mathbf{X}, \mathbf{P}) \quad (2)$$

where $\mathbf{P}=[p_1, p_2, \dots, p_L]$ is the vector of all L parameters included in the RBFN.

The classical RBFNN has a three layer structure, namely *input* layer, *hidden* layer and *output* layer as shown in Fig. 1.

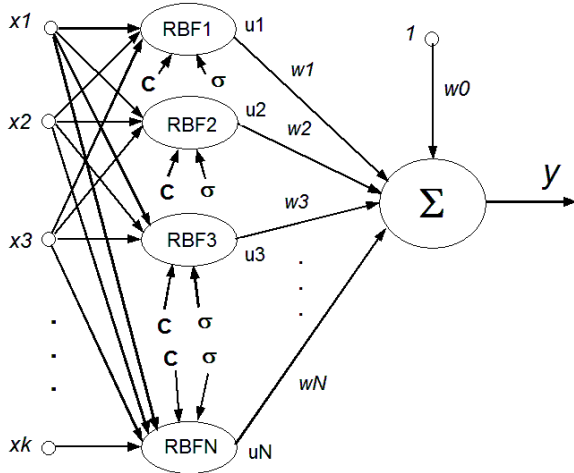


Fig. 1. Structure of the classical RBF network with K inputs and N RBFs

The modeled output from the RBFNN with fixed number of N Radial Basis Functions will be:

$$y_m = w_0 + \sum_{i=1}^N w_i u_i \quad (3)$$

Here $u_i, i=1, 2, \dots, N$ are the outputs of each RBF based on its K inputs x_1, x_2, \dots, x_K and $w_i, i=0, 1, 2, \dots, N$ are the *weights* associated with the RBFs, including the *offset* weight w_0 as seen in the figure.

Each RBF is determined in the K -dimensional space by two groups (vectors) of parameters, namely the *center* (location)

$\mathbf{C} = [c_1, c_2, \dots, c_K]$ and the *width* (spread) $\boldsymbol{\sigma} = [\sigma_1, \sigma_2, \dots, \sigma_K]$.

Then the output u of each RBF is calculated as:

$$u = \prod_{j=1}^K \exp[-(x_j - c_j)^2 / (2\sigma_j^2)] = \exp\left(-\sum_{j=1}^K [(x_j - c_j)^2 / (2\sigma_j^2)]\right) \in [0, 1] \quad (4)$$

It is clear that all parameters form the following 3 groups in the parameter vector \mathbf{P} , namely: *Centers*, *Widths* and *Weights*, as follows:

$$\mathbf{P}=[p_1, p_2, \dots, p_L] = \mathbf{C} \cup \boldsymbol{\sigma} \cup \mathbf{W} \quad (5)$$

For a RBFNN with K inputs and N RBFs, the total number L of the parameters to be tuned will be:

$$L = N \times K + N \times K + (N + 1) = 2(N + K) + N + 1 \quad (6)$$

It is obvious that the number of all L parameters will rapidly grow with increasing the complexity of the RBFNN model, i.e. the number of RBFs and the number of inputs. This possesses a challenge to the selected learning algorithm.

III. MODIFICATIONS OF THE RBFNN MODEL

In order to reduce the total number L of parameters that have to be tuned (optimized), two modifications of the classical RBFNN model from (3) and (4) (Fig. 1) called *Reduced* and *Simplified* RBFNN models are considered and analyzed.

The reduction of the number of parameters here is achieved by assuming that the RBF has a *scalar width* σ instead of a K -dimensional vector width $\boldsymbol{\sigma} = [\sigma_1, \sigma_2, \dots, \sigma_K]$ as in (4). Then the calculation of the output for each RBF is performed according to the Euclidean distance between the input vector \mathbf{X} and the center \mathbf{C} of the RBF, as follows:

$$u = \exp\left(-\sum_{j=1}^K (x_j - c_j)^2 / (2\sigma^2)\right) \in [0, 1] \quad (7)$$

Now the total number L of the parameters in the *Reduced* RBFNN is calculated as:

$$L = N \times K + N + (N + 1) = N \times K + 2N + 1 \quad (8)$$

For further reducing the number L of all parameters of the RBFNN an assumption of one *common width* σ for all N RBFs is made. This means that the calculation of each RBF is performed by the same equation (7), as in the *Reduced* RBFNN, but with one common width σ for all RBFs.

Now the total number L of the parameters in the *Simplified* RBFNN is calculated as:

$$L = N \times K + 1 + (N + 1) = N \times K + N + 2 \quad (9)$$

The idea of creating a model by the *Simplified* RBFNN is that all N RBFs will be located (in general) at different locations (centers) in the K -dimensional input space, but will have one common width σ . It could be expected that a large number of RBFs will be needed (compared with the case of *Reduced* RBFNN) in order to achieve the same or similar model accuracy. However this speculation needs to be proven experimentally.

In Fig. 2 the relations between the number of RBFs and the number of parameters for 2 and 4 inputs are illustrated, where the *Reduced* and the *Simplified* RBFNN models are noted as Model_1 and Model_2 respectively.

As seen the *Simplified* RBFNN model has a clear advantage concerning the number of parameters. This is because of the general assumption that the simpler model is the better model.

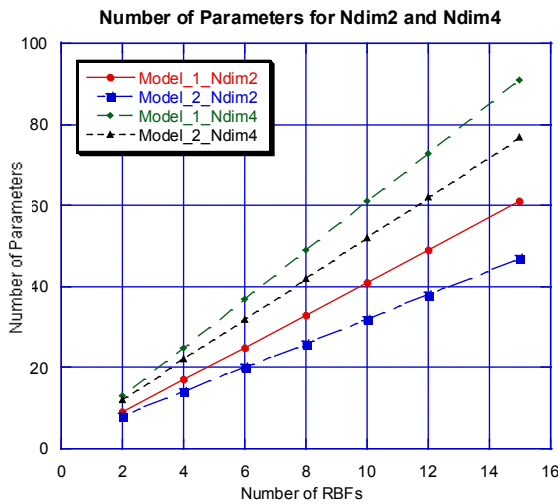


Fig. 2. Number of parameters for 2- and 4-dimensional inputs and different number of RBFs

The answer which is the best model is not obvious. However the problem is that it is often the case when a model with smaller number of parameters produces larger (bigger) approximation error. Therefore sometimes a tradeoff between the number of parameters and approximation error should be done.

It is not straightforward to say that the *Simplified* RBFNN model has similar or even better performance than the *Reduced* one. This needs to be proven experimentally, which is done in the sequel (Section V) in the paper.

IV. PARAMETER TUNING OF THE RBFNN MODELS

Particle Swarm Optimization (PSO) is a novel multi-agent optimization algorithm inspired by social behavior metaphor [6], and based on the simulation of the social behavior of birds within a flock in evolutionary computation. PSO is a swarm intelligence method that roughly models the social behavior of swarms and has been proven to be efficient on many optimization problems in science and engineering [1], [8], [9].

It is a good approach for parameter tuning of the RBFNN models [4].

As mentioned in Section II, there are 3 different groups of parameters in the RBFNN model, namely *centers*, *widths* and *weights*, according to the notations in (3). All L parameters (5) of the RBFNN model are tuned so that to minimize a preliminary formulated performance index. The objective here is to *minimize* the total prediction error (*RMSE*):

$$RMSE = \sqrt{\frac{1}{M} \sum_{i=1}^M (y_i - y_{im})^2} \rightarrow \min \quad (10)$$

For solving this supervised learning problem, we use the *one-step* optimization procedure for simultaneous tuning in *off-line* mode the all 3 groups of parameters. Here the PSO algorithm with constraints from Section 4.2 was used.

In almost all practical engineering problems it is mandatory to impose certain constraints (limits) to the parameters of the input space $[x_1, x_2, \dots, x_K]$ in order to produce an optimal solution with a clear physical meaning that can be practically realized. Therefore we have made a slight modification in the original version of the PSO algorithm with inertia weight in order to consider both constraints (*minimum* and *maximum*) on the input parameters, as follows:

$$[x_{1\min}, x_{2\min}, \dots, x_{K\min}] [x_{1\max}, x_{2\max}, \dots, x_{K\max}] \quad (11)$$

The idea here is very simple, namely the respective input parameter from $[x_1, x_2, \dots, x_K]$ which has violated the input space is *moved back* to its boundary value.

V. EXPERIMENTAL RESULTS OF THE PERFORMANCE EVALUATION

The main goal in this section is to analyze the performance of the above mentioned *Reduced* and *Simplified* RBFNN models.

As seen from (6), (8) and (9), both models have a smaller number of parameters, compared with the parameters in the classical RBFNN model from Section II.

The evaluation was performed on a nonlinear test example with 2 inputs and one output shown in Fig. 3.

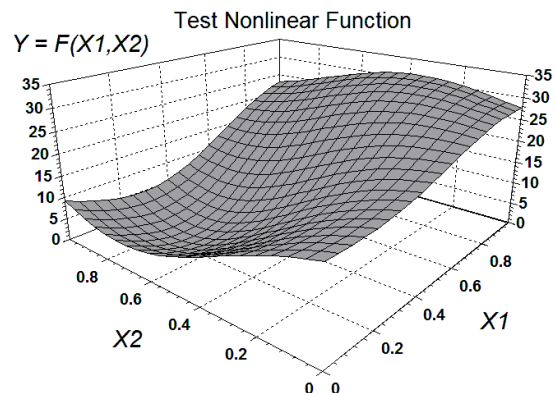


Fig. 3. The nonlinear test example

A set of $M=441$ uniformly distributed experimental data in the two-dimensional space $[X1, X2]$ produced by scanning (Fig. 4) are used for RBFNN training.

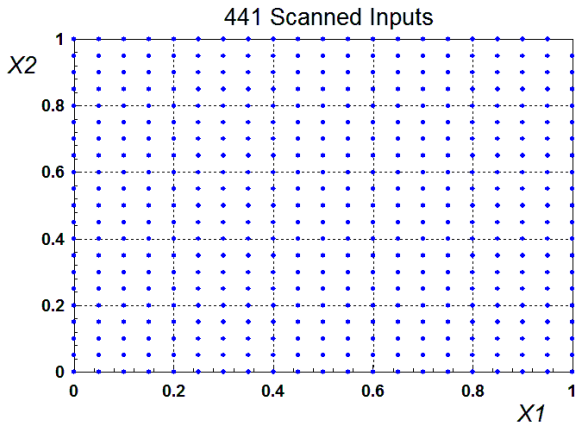


Fig. 4. The scanned inputs used for producing $M=441$ experimental data

All the experiments were performed separately for the *Reduced* and *Simplified* RBFNNs with the following numbers of RBFs: $N = 4, 6, 8, 10, 12$ and 15 . The constraints imposed to each of the 3 groups of parameters in (5) were as follows:

- The group of *Centers*: $C_{min} = -1, C_{max} = 2$;
- The group of *Widths*: $\sigma_{min} = 0.05, \sigma_{max} = 1.2$;
- The group of *Weights*: $w_{min} = -30, w_{max} = 30$.

All the parameters of both models are tuned by using the PSO algorithm with constraints.

This is bio-inspired algorithm with random nature which normally produces at least slightly different solutions from different runs. In order to eliminate the randomness when taking decision about the proper model, we have performed 10 runs of the PSO algorithm for each selected number of RBFs.

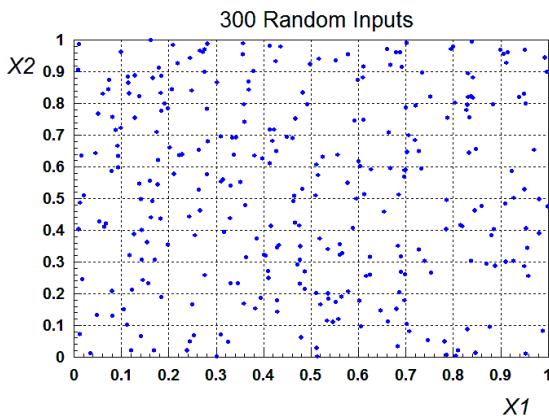


Fig. 5. 300 random generated data

Further on we show the experimental results as plots of the minimum, mean and maximum values of the *RMSE* for both models in Fig. 6 and Fig. 7.

Fig. 6 presents the obtained results for the *Reduced* and *Simplified* RBFNN models with different number of RBFs by using training data set with 441 scanned data in the two

dimensional input space $[0 \div 1]$.

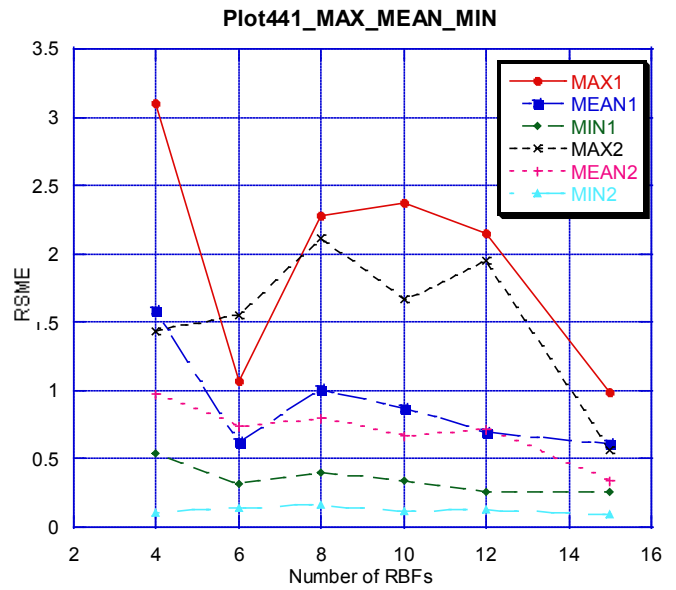


Fig. 6. Minimum, mean and maximum values of the *RSME* for 441 data

In a similar way Fig. 7 shows the respective results by using a training data set with 300 random generated data in the same input space (in Fig. 5).

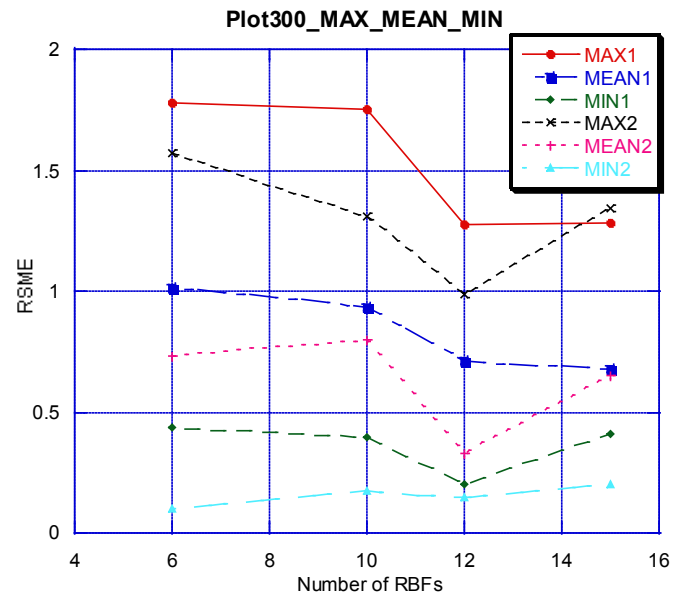


Fig. 7. Minimum, mean and maximum values of the *RSME* for 300 data

The convergence curves for the *Reduced* and the *Simplified* RBFNN models with 6 RBFs for the randomly generated data are presented at Fig. 8 and Fig. 9 respectively.

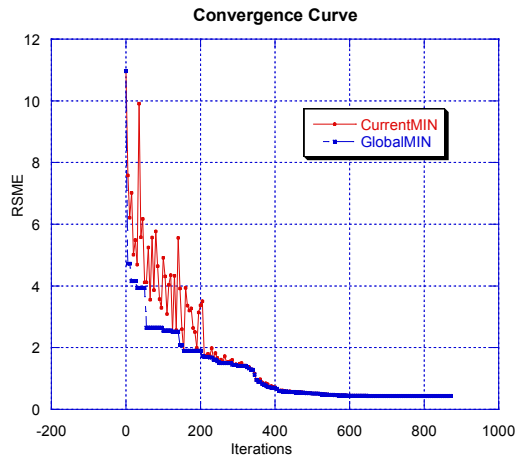


Fig. 8. Convergence curve for the *Reduced* RBFNN model with $N=6$ RBFs

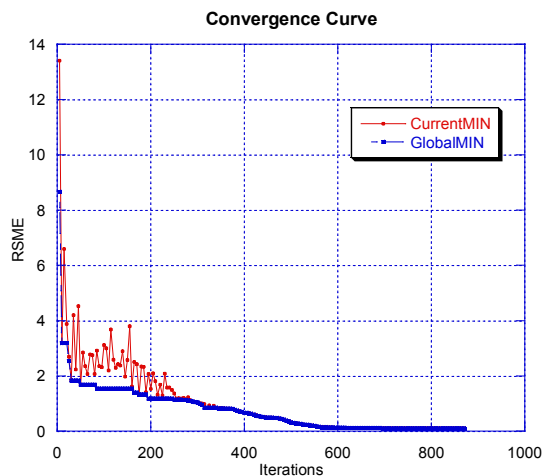


Fig. 9. Convergence curve for the *Simplified* RBFNN model with $N=6$ RBFs

The *Simplified* RBFNN model has 2 advantages:

First, this is a model of smaller number of parameters as seen from Fig. 2.

Second, we have experimentally confirmed that this model has *RSME* that is at least closed to that one of the *Reduced* RBFNN model and in many cases is even better (clearly shown in Fig. 6 and Fig.7).

In addition we have noticed (in Fig. 6 and Fig. 7) that the *Simplified* RBFNN model produces smaller minimal error from all 10 runs for all different number of RBFs compared to the *Reduced* RBFNN model.

VI. CONCLUSIONS

In this paper, two modifications of RBF neural networks have been investigated. The obtained results are conclusive in a sense that the *Simplified* RBFNN model tends to produce a better approximation (minimal *RSME*) for almost all cases.

In addition the smaller parameters number of the optimization procedure increases the possibility to reach the global optimum.

This makes the *Simplified* RBFNN a preferable choice as a structure of the RBFNN models.

Further research is focused on investigation of the merits and performance of other optimization strategies and algorithms as well as on finding a simple and practically applicable method for determination of the optimal number of the RBFs in the RBFNN model.

REFERENCES

- [1] C. L. Lin, S. T. Hsieh, T. Y. Sun, and C. C. Liu, "PSO-based learning rate adjustment for blind source separation", *Proceeding of International Symposium on Intelligent Signal Processing and Communications Systems*, 2005, pp. 181–184.
- [2] T. Poggio, and F. Girosi, "Networks for approximation and learning", *Proceedings of the IEEE*, **78**, 1990, pp. 1481–1497.
- [3] M. Musavi, W. Ahmed, K. Chan, K. Faris, and D. Hummels, "On the training of radial basis function classifiers", *Neural Networks*, **5**, 1992, pp. 595–603.
- [4] V. G. Gudise, and G. K. Venayagamoorthy, "Comparison of Particle Swarm Optimization and Backpropagation as Training Algorithms for Neural Networks", *Proceeding of IEEE Swarm Intelligence Symposium*, 2003, pp. 110–117.
- [5] J. Park, and I. W. Sandberg, "Approximation and radial-basis-function networks", *Neural Computation*, **5**, 1993, pp. 305–316.
- [6] R. C. Eberhart, and J. Kennedy, "Particle swarm optimization", *In: Proc. of IEEE Int. Conf. on Neural Network*, Perth, Australia, 1995, pp. 1942–1948.
- [7] R. Yousef, "Training radial basis function networks using reduced sets as center points", *International Journal of Information Technology*, Vol. 2, 2005, pp. 21.
- [8] J.-R. Zhang, J. Zhang, T. Lok, and M. Lyu, "A hybrid particle swarm optimization, back-propagation algorithm for feed forward neural network training", *Applied Mathematics and Computation*, **185**, 2007, 1026–1037.
- [9] R. Poli, J. Kennedy, and T. Blackwell, "Particle swarm optimization. An overview", *Swarm Intelligence* **1**, 2007, pp. 33–57.
- [10] W. Pedrycz, H. S. Park, and S. K. Oh, "A Granular-Oriented Development of Functional Radial Basis Function Neural Networks", *Neurocomputing*, **72**, 2008, pp. 420–435.

Graphical analysis of robust stability for fractional order time-delay systems and integer order PID controllers

Radek Matušů and Roman Prokop

Abstract—The main goal of this contribution is to present the universal graphical tool for investigation of robust stability and especially its possible application to analysis of feedback control loops which include a fractional order time-delay controlled systems with parametric uncertainty and fixed integer order PID controllers. The robust stability testing is based on plotting the value sets for closed-loop characteristic quasi-polynomial and subsequent application of the zero exclusion condition. The effectiveness but also easy utilization are demonstrated by the set of computational examples for the case of uncertain gain, uncertain time constant and uncertain time-delay term, respectively.

Keywords—Fractional Order Control, PID Controllers, Robust Stability Analysis, Time-Delay Systems, Zero Exclusion Condition.

I. INTRODUCTION

THE fractional order calculus represents more than 300-year-old branch of mathematics that is focused on differentiation and integration under an arbitrary, real or even complex, order of the operation [1] – [7]. Recently, the fractional order has found the real-life application possibilities in many areas such as bioengineering, viscoelasticity, electronics, robotics, control theory or signal processing [8]. Especially in the field of control engineering, it seems that the true fractional order “boom” has exploded lately as many new research works have appeared.

The mathematical model of the controlled system practically never exactly matches its real behaviour. This fact is typically caused by the effort to construct a simple-to-use linear model in which the more complex properties such as nonlinearities, time-variant behaviour or very fast dynamics are neglected. Moreover, the physical parameters of the system can change due to various reasons. All these factors can be taken into consideration by using the uncertain model

The work was supported by the European Regional Development Fund under the project CEBIA-Tech No. CZ.1.05/2.1.00/03.0089. This assistance is very gratefully acknowledged.

Radek Matušů is with the Centre for Security, Information and Advanced Technologies (CEBIA – Tech), Faculty of Applied Informatics, Tomas Bata University in Zlín, nám. T. G. Masaryka 5555, 760 01 Zlín, Czech Republic. The email contact is: rmatusu@fai.utb.cz.

Roman Prokop is with the Centre for Security, Information and Advanced Technologies (CEBIA – Tech), Faculty of Applied Informatics, Tomas Bata University in Zlín, nám. T. G. Masaryka 5555, 760 01 Zlín, Czech Republic. The email contact is: prokop@fai.utb.cz.

instead of the ordinary fixed one. The very popular approach to uncertainty modelling is based on models with fixed structure (order), but not exactly known parameters, which are supposed to lie within given bounds. Such models are called systems with parametric uncertainty and the frequent task is to analyze their robust stability, i.e. if the stability is ensured for all possible values of uncertain parameters. Obviously, several researchers have already combined the issue of robust stability of systems under parametric uncertainty with fractional order systems – e.g. [9] – [14].

This contribution deals with a graphical approach to robust stability investigation for feedback control loops with fractional order time-delay plants and integer order PID controllers. The testing is based on plotting the value sets of a closed-loop characteristic quasi-polynomial and subsequent application of the zero exclusion condition [15]. The computational examples present the analyses for the cases of uncertain gain, uncertain time constant and uncertain time-delay term and they show both robustly stable and unstable events.

II. FUNDAMENTALS OF FRACTIONAL ORDER SYSTEM DESCRIPTION

The fractional order calculus is based on generalization of differentiation and integration to an arbitrary order. This generalization has resulted in the introduction of basic continuous differintegral operator [1], [2], [4], [8]:

$${}_a D_t^\alpha = \begin{cases} \frac{d^\alpha}{dt^\alpha} & \text{Re } \alpha > 0 \\ 1 & \text{Re } \alpha = 0 \\ \int_a^t (d\tau)^{-\alpha} & \text{Re } \alpha < 0 \end{cases} \quad (1)$$

where α is the order of the differintegration (typically $\alpha \in \mathbb{R}$) and a is a constant connected with initial conditions. The differintegral can be defined in various ways. The tree most common are Riemann-Liouville, Grünwald-Letnikov and Caputo definitions.

The Laplace transform of the differintegral is given by [4], [16]:

$$L\{ {}_a D_t^\alpha f(t) \} = \int_0^\infty e^{-st} {}_0 D_t^\alpha f(t) dt = \tag{2}$$

$$= s^\alpha F(s) - \sum_{m=0}^{n-1} s^m (-1)^j {}_0 D_t^{\alpha-m-1} f(t) \Big|_{t=0}$$

where integer n lies within $(n-1 < \alpha \leq n)$.

The (time-delay free) fractional order transfer function can be written as [3], [5]:

$$G(s) = \frac{B(s^{\beta_k})}{A(s^{\alpha_k})} = \frac{b_m s^{\beta_m} + b_{m-1} s^{\beta_{m-1}} + \dots + b_0 s^{\beta_0}}{a_n s^{\alpha_n} + a_{n-1} s^{\alpha_{n-1}} + \dots + a_0 s^{\alpha_0}} \tag{3}$$

where a_k with $(k=0, \dots, n)$ and b_k with $(k=0, \dots, m)$ denote constants, and α_k with $(k=0, \dots, n)$ and β_k with $(k=0, \dots, m)$ are arbitrary real numbers. According to [4], [5], one can assume inequalities $\alpha_n > \alpha_{n-1} > \dots > \alpha_0$ and $\beta_m > \beta_{m-1} > \dots > \beta_0$ without loss of generality. In this paper, the controlled time-delay system is supposed generally as:

$$G(s) = \frac{B(s^{\beta_k})}{A(s^{\alpha_k})} e^{-\Theta s} \tag{4}$$

III. ANALYSIS OF ROBUST STABILITY FOR SYSTEMS WITH PARAMETRIC UNCERTAINTY

The robust stability of the feedback control system will be investigated by means of its closed-loop characteristic polynomial (actually, a quasi-polynomial in the case of this contribution).

The fractional order version of the continuous-time uncertain polynomial with vector of uncertainty q and coefficient functions ρ_k can be written as:

$$p(s, q) = \rho_n(q) s^{\alpha_n} + \rho_{n-1}(q) s^{\alpha_{n-1}} + \rho_1(q) s^{\alpha_1} + \rho_0(q) s^{\alpha_0} \tag{5}$$

Then, the polynomial family is defined by [15]:

$$P = \{ p(\cdot, q) : q \in Q \} \tag{6}$$

where Q is the uncertainty bounding set restricting the uncertain parameters. Commonly, Q is supposed as a multidimensional box, i.e. individual parameters are bounded by intervals.

The polynomial family (6) is robustly stable if and only if $p(s, q)$ is stable for all $q \in Q$. The selection of specific tool for investigation of robust stability depends mainly on the structure of uncertainty. Generally, the higher level of relation among coefficients means more complex robust stability analysis and brings necessity of more sophisticated techniques. Nevertheless, a graphical method based on combination of the value set concept and the zero exclusion condition [15] is unique from the viewpoint of its universal

applicability. It can be applied for wide range of uncertainty structures and it is usable also for various regions of stability (so called robust D -stability). The detailed information on robust stability analysis under parametric uncertainty can be found in [15] and subsequently e.g. in [17], [18]. Finally, the works [9] – [12] extended the idea of the value set concept also to fractional order uncertain polynomials.

According to [15], the value set at given frequency $\omega \in \mathbb{R}$ is:

$$p(j\omega, Q) = \{ p(j\omega, q) : q \in Q \} \tag{7}$$

Practical creation of the value sets can be done by substituting s for $\omega \in \mathbb{R}$, fixing $\omega \in \mathbb{R}$ and letting q range over Q .

The zero exclusion condition for Hurwitz stability of family of continuous-time polynomials (6) is defined [15]: Suppose invariant degree of polynomials in the family, pathwise connected uncertainty bounding set Q , continuous coefficient functions $\rho_k(q)$ for $k=0, 1, 2, \dots, n$ and at least one stable member $p(s, q^0)$. Then the family P is robustly stable if and only if:

$$0 \notin p(j\omega, Q) \quad \forall \omega \geq 0 \tag{8}$$

Authors of the papers [9], [11], [12] construct the value sets for the fractional order families of polynomials mainly on the basis of fact that the fractional power of $j\omega$ can be written as:

$$(j\omega)^\alpha = \omega^\alpha \left(\cos \frac{\pi}{2} \alpha + j \sin \frac{\pi}{2} \alpha \right) \tag{9}$$

and on the subsequent analysis of vertices and exposed edges.

Within this contribution, the value sets are plotted for closed-loop characteristic quasi-polynomials of the feedback control loop with the uncertain time-delay fractional order plant and fixed integer order PID controller. Their visualization is based on sampling the uncertain parameters and on calculation of partial points of the value sets for an assumed frequency range. Thanks to the applied sampling (brute-force) method, the value sets of quasi-polynomials can be easily computed and consequently the robust stability can be analyzed with the assistance of standard zero exclusion condition.

IV. COMPUTATIONAL EXAMPLES

Suppose a fractional order time-delay plant given by transfer function:

$$G(s, K, T, \Theta) = \frac{K}{Ts^{0.9} + 1} e^{-\Theta s} \tag{10}$$

where K represents a gain, T is a time-constant, and Θ stands for a time-delay term. Nominal values of the parameters define the specific system:

$$G_N(s) = \frac{5}{10s^{0.9} + 1} e^{-10s} \quad (11)$$

However, the parameters of really controlled systems are assumed to be uncertain, i.e. they can lie within given intervals. Their specific values will be stated successively in (15)-(18).

The PID controller for nominal plant (11) was obtained by using the FOMCON Toolbox for Matlab [19], [20] and its routine “iopid_tune”. More specifically, as shown in Fig. 1, the Oustaloup filter based [21] approximation resulted in the integer order model:

$$G_A(s) = \frac{4.89523}{14.6777s + 1} e^{-8.86545s} \quad (12)$$

which was then utilized in standard Cohen-Coon method for PID controller design. The obtained compensator is:

$$C(s) = K_p + \frac{K_i}{s} + K_d s = 0.506221 + \frac{0.0278868}{s} + 1.48957s \quad (13)$$

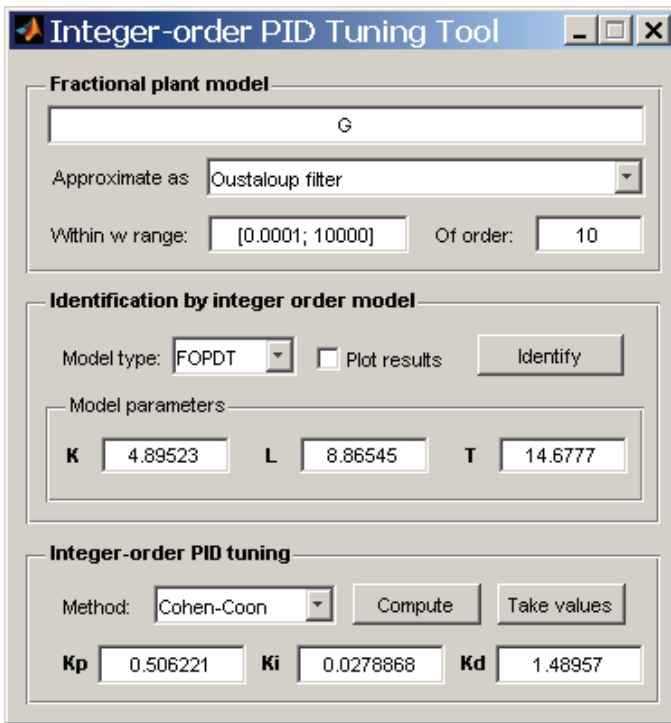


Fig. 1 GUI “iopid_tune” from the FOMCON Toolbox [19]

The graphical comparison of step responses of the original fractional-order nominal model (11) and its integer-order approximation (12) obtained with the assistance of the FOMCON Toolbox is shown in Fig. 2.

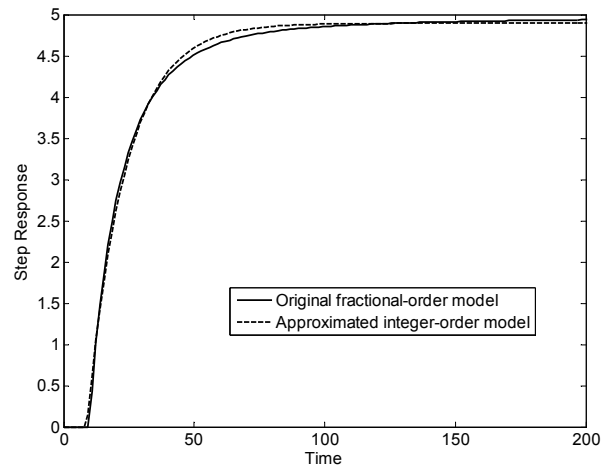


Fig. 2 Step responses of original fractional-order model (11) and approximated integer-order model (12) – visual comparison

The main object of interest, robust stability of the closed-loop control system, will be tested through the family of characteristic quasi-polynomials:

$$p_{cl}(s, K, T, \Theta) = (Ts^{0.9} + 1)s + Ke^{-\Theta s} (K_d s^2 + K_p s + K_i) \quad (14)$$

where one of the plant (10) parameters K , T , Θ can vary according to (15)-(18) and where K_p , K_i and K_d are fixed PID controller parameters taken from (13).

First, only the gain is supposed to lie within the interval while time constant and time-delay term remain fixed, i.e.:

$$K = \langle 4.5, 5.5 \rangle; \quad T = 10; \quad \Theta = 10 \quad (15)$$

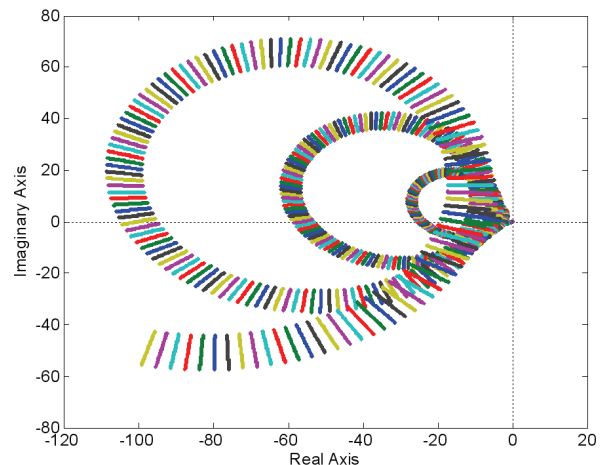


Fig. 3 Value sets for controller (13) and plant with (15)

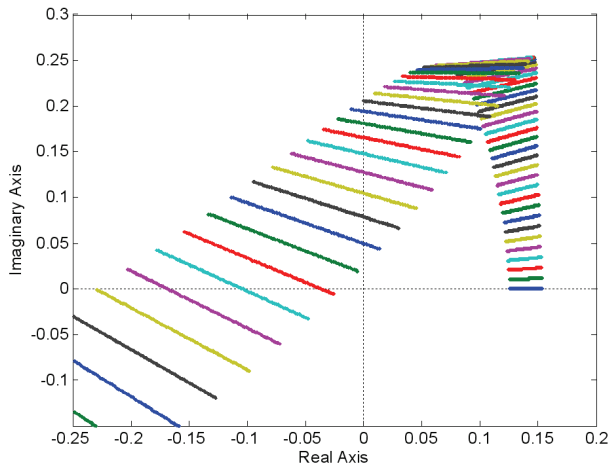


Fig. 4 Value sets for controller (13) and plant with (15) – closer look

The value sets for the corresponding family of closed-loop characteristic quasi-polynomials consist of straight lines. The Fig. 3 shows these value sets for the range of frequencies from 0 to 3 with the step 0.005. At each frequency, K is sampled within given interval with the step 0.01 (that means each line consists of 101 points). Then, the better view of the situation near the origin of the complex plane is provided by closer look in Fig. 4. Obviously, the zero point is not included in the value sets. Consequently, because the family contains at least one stable member and the zero is excluded, the family (14) with parameters (15) is robustly stable, so the closed-loop control system is robustly stable.

Now, the gain is the only uncertain parameter again, but the assumed bounds are a bit wider:

$$K = \langle 4, 6 \rangle; \quad T = 10; \quad \Theta = 10 \tag{16}$$

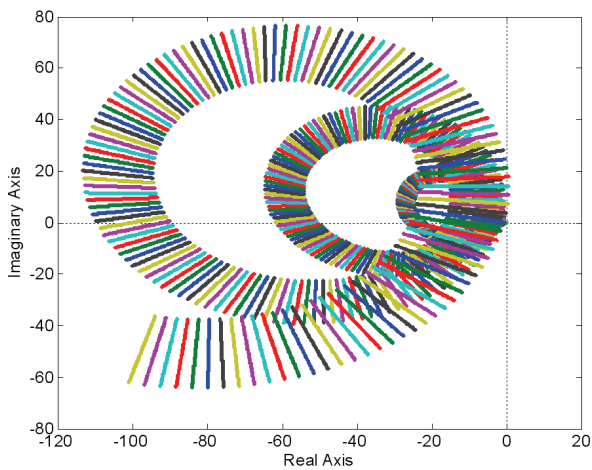


Fig. 5 Value sets for controller (13) and plant with (16)

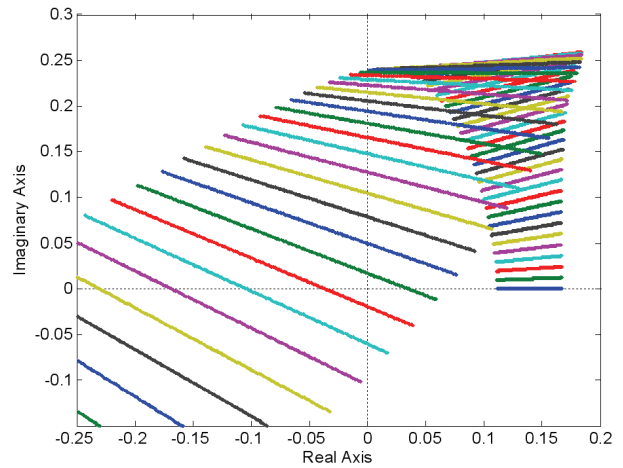


Fig. 6 Value sets for controller (13) and plant with (16) – closer look

The Fig. 5 depicts the value sets for the new interval under the same conditions as in the previous case. The zoomed version is shown in Fig. 6. As can be seen, the origin of the complex plane is included in the value sets and thus the feedback loop with plant parameters (16) is robustly unstable.

Next, the time constant is the uncertain parameter while the gain and time-delay term are fixed:

$$K = 5; \quad T = \langle 9, 11 \rangle; \quad \Theta = 10 \tag{17}$$

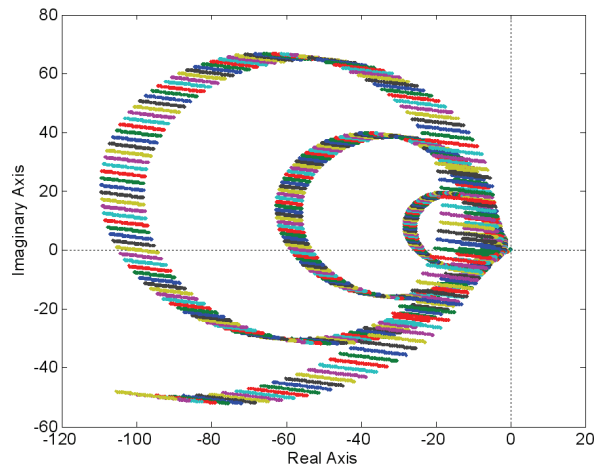


Fig. 7 Value sets for controller (13) and plant with (17)

The relevant value sets can be seen in Fig. 7 and the zoomed view in Fig. 8. The frequency range is $\omega = 0:0.005:3$ and the time constant is sampled $T = 9:0.05:11$. The complex plane origin is excluded from the value sets, the family contains at least one stable member and thus the family is robustly stable.

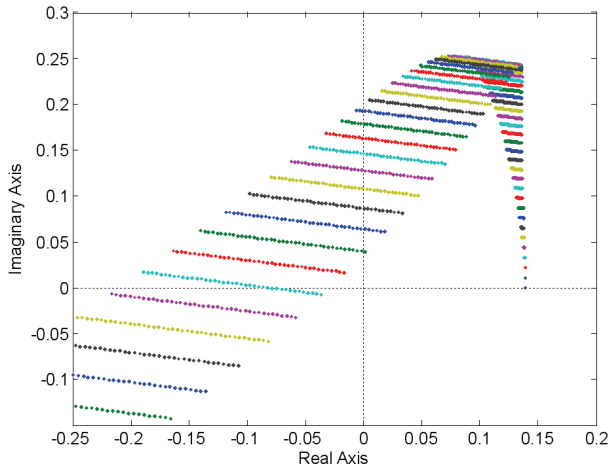


Fig. 8 Value sets for controller (13) and plant with (17) – closer look

Analogically, robustly unstable case can be easily found by taking wider bounds for uncertain time constant.

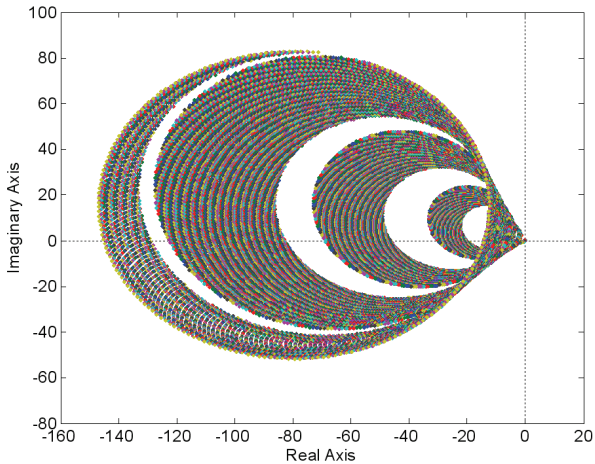


Fig. 9 Value sets for controller (13) and plant with (18)

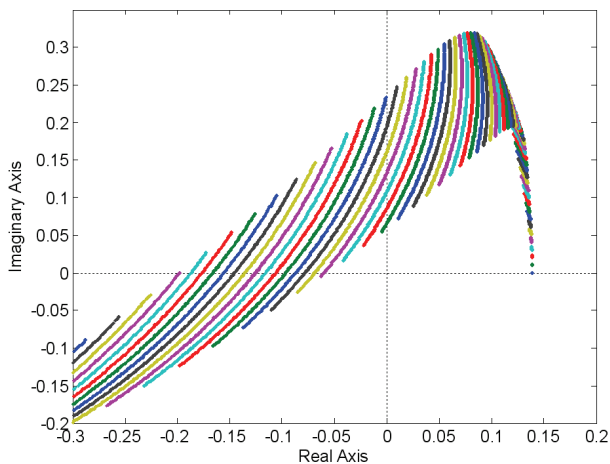


Fig. 10 Value sets for controller (13) and plant with (18) – closer look

Finally, time-delay term is considered as the uncertain one:

$$K = 5; \quad T = 10; \quad \Theta = \langle 9, 11 \rangle \quad (18)$$

The full and zoomed versions of the corresponding value sets for $\omega = 0:0.005:3$ and $\Theta = 9:0.01:11$ are in Figs. 9 and 10, respectively. The zero point is excluded from the value sets, the family has a stable member and so it is robustly stable.

V. CONCLUSION

The paper has been focused on application of very universal graphical approach, based on plotting the value sets of quasi-polynomials and use of the zero exclusion condition, to robust stability analysis for feedback control loops with fractional order time-delay plants and integer order PID controllers. The illustrative examples present the typical shapes of the value sets for the cases of uncertain gain, uncertain time constant and uncertain time-delay term. The future research should deal with the issue in more detail and verify e.g. the cases with more uncertain parameters together.

REFERENCES

- [1] K. B. Oldham, J. Spanier, *Fractional Calculus: Theory and Applications of Differentiation and Integration to Arbitrary Order*, Academic Press, New York – London, 1974.
- [2] K. S. Miller, B. Ross, *An Introduction to the Fractional Calculus and Fractional Differential Equations*, John Wiley and Sons, New York, USA, 1993.
- [3] I. Podlubný, *Fractional Differential Equations*, Academic Press, San Diego, CA, USA, 1999.
- [4] Y. Chen, I. Petráš, D. Xue, “Fractional Order Control – A Tutorial”, in *Proceedings of 2009 American Control Conference*, St. Louis, MO, USA, 2009.
- [5] I. Petráš, “Stability of fractional-order systems with rational orders: A survey”, *Fractional Calculus & Applied Analysis*, Vol. 12, No. 3, 2009, pp. 269-298.
- [6] R. Matušů, “Fractional Order Calculus in Control Theory”, in *Proceedings of the 13th WSEAS International Conference on Automatic Control, Modelling and Simulation*, Lanzarote, Spain, 2011.
- [7] R. Matušů, “Application of fractional order calculus to control theory”, *International Journal of Mathematical Models and Methods in Applied Sciences*, Vol. 5, No. 7, 2011, pp. 1062-1069.
- [8] R. E. Gutiérrez, J. M. Rosário, J. T. Machado, “Fractional Order Calculus: Basic Concepts and Engineering Applications”, *Mathematical Problems in Engineering*, Vol. 2010, 2010, 19 p., DOI: 10.1155/2010/375858.
- [9] N. Tan, Ö. F. Özgüven, M. M. Özyetkin, “Robust stability analysis of fractional order interval polynomials”, *ISA Transactions*, Vol. 48, No. 2, 2009, pp. 166-172.
- [10] B. Şenol, C. Yeroğlu, “Robust Stability Analysis of Fractional Order Uncertain Polynomials”, in *Proceedings of the 5th IFAC Workshop on Fractional Differentiation and its Applications*, Nanjing, China, 2012.
- [11] B. Şenol, C. Yeroğlu, “Computation of the Value Set of Fractional Order Uncertain Polynomials: A 2q Convex Parpolygonal Approach”, in *Proceedings of the 2012 IEEE International Conference on Control Applications*, Dubrovnik, Croatia, 2012.
- [12] C. Yeroğlu, B. Şenol, “Investigation of robust stability of fractional order multilinear affine systems: 2q-convex parpolygon approach”, *Systems & Control Letters*, Vol. 62, No. 10, 2013, pp. 845-855.
- [13] K. A. Moornani, M. Haeri, “Robust stability testing function and Kharitonov-like theorem for fractional order interval systems”, *IET Control Theory and Applications*, Vol. 4, No. 10, 2010, pp. 2097-2108.

- [14] J.-G. Lu, Y. Chen, "Stability and stabilization of fractional-order linear systems with convex polytopic uncertainties", *Fractional Calculus and Applied Analysis*, Vol. 16, No. 1, 2013, pp. 142-157.
- [15] B. R. Barmish, *New Tools for Robustness of Linear Systems*, Macmillan, New York, USA, 1994.
- [16] S. E. Hamamci, "Stabilization using fractional order PI and PID controllers", *Nonlinear Dynamics*, Vol. 51, No. 1-2, 2008, pp. 329-343, DOI: 10.1007/s11071-007-9214-5.
- [17] R. Matušů, R. Prokop, "Graphical analysis of robust stability for systems with parametric uncertainty: an overview", *Transactions of the Institute of Measurement and Control*, Vol. 33, No. 2, 2011, pp. 274-290.
- [18] R. Matušů, R. Prokop, "Robust Stability Analysis for Systems with Real Parametric Uncertainty: Implementation of Graphical Tests in Matlab", *International Journal of Circuits, Systems and Signal Processing*, Vol. 7, No. 1, 2013, pp. 26-33.
- [19] A. Tepljakov, *FOMCON: Fractional-order Modeling and Control*, [online], Available from URL: <http://fomcon.net/>.
- [20] A. Tepljakov, E. Petlenkov, J. Belikov, "FOMCON: Fractional-Order Modeling and Control Toolbox for MATLAB", in *Proceedings of the 18th International Conference "Mixed Design of Integrated Circuits and Systems"*, Gliwice, Poland, 2011.
- [21] A. Oustaloup, F. Levron, B. Mathieu, F. M. Nanot, "Frequency-band complex noninteger differentiator: characterization and synthesis", *IEEE Transactions on Circuits and Systems I: Fundamental Theory and Applications*, Vol. 47, No. 1, 2000, pp. 25-39.

Radek Matušů was born in Zlín, Czech Republic in 1978. He is a Researcher at Faculty of Applied Informatics of Tomas Bata University in Zlín, Czech Republic. He graduated from Faculty of Technology of the same university with an MSc in Automation and Control Engineering in 2002 and he received a PhD in Technical Cybernetics from Faculty of Applied Informatics in 2007. He worked as a Lecturer from 2004 to 2006. The main fields of his professional interest include robust systems and application of algebraic methods to control design.

Roman Prokop, born in 1952, is a Vice-Dean and a Full Professor at Faculty of Applied Informatics of Tomas Bata University in Zlín, Czech Republic. He graduated from Czech Technical University in Prague in 1976 and received a PhD from Slovak University of Technology in Bratislava in 1983. He was an Associate Professor from 1996 and a Full Professor from 2004. He aims his pedagogical and research work to automatic control theory, algebraic methods in control design and optimization. The main interests of the latest period are uncertain and robust systems, autotuning of controllers and time-delay systems.

Building a model of family house heating system using 1-wire sensor network protocol

Dominik Kujawa

Institute of Control and Computation Engineering University of Zielona Góra
ul. Podgórna 50, 65-246 Zielona Góra, Poland
dominikinf@gmail.com, dkujawa@weit.uz.zgora.pl

Abstract— The paper presents the parameter identification of a house heating system using a sensor network based on 1-wire protocol and the Raspberry Pi (RPi) computer. 46 sensors capture measurement data such as temperature, humidity, wind speed and fuel consumption using the 1-wire protocol. A fine-grained displacement of sensors throughout the house provides high measurement resolution. A high number of system inputs and outputs favors using a subspace identification algorithm. The identified model can be used to assess the effectiveness of heating system. To minimize computational burden, sensors delivering the greatest amount of information are chosen. All identification experiments have been carried out in a 270 m², 680 m³ detached uninhabited house, in a period of 30 days.

Keywords— state space models, subspace methods, identification algorithms, parameter estimation.

I. INTRODUCTION

The aim of this paper is searching for energy saving solutions through using a family house heating model obtained via subspace identification. Recently, a profound research effort has been made on identification of buildings condition for the energy saving purposes [1]. A comprehensive results of subspace identification approach are presented in this paper. A high number of inputs and outputs results in a high complexity of the house heating model. Many works present the identification of selected parts of the heating system of building or the entire building by analyzing the individual parts [10], [1]. This paper proposes a new comprehensive approach to the identification using house heating model based on the real measurement data and subspace methods [3]. The house as a whole is treated as a black box and all measurements are acquired from a set of sensors [14], [18]. One possible approach to house heating model identification is to use a 2D model in which in one dimension the information is propagated from day to day and in the other along the day. Repetitive processes are a class of 2D systems in which information in the temporal domain is of

finite duration [12]. Each execution is known as a pass (a day) and its duration as the pass length [4]. Design the house heating system requires a process model and this paper is addressed to the problem of its identification from the input-output data.

Identification of linear repetitive process dynamics is still a challenging problem in the system identification, and [5], [6], and [8] give the only published results. The approach proposed there is based on using an extended input sequence composed of the current pass input and the previous pass output, and the output sequence composed of the current pass output to determine the order of linear repetitive process, its unknown state-space model matrices and the noise covariance matrices [16], [17]. As such identification procedure uses the input output data from two successive passes, it can be restarted consecutively starting from the first pass data and boundary conditions. Therefore, it can be very useful for the identification of time invariant dynamics [2], [7], [21].

The need for fuel-saving results for consumption of natural fuels results both from the environmental and economic reasons. The need to optimize energy consumption, among others, arises from the growing number of buildings (up to 5 % a year in the EU countries). The energy consumption optimization leads to minimization of home maintenance costs. The proposed new approach to building house heating model is based on subspace identification methods. In the overall energy consumption of a residential building, about 50% is used for space heating, and about 19% for hot water heating, the remainder is associated with the use of household equipment. The annual cost of heating is from 30% to 50% of the overall cost of house maintaining. Therefore, the energy consumption reducing for heating residential buildings is important and affects all societies [19].

The house heating system consists of three main elements - a heat source, network pipes, and a heat receiver. To describe house heating system, the following classification features are to be specified:

- 1) Heat source type.
- 2) Heat source location.
- 3) Fuel type.
- 4) Heating medium type.
- 5) Heat dissipation method.

The domestic generation of hot water can be made using installation with or without the heat exchanger. The disadvantage of the first solution is the limited instantaneous maximum flow of hot water, while the other requires maintaining the stored heat energy. This highlights the diversity of simple heating systems in conjunction with different shapes of buildings [1]. The problem of heating is very extensive and therefore it is restricted here to the dwelling house with a central source of heat and a domestic hot water preparation system. An example of house heating system considered in this paper is shown in Fig. 1.

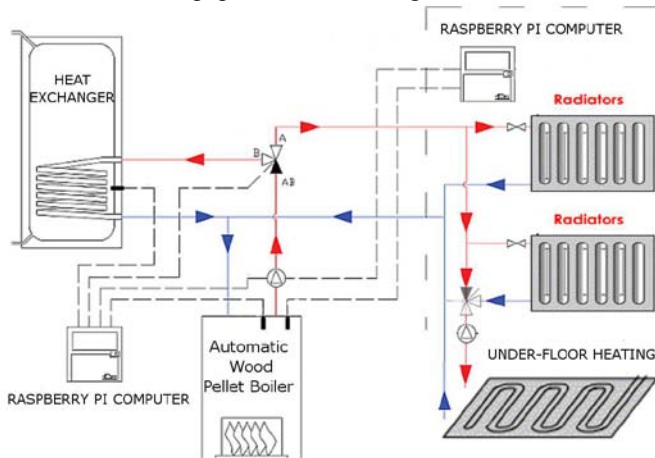


Fig. 1. Central heating with hot water buffer installation.

The physical description of house heating system takes into account the following parameters:

- 1) Thermal resistance.
- 2) Heat transfer coefficients of different elements of the house.
- 3) Heat loss coefficients.
- 4) Heat transfer coefficients by thermal bridges.
- 5) Heat demand of the rooms.
- 6) Heating energy consumption.
- 7) Outdoor temperature.

The heat exchanger, which is a hot water buffer, can be characterized by the following parameters:

- 1) The rate of unit demand for hot water.
- 2) The number of recipients and the coefficient of simultaneity use.
- 3) The required intake water temperature.

The house heat exchanger specification is chosen on the basis of the most adverse weather conditions and the maximum water consumption for a given number of inhabitants [20].

The structure of the paper is as follows: In Section II, the metering building using 1-wire protocol is introduced, description of the test building is given in Section III. In section IV and section V deterministic model of a discrete linear repetitive process is introduced, the identification problem is formulated and its solution based on subspace algorithms is presented. Section VI deals with the stochastic identification problem.

Identification results are shown in Section VII. Finally, conclusions are given in section VIII.

II. METERING BUILDING USING 1-WIRE PROTOCOL

The considered dwelling house is inhabited. Hence, this test site allows parameter identification of building heating system using subspace methods in open loop.



Fig. 2. Experimental building area.

The heat receiver is a dual-circuit system with the reception radiator plugged to the underfloor heating system.

Simple control systems provide low effectiveness because they lack cost effectiveness and energy consumption optimization. The main elements of the proposed control system are three Raspberry Pi (RPI) computers, which have the advantage of small size, low cost and low power consumption, and the GPIO module which allow to gather data from all sensors deployed in the house. For the temperature and humidity measuring, DS18B20 temperature sensors and DHT11 humidity sensor are selected. The DHT11 humidity sensor allows the moisture measurement in the ranges of 10% – 40% and 20% – 90% with the accuracy of $\pm 1\%$.

The weather transmitter WS2800 measures the outside temperature and it also allows to record:

- 1) Wind speed ranged from 0 to 35 m/s and from 0 to 60 m/s with the accuracy of 3%.
- 2) Wind direction ranged from 0 to 360 with the accuracy of 3%.
- 3) Relative humidity ranged from 0 to 100% with the accuracy of 3%.
- 4) Atmospheric pressure in the range from 600 hPa to 1100 hPa.
- 5) Intensity of precipitation and distinguishing the rain and the hail.

The full functionality of the described system is not only limited to collecting measurements. Due to the built-in GPIO module of the RPi computer, it is also possible to configure it with the SRD-05VDC-SL-C Power Relay Modules to control the system. The control system allows to control actuators using GPIO RPi ports. Fig. 3 presents the thermal drive whose action causes RPi computer algorithm to control the valve to save energy.



Fig. 3. Thermal driver allowing to control the valve via RPi computer.

RPis are interconnected through network adapters, which allows to monitor the RPis status. A radio card allows to view, monitor and program RPis from devices equipped with Wi-Fi cards. The RPi collects data from temperature sensors, humidity sensors and the weather station WS2800 using the GPIO module and shielded twisted cable. Having the communication protocol used in a given device, the interpretation of the results can be made after receiving all packages. In total, a set of three RPi computers, with GPIO interface and 1-Wire Dallas Semiconductor protocol, connected to 32 temperature DS18B20 sensors and 9 DHT11 humidity sensors are employed during the measuring experiments. Fig. 4 shows the patch panel which organizes all connections for controlling devices and all sensors placed in the house.



Fig. 4. Patch panel organizing connection of Raspberry Pi computers to sensors.

This configuration allows the input and output temperature measurement of the radiator, boiler and heat exchanger as well as the temperature in different rooms of the building. The measurement system also includes software archiving input and output measurements for the purpose of subspace identification. This software has been developed in PHP, and it provides the tools to easily create data in the form of a website. The program runs in a web browser enabling remote access to measurement data. For the purpose of communication via the RS485 port, the YUKO converter was used. This is an industrial solution, and it allows the choice of low data transmission rate for communication over a distance up to 5 km. Received packets with additional information describing the server status are stored as text files in the form

of logs. This enables verification of the communication correctness. The main archiving is done using the MySQL database. The measurement ranges of physical values received by the server are determined by manufacturing specifications of measuring devices and stored in the respective tables along with the so-called time stamp. The server allows local instantaneous and historical visualization of measuring data in the form of graphs and text files conversion.

III. DESCRIPTION OF THE TEST BUILDING

We distinguish among three types of single-family houses: detached, semi-detached, terraced. The detached house heat losses are greater than those of terraced ones. The test building includes a basement which better insulates heat from the ground. Heating water distribution lines are routed in floors and radiators circulation. Diversity of design features of the building determines its dynamic properties as an identification object. These, in turn, can be determined by examining the mutual relationship between the measured signals. Some of these relationships may prove to be irrelevant, what determines the later choice of a control systems structure.

The test building is a detached house consisting of two apartments with a total area of 270 square meters. It consists of 18 heated rooms and a stairwell. The cubic heated space equals to 630m³. The building was designed as a detached bungalow with a usable floor space attic, entirely cellared with not heated garage located in the cellar part. The building has a single-layered exterior walls made of Porotherm ceramic blocks and 12cm thick styrofoam insulation layer. On the outside, the walls are covered with mesh and glue and a decorative plaster, while on the inside with a mineral plaster. The wall heat transfer coefficient λ is less than 0.25 W/m²K. The floors of the building are made of prestressed concrete panels. The roof is covered with ceramic tiles, insulated with 20cm and 5cm thick mineral wool layer. The insulation layer is protected from the inside by a vapor barrier film, and by a highly permeable foil on the outside. The building has 24 plastic windows, two patio doors, eight roof windows, and one garage gate. The windows heat transfer coefficient λ is 1.1 W/m²K. The ventilation used in the building is natural one and it consists of five channels. In the basement of the house, there is a boiler room in which a central source of heat was placed. It is the solid fuel 25 kW Brass boiler. The house is heated by a floor-mixed installation of radiators. For the water stream distribution, a mixing valve connected to underfloor heating, radiators and water heating is employed. Each of the radiators is equipped with a thermoregulation valve. The water is distributed via a switchboard system (3 sections) and the forced circulation pump. Heating cables are made using the PEX Wavin technology. The system pressure is 0.9MPa. The boiler is equipped with a hot water storage tank of 300l capacity. The building meets the criteria of representativeness associated with the widespread use of technical solutions. The approximate values of heat transfer coefficient for the tested building are given in Table 1.

Table 1. The approximate values of heat transfer coefficient.

No	Bulkhead	Heat transfer coefficient (kW/m ² K)	Area (m ²)
1	Walls	0.22	233
2	Roof	0.27	203
3	Floors	0.68	180
4	Doors	2.01	3.6
5	Windows	1.1	35

A proper design of house heating control system can increase the overall heating system efficiency. The test building was not inhabited during the period of study. The ways of controlling the boiler and an accurate predictability of the noise variability, which are external weather conditions, were limited. Major weather changes during the observation gave a large variety of object excitations. The difficulty in the test was a correct choice of the sampling period of measured continuous signals. The measuring tests included 30 days in the heating season, whereas the next 10 days were reserved only for the efficiency verification of the proposed identification system. The effect of external conditions changes on the thermal state of the building and the performance of heating system were studied. For the experiment, the measuring data were collected at wide variations of weather conditions and constant values of selected heating system parameters such as pump flow, and required temperatures. The outdoor temperature measurement was performed at three points: on the western, southern and eastern side of the house, and the measured values were averaged. Fig. 5 shows the registered temperature, humidity and wind speed. The boiler water temperature and temperatures of individual radiators and floor heating inputs were also measured for the purpose of identification. The output signal is the amount of fuel consumed within 30 minutes. The effectiveness of the heating system is evaluated due to observation of the ZM_H8C-C3-500k ZEMIC extensometer that monitors the boiler fuel consumption. The input signals for identification are temperatures, humidity, and wind force, and the output signal is the amount of consumed fuel. In the context of measuring experiments co-financed by the EU within 30 days of the heating season, more than 2 GB of data were collected. In addition, for comparison a set of weather data gathered by the Wrocław weather station in the years 2006 - 2012, and the year 2012 weather data registered in Szczecin and Zakopane were collected. This allows the reliable identification of the building model and the following simulation studies using registered excitations. In the course of the simulation studies, the model can be stimulated by input signals without any geographical limitations.

IV. DETERMINISTIC DISCRETE REPETITIVE PROCESSES

Consider the state-space model [17] of a discrete linear repetitive process of the following form:

$$x_{k+1}(p+1) = Ax_{k+1}(p) + B_0y_k(p) + Bu_{k+1}(p) \tag{1}$$

$$y_{k+1}(p) = Cx_{k+1}(p) + D_0y_k(p) + Du_{k+1}(p) \tag{2}$$

where:

$0 \leq p \leq \alpha - 1 \in Z_+$ – the independent spatial or temporal variable,

$k \in Z_+$ – the current pass number,

$x_k(p) \in R^n$ – the state vector,,

$y_k(p) \in R^l$ – the pass profile (output) vector,

$u_k(p) \in R^m$ – the input vector,

A, B, B_0, C, D, D_0 – matrices of appropriate dimensions.

To complete process description, it is necessary to specify the boundary conditions [9]:

$$\begin{aligned} x_{k+1}(0) &= d_{k+1} \\ y_0(p) &= f(p) \end{aligned} \tag{3}$$

where $d_{k+1} \in R^n$ is a vector with known constant entries and

$$f(p) \in R^l \tag{4}$$

Define the following input Hankel Block matrix [9]:

$$U_{0|2i-1} \stackrel{def}{=} \begin{bmatrix} u_{k+1}(0) & \dots & u_{k+1}(j-1) \\ y_k(0) & \dots & y_k(j-1) \\ \dots & \dots & \dots \\ u_{k+1}(i-1) & \dots & u_{k+1}(i+j-2) \\ y_k(i-1) & \dots & y_k(i+j-2) \\ \hline u_{k+1}(i) & \dots & u_{k+1}(i+j-1) \\ y_k(i) & \dots & y_k(i+j-1) \\ u_{k+1}(j+1) & \dots & u_{k+1}(i+j) \\ y_k(i+1) & \dots & y_k(i+j) \\ \dots & \dots & \dots \\ u_{k+1}(2i-1) & \dots & u_{k+1}(2i+j-2) \\ y_k(2i-1) & \dots & y_k(2i+j-2) \end{bmatrix} = \begin{bmatrix} U_{0|i-1} \\ U_{i|2i-1} \end{bmatrix} \stackrel{def}{=} \begin{bmatrix} U_p \\ U_f \end{bmatrix} \tag{5}$$

$$U_{0|2i-1} \stackrel{def}{=} \begin{bmatrix} U_{0|i} \\ U_{i+1|2i-1} \end{bmatrix} \stackrel{def}{=} \begin{bmatrix} Y_p^+ \\ Y_f \end{bmatrix} \tag{6}$$

Define also the output block matrix $Y_{0|2i-1}$:

$$Y_{0|2i-1} \stackrel{def}{=} \begin{bmatrix} y_{k+1}(0) & \dots & y_{k+1}(j-1) \\ \dots & \dots & \dots \\ y_{k+1}(i-1) & \dots & y_{k+1}(i+j-2) \\ \hline y_{k+1}(i) & \dots & y_{k+1}(i+j-1) \\ y_{k+1}(i+1) & \dots & y_{k+1}(i+j) \\ \dots & \dots & \dots \\ y_{k+1}(2i-1) & \dots & y_{k+1}(2i+j-2) \end{bmatrix} = \begin{bmatrix} Y_{0|i-1} \\ Y_{i|2i-1} \end{bmatrix} = \begin{bmatrix} Y_p \\ Y_f \end{bmatrix} \tag{7}$$

$$Y_{0|2i-1} \stackrel{def}{=} \begin{bmatrix} Y_{0|i} \\ Y_{i+1|2i-1} \end{bmatrix} = \begin{bmatrix} Y_p^+ \\ Y_f \end{bmatrix} \tag{8}$$

The number of block rows i should be larger than the maximum order of the LRP [11].

Define block Hankel matrices W_p and W_p^+ consisting of Y_p, U_p and Y_p^+, U_p^+ , respectively:

$$W_{0|i-1} \stackrel{def}{=} \begin{bmatrix} U_{0|i-1} \\ Y_{0|i-1} \end{bmatrix} = \begin{bmatrix} U_p \\ Y_p \end{bmatrix} = W_p \quad (9)$$

$$W_p^+ = \begin{bmatrix} U_p^+ \\ Y_p^+ \end{bmatrix} \quad (10)$$

The state-sequence matrix X_i is defined as:

$$X_i \stackrel{def}{=} \begin{bmatrix} x_{k+1}(i) & \dots & x_{k+1}(i+j-1) \end{bmatrix} \quad (11)$$

Define the extended observability matrix Γ_i and the reversed extended controllability matrix Δ_i

$$\Gamma_i \stackrel{def}{=} \begin{bmatrix} C \\ CA \\ CA^2 \\ \dots \\ CA^{i-1} \end{bmatrix} \quad (12)$$

$$\Delta_i \stackrel{def}{=} \begin{bmatrix} A^{i-1}[B \ B_0] & \dots & A[B \ B_0][B \ B_0] \end{bmatrix} \quad (13)$$

Assume also that the pair $\{A, C\}$ is observable and the pair $\{A, [B \ B_0]\}$ is controllable [9]. Finally, define the lower block triangular Toeplitz matrix H_i

$$H_i \stackrel{def}{=} \begin{bmatrix} [D \ D_0] & 0 & \dots & 0 \\ C[B \ B_0] & [D \ D_0] & \dots & 0 \\ CA[B \ B_0] & C[B \ B_0] & \dots & 0 \\ \dots & \dots & \dots & \dots \\ CA^{i-2}[B \ B_0] & CA^{i-3}[B \ B_0] & \dots & [D \ D_0] \end{bmatrix} \quad (14)$$

The block Hankel matrices (5) – (10) along with the extended observability matrix (12), the reversed extended controllability matrix (13) and the lower block triangular Toeplitz matrix play an important role in the development of subspace identification methods [7].

V. IDENTIFICATION PROBLEM

Given α measurements of the input $u_{k+1}(p)$ and the outputs $y_k(p)$ and $y_{k+1}(p)$ generated by the LRP (1) – (2) determine its order and the LRP matrices A, B, B_0, C, D, D_0 up to within a similarity transformation.

Following Theorem 1 [15], the state-space model (1) – (2) can be written in a matrix form

$$\begin{aligned} Y_p &= \Gamma_i X_p + H_i U_p, \\ Y_f &= \Gamma_i X_f + H_i U_f, \\ X_f &= A^i X_p + \Delta_i U_p, \end{aligned} \quad (15)$$

The LRP system matrices can be computed using Algorithm 1 or Algorithm 2 of Van Overschee and De Moor [15], assuming actual pass input and previous pass output as model input [7].

VI. STOCHASTIC DISCRETE REPETITIVE PROCESSES

Consider the state-space model of a discrete linear repetitive process of the following form

$$x_{r+1}(p+1) = Ax_{r+1}(p) + B_0 y_r(p) + Bu_{r+1}(p) + w_{r+1}(p) \quad (16)$$

$$y_{r+1}(p) = Cx_{r+1}(p) + D_0 y_r(p) + Du_{r+1}(p) + v_{r+1}(p) \quad (17)$$

Where the covariance matrix of the zero mean white vector sequences $w_{r+1}(p)$ and $v_{r+1}(p)$ is

$$E \left\{ \begin{bmatrix} w_{r+1}(k) \\ v_{r+1}(k) \end{bmatrix} \begin{bmatrix} w_{r+1}^T(q) & v_{r+1}^T(q) \end{bmatrix} \right\} = \begin{bmatrix} Q & S \\ S^T & R \end{bmatrix} \delta_{rq} \quad (18)$$

and δ_{rq} denotes the discrete Kronecker delta.

The identification problem is: given αK measurements of the input $u_{r+1}(p)$ and the outputs $y_r(p)$ and $y_{r+1}(p)$ generated by (29) – (30) determine the order of this process and the matrices A, B, B_0, C, D and D_0 up to a similarity transformation, and the covariance matrices Q, S and R .

We assume that $u_{r+1}(p)$ and $y_r(p)$ are uncorrelated with $w_{r+1}(p)$ and $v_{r+1}(p)$, $u_{r+1}(p)$ and $y_r(p)$ are persistently exciting of order $2i$, $j \rightarrow \infty$, and $w_{r+1}(p)$ and $v_{r+1}(p)$ are not identically zero.

Based on Theorem 12 [15], the combined Algorithm 1 or its robust version can be applied to determine the process order and the unknown matrices $A, B, B_0, C, D, D_0, Q, S, R$. The combined Algorithm 1 consists of the following steps [13]:

1) Calculate the oblique projection

$$O_i = Y_f / U_f W_p \quad (19)$$

2) Calculate the singular value decomposition

$$W_1 O_i W_2 = [U_1 U_2] \begin{bmatrix} S_1 & 0 \\ 0 & 0 \end{bmatrix} \begin{bmatrix} V_1^T \\ V_2^T \end{bmatrix} = U_1 S_1 V_1^T \quad (20)$$

3) Find the order of the process (16) – (17) by the inspection of the singular values in S_1 .

4) Calculate Γ_i from

$$\Gamma_i = W_1^{-1} U_1 S_1^{1/2} T \quad (21)$$

5) Solve the following set of linear equations in a least squares sense for A, C and K

$$\begin{bmatrix} \Gamma_{i-1}^T Z_{i+1} \\ Y_{ij} \end{bmatrix} = \begin{bmatrix} A \\ C \end{bmatrix} \Gamma_i^T Z_i + K U_f + \begin{bmatrix} \rho_w \\ \rho_v \end{bmatrix} \quad (22)$$

where Z_i and Z_{i+1} are the orthogonal projections:

$$Z_i = Y_f / \begin{bmatrix} W_p \\ U_f \end{bmatrix} \quad (23)$$

$$Z_i = Y_f^- / \begin{bmatrix} W_p^+ \\ U_f \end{bmatrix} \quad (24)$$

6) Determine B, B_0, D , and D_0 from the following over-determined set of equations using least squares method

$$\begin{bmatrix} K_{1|1} \\ \vdots \\ K_{1|i} \\ K_{2|1} \\ \vdots \\ K_{2|i} \end{bmatrix} = N \begin{bmatrix} D & D_0 \\ B & B_0 \end{bmatrix} \quad (25)$$

where

$$N = \begin{bmatrix} -\lambda_{1|1} & M_1 - \lambda_{1|1} & \cdots & M_{i-2} - \lambda_{1|i-1} & M_{i-1} - \lambda_{1|i} \\ M_1 - \lambda_{1|2} & M_2 - \lambda_{1|3} & \cdots & M_{i-1} - \lambda_{1|i} & 0 \\ \cdots & \cdots & \cdots & \cdots & \cdots \\ M_{i-1} - \lambda_{1|i} & 0 & \cdots & 0 & 0 \\ I_l - \lambda_{2|1} & -\lambda_{2|2} & \cdots & -\lambda_{2|i-1} & -\lambda_{2|i} \\ -\lambda_{2|2} & -\lambda_{2|3} & \cdots & -\lambda_{2|i} & 0 \\ \cdots & \cdots & \cdots & -\lambda_{2|i} & 0 \\ -\lambda_{2|i} & 0 & \cdots & 0 & 0 \end{bmatrix} \times \begin{bmatrix} I_l & 0 \\ 0 & \Gamma_{i-1} \end{bmatrix} \quad (26)$$

with

$$\lambda = \begin{bmatrix} A \\ C \end{bmatrix} \Gamma_i^l = \begin{bmatrix} \lambda_{1|1} & \lambda_{1|2} & \cdots & \lambda_{1|i} \\ \lambda_{2|1} & \lambda_{2|2} & \cdots & \lambda_{2|i} \end{bmatrix} \quad (27)$$

$$M = \Gamma_i^l = [M_1 \ M_1 \ \cdots \ M_{i-1}] \quad (28)$$

$$K = \begin{bmatrix} K_{1|1} & K_{1|2} & \cdots & K_{1|i} \\ K_{2|1} & K_{2|2} & \cdots & K_{2|i} \end{bmatrix} \quad (29)$$

7) Determine Q, S and R from the residuals ρ_w and ρ_v

$$\begin{bmatrix} Q & S \\ S^T & R \end{bmatrix} = E \left\{ \begin{bmatrix} \rho_w \\ \rho_v \end{bmatrix} \begin{bmatrix} \rho_w^T & \rho_v^T \end{bmatrix} \right\} \quad (30)$$

VII. IDENTIFICATION RESULTS

The modified subspace identification algorithm has been applied to collected input-output data. The subsequent one-day data have provided the information to build the house heating model. The following input and output signals have been accepted: the house inside temperature, the outdoor temperature as the inputs, and the fuel consumption as the output. Fig. 5 shows the outside temperature, humidity, pressure, and wind force during carrying out the experiments, while Fig. 6 shows the change of inside temperature with changing weather conditions.

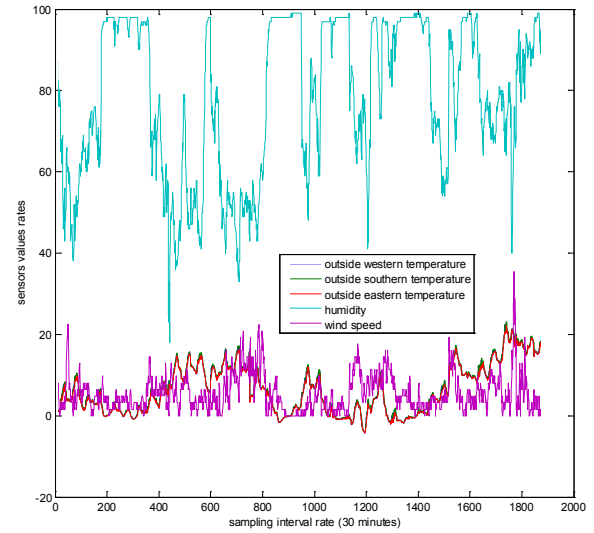


Fig. 5. Sensors values of western temperature, southern temperature, eastern temperature, humidity, and wind force.

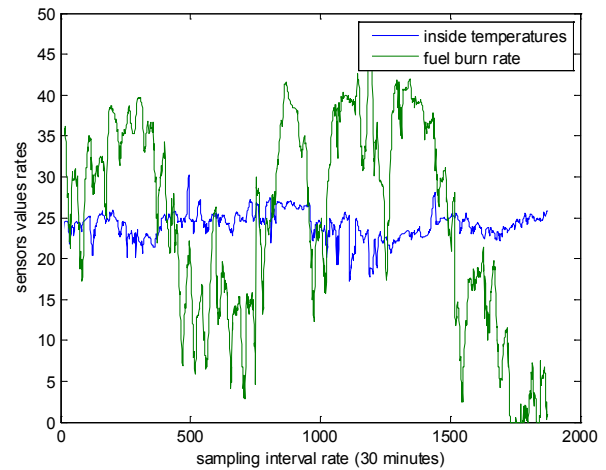


Fig. 6. Change of inside temperature; fuel burn rate [dag/h]

To identify repetitive process model, it is assumed that each pass corresponds to data acquired in 24 hours, and subsequent 24 hours data have been merged. The data are sampled every 30 minutes, hence one pass contains 48 samples. Fig. 7 shows comparison of the second order model response with the actual data. In this case, fitting model response to the actual data achieves 41%. Increasing the order of estimated model to 4, results in the fitting level of 91.61% – Fig. 8.

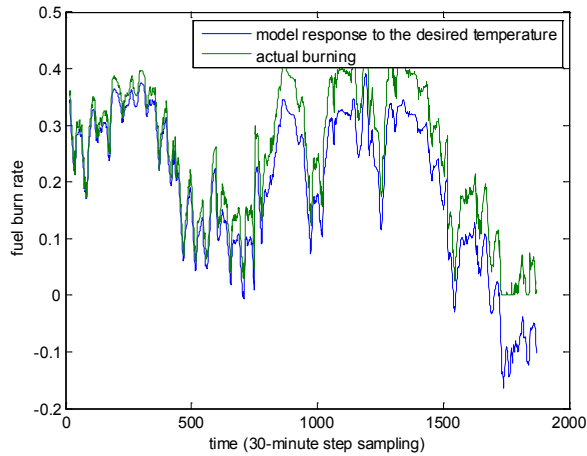


Fig. 7. System fuel burn rate and the second order model response.

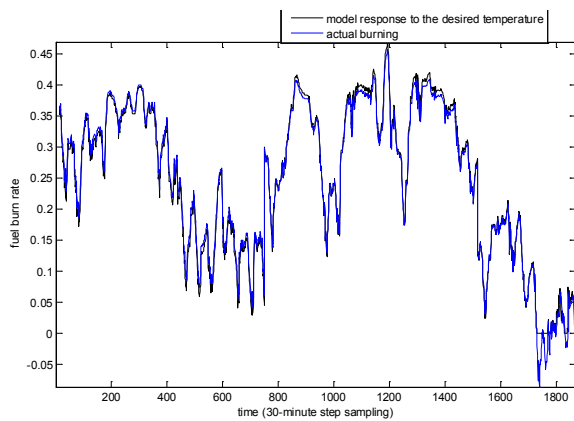


Fig. 8. System fuel burn rate and the fourth order model response.

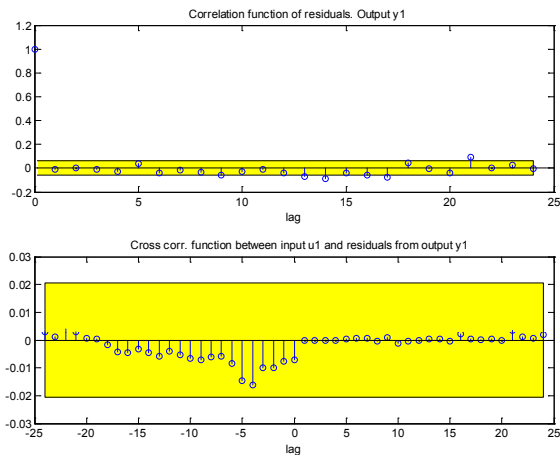


Fig. 9. Correlation function and cross correlation function of the model residuals.

In Fig. 9, the upper plot shows the autocorrelation function of fuel burn rate residuals. The horizontal solid lines correspond to the 95% confidence interval of the corresponding estimates. Any fluctuations within the confidence interval are considered to be insignificant.

Subspace identification approach results in a reliable model as the residual autocorrelation function within the confidence interval indicates that the residuals are uncorrelated. The bottom plot presents the cross-correlation of the residuals with the input. The obtained model residuals are uncorrelated with system inputs.

VIII. CONCLUSIONS

In the paper, the use of 1-wire protocol and Raspberry Pi computers as a useful technology to collect data for the house parameter heating model is proposed and tested.

1-wire protocol by Dallas Semiconductor allows a low-cost data collection from hundreds of sensors measuring temperature, humidity, atmospheric pressure located in the house for a long period of time.

The identification experiments are performed on the basis of real measurement input-output data. To identify the repetitive process model, the modified subspace identification method, in which the actual pass input and the previous pass output are employed as model input, is applied.

IX. ACKNOWLEDGMENT



The author is a scholar participating in Sub-measure 8.2.2. Regional Innovation Strategies, Measure 8.2. Transfer of Knowledge, Priority VIII Regional Human Resources for the Economy Human Capital Operational Programme co-financed by the European Union Social Fund and the State Budget of Poland.

X. REFERENCES

- [1] L. Perez-Lombard, J. Ortiz, and C. Pout, A review on buildings energy consumption information, *Energy and buildings*, vol. 40, no. 3, pp. 394–398, 2008.
- [2] J. Bochniak, K. Galkowski, E. Rogers, and A. Kummert, Robust stabilization of discrete linear repetitive processes with switched dynamics, *Int. Journal of Applied Mathematics and Computer Science*, vol. 16, pp. 441–462, 2006.
- [3] A. Chiuso and G. Picci, Some algorithmic aspects of subspace identification with inputs, *Int. Journal of Applied Mathematics and Computer Science*, vol. 11, pp. 55–75, 2001.
- [4] L. Hladowski, K. Galkowski, Z. Cai, E. Rogers, C. T. Freeman, P. L. Lewin, Experimentally supported 2D systems based iterative learning control law design for error convergence and performance, *Control Engineering Practice*, vol. 18, no. 4, pp. 339–348, 2010.
- [5] A. Janczak and D. Kujawa, Subspace approach to identification of linear repetitive processes, *Proceedings of the 2009 Int. Workshop on Multidimensional (nD) Systems*, Thessaloniki, Greece, pp. 120–123, 2009.
- [6] A. Janczak and D. Kujawa, Identification of linear repetitive processes using subspace algorithms, *Proceedings of 15th Int. Conference on Methods and Models in Automation and Robotics (MMAR 2010)*, Miedzyzdroje, Poland, pp. 371–376, 2010.
- [7] A. Janczak, D. Kujawa, E. Rogers, Z. Cai, Subspace identification of process dynamics for iterative learning control, *Proceedings of the 8th International Workshop on Multidimensional Systems - nDS' 13*. Erlangen, Germany, 2013.
- [8] T. Katayama, *Subspace Methods for System Identification*. Springer, Berlin, 2005.

- [9] L. Ljung, *System Identification: Theory for the User*, 2nd ed, Prentice Hall, Upper Saddle River, N.J., 1999.
- [10] M. Gwerder, B. Lehmann, J. Todtli, V. Dorer, and F. Renggli, "Control of thermally-activated building systems (tabs)," *Applied energy*, vol. 85, no. 7, pp. 565–581, 2008.
- [11] S. J. Qin, An overview of subspace identification, *Computers and Chemical Engineering*, vol. 30, no. 10-12, pp. 1502–1513, 2006.
- [12] E. Rogers, K. Galkowski, and D. H. Owens, *Theory and Applications for Linear Repetitive Processes*, Springer, Berlin, 2007.
- [13] P. Van Overschee and B. De Moor, N4SID: Subspace algorithms for identification of combined deterministic-stochastic systems, *Automatica*, vol. 30, no. 1, pp. 75–93, 1994.
- [14] P. Van Overschee and B. De Moor, A unifying theorem for three subspace identification algorithms, *Automatica*, vol. 31, no. 12, pp. 1853–1864, 1995.
- [15] P. Van Overschee and B. De Moor, *Subspace Identification for Linear Systems: Theory, Implementation, Applications*, Kluwer Academic Publishers, Boston, 1996.
- [16] M. Verhaegen, Application of subspace model identification technique to identify LTI systems operating in closed-loop, *Automatica*, vol. 29, no. 4, pp. 1027–11040, 1993.
- [17] M. Verhaegen, Identification of deterministic part of MIMO state space models given in innovation form from input-output data, *Automatica*, vol. 30, no. 1, pp. 61–74, 1994.
- [18] V. Viberg, Subspace-based methods for the identification of linear time invariant systems, *Automatica*, vol. 31, no. 12, pp. 1835–1851, 1995.
- [19] H. Madsen and J. Holst, Estimation of continuous-time models for the heat dynamics of a building, *Energy and Buildings*, vol. 22, no. 1, pp. 67–79, 1995.
- [20] K. Andersen, H. Madsen, and L. Hansen, Modelling the heat dynamics of a building using stochastic differential equations, *Energy and Buildings*, vol. 31, no. 1, pp. 13–24, 2000.
- [21] Luiza Ocheană, Dan Popescu, Luca Ferrarini, *Euroment, Proc. of the International Conference on Systems, Control and Informatics*, 2013.

Multivariable Control of Unstable Systems – A Matrix Equation Approach

Roman Prokop and Jiří Korbek

Abstract—The contribution is focused on control design and simulation of MIMO linear continuous-time systems. Suitable and efficient tools for description and derivation are algebraic notions as rings, polynomial matrices, and Diophantine equations. Generalized MIMO PI controller design is studied for stable and unstable systems. Unified approach through matrix Diophantine equation can be applied in both cases. All stabilizing feedback controllers are obtained via solutions of a matrix Diophantine equation. The methodology allows defining a scalar parameter for tuning and influencing of controller parameters. A Matlab, Simulink program implementation was developed for simulation and verification of the studied approach. Illustrative examples show the simplicity and flexibility of the proposed method for a simple two input–two output system.

Keywords—Algebraic approach, Diophantine equations, Multivariable systems, Polynomial matrices.

I. INTRODUCTION

THE analysis and control of multi input–multi output (MIMO) systems is a very attractive and interesting research field. Methods and tools of SISO systems cannot be simply and trivially generalized into multivariable cases. The main problem relates to the non-commutativity of the matrix multiplication. However, algebraic notions and tools can be successfully utilized also in the non-commutative case. The main tool for continuous-time systems is the Laplace transform and briefly speaking, multivariable linear continuous-time systems are described and expressed by a set of linear differential equations. So, scalar polynomials describing single input – output linear systems are replaced by polynomial matrices. Algebraic notions and modules remain a suitable and effective tool for analysis and control design of MIMO systems. Transfer functions as a ratio of two polynomials are in MIMO cases considered as matrix fractions and due to non-commutativity of the matrix multiplication the denominator can be left or right. Also, a scalar Diophantine equation is generalized into a matrix one. The contribution is scheduled as follows. The basic notions are mentioned in section II, section III outlines and summarized control design.

This work was supported by the European Regional Development Fund under the project CEBIA-Tech No. CZ.11.05./2.1.00/03.0089.

R. Prokop is with Faculty of applied informatics, Tomas Bata University in Zlín, Nad Stráněmi 4511, Zlín, Czech Republic (phone: 420-57603-5257; e-mail: prokop@fai.utb.cz).

J. Korbek is with Faculty of applied informatics, Tomas Bata University in Zlín, Nad Stráněmi 4511, Zlín, Czech Republic (e-mail: korbek@fai.utb.cz).

Some first order examples and analysis is presented in section IV. The proposed methodology brings one or several scalar which can tune and influence the control behavior in an easy way.

II. MATRICES AND SYSTEM DESCRIPTION

Polynomial matrices are called $l \times m$ matrices where all elements of matrices are polynomials in an indeterminate s . This indeterminate can be considered in linear systems as the Laplace operator and the set of polynomial matrices is $R_{lm}(s)$. If $l = m$, then the set of polynomial matrices constitutes a non-commutative ring. A unit in this ring (an inverse element exists in the ring) is a matrix with real nonzero determinant and all units are called unimodular. Generally, $l \neq m$ set $R_{lm}(s)$ is not more a ring. If $A = BC$ then B is a left divisor of A and A is a right multiple of B , while C is a right divisor of A and A is a left multiple of C . Similarly, greatest common left and right divisors are introduced. Two matrices A, B are left (right) equivalent, if $A = U_1 B$ ($A = B U_2$) with unimodular U_1, U_2 . When $A = U_1 B U_2$ then A, B are simply called equivalent. Matrices with the same number of columns are left coprime if their all left divisors are unimodular matrices and matrices with the same number of rows are right coprime if their all right divisors are unimodular ones.

The known extended (scalar) Euclidean algorithm for can be generalized in multivariable cases. A left greatest common divisor $G_l(s)$ can be calculated for A, B with the same number of rows by

$$\begin{aligned} A(s)P_1(s) + B(s)Q_1(s) &= G_l(s), \\ A(s)R_1(s) + B(s)S_1(s) &= 0, \end{aligned} \quad (1)$$

Moreover, $L = AR_l = -BS_l$ is the least common right multiple of A, B . A right greatest common divisor $G_r(s)$ can be calculated for A, B with the same number of columns by

$$\begin{aligned} P_2(s)A(s) + Q_2(s)B(s) &= G_r(s), \\ R_2(s)A(s) + S_2(s)B(s) &= 0, \end{aligned} \quad (2)$$

Also, $L = R_2A = -S_2B$ is the left common multiple of A, B . Relations (1), (2) are the basic algebraic notions for Diophantine equations, see e.g. [1], [3], [10].

A linear continuous-time multivariable (MIMO) system is described by a set of linear differential equations and then it can be easily expressed by the Laplace transform technique in the form

$$A(s)Y(s) = B(s)U(s), \tag{3}$$

where $A(s), B(s)$ are polynomial matrices. The matrix function can be then expressed by the left or right matrix fraction

$$G(s) = A(s)^{-1}B(s) = B_R(s)A_R(s)^{-1} \tag{4}$$

Note, that both matrices $A(s), B(s)$ are squared but not necessarily of the same dimension. In the case of systems with l inputs and m outputs, the left denominator A has dimension $l \times l$, while the right denominator $A_R(s)$ has the dimension $m \times m$. However, both matrices are associates and the characteristic polynomial following from the state-space description is also associates. It means that all roots of the mentioned polynomials are same. It means

$$\det A(s) \sim \det A_R(s) \sim \det(sI - F) \tag{5}$$

where F is the squared system matrix. With relation (3) the notion of stability is closely connected. A linear system is asymptotic (internal stable), if all determinants in (3) are stable, for continuous-time systems it means that all roots lie in the open left half of the complex plane.

III. CONTROL DESIGN

A basic feedback control system is depicted in Fig. 1.

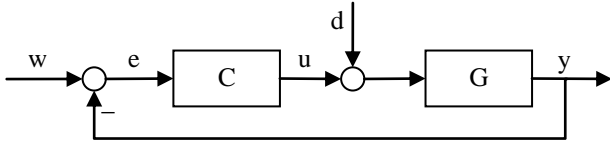


Fig. 1 one degree of freedom (1DOF) control system

Input signals of the feedback system in Fig. 1 is a reference (set point) signal $w = F_w^{-1}(s) G_w(s)$ and a load disturbance signal $d = F_d^{-1}(s) G_d(s)$ defined by their matrix left matrix fractions. All stabilizing controllers for the 1DOF feedback system in Fig. 1 are given by any solution of matrix Diophantine equation

$$A(s)P_R(s) + B(s)Q_R(s) = M(s), \tag{6}$$

where $P^{-1}(s)Q(s) = Q_R(s)P_R^{-1}(s)$ is a left and right matrix fraction of the controller C and $A^{-1}(s)B(s) = B_R(s)A_R^{-1}(s)$ is a left and right matrix fraction of the controlled plant. More details can be found e.g. in [1], [5], [8], [10], [11].

However, for asymptotic tracking and disturbance rejection must be fulfilled further conditions. Briefly speaking, denominator of the controller must be divisible by the denominators of input signals. It is a reason for a pre-compensator F in Fig. 2 which represents the conditions of divisibility. In the case of asymptotic tracking only, it is $F=F_w$. In the case of simultaneous asymptotic tracking and disturbance rejection and attenuation $F=F_wF_vF_n$. The basic

stability and asymptotic tracking in the sense of Fig. 2 is then the controller $Q_R(s)P_R^{-1}(s)$ given by the solution of matrix Diophantine equation

$$A(s)F(s)P_R(s) + B(s)Q_R(s) = M(s), \tag{7}$$

where $M(s)$ is a stable polynomial matrix with prescribed poles of its determinant. Resulting matrices P_R, Q_R represent the right matrix fraction

$$P(s)^{-1}Q(s) = Q_R(s)P_R(s)^{-1} \tag{8}$$

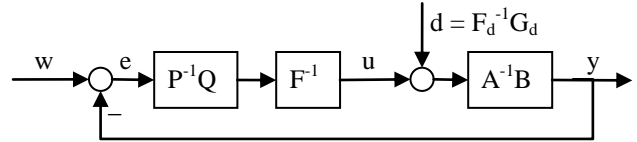


Fig. 2 feedback 1DOF control system with pre-compensator

The control law is then governed by the equation

$$P(s)^{-1}F(s)U(s) = Q(s)(W(s) - Y(s)), \tag{9}$$

which can be easily rewritten into differential equations. Now, it is necessary to propose the method for solution of matrix equation (2). For simpler cases, the solution can be found by means of elementary column operation, according to the scheme

$$\left(\begin{array}{c|c} AF & B \\ \hline I & 0 \\ \hline 0 & I \end{array} \right) \xrightarrow{\substack{\text{elementary column} \\ \text{operations}}} \left(\begin{array}{c|c} M & 0 \\ \hline P_R & Z_1 \\ \hline Q_R & Z_2 \end{array} \right) \tag{10}$$

Elementary column operations (10) may always be lead in the way that the polynomial matrix $P_R(s)$ remains as unit matrix and the conversion (8) is trivial and also a unit one. Then no inversion in (9) is necessary and the realization of the control law is very simple. In more complex cases, the standard techniques based on Euclidean algorithms can be used, see [2], [7], [10]. Polynomial toolbox [12] also provides a user friendly Matlab program for the solution of matrix polynomial equations.

IV. ILLUSTRATIVE EXAMPLES

Illustrative examples 1 - 3 in this contribution are first order stable, unstable and integrating ones two input – two output (TITO) systems are represented by the matrix equation

$$\begin{pmatrix} s+a_1 & a_2 \\ a_3 & s+a_4 \end{pmatrix} \begin{pmatrix} Y_1(s) \\ Y_2(s) \end{pmatrix} = \begin{pmatrix} b_1 & b_2 \\ b_3 & b_4 \end{pmatrix} \begin{pmatrix} U_1(s) \\ U_2(s) \end{pmatrix} \tag{11}$$

The stabilization matrix Diophantine equation (7) takes the form

$$\begin{pmatrix} s+a_1 & a_2 \\ a_3 & s+a_4 \end{pmatrix} \begin{pmatrix} s & 0 \\ 0 & s \end{pmatrix} \begin{pmatrix} p_1 & p_2 \\ p_3 & p_4 \end{pmatrix} + \begin{pmatrix} b_1 & b_2 \\ b_3 & b_4 \end{pmatrix} \quad (12)$$

$$\begin{pmatrix} q_1s+q_0 & q_5s+q_4 \\ q_3s+q_2 & q_7s+q_6 \end{pmatrix} = \begin{pmatrix} (s+m_0)^2 & 0 \\ 0 & (s+m_0)^2 \end{pmatrix}$$

Example 1: Let a TITO linear continuous-time system be expressed by the Laplace transform technique in the form

$$\begin{aligned} y_1'(t) + 2y_1(t) + 0.8y_2(t) &= 5u_1(t) + 6u_2(t) \\ y_2'(t) + 1.5y_2(t) + 0.6y_1(t) &= 2u_1(t) + 3u_2(t) \end{aligned} \quad (13)$$

The Laplace transform of equations (6) gives matrices A, B

$$A(s) = \begin{pmatrix} s+2 & 0.8 \\ 0.6 & s+0.6 \end{pmatrix}, \quad B(s) = \begin{pmatrix} 5 & 6 \\ 2 & 3 \end{pmatrix} \quad (14)$$

The system described in (14) is evidently stable because $\det A = s^2 + 2.6s + 0.72$ is a stable polynomial. Then the scheme (10) can be applied and the result is in the form of generalized PI controller:

$$\begin{aligned} u_1 &= q_1e_1 + q_0 \int e_1(\tau) d\tau + q_5e_2 + q_4 \int e_2(\tau) d\tau \\ u_2 &= q_3e_1 + q_2 \int e_1(\tau) d\tau + q_7e_2 + q_6 \int e_2(\tau) d\tau \end{aligned} \quad (15)$$

where controller parameters were obtained by elementary column operations according scheme (5) in the form:

$$\begin{aligned} q_1 &= 2m_0 - 0.8 & q_5 &= -4m_0 + 2.2 \\ q_0 &= m_0^2 & q_4 &= -2m_0^2 \\ q_3 &= -\frac{4}{3}m_0 + \frac{1}{3} & q_7 &= \frac{10}{3}m_0 - \frac{5.9}{3} \\ q_2 &= -\frac{2}{3}m_0^2 & q_6 &= \frac{5}{3}m_0^2 \end{aligned} \quad (16)$$

In (9) e_i are naturally tracking errors and $m_0 > 0$ is a tuning parameter influencing control behavior.

Example 2: Let an unstable TITO linear continuous-time system can be expressed by differential equations

$$\begin{aligned} y_1'(t) + y_1(t) + y_2(t) &= u_1(t) + 0.5u_2(t) \\ y_2'(t) + 0.5y_2(t) + 2y_1(t) &= 0.8u_1(t) + 2u_2(t) \end{aligned} \quad (17)$$

and the matrix expression has the form

$$\begin{pmatrix} s+1 & 1 \\ 2 & s+0.5 \end{pmatrix} \begin{pmatrix} Y_1(s) \\ Y_2(s) \end{pmatrix} = \begin{pmatrix} 1 & 0.5 \\ 0.8 & 2 \end{pmatrix} \begin{pmatrix} U_1(s) \\ U_2(s) \end{pmatrix} \quad (18)$$

Matrix equation (10) gives the controller matrices P_R, Q_R

$$P_R = \begin{pmatrix} 1 & 0 \\ 0 & 1 \end{pmatrix} \text{ and } Q_R = \begin{pmatrix} q_1s+q_0 & q_5s+q_4 \\ q_3s+q_2 & q_7s+q_6 \end{pmatrix} \quad (19)$$

where parameters are

$$\begin{aligned} q_1 &= 2.5m_0 - 0.65 & q_5 &= -0.6m_0 - 1.1 \\ q_0 &= 1.25m_0^2 & q_4 &= -0.3m_0^2 \\ q_3 &= -m_0 - 0.75 & q_7 &= 1.25m_0 + 0.19 \\ q_2 &= -0.5m_0^2 & q_6 &= 0.625m_0^2 \end{aligned} \quad (20)$$

The form of the control law (15) is again a generalized PI controller.

Example 3: Let an integrating (also unstable) TITO linear continuous-time system can be expressed by differential equations

$$\begin{aligned} y_1'(t) + y_2(t) &= u_1(t) + 0.5u_2(t) \\ y_2'(t) + 0.5y_1(t) &= 0.6u_1(t) + 1.5u_2(t) \end{aligned} \quad (21)$$

Determinant of $A(s) = s^2 - 0.5$ is evidently an unstable one. The controller is derived in a similar way but at the right hand side of (12) is the stable matrix $M(s)$ in the form

$$M(s) = \begin{pmatrix} (s+m_1)^2 & 0 \\ 0 & (s+m_2)^2 \end{pmatrix}, \quad m_1, m_2 > 0 \quad (22)$$

The reason of different m_i is the possibility of different dynamics in both controlled outputs. The control law is again in the form of (15) with the following set of parameters q_i :

$$\begin{aligned} q_1 &= 2.5m_1 + 0.21 & q_5 &= -0.83m_2 - 1.25 \\ q_0 &= 1.25m_1^2 & q_4 &= -0.42m_2^2 \\ q_3 &= -m_1 - 0.42 & q_7 &= 0.5 + 1.67m_2 \\ q_2 &= -0.5m_1^2 & q_6 &= 0.83m_2^2 \end{aligned} \quad (23)$$

Example 4: A controlled system is a two input – single output (TISO) system described by the differential equation

$$y_1'(t) - 0.5y_1(t) = 0.5u_1(t) + 1.2u_2(t) \quad (24)$$

System (24) is evidently an unstable one. The initial and final state of the scheme of stabilizing equation (7) is

$$\left(\begin{array}{c|cc} s^2 - 0.5s & 0.5 & 1.2 \\ \hline 1 & 0 & 0 \\ 0 & 1 & 0 \\ 0 & 0 & 1 \end{array} \right) \sim \left(\begin{array}{c|cc} s^2 + 2m_0 + m_0^2 & 0.5 & 1.2 \\ \hline 1 & 0 & 0 \\ (4m_0 + 1)s & 1 & 0 \\ 0.833m_0^2 & 0 & 1 \end{array} \right)$$

and the control law takes the form of two equations which can be also considered as a generalized PI controller

$$\begin{aligned} u_1(t) &= (4m_0 + 1)e_1(t) \\ u_2(t) &= 0.833m_0^2 \int e_1(\tau) d\tau \end{aligned} \quad (25)$$

An important remark is that there exist an infinite number of feasible stabilizing controllers. It depends how to choose elementary column operations in reduction (10). Control law (25) represents proportional controller in $u_1(t)$ and an integrating one in $u_2(t)$ loop. Also [12] gives a different solution.

V. SIMULATION RESULTS

Matlab and Simulink offer a suitable environment for modeling and simulation of dynamic systems. The Simulink scheme for two input – two output unstable system (7) with controller (10) is depicted in Fig. 3.

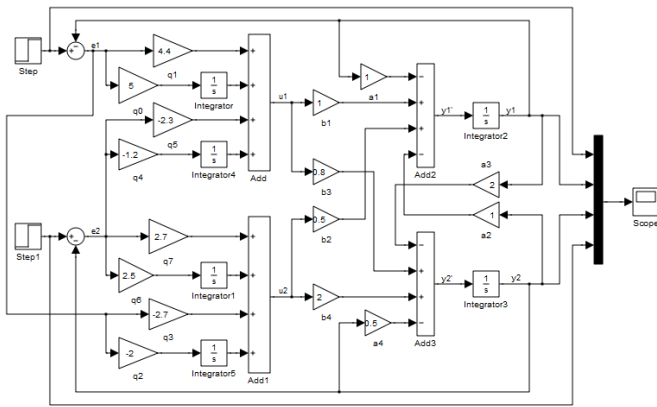


Fig. 3 simulink scheme of feedback unstable system

Control responses of stable TITO system (Example 1) for tuning parameter $m_0=1.5$ and $m_0=3$ are shown in Fig. 4. The control responses of the unstable TITO system (example 2) for tuning parameter $m_0=1.5$ and $m_0=3$ are shown in Fig. 5.

Examples 1 and 2 illustrate that tuning parameter $m_0 > 0$ influences the dynamical behavior of the controlled variable in the stable as well as in the unstable case. The parameter $m_0 > 0$ represents a multiple pole of the feedback characteristic polynomial.

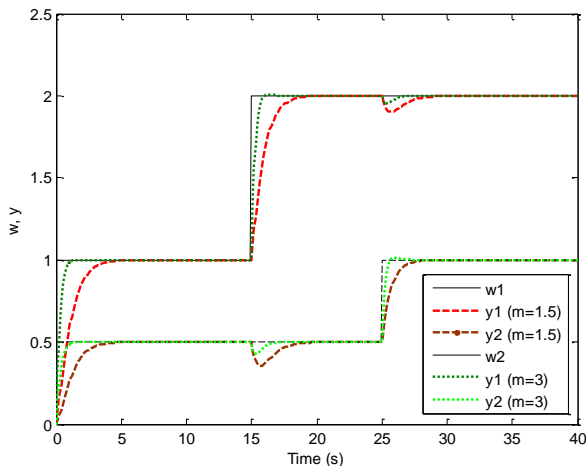


Fig. 4 control responses for $m_0=1.5$ and $m_0=3$ (Example 1)

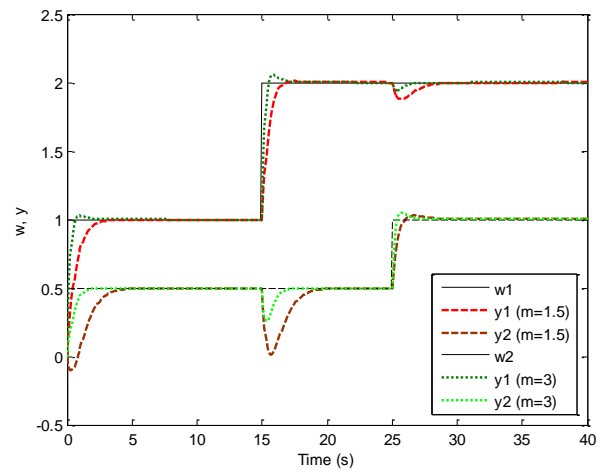


Fig. 5 control responses for $m_0=1.5$ and $m_0=3$ (Example 2)

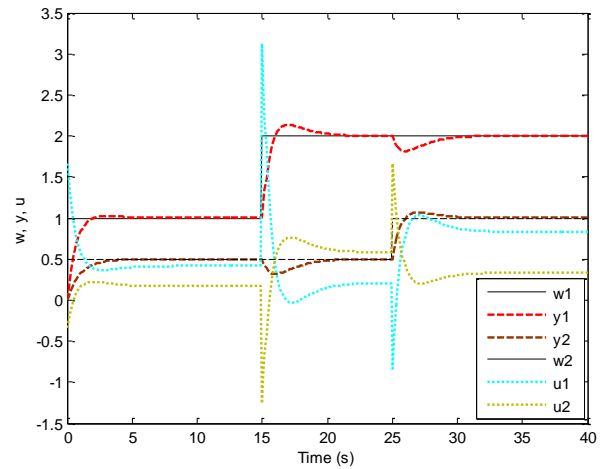


Fig. 6 control responses (Example 3) of integrating system for tuning parameters $m_1 = 1, m_2 = 1$.

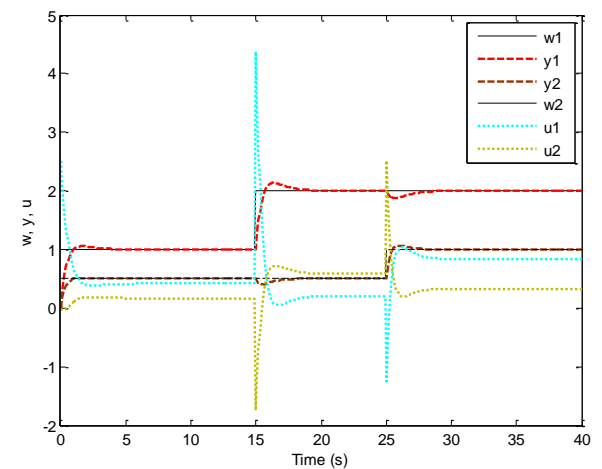


Fig. 7 control responses (Example 3) of integrating system for tuning parameters $m_1 = 1, m_2 = 1$.

In some cases, it can be useful every controlled variable influence in different dynamics. It is easily obtained by a different choice of poles in feedback loops. The situation is

shown in Fig. 6 and Fig. 7 for TITO integrating system. While the response in Fig. 6 is for $m_1 = m_2 = 1$, the responses in Fig. 7 are for the choice $m_1 = 1.5$, $m_2 = 2$. Fig. 8 and Fig. 9 illustrate control responses of the two input – single output system solved in Example 4. Tuning parameter $m_0 > 0$ again influences the control behavior and dynamics.

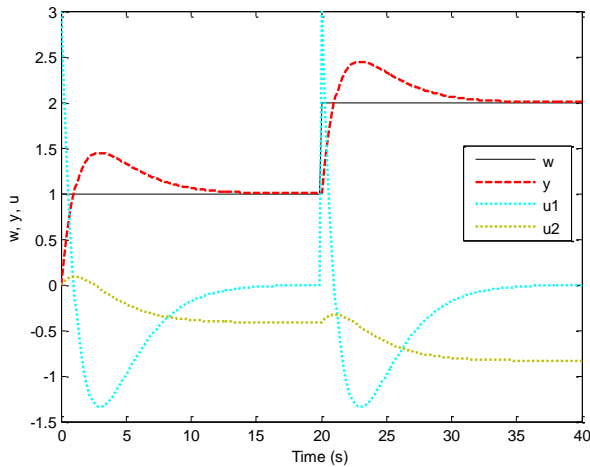


Fig. 8 control responses (Example 4) of TISO system for tuning parameters $m_0=0.5$.

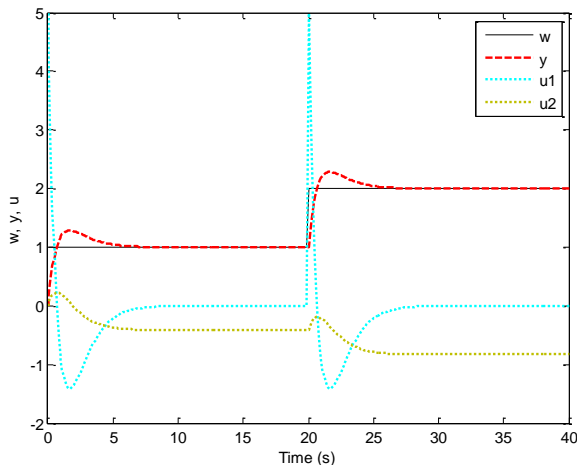


Fig. 9 control responses (Example 4) of TISO system for tuning parameters $m_0=1$.

VI. CONCLUSION

The paper deals with multivariable control of simple continuous-time linear systems. The controller design is performed through a solution of the matrix Diophantine equation. This approach enables to define one or a couple scalar tuning parameters for influencing of control behavior. The tuning parameters represent poles of the characteristic feedback equation. In the first order cases, the solution and a final controller can be obtained in simple and explicit form performing by elementary column operation of the given matrices. All simulations and results are clearly demonstrated in the Matlab-Simulink environment.

REFERENCES

- [1] Kučera, V. *Discrete Linear Control. The Polynomial Equation Approach*. Prague: Academia, 1979.
- [2] Kučera, V. *Analysis and Design of Discrete Linear Control systems*. Prague: Academia, 1991.
- [3] Kučera, V. "Diophantine equations in control - A survey," *Automatica*, Vol. 29, (1993), pp. 1361-75.
- [4] Kaczorek, T. (1985). *Two-dimensional Linear Systems*. Springer-Verlag, Berlin.
- [5] M.J.Grimble and V. Kučera, *Polynomial Methods for Control Systems Design*. London:Springer, 1996.
- [6] A. O'Dwyer, *Handbook of PI and PID controller tuning rules*. London: Imperial College Press, 2003.
- [7] Prokop, R. and J.P. Corriou (1997). "Design and analysis of simple robust controllers," *Int. J. Control*, Vol. 66, pp. 905-921.
- [8] Rosenwasser, E.N. and B.P. Lampe (2006). *Multivariable Computer-controlled Systems*. Springer-verlag, Berlin.
- [9] K.J. Åström and R.M. Murray, *Feedback Systems*. Research Triangle Park, NC: Instrumental Society of America, 1995.
- [10] Vidyasagar, M. (1987). *Control system synthesis: a factorization approach*. MIT Press, Cambridge, M.A.
- [11] Volkova, N. and R. Prokop, R. "Matrix equation approach for MIMO control design," in *Proc. DAAAM Conf., 2011*, p.225-226.
- [12] PolyX, Ltd. *Polynomial Toolbox*. 1998

ROMAN PROKOP was born in Hodonin, Czech Republic in 1952. He graduated in Cybernetics from the Czech Technical University in Prague in 1976. He received post graduate diploma in 1983 from the Slovak Technical University. Since 1995 he has been at Tomas Bata University in Zlín, where he presently holds the position of full professor of the Department of Automation and Control Engineering and a vice-rector of the university. His research activities include algebraic methods in control theory, robust and adaptive control, autotuning and optimization techniques.

JIŘÍ KORBEL was born in Zlín, Czech Republic. He studied automatic control and informatics at the Tomas Bata University and graduated in 2004, now he is assistant at the Faculty of Applied Informatics in Zlín. His research activities include autotuning principles, algebraic and polynomial syntheses and modeling and simulations.

Comparison of Acoustic Barriers Noise Reductions Evaluated by Different Calculation Methods

Claudio Guarnaccia, Joseph Quartieri, Nikos E. Mastorakis

Abstract— The problem of acoustical noise produced by transportation infrastructures is a serious issue to be considered in urban planning and in mitigation actions design. In particular, road traffic is one of the most important source, basically all around the world, in particular in developed countries. Since it is related to several parameters, such as number and typology of vehicles, speed, road conditions, geometry and orography of the site, distance between source and receiver, etc., road traffic noise is very difficult to be properly modelled and predicted at any distance. Even if a serious modelling may be helpful in the design phase, if the road network is already present, the choice and the effectiveness evaluation of several mitigation actions has to be carefully investigated. In this paper, the reduction to noise level produced by the introduction of noise barriers is studied, by means of literature, regulation and software approaches. These three methods will be tested on a case study, where a motorway crosses a residential area, with a new building sets. Results will show that all the methods confirm the better performances of a higher barrier, but it will be shown that diffraction and other parameters have to be carefully taken into account to avoid incorrect evaluation.

Keywords— Acoustics, Noise Control, Barrier, Calculation Methods.

I. INTRODUCTION

PHYSICAL polluting agents, such as air pollution, acoustic noise, electromagnetic field, are a relevant problem for human activities and their assessment is largely studied in literature (see for instance [1], in which the authors proposed a complex index to include several pollutants). Among them, acoustical noise is largely recognized as one of the most important environmental problem in urban areas and has to be carefully assessed, monitored and, when possible, mitigated. The main noise sources that have to be considered in residential areas are related to transportation infrastructures, since it is reasonable to affirm that industrial areas are distant from buildings agglomeration. The same can be assumed for airport and high speed railways, that usually are settled in peripheral zones. These considerations, together with the fact that car is one of the most used transportation mean all around

the world, lead to affirm that road traffic noise is one of the most frequent noise problem for residential areas. Several models have been developed to assess the road traffic noise (see for instance [2] and [3]) and several approaches, both statistical and dynamical, have been largely discussed by the authors in [4-10].

The effects of a regular exposure to noise, in general, and to road traffic noise in particular, are deeply studied in literature. In [11], for instance, both the auditory and non auditory effects of noise are described, motivating the need for mitigation actions in particular exposition cases.

In case of road traffic noise, one of the possible intervention is the installation of acoustical barriers along the roads, in order to reduce the sound levels at the receivers, typically residential buildings, hospitals, schools, etc.. The evaluation of the efficacy of a barrier may be calculated in terms of difference between noise levels in absence of the barriers and noise levels after their installation.

In this paper, a case study of a buildings set beside a motorway is reported, in terms of geometrical and acoustical description. The hypothesis of barriers installation is evaluated, in particular calculating the noise reduction of different possible solutions, in terms of different height of the barriers and different distances from the centre of the roadway. The calculation methods compared are taken from research literature (Maekawa's formula [12]), from international regulation (ISO9613 [13]) and from a commercial software framework. The noise reduction is evaluated per each of the three floors of the buildings, in order to highlight eventual differences of barrier performance.

II. METHODS

The three methods proposed to evaluate the noise barrier reduction are:

- Maekawa formula
- ISO9613 calculation
- CadnaA software simulation

The attenuation, in general, is given by the difference between the acoustic level in absence (L_{dir}) and in presence of the barrier (L_{screen}):

$$\Delta L = L_{dir} - L_{screen} \quad (1)$$

C Guarnaccia, J. Quartieri, are with the Department of Industrial Engineering, University of Salerno, Via Giovanni Paolo II, I-84084 Fisciano (SA) – ITALY (corresponding: cguarnaccia@unisa.it, quartieri@unisa.it).

N. E. Mastorakis is with Technical University of Sofia, English Language Faculty of Engineering, Industrial Engineering, Sofia 1000, Sofia – BULGARIA (mastor@tu-sofia.bg)

A. Maekawa's formula

Maekawa's formula is based on the principle of the difference of path covered by the sound wave. In this scheme, the wave is approximated to a ray and the sound path (shown in Fig. 1) is the connection between source and receiver, in presence and in absence of the barrier.

The attenuation is obtained by the following formulas:

$$\Delta L = 10 \text{ Log}(3 + 20N) \quad (2)$$

$$\Delta L = 10 \text{ Log}(2 + 5.5N) \quad (3)$$

where N is the number of Fresnel. This parameter is defined as follows:

$$N = \frac{2\delta}{\lambda} = \frac{2\delta f}{c} \quad (4)$$

where δ indicates the path difference, i.e. the difference between the path of sound wave in presence and in absence of the barrier, λ is the wave length, f is the frequency and c is the wave speed.

Let us underline that formula (2) is valid in case of pointlike sources, while formula (3) is valid for linear sources. In this study, since road traffic noise, in regular condition of vehicles flow, can be considered a linear source, the authors adopted formula (3).

B. ISO9613 formula

The international regulation ISO9613 [13] defines a formula for the propagation of equivalent sound level, in case of down wind conditions:

$$L_{DownWind} = L_W + D_C - A \quad (5)$$

where L_W is the source power, D_C is the coefficient of directivity and A is the attenuation coefficient. The latter term is the most important for our purpose. The regulation defines the attenuation as a sum of several components, related to geometrical divergence, atmospheric effects, ground absorption, presence of obstacles and other various effects. In this paper, the attention is focused on the attenuation due to the presence of obstacles (barriers), that in [13] is defined as:

$$A_{bar} = D_z - A_{gr} \quad (6)$$

Where A_{gr} is the ground absorption. D_z is defined as follows:

$$D_z = 10 \text{ Log}[3 + (c_2/\lambda)c_3 z K_{met}] \quad (7)$$

with:

- c_2 is a constant that considers the terrain effects;
- λ is again the wave length of the octave under study;
- c_3 is equal to 1 in case of simple diffraction, i.e. in

our case. This means that the width of the barrier is negligible;

- z is the difference between the sound ray direct path and the diffracted path, and is calculated according to [13]:

$$z = [(d_{ss} + d_{rr})^2 + a^2]^{0.5} - d \quad (8)$$

where:

- d_{ss} is the distance between the source and the first edge of diffraction;
- d_{rr} is the distance between the second edge of diffraction and the receiver;
- a is the distance component parallel to the edge of the barrier, between source and receiver.
- K_{met} is the meteorological correction, that is equal to 1 if $z \leq 0$, otherwise is given by:

$$K_{met} = \exp\left[-(1/2000)\sqrt{d_{ss}d_{rr}d/(2z)}\right] \quad (9)$$

C. CadnaA calculation

CadnaA (Computer Aided Noise Abatement) is an environmental noise predictive software. It can be used for calculation, presentation, assessment and prediction of noise in any area designed in its framework. The general approach is the inverse ray tracing technique. This means that the area under study can be divided in horizontal and/or vertical grids (or grids enveloping all facades of buildings), crossing and merging the contributes of each source operating in the environment. The calculation for some special sources, such as roads, railways and airports, is done considering the technical parameter values, according to the international standards related to each typology of source.

The geometry of all objects present in the area, such as roads and buildings, is taken into account, together with the orography of the terrain.

Further applications of the software, in various conditions and for different sources, may be found in [14-21].

III. CASE STUDY

The case study in which the methods described in section 2 have been applied is represented by a set of buildings built beside a motor way in South Italy and it is shown in Fig. 1. The motorway is composed of 4 lanes, two in Avellino direction and two in Salerno direction. Other secondary roads are present, even if, for screening purposes, only the motorway will be considered.

The buildings have approximately the same height and the same number of floors. The distance from the road is different according to which building is considered. The position of the agglomeration suggests a strong impact of the motor way on the acoustic point of view. Let us underline that the aim of this paper is not to assess the noise impact on the buildings, but to compare the noise reduction that can be obtained installing acoustical barriers, with different calculation methods.



Fig. 1: Case study area, taken from Google Maps ©. The buildings under study are numbered from 1 to 6. The motorway is on the left, highlighted in red.

IV. RESULTS AND DISCUSSION

The analysis reported in this section is based on the comparison between noise reduction from barrier insertion, calculated with the three methods presented above, in different conditions of barrier position (d_s , measured with respect to the centre of the roadway) and height (h_b). Results are reported per each floor of the building (z , height of the receiver, 3, 6 or 9 m)

In tables 1, 2 and 3, the different calculations of the attenuation that can be achieved with an hypothetic barrier placed at $d_s = 4.75$ m from the centre of the roadway and with different height (respectively $h_b = 4, 5$ or 6 m), are reported, for all the buildings of the cluster, for each floor (height of the receiver, $z = 3, 6$ and 9 m).

It is easy to notice that Maekawa’s formula furnishes always the highest results, probably because it does not include ground, air and other absorption effects.

In addition, as expected, the growth of barrier height leads to an increase of barrier attenuation. It is interesting to present the maximum and minimum values of this increase, for each calculation method, when raising the height of the barrier from 4 to 5 m (Table 4) and from 5 to 6 m (Table 5). It can be affirmed that increasing the height of the barrier from 4 to 5 m, leads to a minimum increase of the attenuation of about 1-2 dBA (confirmed by all the methods). The same when raising the barrier from 5 to 6 m, obtaining a minimum attenuation of about 1-1.5 dBA.

Tab. 1: Comparison of barrier noise reductions with height $h_b=4m$ and distance from the source $d_s=4,75m$.

$h_b = 4m$	$d_s = 4,75 m$	Noise reduction values [dBA]		
		Height [m]	CadnaA	ISO9613
Building 1	$z=3$	14,6	15,9	18,3
	$z=6$	13,1	14,6	16,7
	$z=9$	10,2	12,9	14,9
Building 2	$z=3$	14,6	16,0	18,3
	$z=6$	13	14,5	16,7
	$z=9$	10	12,8	14,8
Building 3	$z=3$	14,5	16,0	18,3
	$z=6$	12,7	14,5	16,6
	$z=9$	9,8	12,7	14,5
Building 4	$z=3$	13,1	15,3	18,4
	$z=6$	13	14,5	17,5
	$z=9$	11,6	13,6	16,5
Building 5	$z=3$	14,6	15,7	18,3
	$z=6$	14	14,6	17,1
	$z=9$	10,8	13,3	15,6
Building 6	$z=3$	15,3	15,5	18,4
	$z=6$	15	14,6	17,3
	$z=9$	11,9	13,5	16,1

Tab. 2: Comparison of barrier noise reductions with height $h_b=5m$ and distance from the source $d_s=4,75m$.

$h_b = 5m$	$d_s = 4,75 m$	Noise reduction values [dBA]		
		Height [m]	CadnaA	ISO9613
Building 1	$z=3$	16,7	18,0	20,4
	$z=6$	15,9	16,8	19,1
	$z=9$	13,7	15,5	17,7
Building 2	$z=3$	16,7	18,0	20,4
	$z=6$	15,8	16,8	19,1
	$z=9$	13,5	15,4	17,6
Building 3	$z=3$	16,5	18,1	20,4
	$z=6$	15,5	16,8	19,0
	$z=9$	13,1	15,3	17,4
Building 4	$z=3$	14,2	17,2	20,4
	$z=6$	14,4	16,6	19,7
	$z=9$	13,8	15,8	18,9
Building 5	$z=3$	16,0	17,7	20,4
	$z=6$	15,7	16,8	19,4
	$z=9$	13,3	15,7	18,2
Building 6	$z=3$	16,8	17,5	20,4
	$z=6$	16,9	16,7	19,5
	$z=9$	14,6	15,8	18,6

Tab. 3: Comparison of barrier noise reductions with height $h_b=6m$ and distance from the source $d_s=4,75m$.

$h_b = 6m$	$d_s = 4,75 m$	Noise reduction values [dBA]		
		Height [m]	CadnaA	ISO9613
Building 1	$z=3$	18,2	19,5	22,0
	$z=6$	17,8	18,6	21,0
	$z=9$	16,3	17,5	19,8
Building 2	$z=3$	18,2	19,6	22,0
	$z=6$	17,7	18,6	20,9
	$z=9$	16,2	17,4	19,7
Building 3	$z=3$	18,5	19,7	22,1
	$z=6$	18,1	18,6	20,9
	$z=9$	16,7	17,4	19,6
Building 4	$z=3$	15,4	18,7	22,0
	$z=6$	15,3	18,2	21,3
	$z=9$	15,3	17,6	20,7
Building 5	$z=3$	17,1	19,3	22,0
	$z=6$	16,9	18,5	21,1
	$z=9$	15,1	17,6	20,2
Building 6	$z=3$	18,1	19,0	22,0
	$z=6$	18,3	18,4	21,3
	$z=9$	16,8	17,6	20,4

Tab. 6: Comparison of barrier noise reductions with height $h_b=4m$ and distance from the source $d_s=5,75m$.

$h_b = 4m$	$d_s = 5,75 m$	Noise reduction values [dBA]		
		Height [m]	CadnaA	ISO9613
Building 1	$z=3$	12,1	15,4	17,7
	$z=6$	12,2	13,8	15,9
	$z=9$	11,6	11,8	13,7
Building 2	$z=3$	13,8	15,4	17,7
	$z=6$	13,5	13,8	15,8
	$z=9$	12,6	11,7	13,6
Building 3	$z=3$	17,1	15,5	17,7
	$z=6$	16,3	13,7	15,7
	$z=9$	14,4	11,5	13,3
Building 4	$z=3$	14,7	14,7	17,9
	$z=6$	15,0	13,9	16,8
	$z=9$	14,8	12,8	15,7
Building 5	$z=3$	17,7	15,2	17,8
	$z=6$	17,9	13,9	16,3
	$z=9$	15,5	12,3	14,6
Building 6	$z=3$	17,6	15,0	17,8
	$z=6$	17,7	13,9	16,6
	$z=9$	15,6	12,7	15,2

Tab. 4: Maximum and minimum barrier noise reduction values when increasing barrier height h_b from 4m to 5m.

From $h_b = 4m$ to 5m	Noise reduction values [dBA]		
	CadnaA	ISO9613	Maekawa
MAX	3.5	3.0	3.0
MIN	1.1	2.0	2.1

Tab. 5: Maximum and minimum barrier noise reduction values when increasing barrier height h_b from 5m to 6m.

From $h_b = 4m$ to 5m	Noise reduction values [dBA]		
	CadnaA	ISO9613	Maekawa
MAX	3.6	2.0	2.1
MIN	0.9	1.6	1.6

Tab. 7: Comparison of barrier noise reductions with height $h_b=4m$ and distance from the source $d_s=6,75m$.

$h_b = 4m$	$d_s = 6,75 m$	Noise reduction values [dBA]		
		Height [m]	CadnaA	ISO9613
Building 1	$z=3$	12	14,9	17,2
	$z=6$	12,1	13,0	15,1
	$z=9$	11,3	10,8	12,6
Building 2	$z=3$	13,9	14,9	17,2
	$z=6$	13,4	13,0	15,1
	$z=9$	12,2	10,7	12,5
Building 3	$z=3$	17	15,0	17,2
	$z=6$	16,1	12,9	14,9
	$z=9$	13,8	10,4	12,1
Building 4	$z=3$	14,6	14,2	17,4
	$z=6$	14,8	13,3	16,2
	$z=9$	14,4	12,1	14,9
Building 5	$z=3$	18,7	14,7	17,3
	$z=6$	17,7	13,2	15,6
	$z=9$	16,6	11,4	13,7
Building 6	$z=3$	16,2	14,5	17,3
	$z=6$	15,9	13,3	16,0
	$z=9$	13,5	11,8	14,4

Tables 6 and 7 report the calculations of the attenuation that can be achieved with an hypothetical barrier of fixed height ($h = 4 m$) and different distance from the centre of the roadway (respectively $d = 5.75$ and $6.75 m$) for all the buildings of the cluster, for each floor (3, 6 and 9 m). These two tables have to be compared to table 1, in which a barrier with $h = 4 m$ and $d = 4.75 m$ is considered.

The comparison has been performed plotting values of noise reductions versus height of the barrier, for the first three buildings, per each calculation methods. Results are shown in Fig. 2. Let us underline that the lines are not a fit of the data, but just a guide to the eye. Again it is evident that Maekawa's formula furnishes the highest results. In addition, comparing results at the same floor (solid, dashed or dotted lines), they have a very similar slope, while it is exploited that higher floors have a lower reduction, because of lower difference between direct and diffracted sound rays.

Fig. 2 shows that buildings 1, 2 and 3, that are approximately at the same distance from the motorway (see Fig. 1), have a practically equal behaviour of the noise reduction, when varying the height of the barrier and when considering different floors. In addition, Maekawa and ISO9613 calculations are always overestimating the noise reduction, while CadnaA, that considers much more parameters, seems to furnish a more realistic prediction.

Fig. 3 reports the noise reductions calculated by means of CadnaA method, for all the buildings, as a function of the height of the barrier, at the different floor. Buildings 4, 5 and 6 show a different behaviour, probably because of their special position in the buildings lot (see Fig. 1). In particular, building 4 has a lower attenuation, due to the fact that it is covered by other buildings, thus, also in absence of barrier, the level is lower than the other buildings, reducing the barrier effectiveness. This effect is mitigated at the highest floor (z=9m, bottom plot), where the reduction due to the covering of other buildings is lower.

V. CONCLUSION

In this paper, the noise reduction due to the insertion of an acoustical barrier is studied in terms of different calculation methods. A set of buildings built along a motorway in South Italy has been considered as a case study.

Results of attenuation obtained from literature formula (Maekawa), international regulation (ISO9613) and predictive software (CadnaA) have been compared, varying the height and the distance (from the centre of the roadway) of the hypothetical barrier. The differences between the three methods are present but not drastic, as shown in Table 4 and 5. Maekawa's formula usually gave the highest value of barrier attenuation, due to the fact that does not include ground, air and other absorption effects.

In particular, the height of the barrier has been varied from 4 to 6 m, obtaining, as expected, an increase of the attenuation in each floor. This is due to the increase of path to be covered by the sound ray. The distance from the centre of the carriage has been varied from 4.75 to 6.75 m, and the results showed that the closest the barrier is to the motorway, the highest the attenuation is

Further applications of this study could be related to field measurement validation, in order to calibrate the software calculation and to test which methods is more reliable. The eventual results could be used to properly design the barrier that is going to be installed.

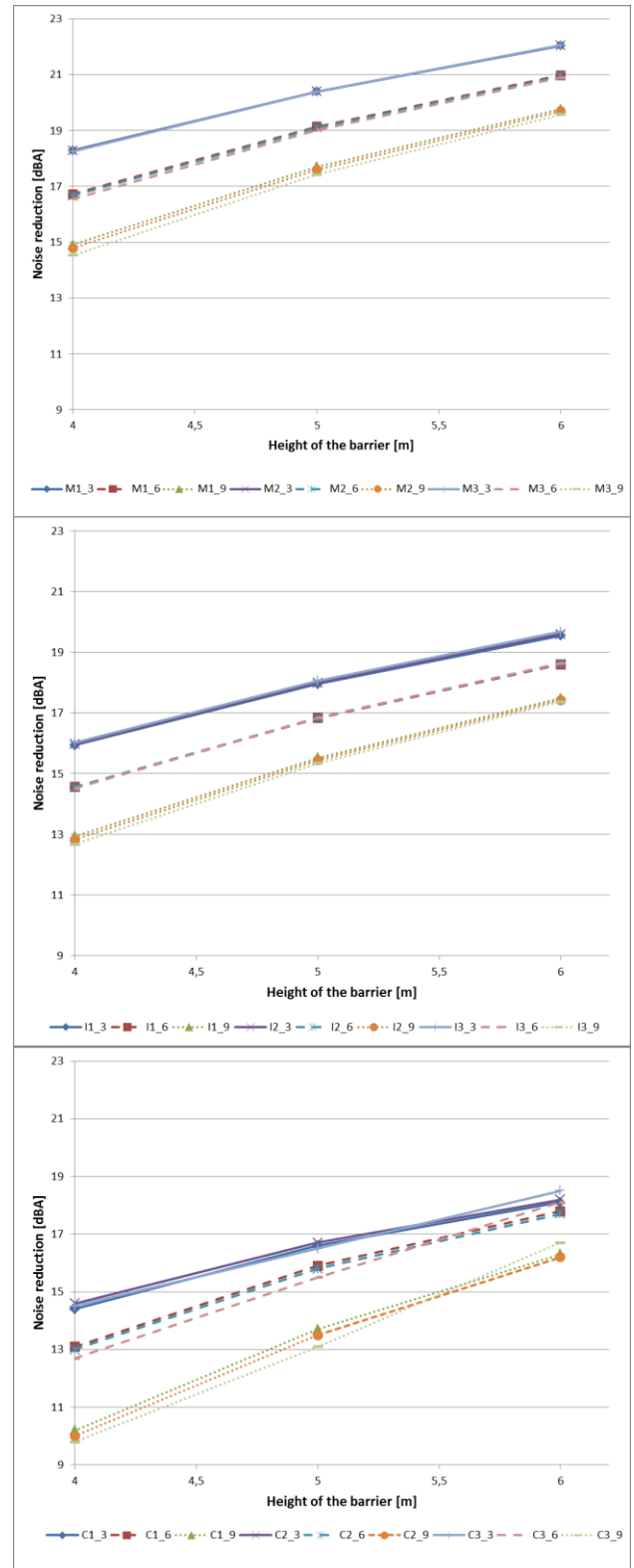


Fig. 2: Noise reduction plotted as a function of the height of the barrier (4, 5 and 6 meters), for buildings 1, 2 and 3. The lines are a guide to the eye. (Top) Maekawa, (Centre) ISO9613, (Bottom) CadnaA. Solid lines refer to the first floor (z=3m); dashed lines refer to the second floor (z=6m); dotted lines refer to the third floor (z=9m).

ACKNOWLEDGMENT

The authors are grateful to Ezio Zappia for the valuable support in this work.

REFERENCES

- [1] Quartieri J., Troisi A., Guarnaccia C., D'Agostino P., D'Ambrosio S., Iannone G., Development of an Environmental Quality Index Related to Polluting Agents, Proceedings of the Int. Conf. on "Environment, Ecosystem and Development", Puerto de la Cruz, Tenerife (Spain), 14-16 December 2009, pp. 153-161.
- [2] Quartieri J., Mastorakis N. E., Iannone G., Guarnaccia C., D'Ambrosio S., Troisi A., Lenza T.L.L., A Review of Traffic Noise Predictive Models, Proceedings of the 5th WSEAS International Conference on "Applied and Theoretical Mechanics" (MECHANICS'09), Puerto de la Cruz, Tenerife, Spain, 14-16 December 2009, pp. 72-80.
- [3] Guarnaccia C., Lenza T.L.L., Mastorakis N.E., Quartieri J., A Comparison between Traffic Noise Experimental Data and Predictive Models Results, International Journal of Mechanics, Issue 4, Vol. 5, pp. 379-386 (2011), ISSN: 1998-4448.
- [4] Guarnaccia C., Advanced Tools for Traffic Noise Modelling and Prediction, WSEAS Transactions on Systems, Issue 2, Vol.12, 2013, pp. 121-130.
- [5] Iannone G., Guarnaccia C., Quartieri J., Speed Distribution Influence in Road Traffic Noise Prediction, Environmental Engineering And Management Journal, Vol. 12, Issue 3, 2013, pp. 493-501.
- [6] Quartieri J., Iannone G., Guarnaccia C., On the Improvement of Statistical Traffic Noise Prediction Tools, Proceedings of the 11th WSEAS International Conference on "Acoustics & Music: Theory & Applications" (AMTA '10), Iasi, Romania, 13-15 June 2010, pp. 201-207.
- [7] Guarnaccia C., Analysis of Traffic Noise in a Road Intersection Configuration, WSEAS Transactions on Systems, Issue 8, Volume 9, (2010), pp.865-874, ISSN: 1109-2777.
- [8] Quartieri J., Mastorakis N. E., Guarnaccia C., Troisi A., D'Ambrosio S., Iannone G., Traffic Noise Impact in Road Intersections, International Journal of Energy and Environment, Issue 1, Volume 4 (2010), pp. 1-8.
- [9] Iannone G., Guarnaccia C., Quartieri J., Noise Fundamental Diagram deduced by Traffic Dynamics, in "Recent Researches in Geography, Geology, Energy, Environment and Biomedicine", Proceedings of the 4th WSEAS Int. Conf. on Engineering Mechanics, Structures, Engineering Geology (EMESEG '11), Corfu Island, Greece, July 14-16, 2011, pp. 501-507.
- [10] Quartieri J., Mastorakis N.E., Guarnaccia C., Iannone G., Cellular Automata Application to Traffic Noise Control, Proc. of the 12th Int. Conf. on "Automatic Control, Modelling & Simulation" (ACMOS '10), Catania (Italy), 29-31 May 2010, pp. 299-304.
- [11] Guarnaccia C., Mastorakis N. E., Quartieri J., Noise Sources Analysis in a Wood Manufacturing Company, International Journal of Mechanics, Issue 2, Vol. 7, pp 37-44 (2013).
- [12] Maekawa Z., Noise reduction by screens, Applied Acoustics, Issue 3, Vol.1, pp 157-173, 1968.
- [13] ISO 9613-2: Acoustics – Attenuation of sound during propagation outdoors – Part 2: General method of calculation, International Organization for Standardization, Geneva, Switzerland, 1996.
- [14] Guarnaccia C., Acoustical Noise Analysis in Road Intersections: a Case Study, Proceedings of the 11th WSEAS Int. Conf. on "Acoustics & Music: Theory & Applications" (AMTA '10), Iasi, Romania, 13-15 June 2010, pp. 208-215.
- [15] Guarnaccia C., New Perspectives in Road Traffic Noise Prediction, in "Latest advances in Acoustics and Music", proceedings of the 13th Int. Conf. on Acoustics & Music: Theory & Applications (AMTA '12), Iasi, Romania, 13-15 June 2012. ISBN: 978-1-61804-096-1, pp. 255-260
- [16] Quartieri J., Troisi A., Guarnaccia C., Lenza TLL, D'Agostino P., D'Ambrosio S., Iannone G., Analysis of Noise Emissions by Train in Proximity of a Railway Station, Proceedings of the 10th International Conference on "Acoustics & Music: Theory & Applications" (AMTA '09), Prague (Rep.Ceca), 23-25 March 2009, pp: 100-107.
- [17] Quartieri J., Troisi A., Guarnaccia C., Lenza TLL, D'Agostino P., D'Ambrosio S., Iannone G., An Italian High Speed Train Noise Analysis in an Open Country Environment, Proceedings of the 10th International Conference on "Acoustics & Music: Theory &

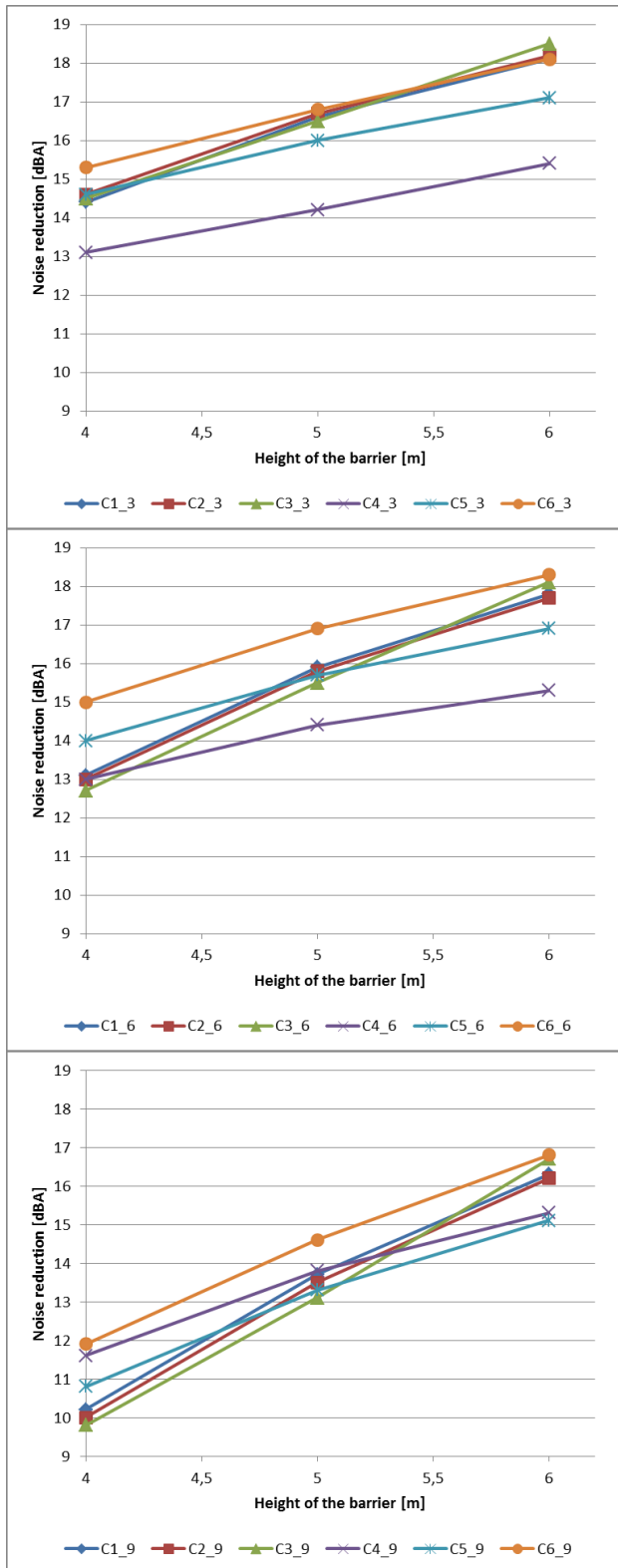


Fig. 3: Noise reduction plotted as a function of the height of the barrier (4, 5 and 6 meters), for all the 6 buildings, evaluated by CadnaA method. The lines are a guide to the eye. (Top) first floor (z=3m), (Centre) second floor (z=6m), (Bottom) third floor (z=9m).

- Applications” (AMTA '09), Prague (Rep.Ceca), 23-25 March 2009, pp: 92-99.
- [18] Quartieri J., Troisi A., Guarnaccia C., Lenza TLL, D'Agostino P., D'Ambrosio S., Iannone G., An Acoustical Study of High Speed Train Transits, WSEAS Transactions on Systems, Issue 4, Vol.8, pp. 481-490 (2009).
- [19] Quartieri J., Troisi A., Guarnaccia C., Lenza TLL, D'Agostino P., D'Ambrosio S., Iannone G., Application of a Predictive Acoustical Software for Modelling Low Speed Train Noise in an Urban Environment, WSEAS Transactions on Systems, Issue 6, Vol.8, pp. 673-682 (2009).
- [20] Quartieri J., Mastorakis N. E., Guarnaccia C., Troisi A., D'Ambrosio S., Iannone G., Road Intersections Noise Impact on Urban Environment Quality, Proceedings of the 5th WSEAS Int. Conf. on “Applied and Theoretical Mechanics” (MECHANICS '09), Puerto de la Cruz, Tenerife, Spain, 14-16 December 2009, pp. 162-171.
- [21] Guarnaccia C., Mastorakis N.E., Quartieri J., Wind Turbine Noise: Theoretical and Experimental Study, International Journal of Mechanics, Issue 3, Vol.5, pp. 129-137 (2011).
- [22] Tronchin L., On the acoustic efficiency of road barriers: The Reflection Index, International Journal of Mechanics, Issue 3, Vol. 7, pp 318-326 (2013), ISSN: 1998-4448.
- [23] Tronchin L., On the acoustic efficiency of road barriers. The Sound Insulation Index, International Journal of Circuits, Systems and Signal Processing, Issue 5, Vol. 7, pp 277-284 (2013).
- [24] Guarnaccia C., Quartieri J., Mastorakis N. E. and Tepedino C., Acoustic Noise Levels Predictive Model Based on Time Series Analysis, in “Latest Trends in Circuits, Systems, Signal Processing and Automatic Control”, proceedings of the 2nd Int. Conf. on Acoustics, Speech and Audio Processing (ASAP '14), Salerno, Italy, June 3-5, 2014 , ISSN: 1790-5117, pp. 140-147.
- [25] Guarnaccia C., Quartieri J., Rodrigues E. R. and Tepedino C., Time Series Model Application to Multiple Seasonality Acoustical Noise Levels Data Set, in “Latest Trends in Circuits, Systems, Signal Processing and Automatic Control”, proc. of the 2nd Int. Conf. on Acoustics, Speech and Audio Processing, Salerno, Italy, June, 2014, pp.171-180.
- [26] Quartieri J., Sirignano L., Guarnaccia C., Equivalence between Linear and Curved Sources in Newtonian Fields: Acoustics Applications, Proc. Of the Int. Conf. on Engineering Mechanics, Structures, Engineering Geology (EMESEG '08), Heraklion, Crete Island, Greece, July 22-24, 2008, pp: 393-395.
- [27] Quartieri J., Guida M., Guarnaccia C., D'Ambrosio S., Guadagnuolo D., Complex Network Applications to the Infrastructure Systems: the Italian Airport Network case, Proc. of the Int. Conf. on Urban Planning and Transportation (UPT'07), Crete Island, Greece, July 22-24, 2008, pp: 96-100.
- [28] Quartieri J., Mastorakis N.E., Iannone G., Guarnaccia C., A Cellular Automata Model for Fire Spreading Prediction, in “Latest Trends on Urban Planning and Transportation”, Proc. of the 3rd Int. Conf. on “Urban Planning and Transportation”, Corfù, Greece, 22-24 July 2010, pp. 173-179.
- [29] Iannone G., Troisi A., Guarnaccia C., D'Agostino P. P., Quartieri J., An Urban Growth Model Based on a Cellular Automata Phenomenological Framework, Int. Journal of Modern Physics C, Volume 22, Issue 05, pp. 543-561 (2011). DOI: 10.1142/S0129183111016427.
- [30] Quartieri J., Guida M., Guarnaccia C., D'Ambrosio S., Guadagnuolo D., Topological Properties of the Italian Airport Network studied via Multiple Addendials and Graph Theory, International Journal of Mathematical Models and Methods in Applied Sciences, Issue 2, Vol.2, pp 312-316 (2008).
- [31] Quartieri J., Sirignano L., Guarnaccia C., Infinitesimal Equivalence between Linear and Curved Sources in Newtonian Fields: Application to Acoustics, International Journal of Mechanics, Issue 4, Vol.1, pp. 89-91 (2007) , ISSN: 1998-4448.
- [32] D'Ambrosio S., Guarnaccia C., Guida D., Lenza T.L.L., Quartieri J., System Parameters Identification in a General Class of Non-linear Mechanical Systems, International Journal of Mechanics, Issue 4, Vol. 1, pp 76-79 (2007).
- [33] Guarnaccia C., Mastorakis N. E., Quartieri J., A Mathematical Approach for Wind Turbine Noise Propagation, in Applications of Mathematics and Computer Engineering, American Conference of Applied Mathematics, Puerto Morelos, Mexico, 29-31 January 2011, pp. 187-194.
- [34] Quartieri J., Mastorakis N.E., Guarnaccia C., Iannone G., Church Acoustics Measurements and Analysis, Proceedings of the 11th WSEAS International Conference on “Acoustics and Music: Theory and Applications” (AMTA'10), Iasi, (Romania), 13-15 June 2010, pp: 216-224.
- [35] Quartieri J., Guarnaccia C., D'Ambrosio S., Iannone G., Room Acoustics Experimental Study: Characterization of the Sound Quality in a New Built Church, Proceedings of the 10th WSEAS Int. Conf. on “Acoustics & Music: Theory & Applications” (AMTA '09), Prague (Rep.Ceca), 23-25 March 2009, pp 108-115.
- [36] Quartieri J., D'Ambrosio S., Guarnaccia C., Iannone G., Experiments in Room Acoustics: Modelling of a Church Sound Field and Reverberation Time Measurements, WSEAS Transactions on Signal Processing, Issue 3, Vol.5, pp. 126-135 (2009).
- [37] Guarnaccia C., Quartieri J., Ruggiero A., Lenza T.L.L., Industrial Settlements Acoustic Noise Impact Study by Predictive Software and Computational Approach, in “Latest Trends in Energy, Environment and Development”, proceedings of the 7th Int. Conf. on Urban Planning and Transportation, Salerno, Italy, June 3-5, 2014 , pp. 80-87.

Relay Feedback Identification of Dynamical SISO Systems – Analysis and Settings

Roman Prokop, Jiří Korbek, and Radek Matusů

Abstract— Autotuning principles usually combine relay feedback tests with a control synthesis. This paper is focused on the first part of this scheme, i.e. relay plant identification for continuous-time plants. The estimation of the controlled system parameters plays the key role in the quality of control. There are many types of relays used in feedback relay schemes. The contribution deals with four ones of them unbiased and biased relays without or with hysteresis.

Most of industrial plants can be satisfactory estimated by a first or second order linear stable with a time delay term. The main relay parameters are the asymmetry, hysteresis and amplitudes. The aim of this paper is to study and analyze the influence of these parameters for the quality of estimation of the gain, time constant and time delay. As a result, some recommendations for settings of relay features can be given.

All simulations were performed in Matlab and Simulink program environment. Identified plant parameters then can be utilized in various autotuning schemes, e.g. with algebraic control design. A program system for automatic estimation, design and simulation was developed.

Keywords—Autotuning, Relay experiment, Limit cycle oscillations, Biased and unbiased relay, Hysteresis, Describing function.

I. INTRODUCTION

THE Åström and Hägglund relay feedback test [1] started in 1984 an important tool for automatic controller tuning because it identifies two main parameters for the Ziegler-Nichols method [3]. Previously, relay was mainly used as an amplifier or as a relay back control. The Åström-Hägglund test is based on the observation, when the output lags behind the input by $-\pi$ radians, the closed loop oscillates with a constant period. Then, the ultimate gain and frequency are identified by a simple symmetrical relay feedback experiment proposed in [1]. From the critical values the controller setting was applied by the Ziegler-Nichols rule which is simple but it suffers from several drawbacks.

This work was supported by the European Regional Development Fund under the project CEBIA-Tech No. CZ.11.05/2.1.00/03.0089.

R. Prokop is with Faculty of applied informatics, Tomas Bata University in Zlín, Nad Stráněmi 4511, Zlín, Czech Republic (phone: 420-57603-5257; e-mail: prokop@fai.utb.cz).

J. Korbek is with Faculty of applied informatics, Tomas Bata University in Zlín, Nad Stráněmi 4511, Zlín, Czech Republic (e-mail: korbek@fai.utb.cz).

R. Matusů is with Faculty of applied informatics, Tomas Bata University in Zlín, Nad Stráněmi 4511, Zlín, Czech Republic (e-mail: rmatuul@fai.utb.cz).

From that time, many studies have been reported to extend and improve both, the relay feedback experiment as well as tuning and control design principles; see e.g. [2] - [4], [9], [14]-[17]. Many of them need an estimation of transfer function parameters and the original approach provides no explicit parameters of the identified transfer function. During the period of almost three decades, the direct estimation of transfer function parameters instead of critical values began to appear. The extension in relay utilization was performed in e.g. [8] - [11], [21] by an asymmetry and hysteresis of a relay. Nowadays, almost all commercial industrial PID controllers provide the feature of autotuning.

This paper brings a study how the asymmetry and hysteresis influence of the quality and accuracy of identification process. Also the length of the experiment and the relay amplitude can influence the quality of the estimation.

Probably Luyben in [5][4] was the first who used the approximate describing function (DF) method to estimate the process transfer function from limit cycle measurements.

The main scheme for the relay estimation and/or identification is depicted in Fig.1.

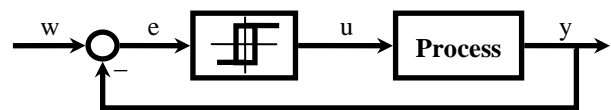


Fig. 1 relay based identification

The goal of the original test was to indicate the critical point in the Nyquist curve of the open loop. However, there are other relays used in identification experiments, e.g. the biased (asymmetrical) relay, main two position symmetrical and asymmetrical (biased) relay without and with hysteresis characteristic are depicted in Fig. 2. A biased (asymmetrical) one characteristic is obtained by a simple vertical moving by an asymmetry shift. Also, the relay without hysteresis is obtained by putting $\epsilon = 0$.

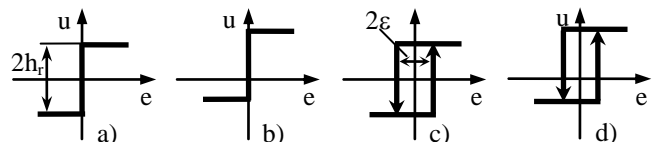


Fig. 2 types of relay

Many research works have been done to improve and refine the effect of fundamental harmonic by using different shapes and structures of the relay element, see [6], [7], [18] - [20]. A limit cycle oscillation for a stable system with positive steady state gain with a biased relay is shown in Fig. 3.

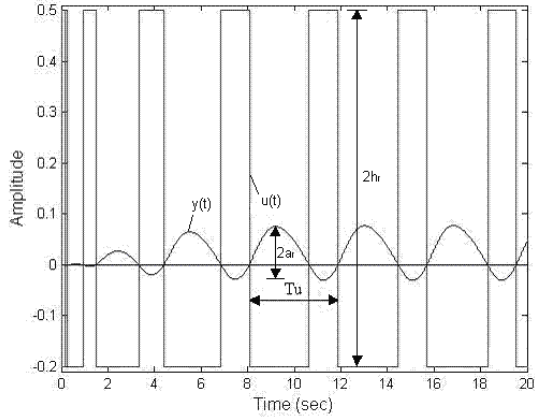


Fig. 3 biased relay oscillation of stable processes

Many stable industrial processes can be approximated by a first or second order linear system with a time delay term. The model for first order (stable) systems plus dead time (FOPDT) is supposed in the form:

$$G(s) = \frac{K}{Ts + 1} \cdot e^{-\Theta s} \quad (1)$$

The second order model plus dead time (SOPDT) is assumed in the form:

$$G(s) = \frac{K}{(Ts + 1)^2} \cdot e^{-\Theta s} \quad (2)$$

II. RELAY FEEDBACK ESTIMATION

A. Critical Values Estimation

Critical values estimation is based on a simple symmetric (unbiased) relay experiment which output is depicted in Fig. 3.

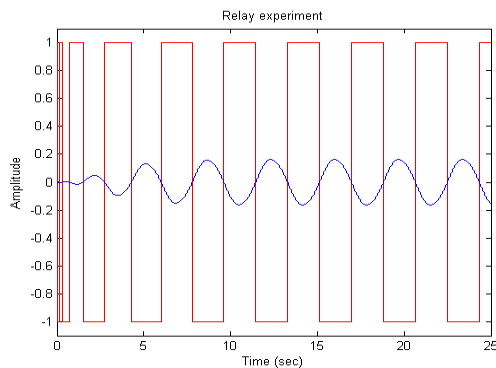


Fig. 4 unbiased relay oscillation of stable processes

The critical gain is then given by the relation (see e.g. [1])

$$r_u = \frac{4}{\pi} \cdot \frac{h_r}{\sqrt{a_r^2 - \varepsilon^2}} \Big|_{\varepsilon=0} = \frac{4}{\pi} \cdot \frac{h_r}{a_r} \quad (3)$$

and the ultimate period T_u can be read according to Fig. 4.

B. Unbiased relay experiment

The relay feedback experiment according to Fig. 1 yields stable harmonic oscillations, i.e. it causes rise of the stable limit cycles (Fig. 3). The describing function method ([5], [11], [13], [24]) is a tool for verification the limit cycle rise. The describing function of the relay $N(a)$ is considered as a complex gain which depends on the harmonic oscillation amplitude a and angular frequency ω in the relay input $e(t)$

$$e(t) = a \sin \omega t \quad (4)$$

The condition for the limit cycle follows from the critical point of non-linear closed-loop system in Fig. 1 which gives

$$N(a)G_p(s) + 1 = 0 \quad (5)$$

where $G_p(s) = A_p(\omega) e^{j\varphi(\omega)}$ is the plant transfer function, $A_p(\omega)$ and $\varphi(\omega)$ are called the (transfer function) magnitude and phase, respectively.

For the symmetric relay without or with hysteresis $\varepsilon > 0$, the describing function and the critical characteristic have the form (see e.g. [8], [11], [24])

$$A_N(a) e^{j\varphi_N(a)} = -\frac{1}{N(a)} \quad \text{for } 0 \leq \varepsilon \leq a \quad (6)$$

otherwise $N(a) = \infty$. Values $A(a)$ and $\varphi_N(a)$ represent the critical magnitude and critical characteristic phase, respectively

$$A_N(a) = \frac{\pi a_r}{4h_r} \quad (7)$$

$$\varphi_N(a) = \arctg \frac{\varepsilon}{\sqrt{a^2 - \varepsilon^2}} - \pi$$

The frequency transfer function $G(j\omega) = A_p(\omega) e^{j\varphi_p(\omega)}$ for the first order system (1) gives

$$A_p(a) = \frac{K}{\sqrt{T^2 \omega^2 + 1}} \quad (8)$$

$$\varphi_p(a) = -\arctg \omega T - \omega \Theta$$

Comparing $A_N(a) = A_p(a)$ and $\varphi_N(a) = \varphi_p(a)$ in (7) and (8) gives two equations for the calculation of T and Θ . The final relations for the time constant and time delay terms for

FOPDT (1) are given by:

$$T = \frac{T_y}{2\pi} \cdot \sqrt{\frac{16 \cdot K^2 \cdot u_0^2}{\pi^2 \cdot a_y^2} - 1}$$

$$\Theta = \frac{T_y}{2\pi} \cdot \left[\pi - \arctg \frac{2\pi T}{T_y} - \arctg \frac{\varepsilon}{\sqrt{a_y^2 - \varepsilon^2}} \right]$$

where a_y and T_y are depicted in Fig.1 and ε is hysteresis.

The second order system SOPDT (2) are estimated by relations

$$T = \frac{T_y}{2\pi} \cdot \sqrt{\frac{4 \cdot K \cdot u_0}{\pi \cdot a_y} - 1}$$

$$\Theta = \frac{T_y}{2\pi} \cdot \left[\pi - 2\arctg \frac{2\pi T}{T_y} - \arctg \frac{\varepsilon}{\sqrt{a_y^2 - \varepsilon^2}} \right]$$

Relations (9), (10) represent a suitable identification tool for computing time and time delay terms but a relay unbiased system is not able to estimate the gain of the controlled system.

C. Biased relay experiment

Asymmetrical relays with or without hysteresis bring further progress, see e.g. [2], [6], [7], [13], [21], [22]. After the relay feedback test, the estimation of process parameters can be performed. A typical data response of such relay experiment is depicted in Fig.5. The relay asymmetry is required for the process gain estimation (11) while a symmetrical relay would cause the zero division in the appropriate formula. In this paper, an asymmetrical relay with hysteresis was used. This relay enables to estimate transfer function parameters as well as a time delay term. The proportional gain can be computed by the relation [11]:

$$K = \frac{\int_0^{\pi} y(t) dt}{\int_0^{\pi} u(t) dt}; \quad i = 1, 2, 3, \dots$$

when the asymmetric relay is used for the relay feedback test, it is shown in Fig.5, the output y converges to the stationary oscillation in one period. These oscillations are characterized by equations (see [8]):

$$A_u = (\mu_0 + \mu) \cdot K \cdot \left(1 - e^{-\frac{\Theta}{T}} \right) + \varepsilon \cdot e^{-\frac{\Theta}{T}}$$

$$A_d = (\mu_0 - \mu) \cdot K \cdot \left(1 - e^{-\frac{\Theta}{T}} \right) - \varepsilon \cdot e^{-\frac{\Theta}{T}}$$

$$T_{u1} = T \cdot \ln \frac{2 \cdot \mu \cdot K \cdot e^{\frac{\Theta}{T}} + \mu_0 \cdot K - \mu \cdot K + \varepsilon}{\mu \cdot K + \mu_0 \cdot K - \varepsilon}$$

$$T_{u2} = T \cdot \ln \frac{2 \cdot \mu \cdot K \cdot e^{\frac{\Theta}{T}} - \mu_0 \cdot K - \mu \cdot K + \varepsilon}{\mu \cdot K - \mu_0 \cdot K - \varepsilon}$$

The normalized dead time of the process ($L = \Theta/T$) is obtained from (14) or (15) in the form (see e.g. [8]):

$$L = \ln \frac{(\mu_0 + \mu) \cdot K - \varepsilon}{(\mu_0 + \mu) \cdot K - A_u}$$

or

$$L = \ln \frac{(\mu - \mu_0) \cdot K - \varepsilon}{(\mu - \mu_0) \cdot K + A_d}$$

Next, the time constant can be computed from (4) or (5) by solving these formulas:

$$T = T_{u1} \cdot \left(\ln \frac{2 \cdot \mu \cdot K \cdot e^{L} + \mu_0 \cdot K - \mu \cdot K + \varepsilon}{\mu \cdot K + \mu_0 \cdot K - \varepsilon} \right)^{-1}$$

or

$$T = T_{u2} \cdot \left(\ln \frac{2 \cdot \mu \cdot K \cdot e^{L} - \mu_0 \cdot K - \mu \cdot K + \varepsilon}{\mu \cdot K - \mu_0 \cdot K - \varepsilon} \right)^{-1}$$

and a time delay term is $\Theta = T \cdot L$.

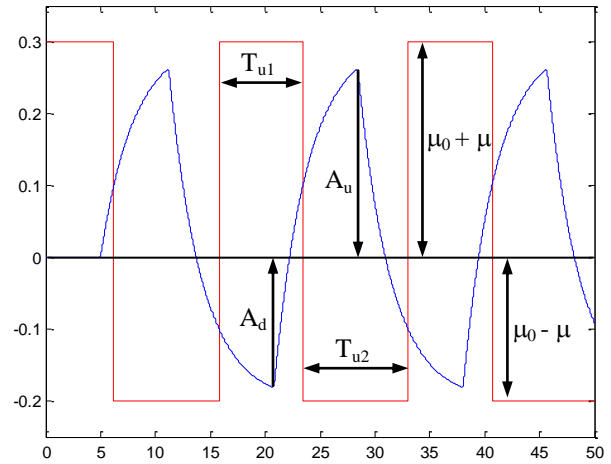


Fig. 5 unbiased relay oscillation of first order stable system

III. EXAMPLES AND DISCUSSION

The relay tests mentioned in the previous section were applied for explicit estimation transfer functions (1), (2). All simulations were performed in the Matlab, Simulink environment by a program, which the main window shown in Fig. 6. This program was described e.g. in [15], [23] and it is aimed for relay experiments as well for control design and control simulations. At the beginning of the simulation, the

controlled transfer function is defined and parameters for the relay experiment must be entered. Then, a relay experiment is performed and it can be repeated with modified parameters if necessary. After the experiment, parameters of the estimated transfer function are calculated automatically and controller parameters are generated after pushing of the appropriate button, details can be found in [15], [17], [23].

In this contribution, the main emphasis was laid on the accuracy of estimated parameters. The aim is to conclude how to set relay parameters and to give some recommendations.

Since the identification relations have to estimate both, time constant as well as a system gain. The time parameters are estimated by a symmetrical relay, while the gain is estimated by a biased relay experiment. Then a contradictory question is concluded: How to utilize a biased relay experiment for estimation of all identified parameters in (1) and (2). The main aim of the research work was to investigate how a biased relay can be used with satisfactory accuracy and how to set up the relay experiment.

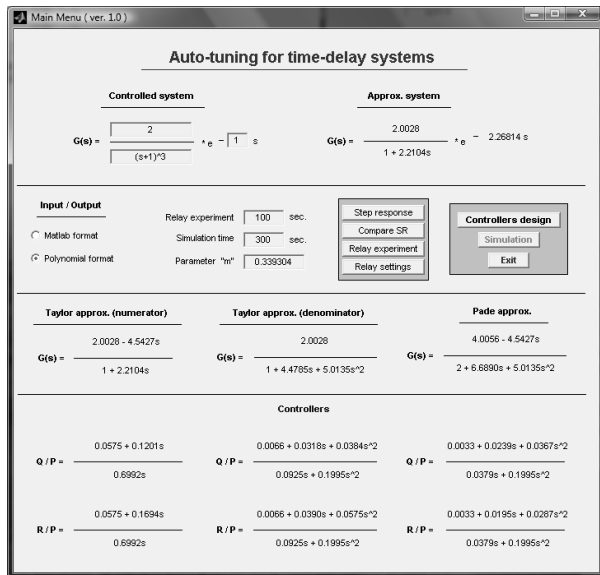


Fig. 6 main menu of program system

The first test transfer function for the first order system is given

$$G(s) = \frac{3}{4s+1} \cdot e^{-6s} \quad (20)$$

Many relay feedback experiments were performed by the simulation program and the following sensitivity was investigated. The accuracy of estimated parameters depends on main parameters of the relay, namely:

- asymmetry
- hysteresis
- relay amplitude

Table I shows the influence of the asymmetry of the relay on the accuracy of estimation. All entries of Table 1 are in differences between the true and estimated values in %. The upper value of the relay output was 0.30.

Asymmetry [%]	10	20	30	40	50	60
ΔK [%]	1.7	1.3	1.3	0.7	0.7	0.7
ΔT [%]	3.5	2.8	2.1	1.2	1.2	1.0
$\Delta \Theta$ [%]	1.2	1.0	0.8	0.5	0.7	0.5

Table I estimation accuracy based on relay asymmetry.

Table II summarizes the sensitivity of the relay hysteresis for transfer function (20). All entries are for comparison in numerical values. The upper relay output was 1.2 lower value - 1.08.

Hysteresis ε	0	0.2	0.4	0.6
Gain K	2.88	2.95	2.95	2.92
Time constant T	3.70	3.88	3.78	3.78
Time delay Θ	6.12	6.05	6.07	6.12

Table II estimation accuracy based on relay hysteresis

In a similar way, according to Table 2 also a set of experiments were for various values of the lower relay output - 0.96, 0.84, 0.72, 0.60, respectively. The following observations and recommendations can be drawn from the obtained analysis:

- bigger values of asymmetry up to 40% caused better accuracy of all parameters
- better accuracy was achieved for smaller values of hysteresis $\varepsilon = 0.1; 0.2$
- values of relay outputs have no relevant influence on the estimation accuracy

The recommended values for a relay experiment were used for the estimation of the higher order system:

$$G(s) = \frac{5}{(s+1)^8} \cdot e^{-3s} \quad (21)$$

The relay parameters with $\varepsilon = 0.1$; asymmetry 40% with upper and lower relay outputs 0.30 and -0.18 were used. The resulting first order estimation takes the form:

$$G(s) = \frac{4.97}{3.58s+1} \cdot e^{-8.19s} \quad (22)$$

Comparison of both step responses of systems (21) and (22) is depicted in Fig. 7. Other results of estimation and autotuning control can be found in [14] - [17], [23].

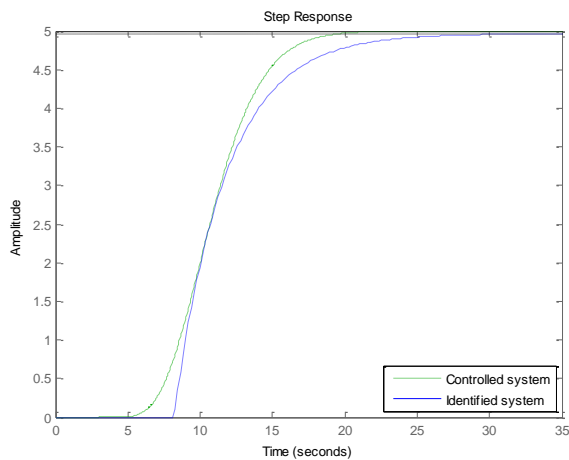


Fig. 7 step responses of systems (21) and (22)

IV. CONCLUSION

The paper describes main methods for parameter estimation by a feedback relay experiment. The proper and accurate parameter identification plays a key role for a control design, especially in autotuning utilization. Various relay improvements and utilization for control design can be found in [12], [13], [17], [25], [23]. The goal of the paper is to investigate how the estimation is sensitive on the relay settings. Main relay characteristics as asymmetry, hysteresis and amplitude can be recommended for the correct adjustment for the relay experiment.

REFERENCES

- [1] K.J. Åström and T. Hägglund, "Automatic tuning of simple regulators with specification on phase and amplitude margins". *Automatica*, Vol.20, 1984, pp.645-651.
- [2] Ch.Ch. Yu, *Autotuning of PID Controllers*. London: Springer Verlag, 1999.
- [3] K.J. Åström and T. Hägglund, *PID Controllers: Theory, Design and Tuning*. Research Triangle Park, NC: Instrumental Society of America, 1995.
- [4] R.F. Garcia and, F.J.P. Castelo, "A complement to autotuning methods on PID controllers". In Preprints of IFAC Workshop PID'00. 2000. s. 101-104. ISBN 0080436242.
- [5] W.L.Luyben, "Derivation of transfer function highly nonlinear distillation column" *Ind. Eng.Chem Res.* 26, 1987, p 2490-2495.
- [6] S. Majhi, Relay based identification of processes with time delay. *Journal of Process Control*. 2007, 17, s. 93-101.
- [7] A. Ingimurdarson and T. Hägglund, Robust automatic tuning of an industrial PI controller for dead-time systems. In Preprints of IFAC Workshop PID'00. 2000. s. 149-154. ISBN 0080436242.
- [8] C.C. Hang, K.J. Åström and Q.C. Wang, Relay feedback auto-tuning of process controllers – a tutorial review, *Journal of Process Control*, Vol.12, No. 6, 2002.
- [9] S. Majhi and D.P. Atherton, Autotuning and controller design for unstable time delay processes, In: *Preprints of UKACC Conf on Control*, 1998, pp. 769-774.
- [10] J.C. Jeng, H.P. Huang and F.Y. Lin, Modified relay feedback approach for controller tuning based on assessment of gain and phase margins. *Industrial and Engineering Chemistry Research*. 2006, 45, s. 4043-4051.
- [11] M. Vitečková, and A. Viteček, Plant identification by relay methods. In: *Engineering the future (edited by L. Dudas)*. Sciyo, Rijeka, 2010, pp. 242-256.

- [12] J. A. Leva, L. Bascetta and F. Schiavo, Model-based PI/PID autotuning with fast relay identification. *Industrial and Engineering Chemistry Research*. 2006, 45, s. 4052-4062.
- [13] W.L. Luyben, Getting more information from relay-feedback tests. *Industrial and Engineering Chemistry Research*. 2001, 40, s. 4391-4402.
- [14] R. Prokop, L.Pekař and J. Korbel, Autotuning for delay systems using meromorphic functions, In: *Prepr. 9th Workshop TDS (IFAC)*, 2010. Prague pp. 51-59.
- [15] R. Prokop, Korbel, J. and Prokopová, Z., Relay based autotuning with algebraic control design, In: *Preprints of the 23rd European Conf. on modelling and Simulation*, Madrid, 2009, pp. 531-536.
- [16] L. Pekař and R. Prokop, Non-delay depending stability of a time-delay system. In: *Last Trends on Systems, 14th WSEAS International Conference on Systems*, Corfu Island, Greece, 2010, pp. 271-275.
- [17] R. Prokop, J. Korbel and O. Liška, A novel principle for relay-based autotuning. *International Journal of Mathematical Models and Methods in Applied Science*, 2011, Vol. 5, No. 7, s. 1180-1188.
- [18] R.C. Panda and Ch.Ch. Yu, Analytical expressions for relay feedback responses. *Journal of Process Control*. 2003, 13, s. 489-501.
- [19] R.R. Pecharrmán and F.L. Pagola, Control design for PID controllers auto-tuning based on improved identification, In: *Preprints of IFAC Workshop PID'00*, pp. 89-94, 2000.
- [20] T. Thyagarajan and Ch.Ch. Yu, Improved autotuning using shape factor from relay feedback, In: *Preprints of IFAC World Congres*, 2002.
- [21] I. Kaya and D.P. Atherton, Parameter estimation from relay autotuning with asymmetric limit cycle data, *Journal of Process Control*, Vol. 11, No4, 2001, pp. 429-439.
- [22] S.H. Shen, J.H. Wu, Ch.hC. Yu, Use of biased-relay feedback for system identification. *American Institute of Chemical Engineers*. 1996, 42, s. 1174-1180.
- [23] R. Prokop, J. Korbel and R. Matušů. Autotuners based on the Smith predictor structures. *International Journal of Mathematical Models and Methods in Applied Sciences*, Vol. 7, No. 3, 2013, pp. 295-302.
- [24] J.H.Taylor, Describing Functions. *Electrical Engineering Encyclopedia*. 1999.
- [25] Z.T. Yaman et al., Improved FODPT model estimation with Delayed-relay feedback for constant time dominant processes. In: *Prepr of UKACC Conf. on Control*, pp. 421-426, 2008.

ROMAN PROKOP was born in Hodonin, Czech Republic in 1952. He graduated in Cybernetics from the Czech Technical University in Prague in 1976. He received post graduate diploma in 1983 from the Slovak Technical University. Since 1995 he has been at Tomas Bata University in Zlín, where he presently holds the position of full professor of the Department of Automation and Control Engineering and a vice-rector of the university. His research activities include algebraic methods in control theory, robust and adaptive control, autotuning and optimization techniques.

JIŘÍ KORBEL was born in Zlín, Czech Republic. He studied automatic control and informatics at the Tomas Bata University and graduated in 2004, now he is assistant at the Faculty of Applied Informatics in Zlín. His research activities include autotuning principles, algebraic and polynomial syntheses and modeling and simulations.

RADEK MATUŠŮ was born in Zlín, Czech Republic in 1978. He graduated from Faculty of Technology of the same university with an MSc in Automation and Control Engineering in 2002 and he received a PhD in Technical Cybernetics from Faculty of Applied Informatics in 2007. Currently, he is a Researcher at the same faculty. The main fields of his research interest include robust systems and application of algebraic methods to control design.

Control of direct-driven PMSG for wind energy system

F. Khater, A. Shaltout, and A. Omar

Abstract—This paper introduces a novel control of wind energy system with directly-driven permanent magnet synchronous generator (DDPMSG) connected to grid. The proposed controller is based on the concept of multi-degree of freedom (MDOF). To obtain the largest wind power and improve the wind energy utilization rate the maximum power point tracking (MPPT) is applied using MDOF. The system is modeled and simulated during wind speed changes. The system includes: variable speed wind turbine, DDPMSG, and full sized voltage source back-to-back converter connected to grid. The control system is developed using PI and MDOF controllers to prove effectiveness of the proposed control in dynamic performance utilizing space vector pulse width modulation (SVPWM).

Keywords—Control, Direct-driven, MPPT, MDOF, PMSG, SVPWM, Wind turbine.

I. INTRODUCTION

Wind energy is one of the most important renewable energy resources because wind power extraction technology is the fastest growing one among various renewable energy generation systems [1]. Several developed generation systems are used to extract wind energy using different wind turbine systems. Using direct-driven permanent magnet synchronous generator (PMSG) is a competitive choice between other generation systems. The direct drive concept is known with its advantages of eliminating the gear train, smaller size, and consequently less weight and losses [2], [3]. PM generator has many competitive advantages, because of its great energy yield, good reliability, and high efficiency [4].

Large scale PMSG are common to be used for grid integration and wind farms installation [5] and they are efficient at high wind speeds [1]. Small scale generator are suitable for medium wind speed sites [6], also has advantage of running stand alone for residential application and micro grids integration [7], [8]. The control of a PMSG with a diode rectifier followed by a dc chopper is proposed in [9] through variation of the duty cycle and maintains appropriate dc

voltage. This arrangement is more practical for small scale PMSG because of its lower cost although with this configuration the control of the generator power factor is not possible and the generator efficiency is affected. Thyristor-based dump-load circuits used in [10] to improve system performance and quality.

Integration of small scale wind turbines with single-phase power supply is introduced in [11] using three-phase PMSG through controlled rectifier and single-phase inverter. Using back-to-back converter is preferred because the control of the machine-side converter can deliver maximum power and increase efficiency of the generation system. This configuration also decouples the wind turbine from grid disturbances.

This paper presents a direct-driven PMSG for variable speed wind turbine system. Back-to-back current controlled converters are controlled utilizing space vector pulse width modulation (SVPWM) to interface the generator and the grid. At the machine-side a novel speed controller is proposed to improve the system performance at wind speed changes. The rotor speed controller uses multi-degree of freedom (MDOF) concept to reduce the changes and duration [12]. This reduces stress at the rotor, while keeping maximum power point tracking (MPPT) with wind speed variation. The grid-side inverter is controlled to keep the dc-link voltage at pre-set value and the current injected to the grid at unity power factor to achieve maximum power delivery to grid as a desired operating condition. Modeling and simulation of the system is developed to insure the enhancement of the performance with the proposed speed controller.

II. SYSTEM DESCRIPTION AND MODELING

A. System Description

In this study, the rotor of the wind turbine is directly coupled to the generator without any gearbox, i.e., through a gearless drive train. A fully controlled back-to-back converter is used as interface between the generator and the grid as shown in Fig.1. SVPWM technique is used for switching both converters. The machine-side converter is controlled so that the generator speed is adjusted to track maximum power operation. Conventional PI controller is used to generate torque reference component, then MDOF controller is used to improve the performance of this control loop at machine-side converter. The dc-link voltage and delivered power to the grid are controlled via PI controllers to achieve unity power factor of the grid injected currents.

This work has been supported by the Electronics Research Institute (ERI) under research grant on direct-driven PMSG for wind energy system.

Faeka M. H. Khater is with the Electronics Research Institute, Dokki, 12622 Giza, Egypt; phone: 202-333105554; fax: 202-33369738; e-mail: khater@eri.sci.eg.

Adel D. Shaltout is with the Electrical Engineering Department, Cairo University, University Street, 12316 Giza, Egypt; e-mail: aashaltout@yahoo.com.

Alaa A. Omar is with the Electronics Research Institute, Dokki, 12622 Giza, Egypt; e-mail: omar8642@eri.sci.eg.

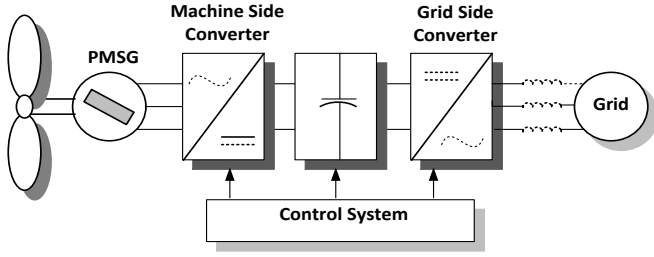


Fig. 1. Main components of DDPMSG wind turbine system.

B. Turbine Mathematical Modeling

The available wind power can be represented by [13],

$$P_{wind} = \left(\frac{1}{2}\rho_{air}\right) \times (\pi R^2) \times V_{wind}^3 \quad (1)$$

where P_{wind} is the total available wind power, ρ_{air} is the air density (kg/m^3), R is the rotor radius (m), and V_{wind} is the wind speed (m/sec).

The extracted power from wind energy by the turbine is given by:

$$P_{mech} = C_p \times P_{wind} \quad (2)$$

The power coefficient (C_p) is a function of the tip speed ratio (λ), and the blade pitch angle (β) as shown in Fig. 2.

This relation can be expressed as

$$C_p = f(\lambda, \beta) \quad (3)$$

The tip speed ratio is defined as:

$$\lambda = \frac{\omega_t R}{V_{wind}} \quad (4)$$

where, ω_t is the rotational speed (rad/sec) of the wind turbine.

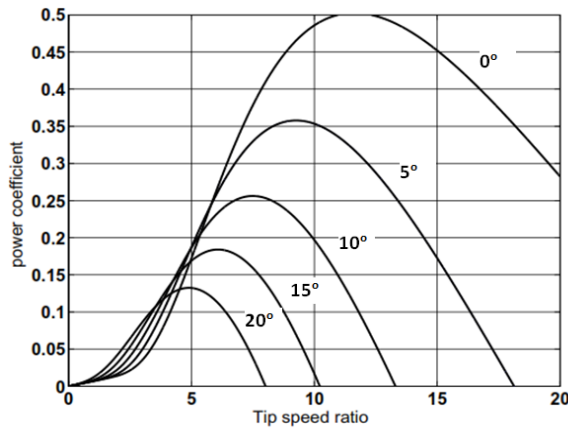


Fig. 2. Typical C_p - λ curves for different pitch angles (from 0° to 20°)

C. Permanent Magnet Synchronous Generator

The mathematical model of the PMSG is considered in per unit quantities. The model equations of the machine are voltages, torque, and mechanical expression [14], [15]. The machine voltage can be expressed in d-q axis as

$$v_{qs} = -R_s i_{qs} - \frac{\omega_e}{\omega_b} \lambda_{ds} + \frac{\omega_e}{\omega_b} \lambda_f - \frac{d\lambda_{qs}}{dt} \quad (5)$$

$$v_{ds} = -R_s i_{ds} + \frac{\omega_e}{\omega_b} \lambda_{qs} - \frac{d\lambda_{ds}}{dt} \quad (6)$$

where i_{ds} , i_{qs} are the stator direct, quadrature currents and R_s is the stator resistance. The base electrical angular frequency is ω_b and ω_e is the actual electrical speed in (rad/sec).

The flux linkages of the machine are

$$\lambda_{ds} = L_{ds} i_{ds} \quad (7)$$

$$\lambda_{qs} = L_{qs} i_{qs} \quad (8)$$

Substituting λ_{ds} and λ_{qs} in the machine voltage equations

$$v_{qs} = -R_s i_{qs} - \frac{\omega_e}{\omega_b} L_{ds} i_{ds} + \frac{\omega_e}{\omega_b} \lambda_f - L_{qs} \frac{di_{qs}}{dt} \quad (9)$$

$$v_{ds} = -R_s i_{ds} + \frac{\omega_e}{\omega_b} L_{qs} i_{qs} - L_{ds} \frac{di_{ds}}{dt} \quad (10)$$

The electromechanical torque can be expressed as

$$T_e = (\lambda_f i_{qs} + i_{qs} i_{ds} (L_{ds} - L_{qs})) \quad (11)$$

The system mechanical equation is expressed as follows,

$$T_e - T_m = 2H \frac{d(\frac{\omega_e}{\omega_b})}{dt} \quad (12)$$

Where H is the system inertia constant $= \frac{1}{2} J \omega_{bm}^2 / S_b$ and J is the system moment of inertia and ω_{bm} is the base mechanical speed in rad/sec and S_b is the base power.

D. Voltage Source Converter

Fully controlled voltage source converter, back-to-back connected configuration, is used in this study. The generator-side converter rectifies the generator output voltage to dc voltage and the grid-side converter converts the dc voltage to ac three-phase grid voltage. The converter switches are IGBT type. For modeling we will consider switch state either on or off and switching losses will be neglected.

The applied voltage at the machine terminal may be expressed as a function of the dc-link voltage and the switches status (Fig. 3).

Therefore the converter can be modeled as follows [16]:

$$\begin{bmatrix} v_{an} \\ v_{bn} \\ v_{cn} \end{bmatrix} = \frac{1}{3} V_{dc} \begin{bmatrix} 2 & -1 & -1 \\ -1 & 2 & -1 \\ -1 & -1 & 2 \end{bmatrix} \begin{bmatrix} S_a \\ S_b \\ S_c \end{bmatrix} \quad (13)$$

MDOF controller as illustrated in Fig. 5 depends on two sub-controllers, one is used for wide-range of error and the other sub-controller is considered for fine tuning of the output. This controller was introduced for fuzzy control improvement in [12], but it is proven to be applicable to PI as used in this work.

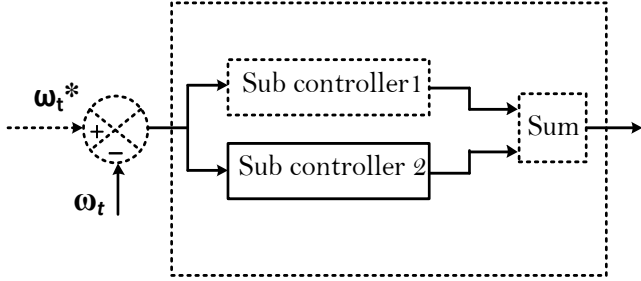


Fig. 5. MDOF sub-controllers

B. MPPT Control

For each wind turbine there are speed-power characteristics which are a function of wind speed and blade angle. Fixed blade angle turbine is considered at 0° as shown in Fig. 6. At each wind speed, operation of the system at maximum power point tracking (MPPT) provides the adequate reference rotor speed (ω_t^*).

Optimal rotational speed of the wind turbine rotor can be estimated based on the following equation [19],

$$\omega_{topt}^* = \frac{V_{wind} \lambda_{opt}}{R} \tag{23}$$

where λ_{opt} is the optimal tip speed ratio and the point of the maximum power operation occurs at this specific speed.

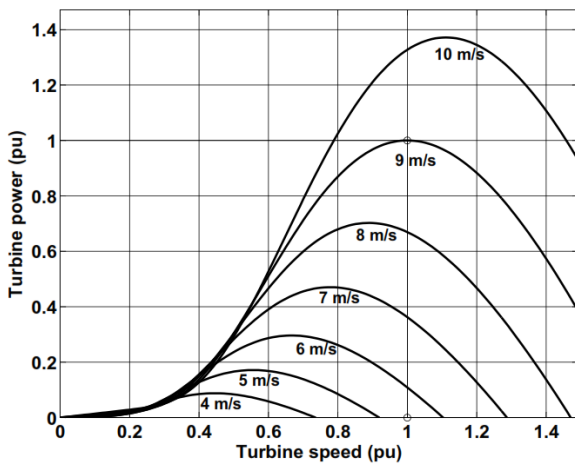


Fig. 6. Turbine power and speed pu curves at different wind speeds and 0° blade angle.

Comparing the actual turbine speed and the estimated optimal reference speed, activates the controller to ensure maximum power capture.

C. Grid-side Converter Control

The grid reference currents i_{dg}^* and i_{qg}^* have been set according to the desired dc-link voltage and the reactive power values, then the reference voltage components are generated by PI current controllers [17] as shown in Fig. 7. The driving signals for grid-side IGBT switches are generated using SVPWM similar to the machine-side converter (subsection 3.1) in order to maximize the range of the inverter output voltage. To ensure unity power factor at the connection to grid, i_{qg}^* is set to zero. Direct current component i_{dg}^* has been generated to keep the dc-link voltage constant at preset reference value. The grid angular frequency ω_g is determined using phase locked loop (PLL). Compensation components ΔV_{dg} and ΔV_{qg} are added to current controller output as illustrated in Fig. 7, where

$$\Delta V_{dg} = V_{dg} - \omega_g L_g i_{qg} \tag{24}$$

and

$$\Delta V_{qg} = \omega_g L_g i_{dg} \tag{25}$$

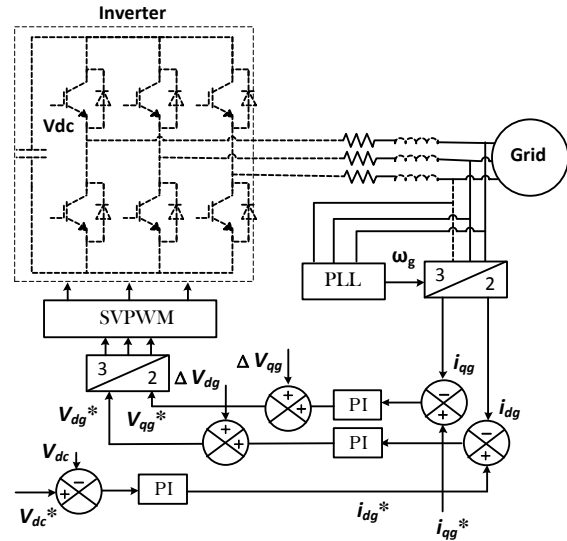


Fig. 7. Grid currents control loops.

IV. SIMULATION RESULTS

Simulation is carried out using Simulink for small wind turbine system that has parameters as given in the appendix. The system has been modeled and simulated under different operating conditions, starting at rated wind speed (9 m/sec). At time 0.6 sec from the starting the simulation wind speed has been changed from 9 m/sec to 8 m/sec, then at 1 sec time the wind speed has been increased to 9.5 as shown in Fig. 8.

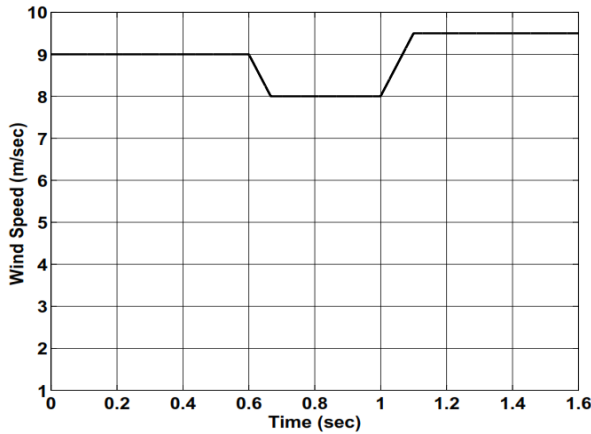


Fig. 8. Wind speed

At starting turbine mechanical torque has increased to reach its rated value, and it follows the wind speed profile at .6 and 1 sec consequently as shown in Fig. 9.

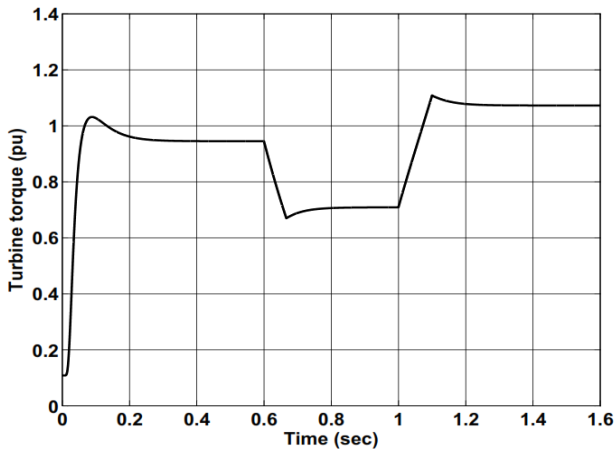


Fig. 9. Wind turbine mechanical torque.

The performance of the conventional PI controller and MDOF controller is shown in Fig. 10. Notice that error value and duration have been decreased with MDOF control strategy. The total efficiency and the system dynamic performance are improved keeping MPPT through modified MDOF controller at changes of wind speed. The effect of the wind gust and torque transients will result in a reduced influence on the system stability using MDOF controller.

The following simulation results for voltage, speed, and current are obtained using modified MDOF controller. Stator

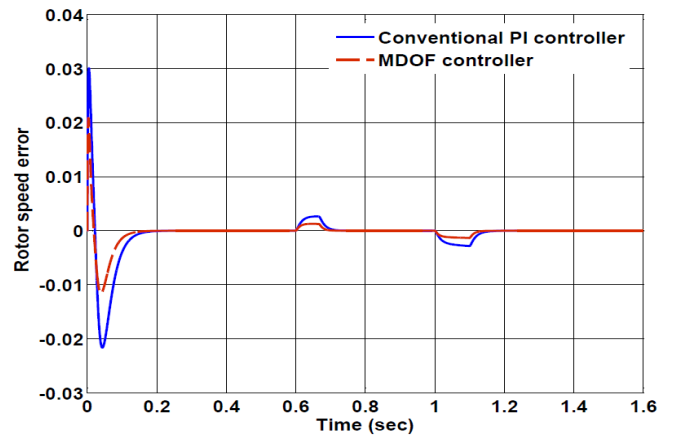


Fig. 10. Change of generator rotor speed.

terminal voltage is shown in Fig. 11, where the voltage depends on the electrical speed which started from zero and increased with the turbine mechanical speed and torque and continues to follow the wind speed changes as illustrated in Fig. 12.

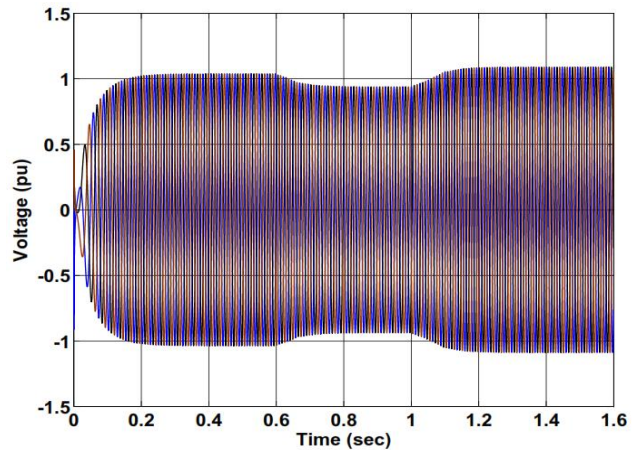


Fig. 11. Generator terminal voltage.

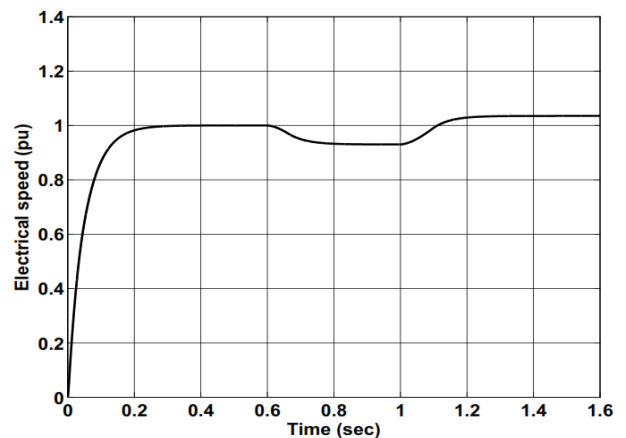


Fig. 12. Electrical speed (rad/sec)

Generator output current is controlled utilizing PI controllers in the rotating frame. The output three-phase current of the generator is shown in Fig. 13.

The dc-link voltage is kept constant at its reference set value using conventional PI controller as illustrated in Fig. 14. The transients of the system appear at dc-link during speed variations, but the controller tracks the reference value which insures system stability. Space vector pulse width modulation strategy is applied at the grid-side converter to deliver maximum power to the grid. Fig. 15 gives the produced voltage at the inverter output under SVPWM strategy. Unity power factor operation of grid-side inverter is clear as shown in Fig. 16, while the actual reactive component current (i_{qg}) is controlled to be around zero.

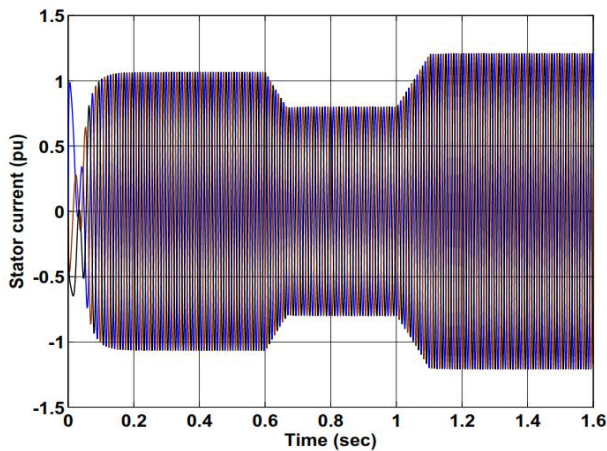


Fig. 13. Generator current.

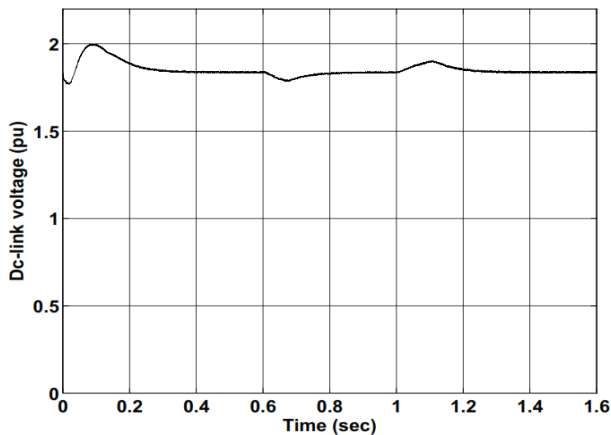


Fig. 14. Dc-link voltage.

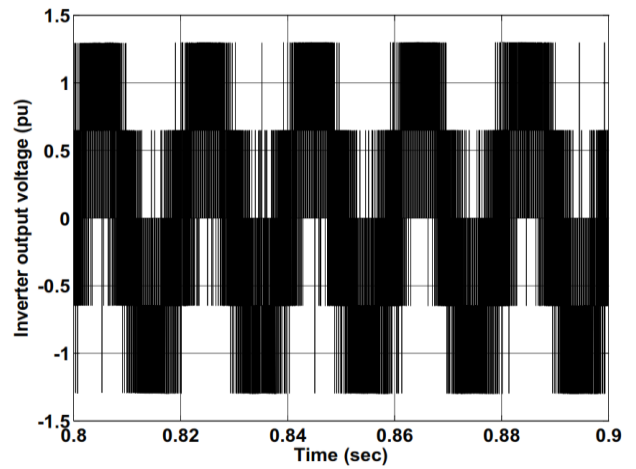


Fig. 15. Inverter output phase-voltage.

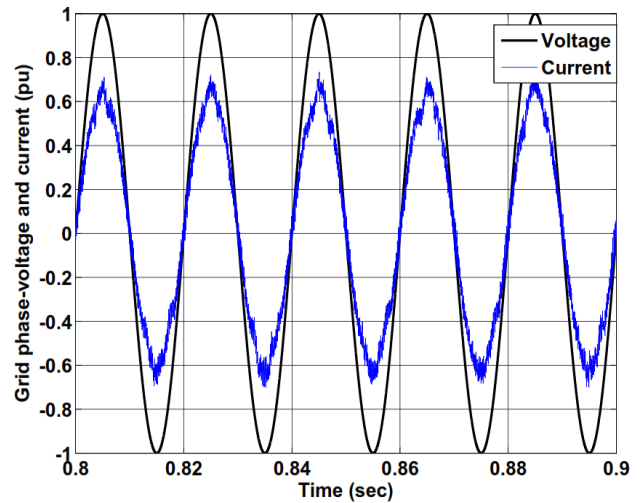


Fig. 16. Grid phase-voltage and current.

V. CONCLUSION

A novel speed controller is presented to improve the DDPMSG system performance at wind speed changes. The rotor speed controller uses MDOF concept to reduce the changes and duration of transients. This reduces stress at the rotor, while keeping maximum power point tracking (MPPT) with wind speed variation. The grid-side inverter has been controlled to keep the dc-link voltage at pre-set value and the current injected to the grid at unity power factor to achieve maximum power delivery to grid as a desired operating condition. The system has been modeled and simulated to realize the proposed controller effect on the performance improvement.

APPENDIX

The used wind turbine and generator parameters are shown in table 1 and 2.

Table 1. Wind turbine parameters [20].

Rated Power (W)	1000
Maximum output power (W)	1500
Start-up wind speed (m/s)	3
Rated wind speed (m/s)	9
Wind speed range (m/s)	3-25
Wind energy utilizing ratio (C_p)	0.45
Blade diameter (m)	3

Table 2. PMSG Parameters [21].

Power(W)	1000
Speed(rpm)	420
ω_m (rad/sec)	44
ω_e (rad/sec)	264
T_m (N.m)	22.7
voltage L-L(V)	220
p (pair poles)	6
Flux (Wb)	0.74
R_s (ohm)	12.6
Inductance L-L (mH)	92.5
$L_d=L_q$ (mH)	61.67
J rotor inertia(mr^2)	0.026
Frequency (Hz)	42

[9] K. Tan, and S. Islam, "Optimum control strategies in energy conversion of PMSG wind turbine system without mechanical sensors," *IEEE Trans. Energy Convers.*, vol. 19, no. 2, pp. 392-399, June 2004.

[10] H. Wang, C. Nayar, S. Jianhui, and M. Ding, "Control and Interfacing of a Grid-Connected Small-Scale Wind Turbine Generator," *IEEE Trans. Energy Convers.*, vol.26, no. 2, pp.428-434, June 2011.

[11] Z. Li, X. Liu, Z. Fan, C. Wen, G.Lu, and P. Wang, "Vector control strategy for small-scale grid connected PMSG wind turbine converter," in *Proc. 2nd PES/IEEE ISGTEurope*, 2011.

[12] F. Khater, F. Ahmed, and M. Abu El-Sebah, "Multi degree of freedom fuzzy controller," in *Proc. IEEE Int. Symp. Intelligent Control*, 8-8 Oct. 2003, pp.293-297, Houston, Texas, USA.

[13] V. Akhmatov, "Analysis of dynamic behavior of electric power systems with large amount of wind power," Ph.D. Thesis, NESA A/S, Technical Univ. of Denmark, 2003.

[14] P. C. Krause, "Analysis of electric machinery and drive systems, 2nd Edition," IEEE Press 2002.

[15] C. ONG, "Dynamic simulations of Electric Machinery: Using MATLAB/SIMULINK," Prentice Hall, 1997.

[16] F. Iov, A. Hansen, P. Sorensen, and F. Blaabjerg, "Wind turbine blockset in matlab/simulink," Tech. Rep., Aalborg Univ. and RISO, March 2004.

[17] Y. Yong, R. Yi, S. Huan-qing, T. Yan-yan, and Y. Ying, "Grid-connected inverter for wind power generation system," *Journal of Shanghai Univ.*, vol. 13, Issue 1, pp 51-56, Feb. 2009.

[18] W. Zheng-Guang, J. Jian-Xun, G. You-Guang, and Z. Jian-Guo, "SVPWM techniques and applications in HTS PMSM machines control," *Journal of Electronic Science and Technology of China*, vol. 6, no. 2, June 2008 .

[19] Y. Errami, and M. Ouassaid, "Modelling and control strategy of PMSG Based Variable Speed Wind Energy Conversion System," in *Proc. ICMS*, 2011, pp. 1-6.

[20] Anhui Hummer Dynamo Co., LTD, "H3.1-1KW wind turbine," Technical datasheet.

[21] DVE-technologies, "PMGI-1K-400," Technical datasheet.

REFERENCES

[1] T. Ackermann, "Wind power in power systems," New York: Wiley, 2005.

[2] S. A. Saleh, M. Khan, and M. A. Rahman, "Steady-state performance analysis and modeling of directly driven interior permanent magnet wind generators," *Renewable Power Generation, IET*, vol. 5, no. 2, pp. 137-147, March 2011.

[3] F. Khater, A. Shaltout, and A. Omar, "Direct driven PMSG for wind energy systems: A review," in *Proc. 11th Int. Conf. WVEC*, 3-5 July, 2012, Bonn, Germany.

[4] M. Rosadi, S. M. mayeen, R. Takashahi, and J. Tamura, "Novel control design of variable speed PM wind generator considering grid code requirement," in *Proc. 15th Int. Conf. ICEMS 2012*, Oct. 22-24, 2012, Sapporo, Japan.

[5] F. V. Hulle, "Large scale integration of wind energy in the European power supply analysis, issue and recommendations," Tech. Rep. EWEA, Dec. 2005.

[6] R. Keypour and R. Ilka, "Permanent magnet synchronous generator design for small wind turbines," *Int. Journal of Advanced Renewable Energy Research*, vol. 1, Issue. 11, pp. 635-641, 2012.

[7] L. Barote and C. Marinescu, "PMSG wind turbine system for residential applications," in *Proc. IEEE Int. Symp. SPEEDAM*, 14-16 June 2010, pp.772-777.

[8] H. Wei, Z. Jianhua, W. Ziping, and N. Ming, "Dynamic modeling and simulation of a Micro-turbine generation system in the micro grid," in *Proc. IEEE Int. Conf. ICSET*, 24-27 Nov. 2008, pp. 345-350.

Signal condition of embedded unit inputs

F.Hruska, M. Navratil, and J. Otahal

Abstract—Systems of informatics and automation use more and more at acquisition of data from sensor of measuring of circuit or informatics perimeters. Primary information is out of scanning sensor in sensor and subsequently this signal goes through process signal condition. This action of signal condition uses technical and program means. The basic technical means perform a verification range, limits effects of disturbing interference of external environment and makes filtration. Other way is software way where value is tested a real range or after existent model, speed of change of rising or dropping, does statistical balancing values, verification of uncertainties and errors of measurement and next operations. Significant application of those areas is used by embedded units.

Keywords—interference disturbance, signal condition, judgment of values, range limitation, statistical balancing, uncertainty and error of measurement.

I. INTRODUCTION

QUALITY of signal condition out of sensors or readers according to measurement on continual production processes in chemistry, on manipulation of petroleum, in power engineering and in other regions of industry significantly influences function of control and monitoring systems. Random fluctuation and errors from measurement incurred in measuring circuit, disturbance of interference in environment of signals and next influences they may depreciate function of advanced control systems as far as to peril safety factor and quality of production.

Which are the possibilities to remove these problems and to ensure the high - quality functions of informatics and control systems? There are on the one hand engineering units and on the other side some programmable methods. A scheme is in “Fig. 1 Block scheme of signal condition of sensors”.

The other look on processes of acquisition and data processing is shown in “Fig. 2 Scheme of input part of signal condition” for processes of measurement of physical quantities and information reading. The processes are divided in function blocks A1- A5, on transmission of signals, data and information up 01 to 05 with additional operations and in blocks SW1 and SW2 of program processing.

F. Hruska is with the Faculty of Applied Informatics, Tomas Bata University in Zlin, Nad Stranemi 4511, CZ 76005 Zlin, Czech Republic.

M. Navratil is with the Faculty of Applied Informatics, Tomas Bata University in Zlin, Nad Stranemi 4511, CZ 76005 Zlin, Czech.

J. Otahal is with the Faculty of Applied Informatics, Tomas Bata University in Zlin, Nad Stranemi 4511, CZ 76005 Zlin, Czech Republic.

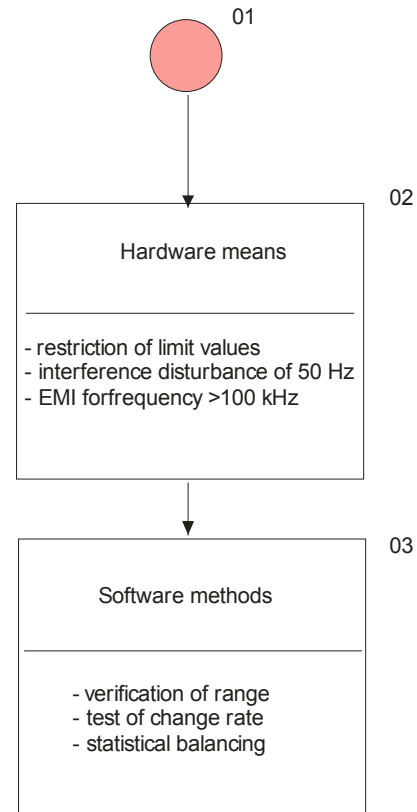


Fig. 1 Block scheme of signal condition of sensors

The block A1 is created of physical environment (temperature, parameters of liquids,..) or data carrier (barcode, tag of RFID, picture, sound) and it is scanned of sensing elements from a block A2 and the primary signals are converted in signals of electric unified voltage. In face of entrance into central unit is registered the block A4 for additional hardware check - up of signal. There is safe no overfullfilment of limit value, removing of disturbance using circuits of galvanic separation and filtration of bad frequency of way of band filter.

Input part of central unit, the block A5, has parts to input signal conditioning mean of PGA, an analog numerical conversion and quantization. Next to the hardware part includes the block also a part of software to verification of range, tendency and setting sampling and to computation accordance with existent functional relation, to statistic processing and to statistic balancing. [1]

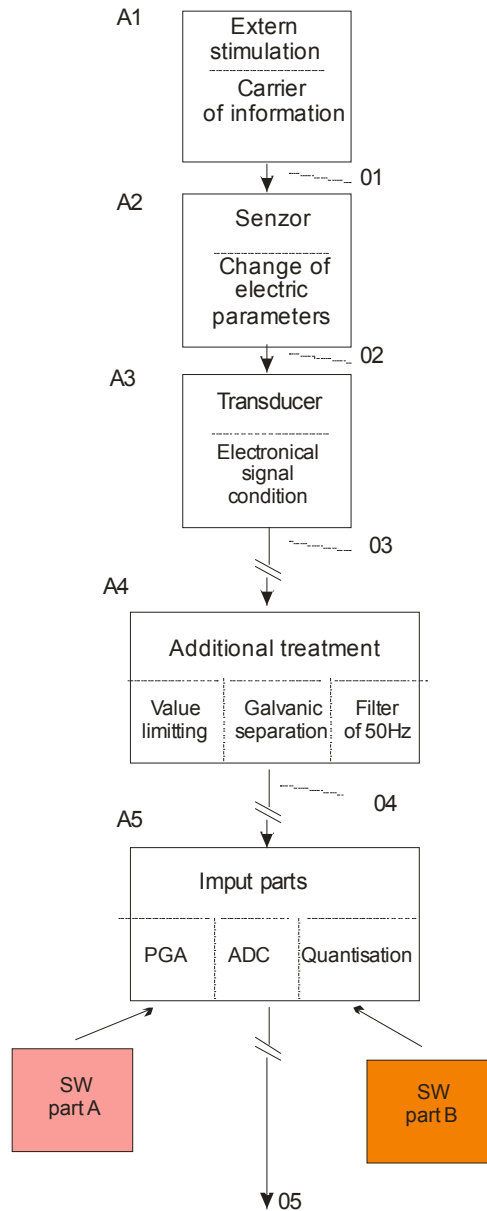


Fig. 2 Scheme of input part of signal condition

II. TECHNICAL MEANS OF SIGNAL CONDITION

Standard technical means provide basic function of instrument from sensors up to embedded or central units. There are at the beginning the sensors working on physical principles, when outer stimulates of measured environment changes most often electrical characteristics or parameters of matter of sensor and systems. The non-unified primary signal out sensors is specific, e.g. alternation of electrical resistance, capacities and inductivities, changes of electric potential or electric charge and there is necessary it electronically set up to unified signal, most frequently as a voltage DC in the range from 0 V up to 10V or current 4- 20 mA. By these operations but there are increased some problems from electric disturbance and therefore this chain has to add specific elements, like to limit maximum signal value, galvanic separation etc.

Specific operation is affected already in electronic circuit on exit of sensors or at connection with converter. There is e.g. and wiring to compensation of longitude of cables, correction of other parallel influences,. There is also a limitation of influence of electromagnetic interference, by using twisting and shielded cables. [2,3,4]

A. Limitation of signal maximum

Enter data are in real environment effected by many factors first of all influences of other electric systems. One from many consequences there is unfair or and dangerous increasing signal level. Like first and basic procuracy is limitation of value of amplitude of signal via using added electronic circuits.

As a tested solution can be bring in wiring accordance with “Fig. 3 Circuit with the voltage reference TL431”.

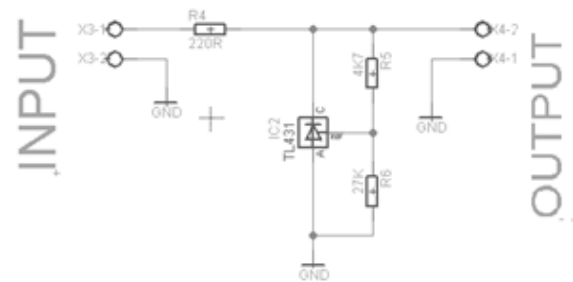


Fig. 3 Circuit with the voltage reference TL431

The circuit serves has a protective or regulative function on input. The circuit with programmable voltage reference LM431 was experimentally created for behaving as an ideal Zener diode. Saturation voltage of IC was set to 2.9V. The output has a maximum constant voltage according to values of resistors of R5 and R6.

This circuit was tested and simulated, its static and dynamic behaviors in the environment of Matlab Simulink and was compared with real circuit of data measurements.

B. Remove and limitation influence of electric interference

A source of electric disturbance and overrunning limit values there is the electromagnetic interference. Electromagnetic interference (EMI) is a process of emission and immission of electromagnetic field or electromagnetic radiation. Emission generates electromagnetic field or radiation from electric devices or electrical lines into free space. Immission is a state of environment where is created field and accordance with concrete conditions this field affects other electrical equipment. [2]

Coupling between elements of EMI is realized by cable as galvanic structure or in environment as capacitive or inductive structure. General view on EMI shows “Fig.4 Scheme of general view on EMI”. [1]

Scheme of generating of disturbing harmonic voltage under EMI and their incidence on measuring circle is showed in “Fig.5 Influence of interference voltage to measured signal”. Source of data signal has voltage U_m and it is carried over signal in unit A2 with load resistance R_i of unit of signal

processing and carry over signal give upon input device A2 load angle resistance Ri troop for signal processing.

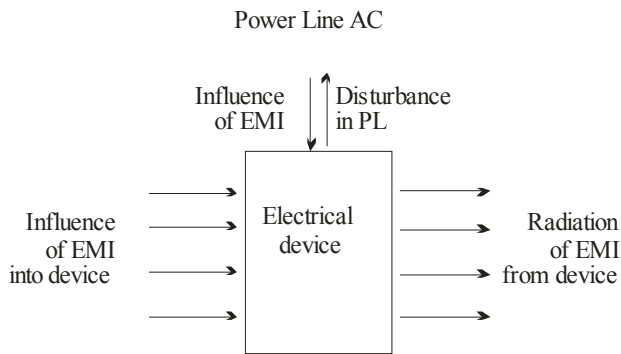


Fig.4 Scheme of general view on EMI

Power phasic lead uses electric current I_{inter} about voltage U_{inter} . Power control interferential field functions over capacity coupling C_1, C_2 on signal lead. Magnetic interferential field B_1 is transformed to the signal circuit. This harmonic disturbance forms disturbing series mode voltage U_{SM} and common mode voltage near U_{CM} . Influences of differences of earth current rises another disturbing harmonics tension, which adds to conformable voltage U_{CM} . On input device there are disturbing voltage superposed on voltage measuring signal U_{land} .

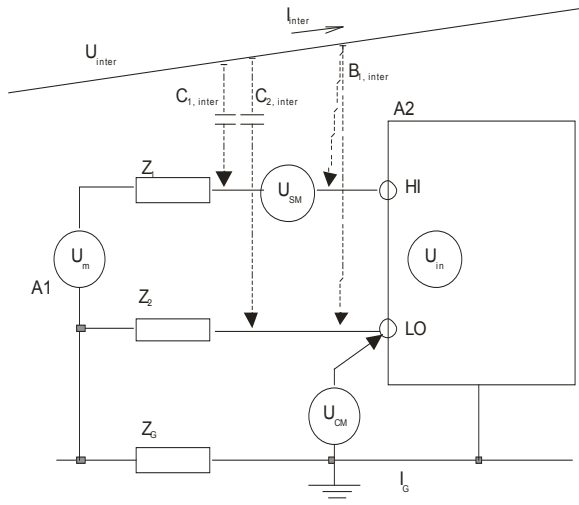


Fig.5 Influence of interference voltage to measured signal

Very important aspect at composition of technical means there is electric parameters of binding periphery it is output and input of following element. At those structures correct voltage level, kind of voltage, correct output and input impedance of interconnected periphery and frequency characteristic have be realized.

C. Limitation of EMI

Distance of lead with data from cables AC of limitation of influence of disturbance of EMI is possible achieve: of distance of data cables from radius of power cables AC, of using the high - quality signal and data cables with twisting pairs for elimination of frequency of 50Hz, of shielding of

cables against a strong electric field and of galvanic separation.

The galvanic separation is possibility to isolate mainly the earthy currents. There has been tested a module. The linear optocoupler IL300 was used in the same schematic as in the datasheet for IL300. The scheme in “Fig.6 Circuit with the optocoupler IL300” shows the tested connection and the results of tests confirmed the circuit. The output is strictly linear.

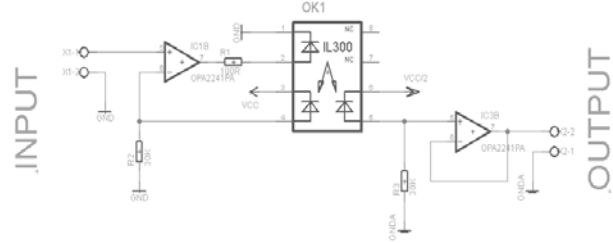


Fig.6 Circuit with the optocoupler IL300

D. Sampling and quantizing

Analog continuous signal from sensors on entrance have to be converted in technical circuits on binary number. The conversion runs in two phases. At first there is will performed sampling of signal and then quantitation follows quantization. This operations are very important during the processes of signal condition.

The error of sampling can able indeed yet very worse. If namely in original analog signal is occurred frequency higher than is half of sampling rate (given a name also Nyquist frequency), will get accordance with Shannon theorem to total and irrevocable distortion signal thanks effect aliasing. The aliasing can be prevented only so - called anti - aliasing filter, which is low-pass filter registered before converter. The low-pass filter will forbid to input frequencies higher than is Nyquist frequency into the AD converter.

Because digital signal as a rule is processed on equipment working in binary numeric system, there are the numbers of quantized levels of A/D converters as a rule equal with N the power of number 2, and the quantized signal can be imply in N bits.

If would give up the sizes of errors of particular samples into chart, it would come into being random signal, which is named quantized noise. The size of noise is emitted as index number in decibels, namely as a relation of useful signal to noise. Because number in denominator of fragment - quantitated error is near of all linear converters the same (interval +1/2 up to 1/2 quantified levels), it depends size of quantified noise only on numerator of fragment, it is on the size of useful signal, which is maximum number of quantified levels of existent converter.

III. SOFTWARE METHODS

Software means can affect significantly processes signal condition. There are in the main operations computation of

measured values to equivalent physical quantity, checking errors and uncertainties in measurement, calculations of indirect measurement, statistical balancing.

Recomputation of measured values to data and values of physical quantity after AD conversion are first software operation together with rounding. Recalculation uses statistic transform function the general formula is:

$$y = f(x) + \sum_{j=1}^n g_j(v_1, v_2, \dots, v_p) \quad (1)$$

where is y output of function, f(x) transform function with measured value x, g function of disturbing from influences v₁ up to v_p.

A. Uncertainty and errors in measurement

Process of measurement is process of stochastic system. It is impressed with rising random, systematic eventually rude errors.

Random errors have reasons in stochastic actions. Absolute value and mark of these errors is described according to law of probability. These errors it is impossible except. At their determination there is necessary to evaluate repeated measurement behind same conditions by the help of statistic methods. Evaluation of result of measurement employs calculations:

The arithmetical average:

$$\bar{x} = \frac{1}{n} \sum_{i=1}^n x_i \quad (2)$$

where is x_i value measured in step i, n number of repetition of measurement.

The selection variance of repeated measuring:

$$s^2 = \frac{1}{n-1} \sum_{i=1}^n (x_i - \bar{x})^2 \quad (3)$$

which determines deviation of random error for explicit probability

The selection variance of the arithmetical average:

$$s_{\bar{x}}^2 = \frac{s^2}{n} \quad (4)$$

Systematic errors have some reasons at suggestion and implementation of measurement system. They exist then, when at suggestion there are not detected their causes, there are not compensated their influence and not performed necessary correction. Not detected systematic errors are assessed at determination of uncertainties in measurement.

Uncertainties in measurement define values as parameter of measurement accordance with real conditions. Perfect knowledge requires to obtain relevant information in the process of measurement. To primary resources of uncertainties in measurement there are placed e.g. incomplete definition of metered quantity, non-representative range of samples of measurement, unknown conditions of measurement, errors of human factor at hand data collection, incorrectly intended

accuracy of instrument, inaccurate values of constants for evaluation of signals and other.

Uncertainty in measurement for concrete metering is determined uncertainties of type A of date according to statistic methods and uncertainties of type B, which are non-measurable and which are expertly estimated.

Uncertainty of type A equals with standard deviation of arithmetic average of sample of measurement at n>10 number of measurement and has the formula :

$$u_{A,x} = s_{\bar{x}} = \sqrt{\frac{1}{n(n-1)} \sum_{i=1}^n (x_i - \bar{x})^2} \quad (5)$$

Uncertainties of type B is estimated for every source of uncertainties accordance with range of possible changes of deviation from nominal value +/- z_{and,max}. Concrete calculation uncertainties of type B are:

$$u_{B,z_i} = \frac{z_{j,max}}{k} \quad (6)$$

where is k value for selected approximation of probability distribution, for normal (Gauss) partition (N) is k= 3, for equable rectangular partition (C) is k=3^{0,5}, for triangular partition (S) them to= 2,45, for bimodal partition (U) is k= 1.

Total uncertainty of measurement is according to formula:

$$u_x = \sqrt{u_{A,x}^2 + u_{B,x}^2} \quad (7)$$

On entry of system there is come signal of dynamic changing and rise other errors. Problem of dynamics is given according with inertia of system. The base of description is dynamic characteristics, which takes in consideration all dynamic influences. Description is via form of differential equation, image or frequency transmission, and logarithmic frequency characteristics.

B. Statistic balancing of measurement

Statistical balancing of measured data (data reconciliation - DR) is effective method for total improvement of file of measured data. Make use of mathematical models and natural laws. [5,6]

Models of measurement is come - out from static characteristics of dependence of exit/entrance. There is able to partly model of polynomial relation (reduction of measured temperature at sensor Pt100) or model of exponential relation at evaluation of sensor NTC or about common matrix model.

Statistical balancing of data was developed in effective and extensive method of complex elaboration of measured data, there is utilized all information included in information. The DR method (obtaining of consistent data) is also base to data validation (exclusion of rude and systematic errors of measurement). The method DR is possible apply only in cases of redundant measurement.

The basic idea of DR is repair (balance) measured values so, that date has to bring near mostly to (unknown) correct values of measured quantity. Well - balanced values x_{and}' are obtained from relation:

$$x_i = x_i^+ + v_i \quad (8)$$

where to measured values are added so - called corrections v_{ind} . In ideal case the corrections would have to be equal with in the negative taken errors; these however aren't known. If is if but I known a mathematical model, to which correct values agree with, there is the best possible solving its, which is based in method of maximum credibility.

Well - balanced values conform to two basic conditions:

1. Balanced values of metered quantities are agreed with physical laws, so they are consistent with them, whereas this condition is possible write down in form

$$F(x', y', c) = 0 \quad (9)$$

where is F a vector of formulas according to mathematical model of technological process, x' vector directly plumbed quantities, y' vector of indirectly of metered (derived) quantities, c vector of exactly known constants.

2. Sum of all corrections of measured data is minimal, whereas corrections are defined so, in order to sum of squares of weighted corrections (weight oh) which has to be minimum, and pays

$$Q_{\min} = \sum \left(\frac{(x^+ - x_i)}{\delta} \right)^2 \Rightarrow \min \quad (10)$$

Sizes of corrections have to grant a inequality:

$$Q_{\text{krit}} > Q_{\min} \quad (11)$$

where is Q_{krit} critical value χ^2 partition with v steps of freedom assessed accordance with Gauss theory of errors (value Q_{krit} for existents v is introduced in statistic tables).

If inequality (5) isn't fulfilled, it means , that the DR detected present of rough error in measurement. In such a case it is impossible balanced data further to use, although the agreement with physical laws, because isn't fulfilled the criterion of Gauss's error distribution.

IV. CONCLUSION

The paper deals with aspects of improving the operations of signal condition at inputs side of embedded system. There is the possibility via hardware means and software methods. In the software there is very important the statistical date reconciliation.

Statistical reconciliation of measured data is the prospective method and leads practically to optimization of technological arrangement, reduce to operating costs, service costs, increases responsibility and safety factor of function system.

REFERENCES

- [1] F.Hruska, "Aspects of electromagnetic interference", in *Proc. 4th International Conference on Circuits, Systems, Control, Signals (ICSCS '13)*. Valencia, 2013, pp. 33-36.
- [2] J.Otahal et al, "Protections of embedded system inputs", in *Proc. 13th WSEAS International Conference on Automatic Control, Modelling and Simulation (ACMOS '11)*. 2011, pp. 407-411.
- [3] J.Otahal and F.Hruska, "The reasons for use and description of the circuit with linear optocoupler IL300", in *Proc. 22nd International DAAAM Symposium*, Vienna 2011, pp 0815-0816.

- [4] J.Otahal and F.Hruska, "Possible protections of embeded systems inputs", in *Proc.22nd International DAAAM Symposium*, Vienna 2011, pp 0813- 0814.
- [5] J.Otahal and F.Hruska, "Dynamic identification of circuit with linear optocoupler IL300", in *Proc. 22nd International DAAAM Symposium*, Vienna 2011, pp 0809-0810.
- [6] F. Madron, V.V.Veverka, and M.Hostalek, "Process optimization in power industry", in *Conf. Rec. IEEE Int. Conf. Communications*, 1995, pp. 3-8.

An operational model of bus terminal management based on daily passengers demands

José A. M. de Gouveia, Maurício L. Ferreira, Maria L. R. P. Dias, Melissa S. Porkorny, Eduardo M. Dias

Abstract—This article aims to tackle management operational model of public transport as a guideline with the consolidation of the operating efficiency of the municipal bus terminals, based on the use of ubiquitous technology [1] and concept of Big Data [2]. As well to be used in obtaining and processing information of passenger demand, to be collected and processed in real time, in order to maximize resource utilization and fleet operators, to meet the needs of users of the displacement of the system, reducing the waiting time on platforms, shipments and travel providing a better quality of life for the population, as well as the improvement of environmental conditions through the reduction of pollutants into the atmosphere. In this proposed model the main purpose is to qualify transportation services with the enhancement of the use of RFID [3] technology and Big Data [2] for the collection and processing of information by ensuring the implementation of activities based on standards developed by adopting the best practices of work. As well aiming at increase of satisfaction and quality of transportation service.

Keywords—Technology ubiquitous concept of Big Data, needs displacement, quality transportation service, environmental conditions.

I. INTRODUCTION

THE city of São Paulo with already industrial city profile, today can be considered as a major pole of attraction for businesses and services, in this way transport systems face each day a greater demand for offsets without the traditional transport planning which can follow this growing trend with proper implementation of urban infrastructure and other necessary investments.

Currently the manager and operator of transport do not have the information in real time about conditions of

J. A. de Golveia is systems analyst of São Paulo Transporte - SPTrans, R. Boa Vista n.236, São Paulo/SP, Brazil, CEP 01014-000 (e-mail: jose.golveia@gmail.com).

M. Lima is project coordinator of São Paulo Transporte - SPTrans and a PhD student at Escola Politécnica of the Universidade de São Paulo (Polytechnic School of the University of São Paulo) (mauriciolima7@usp.br).

M. L. R. P. Dias is a PhD student at Escola Politécnica da Universidade de São Paulo (Polytechnic School of the University of São Paulo) (lidiadias@pea.usp.br).

M. S. Pokorny is a PhD student of Polytechnic School, University of São Paulo – USP and a researcher of GAESI (melissapokorny@pea.usp.br)

E. M. Dias is full professor of the Escola Politécnica of the Universidade de São Paulo and coordinator of GAESI - Grupo de Automação Elétrica em Sistemas Industriais, a reseach group of the Electrical Energy and Automation Department, Escola Politécnica, Universidade de São Paulo, Av. Prof. Luciano Gualberto, trav. 3, n. 158, São Paulo/SP, Brazil, CEP 05508-970 (emdias@pea.usp.br).

manning of vehicles and platforms in order to provide available resources at runtime in a rational way, providing better service and flow of movement of vehicles and passengers.

Considering municipal terminals as elements of regional integration, the City's proposed model aims to collect and process data on the daily movement of users in access, shipments, vehicles and the effective use of services (destinations) offered, aiming to reduce the time of passengers waiting on the platform, better use of resources fleet in order to avoid accumulation of vehicles at its facilities and access, providing better fluidity of movement, maximizing performance and avoiding saturation, and this (model) is geared to efficiency, productivity and quality of operation that is extended to the entire mass transit system.

Operational management of the terminal should enforce the use of the information of passengers commuting via public transportation, properly addressed in ITS applications - (Intelligent Transportation System) and Big Data at runtime which in turn rely the advances in telecommunication and positioning via GPS. Taking into consideration the use of other technologies such as Radio Frequency identification (RFID) in the identification of travel profiles through the use of tag in smart card payment (Billete Unico) cards and readers / antennas installed in vehicles, accesses, platforms and crossing points extending to the terminal corridors and other stopping points of the bus.

The mobility data collected will be used in real time by management, supervision and planning teams in solving performance problems of the system through improving both terminal functioning and services provided by external actors.

The elaboration and systematization of measures of operating performance was only possible by performing costly field surveys, since data regarding the regional mobility of the population does not include municipal passenger terminals.

The organization of travel distribution will be essential to meet the mobility needs of the city. This management model aims to increase the capacity of transport systems in terminals correlating the various operational elements, creating indexes of fluidity and performance of the operation, based on the conditions of platforms occupancy, access and vehicles considering the best service to be

provided. The model is also guided by a combination of historical data and the profile of dislocations of users, the occupancy rate of vehicles and points charts that meet the lines involved in axis scroll managed, as well as projections of traffic, in order to increase the commercial speed of buses, safety displacement and reduce the negative impacts of mass transit operations on the environment and mobility in the city.

Such objectives can be achieved by collecting and processing information at runtime, from the integration and interoperability of joint systems and embedded devices as well as in providing a planning framework based on historical data around which can develop permanent interaction between those responsible for monitoring and fleet management, guiding the actions of regulation of the transport system by bus terminals.

Simultaneously, it is proposed to increase the capacity of the remaining operational control centers (Central, Regional and Operator and future Mobility Centre) to track, monitor and integrate preventive actions, especially in sections where saturation of vehicles and road system may occur, or any other type of conditions that may pose risks to the operation of the buses.

Even though the potential for covering various classes of transport, this proposal focuses on management mode of The Passengers Bus Terminal, with the aim of providing improvements in management and care of the user needs and other stakeholders.

A. Context

The city of Sao Paulo has a population of over 10 million inhabitants. If 38 surrounding counties will be added, the result will reach almost 17 million people. In the metropolitan area, about 55% of motorized trips are made by public transport, a total of 6.3 million passengers per working day [4].

To meet the such demand, the city currently maintains 30 municipal bus terminals, 10 of which are equipped with technology (smart terminals) and bus lines operated by private companies, under the management of Sao Paulo Transporte SA - SPTrans. The system is operated by 16 consortia formed by companies and cooperatives, responsible for the operation of 15 thousand vehicles which operate in more than 1300 lines [4].

In accordance with the Law 13.241/01 and Decree No. 43.582/03 is for the city of São Paulo, through the Municipal Transportation - SMT organize, operate and supervise the public transport services in its various modes [4].

The Municipal Transportation System is composed of an integrated network, created by the City Department of Transportation, in conjunction with SPTrans in 2003. Such a network allows quicker shifting and rational use of means of transport in the city. [4]

To better meet the demands of bus transportation in the

city mass transit system was divided into two auxiliary and complementary systems:

1) Structural subsystem

Aimed to meet the high demands of displacement that target from various regions and regional centers to the city central areas. To fully meet these connections, this subsystem main characteristic is to operate on the main axes of displacement and transport corridors with vehicles of medium and large size (articulated and bi-articulated).

In the general structure this integrated network service is considered as the backbone of public transport as it provides the connection to the various regions, as well as connects several regional centers to the city center.

2) Local subsystems

Aimed to meet the demands with short displacements needed in outlying areas, especially in places with limited road vehicles and feed the system of structural mesh, allowing the attendance to points of connection with the structural subsystem and/or sub-centers through lines operated by public buses and smaller vehicles, such as: minibuses, small buses and midi-buses.

To facilitate the organization of the lines, the city was subdivided into eight areas, each with a different consortium and cooperative, and the vehicles follow the same color pattern, according to adopted visual identity.

Nevertheless, the implementation of the activity of the public transportation planning at the level of specification is needed. Having in mind that various elements influence the planning process, such as the identification of the basic relationships between the main needs of population, in context of the physical conditions of the neighborhood and other characteristics of the city; the influence of the operating conditions of the transport system and its permeability in the road system.

In order to regulate, guide and monitor the implementation of the provided services OSO's-Service Orders by the Managing Operating System are issued which stipulate the amount of matches, fleet type and other characteristics for the performance of the activity by the dealer or grantee of public transportation system.

B. Problem

With a lack of knowledge of the relationships between displacements and the other conditions of the city as well as its influences on the services of public transport, regulation through the execution of orders (OSO) is insufficient to understand due to the unfavorable conditions to the transaction, whether in a particular terminal or in its background and feeder systems (structural and local).

Regarding the complementary operational measures, which must be taken into account to restore normal operation, the indicators of production and productivity should be considered (capacity and demand; occupation of platforms and intermediate points; contracted level of service and commercial medium speed).

Exceptionally service orders do not show adaptability in adverse situations (meteorological factors, heavy traffic, strikes and other events) that may alter the conditions of service causing discomfort to users.

There are currently no means of telling with the online Monitoring System SPTrans if any service is being impaired, in this case those responsible for the supervision and control of the fleet, communicate to teams of monitoring and management, to the operator to replace certain vehicle (broken or damaged in a traffic accident) or forwarding a particular service to a particular point of the line or terminal, in order to avoid losses on the needs of displacements of the system users.

Do not always the decisions taken by the management team of operation produce an effective monitoring, as determined correction action of a specific problem in a line, may trigger sequence of adverse events that may cause deregulation of the system, including: increased waiting time at bus stop, increase in travel time, increase of saturation levels of service in bus terminals and the worsening of unfavorable conditions of the flow due to the insertion of a service on a road already saturated.

Besides these situations, the operations of terminals in the central areas of cities are influenced by scarcity of physical space for operation and internal circulation, as well as the traffic conditions and access. Such factors may cause delays in the scheduled departures due to greater accumulation of passengers on platforms and increasing the waiting time and boarding the vehicles.

During morning peaks central terminals have large flow of vehicles approaching the bus lines more frequently operating, with platforms space not sufficient to accommodate all the buses arriving in the terminal and passenger demand relatively lower compared to the peripheral terminals in the same time.

In this case, the vehicles tend to wait for the departure time while the others move between platforms waiting for space parking. In this situation, operators have capacity of peripheral terminals reduced to the maintenance of the scheduled fleet, generating the accumulation of users on the platform, and in some cases the vehicles are only released for departure after the arrival of another vehicle of the same line, causing the cascading effect.

Depending on the geographic location of the terminal in the city and the design of the public transport network, the fluctuation of supply in various parts of the system results in greater movement in the terminal, often surpassing its ability to meet the pent-up demand in platforms. The traffic generated as a result of these facts affect the circulation of buses and vehicles in their vicinity in general.

Another fact to be added to understand the behavior patterns of users in a given terminal, in some cases it is observed that during the morning boarding peak passengers use the first vehicle available, while in the afternoon peak there is trend to wait in line for less crowded bus to travel

sitting.

C. Purpose

This article aims to apply the methodology and use of ITS (Intelligent Transportation System) tools, integrating the information acquired in the module for monitoring and controlling the fleet together with the adoption of new models of operational management.

Furthermore, it allows the adoption of knowledge for the operational management from Terminal Transfer, allowing these urban facilities greater autonomy in control of the services, with the use of monitoring information across spatial location latitude and longitude of embedded devices (GPS / AVL [5]), the data collected and processed in real time, using the technologies of data collection, radio frequency - RFID, using tag (to be installed in public terminal equipments, breakpoints and corridors and Smart's charge cards - Bilhete Único) combined with historical data of the displacements of users via public transportation [7].

The information provided to assist management teams in system operation and decision making adjustments to the regulation of services, determined by the orders of operation service (OSO), taking into account the level of current service in vehicles and approximate ratio of users on the platforms of the terminal.

The proposed model will maintain correlations with the conditions of fluidity of regional transit and other related factors that can change the characteristic of the operation or the commercial speed, with the premise of providing information to users about the conditions of manning of vehicles approaching and alternative displacement, based on the application of the concept of systems with big data.

The proposed these technologies in conjunction with the new management model may provide a better understanding of the behavior of the transport system, allowing the validation of proposed models with the current conditions (reprogramming, changes lines), filling partially empty gap within the existing literature with regard to the basic principles of planning and operation with the reality of the system.

D. Relevance

The relevance of this topic is given to the fact that the system monitor the real-time location of buses, following the evolution of its service level according to the behavior profile of demands over the route of the line. The quality of transport is also related to the capacity of the vehicles, and the users' perception, the last parameter depends on the period in which passengers use the system.

In this case, the evaluation of the capacity factor is through the relationship between the number of passengers inside the bus and its stretch and critical period, to maximum capacity and vehicle capacity.

With the identification of tag of payment cards and other embedded devices (AVL / GPS [5]) any change of pattern in

the level of service in operation, saturation of demand in terminals or intermediate points of the bus lines will be communicated to the teams of System Management and monitoring.

The management model can provide alternative service based on:

- 1) Current conditions of displacement of passengers compared with historical data source and destination [7] and the evolution of the displacements at runtime of tags;
- 2) Application of projection level of service using parameters employed by the management of services, which will be calculated based on a combination of established quality standard data of manning of vehicles in operation lines (Ferraz, 1990), monitored at runtime collected from tags (Mauricio Lima 2013) emerged with historical data for demand response in the intermediate and terminal points;
- 3) Recommendation of measures to regulate the operation of services allocated in accordance with the minimum standards for occupancy of the terminal platforms, based on the provisions of the Transit Capacity and Quality of Service Manual 2nd Edition (Part 7/Station and Terminal Capacity) including fleet availability and operational costs;
- 4) Provision of information for the planning teams and managers of service provider, to improve the adequacy of the terms of schedules of work orders (OSO) according to changes in demand or other factors arising;
- 5) Indication of teams that have irregular operating

conditions or level of service at runtime in order to be monitored, as well as finding irregularities, and further penalisation;

- 6) Service of contingency systems until a situation of discrepancy can be bypassed (eg strikes, high capacity, adverse weather conditions, demonstrations, blocked traffic, and other system failures).

II. DEVELOPMENT

Terminals allow passengers to make bus travel between points of interest so they can freely choose between various combinations in order to reach destination. Performance measurements can be made on the operational conditions of the whole system, since that is where greater intensity the problems of operation of lines and corridors are reflected with.

The proposed model of management operation terminal provides with information displacements of users at runtime, based on data collected by the antennas RFID readers installed at the access and circulation areas of people and vehicles.

This process of automatic exchange of data between the device middleware [6] RFID system, filters, and aggregate identification labels tag that RFID reader processed with spatial reference latitude and longitude of embedded devices (GPS / AVL [5]).

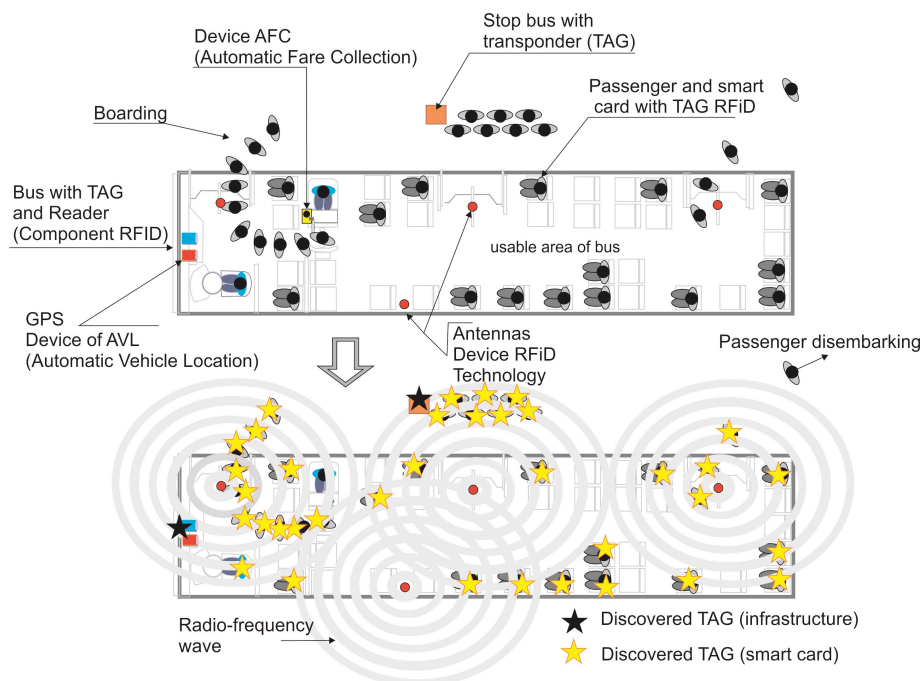


Fig. 1 - Proposed model for data collection by tags – Mauricio Lima 2013

Source: M. Lima, E. Dias, 2014, Real time monitoring of public transit passenger flows through Radio Frequency Identification - RFID technology embedded in fare smart cards, (in print)

For determining the level of service contracted, combination of the following procedures should be applied:

- 1) The proposed data collection by tags - Maurício Lima (2013);
- 2) Historical values of the exchange supply and demand;
- 3) Conditions for saturation of platforms and standards levels of service as the manning of vehicles Ferraz (1990) [8], which in Table 01, the lower the density of passengers, the better the quality of the transport service.

Table 01 - Standard quality manning of vehicles [8]

Level of Service	Density (Passenger/m ²)
A	Only sitting
B	0 a 1,5
C	1,5 a 3,0
D	3,0 a 4,5
E	4,5 a 6,0
F	>6,0

Source: Ferraz (1990)

- 4) For the conditions of saturation of the terminal platforms on the proposed study the adaptation of service-level model is needed for common circulation area (TCQSM, 2003) [9] with:

- Level of Service "A" - Walking speeds freely selected; conflicts with other pedestrians unlikely.

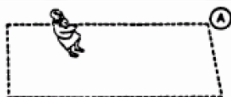


Fig. 2 - Level of Service 'A'
Source: TCQSM, 2003

- Level of Service "B" - Walking speeds freely selected; pedestrians respond to presence of others.



Fig. 3: Level of Service 'B'
Source: TCQSM, 2003

- Level of Service "C" - speed walk freely selected; unidirectional flows there can be shocks; minor

conflicts in the opposite direction and crusaders motion.



Figure 4: Level of Service 'C'
Source: TCQSM, 2003

- Level of Service "D" – Freedom to select walking speed and pass others is restricted; high probability of conflicts for reverse or cross movements.



Figure 5: Level of Service 'D'
Source: TCQSM, 2003

- Level of Service "E" – Walking speeds and passing ability are restricted for all pedestrians, only forward movement is possible; reverse or cross movements are possible only with extreme difficulty; volumes approach limit of walking capacity.



Fig. 6: Level of Service 'E'
Source: TCQSM, 2003

- Level of Service "F" – unavoidable contact with others; reverse or cross movements are virtually impossible; flow is sporadic and unstable.



Figure 7: Level of Service 'F'
Source: TCQSM, 2003

With the use of all information collected allied to parameters defined by the management of services, the

breakeven point for the management of the terminal will be established, taking into account the economic and financial aspects applied to each operation of the bus lines involved.

In addition to the information relevant to the operation of the terminal, with each pass of the vehicles equipped with the system of collection in a particular notable point (bus stop, transfer or terminal control line-TP/Ts station), new data submitted by equipment embedded (GPS / AVL [5]) being sent to update the system.

This update will be performed based on the concepts of Big Data technology, the processing of data collected from vehicle to vehicle from point to point of its operation, with the other information coming from other related systems (fleet management and tracking of buses, traffic and information system planning with origin and destination of travel [7]), statistical data for composition that will form the basis for generation of alerts inconsistency of the transport system at runtime.

All alerts are associated with operation indicators and other parameters of calculations that focus on saturation of the bus service, as well as monitoring the general profiles of dislocation (demand) through the alignment of data users at the point of capture or transfer stations where serve as input to guide the actions of regulating the public transport service by the management teams of transportation and transit.

Consignments of such information and alerts to the monitoring system will be handled through the respective control centers by management teams operating. The purpose of this procedure is to enhance supervision of services and fleet management and monitoring of the situation of the road, rows of terminals and corridors that offer greater risks degradation of service by the public officials and operators of the system.

The information system will maintain historical conditions and the movement of vehicles on the data lines, as well as monitoring through management reports and indicators in order to guide the planning actions aimed at continuous improvement of the service specification and the development of specialized routines for performance of inspection teams in the field of transport system.

This proposal aims to assist the management of the main system in the monitoring of potential risks based on:

- 1) Treatment alerts cartographic databases (points charts with zoom levels and saturation);
- 2) Temporal transmission parameterized by the monitoring system data concerning the probable movement of the demands aiding decision making processes in the implementation of fleet resources rationally and effectively, considering the performance indicators, resource availability and costs;
- 3) Identification of control data events, with possible "bottlenecks" in the operation of commercial speed or fall because of road impedances and propose based on the demand profile and historical data and load flow solutions;

- 4) Serve as the basis of knowledge in the application of contingency operations in situations of deadlock of other modes of public transport or other adverse;
- 5) Preparation of management reports for analysis planning teams and costs for improving the applied models;
- 6) Providing information on system conditions in real time to the general public.

III. IMPROVEMENTS

Besides knowing the location of public transport vehicles the user can check the conditions of occupation of vehicles approaching in order to get more comfortable ride.

Using data collected from embedded devices, system managers can evaluate the performance of the operation, plan interventions through estimates of arrival rates of the lines and the conditions of arrival of demands in a particular stop point or terminal.

Recognizing the critical points of the bus lines and suggest service solutions, considering the array of destinations [7], elaborating scenarios of changes in demand profiles for each modification or correction of work orders (OSO).

Provide support to managers and urban planners to develop guidelines for transportation plans through management of indicators of services.

Monitor system performance in the context of actions taken to further analysis of the results.

Make public the information of system performance to all stakeholders by issuing periodic reports.

Suggest new bus lines/connections rationally based on displacement [7] array to improve the quality of care, with better use of staff resources and vehicles.

IV. CONCLUSION

The management model for measurement of performance function support the planning and management of specific and adverse problems, logistical support for decision-making processes, promote continuous improvement of the system as well as improved operational control using as reference historical database.

The proposed study aimed to present the analysis of data with relevant information on the density, flow and displacement of passenger terminals in the public mass transit system, that will:

- 1) Reduce the cost caused by waste or mis-sizing of the terminal features;
- 2) Make the provision of services closer to the need to travel for passengers;
- 3) Allow pro-active rescheduling of services based on the systematic evaluation of recurrent changes in the use of supply;
- 4) Develop new tools for informing users about the conditions and occupation of vehicles and other public

transport facilities;

- 5) Application of technology in places of embarking and disembarking in order to contribute to the operational services regulation avoiding the saturation of the terminal;
- 6) Produce database with inputs for the composition of inspection plans of the bus lines, which include higher accuracy and improved use of inspection teams;
- 7) Promote the allocation of resources and services according to the need to travellers in critical situations;
- 8) Systematically collect and analyse the data on the conditions of the platforms, points of stops and passenger capacity in the vehicles of the public transport system;
- 9) Reduce the points of congestion caused due to long embarking and disembarking due to excess of demand and intermediate stops;
- 10) Provide greater flexibility in the allocation of resources based on the assessment of demands, available resources and space allocation;
- 11) Undertake immediate correction of data aimed at increasing the commercial speed and comfort of the user.

The ubiquitous technology can be adapted both in the concept and design, to use other personal communication devices such as mobile phones, tablets and other devices or with Bluetooth technology to collect data essential for management teams operation for organization and monitoring of the system, providing however, that the user can provide information in real-time about the conditions of the transportation system.

Drafting new management model similar to those applied in activities of port terminals, using identification of approaching vehicles and their levels and quality of service with the purpose to optimize the use of physical space and streamline operations through the provision of bus bays or in response to different traffic flows and demand.

Within the contrasts with the conventional schemes, where all lines have pre-designated bays, the new systems function under normal circumstances. However when one bus is late, triggering high density of passengers on the platform, the dynamic system can automatically relocate other vehicle to a nearby free bay, accommodating passengers waiting of the platform.

REFERENCES:

- [1] CIRILO, C. E. , (2011) - **Computação Ubíqua: Definição, Princípios e Tecnologias**, Departamento de Computação Universidade Federal de São Carlos – SP. Ubiquitous computing encompasses a computing model in which mobile users, services and resources are able to find other users, services and resources. The basic idea is that computing move out of work stations and personal computers and become pervasive in our everyday life. A number of principles and technologies behind this computational paradigm must be kept in mind for the development of applications and devices. <http://www.academia.edu/1733697>
- [2] <http://oglobo.globo.com/infograficos/bigdata/> (Accessed: May 2014) Big Data is the set of technological solutions capable of handling digital data volume, variety and velocity unpublished until today. In practice, the technology allows us to analyze any type of digital information in real time and is central to decision making, it is able to handle unstructured data included in these geolocation and behaviors that depend on a context to have meaning.
- [3] <http://www.gta.ufri.br/grad/071/rfid/RFIDarquivos/Index.htm> (Accessed: May 2014) RFID technology (radio frequency identification - Radio Frequency Identification) is nothing more than a generic term for technologies that use radio frequency for data capture. So there are several methods of identification, but the most common is to store a serial number that identifies a person or object, or other information, on a microchip. This technology allows automatic data capture, to identify objects with electronic devices, known as electronic tags, tags, RF tags or transponders that emit radio frequency signals to readers that capture this information. She has been there since the 40s and came to complement the technology of bar code, widespread in the world.
- [4] http://www.sptrans.com.br/pdf/biblioteca_tecnica/ (Restricted access, accessed: May 2014)
- [5] <http://www.mundogeo.com> (accessed: Jan 2014) The Acronym AVL (Automatic Vehicle Location which means, ie, automatic vehicle location), defines systems where GPS technology is used for monitoring vehicles. Since GPS is designed to provide primarily expresses the vehicle's position in geographic coordinates. The system consists of a network of satellites in various orbits arranged so that any point on the planet.
- [6] WILEY, JOHN & SONS, (2003) **RFID Handbook Fundamentals and Applications in Contactless Smart Cards and Identification**, Second Edition.
- [7] Project developed in partnership between the São Paulo Transporte and Grupo GAESI da Escola Politécnica da Universidade de São Paulo -USP, which is the development of Matrix Travel (Origin / Destination) municipal bus based on the systematic processing of data from Smart's cards used to pay fare (Bilhete Único), combined with geographical location information of vehicles, collected by onboard equipment (GPS / AVL).
- [8] FERRAZ, A.C.P., (1990) - **Sobre a eficiência e a eficácia do transporte público nas cidades médias**. Tese de Livre Docência, Escola de Engenharia de São Carlos - EESC, São Carlos.
- [9] **TRANSIT CAPACITY AND QUALITY OF SERVICE MANUAL** TCRP Report 100, (2003), Second Edition, Federal Transit Administration, Part 7/Stop Station,And Terminal Capacity, Chapter 3-Passenger Circulation and Level of Service, p. 7-15.

Holonic concept in the heat production and distribution control systems

Lubomir Vasek, Viliam Dolinay, and Tomas Sysala

Abstract—This contribution shows the idea of the application of holonic concept for decentralized systems in district heating systems. Modern heating networks, referred as smart heat grids, require quality control and communication infrastructure and the holonic concepts appear to be appropriate for this purpose. District heating network can be divided into the autonomous elements and it is possible to define tasks and relationships between them. To manage such kind of systems bring many benefits in comparison with centralized systems. The first task of this research is to analyze the behavior of each heating network element in detail and define hierarchies and mutual bindings. The preparation of this holonic application has already been started for the key elements of the distribution network. The analysis focuses on operational data of individual heat exchanger stations and their binding on other system elements.

Keywords—Heat distribution, heat consumption, energy, holarchy, holon.

I. INTRODUCTION

THE important aspect, leading to efficient energy consumption is undoubtedly effective management of heat production and distribution. Heat supply in the scale of the municipality, termed district heating, means to provide the transfer of heat energy from source into the place of consumption in time when it is required and in the expected quantity and quality. Quality of supplied heat energy is expressed in the temperature of heat transferring media. Quantity and quality of heat energy must go hand in hand with minimal distribution costs [1]. It is obvious that the heat distribution is inextricably linked to heat consumption, therefore the management strategies of the heat production, distribution and consumption must be solved as one unit. Nowadays, modern low-energy, passive or even active buildings are developed, smaller local sources are set up - such as waste incinerators, extensively grows the use of renewable

This work was supported by the European Regional Development Fund under the project CEBIA-Tech No. CZ.1.05/2.1.00/03.0089)

Lubomir Vasek is with the Department of Automation and Control Engineering, Tomas Bata University in Zlin, Faculty of Applied Informatics, nám. T. G. Masaryka 5555, 76001 Zlin, Czech Republic (e-mail: lvasek@fai.utb.cz).

Viliam Dolinay is with the Department of Automation and Control Engineering, Tomas Bata University in Zlin, Faculty of Applied Informatics, nám. T. G. Masaryka 5555, 76001 Zlin, Czech Republic (e-mail: vdolinay@fai.utb.cz).

Tomas Sysala is with the Department of Automation and Control Engineering, Tomas Bata University in Zlin, Faculty of Applied Informatics, nám. T. G. Masaryka 5555, 76001 Zlin, Czech Republic (e-mail: sysala@fai.utb.cz).

resources. At the same time, there are a large power plants producing electricity with potential large residual heat production. All of these factors change the view of the management strategies. Current strategy and concepts have to be upgraded or replaced by new one. Such modern concept is the Smart Heat Grid [2]. To control such complex system as smart heat grid it is advisable to use one of the distributed management methods. The method based on holonic architecture was selected and is presented in this contribution.

II. BASIC FEATURES AND PRINCIPLES OF THE HOLONIC SYSTEMS

The term "holon" and "holonic system" appeared more than 40 years ago, it was introduced by Herbert Simon and Arthur Koestler [4]. In recent years the concept of holonic systems expanded, elaborated and applied inter alia in the field of production systems, especially in discrete manufacturing. It is one of the concepts applicable to distributed systems and their management, but it has also potential for use in other areas.

This paper describes an application of this concept for the production and distribution of energy, especially heat energy. Modern trend in this area is the concept of Smart Grid, respectively. Smart Heat Grids are based on the application of the distributed systems ideas and it is therefore suitable to apply holonic concept.

Holon, in this context, could be defined as an autonomous and co-operative building block of a production system for transforming, transporting, storing and/or validating information and physical objects. The holon consists of an information processing part and often a physical processing part. A holon can be part of another holon. It is also possible to see it as a model of a particular element, i.e. part of the model of the entire system. In this sense is holon used in this article.

The Fig. 1 shows designed holarchy for the district heating system. The term holarchy refer to a set of holons including their mutual relations. Holarchy is a system of holons that can co-operate to achieve a goal or objective. The holarchy defines the basic rules for co-operation of the holons and thereby limits their autonomy [8]. The abbreviations used in the above figure mean the following:

HSH – Heat Sources Holon
LHSH - Large Heat Source Holon
HDH – Heat Distribution Holon
HAH – Heat Accumulator Holon
HCH – Heat Consumption Holon

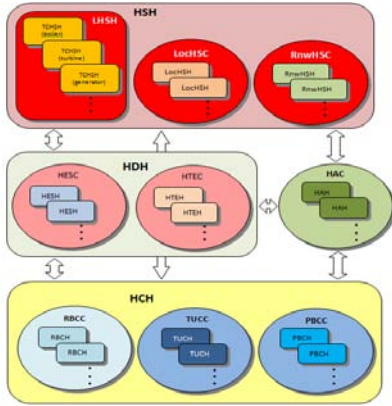


Fig. 1 Hierarchy for District Heating System

The internal structure of holons can be made up of a group of other holons, which can be described as "subholons". Any such subholon is, of course, full holon. This allows a very flexible way to define entire holonic system.

The most important features of holon are autonomy and cooperation. Autonomy is characterized by its ability of self-regulation, i.e. the capability to apply the flexible strategy which allows holon to respond differently to changes in their relevant environment. This ability to respond individually to changing conditions in which holon work, must be connected with a certain degree of intelligence to its reaction to change and adapt to the demands of the environment to be efficient and effective. Cooperation takes place between holons using the corresponding parts "subholons" of each holon - the parts that have the ability to implement relevant cooperation.

Good co-operation requires good communication between holons. Holon exchange information with other holons throughout holarchy. This direct, mutual communication between holons manifests an important distinction between distributed systems management and centralized management systems. In centralized systems, all communication takes place via a central element of the control system.

III. HOLONS AND HOLARCHY IN DISTRICT HEATING

The production, distribution and consumption of heat can be characterized as a set of individual elements of different types, which are linked together in a certain way - see Fig 2. These elements of the system can be divided into several groups and each group then into several subgroups.

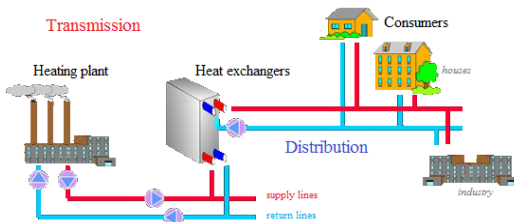


Fig. 2 Heat transmission and distribution system [9]

Heat sources

Structure of heat source holons (HSH) depends on the type and the structure of the source. It is important to build the structure of HSH in very flexible way to be able to match the given source. Individual subholons of HSH model the particular technological equipments of the heat source.

The resulting structure corresponds to the level of HSH intelligence. It is implemented by a set of methods, which is the union of the individual methods of subholons and HSH itself. Basic service, offered by HSH to other parts of the system, is the timing of the possible energy supplies (heat and for the case of cogeneration also an electricity) including relevant economic parameters.

Heat sources can be classified into following groups:

- Large centralized sources, which usually produce thermal and electrical energy (cogeneration systems). Their management depends on priority forms of produced energy or the ratio of their volumes. Individual variants of these resources will also differ as to the used energy technologies and source of energy.
- Smaller local sources produce only heat in the traditional way - by burning fossil fuels or biomass.
- Renewable energy sources that use different forms of renewable energy (photovoltaic sources, solar heaters, geothermal, heat pumps etc.)

Distribution network

Its implementation will vary depending on the heat transfer medium and it corresponds to the structure of the corresponding holarchy, which is modeling the distribution network. In this case it is not possible to talk about one holon of the distribution network but about part of holarchy. Individual holons of the distribution network holarchy correspond to elements of the distribution network, which will be listed below. The basic function of used holons is to monitor and control the hydraulic and thermal conditions in individual parts of the distribution network. The distribution network itself consists of the following parts:

- Heat exchanger, which is used for separating the primary and secondary parts of the distribution network (transmission and distribution) and to transfer heat between them. There are several structurally and technologically different types.
- Object transfer stations - have a similar function as heat exchangers, the difference are that it serves to connect the secondary and tertiary part of distribution network.
- The components of the distribution network for the transport of heat transfer medium between the source and consumers, such as various parts of pipe (straight, forming a branch network junctions forming network nodes), valves, pumps, etc.

Appliances – heat consumers

The individual types of consumers vary in their technical design its properties and characteristics. This is reflected in the group of holons for modeling this part of the system. Basic

characteristics, and thus offered service of modeling holons, are a timing diagram of heat consumption based on the temperatures around the appliance. This will be different for different types of consumers - heating residential building, office building, schools, retail premises or industrial building, or supplies heat for technological processes in various types of production, etc. To determine required heating diagrams, the modeling holons will use the functions for analysis of historical operating data and to update the consumption diagram will use learning process based on artificial intelligence methods.

Accumulator (storage tanks) of thermal energy

Accumulators allow eliminate differences in timing of the availability of heat production on the one side and timing of heat demand on the other side. An accumulator operates at certain time intervals as the source and at other time intervals as consumer. This corresponds to features and services of the relevant holons modeling accumulators of thermal energy.

IV. SPECIFICATION OF THE HOLON PROPERTIES

Preparation of individual holons covering elements in the heat supply system is based on their physical properties and analysis of operational data. An example will be shown on heat exchange station.

A. Heat exchange station

An important element of the heating system - heat exchange station HES, is selected as an example. In practice, many types of heat exchangers are used which vary for example in size or purpose in the heat distribution system. However, their behavior is very similar.

The elementary part of the heat exchanger station is heat exchanger, see fig. 3 and the appropriate control system or mechanism.



Fig. 3 Double pipe heat exchanger [7]

The heat exchanger station holon and corresponding subholons are shown on Fig. 4

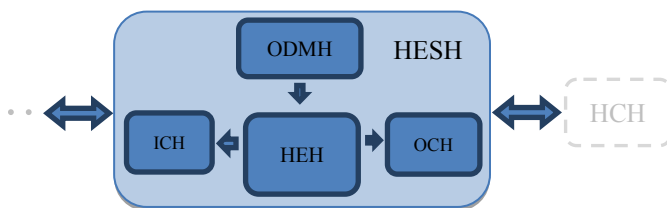


Fig. 4 Heat exchange station holon

The abbreviations used in the above figure mean the following:

- HESH – Heat Exchange Station Holon
- HEH – Heat Exchanger Holon
- ODMH – Operation Data Measurement Holon
- ICH – Inlet Control Holon
- OCH – Outlet Control Holon
- HCH – Heat Consumption Holon

Heat exchangers work based on convective heat transfer. In this heat transfer mechanism, the transfer rate depends on many factors such as flow velocity, pipe or tube surface, flow arrangement, etc.

The heat duty can be defined as the heat gained by cold fluid which is equal to the heat loss of the hot fluid. It can be calculated as (heat loss in heat exchanger is ignored):

$$Q = m_c \cdot C_c \cdot \Delta T_c = m_h \cdot C_h \cdot \Delta T_h \tag{1}$$

In equation (1), the subscript *c* indicates the parameters related to cold flow and *h* relates to hot flow. *m* is the mass flow rate of streams, *C* is the specific thermal heat capacity and ΔT is the difference of the flow input and output temperatures [5].

According to Newton's Law of Cooling heat transfer rate is related to the instantaneous temperature difference between hot and cold media. In a heat transfer process the temperature difference vary with position and time. The rise in secondary temperature is non-linear and can best be represented by a logarithmic calculation. Typically the calculation of convective heat transfer the LMTD (logarithmic mean temperature difference) is used:

$$LMTD = \frac{|T_c - T_h|}{\log(T_c/T_h)} \tag{2}$$

With definition (2), the LMTD can be used to find the exchanged heat in a heat exchanger:

$$Q = U \cdot A_r \cdot LMTD \tag{3}$$

Where: *Q* is the exchanged heat duty (in watts), *U* is the heat transfer coefficient (in watts per kelvin per square meter) and *A_r* is the exchange area.

Equations (1) – (3) describe main rules for HES. Detailed analyses of the relationships are in [5, 6, 9]. Used equations are also for HES models – i.e. holons. The parameters in model will be determined from operational data analysis.

V. OPERATION DATA ANALYSIS

The following analysis is based on data from the heat exchanger station. Fig. 5 shows the consumption of heat in two working days with similar course of external temperature. The Fig. 6 show their course of flow and the temperature in the return line (Fig. 7) This measured operational data and their evaluation are a source of information for determining the necessary characteristics of the individual components of the system, so also holons, forming the model. As expected, pattern of consumption of heat are quite similar - the nature

and quantity (red curve shows the day when night and the morning temperature were slightly cooler and therefore higher compliance in external temperatures would probably mean even greater compliance in the consumed heat). The used control strategy of the HES is based on the use of heating curve for determining the water temperature in both, the primary and the secondary circuit.

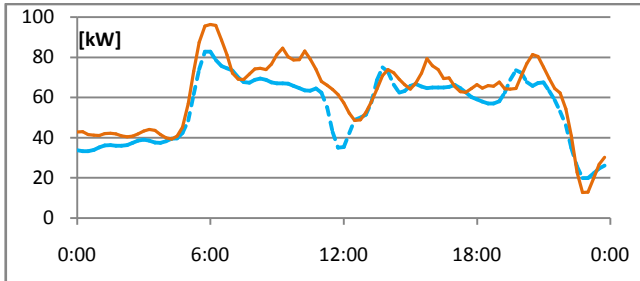


Fig. 5 Heat consumption

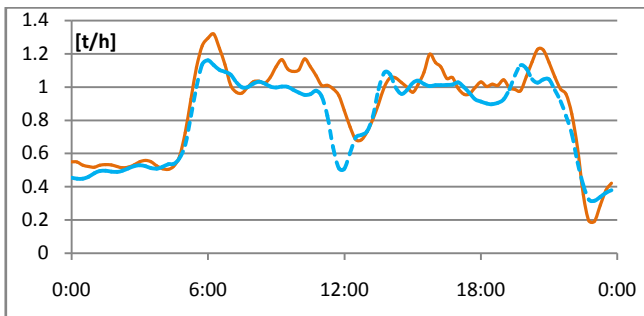


Fig. 6 Mass flow - primary circuit

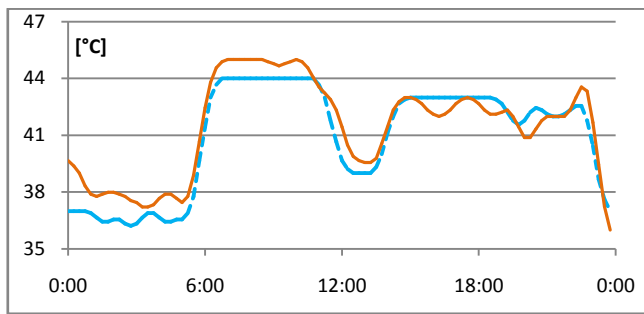


Fig. 7 Temperature of the output water from the primary circuit

The analysis of the presented data is the basis for defining the properties of the Holon. Apparently, it is binding on the outdoor temperature, time - day period.

In the above described method of control is also necessary to consider the transport delay. Generally this delay for the primary circuit is several hours, in the secondary circuit it is a few minutes.

The holonic model, that has the character of a simulation model, can be used in two ways:

- To determine the suitable strategy for district heating system management. From the measured data is apparent, that the selected and applied control strategy results in relatively significant variations in the operating state of the system. This may not always be appropriate – e.g.

cogeneration electricity production has to achieve the desired course of electricity supplied is crucial to have a stable behaviour of the whole system, therefore also its thermal part. This can be achieved by changing the management strategy.

- As an aid for the control process in specific conditions - to allow verify the suitability of control actions by the simulation, especially when dealing with unusual situations - what-if analysis.

The task for the future holons (group of holons), is to solve above described deficiencies of classical HES control strategies. Based on the knowledge gained from the analysis of HES operational data, and in cooperation with others holons in entire system, dynamically select appropriate strategies and parameters for HES control.

VI. CONCLUSION

The holonic distributed system for the modeling and control of production, distribution and consumption of heat has been designed and initiated its development. This concept is fully consistent with modern structures used recently in power systems - Smart Heat Grid and Smart Grid.

The holarchy system of production, distribution and consumption of heat was created and different types of holons, including their basic features were specified. The work also focuses on methodology for the design, specification and implementation of individual holons.

REFERENCES

- [1] Navratil P., Klapka, J., Balate J., Konecny, P. (2012). "Optimization of load of heat source described by nonlinear mathematical model." In: Proceedings of the 18th International Conference on Soft Computing MENDEL 2012. Editor: Matousek, R., Published by Brno University of Technology, Brno, CR, p. 356-362. [June 27-29].
- [2] Johansson, C. (2012). Smart Heat Grids, Sustainable district heating and cooling for the future [Online]. Available: <http://innoheat.eu/wp-content/uploads/2012/04/Guest-Writer-NODA.pdf>
- [3] Koestler A. *The Ghost in the Machine*, Penguin Books (reprint 1990), ISBN-13: 978-0140191929
- [4] Sadik Kakaç and Hongtan Liu. *Heat Exchangers: Selection, Rating and Thermal Design (2nd ed.)*. CRC Press, 2002.
- [5] Heat exchanger [Online]. Available: <http://scopewe.com/double-pipe-heat-exchanger-design-part-2>
- [6] Alfa Laval [Online], Available: <http://local.alfalaval.com/cs-cz/produkty/prenos-tepla/teorie-prenosu-tepla/pages/teorie-prenosu-tepla.aspx>.
- [7] Heat exchanges in district heating systems [Online]. Available: <http://www.tzb-info.cz/5236-predavaci-stance-tepla-v-soustavach-czt-iii>
- [8] Kwangyeol, R. 2004, "Fractal-based Reference Model for Self-reconfigurable Manufacturing Systems". Ph.D. dissertation, University of Science and Technology. Pohang, Korea, 2004.
- [9] DBDH, District heating technology, Available: <http://www.dbdh.dk/artikel.asp?id=462&mid=24>
- [10] Ansvers™ [Online]. Available: <http://www.answers.com/topic/log-mean-temperature-difference>

Automatic complexity estimation based on requirements

Radek Silhavy, Petr Silhavy, and Zdenka Prokopova

Abstract—This article disuses the automatic complex estimation of a software project and the “effort measurement” of the development process. The proposed methodology is based on a requirements document and can therefore be used in requirements-based development methods. The positive and negative impacts of the proposed methodology, requirements associations’ influence and requirements structure are also discussed. Moreover, requirement’s writing style and the of influence personal consultants are also investigated.

Keywords—Software estimation, complexity measurement, requirements, algorithmic methods, requirements engineering, system engineering.

I. INTRODUCTION

COMPLEXITY Estimation is an important task for system projects planning. Software-intensive systems dominate in the system development sector. Therefore, the principles of Complexity Estimation are investigated in this paper.

In the software engineering field, there are several principles which have already been adopted. Probably the most important of them is Functional Points Analysis. This method can be used in the early stages of system projects. Albrecht first introduced the method in 1979 [1]. Further development led to the international standardized version [2], which is used for various research purposes in the software engineering measurement field.

In System Engineering, methods are used, which are similar to Functional Points Analysis.

Therefore, in the following text, we describe our algorithmic method - called “The System Size Estimation Method [3], which is described and redefined in Section II. Several authors have investigated and proven that factors like, team size [4], project type [5], or technological platform have a significant impact [6].

The actual system complexity is derived as being the relationship between the number of functional points and the input effort necessary for a system’s development [7].

R. Silhavy, Tomas Bata University in Zlin, nám. T. G. Masaryka 5555, 760 01 Zlín, Czech Republic (phone: +420 57 603 5015; e-mail: rsilhavy@fai.utb.cz).

P. Silhavy, Tomas Bata University in Zlin, nám. T. G. Masaryka 5555, 760 01 Zlín, Czech Republic (phone: +420 57 603 5015. e-mail: psilhavy@fai.utb.cz).

Z. Prokopová, Tomas Bata University in Zlin, nám. T. G. Masaryka 5555, 760 01 Zlín, Czech Republic (phone: +420 57 603 5011. e-mail: prokopova@fai.utb.cz).

The traditional concept of Functional Points Analysis describes a system as a set of transactions: Entry, Exit, Read, Write. [8].

II. THE ESTIMATION APPROACH - DEFINITION

For estimation purposes, an analysis of the requirements is necessary. The estimation process consists of the following steps:

- 1) Set the importance of the requirement
- 2) Set the complexity level of the requirement
- 3) Set the complexity level of the non-functional requirements
- 4) Calculate the Technical Factor
- 5) Calculate the Environment Factor

The requirements are clustered into three groups. The complexity of the each group can be expressed as:

$$\text{complexity} = \{\text{simple; average; complex}\} \quad (1)$$

The simple set contains the requirements which software-based implementation needs and these are solved by 1 individual subsystem. The calculation weighting value is 5, as can be seen in Table I.

Table I Complexity List

Complexity	Calculation Weight (C_f)
Simple Non-Functional RQ (NF)	5
Average System Characteristics (SC)	10
Complex Constrain RQ (CR)	15

The average set contains the requirements that the hardware user interface or data-processing need to be met. The

calculation weighting value is 10.

The complex set contains the requirements, which involve technological control, mechanical user interface or very complex data processing. Here, implementation involves more than 1 subsystem. The calculation weighting value is 15.

The total value of the parameters is calculated as follows, for each group:

$$\text{Simple: } \sum (NF \times Cf) \quad (2)$$

$$\text{Average: } \sum (SC \times Cf) \quad (3)$$

$$\text{Complex: } \sum (CR \times Cf) \quad (4)$$

These values, when summed, determine the Raw Requirements Points (RRP). According to the following formula:

$$\text{RRP} = \sum(NF \times Cf) + \sum(SC \times Cf) + \sum(CR \times Cf) \quad (5)$$

III. TECHNICAL FACTORS

There are 15 technical factors. These factors can be seen in Table II. The factors are a revised version of an earlier-published work [4].

Table II Technical Factors

TF	Description	Value (V _c)
T1	Distributed Architecture	2
T2	Business Critical	5
T3	Performance	1
T4	End User Efficiency	1
T5	Complex Internal Processing	1
T6	Reusability	1
T7	Usability	0,5
T8	Safety	5
T9	Security	1
T10	Sociotechnical Aspect	2
T11	Modular Architecture	2
T12	Maintenance	2
T13	Upgradability	2
T14	Graphical User Interface	5
T15	Long Life-time	2

The role of the impact is to provide a description of the problem domain form from a technical point of view.

Each factor is weighted according to its relative impact. A weighting of zero indicates the factor is irrelevant; and the value 5, means that the factor has the greatest impact.

The technical factors are used for calculating the Total Technical Factor Value (TTV). Each TF value is multiplied by the value of its significance (TFs):

$$\text{TFs} = \langle 0, 10 \rangle, \text{ for each TF} \quad (6)$$

The Technical Factors Value (TFV) is calculated as follows:

$$\text{TFV} = \sum (\text{TFs} \times \text{Ve}) \quad (7)$$

As can be seen, TFV represents the weighted value of each TF (T1 – T15).

IV. ENVIRONMENTAL FACTORS

Environmental Factors (EF), estimates the impact on productivity that various environmental factors have during the system development process. Their role is to describe the development environment and, moreover, the problem domain itself.

The list of proposed environmental factors can be seen in Table III. The factors are evaluated and weighted according to their perceived impact and are assigned a value between 0 and 10. A value of 0 means the environmental factor is irrelevant for this project; 5 is an average; and 10 means it has great impact.

Table III Environmental Factors

EF	Description	Value (V _e)
E1	System Designer Experience	2
E2	Domain Experience	1
E3	Modelling Experience	2
E4	Analysis Capability	2
E5	Motivation	1
E6	Stable Requirements	2
E7	Subcontractors	5
E8	Integration Complexity	5
E9	Ecological Impact (development)	3
E10	Public Importance	1
E11	Cost of the Shelf	5
E12	Regular Cooperation	-1
E13	National Level Evaluation	1
E14	Methodology Experience	5
E15	Certification	2

The Environmental Factors are used to calculate the Total Environmental Factor Value (EFV). Each EF value is multiplied by the value of its significance (EFs):

$$\text{EFs} = \langle 0, 10 \rangle, \text{ for each EF} \quad (8)$$

The Environmental Factors Value (EFV), is calculated as follows:

$$\text{EFV} = \sum (\text{EFs} \times \text{Ve}) \quad (9)$$

As can be seen, EFV represents the summed weighted value of each EF (E1 – E15).

V. CALCULATION FORMULAS

The final result of calculation is the Total Requirements Points (TRP), which are calculated according to the following formula:

$$TRP = RRP \times ((CR1 \times TFV/100) + (CR2 \times EFV/100)) \quad (10)$$

The values CR1 and CR2, are used for tuning the method. These values are set according to historical project measurement or statistical evaluation data.

The TRP value represents the coefficient of the system size. Project Costs (PC), can be determined according to the following formula:

$$PC = TRP \times PP \quad (11)$$

Where, PP is Price Per on TRP. The value of the PP is individual for each system engineering company.

Development Time (DT) can be predicted in a similar way. The only difference is that TRP is multiplied by the coefficient: man-hour per one TRP (MHP):

$$DT = TRP \times MHP \quad (12)$$

VI. CASE STUDY

The proposed methodology will be described on the sample project, which was adapted from [6].

In this sample, the development process of a pocket audio player is described. The main, important project goal was to offer a solution which was successful and usable and which offered the appropriate functionality.

The Specification Package can be seen below. The requirements are grouped into four basic groups:

1. User Friendliness
2. Durability
3. Performance
4. Media Capacity

The User Friendliness group defines the set of requirements which deal with the quality of service of the audio player – e.g. Keys Layout, Graphical User Interface and Scroller are the primary requirements which play an important role in user satisfaction.

Fourteen requirements can be found in the project. These requirements can be clustered into Simple, Average or Complex groups:

- Simple: 5
- Average: 5
- Complex 4

The complexity for each group can be calculated as follows:

$$\text{Simple: } \sum (5 \times 5)$$

$$\begin{aligned} \text{Average: } & \sum (5 \times 10) \\ \text{Complex: } & \sum (4 \times 15) \end{aligned}$$

Thus, the Raw Requirements Points are:

$$\begin{aligned} RRP &= 25 + 50 + 60 \\ RRP &= 135 \end{aligned}$$

The next step is to prepare the Technical Factors and Environmental Factors. Tables II and III will be used for this purpose. The TFs and EFs values have to be set.

The significance levels for each of the Technical Factors can be found in Table IV.

The Technical Factors Value (TFV) is calculated according

Table IV Technical Factors Significance

TF	Description	(V _e)	TFs
T1	Distributed Architecture	2	0
T2	Business Critical	5	0
T3	Performance	1	10
T4	End User Efficiency	1	10
T5	Complex Internal Processing	1	5
T6	Reusability	1	0
T7	Usability	0.5	10
T8	Safety	5	2
T9	Security	1	0
T10	Sociotechnical Aspect	2	5
T11	Modular Architecture	2	0
T12	Maintenance	2	0
T13	Upgradability	2	0
T14	Graphical User Interface	5	6
T15	Long Life-time	2	4

to the formula: $(\sum(TFs \times V_e))$. In the case study, TFV = 88.

The Environmental Factors can be found in Table V, where the (EFs) values of the significance of the environmental factors can be seen.

The EFV value – according to the Table V is 66.

The TRP is calculated according to the following formula (10), $TRP = 135 \times ((0.7 \times 88/100) + (0.5 \times 66/100))$.

The Total Requirements Points are: 83.43

The value CR1 is set to 0.7 and CR2 is set to 0.5. These values are based on the average values of the correction values – based on empirical research, which were based on historical project measurement evaluations.

The Project Cost for the sample project is:

$PC = 83.49 \times 8500$, where PP in (11) is in an undefined currency. The result is: 709 665.

Table V Environmental Factors Significance

EF	Description	(V _e)	EFs
E1	System Designer Experience	2	0
E2	Domain Experience	1	5
E3	Modelling Experience	2	5
E4	Analysis Capability	2	4
E5	Motivation	1	4
E6	Stable Requirements	2	0
E7	Subcontractors	5	0
E8	Integration Complexity	5	5
E9	Ecological Impact (development)	3	0
E10	Public Importance	1	0
E11	Cost of the Shelf	5	0
E12	Regular Cooperation	-1	10
E13	National Level Evaluation	1	2
E14	Methodology Experience	5	4
E15	Certification	2	1

The Development Time (DT) can be predicted in a similar way.

$DT = 83.49 \times 100$. This resulted in 8,349 man-hours for the proposed project.

VII. AUTOMATIC ESTIMATION ARCHITECTURE

In the section above, there was an estimation approach case study. For real-life usage of the proposed methodology what is important is to create Automatic Estimation Solution architecture.

In the methodology section, the correction values (CR1, CR2) are implemented. These two values can be used for computational model tuning, based on historical data. This ability makes a model versatile in different problem domains and for various system engineering projects.

The calculation component can be implemented using various approaches – e.g. Neural Networks or Genetic Programming can be used or even, methods based on classical Optimization principles can be used.

VIII. CONCLUSION

In this article, we introduce a System Size Algorithm, based on System Requirements. The theoretical background is adopted from Functional Points Analysis and the Use Case Points' Method.

In Functional Points Analysis, the basic system-transactions are analyzed. The Requirements List is used for such analysis. This process is complex and non-trivial, which also has a tendency to lose accuracy. Accuracy is influenced by Requirements Writing Style and by the ability to calculate the Functional Points.

In the System Size Algorithm, only the number of requirements is taken and the project is described more precisely by using the Technical and Environmental Factors (TF and EF). The factors describe the relationship in the

Requirements and the Describe Problem domain in which the project is developed.

The Correction Values – are coefficients which allows for tuning calculations. These can be used to adjust the calculation models within the scope of an individual project team, or at the company level.

REFERENCES

- [1] A.J. Albrecht, "Measuring Application Development Productivity", in *Proceedings IBM Applications Development Symposium*, Monterey, California, October 1979, pp. 14-17.
- [2] ISO/IEC 14143-1:1998 Information Technology - Software Measurement - Functional Size Measurement - Part 1: Definition of Concepts, 1998.
- [3] R. Silhavy, P. Silhavy, Z. Prokopova, "Clustered requirements in system engineering project estimation", *International Journal of Mathematical models and Methods in Applied Sciences*, vol. 5, no.1, pp. 1052-1059. 2011.
- [4] L. Angelis, I. Stamelos, M. Morisio, "Building a Cost Estimation Model Based on Categorical Data", in *Proc. 7th IEEE Int. Software Metrics Symposium (METRICS 2001)*, London, April 2001.
- [5] R. Premraj, M. J. Shepperd, B. Kitchenham, P. Forselius, "An Empirical Analysis of Software Productivity over Time", in *Proc. 11th IEEE International Symposium on Software Metrics (Metrics 2005)*, IEEE Computer Society, 2005.
- [6] P. Forselius, "Benchmarking Software-Development Productivity", *IEEE Software*, vol. 17, no. 1, Jan./ Feb. 2000, pp. 80-88.
- [7] C. Gencel, "How to Use COSMIC Functional Size in Effort Estimation Models?", in *Software Process and Product Measurement*, Springer Berlin Heidelberg, 2008. pp. 196-207.
- [8] F. Zickert, R. Beck, "A mapping model for assessing project effort from requirements", *Information Systems and e-Business Management*, 2013, vol. 11, no. 3, pp. 377-401.
- [9] D. Tran-Cao, G. Lévesque, J. G. Meunier, "A Function Point Method for Software Complexity Measurement". 2013.

Radek Silhavy was born in Vsetin in 1980. He received a B.Sc. (2004), M.Sc. (2006), and Ph.D. (2009) in Engineering Informatics from the Faculty of Applied Informatics, Tomas Bata University in Zlin.

He is a Senior Lecturer and researcher in the Computer and Communication Systems Department.

His Ph.D. research was on The Verification of the Distributed Schema for the Electronic Voting System. His major research interests are software engineering, empirical software engineering and system engineering.

Petr Silhavy was born in Vsetin in 1980. He received a B.Sc. (2004), M.Sc. (2006), and Ph.D. (2009) in Engineering Informatics from the Faculty of Applied Informatics, Tomas Bata University in Zlin.

He is a Senior Lecturer and researcher in the Computer and Communication Systems Department.

His Ph.D. research was on Electronic Communication and Services in Medical Information Systems. His major research interests are data mining, database systems and web-based services.

Zdenka Prokopova was born in Rimavska Sobota, Slovak Republic in 1965. She graduated from the Slovak Technical University in 1988, with a Master's degree in Automatic Control Theory.

She received her Technical Cybernetics Doctoral degree in 1993 from the same university.

She worked as an Assistant at the Slovak Technical University from 1988 to 1993. During 1993-1995, she worked as a programmer of database systems in the Datalock business firm. From 1995 to 2000, she worked as a Lecturer at Brno University of Technology. Since 2001, she has been at Tomas Bata University in Zlin, in the Faculty of Applied Informatics. She presently holds the position of Associate Professor at the Department of Computer and Communication Systems.

Her research activities include programming and applications of database systems, mathematical modeling, computer simulation and the control of technological systems.

Dynamic patients scheduling in the Pediatric Emergency Department

Sara Ben Othman¹, Nesrine Zoghlami¹, Slim Hammadi¹, Alain Quillot², Alain Martinot³, Jean-Marie Renard⁴
¹LAGIS UMR CNRS 8219 Ecole Centrale de Lille – France; ²LIMOS UMR CNRS 6158; ³PED of CHR Lille; ⁴EA2694 University Lille 2

Abstract—Due to the complexity of Pediatric Emergency Department, health care management has attracted the attention of many researches which has led to intensive research in agent technology. Multi-agent systems seem to be an effective approach to design complex distributed applications. As the structure of hospitals is divided into several autonomous and ancillary units, we propose a new approach integrating jointly agent-based modeling and optimization tools. In this context, mobile agent paradigm is also very efficient once used through an optimization approach. In this paper, we suggest a three-level agent-based architecture to solve a distributed scheduling problem for resources allocation during patient journey. Our interest is minimizing the waiting time of patients to improve the quality of care process management as well as optimizing resources allocation. This contribution is included in the project ANR HOST (ANR-11-TecSan-010).

Keywords—Pediatric Emergency Department, Health Care Management, Multi-agent Systems, Mobile Agents, Optimization, A Three-Level Agent-based Architecture, Waiting Time, Resources Allocation.

I. INTRODUCTION

Emergency services have a critical mission in health care facilities. They feature the ability to satisfy the different needs of every patient. In addition to the purely medical terms, emergency medicine requires logistics (having the right equipment and the right medical staff at the right time and the right place) [1] and cooperation with other organizations. This may involve modeling and simulation concepts necessary to control and optimize patients flow. Planning and resources scheduling are also responsible for performance management and system control.

Health care facilities are facing more and more difficulties to manage the rising patients flow. In emergency departments, these difficulties consisted of overcrowding caused by chaotic patients' arrivals. Indeed, several studies have shown that one of two emergency services work in overdrive, which means that all patients do not have the privilege of being supported in optimal conditions with extended waiting times [2]. Emergency services can be exploited in an optimal way by an improvement in the services provided to patients and operating costs reduction. Indeed, patient waiting time improvement is a critical performance indicator related to the

quality of care in the emergency department settings. This parameter has also an influence on costs.

Emergency Logistics system refers to a set of logistics elements which interact and coordinate with each other in order to complete emergency logistics requirements [3]. Therefore the system relies on a new set of distributed applications using a huge amount of data spread on different sites geographically separated). In such systems, data may undergo various simultaneous actions (requests, storage, update, etc.) which requires the access to different remote information sources. This dynamic, distributed and open aspect of the problem can be treated through different interacting individual entities. Thus, Multi-Agent Systems (MASs) have shown their relevance to this complex distributed applications design [4]. The concept of agent is not only an efficient technology, but it is also a new paradigm for software development in which the agent is an autonomous entity operating in a dynamic environment [5] and interacting with other agents using languages and protocols.

In addition to the distributed aspect of the studied problem, in the PED, actors behave in a critical and stochastic environment where an optimal solution must be deployed as quickly as possible in order to avoid the dramatic consequences especially on patients.

In this context, mobile technology can be a major advantage along with the artificial intelligence in the optimization of patients scheduling due to their adaptability and efficiency in heterogeneous and dynamic environments. The main objective of mobile agent (MA) paradigm to navigate through system's functions and also to extend its functionality by supporting disconnected operations. When the active mobile execute a remote operation, it disconnects the client and reconnect later to retrieve the results [6].

This option is based on the ability to move according to their own needs to best accomplish accorded tasks. In fact, medical staff which is the most critical resources can be treated carefully using mobile technology. The goal here is to simulate medical staff behaviors in the PED using MAs which, unlike "stationary" agents, have mobility. Certainly, these agents may move from one medical team to another, operating alternately on different patients, according to the skills required for the corresponding treatments. The paradigm of MA has been discussed in many studies. They are shown to be efficient [7] [8] [9] [10]. In this paper, we propose a proficient using of MA paradigm through a MAS designed for

patient journey management where actors provide smart negotiation in order to execute and control patient's treatment tasks scheduling. More precisely, our study presents a set of tools and approaches for optimizing patients flow in a PED. Our goal is to model and implement a robust system for patients' treatment which is able to support a huge number of simultaneous requests, optimizing the services management, in order to satisfy patients with minimum costs and respecting emergencies degrees. In fact, we will detail the optimization models we used for the entire treatment of patients in the best conditions based on needed resources scheduling such as medical staff, beds, medicines, etc.

We will go through decisions regarding patients' emergency degree, resources availabilities and costs as well as the choice of medical staff based on their skills and planning. The presented solution comprises the use of a three-level agent-based framework including an optimization and negotiation scheme to resolve resources and patients scheduling.

This paper is organized as follows: a general formulation of the problem is illustrated in the following section. After that, an overall architecture of the MAS is proposed in section 3. The global scheduling approach is given in section 4. Experimentation and results are given in section 5. Conclusion and possible future works are addressed in last section.

II. PROBLEM DESCRIPTION

During periods of peak activity, the PED, main entrance of sick children in hospital regardless their severity, overflows. The waiting room is not large enough, parents crowded into the narrow corridors of the service with their infants and waiting time dramatically increases. The service then switches into a new phase of operation, which we call "overcrowding" to streamline the flow of patients.

The idea is to get a rigid and theoretical framework for the service operation that would delight probably a specialist bureaucratic organization, but who has the terrible drawback of "waste" of resources. Thus, during peak activity, the medical staff takes the initiative to commandeer randomly all available resources, regardless of their theoretical characteristics.

The main interest of the PED is to satisfy patients, respecting responses delays according to emergency degrees and minimizing treatment costs; the problem to be solved is to ensure patients care quality as taking into account the severity of their pathologies. The main goal of our work is to manage patients flows by supporting and prioritizing the most serious cases. Care must mobilize both human and material resources in relation to (/with) their availabilities. Medical staff should be deemed "most expert" for a given care task to get allocated for treatment tasks.

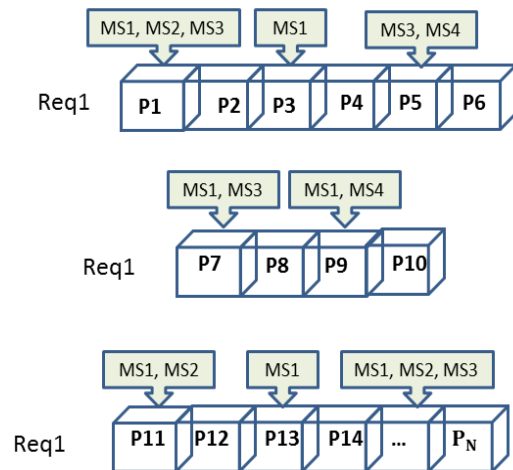


Figure 1: Medical Staff movement

The integration of mobile paradigm into our software agent gives the possibility to migrate towards the different boxes of the PED where patients are waiting for treatment and which can receive mobile entities (Medical Staff). In our proposed system, we use mobile medical staff agents to travel through the PED architecture to treat patients and to collect intelligently needed information related to patient health state in order to update the system data.

A task can belong to one or various patients. Medical staff agents receive many requests for different patients' treatment and according to their availabilities and to the emergency degree of patients they go for their treatment in the different boxes of the PED.

The reliability of the services delivered by the PED requires providing the necessary equipment to meet the requirements of the emergency mission. For the material resources, the issue is to deliver the resources avoiding stock-outs that can paralyze the functioning of whole the PED. This is called the procurement policy. It requires knowledge and total control of treatment time and amount of resources to allocate. So delays should be predicted and resolved earlier to minimize penalties and resources quantities should be optimized to avoid stock-outs and high wastage rates. On the other hand, before assigning one of the medical staff for patient treatment, a whole study should be done. Indeed, each medical assistant must be qualified to be charged of patients. Their availabilities must also be taken into account and their planning should be optimized by reducing their idle time.

The main concern is to satisfy the demand of the different actors of the studied health care circuit by providing efficient management and high care service level. Accuracy is one of the key objectives of the operations administration in health emergency institution management.

III. SYSTEM ARCHITECTURE

In a scheduling problem, four basic concepts are involved: tasks (or Jobs), resources, constraints and objectives. In our case, to execute patients' treatment tasks we have to consider the resources (medical staff, boxes, beds, medicines, etc.) to

assign, time needed for task execution which depends on the emergency degree of patients. Additionally, we have to take into consideration some constraints such as waiting time and some objectives like costs minimizing as well as the complexity of the environment characterized by uncertainty and large number of actors in case of an overcrowding situation that make the scheduling task in emergency health care management highly complex.

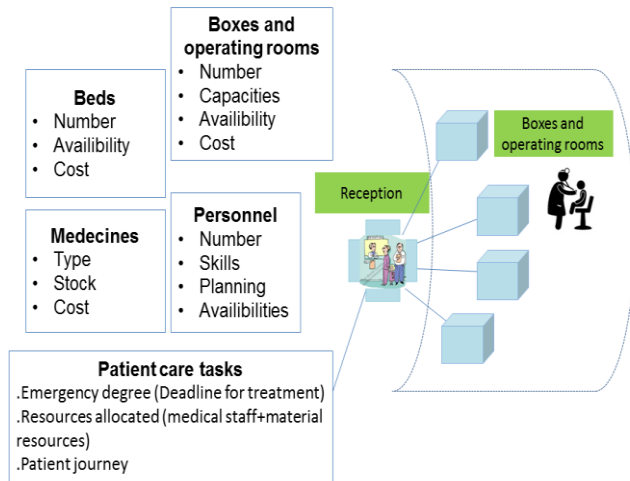


Figure 2: Typical model of a patient treatment scheduling system

We propose to consider each actor of the PED as an autonomous agent, able to interact with other actors [11]. Our proposition is to resolve the problem described previously through a system based on the coordination and cooperation between different kinds of software agents.

- Gui Agent (GA): This agent interacts with system users particularly the medical staff of the PED allowing them to know different demands sent to them as well as patients monitoring and the global state of the PED including the number of patients waiting, so they manage requests, go for patient treatment and then update the system data. When a patient arrives to the PED, an agent Home Agent (HA) responsible receiving the patients and their orientation and for the pathology identification is created. HA has all the skills required by the rules of registration plan, medical diagnosis plan and patient orientation plan. It deals with the formulation of the problem and then sends it to the Identifier Agent. This corresponds to the creation of a medical record through the Identifier Agent (IA) triggered by an administrative nurse.
- IA: it receives the different information from HA about the medical problem and identifies the skills needed for the treatment referring to the medical protocols. It consults the database of the different pathologies and the needed resources for their (patients') treatment.
- Scheduler Agent (SA): This agent has to optimize the choice of resources for patients' treatment taking into account some of the constraints of our system. It has to assign resources to patients' treatment tasks minimizing total cost and patients waiting time in order to respect emergency degrees. First of all it organizes the queue of patients who

need treatment taking into account their emergency degree then it assigns resources to different task.

- Resource Agent (RA): this agent is responsible of the monitoring and management of different resources available for treatment tasks. It also detects whenever there are stock-outs of medicines and informs the user through the IA about requested supply.
- Monitoring Agent (MoA): this agent is notified for every taken decision and every task completed. It represents the coordinator between all software agents and an informer for the physical agents about actions and patients status.
- Integration and Evaluation Agent (IEA): this agent is responsible for the whole system performance control. It calculates the performance indicators of the system such as waiting time of patients and treatment costs in order to evaluate the overall schedule of patients in the PED.
- Medical Staff Agents (MSA): An agent MSA is a mobile software agent which can move intelligently from one treatment room to another in the PED in order to treat patients. It is characterized by two variables (skills and availability). This special kind of agent is composed of data, states and a code and has a smart behavior. Once MSA achieves a treatment task it can shift to another treatment room for a new task execution. Therefore, the agent SA must take into account this aspect when assigning human resources to tasks. Each task represents a service which can be performed by different possible MSAs, with different cost. To respond to tasks, it needs data about MSAs availabilities and available skills through the RA. Therefore, the SA agent must optimize the assignments of resources to tasks. For this assignment problem, we propose a three-level architecture as an optimizing solution based on the alliance between MASs and optimization tools. This architecture is described in the next section.

IV. THE AGENT-BASED DISTRIBUTED SCHEDULING SYSTEM

The system algorithm created for the scheduling based on interacting agents is as follows (Figure 3):

- a. Once a patient arrives, we create our system's agents; HA is created for patient receiving and orientation and also for pathology identification. After registration, the information about patient is passed to MoA and to the IA.
- b. The IA establishes which kind of resources is necessary for patient's pathology treatment using data histories. In addition to the material resources, it identifies the needed skills for every treatment task. Then, the SA is notified of information about material and human resources to be allocated.
- c. SA treats the patients care requests received and asks for resources allocation from RA.
- d. RA uses patient and pathology information received from IA to allocate the needed resources for the SA to start the scheduling of treatment tasks.
- e. SA then goes for tasks scheduling. If it is about human resources, it identifies the needed skills for every task and medical staff availability. Patients' emergency degrees are given priority in this

- g. MoA control the patients' physiological signs and location.

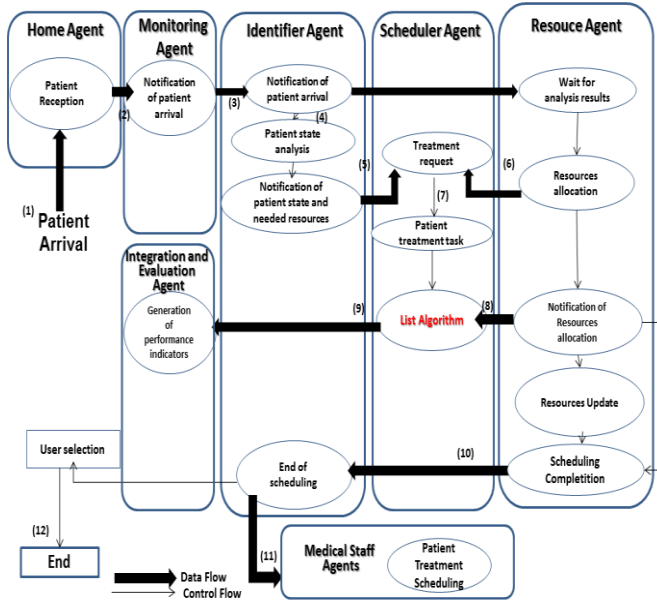


Figure 3: The Synchronized Distributed Patients Scheduling

A. A three-level agent based architecture

There are several scheduling optimization algorithms that can be involved in scheduling applications. But we can't find an agreeable and efficient scheduling strategy that is common to each and every patient's treatment tasks. In addition, resources in health care field are various and for each type we have to choose a different algorithm. In fact, operating rooms can't be scheduled like human resources for example. These are different and their differences are due to their skills. Thus, taking into account the characteristics of each type of resources, we propose a three-level framework. Figure 4 shows the three levels representing the architecture suggested. The main level contains the MAS modeling actors involved during patients' journey. In this level agents are collaborating and negotiating in order to make decisions on scheduling strategies. The made decisions depend on data received from the bottom level (PED). The higher level contains scheduling optimization tools including different mathematical models.

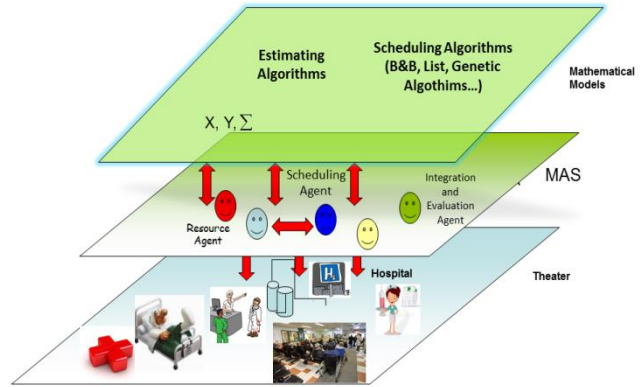


Figure 4: A three level scheduling architecture

As agents are autonomous entities characterized by decision-making capabilities, we propose to implement in this level a set of scheduling optimization algorithms, and according to the complexity of the situation, agents evaluate the global preference of a proposal to find out which scheduling algorithm should be used in order to better respond to the needs of lower level. The global preference is based on the performance indicators calculated.

The assignment of resources is an NP-complete problem. This complexity makes difficult the development and use of schedules planning systems generation. Planning system must consider organizational, treatment methods of resources and legal programming rules and individual preferences (in case of human resources scheduling).

B. Agent-based algorithm for patients scheduling

To execute treatment tasks, agents may decide to go for list algorithm, particularly suited to the studied system due to its dynamic priority rules. This algorithm is characterized by its flexibility and is easy to implement in real time. The problem is solved by static or dynamic priority rules.

The standard of this approach is to perform a scheduling of treatment tasks using lists algorithms based on dynamic priority rules. Specifically, at a given time T_0 , among the ready treatment tasks to execute, the task of highest priority is scheduled. More generally, list algorithms develop first a priority list, which is then used to build a solution. In our problem the priority rule is dynamic. It is chosen by HA. Depending on the pathology and the emergency degree, it may be the smaller latest start date or lesser execution time.

The objective is to reduce waiting time of each patient; the objective function is as follows:

$$Min (\sum_{j=1}^l \max(0, c_j - d_j))$$

With:

- c_j = the completion time of the treatment task t_j
- d_j = the theoretical treatment time for the task t_j
- l = the total number of treatment tasks.

List Algorithm

In: T (set of tasks to schedule)
Out: S
Begin
 S={};
While T ≠ ∅ (set of ready tasks T is not empty) **do**
 Begin
 Determine among the set T, the task t_i of highest priority;
 S: = S ⊕ t_i
 End
End
End

S is a sequence of partial (or total) solution for tasks scheduled.

S = t_i ⊕ S; means to insert the task t_i in the sequence S, in the position intended by the scheduling.

C. Mathematical Formulation of the scheduling problem

The main concern of our proposed system is to satisfy the patients' needs, respecting emergency degrees and minimizing their costs and waiting times. At first, patients' treatment schedules are built by assigning material resources and medical staff to the needing patient. Then, performance indicators are generated to evaluate the overall performance of the PED and to identify the assignments that need to be readjusted, in order to get at the end patients satisfaction and safety as well as medical staff idles and overdrive elimination. A patient is satisfied if his request for treatment is answered rapidly with quality services. We start the description of the mathematical model of the treatment tasks scheduling problem by introducing the necessary sets:

Let R be the set of material resources to be allocated.

R = {r₁, r₂, ..., r_u}, with u the total number of these resources.

Let P be the set of patients.

P = {P₁, P₂, ..., P_h}, with h the total number of patients.

Let K be the set of skills that can characterize each MSA.

K = {K₁, K₂, ..., K_f}, where f is the total number of skills that medical staff can have.

Let D be a boolean variable for MSA availability. If it is free, D=true, otherwise D=false.

Let A be the set of MSAs Ag_x, where x is his position in the PED. Each MSA is characterized by Skills and availability, Ag_x=f(K, D).

Let T be the set of treatment tasks to be executed. T = {t₁, t₂, ..., t_L}, with L the total number of tasks to be scheduled. A treatment task t_i ∈ T consists in the allocation of a number {numberAllocated} of medical resources (resourceID) to treat a specific patient (patientID) under some constraints (the deadline for patients treatment: d_i and the treatment time p_i).

A task is formalized as follows:

T_i: <patientID; MedicalStaffID; materialResourceID; amount; d_i; p_i>

D. Performance indicators evaluation

We choose to assign to patients treatment in the PED a cost that represents the total treatment cost for satisfying the patients. It is composed of fixed performance indicators. To

formulate these indicators, we need some sets of binary variables.

Let m be a member of Medical Staff A.

Let i be the index of treatment operation.

Let j be the index of patient.

X_{m,k,i,j} = affectation of Medical Staff having the skill k for treatment task i of patient j.

X_{m,k,i,j} = $\begin{cases} 1 & \text{if Medical Staff is used} \\ 0 & \text{otherwise} \end{cases}$

The variable representing the use of material can be as:

Y_{r,i,j} = use of material resource r for treatment task i of patient j.

Y_{r,i,j} = $\begin{cases} 1 & \text{if Medical material resource is used} \\ 0 & \text{otherwise} \end{cases}$

The performance indicators can then be defined as follows:

C^{MS_{Staff}} = Medical staff cost for patients treatment,

C^{MatResources} = Material resources cost allocation,

C^{Waiting time} = Penalty of delay in treatment.

Let C_i be the cost of one working hour of one of the Medical Staff m.

$$C^{MS_{Staff}} = \sum_{mi \in A} C_{m_i} * X_{m,k,i,j}$$

Let C_p be the cost of delay in treatment per minute for patient r.

$$C^{delay} = \sum_{p \in P} C_p * D_p$$

With D_p the total minutes of delay.

Let C_i be the cost of the material resource r_i.

$$C^{MatResources} = \sum_{ri \in R} C_i$$

Once each cost is calculated, a comparison with reference costs will be done: C^{MS_{Staff}}_{Ref}, C^{delay}_{Ref} and C^{MatResources}_{Ref}.

V. SIMULATION

To better explain our approach to resolution, we propose the following illustrative example:

Representing an initial scheduling (Figure 5) consists of 9 care operations assigned to two medical staff "nurse" and "doctor" able to execute them. Medical care procedures can be done at the same time (for example, in case of Concussion, a doctor makes a diagnosis while a nurse is doing a carefully Neurological Exam for the same patient). Therefore, the operation can be performed carefully by mobilizing members of the Medical Staff at the same time and with the same duration or with varying execution times according to the skills required for the treatment realization.

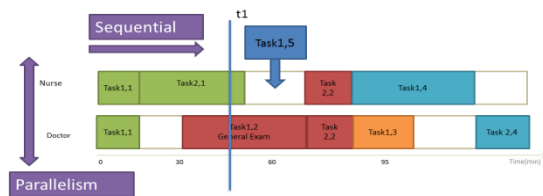


Figure 5: Tasks scheduling

At $t=t_1$, a new patient arrives. A doctor is needed for his treatment. Thus, the doctor (MSA) leaves the box where patient 1 is being treated to go to another box to treat patient 5. An operation may also be accomplished or interrupted by an emergency.

A. JADE PLATFORM

We are developing our system with JADE (Java Agent DEvelopment framework) platform [12]. JADE simplifies the implementation of MAS through a middleware that complies with the FIPA (Foundation for Intelligent Physical Agents) specifications and provides a set of graphical tools supporting the debugging and deployment phases. JADE system supports coordination between several agents FIPA and provides a standard implementation of the communication language agents which complies with FIPA specifications [13]. JADE is written in java language, supports mobility, evolves rapidly and until there, it is the only existent multi-agent platform which tolerates web services integration [14]. In this paper, we used a JADE graphical tool which sniffs message exchange between agents. This tool is useful to debug a conversation between agents.

Figure 6 shows the evolution of message exchange between the different agents through the “sniffer” tool useful for debugging.

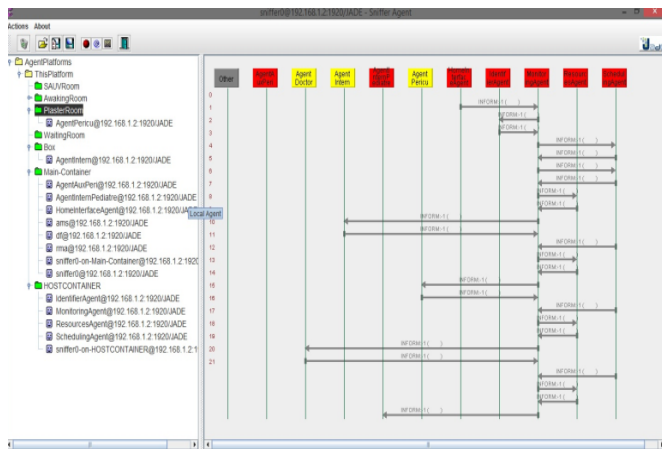


Figure 6: Communication between agents

B. Scheduling system implementation

The final assignment solution of MSAs to tasks is deduced from diagnosis generated by IA and our list algorithm results. On the Sniffer graphic tool (see Figure 6), “SAUVROOM”, “AwakingROOM”, “PlasterRoom”, “waitingRoom”, “Box” represent available PED department containers, where MSAs can move in order to treat patients according to the adopted contract model.

```
C:\WINDOWS\system32\cmd.exe
INFO: Listening on intra-platform commands on address:
- jicp://197.28.120.52:1920
juin 30, 2014 3:26:56 PM jade.core.BaseService init
INFO: Service jade.core.management.AgentManagement initialized
juin 30, 2014 3:26:56 PM jade.core.BaseService init
INFO: Service jade.core.messaging.Messaging initialized
juin 30, 2014 3:26:56 PM jade.core.BaseService init
INFO: Service jade.core.resource.ResourceManagement initialized
juin 30, 2014 3:26:56 PM jade.core.BaseService init
INFO: Service jade.core.mobility.AgentMobility initialized
juin 30, 2014 3:26:56 PM jade.core.BaseService init
INFO: Service jade.core.event.Notification initialized
juin 30, 2014 3:26:56 PM jade.core.PlatformManagerImpl localAddNode
INFO: Adding node <PLASTERROOM> to the platform
juin 30, 2014 3:26:56 PM jade.core.AgentContainerImpl joinPlatform
INFO:
Agent container PLASTERROOM@197.28.120.52 is ready.
-----
juin 30, 2014 3:26:56 PM jade.core.PlatformManagerImpl nodeAdded
INFO: --- Node <PLASTERROOM> ALIVE ---
INFO: Service jade.core.mobility.AgentMobility
juin 30, 2014 3:40:19 PM physicalAgents.AgentDoctor setup
INFO: AgentDoctor@Main-Container
Agent AgentDoctor moved to OFFICE@197.28.120.52:1920
INFO: Service jade.core.mobility.AgentMobility initialized
juin 30, 2014 3:40:16 PM jade.core.BaseService init
INFO: Service jade.core.event.Notification initialized
juin 30, 2014 3:40:16 PM jade.core.PlatformManagerImpl localAddNode
INFO: Adding node <WAITINGROOM> to the platform
juin 30, 2014 3:40:16 PM jade.core.PlatformManagerImpl nodeAdded
INFO: --- Node <WAITINGROOM> ALIVE ---
juin 30, 2014 3:40:16 PM jade.core.AgentContainerImpl joinPlatform
INFO:
Agent container WAITINGROOM@197.28.120.52 is ready.
```

Figure 7: Agent migration

VI. CONCLUSION

In this paper, we have proposed an intelligent system for the care of patients in the PED based on framework for dynamic scheduling. The proposed solution introduces the possibility to satisfy the needs of patients while minimizing the costs related to delays in treatment, human and material resources allocation and waiting time of patients. This application proves the efficacy of the approaches proposed by the multi-agent community to attain some of our objectives. In a future work, we aim to detail the behavior of MSAs.

REFERENCES

- [1] M.C. Pham, *Care of the patient in the hospital to better manage the complexity of the coordination of actors*. Dissertation of the National School of Public Health, Renne, 2002.
- [2] 2. X. Bertrand. Press Kit, « *Emergencies* », Ministry of Health and Solidarity, 23 may 2006.
- [3] J. Sauer, *Knowledge-Based Scheduling Techniques in Industry*, CRC Press, Boca Raton, 1999.
- [4] Ni, Wang, Y. Chen, L. Zhang, *Design of Multi-agent based Distributed Scheduling System for Bus Rapid Transit*. Third International Conference on Intelligent Human-Machine Systems and Cybernetics, 111-114, 2011.
- [5] N. Zoghliani and S. Hammadi, “Estimator Agent approach for distributed logistic chain optimization”, In Proceedings of the 50th IEEE International Conference ANIPLA’2006, Rome (Italy), 13-15 November 2006.
- [6] G. Bernard. *Technology of Mobile Code: State of art and perspectives*. National Institute of telecommunications, 1999.
- [7] G. P. Picco & al, "Designing distributed applications with mobile code paradigms", Proc. Of 19th Int'l Conf. on Software Engineering, July 1997.
- [8] H. Zgaya, S.Hammadi, K. Ghedira "WorkPlan Mobile Agent for the Transport Network Application", IMACS'2005, Paris, 11-15 July 2005.
- [9] H. Zgaya, S. Hammadi, K. Ghedira "Evolutionary method to optimize Workplan mobile agent for the transport network application", IEEE SMC'2005, Hawaii, USA 10-12 October 2005.
- [10] www.fipa.org
- [11] H. van der Linden, D. Kalra, A. Hasman, J. Talmon, Inter organizational future proof EHR systems: a review of the security and privacy related issues, International Journal of Medical Informatics 78 (3) (2009) 141–160.
- [12] <http://jade.titlab.com/doc>
- [13] www.fipa.org
- [14] D. Greenwood. "JADE Web Service Integration Gateway (WSIG)". Whitstein Technologies. Jade Tutorial, AAMAS 2005.

Program modules for control applications of microcontrollers

Jan Dolinay, Petr Dostálek and Vladimír Vašek

Abstract—This paper describes software library for microcontrollers intended for control applications. The library was created to make it easier to develop control applications for microcontrollers using modular approach - putting together modules provided in the library. The library is written in C language and works with Freescale HCS08 8-bit microcontrollers and the Kinetis series 32-bit ARM-based microcontrollers. However, it is easy to port it to other platforms.

Keywords—discrete controller, microcontroller, kinetis, hcs08.

I. INTRODUCTION

IN present time microcontrollers (MCU) are found in virtually any area of our life. Their applications range from simple devices such as flashlights or toys to complex embedded systems such as car and aircraft control units. In many applications it is required to implement some control algorithm on the MCU.

One of the greatest challenges in software development, and especially for embedded systems, is the reuse of existing code. Such reuse can save considerable time and money, but it requires wisely designed and implemented code modules, which are not focused just on fulfilling the task on given MCU, but which also consider the possible reuse on a different MCU. In microcontroller programming big part of the code seems to be developed from the scratch for every application [1]. This has some rational reasons, such as that the hardware differs much across the applications, but may be in part also caused by the lack of effort to write portable code. This is probably consequence of the tight deadlines and pressure for high performance from the employers and perhaps also small effort from the developers – it is easier to write hardware-specific code for single MCU than write more generic

This work was supported by the European Regional Development Fund under the project CEBIA-Tech No. CZ.1.05/2.1.00/03.0089)

Jan Dolinay is with the Department of Automation and Control Engineering, Tomas Bata University in Zlin, Faculty of Applied Informatics, nám. T. G. Masaryka 5555, 76001 Zlin, Czech Republic (e-mail: dolinay@fai.utb.cz).

Petr Dostálek is with the Department of Automation and Control Engineering, Tomas Bata University in Zlin, Faculty of Applied Informatics, nám. T. G. Masaryka 5555, 76001 Zlin, Czech Republic (e-mail: dostalek@fai.utb.cz).

Vladimír Vašek is with the Department of Automation and Control Engineering, Tomas Bata University in Zlin, Faculty of Applied Informatics, nám. T. G. Masaryka 5555, 76001 Zlin, Czech Republic (e-mail: vasek@fai.utb.cz).

code which is ready for future porting to another MCU. Whatever the reasons are, the result is that the cost of embedded software is high and time-to-market is long. Or, in some cases, the quality of the software is poor.

The solution is in the usage of program libraries, which provide code usable in different applications. In the area of embedded programming, however, the problem is that the hardware may be very diverse in different applications and therefore it is hard to create program libraries, which would be usable on several types of microcontrollers. Nevertheless, there are kinds of problems which are virtually hardware independent. For such areas it is possible to create a library which will work on wide range of devices [2].

One such area is system control. The control algorithms may be relatively complex, which makes it hard and time-consuming to implement and debug them, but on the other hand, once the code is written and debugged in a portable programming language, such as C, it can be used on many devices without change.

In this paper such a program library for control applications is described. The main part of the library consists of discrete controllers, but it also proposes the framework for the whole control application which allows separating the hardware-dependent code from the independent and thus makes the application easily portable to new MCUs. As a byproduct of creating the library also some supporting code (such as hardware drivers) was developed.

The described library was developed for Freescale HCS08 8-bit microcontrollers [4] and for Freescale Kinetis family, which are 32-bit MCUs with ARM architecture [5], [6]. The idea of such a library originates from our previous work [8] [9], but the design and code is completely new.

II. LIBRARY CONCEPTS

The requirements considered when designing the library can be summarized as follows:

- Provide discrete controllers usable in many common MCU applications
- Easy to use programming interface
- Easily portable to different MCUs

From the logical point of view the library can be divided into three main parts:

- controller modules (functions)
- template code for user application

- software-PWM generator
- supporting code (drivers)

A. Controller modules

Controller modules are the core part of the library. The word module is used here in the meaning common in C-language programming, that is, a set of functions and the data used by those functions wrapped into a source and header file. From the logical point of view a module is one type of a controller, e.g. a discrete PID controller. Typically it contains two C functions: the 1st one takes care of the initialization of the controller and the 2nd function computes the controller output in each step.

B. Template for user application

The library not only provides the modules (controllers) but it also suggest a preferred way of using these controllers. This is achieved by providing template files, which contain skeleton code of a control application. The user is advised to include these template files in his/her program and implement the application-specific and hardware-specific code as outlined in the templates. Example applications are also provided which show how to implement this code.

However, the user is not forced to use this application template or any other particular style of programming. He is free to use any part of the library separately, e.g. just the controller module(s), which are C functions and therefore can be simply called from any C program.

C. Software PWM generator

The library also contains simple multi-channel generator of pulse-width-modulated (PWM) signal. This signal can be used as a simple replacement for digital-to-analogue converter and therefore is used in many control applications for driving the actuators, e.g. for turning a heating element on and off in applications which control temperature.

In an application where there the period of the PWM signal can be relatively long (about 1s or more), the user can take advantage of this software PWM generator provided by the library, which is easier to use than hardware PWM generator contained within most MCUs.

D. Supporting code

The library also contains supporting code, which was developed in during the development of the library for testing its functions on real hardware. An example of such a supporting code is driver for serial communication interface (UART).

The support code can be directly used in applications targeting one of the MCUs supported by the library, or it may provide starting point and working examples of the code which will be very likely needed when using the library on a different MCU.

E. Typical use

The preferred way of using the library is as follows: the user will create an 'instance' of a controller by defining one

variable (a C structure which holds the private data of this instance of the controller). The fact that the user provides the memory for storing these data is advantageous for embedded systems with limited amount of RAM, because only as much memory is occupied as is needed. Other approaches which provide the memory internally and automatically in the library may be somewhat easier to use, but they require more resources. Either the memory needs to be statically allocated inside the library which limits the number of available controllers and wastes memory of the unused controllers. Or there needs to be dynamic memory management used, which bring large overhead to the code.

After creating the variable for controller data, user passes this variable into the controller initialization function.

Then he/she ensures that controller 'step' function is called regularly with the period equal to sampling period of the system. This can be done using simple busy loop in the main function, or (preferably) by using hardware timer.

The user is assumed to add to his/her project the template files `ucp_app.h` and `.c` and `ucp_hal.h` and `.c` and implement the application and hardware specific code in these files. The application logic including the controller variable(s) is contained in `ucp_app.c` file.

The following figure shows very basic user program:

```
#include "ucp_app.h"

void main()
{
    ucp_app_init();

    for(;;) {
        ucp_app_on_sample();
        delay();
    }
}
```

Fig. 1 minimal version of control application with the library

As can be seen in the figure, there is standard C-language main function, which calls function `ucp_app_init()` at the beginning and then periodically calls `ucp_app_on_sample()`. Both these functions are implemented in the template file `ucp_app.c`. The `ucp_app_init` function performs any initialization necessary, mainly the initialization of the controller(s), but also initialization of the hardware, such as AD converter or I/O ports. This is obviously application-specific and the code itself should be written by the user. The library offers standardized approach to the hardware-specific code by providing hardware abstraction layer (HAL) files `ucp_hal.h` and `.c`. The HAL defines functions for hardware initialization (`ucphal_init`), reading input (`ucphal_read_input`) and writing output (`ucphal_write_output`) and also reading the set point (`ucphal_read_setpoint`). Naturally, the library cannot provide implementation of these functions, but if the user(s)

adhere to this proposed API, it makes the implementation straightforward and simplifies possible porting to different hardware, as the hardware-specific code is isolated in one place (the `ucphal.c` file) and at low level of the application. The implementation of the HAL API itself depends greatly on the application, for example, the `ucphal_read_input` can obtain the measured input from AD converter, or from a software driver which communicates with external smart sensor. Similarly, the `ucphal_write_output` can produce the desired actuating signal using DA converter, PWM or some external device. And the `ucphal_read_setpoint` provides uniform method of obtaining the desired value of the controlled signal no matter if this value is obtained from a single potentiometer, internal variable of the GUI code, etc. This is all hidden from the control app, which just calls the HAL API functions.

III. TARGET HARDWARE

The library aims to be as much hardware-independent as possible with the hardware-specific code easily portable to other MCUs. However, it did need to be created and tested on some hardware. We selected HCS08 MCUs and Kinetis series MCUs as two candidates of relatively different MCU platforms. Important role in the selection played the availability of the device in a development kit. For these reasons we used the development kit from the MCU-programming lessons at our institute, which contains HCS08 GB60 MCU and new ultra-low-cost development kit FRDM-KL25Z with the Kinetis MCU [6].

A. HCS08 8-bit microcontrollers

For testing the library on 8-bit MCUs we used development kit M68EVB908GB60. This kit is no longer manufactured but still used in our lessons. The GB60 MCU itself is still a live part and besides that, it should require very little effort to use the code for the GB family on another member of the HCS08 product line, e.g. the QG or SH.

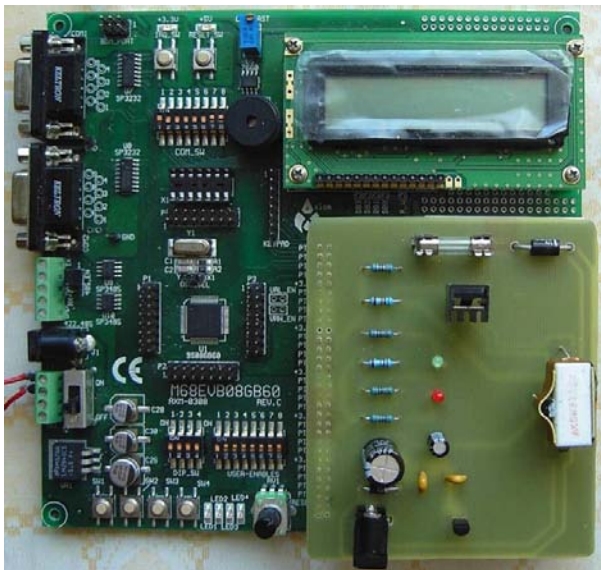


Fig. 2 HCS08 development kit with heating-plant model attached

In the figure 2 the evaluation kit can be seen together with model of a heating plant [7], which was used for experimental verification of the library.

B. Kinetis 32-bit microcontrollers

Another hardware platform for which the library was developed is Freescale Kinetis series of 32-bit microcontrollers. Compared to the HCS08 microcontrollers the 32-bit MCUs offer higher computing power and more memory, which makes them suitable even for complex control applications.

There is a line of low cost evaluation boards available for these microcontrollers called Freedom platform [6]. In our case FRDM-KL25Z board was used. This board contains KL25Z128VLK4 microcontroller with 128 kB of Flash and 16 kB of RAM memory together with programming and debugging interface (openSDA). The layout of the board is compatible with the layout of popular Arduino platform [11] which makes it possible to connect expansion boards (so called shields) for Arduino to this board.

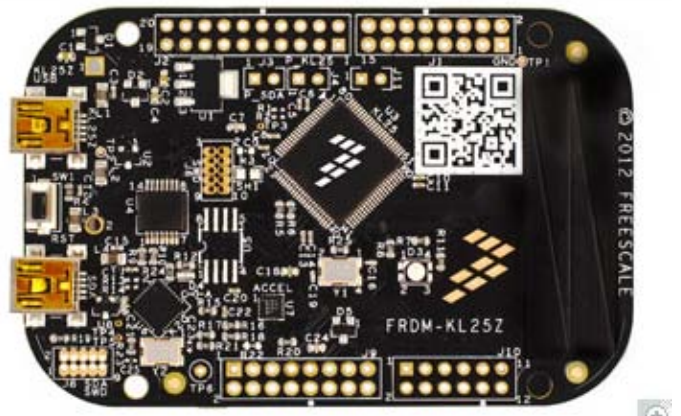


Fig. 3 FRDM-KL25Z board used for tests (32-bit ARM MCU) [5]

IV. CREATED MODULES

Currently two control algorithms are implemented in the library – discrete PID controller (PSD) and a simple on-off controller with hysteresis.

A. Discrete PID controller (PSD controller)

This module implements the well-known incremental version of the discrete PID algorithm. The recursive equation used to compute the control signal in each sample period is:

$$u(k) = u(k-1) + q_0 e(k) + q_1 e(k-1) + q_2 e(k-2) \quad (1)$$

Where k denotes the step, so for example, $e(k)$ is the error in current step and $e(k-1)$ is the error in previous step. The coefficients of the controller q_0 , q_1 and q_2 can be obtained by methods for controller tuning, such as [3].

From the programmer's perspective, the interface of this module is represented by data structure `UCP_PSD_REG` and

functions `ucp_psd_init` and `ucp_psd_step`. Signatures of these functions can be seen in the figure 4:

```
uint8_t ucp_psd_init(UCP_PSD_REG* pReg,
                   float q0, float q1, float q2, float q3);
float ucp_psd_step(UCP_PSD_REG* pReg,
                  float y, float setpoint, float minval, float maxval);
```

Fig. 4 Interface of the discrete PID controller

As mentioned earlier, there is “init” function, which the user program calls one at the beginning to initialize the controller and there is “step” functions which should be called in every sample period to obtain new value of the control signal. Both these functions receive pointer to the data structure of the controller as the 1st parameter. Parameter `y` is the current output of the controlled plant; the `minval` and `maxval` are the boundary values for the control signal (e.g. 100% for PWM). These are needed as the input of the controller because the old values of `u(k)` stored inside the controller must correspond to control signal really applied to the plant. The other parameters are rather self-explanatory.

B. On-off controller

This module implements simple on-off type of controller with optional hysteresis. The data structure for this controller is called `UCP_ONOFF_REG`. Similarly as in the discrete PID controller, there are 2 functions as shown in the figure 5.

```
uint8_t ucp_onoff_init(UCP_ONOFF_REG* pReg,
                      float up_hysteresis, float down_hysteresis);
uint8_t ucp_onoff_step(UCP_ONOFF_REG* pReg,
                       float y, float setpoint);
```

Fig. 5 Interface of the on off controller

As can be seen in the figure, the user can specify two values of the hysteresis; one for the “up” direction of the controlled signal and one for the “down” direction.

V. EXPERIMENTAL VERIFICATION

To verify the functionality of the library, we created several control applications. As the controlled system a model of heat plant was used [7]. This model represents a 2nd order system with transfer function approximately:

$$G(s) = \frac{0.8}{(86.5s + 1)(18.2s + 1)} \quad (2)$$

Figure 6 shows result of control with the discrete PID controller module. This is very simple control process, but it demonstrates the correct function of the program modules. The parameters of the controller were designed using method [3]. The control signal is created using the software PWM module contained also in the library. In the figure, the set point and output of the plant are depicted in degrees Celsius; the control signal is shown in percent. The set point was fixed at 50 °C.

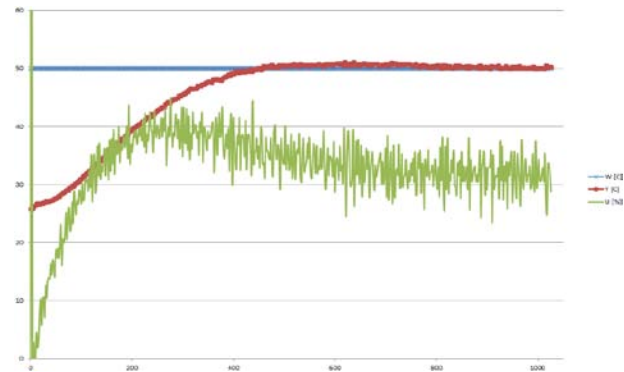


Fig. 6 Experimental verification of the PID controller

VI. CONCLUSION

This article described our program library for control applications. The library makes it easier and faster to create microcontroller applications for control systems. This is achieved by set of hardware-independent modules, which are ready-to-use and also by providing framework for writing the whole application including hardware-dependent code and its interface with the rest of the application. The library is written in C language and currently implemented and tested on two types of microcontrollers: 8-bit HCS08 core and 32-bit Kinetis (ARM) cores. It is possible to port it to other microcontrollers easily.

REFERENCES

- [1] T. D. Morton, *Embedded Microcontrollers*. Prentice Hall, 2001.
- [2] D. Ibrahim, *Microcontroller-based temperature monitoring and control*, Oxford: Newnes. 2002.
- [3] A. Viteček, M. Vitečková, “Inverse Dynamics Method Tuning and Basic Quality Indices”, *9th International Scientific Conference CO-MAT-TECH 2001*, Slovenská technická univerzita, 2001, pp. 412-417. ISBN 80-227-1591-3.
- [4] *Freescale Semiconductor, CPU08 Central Processor Unit Reference Manual, rev.4*. Available: <http://www.freescale.com>
- [5] *Freescale Semiconductor, Freescale Freedom Development Platform*. Available: <http://www.freescale.com/webapp/sps/site/overview.jsp?code=FREDEV PLA>
- [6] *Freescale Semiconductor, FRDM-KL25Z: Freescale Freedom Development Platform for Kinetis KL14/15/24/25 MCUs*. Available: http://www.freescale.com/webapp/sps/site/prod_summary.jsp?code=FRDM-KL25Z.
- [7] J. Dolinay, P. Dostálek, V. Vašek, “Educational models for lessons of microcontroller programming”, in *Proc. 11th International Research/Expert conference TMT 2007*, Hammamet 2007, pp. 1447-1450.
- [8] P. Dostálek, V. Vašek, J. Dolinay, “Design and implementation of portable data acquisition unit in process control and supervision applications”, in *Proc. 13th WSEAS International Conference on CIRCUITS*, Rhodes 2009, pp. 799-808.
- [9] J. Dolinay, V. Vašek, P. Dostálek, “Implementation and Application of a Simple Real-time OS for 8-bit Microcontrollers”, in *Proc. 10th WSEAS International Conference on ELECTRONICS, HARDWARE, WIRELESS and OPTICAL COMMUNICATIONS (EHAC '11)*, Cambridge 2011, pp. 023-026, ISSN 1792-8133.
- [10] J. Dolinay, P. Dostálek, V. Vašek, P. Vrba, “Platform for teaching embedded programming”, *International journal of mathematical models and methods in applied sciences*, vol. 5, no. 6, pp. 1110-1117, 2011.
- [11] *Arduino, Open-source electronics prototyping platform*, Available: arduino.cc.

Evaluation of SolidWorks Flow Simulation by ground-coupled heat transfer test cases

S. Sehnalek, M. Zalesak, J. Vincenec, M. Oplustil, and P. Chrobak.

Abstract — In this article validation of SolidWorks Flow Simulation with IEA BESTEST Task 34 is presented. Firstly are described steady-state cases used for validation. Afterward is mention implementation of these cases on SolidWorks Flow Simulation. Article is concluding with presenting the simulated results with comparison of those from already validated simulation software by IEA. At the end is presented discussion with outline of future research.

Keywords — Heat transfer, Finite Element Method, SolidWorks Flow Simulation, Software validation, Benchmark, Building simulation

I. INTRODUCTION

Share of glass used in façades of buildings is logarithmically increasing during the last two centuries.

This results from some valuable features of glass, which are transparency, low weight and ability to separate different environments. Since Le Corbusier's era, glass is becoming dominant in usage for façades at the expense of conventional materials. This fact could prove Scheerbart's paraphrased words "Bricks are only good to hurt". In the way of usage of glass for façades there is one important issue, which should be always taken into account. Temperature gains caused by internal and external heat sources. These gains affect comfort of people inside these "plant house" buildings. A long-term research of people's comfort in 26 office buildings in five European Union countries was executed [1]. Interior comfort can be provided by ventilation systems, by shading systems or

This work was supported in frame of Internal Grant Agency of Tomas Bata University in Zlin, Faculty of Applied Informatics IGA/FAI/2014/015, IGA/FAI/2014/047, IGA/FAI/2014/050, and IGA/FAI/2014/057 and under the project CEBIA-TECH NO. CZ.1.05/2.1.00/03.00089

S. Sehnalek is with the Tomas Bata University in Zlin, Faculty of Applied Informatics, Department of Automation and Control Technologies, Zlin, 76005 Czech Republic (e-mail: sehnalek@fai.utb.cz, phone: +420 576 035 231).

M. Zalesak, is with the Tomas Bata University in Zlin, Faculty of Applied Informatics, Department of Automation and Control Technologies, Zlin, 76005 Czech Republic (e-mail: zalesak@fai.utb.cz).

J. Vincenec is with the Tomas Bata University in Zlin, Faculty of Applied Informatics, Department of Automation and Control Technologies, Zlin, 76005 Czech Republic (e-mail: vincenec@fai.utb.cz).

M. Oplustil is with the Tomas Bata University in Zlin, Faculty of Applied informatics, Department of Automation and Control Technologies, Zlin, 76005 Czech Republic (e-mail: oplustil@fai.utb.cz).

P. Chrobak is with the Tomas Bata University in Zlin, Faculty of Applied informatics, Department of Automation and Control Technologies, Zlin, 76005 Czech Republic (e-mail: chrobak@fai.utb.cz).

by their combination, which are not always energetically sustainable. In recent years, there is a particular interest in sustainability of buildings [2], [3]. Currently, there has been growing interest in lowering energy performance of buildings. This effort is also reflected in a new European directive, which instructs to construct near to zero energy sufficient buildings since year 2020. Regardless of our experience and knowledge, there are always a risks of constructing an inconvenient building. To prevent this, appropriate design of building should be achieved. Thermal properties of a building could be calculated in a development phase, but it is limited to one-dimensional and rarely as two-dimensional problem solutions thanks to the complexity of buildings and the mathematical apparatus available. As a result of computational power increase in last decades, it is possible to design a model and implement mathematical simulation of thermal behavior of a building also in three-dimensional space. For such mathematical simulation it is used finite element method (FEM). Thanks to the expanding performance of computers, FEM is used for partial differential equations solutions as a convenient way to validate building's behavior. However, first of all it is important to validate thermal simulation programs (DTSP) [4], which is used. The solution can be achieved by several ways. Judkoff and Neymark developed a methodology for such intention in the middle of 90s [5]. Their approach is based on the analytical solution for steady-state heat flow through the floor slab. Although it was developed by Delsante, Stokes and Walsh [6], although this problem has been in focus of researchers for some time [7]. It is worth to mention a simplified model by American Society of Heating, Refrigerating and Air Conditioning Engineers (ASHRAE), which calculates slab-on-grade perimeter heat-loss, operates with perimeter length and an F-factor heat loss coefficient. Delsante's methodology focuses only on heat flow through floor slab and omits above grade constructions. Standard established by ASHRAE improved Judkoff's and Neymark's methodology by adding cases which focus mainly on above grade constructions and solar radiation [7], [9].

All mentioned methods and standards are based on finite element analysis (FEA). In this paper, an application of International European Agency Building Energy Simulation Test (IAE BESTEST) Task 34 is described on SolidWorks Flow Simulation (SW-FS). This task is already approved on DTSP like are TRNSYS, Fluent, EnergyPlus and ESP-r/BASESIMP. Besides that, investigation of COMSOL Multiphysics on Task 34 was done by Gerlich [10].

In the section methods is included outline of 6 cases from IAE BESTEST Task 34 along with a description of SW-FS.

This chapter is followed by results section with description of implementation of cases on SW-FS and finally with results from simulation. Article is summarized by conclusion section with discussion about results and outline of further research.

II. METHODS

This section of the paper cover several topics and is divided in two parts. At the beginning of the section, Ground Coupling In-Depth Diagnostic Cases is described. More specifically: geometry, physical properties, initial conditions and boundary conditions. In the second section the outline capabilities of SolidWorks Flow Simulation 2012 SP 5 (SW-FS) is tested.

A. IEA BESTEST cases

International Energy Agency Building Energy Simulation Test methodology was developed by Judkoff [5] in the middle of 90s. Combination of empirical validation, analytical verification and comparative analysis techniques are main proceedings of this methodology. It operates only with slab-on-grade heat transfer and became a stepping-stone for the other approaches, such as ANSI/ASHRAE Standard 140 improved adaptation developed by ASHRAE accordingly with American National Standards Institute (ANSI).

Methodology describes 6 cases of ground-coupled heat transfers designed to be compared with verified whole-building energy simulation software. Several of those already tested by IEA are EnergyPlus, FLUENT, Matlab, TRNSys and GHT. The first case, GC10a has its base in analytical solution and it is the simplest one of all six cases. Furthermore, these cases are subdivided into three series, each with its own specification.

- Series a
 - The main purpose of this series is to use to validate whole-building simulation programs.
 - Namely: TRNSYS, SUNREL-GC, FLUENT and MATLAB.
 - It is recommended to apply this series as the first one, if a tested software can run it.
- Series b
 - In this series, parameters are adjusted for more limited whole-building simulation programs or standard.
 - Namely: EnergyPlus and ISO 13 370.
 - Provides basis for series “a” and “c”.
- Series c
 - This series is most narrowed in use of boundary conditions, because it serves only for comparison of BASESIMP with other software.

1) Geometry

Geometry is similar in most cases, except for several models, which will be described later. Figure 1 depicts the elevation section of the examined test model, where F represents far field boundary distance, E stands for deep ground boundary depth, T_{dg} is deep ground temperature, $T_{o,a}$ is

the outside air temperature, $T_{i,a}$ is the inside temperature and h_{int} and h_{ext} represents surface coefficients of convection [5].

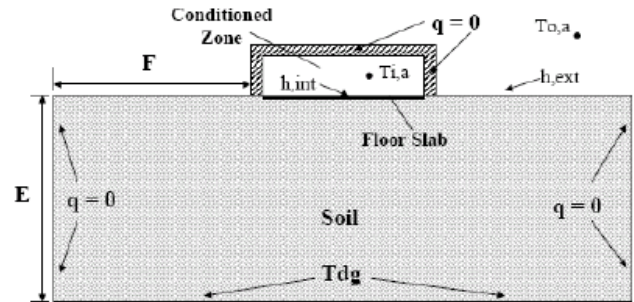


Fig. 1 Elevation section [11]

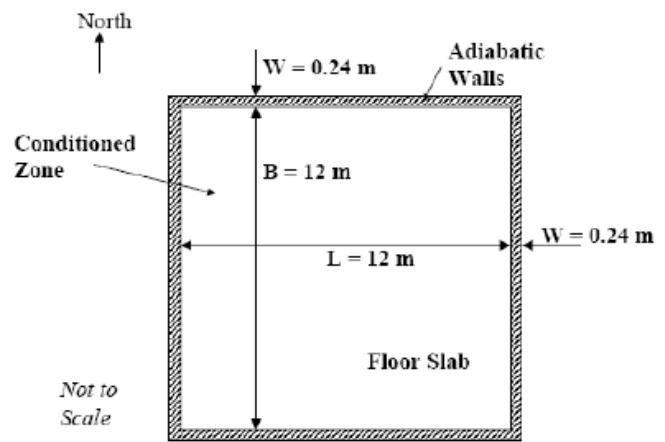


Fig. 2 Plan view [11]

Figure 2 shows plan view of the proposed building with slab dimensions. These parameters are similar for all cases. The last dimension parameter worth mentioning is the height of the conditioned zone. Table I enlists geometrical properties for proposed cases, with inequality in GC10a, GC30a and GC30c, which vary in ground depth and far-field boundary distance [5].

Table I Geometry properties

Parameter	Value [m]
B	12
E	15
F	15
L	12
W	0,24
Building height	2,7

2) Thermal properties

Besides surface coefficients of convection, the rest of thermal properties are the identical for all test cases. These are enlisted in table 2 where surface coefficients of convection are applied on all surfaces with a value $100\text{ W}/(\text{m}^2\text{ K})$, within exception of specific cases which are mentioned later.

Table II Thermal properties for soil, slab and above grade construction

	Soil and Slab	Above-Grade Construction
Temperature [°C]	10	30
Convective surface coefficients [W/(m ² K)]	100	100
Thermal conductivity [W/(m K)]	1,9	0 or 0,000001
Density [kg/m ³]	1490	0 or 0,000001
Specific heat [J/(kg K)]	1800	0 or 0,000001

Several parameters which are not present in table IIza also have to be taken into account: use slab thickness as low as software allows for a stable calculation; for software demanding below-grade foundation walls, use the same thermal properties as soil; surface radiation exchange is not included (if necessary set radiation to 0 or as low as possible); the ground surface and floor slab are on the same height level and both are considered to be flat and homogenous; for all cases water transmission via material should be turned off or reduced to its lowest level; adiabatic walls of the above construction are in contact with soil but do not penetrate it; no windows; no infiltration or ventilation; no internal gains.

If the software does not allow entering direct surface temperatures, user can apply very high surface coefficients of convection with ambient air temperature. It is recommended to set $h \geq 5000 \text{ W/(m}^2 \text{ K)}$ if the program allows such surface coefficient, if it be to the contrary use maximum h value that tested software accepts. In some cases such a great number can cause instability of some simulation software [5].

3) *Case GC10a – Steady-State Analytical Verification Base Case*

Result from this case is verified by analytical solution method and comparison with test numerical simulation software can be considered as secondary mathematical truth standard. Such approach is beneficial for later cases, where exact analytical solution is unknown.

Changes to surface geometry is given

- This case has similar main geometrical and thermal properties with exception of dimension. In this case, ground surface is considered to be semi-infinite both in downward and horizontal direction.

This case is based on Analytical Solution for Steady-State Heat Flow through the Floor Slab in 3 dimensional space conditions, which was developed by Delsante [6]. The total heat flow through the slab into the ground is:

$$q = k(T_i - T_o) \frac{1}{\pi} F(L, B, W) \tag{1}$$

Where: T_i is surface temperature of the floor
 T_o surface temperature of the outside ground
 k conductivity of floor slab and soil
 $F(L, B, W)$ dimension function of L, B and W

4) *Case GC30a – Steady-State Comparative Test Base Case with Direct Input of Surface Temperatures*

This test case method compares steady-state heat flow results with verified numerical-model results. In this case surface boundary conditions could be tricky for some simulation software. Comparison of this case with GC10a (GC30a–GC10a) reveals the sensitivity to perimeter surface boundary.

Changes to surface geometry are given

- Deep ground boundary depth (E) 30 m
- Far-field boundary distance (F) 20 m

5) *Case GC30b – Steady-State Comparative Test Base Case*

Steady-State Comparative Test is used to compare temperature divergence of zone air and ambient air with a use of adiabatic zone interface boundary. This case compares GC30a (GC30b–GC30a) checking sensitivity to steep surface coefficients of convection versus direct-input surface temperature boundary.

Changes to surface geometry is given

- $h_{,int} = 100 \text{ W/(m}^2 \text{ K)}$
- $h_{,ext} = 100 \text{ W/(m}^2 \text{ K)}$

6) *Case GC60b – Steady State with Typical Interior Convective Surface Coefficient*

In this case more realistic interior convective surface heat transfer coefficient is used. Zone floor surface temperature will be barely identical when more realistic coefficient is used. Also, increment in outward temperature in direction from the center can be expected. This case will be compared with result from GC30b (GC60b–GC30b) to check sensitivity of decreased h .

Changes to surface parameter is given

- $h_{,int} = 7.95 \text{ W/(m}^2 \text{ K)}$

7) *Case GC65b – Steady State with Typical Interior and Exterior Convective Surface Coefficients*

With this case is used similar conditions as with GC60b only taking account one exception and that is lower $h_{,ext}$. Similar increment in outward temperature can be estimated and results from this case will be compared with GC60b (GC65b–GC60b), where sensitivity on $h_{,ext}$ is compared. And also will be compared result with GC30b (GC65b–GC30b) where compared sensitivity on $h_{,ext}$ and $h_{,int}$ are checked.

Changes to thermal properties are given

- $h_{int} = 7.95 \text{ W}/(\text{m}^2 \text{ K})$
- $h_{ext} = 11.95 \text{ W}/(\text{m}^2 \text{ K})$

8) Case GC30c – Steady-State Comparative Test Base Case with BASESIMP Boundary Conditions

Purpose of this case is to compare numerical simulation programs of boundary conditions compatible with BASESIMP. With this model will be comparison of GC30b (GC30c–GC30a) to check reduced interior surface coefficient sensitivity.

Changes to surface geometry and parameter are given

- $h_{int} 7.95 \text{ W}/(\text{m}^2 \text{ K})$
- Far field boundary distance (F) 8 m

B. SolidWorks Flow Simulation

SolidWorks Flow Simulation 2012 (SW-FS) is a fluid flow analysis add-in package that is available for SolidWorks in order to obtain solutions to the full Navier-Stokes equations that govern the motion of fluids. SW-FS is tool which can be used for wide range of fluid flow and heat transfer studies. Some of physical calculation capabilities are [12]:

- External and internal fluid flows
- Steady-state and time-dependent fluid flows
- Fluid flows with boundary layers, including wall roughness effects
- Multi-species fluids and multi-component solids
- Heat conduction in fluid, solid and porous media with/without conjugate heat transfer and/or contact heat resistance between solids and/or radiation heat transfer between opaque solids (some solids can be considered transparent for radiation), and/or volume (or surface) heat sources, e.g. due to Peltier effect
- Joule heating due to direct electric current in electrically conducting solids
- Various types of thermal conductivity in solid medium, *i.e.* isotropic, unidirectional, biaxial/axisymmetrical, and orthotropic
- Fluid flows and heat transfer in porous media
- Periodic boundary conditions.

1) The Navier-Stokes Equations for Laminar and Turbulent Fluid Flows

SW-FS are solving Navier-Stokes equations formulated with mass, momentum and energy conservation laws. They are supplemented with nature of the fluid and with empirical dependencies of fluid density, viscosity and thermal conductivity. Finally the definition of geometry, boundary and initial condition is specifying particular problem.

Several boundary conditions can be setup. Internal Flow Boundary Conditions can be managed as same as External Flow Boundary Conditions. The last of three is Wall Boundary Conditions that can be managed as impermeable in case of solid walls. There is also option to manage wall as Ideal Wall, which corresponds to the well-known slip condition.

SW-FS employed numerical solution technique so it is usable for less knowledge about the computational mesh and

numerical methods. But there are also included options to adjustment values of parameters governing the numerical solution technique to lower computer resources or to provide superior results. Finite volume method is used on a cubic Cartesian coordinate system with planes orthogonal to its axes. If necessary it can be refined locally in specific region during calculation [12].

Mesh in SW-FS is rectangular everywhere in the computational domain. That means that cells sides are orthogonal to specific axes. That means that boundary between fluid and solid may have partial cells. The computational mesh is constructed in the several stages. Basic mesh is constructed firstly, dividing computational domain into slices where user can specify number and spacing of the planes in each axes. Intersection between solid and fluid are divided uniformly into smaller cells to provide more appropriate result in this boundary. Meshing procedures are executed before the calculation so SW-FS is unable to resolve all solution features well. To abandon this disadvantage there is option during the calculation to change mesh in accordance with the solution spatial gradients. That means that regions with high-gradient are divided in more cells while in low-gradient regions are cells merged. This feature is called **refinement** and it can be imposed manually or automatically, at any state of the calculation process [13].

Validation examples can be found in documentation or elsewhere [13].

III. RESULTS

Result section will provide outcome of appropriate application of IEA BESTEST cases on SW-FS software and findings will be discussed in the second part of this chapter.

A. Application of cases on SW-FS

This chapter deals with implementation of IEA BESTEST on SW-FS. Cases' main parameters initiation will be provided in subsections. First case is considered as parental for all the other cases and only changes in those will be mentioned.

Geometry model was established as assemblies in SolidWorks consisting of three parts. These are soil, slab and Above-Grade Construction (cubicle), and each part corresponds with model's physical property. They were modelled from center of the Cartesian coordinates and mates together.

A new project in Flow Simulation by Wizard tool was created for simulation. Selection of Unit Systems, in this case SI units, follows the choice of appropriate name. The only change made was a switch on temperature; from K to °C. Heat conduction in solids as the only option was selected for external analysis type. For a default solid material was created a new entry in the Engineering database with thermal properties of soil and slab described in Table 2. Initial conditions of solid parameters were changed from 20 °C to 10 °C. The last adjustment in Wizard tool was made on initial mesh, which was set to 8 along with manual input of gap size value 2.7m and wall thickness 0.24m. Setup of the study continues with an insertion of thermal properties for the cubicle. This can be done by Solid Material option and by

creating a new entry in the Engineering database together with a selection of appropriate geometry. Boundary conditions were established separately for each surface with an entry of appropriate convective surface coefficients and fluid temperature. Finally, computational goals were selected.

B. Simulation outcome

After appropriate setup of the cases on SW-FS simulation of each case was executed.

Results from simulation are shown in figure 3. Axis Y represents heat flows in W, on axis X are displayed used cases. The line at the top of each case is average without SW-FS taken in account. Results for EnergyPlus, FLUENT, Matlab and TRNSYS was taken from [5], results for COMSOL Multiphysics was taken from [10]. Results of case GC10a and GC30a was not provided for EnergyPlus.

As can be seen in figure 3, results of SW-FS vary from average by small percentage. Only in case GC10a is result lower than was desirable, particular because this case is validate by analytical solution. This difference could be cost by impossibility to make the perimeter infinite. The rest of cases achieved satisfactory values, which differ almost in all instants by 1% and case GC65b differ in positive direction almost by 4% as reveals table III.

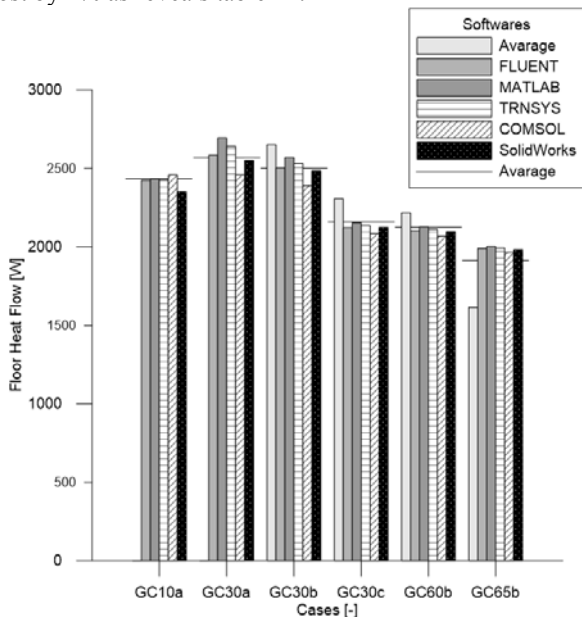


Fig. 3 IEA BESTEST Ground Coupling: In-Depth Floor Slab Steady-State Floor Conduction

Table III Stationary test cases calculated by SW-FS

Case	Solid Works [W]	Average [W]	Absolute difference [W]	Relative difference [%]
GC10a	2416,96	2431,59	14,63	0,6
GC30a	2552,28	2567,48	15,20	0,6
GC30b	2487,54	2498,73	11,18	0,4
GC30c	2125,12	2161,20	36,09	1,7
GC60b	2097,30	2126,70	29,40	1,4
GC65b	1983,93	1914,11	-69,82	3,6

Comparison of cases is displayed in figure 4. Axis Y is similar to figure 3, axis x represents odds between cases. Values were taken from same source as for figure 3. For this comparison was EnergyPlus excluded because of missing results for cases GC10a and GC30a. The evaluation for this comparison is presented in table IV. As can be seen difference vary from approximately 1% to 32%. Difference between cases GC10a – GC30a in about 15% reveals that the sensitivity to perimeter boundary of SW-FS is slightly worse than it should be. The comparison of GC30a – GC30b illustrates that SW-FS is imbalance for steep surface coefficients. On the other hand sensitivity to decreased *h* is very positive, which proves comparison of cases GC30b – GC60b and GC30b - GC65b.

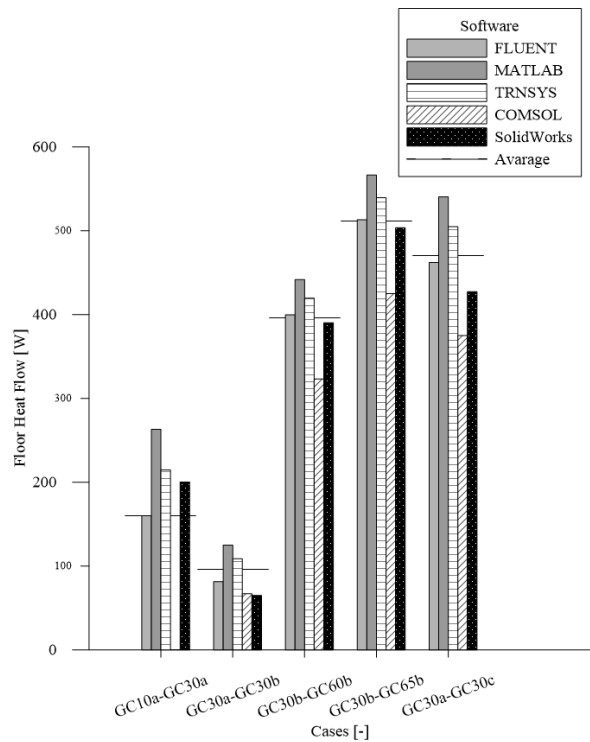


Fig. 4 IEA BESTEST Ground Coupling: In-Depth Floor Slab Steady-State Floor Conduction Sensitivity

Table IV Stationary test case comparison calculated by SW-FS

Case comp.	Solid Works [W]	Average [W]	Absolute difference [W]	Relative difference [%]
GC10a – GC30a	135,33	159,41	-24,09	15,1
GC30a – GC30b	64,74	95,49	-30,75	32,2
GC30b – GC60b	390,24	395,96	-5,71	1,4
GC30b – GC65b	503,61	510,94	-7,32	1,4
GC30a – GC30c	427,17	470,65	-43,48	9,2

During the simulation preparation phenomenon of SW-FS have been discovered. That is inappropriate behavior when SW-FS refining the mesh. When settings of mesh and refinement kept on default, software are generates basic mesh properly, after several iteration it starts to refine and phenomenon occur. Several options were changed along with geometry to figure what this asymmetry causing, without positive answer.

For the proper calculations was mesh configured manually to obey automatic refinement problem. This was done by control planes, which divide geometry to parts and then spread mesh between. The appropriate settings, which were use, can be find in table V. The comparison of basic mesh with refined mesh is depicted in figure 5. Basic mesh had totally 38 400 cells, where in direction X and Z had 40 cells and direction Y had 24 cells. After refinement, number of cells increased to 331 553.

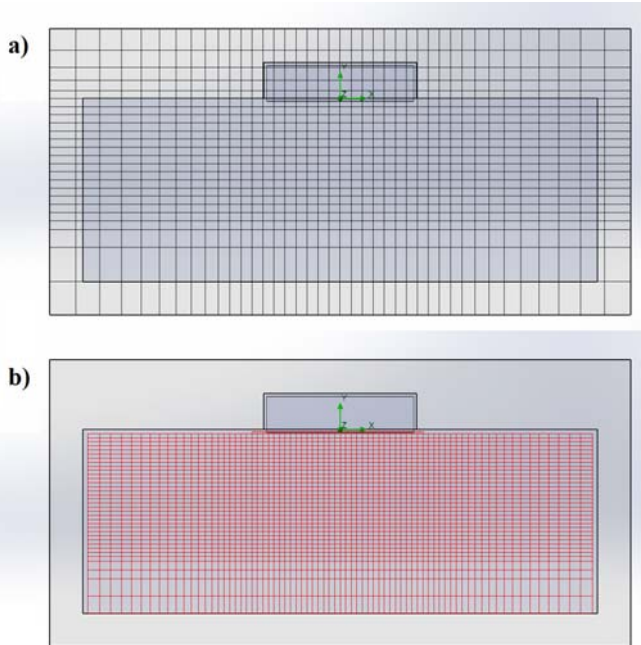


Fig. 5 Generated mesh by manual settings: a) basic mesh, b) refined mesh for solids

Table V Control planes settings

Control planes in	Name	Minimum	Maximum
X direction	X1	-23,7	-10,0
	X2	-10,0	10,0
	X3	10,0	23,7
Y direction	Name	Minimum	Maximum
	Y1	-17,7	-10,0
	Y2	-10,0	-3,0
	Y3	-3,0	0,0
Z direction	Name	Minimum	Maximum
	Z1	-23,7	-10,0
	Z2	-10,0	10,0
	Z3	10,0	23,7

Side view of temperature distribution is disclosed in figure 6. This state is for case GC30b with basic conditions. Other cases are similar to this only with little differences in distribution and geometry sizes. Displayed temperature are in °C and vary from 10 °C for exterior to 30 °C for investigated slab.

Figure 7 represent heat flux on interior and exterior ground surface from top view. Values reaching more than 83 W/m² in corners of above-grade construction in opposition to exterior surface where reaching almost zero.

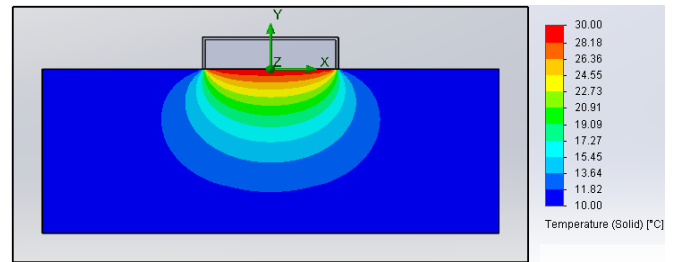


Fig. 6 Side view of temperature distribution

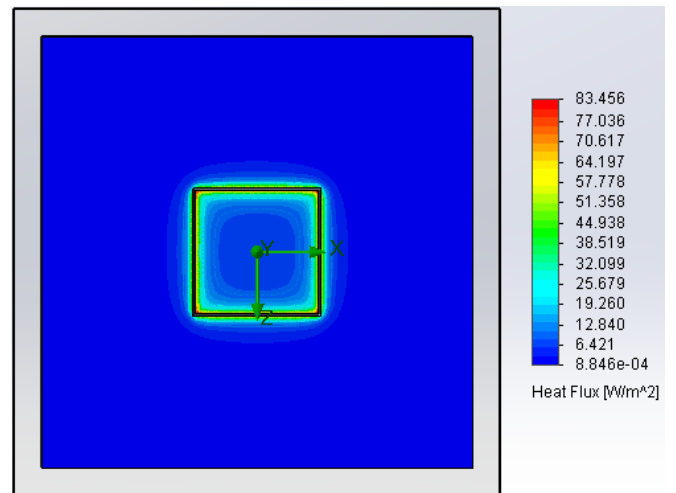


Fig. 7 Top view of heat flow

IV. CONCLUSION

The results indicate, overall, that SW-FS is capable of mathematical simulation of heat flow through the floor slab. Variation of 1% to 4% is very positive for such type of benchmark. As is documented in [11], there was variety from 9% to 55% disagreement between firstly tested software with the analytical solution. Afterward improvement in software lowering that difference to the highest value of 24%. Although version of SW-FS was 2012 and in present time is version 2014 on the market, it would be interesting to benchmark and compare results of that version with tested version.

However, appropriate setup of mesh should be considered along with proper analysis after generation. Also refinement option should be acknowledge as results showed big differences. Interest with refinement should be also in symmetrical object where SW-FS showed high disproportions.

As next step should be to do testing on remaining 10 cases from IAE BESTEST. These are similar to already tested one, but they have sinusoidal variation of outside temperature. Also condition to store every hour of ten year simulation make it hard for storage space. Just for interest there was accomplished case GC40b and whole data computed had more than 1TB of storage space.

Further research should aim comprehensive ANSI/ASHRAE Standard 140, and properly validate SW-FS with it. Although, SW-FS is not mainly for building applications, there is no snag why not to use it for such industry. Moreover as results prove it is suitable and in some cases more than other program adjusted mainly on it.

REFERENCES

- [1] F. Nicol and M. Humphreys, "Maximum temperatures in European office buildings to avoid heat discomfort," *Sol. Energy*, vol. 81, no. 3, pp. 295–304, Mar. 2007.
- [2] F. M. Butera, "Glass architecture: is it sustainable?," in *Passive and Low Energy Cooling for the Built Environment*, 2004, no. May 2005, pp. 161–168.
- [3] H. Poirazis, 2004. Double Skin Façades for Office Buildings – Literature Review, Report EBD-R--04/3, Lund University.
- [4] K. J. Lomas, H. Eppel, C. J. Martin, and D. P. Bloomfield, "Empirical validation of building energy simulation programs," *Energy Build.*, vol. 26, no. 3, pp. 253–275, Jan. 1997.
- [5] R. Judkoff and J. Neymark, (1995). *International Energy Agency Building Energy Simulation Test (IEA BESTEST) and Diagnostic Method*. NREL/TP-472-6231. Golden, Colorado, US: National Renewable Energy Laboratory. www.nrel.gov/docs/legosti/old/6231.pdf.
- [6] A.E. Delsante; A.N. Stokes; P.J. Walsh, (1983). Application of Fourier Transforms to Periodic Heat Flow into the Ground under a Building. *International Journal of Heat Mass Transfer*, 26(1): 121-132.
- [7] Four-Year On-Site Measurement of Heat Flow in Slab-on-Ground Floors with Wet Soils. In: *Thermal performance of the exterior envelopes of buildings VII: December 6-10, 1998, Sheraton Sand Key Hotel, Clearwater Beach, Florida: conference proceedings*. Atlanta, Ga.: American Society of Heating, Refrigerating and Air-Conditioning Engineers, Inc., c1998, s. 14. ISBN 1883413702.
- [8] ANSI/ASHRAE Standard 140-2007. 2007. Standard Method of Test for the Evaluation of Building Energy Analysis Computer Programs, Atlanta, Georgia, USA: American Society of Heating, Refrigerating and Air-Conditioning Engineers.
- [9] R. Judkoff and J. Neymark, "Model validation and testing: The methodological foundation of ASHRAE Standard 140," in *ASHRAE Transactions*, 2006, vol. 112 PART 2, pp. 367–376.
- [10] V. Gerlich, K. Sulovská, and M. Zálešák, "COMSOL Multiphysics validation as simulation software for heat transfer calculation in buildings: Building simulation software validation," *Measurement*, vol. 46, no. 6, pp. 2003–2012, Jul. 2013.
- [11] R. Judkoff and A. Wijsman, "IEA BESTEST In-Depth Diagnostic Cases for Ground Coupled Heat Transfer Related to Slab-on-Grade Construction," no. July, 2009.
- [12] DASSAULTS SYSTEMES, S.A. *SolidWorks Flow Simulation 2012 Technical Reference*. 2012.
- [13] DASSAULTS SYSTEMES, S.A. *Solving Engineering Problems with Flow Simulation 2012*. 2012.

Time Series Predictive Model Application to Air Pollution Assessment

Claudio Guarnaccia, Julia Griselda Cerón Bretón, Joseph Quartieri, Carmine Tepedino and Rosa Maria Cerón Bretón

Abstract—Physical polluting agents monitoring and control is a relevant problem to be considered in all areas where human activities take place. Air pollution, acoustical noise, electromagnetic fields, etc., should be carefully assessed in order to protect human health. Regarding air pollution, the importance of developing proper mathematical models, able to fit observed data and predict future behavior of pollutants is obvious. Among all the possible approaches, regression methods seem to be feasible when a large dataset is available and the trend and eventual periodicities can be evaluated. In this paper, a Time Series Analysis model is developed and applied to hourly CO concentrations in the urban site of San Nicolas de los Garza, Nuevo Leon, Mexico. The calibration made on one year dataset will show a 24 hours seasonal effect and a quite stable trend. The validation on two different periods, not used in the calibration phase, will exploit quite different results, showing that the general slope of the data is quite good reconstructed, while the local oscillation are difficult to be predicted.

Keywords— Air Pollution, Criteria Pollutants, CO Concentration, Regression Analysis, Time Series.

I. INTRODUCTION

THE physical and chemical processes of atmospheric pollutants gases, particularly nitrogen oxides (NO_x), CO and volatile organic compounds (VOC), in the low atmosphere result in the formation of secondary oxidized products. Since many of these processes are regulated by the presence of sunlight, the oxidized products are commonly referred to as “secondary photochemical pollutants” being Ozone (O₃), the most important oxidant at the troposphere [1].

Tropospheric ozone has been recognized as one of the principal pollutants that degrades the air quality in urban areas ([2], [3]). The production of high levels of ground ozone is of particular concern, as it is known to act as the primary source of OH radicals (the main atmospheric oxidant) and it is the third most important greenhouse gas behind CO₂ and CH₄. In the upper layers of the atmosphere, ozone blocks an excessive ultraviolet irradiation of the earth but at the ground level in the troposphere, this pollutant has been related to adverse effects

C Guarnaccia, J. Quartieri, C. Tepedino are with the Department of Industrial Engineering, University of Salerno, Via Giovanni Paolo II, I-84084 Fisciano (SA) – ITALY (corresponding: cguarnaccia@unisa.it, quartieri@unisa.it, ctepedino@unisa.it).

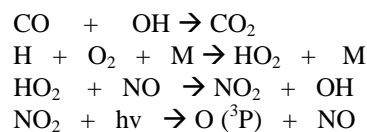
J. G. Cerón Bretón and R. M. Cerón Bretón are with the Environmental Sciences Research Center, Autonomous University of Carmen City (UNACAR), Av. Abasolo s/n Col. Renovación 2da Sección, CP 24180, Ciudad del Carmen, Campeche – MEXICO (jceron@pampano.unacar.mx, rceron@pampano.unacar.mx).

on human health, vegetation and materials ([4-11]).

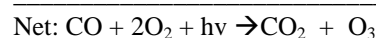
In urban areas, CO is one of the most important ozone precursors as it is known to be a tracer of vehicle exhaust emissions. Its outdoor sources include diverse anthropogenic activities such as power station burning coal, combustion of fossil fuels, making steel, etc.. Indoor sources of this pollutant include tobacco smoke and biomass burning from cooking and houses warming systems. In addition, CO it is known to be toxic and cause several health affections. CO poisoning is the most common type of fatal poisoning in many countries. Symptoms of mild poisoning include headaches, vertigo, and flu-like effects. Larger exposures can lead to significant toxicity of the central nervous system, heart and even death. Following poisoning, long-term sequelae often occurs. Carbon monoxide can also have severe effects on the fetus of a pregnant woman [12]. In developed countries, as for instance United States, it has been estimated that more than 40000 people per year seek medical attention for carbon monoxide poisoning [13].

For all these reasons it is important to know the behavior and trends of CO in a given site and to understand the role that this pollutant plays in the tropospheric ozone formation. The main atmospheric sink process for CO is by reaction with OH, and this mechanism also makes CO a major precursor to photochemical ozone [14].

The day time increase in ozone concentration, which is a pronounced feature of a polluted site, it is basically due to the photo-oxidation of the precursor gases such as CO, CH₄ and NMHC (non methane hydrocarbons) in the presence of sufficient amount of NO_x. In this process NO_x acts as a catalyst and continues to do so until physical processes permanently remove it or it gets transformed to other oxides of nitrogen. The well-known photo-oxidation cycle of CO can be represented as [15]:



$$\lambda < 420 \text{ nm}$$



Therefore, accurate characterization of CO is extremely important for understanding tropospheric ozone formation and accumulation, and crafting effective control strategies to better address ozone air quality management issues. However, the continuous monitoring of air pollutants is generally expensive; most of the times it is limited only to big urban areas and usually the number of the stations of the air quality monitoring networks are not enough. Therefore, there is growing need to implement predictive models that can provide a reliable assessment in an economical way of air pollution levels and other polluting agents (see for instance [16-25]). Among these models, Time Series Analysis (TSA) models ([26], [27]) have been largely adopted in several disciplines and have showed good performances and adaptability to polluting agents levels prediction ([28-31]).

This paper aims to apply TSA models to the hourly CO concentrations dataset collected in an urban site of San Nicolas de los Garza, Nuevo Leon, Mexico. Once the model is calibrated on a given dataset, a validation on more than one range of observed values (not used in the calibration) will be performed, in order to estimate the predictive performances and to understand the criticalities of the model.

II. METHODS

The model adopted in this paper has been presented by some of the authors in [28]. It is based on the Time Series analysis (TSA) models idea. These TSA are mathematical models largely adopted in Economics, Physics, Engineering, Mathematics, etc.. (see for instance [32-34]), that are used to reproduce the behaviour of data series and to predict future slope.

The main aims of these kind of models are basically the recognition of the phenomenon under study by means of data trend and periodicity reconstruction, and the prediction of future values of the time series. Thus, a general procedure may be resumed as follows:

- Eventual seasonal effect detection in the data set
- Lag (periodicity) evaluation
- Smoothing (removal of periodicity) of the calibration data time series
- Trend and seasonality evaluation
- Error evaluation (difference between observed and forecasted values in the calibration dataset)
- Final model drawing

The details of how perform the steps listed above can be found in [28] and references therein, where different approaches, in particular additive and multiplicative, are presented and briefly discussed. The choice for this dataset is a mixed approach, that is multiplicative between trend and seasonality, and additive for the error component:

$$F_t = T_t \bar{S}_i + m_e \quad (1)$$

where F_t is the model prediction, T_t is the trend, \bar{S}_i is the seasonal coefficient, m_e is the mean of the error e_t , defined as actual value (A_t) minus forecast (F_t):

$$e_t = A_t - F_t \quad (2)$$

Let us underline that TSA models are mostly adopted when the data sets follow recurring seasonal patterns. The attempt to adopt this kind of models in a so variable and random physical phenomenon, such as air pollution, is extremely challenging. Results shown in Section 4 will underline these difficulties and open new ways to further improvement of this model.

III. CASE STUDY

In Mexico there is not enough information about air pollution and most of the studies about spatial and temporal levels of criteria air pollutants have been focused to Mexico City whose air quality monitoring network began operating in 1966. However, other important urban zones like the Metropolitan Areas Monterrey and Guadalajara started measuring of air pollution until 1992, thus the lack of air quality information is even greater.

This study is focused on San Nicolas de Garza, one of the twelve municipalities of the Metropolitan Area of Monterrey (MAM), which constitutes the third largest urban area in Mexico. MAM is a high profile center of education, tourism and business with a population of 4,000,000 habitants. This city is located at 25°40'N and 100°18' W at 537 masl and covering an area of 580.5 km². This area is characterized by the presence of important education and research centers, business activities and industrial development. Road transportation and area sources (evaporative emissions from solvents, storage tanks, coatings, fuel marketing and other miscellaneous sources) are the dominant sources of O₃ precursors in MAM [35].

The Nuevo León State Government has been committed to undertaking all necessary steps to protect public health from air pollution, with sensitivity to the impacts of its actions on the community and industrial activities. Although air pollutants and weather conditions have been measured from 90's and some actions have been taken in order to improve air quality, some pollutants may reach unhealthy levels during air pollution episodes. In Mexico, with respect to carbon monoxide, significant advances have been made since the implementations by 2012 of a emissions limit from vehicles (ranged from 3.418 to 4.536 g/km depending on the net weight of the vehicle and fuel type) [36]. In addition, a standard to protect population health against CO was implemented in 1993, which regulates the ambient air levels of this pollutant within a limit of 11 ppm (12.595 µg/m³) in an 8-h mobile average once a year as maximum [37]. Nevertheless, a better understanding of the behavior and trends of this pollutant in MAM is required in order to develop effective strategies focused to ozone abatement in this area.

This paper describes the methodology for time series analysis of air quality data and the development of a predictive model for daily mean concentrations of CO, and gives an example of this model application in order to predict CO levels from data obtained at the air quality monitoring network of the Integrated System of Environmental Monitoring (SIMA) of Monterrey, Nuevo Leon, Mexico.

A. Case study area description

San Nicolas de los Garza, Nuevo León, Mexico is located at the northeast of the Metropolitan Area of Monterrey (Figure 1). Climate in this area is classified as semi-arid warm being hot in summer (temperature reaches 35 °C in August), though reasonably pleasant in spring and autumn. The average temperature in winter is 8 °C. Rainfall is scarce, but more prominent during May to September. Humidity in winter can be high, although without showers. Snowfall is a very rare event. The annual average precipitation is 615 mm and this area is commonly influenced by frontal systems coming from the north of the continent. The specific sampling site was located within the facilities of Northeast Station of the SIMA, located in the Laboral Unity District in San Nicolas de los Garza, N.L. at 25° 43' 30 "N and 100° 18' 48" W at 500 m above sea level, within an area with high density of population (Figure 2).

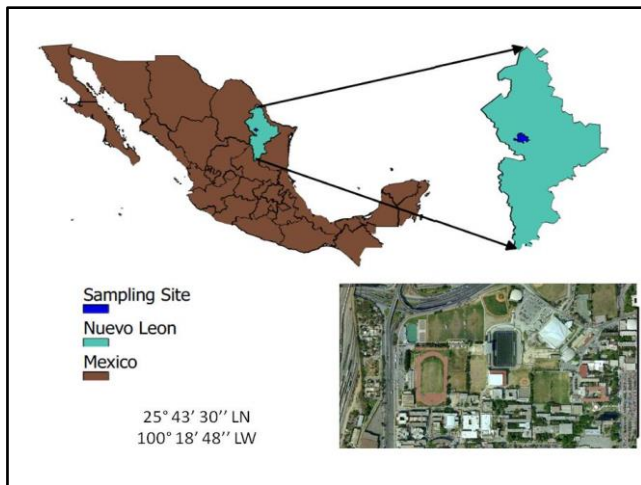


Fig. 1: Case study Location

B. Air pollution and meteorological parameters monitoring

The air quality monitoring network of MAM is operated by the Integrated System of Environmental Monitoring (SIMA) of the Mexican Environmental Protection Agency (APMARN). This network has 8 fixed monitoring stations and a Sodar Doppler System for meteorological conditions measuring. Each monitoring station generates hourly information of the ambient air concentrations of criteria air pollutants and meteorological parameters [38]. Table 1 lists the criteria air pollutants (O₃, NO, NO₂, NO_x, CO, PM10, and SO₂) and meteorological parameters (wind direction, wind speed, relative humidity, temperature, solar radiation and

barometric pressure) usually measured in the air quality monitoring stations and measurement techniques. The data set used in this paper was limited to hourly CO ambient air concentrations during 2012, obtained from the Northeast Station of the SIMA whose location is indicated in Figure 2.

Tab. 1: Criteria air pollutants and meteorological parameters usually measured in the air quality monitoring network of MAM

Variable	Measurement Technique	Units
Carbon monoxide (CO)	IR non dispersive attenuation GFG	ppm
Ozone (O ₃)	UV spectrophotometer	ppb
Nitrogen dioxide (NO ₂)	chemical luminescence	ppb
Sulfur dioxide (SO ₂)	UV pulsed fluorescence	ppb
Particulate matter with aerodynamic radius equal or lower than 10 μm (PM10)	Beta ray attenuation	μg/m ³
Wind speed	Conventional anemometer	km/h
Wind direction	Conventional vane	Azimuth grades
Ambient temperature	Solid state thermostat	Celsius grades
Solar radiation	Pyranometer	kW/m ²
Barometric pressure	Barometric pressure sensor	mm Hg

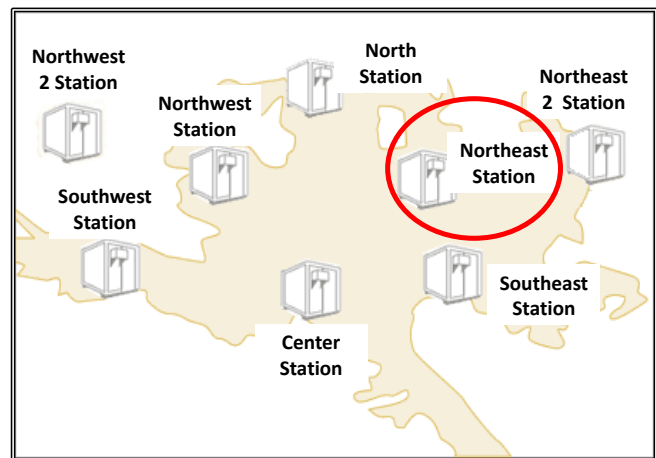


Fig. 2: Specific location of the northeast station within the air quality monitoring network in MAM.

IV. DATA ANALYSIS AND RESULTS

The first step, in order to build the model, is to analyse the dataset to be used in the calibration phase. The choice was to consider the CO concentrations, during all the year 2012.

The calibration dataset is made of 8784 hourly CO concentrations, measured in ppm, and the summary statistics

are resumed in Table 2. As it can be noticed from skewness and kurtosis values, the distribution is not normal. In addition, the high value of standard deviation with respect to the mean, together with the maximum and minimum values, exploits a very spread distribution.

Looking at the time slope of the data, these CO concentrations show a daily periodic pattern, together with an average decrease in spring and summer. The daily periodic pattern can be explained from distinct peaks which correspond to morning rush hours. This is consistent with the assumption that on-road vehicles dominate CO emissions.

The seasonal pattern of tropospheric CO, with its maximum in winter and its minimum in summer and spring, has been reported before by other authors ([39-43]). The boundary layer usually becomes deeper in late spring and summer because of greater solar insolation and stronger turbulent eddies. This condition promotes released pollutants dilution at the surface and results in lower ambient concentrations [39]. Therefore, during summer, photochemical activity is increased and OH concentrations are higher. In the presence of sunlight and sufficient amount of NO_x (urban atmospheres), photo-oxidation cycle of CO begins with its reaction with OH leading to the tropospheric ozone formation. The lifetime of CO is sufficiently long (from some days over continents in summer to over a year at high latitudes in winter) [40]. Thus, higher OH concentrations and hence a decrease in the lifetime of CO during late spring and summer result in a decrease in tropospheric CO levels. On the other hand, during winter, a longer lifetime of CO result in an accumulation of this pollutant toward late spring until loss by OH surpasses inputs of CO (emissions and photochemical production) [41]. In addition, during winter months, thermal inversions and a decrease in the boundary layer depth contribute to higher CO levels.

The autocorrelation analysis on the entire calibration dataset, made by means of correlogram, highlights the presence of a 24 hours periodicity, as shown in Fig. 3. The autocorrelation value corresponding to a lag of 24 hours is 0.371 .

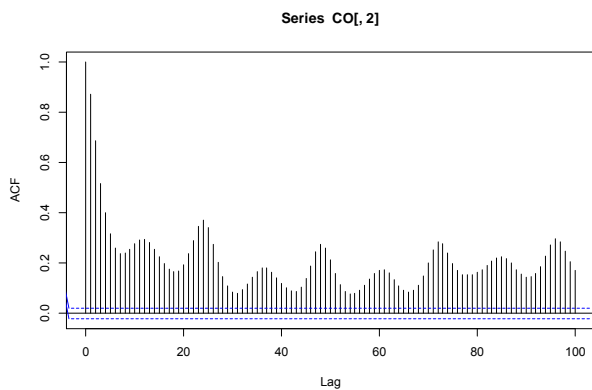


Fig. 3: Autocorrelation plot (correlogram) as a function of the lag (periodicity).

Once the lag has been detected, the model has been built according to procedure described in Section 2 and in [28]. The results of the model are plotted in Figure 4, together with the observed CO concentrations. In Table 2, the model parameters are reported. It can be highlighted that the trend line is almost constant and that the seasonal coefficients increase in rush hours, since they are affected by vehicles emissions.

Tab. 2: Model parameters estimated on the 2012 CO concentration data. b_0 and b_1 are respectively the intercept and the slope of the trend line, while \bar{S}_i is the seasonal coefficient in the time range from $i-1$ to i hour.

Time Series Model parameters			
b_0	0,64383730	b_1	0,00000147
\bar{S}_1	0,805094	\bar{S}_{13}	0,886475
\bar{S}_2	0,723286	\bar{S}_{14}	0,847639
\bar{S}_3	0,680476	\bar{S}_{15}	0,839873
\bar{S}_4	0,644032	\bar{S}_{16}	0,835991
\bar{S}_5	0,657638	\bar{S}_{17}	0,8627
\bar{S}_6	0,845082	\bar{S}_{18}	0,9359
\bar{S}_7	1,23911	\bar{S}_{19}	1,075612
\bar{S}_8	1,542119	\bar{S}_{20}	1,24604
\bar{S}_9	1,469525	\bar{S}_{21}	1,274936
\bar{S}_{10}	1,237873	\bar{S}_{22}	1,182683
\bar{S}_{11}	1,038506	\bar{S}_{23}	1,08388
\bar{S}_{12}	0,939687	\bar{S}_{24}	0,953364

It is interesting to notice that the general trend of the time series is achieved by the model, even if the local strong variations are not predicted by the model. These local strong oscillations may be due to day to day variations related to meteorological conditions (transport) and emission local sources strength. The good performance of the model is confirmed by the error distribution, evaluated according to formula (2), whose mean is close to zero but whose maximum value is 9.57 ppm. Thus the first consideration that can be drawn is that this model is not able to locally predict the exact behaviour of the CO concentration, but it can give interesting results on a long term analysis basis and it can give reliable predictions in periods in which there are not strong variations with respect to the general trend. For instance, the comparison between observed values and model predictions in the range between 7000 and 7500 hours (Figure 5) is encouraging, even if the single peaks are not reconstructed by the model. On the contrary, during the summer time, the model clearly overestimates the observed values.

Tab. 3: Summary of statistics of the complete data set, 8784 data, in ppm.

Mean [ppm]	Std.dev [ppm]	Median [ppm]	Min [ppm]	Max [ppm]	skew	kurt
0.66	0.67	0.47	0.08	10.01	5.22	40.96

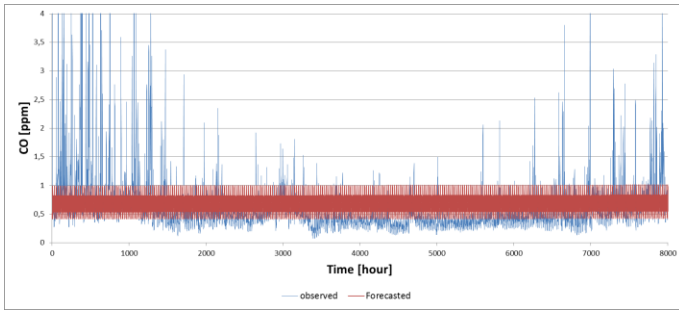


Fig. 4: Observed and predicted CO concentrations, during 2012 (i.e. calibration dataset).

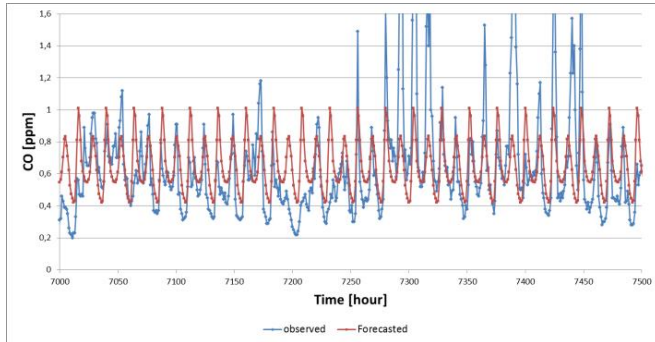


Fig. 5: Observed and predicted CO concentrations, during 2012: zoom on the time range from 7000 to 7500 hours.

Tab. 4: Summary of statistics of the error distribution, evaluated on the calibration dataset, in ppm.

Mean [ppm]	Std.dev [ppm]	Median [ppm]	Min [ppm]	Max [ppm]
0.01	0.65	-0.15	-0.79	9.57

In order to validate the model and to check its performances, a comparison between model predictions and observed CO concentrations has been made on two sample datasets in 2013.

The first validation has been made on January 2013 data (Figure 6): the model hardly predicts the peaks, while the trend seems to be confirmed.

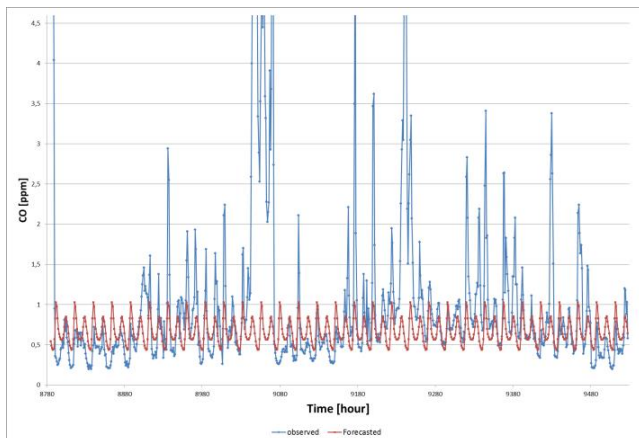


Fig. 6: Observed and predicted CO concentrations, during January 2013 (i.e. first validation dataset).

Tab. 5: Summary of statistics of the error distribution, evaluated on the first validation dataset (January 2013).

Mean [ppm]	Std.dev [ppm]	Median [ppm]	Min [ppm]	Max [ppm]
0.34	1.09	0.03	-0.75	8.00

Moreover, when comparing results of the model with observed values in May 2013, the obtained agreement is evident (Figure 7) and confirmed by error distribution statistics (Table 5).

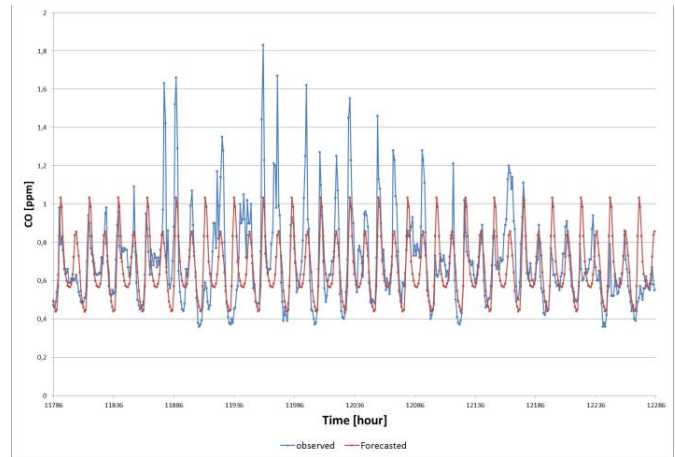


Fig. 7: Observed and predicted CO concentrations, during May 2013 (i.e. second validation dataset).

Tab. 6: Summary of statistics of the error distribution, evaluated on the second validation dataset (May 2013).

Mean [ppm]	Std.dev [ppm]	Median [ppm]	Min [ppm]	Max [ppm]
0.03	0.20	0.03	-0.58	0.84

Let us underline that the median of error distribution evaluated on the two different validation dataset is basically the same (0.03 ppm). This is due to the fact that the median is much less sensitive to distribution outliers than the mean, i.e. in our case, it is not strongly affected by local CO concentration peaks.

Another consideration is that one should expect that the model works better on validation periods closer to calibration dataset. In this case, the model shows better performances on the May 2013 validation period, even if the calibration is done on 2012 data. This is probably due to the fact that in this period there is a lower variability in the data and the slope is closer to the model trend and periodicity, evaluated on 2012 data.

V. CONCLUSIONS

In this paper the authors deal with the problem of modelling the time series of CO concentrations in the urban site of San Nicolas de los Garza, Nuevo Leon, Mexico. A mixed Time Series Analysis (TSA) model, i.e. a model that considers a multiplicative relation between trend and seasonality of the

data, and an additive correction related to the calibration error, has been adopted. This model has been calibrated on the 2012 CO concentration data, obtaining a 24 hours periodicity and an almost constant trend. The error in the calibration has been evaluated as the difference between observed and forecasted values, and its mean has been added to the product between trend and seasonality, in order to obtain the final model. The validation of the resulting model has been performed on two different periods (January and May) of 2013 CO concentration dataset, giving different results. Even though the graphical comparison and the error means are quite different, the median of the error distribution is the same for both periods. The median, in fact, is a better measure of central tendency with respect to the mean, in case of random peaks presence in the dataset.

Thus, the TSA model presented in this paper is able to predict the general slope of the data, while local variations and random peaks are difficult to be predicted. Further studies on multiple periodicity or different regression methods represent the next steps of this analysis, and will be postponed to future works.

ACKNOWLEDGMENT

The authors are grateful to the local Government of San Nicolas de los Garza, Nuevo Leon, especially to the Integrated System of Environmental Monitoring (SIMA), for having made available the air pollutants levels data measured in MAM used in this paper

REFERENCES

- [1] Sousa, S.I.V., Martins, F.G., Pereira, M.C., and Alvim-Ferraz, M.C.M. 2006. Prediction of ozone concentrations in Oporto City with statistical approaches. *Chemosphere* 64, 1141-1149.
- [2] Van Eijkeren, J.C., Freijer, J.I., and Van Bree, L. 2002. A model for the effect on health of repeated exposure to ozone. *Environmental Modelling and Software* 17, 553-562.
- [3] Xu, J., and Zhu, Y. 1994. Some characteristics of ozone concentrations and their relations with meteorological factors in Shanghai. *Atmospheric Environment* 20, 3387-3392.
- [4] Lee, D.S., Holland, M.R., and Falla, W. 1996. The potential impact of ozone on materials in the U.K. *Atmospheric Environment* 30 (7), 1053-1065.
- [5] Cass, G.R., Nazarof, W.W., Tiller, C., and Whitmore, P.M. 1991. Protection of works of art from damage due to the atmospheric ozone. *Atmospheric Environment* 25A, 441-451.
- [6] Wang, S.W. and Georgopoulos, P.G. 2001. Observational and mechanistic studies of tropospheric studies of ozone, precursor relations: photochemical models performance evaluation with case study. Technical Report ORC-TR99-03.
- [7] Cerón-Bretón, J.G., Cerón-Bretón, R.M., Guerra-Santos, J.J., Córdova-Quiroz, A.V., Vargas-Cáliz, C., Aguilar-Bencomo, L.G., Rodriguez-Heredia, K., Bedolla-Zavala, E., and Pérez-Alonso, J. 2010 a. Effects of simulated tropospheric ozone on soluble proteins and photosynthetic pigments levels of four woody species typical from the Mexican Humid Tropic. *WSEAS Transactions on Environment and Development* 6 (5), 335-344.
- [8] Cerón-Bretón, J.G., Cerón-Bretón, R.M., Rangel-Marrón, M., Vargas-Cáliz, C., Aguilar-Bencomo, L.G., and Muriel-García, M. 2010 b. Effects of simulated tropospheric ozone on foliar nutrients levels (Ca²⁺, Mn²⁺, Mg²⁺, and K⁺) of three woody species of high commercial value typical from Campeche, Mexico. *WSEAS Transactions on Environment and Development* 6 (11), 731-743.
- [9] Aris, R.M., Christian, D., Hearne, P.Q., Kerr, K., Finkbeiner, W.E., and Balmes, J.R. 1993. Ozone-induced airway inflammation in human subjects as determined by airway lavage and biopsy. *Am. Rev. Respir. Dis.* 148, 1363-1372.
- [10] Coleridge, J.C., Coleridge, H.M., Schelegle, E.S., and Green, J.F. 1993. Acute inhalation of ozone stimulates bronchial C-fibers and rapidly adapting receptors in dogs. *J. Appl. Physiol.* 74, 2345-2352.
- [11] Cashel, P., Newhouse, B.S., and Leventin, E. 2004. Correlation of environmental factors with asthma and rhinitis symptoms in Tulsa, OK. *Ann. Allergy, Asthma & Immun.* 92, 356-366.
- [12] Hampson, N.B. 1998. Emergency Department visits for carbon monoxide poisoning. *Journal of Emergency Medicine* 16, 695-698.
- [13] U.S. EPA. Environmental Protection Agency Office of Mobile Sources. Motor vehicles and the 1990 Clean Air Act, August, 1994.
- [14] Crutzen, J. 1974. Photochemical reactions initiated by and influencing ozone in unpolluted tropospheric air. *Tellus*, Vol. 26, 47-56.
- [15] Finlayson-Pitts, B.J., and Pitts, J.N. Jr. 1999. Chemistry of the upper and lower atmosphere: Theory, Experiments and Applications. Academic Press, San Diego, CA, USA, 90-96.
- [16] Guarnaccia C., Advanced Tools for Traffic Noise Modelling and Prediction, *WSEAS Transactions on Systems*, Issue 2, Vol.12, 2013, pp. 121-130.
- [17] Quartieri J., Mastorakis N. E., Iannone G., Guarnaccia C., D'Ambrosio S., Troisi A., Lenza T.L.L., A Review of Traffic Noise Predictive Models, Proceedings of the 5th WSEAS International Conference on "Applied and Theoretical Mechanics" (MECHANICS'09), Puerto de la Cruz, Tenerife, Spain, 14-16 December 2009, pp. 72-80.
- [18] Quartieri J., Troisi A., Guarnaccia C., Lenza T.L.L., D'Agostino P., D'Ambrosio S., Iannone G., An Acoustical Study of High Speed Train Transits, *WSEAS Transactions on Systems*, Issue 4, Vol.8, pp. 481-490 (2009).
- [19] Quartieri J., Troisi A., Guarnaccia C., Lenza T.L.L., D'Agostino P., D'Ambrosio S., Iannone G., Application of a Predictive Acoustical Software for Modelling Low Speed Train Noise in an Urban Environment, *WSEAS Transactions on Systems*, Issue 6, Vol.8, pp. 673-682 (2009).
- [20] Guarnaccia C., Lenza T.L.L., Mastorakis N.E., Quartieri J., A Comparison between Traffic Noise Experimental Data and Predictive Models Results, *International Journal of Mechanics*, Issue 4, Vol. 5, pp. 379-386 (2011), ISSN: 1998-4448.
- [21] Guarnaccia C., Mastorakis N.E., Quartieri J., Wind Turbine Noise: Theoretical and Experimental Study, *International Journal of Mechanics*, Issue 3, Vol.5, pp. 129-137 (2011).
- [22] Guarnaccia C., Analysis of Traffic Noise in a Road Intersection Configuration, *WSEAS Transactions on Systems*, Issue 8, Volume 9, (2010), pp.865-874, ISSN: 1109-2777.
- [23] Iannone G., Guarnaccia C., Quartieri J., Speed Distribution Influence in Road Traffic Noise Prediction, *Environmental Engineering And Management Journal*, Vol. 12, Issue 3, 2013, pp. 493-501.
- [24] Rodrigues, E.R., Achcar, J.A., and Jara-Ettinger, J. A Gibbs sampling algorithm to estimate the occurrence of ozone exceedances in Mexico City. In: *Air Quality: Models and Applications*, Popovic D (ed.), In Tech Open Access Publishers, 131-150, 2011.
- [25] Achcar, J.A., Fernandez-Bremauntz, A.A., Rodrigues, E.R., and Tzintzun, G., Estimating the number of ozone peaks in Mexico City using a non homogeneous Poisson model, *Environmetrics*, 19, 469-485, 2008.
- [26] Box, G. E. P., and Jenkins, G., *Time Series Analysis: Forecasting and Control*, Holden-Day, 1976.
- [27] Chatfield, C., *The Analysis of Time Series: an Introduction*, Chapman & Hall, New York, 1975.
- [28] Guarnaccia C., Quartieri J., Mastorakis N. E. and Tepedino C., Acoustic Noise Levels Predictive Model Based on Time Series Analysis, in "Latest Trends in Circuits, Systems, Signal Processing and Automatic Control", proceedings of the 2nd Int. Conf. on Acoustics, Speech and Audio Processing (ASAP '14), Salerno, Italy, June 3-5, 2014, ISSN: 1790-5117, ISBN: 978-960-474-374-2, pp. 140-147.
- [29] Guarnaccia C., Quartieri J., Rodrigues E. R. and Tepedino C., Time Series Model Application to Multiple Seasonality Acoustical Noise Levels Data Set, in "Latest Trends in Circuits, Systems, Signal Processing and Automatic Control", proceedings of the 2nd Int. Conf. on Acoustics, Speech and Audio Processing (ASAP '14), Salerno, Italy, June 3-5, 2014, ISSN: 1790-5117, ISBN: 978-960-474-374-2, pp. 171-180.

- [30] Pope C. A., Dockery D. W., Spengler J. D., and Raizenne M. E., Respiratory Health and PM10 Pollution: A Daily Time Series Analysis, *American Review of Respiratory Disease*, Vol. 144, No. 3_pt_1 (1991), pp. 668-674.
- [31] Dominici F., McDermott A., Zeger S. L., and Samet J. M., On the Use of Generalized Additive Models in Time-Series Studies of Air Pollution and Health, *American Journal of Epidemiology*, 156 (3), pp 193-203, 2002.
- [32] Di Matteo T., Aste T., Dacorogna M.M., Scaling behaviors in differently developed markets, *Physica A: Statistical Mechanics and its Applications*, Vol. 324, Issues 1-2, 2003, pp. 183-188.
- [33] Milanato D., Demand Planning. Processi, metodologie e modelli matematici per la gestione della domanda commerciale, Springer, Milano, 2008, in Italian.
- [34] Chase R. B., Aquilano N. J., Operations Management for Competitive Advantage, Irwin Professional Pub, 10th edition, 2004.
- [35] SEMARNAT-INE. 2005. Emissions Inventory for the Metropolitan Area of Monterrey.
- [36] SEMARNAT. Mexican Environmental Protection Agency. 2012. NOM-076-SEMARNAT-2012: Mexican standard to regulate maximum permissible levels of hydrocarbons, carbon monoxide and nitrogen oxides in vehicle exhaust.
- [37] SSA. Mexican Public Health Agency. 1993. NOM-021-SSA1-1993. Mexican standard to regulate air quality for carbon monoxide ambient air concentrations.
- [38] SIMA. 2014. Monitoring Program of Nuevo Leon State. http://www.nl.gob.mx/?P=med_amb_mej_amb_sima_municipal
- [39] Chen L.W.A., Doddridge B.G., Dickerson R.R., Chow J.C., Mueller P.K., Quinn J., Butter W.A., Seasonal variations in elemental carbon aerosol, carbon monoxide and sulfur dioxide: implications for sources, *Geophysical Research Letter*, Vol. 28, No. 3 (2001), pp. 1711-1714.
- [40] Holloway T., Ley II H.L., Kasibhatla P., Global distribution of Carbon monoxide, *Journal of Geophysical Research: Atmospheres*, Vol. 105 (2000), pp. 12123-12147.
- [41] Koike M., Jones N.B., Palmer P.L., Matsui H., Zhao Y., Kondo Y., Matsumi Y., Tanimoto H., Seasonal variation of carbon monoxide in northern Japan: Fourier transform IR measurements and source-labeled model calculations, *Journal of Geophysical Research*, Vol. 111 (2006), pp. 1-15.
- [42] Novelli P.C., Masarie K.A., Lang P.M., Distributions and changes of carbon monoxide in the lower troposphere, *Journal of Geophysical Research: Atmospheres*, Vol. 103 (1998), pp. 19015-19033.
- [43] Rinsland C.P., Mahieu E., Zander R., Demoulin P., Forrer J., Buchmann B., Free tropospheric CO, C2H6 and HCN above central Europe: Recent measurements from the Jungfraujoch station including the detection of elevated columns during 1998, *Journal of Geophysical Research: Atmospheres*, Vol. 105 (2000), pp. 24235-24249.
- [44] Quartieri J., Troisi A., Guarnaccia C., D'Agostino P., D'Ambrosio S., Iannone G., Development of an Environmental Quality Index Related to Polluting Agents, Proceedings of the WSEAS International Conference on "Environment, Ecosystem and Development" (EED'09), Puerto de la Cruz, Tenerife (Spain), 14-16 December 2009, pp. 153-161.
- [45] Quartieri J., Iannone G., Guarnaccia C., On the Improvement of Statistical Traffic Noise Prediction Tools, Proceedings of the 11th WSEAS International Conference on "Acoustics & Music: Theory & Applications" (AMTA '10), Iasi, Romania, 13-15 June 2010, pp. 201-207.
- [46] Quartieri J., Mastorakis N. E., Guarnaccia C., Troisi A., D'Ambrosio S., Iannone G., Traffic Noise Impact in Road Intersections, *International Journal of Energy and Environment*, Issue 1, Volume 4 (2010), pp. 1-8.
- [47] Iannone G., Guarnaccia C., Quartieri J., Noise Fundamental Diagram deduced by Traffic Dynamics, in "Recent Researches in Geography, Geology, Energy, Environment and Biomedicine", Proceedings of the 4th WSEAS Int. Conf. on Engineering Mechanics, Structures, Engineering Geology (EMESEG '11), Corfù Island, Greece, July 14-16, 2011, pp. 501-507.
- [48] Quartieri J., Mastorakis N.E., Guarnaccia C., Iannone G., Cellular Automata Application to Traffic Noise Control, Proc. of the 12th Int. Conf. on "Automatic Control, Modelling & Simulation" (ACMOS '10), Catania (Italy), 29-31 May 2010, pp. 299-304.
- [49] Guarnaccia C., Acoustical Noise Analysis in Road Intersections: a Case Study, Proceedings of the 11th WSEAS International Conference on "Acoustics & Music: Theory & Applications" (AMTA '10), Iasi, Romania, 13-15 June 2010, pp. 208-215.
- [50] Guarnaccia C., New Perspectives in Road Traffic Noise Prediction, in "Latest advances in Acoustics and Music", proceedings of the 13th Int. Conf. on Acoustics & Music: Theory & Applications (AMTA '12), Iasi, Romania, 13-15 June 2012. ISBN: 978-1-61804-096-1, pp. 255-260
- [51] Quartieri J., Troisi A., Guarnaccia C., Lenza TLL, D'Agostino P., D'Ambrosio S., Iannone G., Analysis of Noise Emissions by Train in Proximity of a Railway Station, Proceedings of the 10th International Conference on "Acoustics & Music: Theory & Applications" (AMTA '09), Prague (Rep.Ceca), 23-25 March 2009, pp: 100-107.
- [52] Quartieri J., Troisi A., Guarnaccia C., Lenza TLL, D'Agostino P., D'Ambrosio S., Iannone G., An Italian High Speed Train Noise Analysis in an Open Country Environment, Proceedings of the 10th International Conference on "Acoustics & Music: Theory & Applications" (AMTA '09), Prague (Rep.Ceca), 23-25 March 2009, pp: 92-99.
- [53] Quartieri J., Mastorakis N. E., Guarnaccia C., Troisi A., D'Ambrosio S., Iannone G., Road Intersections Noise Impact on Urban Environment Quality, Proceedings of the 5th WSEAS International Conference on "Applied and Theoretical Mechanics" (MECHANICS '09), Puerto de la Cruz, Tenerife, Spain, 14-16 December 2009, pp. 162-171.
- [54] Quartieri J., Sirignano L., Guarnaccia C., Equivalence between Linear and Curved Sources in Newtonian Fields: Acoustics Applications, Proc. Of the Int. Conf. on Engineering Mechanics, Structures, Engineering Geology (EMESEG '08), Heraklion, Crete Island, Greece, July 22-24, 2008, pp: 393-395.
- [55] Quartieri J., Sirignano L., Guarnaccia C., Infinitesimal Equivalence between Linear and Curved Sources in Newtonian Fields: Application to Acoustics, *International Journal of Mechanics*, Issue 4, Vol.1, pp. 89-91 (2007), ISSN: 1998-4448.
- [56] Guarnaccia C., Mastorakis N. E., Quartieri J., A Mathematical Approach for Wind Turbine Noise Propagation, in Applications of Mathematics and Computer Engineering, American Conference of Applied Mathematics (AMERICAN-MATH '11), Puerto Morelos, Mexico, 29-31 January 2011, pp. 187-194.

Educational microprocessor development kit – low-cost access system application

Tomas Sysala, Petr Neumann, Filip Zanka, and Lubomir Vasek

Abstract—The article deals with a low cost development kit based on the Atmel microprocessor. That development kit is supposed to serve as an educational support for microcomputer programming classes within the scope of subjects oriented at microcomputers and PLCs. As that designed kit model application, a low cost access system is described. The iButton family members by Maxim Integrated Products are used for door lock opening identification elements.

Keywords—Microprocessor development kit, Education, Access system, Microprocessor programming.

I. INTRODUCTION

MICROCOMPUTERS and microcontrollers constitute a common ingredient in our daily life. We are meeting them without noticing it.

Microcomputers as a cheap and small form of digital devices (computers) lived through their rapid development in early 80-ties of the last century. Those microcomputers were first in 8-bit version and later in 16-bit version then. The model Intel8080 [1] and/or Zilog Z80 [2] may be mentioned as the most popular models at that time.

Microcomputers in 32-bit version with the ARM core gained popularity in more challenging application during 90ties of the last century [3].

One of our former projects was aimed at the 32-bit version of a development kit with a color display and many options oriented in the multimedia application field [4].

The low cost attribute of this project prefers the 8-bit processor.

II. GOAL AND SPECIFICATIONS

Many subjects taught at Tomas Bata University, Faculty of Applied Informatics, are oriented at technological processes control. The microcomputer presents one of alternatives for

The authors wish to thank to the Ministry of Education, Youth and Sports of the Czech Republic (the European Regional Development Fund under the project CEBIA-Tech No. CZ.1.05/2.1.00/03.0089) for financial support.

Tomas Sysala is with Tomas Bata University in Zlin, Faculty of Applied Informatics, nam. T.G.Masaryka 5555, 760 01 Zlin, Czech Republic (corresponding author to provide phone: +420 57 603 5260; fax: +420 57 603 2716; e-mail: sysala@fai.utb.cz).

Petr Neumann and Lubomir Vasek are with Tomas Bata University in Zlin, Faculty of Applied Informatics, nam. T.G.Masaryka 5555, 760 01 Zlin, Czech Republic (e-mail: neumann@fai.utb.cz, lvasek@fai.utb.cz).

Filip Zanka was with Tomas Bata University in Zlin, Faculty of Applied Informatics, nam. T.G.Masaryka 5555, 760 01 Zlin, Czech Republic.

such processes control.

The goal of one our project was to design a development kit based on a 8-bit microcontroller with the AVR core which should comply with following requirements:

- Low costs,
- Extended peripheral equipment for interfacing technological processes,
- Extended peripheral equipment for various communication modes,
- Dual line text display unit (2 x 16 characters),
- Peripheral modularity for a flexible expansion and/or modification according to the particular purpose.

III. MICROPROCESSOR DEVELOPMENT KIT

A. Microprocessor

Processor is a core of each development kit. In our case, we have opted for 8-bit processor from Atmel product range, namely the Atmel® AVR® ATmega128.

This processor is a low-power CMOS 8-bit microcontroller based on the AVR enhanced RISC architecture. By executing powerful instructions in a single clock cycle, the ATmega128 achieves throughputs approaching 1MIPS per MHz allowing the system designer to optimize power consumption versus processing speed.

The Atmel® AVR® core combines a rich instruction set with 32 general purpose working registers. All the 32 registers are directly connected to the Arithmetic Logic Unit (ALU), allowing two independent registers to be accessed in one single instruction executed in one clock cycle. The resulting architecture is more code efficient while achieving throughputs up to ten times faster than conventional CISC microcontrollers [5].

The ATmega128 provides the following features: 128Kbytes of In-System Programmable Flash with Read-While-Write capabilities,

- 4Kbytes EEPROM,
- 4Kbytes SRAM,
- 53 general purpose I/O lines,
- 32 general purpose working registers,
- Real Time Counter (RTC), four flexible Timer/Counters with compare modes and PWM,
- 2 USARTs, a byte oriented Two-wire Serial Interface, an 8-channel, 10-bit ADC with optional differential input stage with programmable gain,

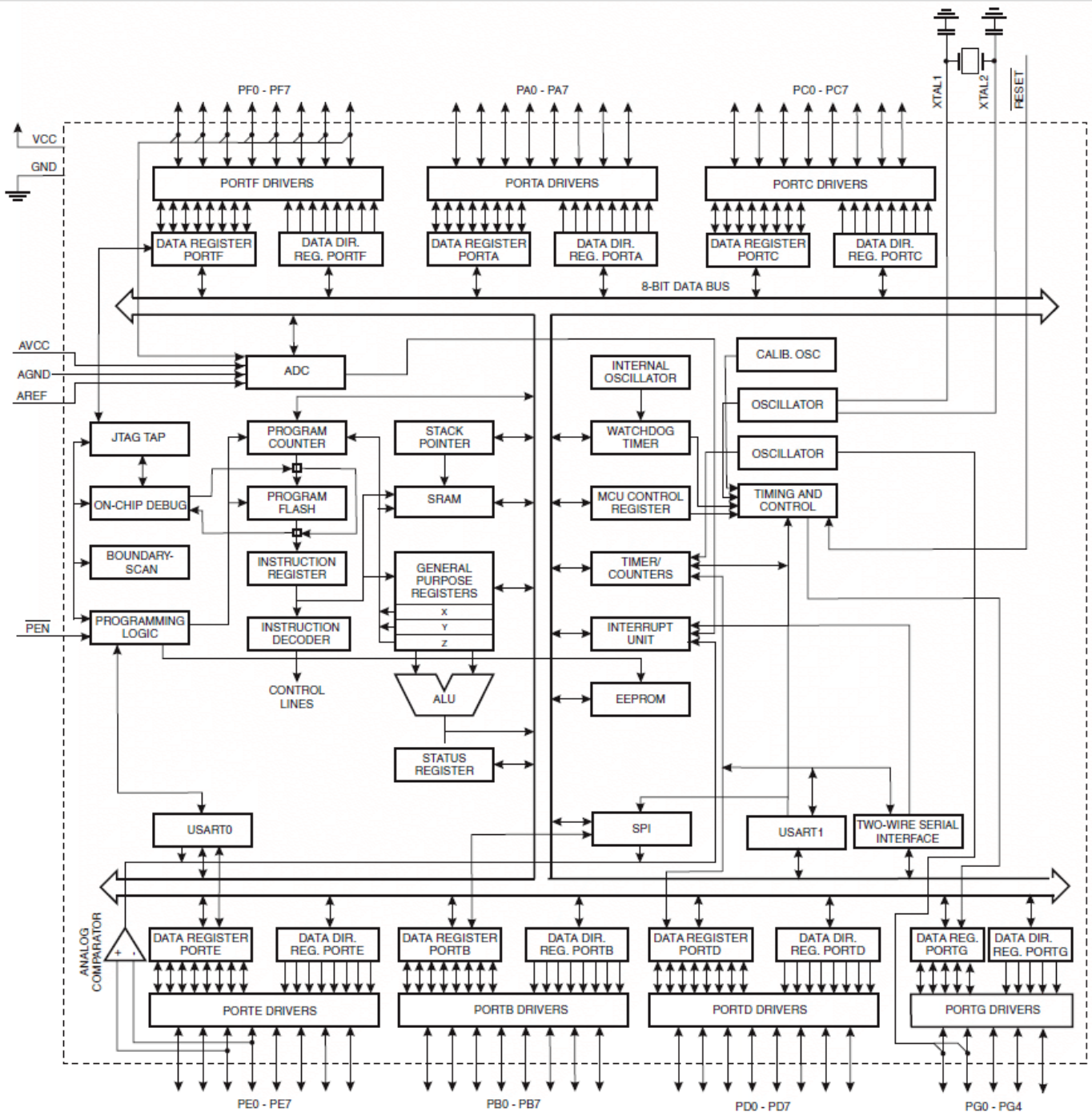


Fig. 1 Block Diagram of the AVR Architecture [5]

- programmable Watchdog Timer with Internal Oscillator,
- an SPI serial port, IEEE std. 1149.1 compliant

The device is manufactured using Atmel’s high-density nonvolatile memory technology. The Onchip ISP Flash allows the program memory to be reprogrammed in-system through an SPI serial interface, by a conventional nonvolatile memory programmer, or by an On-chip Boot program running on the AVR core. The boot program can use any interface to download the application program in the application Flash memory. Software in the Boot Flash section will continue to run while the Application Flash section is updated, providing

true Read-While-Write operation. By combining an 8-bit RISC CPU with In-System Self-Programmable Flash on a monolithic chip, the Atmel ATmega128 is a powerful microcontroller that provides a highly flexible and cost effective solution to many embedded control applications [5].

The ATmega128 device is supported with a full suite of program and system development tools including: C compilers, macro assemblers, program debugger/simulators, in-circuit emulators, and evaluation kits.

A. AVR CPU Core

The ATmega128 has an AVR® core architecture. The main function of the CPU core is to ensure correct program execution. The CPU must therefore be able to access memories, perform calculations, control peripherals and handle interrupts.

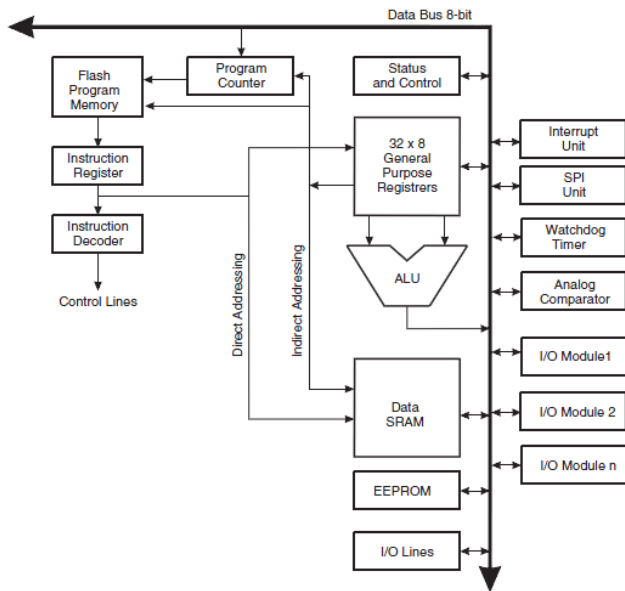


Fig. 2 Block Diagram of the AVR Architecture [5]

In order to maximize performance and parallelism, the AVR uses a Harvard architecture – with separate memories and buses for program and data. Instructions in the program memory are executed with a single level pipelining. While one instruction is being executed, the next instruction is pre-fetched from the program memory. This concept enables instructions to be executed in every clock cycle. The program memory is In-System Reprogrammable Flash memory.

The fast-access Register file contains 32 x 8-bit general purpose working registers with a single clock cycle access time. This allows single-cycle Arithmetic Logic Unit (ALU) operation. In a typical ALU operation, two operands are output from the Register file, the operation is executed, and the result is stored back in the Register file – in one clock cycle [5].

The ALU supports arithmetic and logic operations between registers or between a constant and a register. Single register operations can also be executed in the ALU. After an arithmetic operation, the Status Register is updated to reflect information about the result of the operation.

B. LCD Display

For the sake of device compactness, low price, and availability, the LCD2L4P02A [6] module has been selected as a device management unit and as an input interface for simple user data entering. That module is equipped with a dual line text LCD display (2 x 16 characters), and it is controlled by the Hitachi HD44780 controller. The user interface consists of four buttons and of a piezoelectric element for pertinent sound signalization what is well

sufficient for basic operation.

C. Real Time Clock Module

The RTC module for actual datum and time retention is not a part of that microcontroller. It was necessary to design and realize it. The integrated circuit DS1307 by Maxim Integrated Products seemed to be a convenient basic element for the RTC module. The circuit design has respected the application circuitry recommended in the data sheet [7]. The RTC beat is controlled by an external crystal with the resonance frequency of 32.768 kHz. When the power supply is off, the time and data memory content is secured with a battery. In such back up mode, the current consumption is only 500 nA what means that the time and memory content can be kept for more than 10 years (the battery capacity 48 mAh at the room temperature +25 °C).

The ease availability of datum and time represents a remarkable advantage of that circuit family. They are coded in the BCD, and it is possible to read the from internal shift registers.

D. Other development kit parts

That designed device set includes some other modules, namely:

- The memory card data storing module
- The Voltage Level Translator
- The power switch for external devices control
- Power supply
- The USART/USB conversion module.

The whole device set is of a modular design. That corresponds with the low cost requirement because only relevant modules for a particular application are connected and installed.

IV. LOW-COST ACCESS SYSTEM

A security oriented composition was created for the developed kit functionality and applicability evaluation. That composition represented an autonomous system for access security control. That security control application is oriented at family houses and apartment houses where it attends one entrance point (the electromagnetic gate). There is up to 20 such entrance points with a prospect for future increasing. It is supposed that each device has a different approved set of identification elements (tokens), and that it operates independently. The memory stored identification elements counts in tens at maximum.

A. The system requirements

The above mentioned security application identification elements selection asks for a mechanically robust, cheap and passive design. From the security point of view, such ID elements counterfeiting should be much more complicated than key imitating, and the ID elements misinterpretation should be also quite unlikely during authorization process. The access history evaluation, in case of a theft in commonly shared rooms, for instance, should be possible with current

design because it could retrospectively specify the access ID and access time. The device control should be simple, preferably without necessity to connect any other devices, like programmers, computers, etc. However, that device is supposed to be placed near the entrance point so that the authorization interface should be protected correspondingly. Further requirement relates to the device operability in case of energy supply drop-out. The device power supply is either the public electricity distribution network, or alternatively the building local electricity distribution and/or battery back-up power supply, for instance.

If we summarize the above mentioned requirements, the developed device should fulfill the following features:

- Exploitation of microcontroller technology.
- User friendly design.
- Lost ID element quick and simple removal and new ID element registration.
- ID elements selection with regard to counterfeiting prevention.
- Storing data about authorized and unauthorized accesses.
- Unauthorized access to the control interface protection.
- Emergency access alternative without identification, for instance protected emergency button, or a remote electronic gate keeper.
- Price comparable to the common door lock replacement in case of a lost key.

B. Identification element

The iButton contact elements have been selected because of their interesting price to utility value ratio [8]. The only disadvantage of those elements is the absence of direct communication with microcontroller possibility. Those elements exploit the “1 Wire Bus” which is to be emulated by software.



Fig. 3 ID element iButton [9]

Maxim Integrated Products produces a wide assortment of identification elements (tokens) under iButton family name. The scope of application covers various access control system, attendance systems, etc. Such element consists of a

microcontroller chip encapsulated in a stainless steel package with the diameter of 16 mm. The iButton elements make use of their metal packages as an electrical contact interface to 1-Wire bus and for power supply. Each element is identified with a unique 64 bit identification code which is laser engraved in the package surface.

The particular token identification safety provides the CRC check sum with $X^8+X^5+X^4+1$ polynomial. The authorization reading is valid if the first 56 bits check sum is coincident with the value stored in the seventh byte.

The iButton elements [8] are produced in about twenty variants, and besides the ID number they can hold further functions. The ID element basic version iButton DS1990A holding ID code only has been selected for our project.

C. Access point interface

The access point interface is comprised of an iButton sensing module and of an electromagnetic lock (door open system). With regard to 1-Wire bus software emulation, the sensing module does not need to be equipped with data processing logic. It could be just an electromechanical contact. An arbitrary electromagnetic lock system with direct current power supply of 12 V is convenient for the access point unlocking. It is not important whether there will be used a lock system with memory (activated by an impulse and deactivated mechanically after door is open), or if there will be used a standard lock system (deactivated with the electromagnet supply termination).

D. Other part of system

Although there is possible to use a standard two wire serial communication interface for the device management like many other systems do, we have decided differently in this case. There is necessary to connect a PC in standard situations mentioned above. Such manipulation is not always user friendly. In our case, we are using the serial interface only for special and rare diagnostic purposes. Any regular device management in our case is realized LCD display with a few buttons.

The process of storing transactions data (entrance permission or entrance denial) is realized as a data storing in a text file on a SD/MMC memory card.

E. System block diagram

The system block diagram has been created for particular device component interconnection design:

- Microcontroller
- Programmer
- USART/USB converter
- Control interface – LCD display
- Real time clock (RTC)
- Access transactions storing – SD card
- Voltage Level Translator
- iButton reader
- Access point interface – power switch
- Power supply

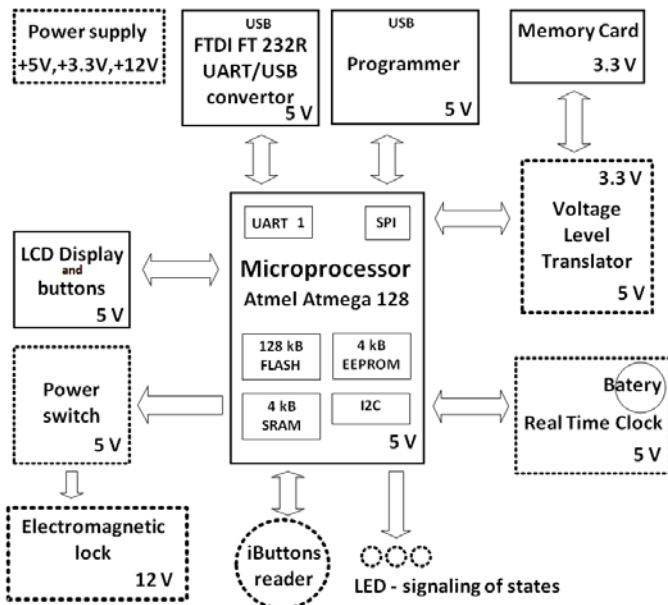


Fig. 4 Block Diagram of the Access System

F. Selected functions

From security reasons, there is an urgent need to arrange passage for authorized persons even in case of energy drop-out. That can be ensured either with a centralized sector and its energy backup or with a local USP and/or a backup battery.

Administrator has to keep an updated register of issued token ID codes with regard to lost token cases and token blockage process. An urgent blockage minimizes the risk of token misusing, however, the ID code records are to be protected against theft or copying because an emulator can be created with the knowledge of them.

Same strict measures apply to control interface administration access PIN. Provided the administrator forgets that PIN, it is possible to reset it by RTC battery removal after the device cabinet opening.

In case of a security incident, there is possible to analyze that data stored on a memory card and gain an overview about individual entering a protected area. The memory card can be removed even during a device operation. That device continues in operation mode and serves users. It is of course unable to record transaction data. Such memory-less state is indicated by a quickly flashing blue LED [15].

The device can be switched off with a button at any time. No action is necessary to perform before switching off.

V. CONCLUSION

The project main goal was to design and create a kit for the verification of microcomputer programming student education possibilities.

That designed device was verified for a security application, namely for an autonomous entrance guard system. The result corresponds with task assignment, and it fulfills the economic goal as well. Our design is cheaper and carries more functionality than commercial ones. The task solution

composes from two parts, the hardware part and the software part. The software part has been created in the AVR Studio 4 development environment in C language.

The hardware part is realized as a complete set including electromagnetic lock system and iButton reader.

An economic analysis proved that our device set can be manufactured with half of the costs of those existing commercial products, and its functionality can be even better. In comparison with a standard security lock, our device set is more expensive, but it is true only until the first key loss.

REFERENCES

- [1] Intel Museum: Journey through decades of innovation, Intel Corporation, [Online] 2012. Available: <http://www.intel.com/content/www/us/en/company-overview/intel-museum.html>.
- [2] Zilog Embedded in Life, Zilog, Inc., [Online] 2012. Available: <http://www.zilog.com/>
- [3] A. Qamar, J. Iqbal, I. Javed, Ishaque, H. Rehan, "Design and manufacturing of a real time imitation based robotic arm using low cost microcontroller", *Proceedings of the 6th WSEAS International Conference on Applied Informatics and Communications*, Elounda, Greece, August 18-20, 2006 (pp363-368).
- [4] T. Sysala, P. Neumann, J. Pribyslavsky, M. Adamek, "Tutorial development kit for 32-bit ARM microcontrollers with a focus on multimedia", *International Journal of Circuits, Systems and Signal Processing*, Issue 2, Vol. 7, 2013, North Atlantic University Union.
- [5] Atmel Corporation, "8-bit Atmel microcontroller with 128Kbytes in-system programmable flash." [Online] 2011. Available: <http://www.atmel.com/Images/doc2467.pdf>.
- [6] MLAB online, "Module with LCD 2 line display and 4 buttons (in Czech)." [Online] 2014. Available: <http://www.mlab.cz/Modules/HumanInterfaces/LCD2L4P01A/DOC/LCD2L4P01A.cs.pdf>.
- [7] Maxim Integrated online, "DS1307 real-time clock." [Online] 2008. Available: <http://datasheets.maximintegrated.com/en/ds/DS1307.pdf>.
- [8] Maxim Integrated online, "1-Wire and iButton." [Online] 2014. Available: http://www.maxim-ic.com/auto_info.cfm.
- [9] Kassen Computer Wagner. "Dallas iButton standard." [Online] 2014. Available: <http://kacowa.de/kellnerschlüssel/203-dallas-ibutton-standard-kellnerschlüssel-schwarz.html>.
- [10] J. Navratil, M. Stanek, M. Manas, D. Manas, K. Kvas, V. Senkerik, A. Skrobak, "Recyclation of irradiated HDPE - influence on tensile toughness", in *Proc. 17th WSEAS International Conference on Systems*, Rhodes Island, Greece, 2013, pp. 186-189.
- [11] D. Manas, M. Ovsik, M. Manas, M. Stanek, P. Kratky, A. Mizera, M. Bednarikl, "Effect of Beta low irradiation doses on the microhardness of PA 66," in *Proc. 17th WSEAS International Conference on Systems*, Rhodes Island, Greece, 2013, pp. 190-195. ISBN 978-960-474-314-8.
- [12] V. C. Petre, „Microcontroller based measurements : how to take out the best we can of them”, *Proc. of the 8th WSEAS Int. Conf. on Mathematical Methods and Computational Techniques in Electrical Engineering*, Bucharest, October 16-17, 2006.
- [13] S. Y. Cho, "A virtual development environment for smart card applications", *Proceedings of the 12th WSEAS International Conference on Automatic Control, Modelling & Simulation*, Catania, Sicily, Italy, May 29-31, 2010.
- [14] P. Navratil, L. Pekar, "Combined production of heat and electric energy – linear mathematical model", *Proc. of the 16th WSEAS International Conference on Circuits*, Kos Island, Greece, July 14-17, 2012.
- [15] F. Zanka, "Implementation of autonomous access control system using MCU Atmel (in Czech)", *diploma thesis*, Faculty of Applied Informatics, Tomas Bata University in Zlin, Zlin, 2011.
- [16] J. Pribyslavsky, "Development kit for 32-bit ARM micro-controllers with a focus on multimedia applications (in Czech)", *diploma thesis*, Faculty of Applied Informatics, Tomas Bata University in Zlin, Zlin, 2012.

Fuzzy logic controller in servo drive control system with speed limitation

Nikita Smirnov, Dmitry Lukichev
ITMO University

Abstract – The paper considers problem of a servo drive speed limitation within the permissible values rate in condition of different impacts types. A fuzzy logic controller with speed limitation suggested for such electric drive. Control system with tis controller was tested on the laboratory stand of telescope rotary support axis.

Keywords – Fuzzy Controller, Servo Drive, Electric Drive, Speed Limitation.

I. INTRODUCTION

High precision direct servo drive systems are widely used in laser ranging systems. Rotary support of this laser ranging systems with embedded synchronous motors and optical equipment is characterized by low speeds at relatively high moments of inertia. If rotary support emergency strikes on the angle limiters, it should not get irreversible mechanical deformation. Also there are limits for maximum acceleration of telescope optical equipment. Both of these requirements impose a limit on the rotary support maximum speed.

To prevent failure in the telescope drive controller integrated overspeed protection. If the maximum permitted rotating speed was exceeded - protection works and off power supply of rotary support electric motor. Thus, there is an emergency situation that requires human intervention, and fails object tracking cycle. In this regard, the electric drive control system tasked rotary support angle speed not exceeding the allowable limits both at working by reference signal and when there is external disturbance.

There are various techniques for limiting of angle speed of rotary support. At the Electrical Engineering and Precision Electromechanical Systems Department (EEPEMS), ITMO University, developed algorithm [1], that builds reference signal with defined limits of the speed and acceleration values. This algorithm successfully copes with reference signal smoothing and holds drive angle speed within the specified limits, if external disturbances are absent.

Control system doesn't differentiate external disturbance and reference signal and tasked to reduce mismatch error of feedback signal with reference. In single-loop positioning control system, the speed limit task is difficult because in these systems regulator works on angle error and ignores the information about object velocity. Restriction of the control signal is not effective as a control signal sets current value in the synchronous

motor that slew rotary support, so it defines the object acceleration. Introducing of the second speed loop has the following disadvantages: 1) saturation of the position controller output reduces the sensitivity of the system to position error, and 2) the possible overshoot in speed loop does not exclude overspeed accident even there are constraints on the speed reference signal, and 3) the time constant of a two-loop system increases compared with single-loop.

Due to the positive experience of the fuzzy logic application in solving problems of motor control [2,3], it was decided to develop controller based on fuzzy logic with speed constraint. The proposed single-loop positioning control system has a fuzzy controller with additional input on the object's speed in the forward control channel. It solves task of telescope rotary support angle speed retention within acceptable limits. Maximum allowable object speed is given by the coefficient of speed feedback.

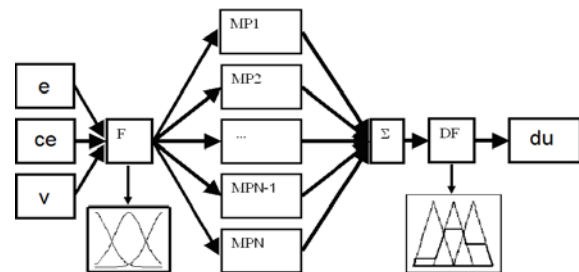


Fig. 1. Fussy controller structure

II. SYNTHESIS OF FUZZY CONTROLLER

The internal structure of fuzzy controller is shown in Fig. 1. Developed regulator includes three input linguistic variables: error e , the error derivative ce and the object speed v ; and one output linguistic variable - control signal du (Fig. 2a). Linguistic variables e , ce and du have five terms with fuzzy values “big negative” (bn), “medium negative” (mn), “zero” (z), “medium positive” (mp) and “big positive” (bp). That’s number of terms is the most convenient and provides satisfactory regulator sensitivity [3]. As membership functions were chosen triangular functions defined by three numbers (a, b, c). Term boundaries are selected from the conditions of their symmetry with respect to the positive and negative values of the input signals. In the defuzzification stage was used the center of gravity method [4].

The object angular velocity (variable v) is used as an additional parameter. If the object velocity does not go

out of the specified range, output value of the regulator is determined only by the value of the error and error derivative. If object velocity exceeds the specified range, the output value of the regulator limited. Based on these requirements linguistic variable v defined by three terms with fuzzy values “big negative” (bn), “zero” (z) and “big positive” (bp). Terms bn and bp are defined by triangular membership functions defined by the triple (a, b, c). To localize the zone of influence of speed limits on the control value the term z has trapezoidal membership function, that defined by four numbers (a, b, c, d).

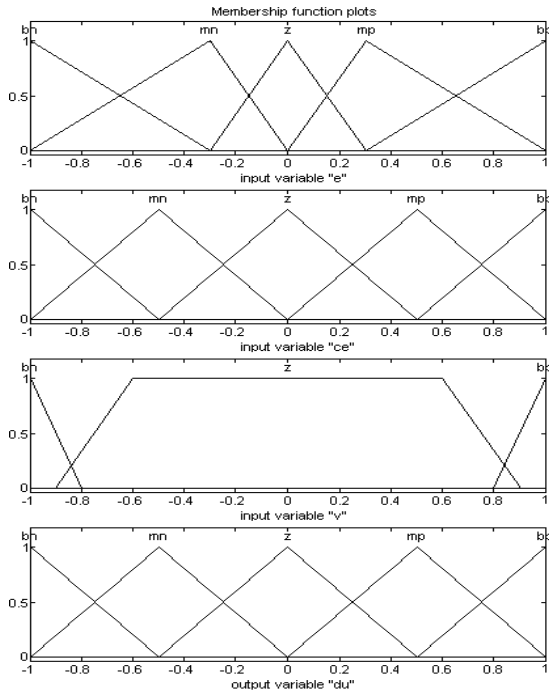


Fig. 2. Initial membership functions of the terms of the linguistic variables e , ce , v and du

Fuzzy rules were synthesized after determining the terms number of each linguistic variable and the distribution of the membership functions. That rules are shown below:

$$R_i : \left(\begin{array}{l} \text{IF } e = A_{i1} \text{ AND } ce = A_{i2} \text{ AND } v = A_{i3} \\ \text{THEN } du = B_i \end{array} \right), \quad (1)$$

where A_{ij} – set of a membership functions of a j -th variable to a i -th term; B_i - set of membership functions to the term i -th output variable. The total number of fuzzy rules is the product of terms number on input variables, i.e. 75 (Fig. 3). Divide the synthesis of fuzzy rules into several stages.

First of all, fuzzy rules were developed excluding limits by object speed, i.e. for the case when the variable v corresponds to the term I (Fig. 3b). The greater angle error between rotor position and reference signal corresponds to the greater output signal of the regulator. Control is also dependent on error derivative. If it decreases, controller output signal decreases too even win a big error. Conventionally, the shown system of 25 rules can be divided into two halves: positive and negative

error. In the first case, the controller generates a positive output signal, in the second - negative.

Then the object velocity keeping was introduced and advanced block rules was developed. Rotary support movement was considered depending on the reference signal. Variety of input variables combinations of the controller can be qualitatively divided into eight modes:

1. $e \geq 0, ce \geq 0, v \geq 0$;
2. $e \geq 0, ce \geq 0, v \leq 0$;
3. $e \geq 0, ce \leq 0, v \geq 0$;
4. $e \geq 0, ce \leq 0, v \leq 0$;
5. $e \leq 0, ce \geq 0, v \geq 0$;
6. $e \leq 0, ce \geq 0, v \leq 0$;
7. $e \leq 0, ce \leq 0, v \geq 0$;
8. $e \leq 0, ce \leq 0, v \leq 0$;

Graphical representation of the possible system modes (Fig. 4, where z – reference signal, α – angle by feedback signal, e_k, e_{k-1} – error on k and $k-1$ step) simplifies understanding of the desired behavior of the controller. In drawing up the remaining rules situation with positive and negative angle velocity must be consider separately.

e \ ce	bn	mn	z	mp	bp
bn	z	z	z	z	z
mn	z	z	z	z	z
z	z	z	z	mp	bp
mp	z	mp	mp	bp	bp
bp	mp	mp	bp	bp	bp

a)

e \ ce	bn	mn	z	mp	bp
bn	bn	bn	bn	mn	mn
mn	bn	bn	mn	mn	z
z	bn	mn	z	mp	bp
mp	z	mp	mp	bp	bp
bp	mp	mp	bp	bp	bp

b)

e \ ce	bn	mn	z	mp	bp
bn	bn	bn	bn	mn	mn
mn	bn	bn	mn	mn	z
z	bn	mn	z	z	z
mp	z	z	z	z	z
bp	z	z	z	z	z

c)

Fig.3 Fuzzy rules for the cases: $v = bn$ (a), $v = z$ (b), $v = bp$ (c).

Upon reaching dangerous values of rotary support speed speed controller must stop the its acceleration and, if necessary, slow it down. So the control signal must have negative sign to the value of rotary support speed. Based on these considerations the rules matrix transforms as follows: control signal set to zero when its sign coincides with the object speed sign and remains nonzero with opposite signs (Fig.3, a, c) . Suchwise, the controller resets output signal when the speed of the object exceeds the allowable values and the object behind the reference signal (Fig.4, scheme 1, 3 for positive speed and 6, 8 for negative speed). The controller also prevents the object target position deviation by external forces and subsequent excessively sharp adjustment of the deviation (Fig. 4, schemes 5, 7 for a positive speed and 2, 4 for negative).

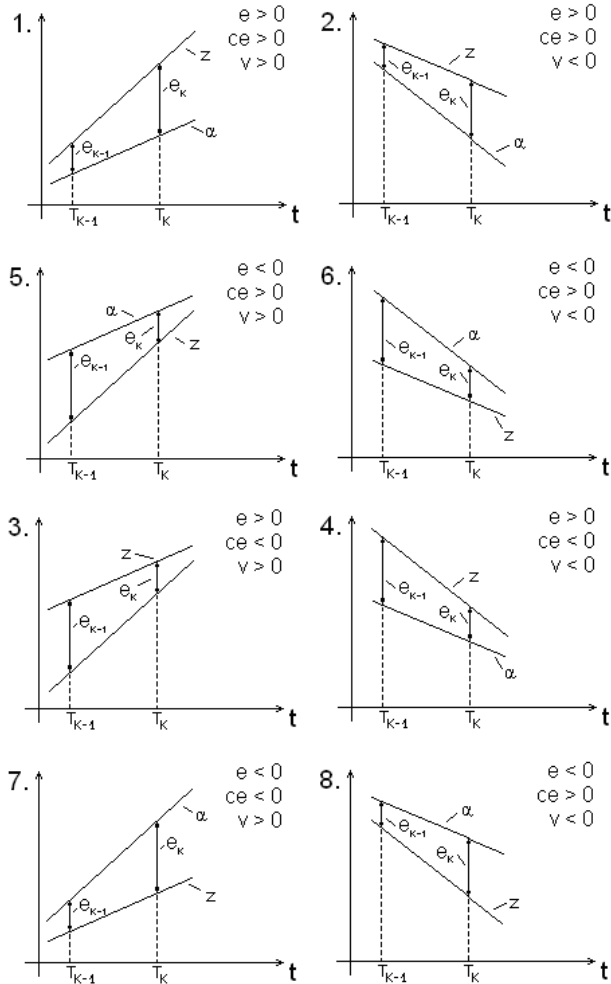


Fig.4. Diagrams of the rotary support movement.

III. BUILDING OF FUZZY CONTROL SYSTEM

Control system with suggested fuzzy controller was built for electromechanical stand which is available to the EEPEMS Department. This stand represents a telescope elevation axis with moment of inertia, equals 0.39 kg.m^2 . Stiffness of the mechanical characteristic of

this object is $1.6 \text{ kg.m}^2/\text{s}$. Stand also has mechanical resonances around 80 and 200 Hz, which imposes additional constraints on the control system for suppression of mechanical vibrations, manifested as acoustic noise.

Identification problem for this electromechanical system presented [5,6]. In [5] stand, discussed in the article presents by single-mass model and describes as second-order aperiodic link with output as object speed and additional integrator to object angle (2).

$$W_{ob} = \frac{K}{(T_1 \cdot s + 1)(T_2 \cdot s + 1)} \cdot \frac{1}{s} = \frac{b_0}{s^2 + a_1 \cdot s + a_0} \cdot \frac{1}{s} \quad (2)$$

Where $b_0 = 1173 \cdot 105 \text{ deg} \cdot \text{s}^{-3}/\text{V}$; $a_1 = 512,3 \text{ s}^{-1}$; $a_0 = 1173 \text{ s}^{-2}$. T_1, T_2 – time constants, K – transfer ratio.

Closed single-mass fuzzy control system of angle regulation was developed in the Matlab software based on the above considerations and the proposed method of synthesis fuzzy controller (Fig. 5).

Real object as a feedback sensor uses optical incremental encoder and velocity is calculated by an electric drive controller. Therefore, the model uses the same principle: the output angle from analog integrator quantized in steps of the encoder scale factor. Speed value at k -th step is calculated by the formula:

$$v(k) = \frac{\alpha(k) - \alpha(k-1)}{T_d}, \quad (3)$$

where v – speed, α – angle, k – discrete step, T_d – discrete epoch. In the block of velocity calculating also applied smoothing by averaging over the last two frames.

Fuzzy controller is implemented in a block *FuzzyReg*. The rule base and the information about terms stored on the block *Fuzzy Logic Controller*. Speed error is calculated from the error signal on the basis of a similar computation of the object speed.

Control input signals are normalized with coefficients $k5, k6, SpeedLimit$. The control signal is amplified by a factor $k7$. *SpeedLimit* equals to the reciprocal value of the maximum allowable speed of 10 deg/s. Coefficients $k5, k6, k7$ were tuned via a function block “Signal Constraint” from Design Optimization Simulink library.

IV. THE SIMULATION AND TESTING RESULTS

Matlab simulation with closed-loop speed showed, when speed reaches the maximum permissible values high ripples of the control signal and object speed are appear (Fig. 6, curve 1). Testing on a laboratory stand, confirmed the presence of pulsations, manifested in increased acoustic noise. Correction of coefficients $k5, k6, k7$ has not led to a positive result.

Analysis of the feedback signals with controller output signal showed that a velocity step change occurs when the angle error value transiting through the value 0.3 - switching boundary terms of the linguistic variable. Triangular membership function of the linguistic variable v may cause velocity fluctuations and associated with its acoustic noise.

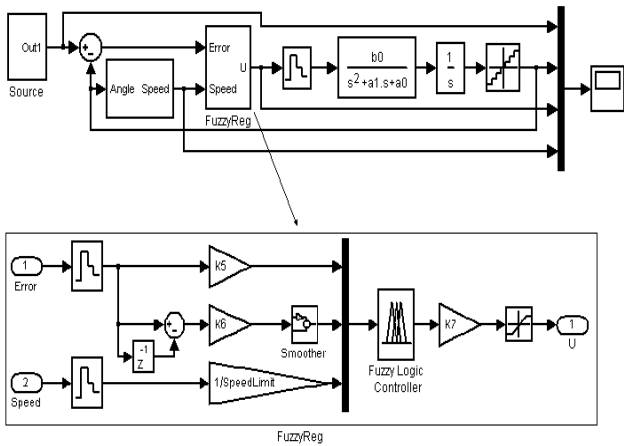


Fig.5 Fuzzy control system implemented in the Matlab

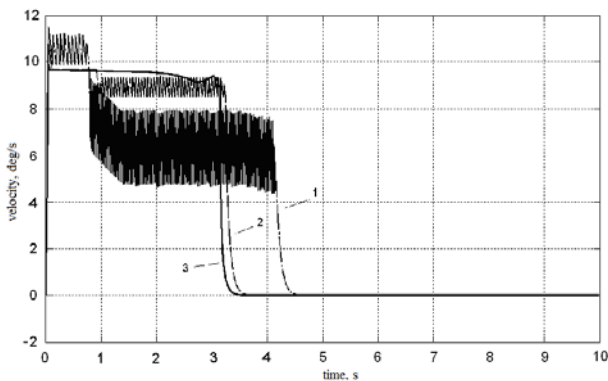


Fig.6 Modeled rotary speed with controller rules from Fig.2 (1), with corrected rules of v (2) and rules from Fig.7 (3).

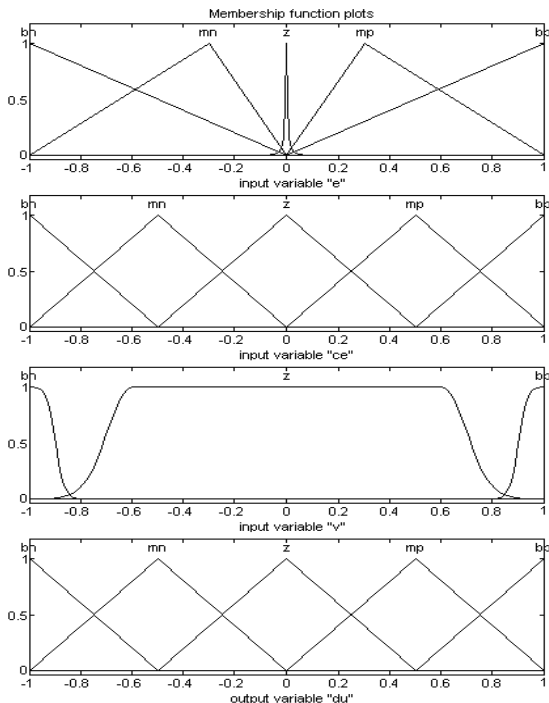


Fig.7 Corrected membership functions of the terms of the linguistic variables e , ce , v and du

Based on these findings, the terms boundaries were adjusted and new functions of linguistic variables, shown at Fig.7. Modeling in Matlab package revealed a marked improvement of the feedback signals. Presented on Fig.6

curve 3 has not velocity pulsation and a step. Subsequent testing on a laboratory stand confirmed modeling results.

On the laboratory stand was confirmed acoustic noise absentness and tested system reaction on external disturbance (Fig.8, 25-th second). On the 25th second of the experiment (Fig.8) external active torque was attached to the motor shaft for eight seconds. Under the action of the active torque shaft is deviated from the predetermined value by more than 20 degrees. After closure of the external torque controller compensated mistake and returned rotary support target position with speed not exceeding the maximum allowed value. Then the external torque was applied in the opposite direction with the same result.

At experimental test the control system has successfully coped with the speed limiting within 10 deg/s and mean square error (MSE) does not exceed 30 arc seconds. But its value depends on the position of the rotary support and of resistance torque value at this point. This MSE value is unsatisfactory for a optical guidance systems. Aiming to reduce the MSE, it was decided to close the inner current loop with PI controller, that was increased the transmission coefficient for the control signal of fuzzy controller and increased sensitivity of the system to position error. It is not needed to retune the controller coefficients and MSE decreased to a few seconds of arc, which is a satisfactory result.

The constant component of the instantaneous MSE value depends on the resistance moment, which says about low astatism of control system.

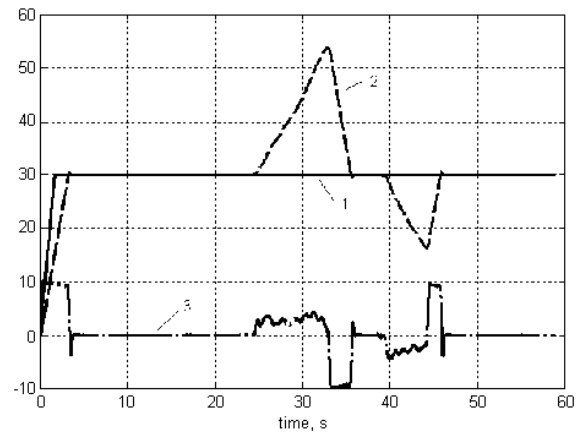


Fig.8 Reaction of the stand with fuzzy controller on active external torque, where 1 – reference signal, 2 – feedback angle, 3 – feedback speed.

V. CONCLUSION

Designed fuzzy controller solves the speed limit problem of telescope rotary support. In an experimental investigation, we can draw the following conclusions:

1. Application of fuzzy controller can effectively limit the angle speed of rotary support in positioning electric drive, when reference signal has derivative higher than the maximum allowable speed or when has place large disturbing external influence.

2. To reduce errors in a real system is required to enter the inner current loop. The system remains stable without retuning fuzzy controller, which indicates its robustness.

3. Zero astatism by disturbance of the developed system requires including of compensation in the control channel.

ACKNOWLEDGEMENT

This work was financially supported by Government of Russian Federation, Grant 074-U01.

REFERENCES

- [1] S. Yu. Lovlin, M.Kh.Tsvetkova, I.N. Zhdanov, Programming trajectory former of servo drive movement. *Scientific and Technical Journal of Information Technologies, Mechanics and Optics*. Vol.72, 2011, pp. 113-117.
- [2] K. M. Denisov, D.V. Kuprianchik, Electric drive control system of a telescope azimuthally axis with fuzzy controller. *Scientific and Technical Journal of Information Technologies, Mechanics and Optics*. Vol.20, 2005, pp. 116-122.
- [3] O.V. Goryachev, M.A. Sharapov, E.S. Ivanova, Synthesis of Fuzzy Regulator for Guidance and Stabilization Drive with Multimass Mechanical Subsystem, *Mechatronics, Automation, Control*, 2011, № 11, pp. 30-35.
- [4] A.V. Leonenkov, Fuzzy modeling in Matlab and fuzzyTECH, *BHV – Saint Petersburg*, 2003, 736 pages.
- [5] S.V. Aranovskiy, V.M. Bardov, The Motor Leads two Masses Equipment System's Parameters Identification Algorithm, *Mechatronics, Automation, Control*, 2010, № 5, pp. 15-18.

Chaos enhanced differential evolution with the dissipative map for the PID tuning problem

Roman Senkerik, Michal Pluhacek, and Zuzana Kominkova Oplatkova

Abstract— This paper presents results of the utilization of selected discrete chaotic map, which is Dissipative standard map, as pseudo-random number generator for the differential evolution (DE) optimization algorithm in the task of PID controller design for the 4th order dynamical system. The results are compared with previously published results and discussed.

Keywords—Evolutionary algorithms; Differential evolution; Chaos, PRNG, PID controller, Optimization

I. INTRODUCTION

THESE days the methods based on soft computing such as neural networks, evolutionary algorithms, fuzzy logic, and genetic programming are known as powerful tool for almost any difficult and complex optimization problem.

In the past decades, PID controllers became a fundamental part of many automatic systems. The successful design of PID controller was mostly based on deterministic methods involving complex mathematics [1, 2].

Recently, different soft-computing methods were used with promising results for solving the complex task of PID controller design [3]. These techniques [5-8] use random operations and typically use various kinds of pseudo-random number generators (PRNGs) that depend on the platform the algorithm is implemented. More recently it was shown that chaotic systems could be used as PRNGs for various stochastic methods with great results. Some of these chaos driven stochastic methods were tested on the task of PID controller design in [4]. In [3] it was shown that Particle Swarm optimization (PSO) algorithm could deal with the task of PID controller design with very good results. Following that in [9 - 12] the performance of chaos driven PSO algorithm was tested on this task with great results.

In this paper, the influence of promising discrete dissipative chaotic system to the performance of chaos driven heuristic algorithm, which is DE, is investigated and results are compared with previously published results of chaos driven

R.Senkerik, M. Pluhacek and Z. Kominkova Oplatkova are with the Department of Informatics and Artificial Intelligence, Faculty of Applied Informatics, Tomas Bata University in Zlin, Nam. T.G. Masaryka 5555, 760 01 Zlin, Czech Republic, (phone: +420576035189; fax: +420576035279; e-mail: senkerik@fai.utb.cz).

This work was supported by European Regional Development Fund under the project CEBIA-Tech No. CZ.1.05/2.1.00/03.0089; and by Internal Grant Agency of Tomas Bata University under the project No. IGA/FAI/2014/010.

evolutionary algorithm PSO [9 - 12] and with other techniques [3,4] as well as with the canonical versions of DE (without chaotic pseudo-random number generator - CPRNG).

II. MOTIVATION

Till now the chaos was observed in many of various systems (including evolutionary one) and in the last few years is also used to replace pseudo-number generators (PRNGs) in evolutionary algorithms (EAs).

This research is a continuation of the previous successful initial application based experiment with chaos driven DE [4]. In this paper the DE/rand/1/bin strategy driven by Dissipative chaotic map (system) was utilized to solve the issue of evolutionary optimization of PID controller settings. Thus the idea was to utilize the hidden chaotic dynamics in pseudo random sequences given by chaotic Dissipative map system to help Differential evolution algorithm in searching for the best controller settings.

Recent research in chaos driven heuristics has been fueled with the predisposition that unlike stochastic approaches, a chaotic approach is able to bypass local optima stagnation. This one clause is of deep importance to evolutionary algorithms. A chaotic approach generally uses the chaotic map in the place of a pseudo random number generator [13]. This causes the heuristic to map unique regions, since the chaotic map iterates to new regions. The task is then to select a very good chaotic map as the pseudo random number generator.

The primary aim of this work is not to develop a new type of pseudo random number generator, which should pass many statistical tests, but to try to test, analyze and compare the implementation of different natural chaotic dynamics as the CPRNGs, thus to analyze and highlight the different influences to the system, which utilizes the selected CPRNG (including the evolutionary computational techniques).

III. DIFFERENTIAL EVOLUTION

DE is a population-based optimization method that works on real-number-coded individuals [8]. For each individual $\bar{x}_{i,G}$ in the current generation G , DE generates a new trial individual $\bar{x}'_{i,G}$ by adding the weighted difference between two randomly selected individuals $\bar{x}_{r_1,G}$ and $\bar{x}_{r_2,G}$ to a randomly selected third individual $\bar{x}_{r_3,G}$. The resulting

individual $\bar{x}'_{i,G}$ is crossed-over with the original individual $\bar{x}_{i,G}$. The fitness of the resulting individual, referred to as a perturbed vector $\bar{u}_{i,G+1}$, is then compared with the fitness of $\bar{x}_{i,G}$. If the fitness of $\bar{u}_{i,G+1}$ is greater than the fitness of $\bar{x}_{i,G}$, then $\bar{x}_{i,G}$ is replaced with $\bar{u}_{i,G+1}$; otherwise, $\bar{x}_{i,G}$ remains in the population as $\bar{x}_{i,G+1}$. DE is quite robust, fast, and effective, with global optimization ability. It does not require the objective function to be differentiable, and it works well even with noisy and time-dependent objective functions. Description of used DERand1Bin strategy is presented in (1). Please refer to [8], [14], [15] and [16] for the description of all other strategies.

$$u_{i,G+1} = x_{r1,G} + F \cdot (x_{r2,G} - x_{r3,G}) \quad (1)$$

IV. THE CONCEPT OF CPRNG

The general idea of CPRNG is to replace the default PRNG with the chaotic system. As the chaotic system is a set of equations with a static start position, we created a random start position of the system, in order to have different start position for different experiments. This random position is initialized with the default PRNG, as a one-off randomizer. Once the start position of the chaotic system has been obtained, the system generates the next sequence using its current position.

Generally there exist many other approaches as to how to deal with the negative numbers as well as with the scaling of the wide range of the numbers given by the chaotic systems into the typical range 0 – 1:

- Finding of the maximum value of the pre-generated long discrete sequence and dividing of all the values in the sequence with such a maxval number.
- Shifting of all values to the positive numbers (avoiding of ABS command) and scaling.

V. SELECTED CHAOTIC SYSTEM

This section contains the description of discrete dissipative chaotic map, which was used as the chaotic pseudo random generator. In this research, direct output iterations of the chaotic map were used for the generation of the both integer numbers and real numbers scaled into the typical range for random function: <0 - 1>. Following chaotic system was used: Dissipative Standard Map (2).

The Dissipative Standard map is a two-dimensional chaotic map. The parameters used in this work are $b = 0.6$ and $k = 8.8$ as suggested in [17]. The map equations are given in (2).

$$\begin{aligned} X_{n+1} &= X_n + Y_{n+1} \pmod{2\pi} \\ Y_{n+1} &= bY_n + k \sin X_n \pmod{2\pi} \end{aligned} \quad (2)$$

The x,y plot of Dissipative map is depicted in Fig. 2. The

typical chaotic behavior of the utilized chaotic map, represented by the example of direct output for the variable x is depicted in Fig. 2. Whereas Fig. 3 represents the discrete direct outputs of the chaotic system.

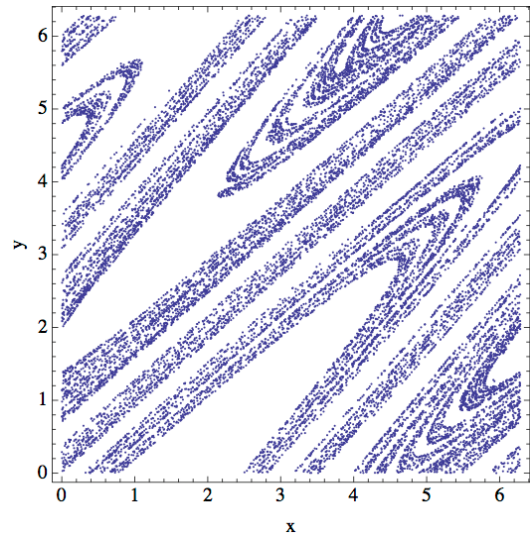


Fig. 1 x, y plot of the Dissipative standard map

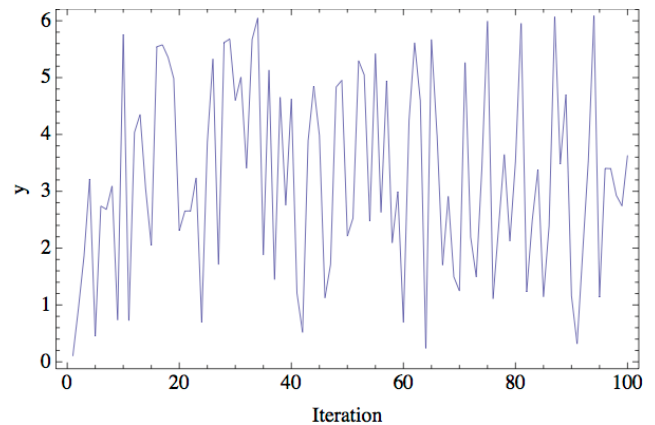


Fig. 2 Simulation of the Dissipative map (variable y – line-plot)

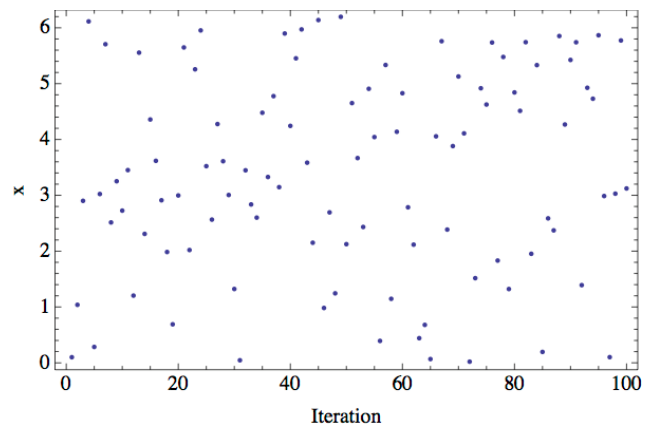


Fig. 3 Direct output iterations of the Dissipative map – variable x

The illustrative histograms of the distribution of real numbers transferred into the range <0 - 1> generated by means of studied chaotic system is in Fig. 4.

Finally the Fig. 5 shows the example of dynamical sequencing during the generating of pseudo number numbers by means of studied CPRNG.

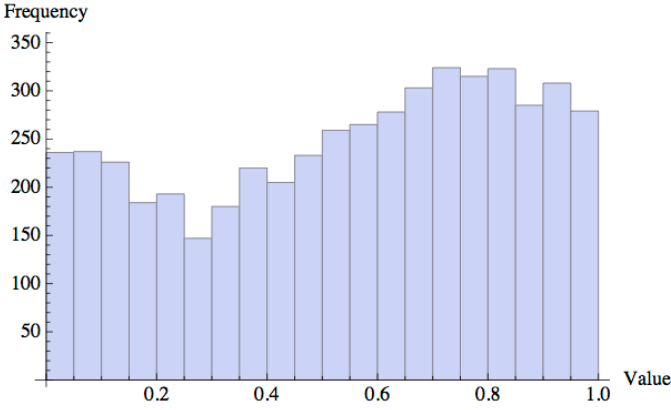


Fig. 4 Histogram of the distribution of real numbers transferred into the range <0 - 1> generated by means of the chaotic Dissipative standard map – 5000 samples

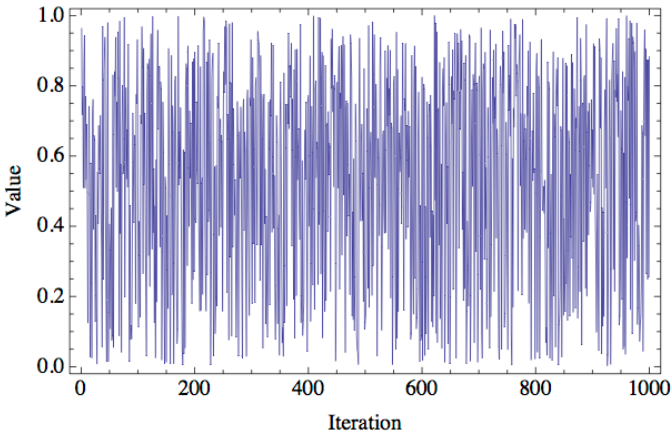


Fig. 5 Example of the chaotic dynamics: range <0 - 1> generated by means of the chaotic Dissipative standard map

VI. PROBLEM DESIGN

A. PID Controller

The PID controller contains three unique parts; proportional, integral and derivative controller [1-4]. A simplified form in Laplace domain is given in (3).

$$G(s) = K \left(1 + \frac{1}{sT_i} + sT_d \right) \quad (3)$$

The PID form most suitable for analytical calculations is given in Eq. 4.

$$G(s) = k_p + \frac{k_i}{s} + k_d s \quad (4)$$

The parameters are related to the standard form through:

$k_p = K$, $k_i = K/T_i$ and $k_d = KT_d$. Acquisition of the combination of these three parameters that gives the lowest value of the test criterions was the objective of this research.

Selected controlled system was the 4th order system that is given by Eq. 5.

$$G(s) = \frac{1}{s^4 + 6s^3 + 11s^2 + 6s} \quad (5)$$

B. Cost function

Test criterion measures properties of output transfer function and can indicate quality of regulation [1-4]. Following four different integral criterions were used for the test and comparison purposes: IAE (Integral Absolute Error), ITAE (Integral Time Absolute Error), ISE (Integral Square Error) and MSE (Mean Square Error). These test criterions (given by Eq. 6 – 9) were minimized within the cost functions for the enhanced PSO algorithm.

a) Integral of Time multiplied by Absolute Error (ITAE)

$$I_{ITAE} = \int_0^T t |e(t)| dt \quad (6)$$

b) Integral of Absolute Magnitude of the Error (IAE)

$$I_{IAE} = \int_0^T |e(t)| dt \quad (7)$$

c) Integral of the Square of the Error (ISE)

$$I_{ISE} = \int_0^T e^2(t) dt \quad (8)$$

d) Mean of the Square of the Error (MSE)

$$I_{MSE} = \frac{1}{n} \sum_{i=1}^n (e(t))^2 \quad (9)$$

VII. RESULTS

In this section, the results obtained within experiments with ChaosDE algorithm driven by Dissipative standard map are compared with previously published works [3, 4, 9 - 12]. Table 1 shows the typical used settings for the both ChaosDe and Canonical DE.

TABLE I. DE SETTINGS

DE Parameter	Value
PopSize	25
F	0.8
CR	0.8
Generations	50
Max. CF Evaluations (CFE)	750

Best results obtained for each method are given in Table 2. The statistical results of the experiments for one selected

criteria are shown in Table 3, which represent the simple statistics for cost function (CF) values, e.g. average, median, maximum values, standard deviations and minimum values representing the best individual solution for all 50 repeated runs of canonical DE and ChaosDE. The bold values within the all Tables 2 and 3 depict the best obtained results.

Furthermore an example of the step responses of the system with PID controllers designed by means of Chaos DE is depicted in Fig 6.

TABLE II. COMPARISONS OF RESULTS FOR OTHER HEURISTICS – 4th ORDER SYSTEM PID CONTROLLER DESIGN

Criterion	ZN Step Response	Canonical DE	Chaos DE	Chaos SOMA	PSO	Chaos PSO
IAE	34.9413	12.3262	12.3260	12.3305	12.3738	12.3479
ITAE	137.5650	15.1935	15.1919	15.3846	16.4079	15.5334
ISE	17.8426	6.40515	6.40515	6.41026	6.40538	6.40516
MSE	0.089213	0.032026	0.032026	0.032027	0.032030	0.032026

TABLE III. STATISTICAL RESULTS OF ALL 50 RUNS OF CHAOS DE AND CANONICAL DE -ITAE CRITERION

DE Version	Avg CF	Median CF	Max CF	Min CF	StdDev
Canonical DERand1Bin	15.2292	15.2171	15.3834	15.1935	0.0413201
Chaos DE with Dissipative Map	15.2251	15.2127	15.3212	15.1919	0.0337992

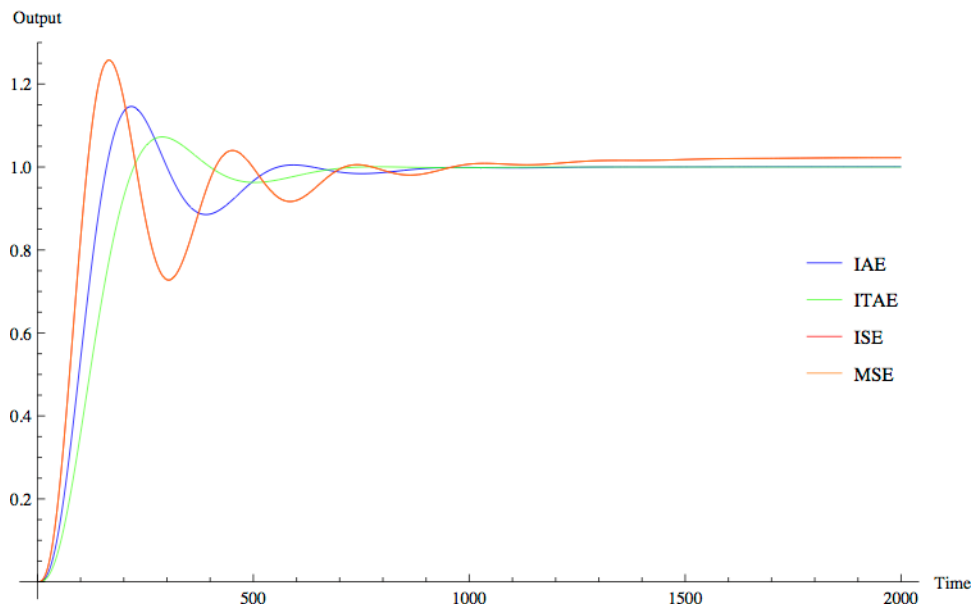


Fig. 6 Comparison of system responses – 4th order system - ITEA criterion

VIII. CONCLUSION

In this paper the chaotic dissipative standard map was presented and investigated over their capability of enhancing the performance of DE algorithm in the task of PID controller design.

From the comparisons, it follows that through the utilization of chaotic systems; the best overall results were obtained and entirely different statistical characteristics of CPRNGs-based

heuristic can be achieved. Thus the different influence to the system, which utilizes the selected CPRNG, can be chosen through the implementation of particular inner chaotic dynamics given by the particular chaotic system.

Promising results were presented, discussed and compared with other methods of PID controller design. More detail experiments are needed to prove or disprove these claims and explain the effect of the chaotic systems on the optimization and controller design.

REFERENCES

- [1] K. J. Åström. (2002). *Control System Design - Lecture Notes for ME 155A*. Available: <http://www.cds.caltech.edu/~murray/courses/cds101/fa02/caltech/astrom.html>
- [2] I. D. Landau and Z. Gianluca, *Digital Control Systems*: Springer London, 2006.
- [3] B. Nagaraj, S. Subha, and B. Rampriya, "Tuning Algorithms for PID Controller Using Soft Computing Techniques " *International Journal of Computer Science and Network Security*, vol. 8, pp. 278-281, 2008.
- [4] D. Davendra, I. Zelinka, and R. Senkerik, "Chaos driven evolutionary algorithms for the task of PID control," *Computers & Mathematics with Applications*, vol. 60, pp. 1088-1104, 2010.
- [5] J. Kennedy and R. Eberhart, "Particle swarm optimization," in *IEEE International Conference on Neural Networks*, 1995, pp. 1942-1948.
- [6] M. Dorigo and G. Di Caro, "Ant colony optimization: a new meta-heuristic," presented at the CEC 99. Proceedings of the 1999 Congress on Evolutionary Computation, 1999.
- [7] D. E. Goldberg, *Genetic Algorithms in Search, Optimization, and Machine Learning*: Addison-Wesley, 1989.
- [8] R. Storn and K. Price, "Differential Evolution – A Simple and Efficient Heuristic for global Optimization over Continuous Spaces," *Journal of Global Optimization*, vol. 11, pp. 341-359, 1997.
- [9] M. Pluhacek, R. Senkerik, D. Davendra, I. Zelinka, "Designing PID Controller For DC Motor System By Means Of Enhanced PSO Algorithm With Discrete Chaotic Lozi Map", in *Proc. 26th European Conference on Modelling and Simulation, ECMS 2012*, pp. 405 - 409, 2012, ISBN 978-0-9564944-4-3.
- [10] M. Pluhacek, R. Senkerik, D. Davendra, I. Zelinka, "PID Controller Design For 4th Order System By Means Of Enhanced PSO algorithm With Lozi Chaotic Map", in *Proc. 18th International Conference on Soft Computing, MENDEL 2012*, pp. 35 - 39, 2012, ISBN 978-80-214-4540-6.
- [11] M. Pluhacek, R. Senkerik, D. Davendra, I. Zelinka, "Designing PID controller for DC motor by means of enhanced PSO algorithm with dissipative chaotic map". In: Snasel, V., Abraham, A., Corchado, E.S. (eds.) *SOCO Models in Industrial & Environmental Appl. AISC*, vol. 188, pp. 475-483. Springer, Heidelberg (2013)
- [12] M. Pluhacek, R. Senkerik, D. Davendra, I. Zelinka: "Designing PID Controller for 4th Order System By Means of Enhanced PSO Algorithm with Discrete Chaotic Dissipative Standard Map". in *Proc. 24th European Modeling & Simulation Symposium, EMSS 2012*, pp. 396-401 (2012) ISBN 978-88-97999-09-6
- [13] R. Caponetto, L. Fortuna, S. Fazzino, and M. G. Xibilia, "Chaotic sequences to improve the performance of evolutionary algorithms," *IEEE Transactions on Evolutionary Computation*, vol. 7, pp. 289-304, 2003.
- [14] K. Price, "An Introduction to Differential Evolution", In: *New Ideas in Optimization*, (D. Corne, M. Dorigo and F. Glover, Eds.), pp. 79-108, McGraw-Hill, London, UK, ISBN 007-709506-5, 1999.
- [15] K. Price and R. Storn, "Differential evolution homepage" (2001) [Online]. Available: <http://www.icsi.berkeley.edu/~storn/code.html>.
- [16] K. Price, R. Storn and J. Lampinen, "Differential Evolution - A Practical Approach to Global Optimization", 2005, Springer, ISBN: 3-540-20950-6.
- [17] J. C. Sprott, *Chaos and Time-Series Analysis*: Oxford University Press, 2003.

A VSC approach for Wave Energy Converters

Aitor J. Garrido, Izaskun Garrido, Mikel Alberdi, Modesto Amundarain and Edorta Carrascal

Abstract—In this paper it is presented a Variable Structure Controller (VSC) applied to the Rotor Side Converter (RSC) of a typical Doubly Fed Induction Generator (DFIG) mounted on on-shore Wave Energy Converters. Within the different types of on-shore wave devices, OWC converters are one of the most widely used ones. This is the case of Mutriku Breakwater Wave Plant located in the Basque Country, which incorporates 16 turbo-generator modules. This work proposes a VS control scheme that improves the energy extraction in presence of disturbances and system uncertainties. The validity of this approach has been proven both via simulation and experimentally, showing an increment of the power generated by traditional controllers.

Keywords—Ocean Energy, WECs, Power system control, Variable structure control.

I. INTRODUCTION: OWC PLANT DESCRIPTION

The aim of the NEREIDA MOWC project, promoted by the Basque Energy Board (EVE), is to demonstrate the feasibility of the OWC technology with Wells turbine power take-off into a newly constructed breakwater in Mutriku, in the north coast of Spain. It consist of of 16 18.5kW turbines that provide a total power of 296kW [1,2]. See Fig 1. It was inaugurated in July 2011 and produced 200.000kWh during the first year while it was estimated a 600.000kWh production per year. Although the difference if mainly due to a storm that damaged the control room and kept the facility closed during the best wave months, an improvement in the power generation could highly benefit the system.

II. VS APPROACH

As it has been indicated, the turbo-generator modules use Wells turbines, which provides unidirectional rotation despite of the air flow direction [3], combined with DFIGs. This kind of AC drives is usually controlled using a vector control

This work was supported in part by the University of the Basque Country (UPV/EHU) through Research Project GIU11/02 and the Research and Training Unit UF111/07, by the Ministry of Science and Innovation (MICINN) with Research Project ENE2010-18345, by the Basque Government through S-PEI3UN042 and by the Euregion Aquitaine-Euskadi through Project 2013/GR1/11.

Aitor J. Garrido, Izaskun Garrido, Mikel Alberdi and Modesto Amundarain are with the Automatic Control Group, Department of Automatic Control and Systems Engineering, EUITI de Bilbao, University of the Basque Country (UPV/EHU), Paseo Rafael Moreno 3, 48013 Bilbao, Spain (corresponding author: aitor.garrido@ehu.es).

Edorta Carrascal is with Advanced Control Group, Department of Thermal Engineering, ETSI de Bilbao, University of the Basque Country (UPV/EHU), Alameda Urquijo S/N, 48013 Bilbao, Spain.



Fig. 1. Turbines in Mutriku MOWC breakwater

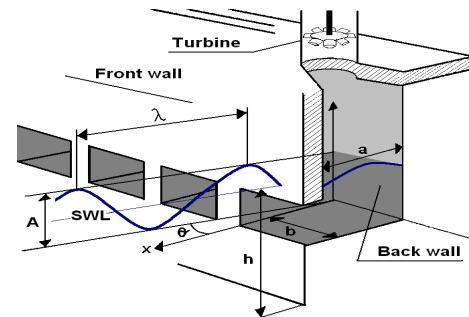


Fig. 2. Wave and OWC capture chamber parameters

scheme and cascaded PI-current and power loops [4]. Nevertheless, since the actual system parameters always differ from those from the data sheet used for PI tuning, a fine tuning over the real equipment is generally required to achieve an adequate performance [5]. Besides, some tuning methods require a detailed modelling of the system, and it is well known that, depending on the tuning method used, PI controllers may present a considerable lack of robustness [6]. To avoid these drawbacks, a suitable option is to consider some kind of robust control scheme as it is the case of the Sliding Mode Control (SMC) initially developed by Utkin [7] and successfully applied to diverse types of induction machine drives [8].

Taking into account the wave and the OWC chamber parameters, it is possible to obtain the power available from the airflow in the OWC chamber as (see [9] and Fig. 2):

$$P_m = (dp + \rho v_x^2 / 2) v_x a .$$

On the other hand the equations used for the modelling of the turbine are given by (see [10]):

$$\begin{aligned} dp &= C_a K (1/a) [v_x^2 + (r\omega_r)^2]; \quad T_t = C_t K r [v_x^2 + (r\omega_r)^2] \\ T_t &= dp C_t r a / C_a; \quad \phi = v_x / r\omega_r; \quad K = \rho b n l / 2 \\ q &= v_x a; \quad \eta_t = T_t \omega_r / dp q . \end{aligned} \quad (1)$$

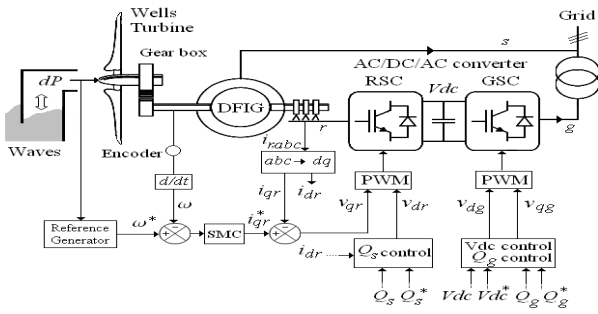


Fig. 3. Control design

The proposed SMC scheme is used within the rotational speed controller to regulate the slip of the generator, while maintaining the traditional air valve controller, as it is shown in Fig. 3 (see [4]).

It is known that the dynamic equation of the IM drive system may be expressed as: $\dot{\omega}_r = 1/H(T_t - K_T i_{qr} - F\omega_r)$, where K_T is the torque factor and H and F the inertia and the friction factor the system respectively, so that the generator slip can be controlled by regulating the q-axis rotor current i_{qr} .

Now, adequately managing this expression, it is possible to obtain the speed tracking error $e(t)$, that in turn allows to define a sliding variable:

$$S(t) = e(t) + \int_0^t (k + a)e(\tau) d\tau \quad (2)$$

and the SMC law as:

$$u(t) = -k e(t) - \beta \text{sgn}(S), \quad (3)$$

Where, $a = F/H$, k is a constant gain, β represents the switching variable and $\text{sgn}(\cdot)$ is the signum function (see [10]).

Then, it is demonstrated using the Lyapunov stability theory that tracking error converges to zero exponentially as time tends to infinite, so that the desired current command i_{qr}^* can be expressed as (see [11]):

$$i_{qr}^* = 1/b \left(k e + \beta \text{sgn}(S) + f - a \omega^* - \dot{\omega}^* \right). \quad (4)$$

Therefore, the VS controller designed solves the power tracking problem for DFIG-based OWC power plants in the presence of uncertainties.

III. RESULTS

In order to prove the proposed control scheme, it has been compared with the traditionally used PI-based vector control for the same pressure drop input, including a 30% of uncertainties. As it may be observed in Fig. 4, the result of the PI-based control presents a considerable steady state error due to the deviation of the actual machine parameters. In contrast, the SMC is able to assume these uncertainties providing a higher power generation, as it may be seen in Fig. 5.

IV. CONCLUSION

A robust SM control for OWC devices has been presented. The stability of the proposed controller has been proven using the Lyapunov theory. It may be demonstrated that the control scheme allows overcoming parameter uncertainties and system disturbances, providing a higher power production than the traditional PI-based vector control.

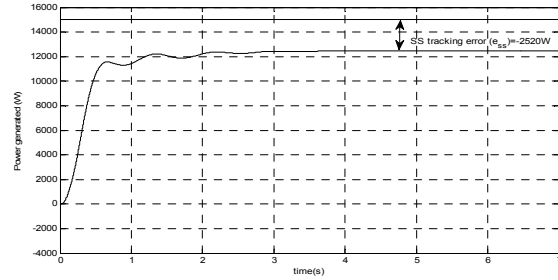


Fig. 4. PI generated power (|6500|Pa dP input, 30% uncert.)

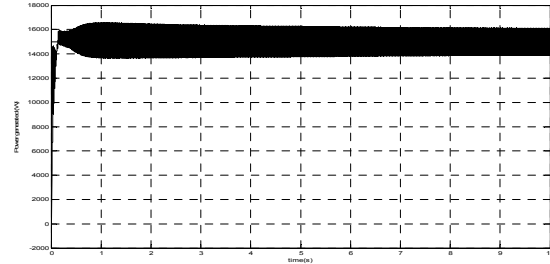


Fig. 5. SMC generated power (|6500|Pa dP input, 30% uncert.)

ACKNOWLEDGMENT

The authors would like to thank the collaboration of the Basque Energy Board (EVE) through Agreement UPV/EHUEVE23/6/2011 and the Spanish National Fusion Laboratory (CIEMAT) UPV/EHUCIEMAT08/190.

REFERENCES

- [1] Basque Energy Board (EVE): <http://www2.eve.es/web/Energias-Renovables/Energia-marina.aspx>
- [2] Y. Torre-Enciso "Mutriku Wave Power Plant: From Conception to Reality", European Federation of Regional Energy and Environment Agencies (FEDARENE) [Online]. Dec. 2009. Available: http://www.fedarene.org/documents/projects/Nereida/Document/01_Mutriku-OWC_plant.pdf
- [3] Thakker and R. Abdulhadi, "Effect of blade profile on the performance of Wells turbine under unidirectional sinusoidal and real sea flow conditions," *Int. J. Rotating Machinery*, vol. 2007, pp. 1–8, Jan. 2007.
- [4] M. Amundarain, M. Alberdi, A. J. Garrido, and I. Garrido, "Modeling and simulation of wave energy generation plants: Output power control," *IEEE Trans. Ind. Electron.*, vol. 58, no. 1, pp. 105–117, Jan. 2011.
- [5] K. J. Astrom and T. Hagglund, *Advanced PID Control*, ISA-The Instrumentation, Systems, and Automation Society, 2009.
- [6] R. Vilanova, V. M. Alfaro, O. Arrieta, C. Pedret, "Analysis of the claimed robustness for PI/PID robust tuning rules," in *Proc. 2010 IEEE Mediterranean Conference on Control & Automation (MED)*, pp.658-662.
- [7] V. I. Utkin, "Sliding mode control design principles and applications to electric drives," *IEEE Trans. Ind. Electron.*, vol. 40, no. 1, pp. 23–36, Feb. 1993
- [8] Barambones, O.; Alkorta, P.; De La Sen, M., "Wind turbine output power maximization based on sliding mode control strategy," *Industrial Electronics (ISIE), 2010 IEEE International Symposium on*, vol., no., pp.364,369, 4-7 July 2010
- [9] A. El Marjani, F. Castro Ruiz, M. A. Rodriguez, and M. T. Parra Santos, "Numerical modelling in wave energy conversion systems," *Energy*, vol. 33, no. 8, pp. 1246–1253, Aug. 2008.
- [10] S. Muthukumar, "Design of a stand alone wave energy plant," in *Proc. 15th Int. Offshore Polar Eng. Conf.*, 2005.
- [11] O. Barambones and A. J. Garrido, "An adaptive variable structure control law for sensorless induction motors", *European J. of Control*, vol. 13, no. 4, pp. 282–392, Jul./Aug. 2007.

Control system for chemical thermal processes

Petr Chalupa, Martin Beneš, Jakub Novák, and Michaela Bařinová

Abstract—This paper describes a hardware controller designed for a real-time control of laboratory thermal processes. Both hardware and software is presented in the paper. The controller can be applied to temperature control of various chemical and technological processes. The controller contains a temperature sensor and a pulse width modulation actuator for the AC power supply of a thermal process. Several control strategies are available for the temperature control including adaptive control. Control of heating mantle is presented as an example of a real-time application of the controller. Temperature control as a main part of measurement of shrinkage of collagen materials is also presented.

Keywords—temperature control, thermal process, adaptive control.

I. INTRODUCTION

TEMPERATURE control is a common task in many technological processes. Almost all chemical processes are temperature dependent and temperature control is required to obtain precise results. One of the simplest pieces of temperature control equipment consists of an electric heater and a temperature sensor used as a feedback. Such instruments are very common in chemical laboratories: a hot plate, an immersion heater, heating mantle.

Common drawbacks of most of available laboratory heaters, especially the low-cost ones, can be seen in the following areas:

- There is no temperature sensor providing a feedback.
- The temperature sensor measures temperature of the heating element itself, not the part that actually is to be heated (usually some liquid).
- Only a control with constant reference signal is provided. The required temperature level can be set manually.

This work was supported by the European Regional Development Fund under the project CEBIA-Tech No. CZ.1.05/2.1.00/03.0089. This support is greatly acknowledged.

Petr Chalupa is with the Tomas Bata University in Zlin, Faculty of Applied Informatics, Regional Research Centre CEBIA-Tech, nam. T. G. Masaryka 5555, 760 01 Zlin, Czech Republic (phone: +420 57603 5204, e-mail: chalupa@fai.utb.cz).

Martin Beneš is with the Tomas Bata University in Zlin, Faculty of Applied Informatics, Department of Automation and Control Technologies.

Jakub Novák is with the Tomas Bata University in Zlin, Faculty of Applied Informatics, Regional Research Centre CEBIA-Tech (email: jnovak@fai.utb.cz).

Michaela Bařinová is with the Tomas Bata University in Zlin, Faculty of Applied Informatics, Regional Research Centre CEBIA-Tech (email: barinova@fai.utb.cz).

- Controller behavior cannot be changed. The controller is hard-wired and it is not possible to define transient response of the system in terms of e.g. defensive, slow and smooth control vs. aggressive fast control with overshoots.
- The course of the reference signal (required temperature), controlled signal (actual temperature) and control signal (power of the heater) is not recorded for further evaluation.

To cope with these drawbacks a universal controller was designed and manufactured. This controller and is presented in the paper. The paper is organized as follows. Section II describes the controller from the hardware point of view; section III shortly presents controller's software. A heating mantle as an example of a controlled system is presented in section IV. The temperature control of the heating mantle and a measurement of shrinkage of collagen materials are presented in sections V and VI respectively. A short conclusion is provided in section VII.

II. HARDWARE OF THE CONTROLLER

A. Controller overview

The controller is intended for usage with simple heating elements that can be controlled by switching their power supply on and off. Advanced heating systems equipped with microcontrollers are not, in general, suitable for usage with the proposed controller.

A simple scheme of the controller is presented in Fig. 1.

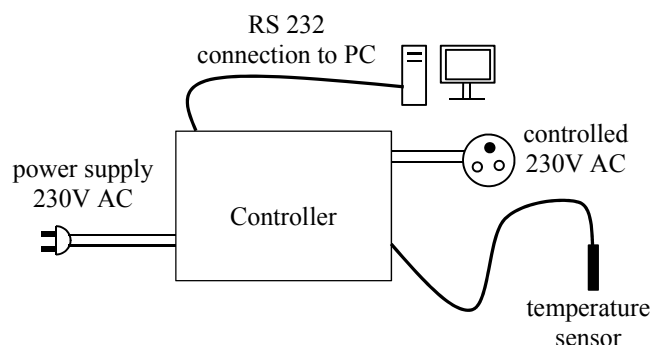


Fig. 1 Scheme of the controller

The controller is supplied by 230V AC and controls 230V AC socket which is used to plug-in the heating equipment. A pulse width modulation (PWM) is applied to this socket to control the output power of the heater. A temperature sensor

Pt1000 is connected to the controller to provide feedback for the control system. A personal computer (PC) or a laptop can be connected to the controller to achieve the ability of on-line recording of controller input, output, states and time. The controller itself contains very simple user interface as can be seen from the photograph of the controller which is presented in Fig. 2.



Fig. 2 Photo of the controller

B. Hardware elements

The following main components were used to manufacture the controller.

- **Power supply.** A transformer was used to obtain 9V DC to supply for CPU and other electronic parts.
- **CPU.** A Freescale MC9S08AC128 microcontroller was used as heart of the controller. It operates at 40 MHz and contains 128 kB of FLASH memory and 8kB of RAM memory. Peripheral devices can be connected via SPI or SCI serial interfaces. This CPU is equipped with 16-channel AD converter with 10 bit resolution. Moreover it contains one dual-channel and two 16-channel timers which can be used for PWM. More detail can be found in [1].
- **External AD convertor.** The controller is equipped with MCP3551 AD converter produced by Microchip Technology. It communicates with CPU using SPI interface. The resolution of the converter is 22 bits which ensures sufficient preciseness of temperature control even for wide range of operating points [5]. Detail concerning connection of the AD converter can be found in [2]
- **EEPROM.** A 32kB EEPROM memory by ATMEL is

used to store controller parameters and other user settings. It is connected to SPI. Details are available in [3].

- **RS232 convertor.** A MAXIM RS232 converter is used for interface of the controller and a PC.
- **SSR.** A solid state relay (SSR) by Carlo Gavazzi company is used as an actuator for the 230V AC output of the controller [4]. The maximal switched current of the relay is 25A which is enough for a laboratory deployment of the controller. The changing of state of SSR (switching on or off) is performed in synchronous way: the switching is delayed until the power-line voltage is passing through zero.

The controller contains several printed circuit boards (PCB). All of them were designed using CadSoft EAGLE PCB Design Software.

III. SOFTWARE OF THE CONTROLLER

This section briefly describes software equipment of the controller. The first subchapter is focused on user interface, remaining two subchapters cope with controller algorithms and on-line identification.

A. User Interface

The user interface of the controller consists of the following items as depicted in Fig. 2:

- display
- three LEDs (power on indicator, output indicator, malfunction)
- on/off switch
- master stop button
- Esc and OK buttons
- arrow buttons

The arrow buttons together with Esc and OK buttons are used to browse the menu and to change settings.

The setting sections serves for defining various parameters of the controller. The sample time is used in measurement and RS232 communication; each controller has its own sample time. It is possible to define up to 10 reference signal courses. Each reference signal is piecewise linear consisting of up to 15 sections. It is also possible to define up to 10 settings for each of the three types of the controller. Controller types are discussed in the next subsection. The thermometer calibration can be used to precisely define relation between resistance of the Pt1000 sensor and the temperature in °C.

The controller submenu is used to select appropriate reference signal, controller and to start the control process.

The measurement menu is used to measure the temperature only. This function can be used for example for step response measurement.

The menu structure is presented in Fig. 3.

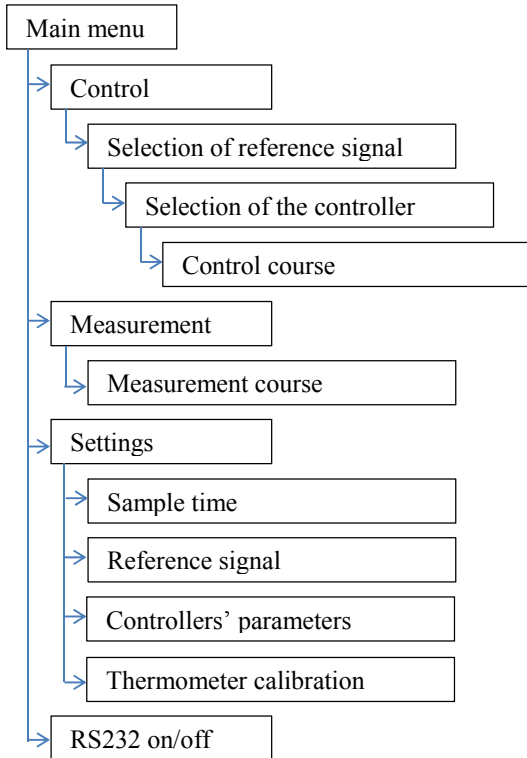


Fig. 3 Menu structure

B. Control Algorithms

The controller contains the following three different control algorithms:

- adaptive dead-beat controller
- adaptive pole-placement controller
- discrete PID controller

The first two controllers belong to a self-tuning controllers group [7], [8]. An on-line identification is used to obtain ARX model of the controlled system. The structure of the control loop is depicted in Fig. 4.

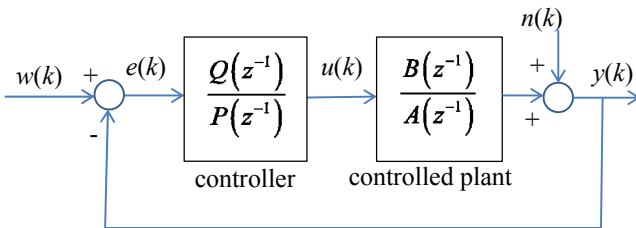


Fig. 4 Control loop

The reference signal is represented by $w(k)$; symbols $e(k)$, $u(k)$, $y(k)$ and $n(k)$ represent control error, control signal, output signal and disturbance respectively. $Q(z^{-1})$ and $P(z^{-1})$ are polynomials of the controller and $B(z^{-1})$ and $A(z^{-1})$ are polynomials of the model of the controlled system. The coefficients of controller polynomials are computed in each sample step when adaptive controllers are used. The discrete PID controller uses constant coefficients. The transfer function

of both adaptive controllers is as follows:

$$G_r(z^{-1}) = \frac{Q(z^{-1})}{P(z^{-1})} = \frac{q_0 + q_1 z^{-1} + q_2 z^{-2}}{(1 - z^{-1})(p_0 + p_1 z^{-1})} \quad (1)$$

The following transfer function describes discrete PID controller:

$$G_r(z^{-1}) = \frac{Q(z^{-1})}{P(z^{-1})} = \frac{q_0 + q_1 z^{-1} + q_2 z^{-2}}{1 - z^{-1}} \quad (2)$$

C. On-line Identification

Parameters of adaptive controllers are computed on basis of the ARX model of the controlled system. These adaptive controllers are based on the self-tuning approach where on-line identification is used to obtain ARX model [6]. The ARX model is described by equation (3)

$$y(k) = \phi^T(k)\theta(k) + e_s(k) \quad (3)$$

where $\phi^T(k)$ is the data vector and $\theta(k)$ is the vector of model parameters

Parameter estimates are updated in each step:

$$\hat{\theta}(k) = \hat{\theta}(k-1) + \frac{C(k-1)\phi(k)}{1 + \xi(k)} \hat{e}(k) \quad (4)$$

where

$$\xi(k) = \phi^T(k)C(k-1)\phi(k) \quad (5)$$

and $\hat{e}(k)$ is prediction error

$$\hat{e}(k) = y(k) - \hat{y}(k) \quad (6)$$

Covariance matrix is updated in each step:

$$C(k) = C(k-1) - \frac{C(k-1)\phi^T(k)\phi(k)C(k-1)}{1 + \xi(k)} \quad (7)$$

This basic form of on-line least squares method can be further enhanced by exponential or adaptive forgetting [9] to obtain more precise model of the current behavior of the system. These modifications are useful especially in case of nonlinear or time-varying controlled system.

IV. HEATING MANTLE

A. Description of the Heating Mantle

The heating mantle is one of the often used pieces of equipment in chemical laboratories. It consists of spherical heating element connected to electric power supply, a case and optionally a temperature sensor with hysteresis which is used to switch the power supply on or off. Such a heating mantle can be used in connection with the proposed controller.

There are also more sophisticated heating mantles in the market which are controlled by microcontrollers but there are not suitable for the proposed controller.

A scheme of heating mantle is depicted in Fig. 5.

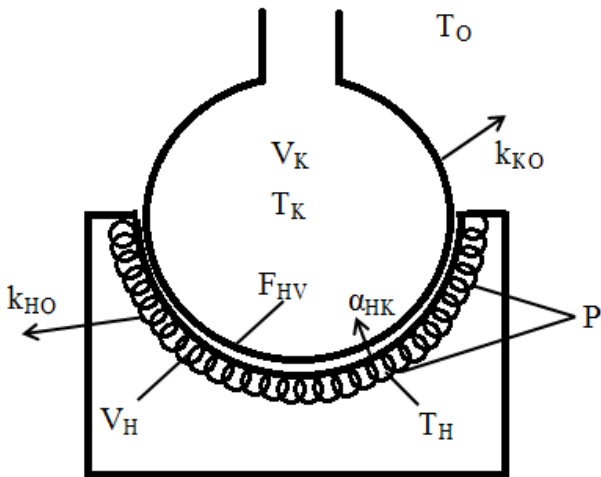


Fig. 5 Heating mantle scheme

The following parameters of the mantle are presented in the Fig. 5:

- T_O – ambient temperature [K]
- T_H – temperature of heating element of the mantle [K]
- T_K – temperature of the liquid [K]
- V_H – volume of the heating element [m³]
- V_K – volume of the liquid [m³]
- P – electric power of the mantle [W]
- F_{HK} – area of the bulb which is in contact with the mantle [m²]
- k_{HO} – constant representing heat transfer from the mantle to its environs. It contains transfer from the heating element to the inner space of the mantle, accumulation of the heat inside the mantle as well as transfer from the heat case to its environs. [W·K⁻¹]
- k_{KO} – constant representing heat transfer from the liquid to the environs. It is dependent on the level of the liquid. [W·K⁻¹]
- α_{HK} – constant representing heat transfer from the heat element to the liquid. Heat capacity of the bulb is neglected which is valid in case if water level is not bellow the mantle margin [W·m⁻²·K⁻¹]

The first principle model of the mantle contains also some other parameters:

- ρ_H – density of the heating element [kg·m⁻³]
- ρ_K – density of the liquid [kg·m⁻³]
- c_{pH} – specific heat capacity of the heating element [J·kg⁻¹·K⁻¹]
- c_{pK} – specific heat capacity of the liquid [J·kg⁻¹·K⁻¹]
- m_H – weight of the heating element [kg]
- m_K – weight of the liquid [kg]

Typical laboratory heating mantle is depicted in photograph in Fig. 6.



Fig. 6 Heating mantle

B. Mathematical model of the heating mantle

The first principle model [10] of the heating mantle is based on heat transfer balances. The heat balance of the mantle:

$$\left\{ \begin{array}{l} \text{Heat from the} \\ \text{heating element} \end{array} \right\} = \left\{ \begin{array}{l} \text{Heat transferred} \\ \text{to the liquid} \end{array} \right\} + \left\{ \begin{array}{l} \text{Heat transferred} \\ \text{to environs} \end{array} \right\} + \left\{ \begin{array}{l} \text{Heat accumulated in} \\ \text{the heating element} \end{array} \right\}$$

$$P = F_{HK} \cdot \alpha_{HK} \cdot (T_H - T_K) + k_{HO} \cdot (T_H - T_O) + V_H \cdot \rho_H \cdot c_{pH} \cdot \frac{dT_H}{dt} \quad (8)$$

Heat balance of the bulb is described by the following equation:

$$\left\{ \begin{array}{l} \text{Heat transferred} \\ \text{from the mantle} \end{array} \right\} = \left\{ \begin{array}{l} \text{Heat transferred} \\ \text{to environs} \end{array} \right\} + \left\{ \begin{array}{l} \text{Heat accumulated} \\ \text{in the liquid} \end{array} \right\}$$

$$F_{HK} \cdot \alpha_{HK} \cdot (T_H - T_K) = k_{KO} \cdot (T_K - T_O) + V_K \cdot \rho_K \cdot c_{pK} \cdot \frac{dT_K}{dt} \quad (9)$$

This simplified model can be used to create dynamic linearized model of the system, which can serve as a fundament for the control design. It is obvious that the linearized model should be of the second order because the first principle model has two states.

The real system contains several nonlinearities and is time dependent contrary to simplified first principle model.

V. CONTROL OF HEATING MANTLE

The controller was verified using several heating mantles and various liquids were heated. An example of temperature control of propylene glycol in a 480W heating mantle is presented in Fig. 7. A pole placement adaptive controller was used in this case.

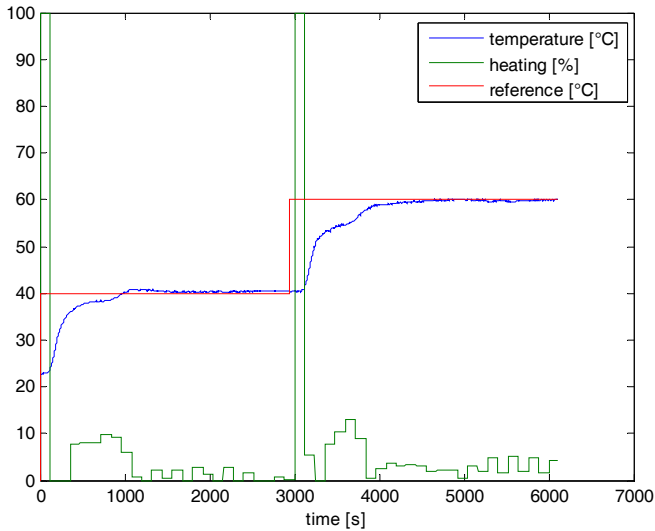


Fig. 7 Pole placement control of 1000ml of propylene glycol (480W mantle)

Heating of water in the same mantle is presented in Fig.8. In this case a discrete PID control algorithm was selected.

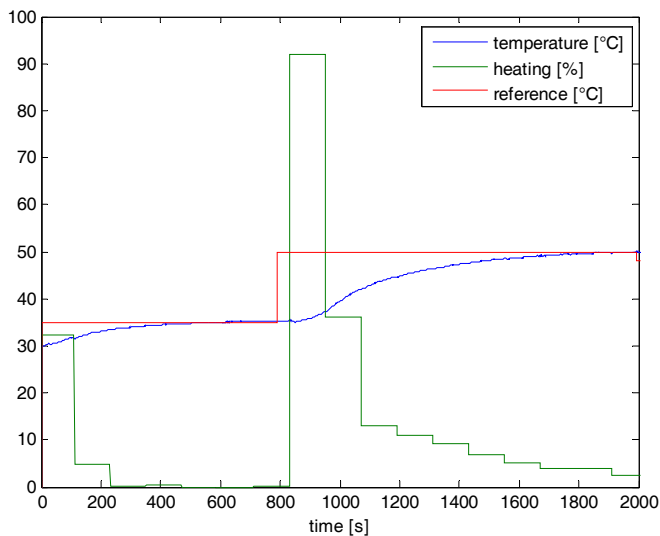


Fig. 8 Discrete PID control of 1500ml of water (480W mantle)

It can be observed, that in both cases the control algorithms coped with the task well.

VI. SHRINKAGE OF COLLAGEN MATERIALS

The controller was also used for control of water temperature in task of measurement of shrinkage of collagen materials. This task has been studied by many scientists and remains interesting till today [11], [12], [13].

The laboratory control setup photograph is presented in Fig. 9.



Fig. 9 Setup for measurement of shrinkage of collagen materials

The water was heated by electric plate. The plate power supply was connected to the output of the controller. The water inside the beaker was mixed to obtain approximately the same temperature inside its whole volume. Temperature was measured by Pt1000 sensor connected to the controller and the accuracy of the temperature reference tracking was verified by classical laboratory thermometer.

In this case, the temperature should rise slowly to be able to observe the shrinkage. An increase of temperature by 2°C/min was requested and a discrete PID controller was used to cope with this task. The controller was tuned using nonlinear optimization method to incorporate saturation to the control design. A control course is presented in Fig. 10.

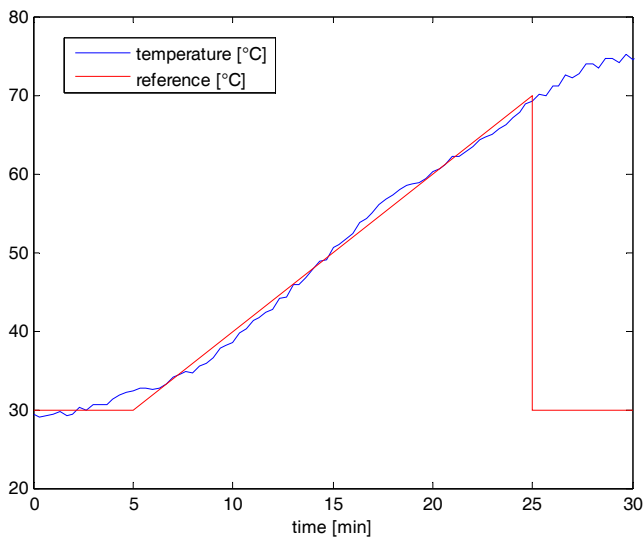


Fig. 10 Temperature control – shrinkage of collagen materials

The reference was set to 30°C in the last part of its course (after 25 min). This represents the end of experiment as the shrinkage was always observed before. The temperature of the water cannot follow this reference because no cooling was applied. Moreover, reference tracking is not important in this part as the experiment has already ended.

VII. CONCLUSION

A controller for laboratory thermal processes was presented in this paper. Both hardware and software of the controller were described. Real time experiments of control of heating mantle and control of water temperature as a part on measurement of shrinkage of collagen material were presented. Real-time experiments proved applicability of the controller in chemical laboratory.

REFERENCES

- [1] Freescale Semiconductor. *MC9S08AC128 Series Reference Manual Rev. 3*. [Online]. Available: http://cache.freescale.com/files/microcontrollers/doc/ref_manual/MC9S08AC128RM.pdf
- [2] Microchip. *Precision RTD Instrumentation for Temperature Sensing* [online]. Available: <http://ww1.microchip.com/downloads/en/AppNotes/01154a.pdf>
- [3] Atmel. *SPI Serial EEPROMs AT25128A_256A* [online]. Available: <http://www.gme.cz/dokumentace/414/414-057/dsh.414-057.1.pdf>
- [4] Carlo Gavazzi. *Solid State Relays Industrial* [online]. Available: <http://www.gme.cz/dokumentace/635/635-241/dsh.635-241.1.pdf>
- [5] Microchip. *MCP3550/1/3: Low-Power, Single-Channel 22-Bit Delta-Sigma ADCs* [online]. Available: <http://ww1.microchip.com/downloads/en/DeviceDoc/21950e.pdf>
- [6] L. Ljung, *System identification: theory for the user*. Upper Saddle River, NJ : Prentice Hall PTR, 1999.
- [7] V. Bobál, J. Böhm, J. Fessl, and J. Macháček, *Digital Self-tuning Controllers: Algorithms, Implementation and Applications*. Springer - Verlag London Ltd., 2005.
- [8] K. J. Åström and B. Wittenmark, *Adaptive Control*. Addison Wesley, 1989.
- [9] R. Kulhavý, "Restricted exponential forgetting in real time identification," *Automatica*, vol. 23, pp. 586-600, 1987.
- [10] D. M. Himmelblau and J. B. Riggs, *Basic principles and calculations in chemical engineering*. Upper Saddle River, N.J. : Prentice Hall, 2004.

- [11] F.G. Lennox, "Shrinkage of collagen", *Biochimica et Biophysica Acta*, vol. 3, pp. 170-187, 1949.
- [12] J.M. Ruijgrok, J.R. de Wijn, and M.E. Boon, "Glutaraldehyde crosslinking of collagen: Effects of time, temperature, concentration and presoaking as measured by shrinkage temperature" *Clinical Materials*, vol. 17, pp. 23-27, 1994.
- [13] P. K. Beredjiklian and M. Rivlin, "Electrothermal Collagen Shrinkage" *The Journal of Hand Surgery*, 37, pp. 2165-2167, 2012.

Galvanically isolated interface for an oscilloscope

Martin Pospisilik, Petr Neumann, Roman Honig, and Peter Scheibenreiter

Abstract— The paper describes an approach to design and construction of a galvanically isolated interface for an oscilloscope. The device has been drawn in two samples showing how helpful the galvanic isolation of the oscilloscope can be at certain service operations. The monitored signals are transferred by means of a capacitive coupling through an isolation barrier inside a custom integrated circuit, described hereby as well.

Keywords—Differential Measurement, Oscilloscope, Isolating Amplifier, Galvanic Isolation

I. INTRODUCTION

MOST oscilloscopes use single ended input [2] the negative pole of which is usually grounded to a common ground. This construction allows the operator to measure only those waveforms that are referenced to the ground. If there is a need for differential measurements, two inputs must be involved and the oscilloscope must be switched into a differential measurement mode. Although this practice is satisfactory in most cases, it brings several disadvantages as enlisted below:

- Measurement of one waveform employs two oscilloscope's channels,
- Errors in measurement are cumulated from both channels,
- Common mode rejection ratio is considerably low, especially when the differential voltage is quite low compared to the potential of the measurement points relative to the ground.

As it turned out during service measurements, the differential input is often needed. Therefore the authors decided to construct the proper interface that is described

This work was supported in part by the European Regional Development Fund under the project CEBIA-Tech No. CZ.1.05/2.1.00/03.0089, and by OPVK project CZ.1.07/2.3.00/30.0035.

Martin Pospisilik is with Tomas Bata University in Zlin, Faculty of Applied Informatics, Nad Stranemi 4511, 760 05 Zlin, Czech Republic. He is now at the department of Computer and Communication Systems (e-mail: pospisilik@fai.utb.cz)

Tomas Dulik is with Tomas Bata University in Zlin, Faculty of Applied Informatics, Nad Stranemi 4511, 760 05, Zlin, Czech Republic. He is now a researcher at the Department of Informatics and Artificial Intelligence (e-mail: dulik@fai.utb.cz)

Roman Honig is with AM Test, Uherske Hradiste, Czech Republic. He is a senior specialist on measurement technology services.

Peter Scheibenreiter is with BEV – Federal Office of Metrology and Surveying, laboratory of Electrical Quantities, Vienna, Austria.

within the framework of this paper.

II. REQUIREMENTS AND PREREQUISITIES

The initial requirements were as follows:

- Two different channels for voltage and current measurements,
- Possibility of the zero level correction,
- Measured voltage range ± 20 V,
- Measured current range ± 1 A,
- Isolation strength between input and output at least 1.5 kV,
- Frequency range DC to 30 kHz.

On the basis of the above mentioned requirements it was decided to apply the isolation amplifier ISO124 [3] and to equip it with additional output low pass filter. The construction of the differential inputs and the output low pass filters is based on JFET operating amplifiers TL081 [4].

A. Isolating amplifier ISO 124

The ISO124 is a precision isolation amplifier incorporating a duty cycle modulation-demodulation technique. The signal is transmitted digitally across a 2pF differential capacitive barrier. With digital modulation the barrier characteristics do not affect signal integrity, resulting in excellent reliability and good high frequency transient immunity across the barrier. Both barrier capacitors are imbedded in the plastic body of the package. No external components are required for operation. The key specifications are 0.010 % max nonlinearity, 50 kHz signal bandwidth, and 200 $\mu\text{V}/^\circ\text{C}$ V_{OS} drift. A power supply can lie in the range of ± 4.5 V to ± 18 V [3].

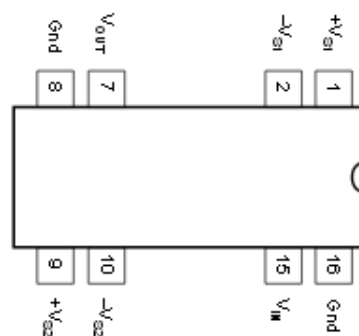


Fig. 1 DIP package connection diagram of ISO124 (top view) [3]

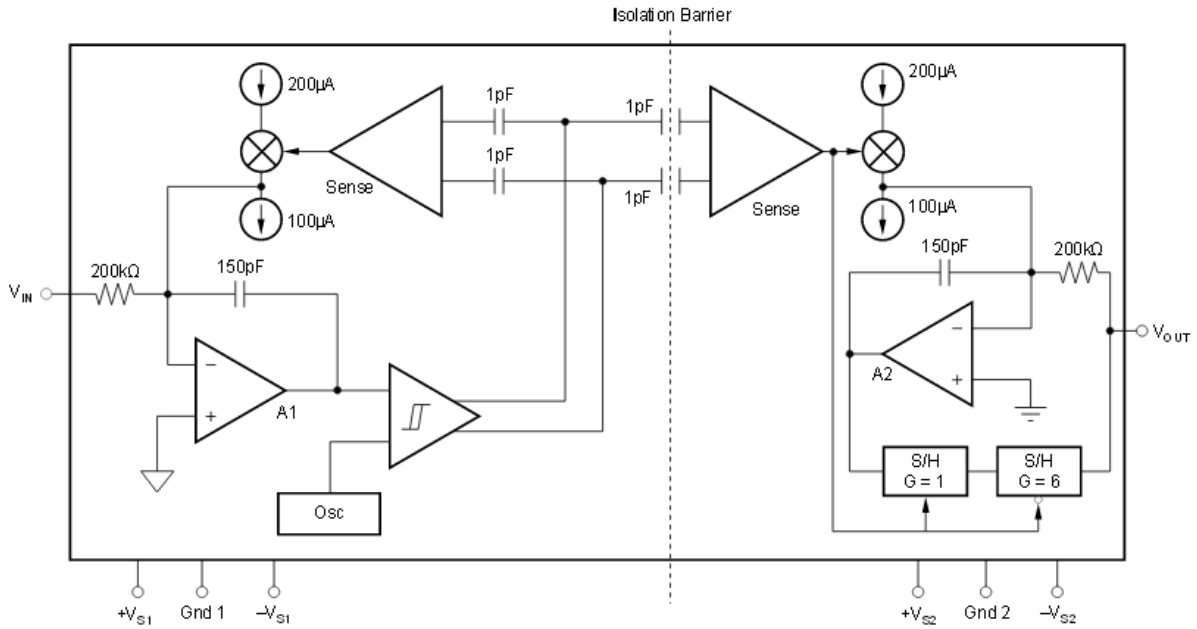


Fig. 2 Block diagram of internal circuits in ISO124 [3]

The package of the device is adjusted to allow achieving the continuous isolation voltage of 1,500 V_{RMS} . Therefore the amplifier is encapsulated in 16-pin plastic DIP or 28-lead plastic SOIC package. The connection of pins is described in Fig. 1.

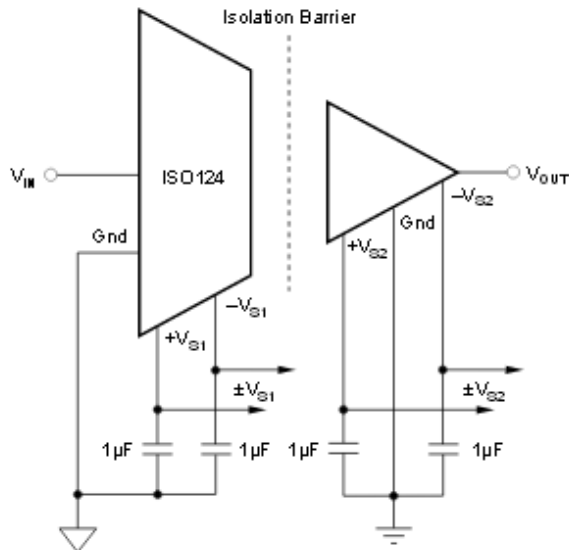


Fig. 3 Basic signal and power connections of ISO124 [3]

In Fig. 2 the block diagram of internal circuits in ISO124 can be found. The input amplifier A1 integrates the difference between the input current and the switched $\pm 100 \mu A$ current source. The internal oscillator forces the current source to switch at the frequency of 500 kHz. The complete block at the front-end of the isolation barrier creates a modulator that produces triangular wave at the frequency forced by the

internal oscillator and the duty cycle proportional to the voltage at the input pin V_{IN} . At the back-end of the isolation barrier there is a sense amplifier that detects the signal transitions across the barrier and drives a switched current source into the integrator A2. The output stage balances the duty-cycle modulated current against the feedback current through the 200 kΩ feedback resistor, resulting in an average value at the V_{OUT} pin. [3]. As a result of the operation, 20mV ripple at the frequency of 500 kHz is present at the output of the circuit. This can be removed by additional low pass filter. The basic signal and power connections of the amplifier are depicted in Fig. 3.

In figures 4 to 7 the typical performance of the amplifier according to its datasheet [3] is depicted.

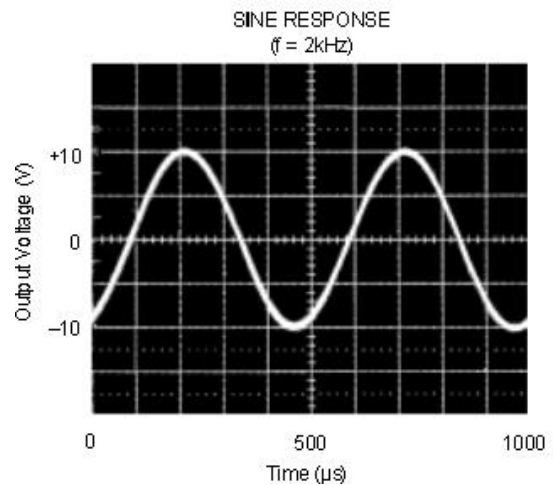


Fig. 4 Sine response of ISO124 on the signal with $f = 2 \text{ kHz}$ and $V_{PP} = 20 \text{ V}$ [3]

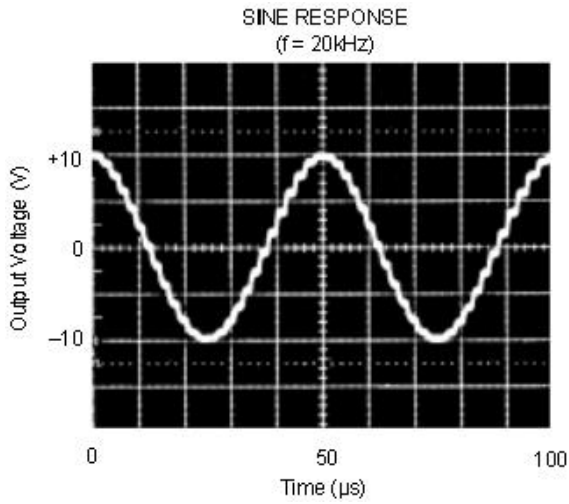


Fig. 5 Sine response of ISO124 on the signal with $f = 20 \text{ kHz}$ and $V_{PP} = 20 \text{ V}$ [3]. The effect of sampling can be observed here.

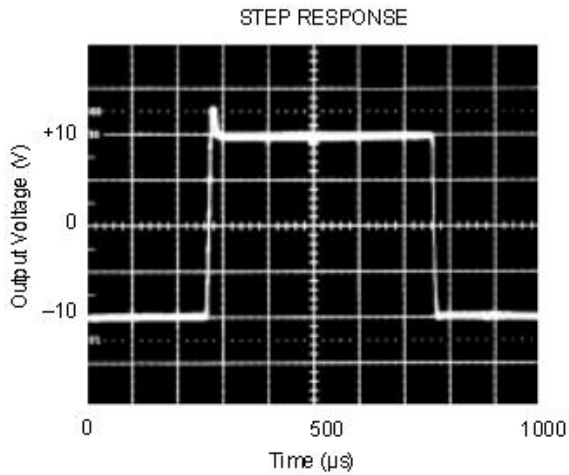


Fig. 6 Step response of ISO124 to a pulse wide 500 μs [3]

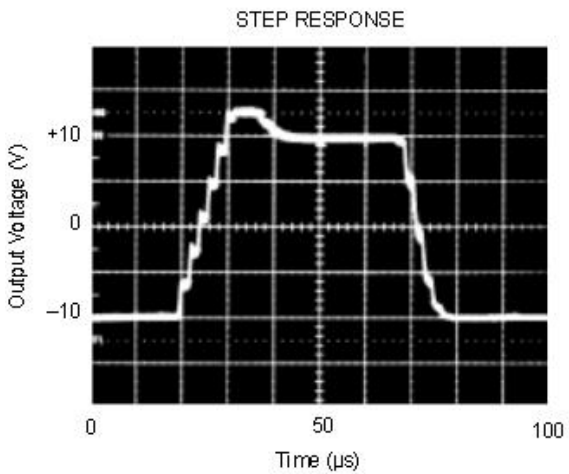


Fig. 7 Step response of ISO124 to a pulse wide 50 μs [3]

B. Operating amplifier TL081

The TL081 is a low cost high speed JFET input operational amplifier with an internally trimmed input offset voltage. The device maintains a large gain bandwidth product and fast slew rate. The noise and offset voltage drift is also at low levels. The absolute voltage offset can be set by an external trimmer. According to [4], the parameters of the device are as described in Table I.

Table I Parameters of TL081 [4]

Parameter	Value
Input bias current	50 pA
Input noise voltage	25 nV/ $\sqrt{\text{Hz}}$
Gain bandwidth	4 MHz
Slew rate	13 V / μs
Supply current	1.8 mA
Input impedance	$10^{12} \Omega$

The typical connection of TL081 including the zero level correction is depicted in Fig. 8. The internal connection of the amplifier is depicted in Fig. 9.

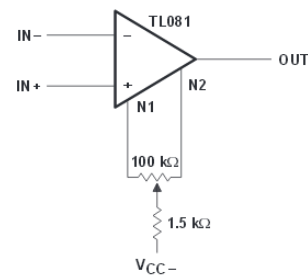


Fig. 8 Basic connection diagram including zero level setting [4]

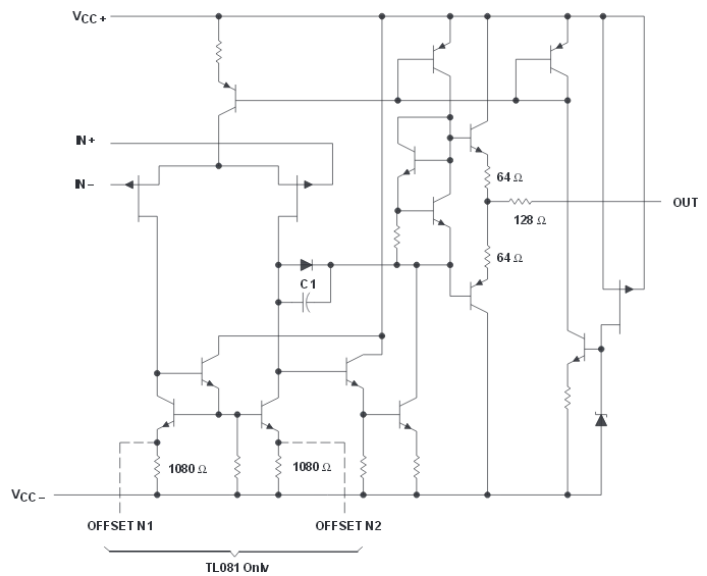


Fig. 9 Internal connection of TL081 [4]

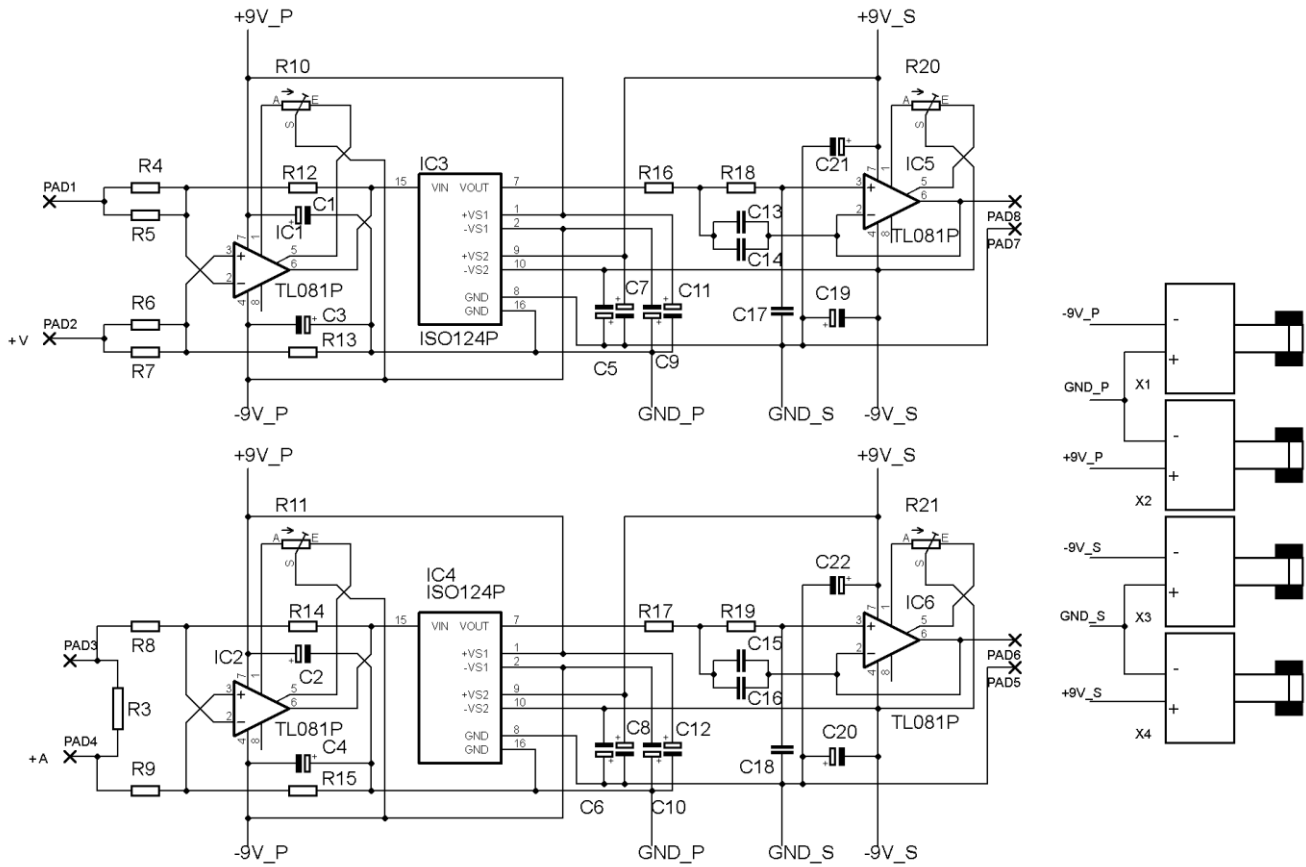


Fig. 10 Isolating interface circuit diagram

III. THE CONSTRUCTION

The dual channel isolating amplifier was constructed in two versions. One of them require an external power source while the second one, the circuit diagram of which is depicted in Fig. 10, employs four independent 9 V batteries. This solution is more convenient for using the device at servicing outside the laboratory.

The device is constructed on a single double sided printed circuit board, including the battery holders. The inputs and outputs of the channels are equipped with pins to which the cables with crocodile clips can be attached. In the neighborhood of each of the operating amplifiers there are precise trimming resistors allowing accurate zero level setting. The printed circuit board is strictly divided into primary and secondary part. These parts are coupled only by means of the ISO124 isolating amplifiers.

Four 9V batteries are mounted in appropriate holders X1 to X4. The power supply nets are different for the “primary” (frontend of ISO124) and the “secondary” (backend of ISO124) part. Also the grounds are strictly separated. The “primary” power supply nets are marked with the letter P (+9V_P, GND_P, -9V_P) while the “secondary” power supply nets are marked with the letter S (+9V_S, GND_S, -9V_S). All power supply inputs of the pertinent integrated circuits are blocked by tantalum capacitors as close to the appropriate pins as possible. The power paths on the printed circuit board were

designed carefully in order to protect the output of the device from noise caused by switching of the circuitry inside the isolating amplifiers (see Fig. 2).

The input of the “voltage” channel is at pins PAD1 and PAD2. The sign “+” shows the polarity of the input. This sign is also depicted at the printed circuit board. The input of the “current” channel is at pins PAD3 and PAD4, also marked with the appropriate sign. The input stages are realized by means of operating amplifiers IC1 and IC2 in a conventional connection. The input resistance of the “voltage” channel is approximately 50 kΩ. The current is measured by means of the shunt resistor R3 the resistance of which is 0.1 Ω.

The output filters are based on the operating amplifiers IC5 and IC6. The values of the appropriate devices were set so the 2nd order Butterworth’s transfer function was achieved. Consequently, smooth modification of the device values were made so higher Q was achieved close to the corner frequency. The corner frequency is tuned to approximately 35 kHz. The measured frequency response of the channels is depicted in Fig. 11.

The outputs of the relevant channels are connected at pads 5, 6, 7 and 8.

In Fig. 12 there is a photo of the battery-powered device. The device list is enlisted in Table II. Some of the positions are omitted for the battery-powered version that is described within the framework of this paper.

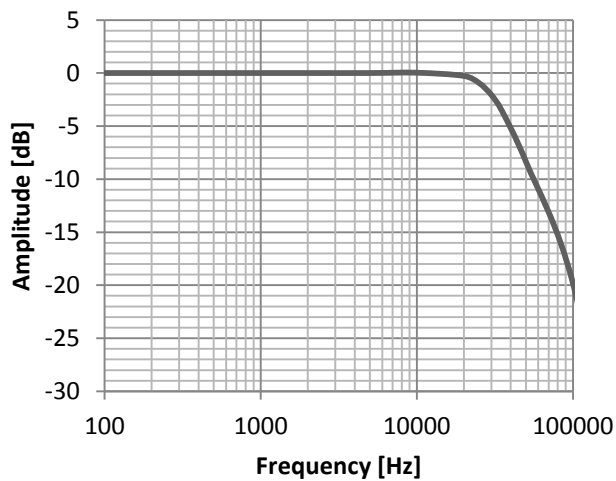


Fig. 11 Typical frequency response of the isolating interface

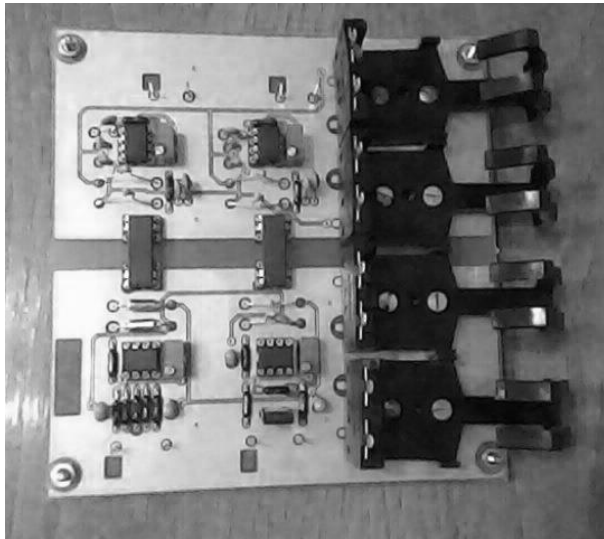


Fig. 12 Battery powered version of the isolating interface

Table II Device list

Position	Value	Note
R3	0.1 Ω	1 %, 1 W
R4, R5, R6, R7, R14, R15	100 k Ω	1 %
R8, R9	1 k Ω	1 %
R10, R11, R20, R21	100 k Ω	Multiturn trimmer
R12, R13, R16, R17, R18, R19	10 k Ω	1 %
C1 to C12, C19 to C22	1 - 10 μ F	tantal
C13, C15	68 pF	ceramic
C14, C15	680 pF	ceramic
C17, C18	330 pF	ceramic
IC1, IC2, IC5, IC6	TL081	See [4]
IC3, IC4	ISO124	See [3]
X1 to X4	9V battery holders	

IV. CONCLUSION

This paper provides a description on a construction of a dual channel galvanically isolated interface for an oscilloscope that enables measurement of differential voltages or currents of those waveforms the bandwidth of whose does not exceed approximately 30 kHz. The device utilizes the isolating amplifier ISO124 with discrete-time modulation.

The device has been built in two versions. One of them requires external power supply while the second one is powered from batteries mounted directly on the device. This version is successfully used at service operations outside the laboratory.

REFERENCES

- [1] Z. Trnka, *Theory of Electrical Engineering* [Teoretická elektrotechnika], SNTL Alfa, Bratislava, 1972, Czechoslovakia
- [2] V. Haasz, M. Sedlacek, *Electrical measurements* [Elektrická měření], Czech Technical University in Prague, 1998, ISBN 80-01-01717-6
- [3] ISO124, datasheet
- [4] TL081, datasheet
- [5] J. Svacina. *Electromagnetic compatibility: Principles and notes* [Elektromagnetická kompatibilita: Principy a poznámky], 1st edition. Brno: Vysoké učení technické, 2001. ISBN 80-214-1873-7.

Identification and control of oscillatory dynamical systems using recurrent complex-valued neural networks

Ieroham S. Baruch and Víctor M. Arellano-Quintana

Abstract—The present paper used the obtained results of Recurrent Complex Valued Neural Network (RCVNN) identification and extend these results to direct complex value control of nonlinear oscillatory plants. After the introduction, the paper gives a short description of the used RCVNN topology and BP learning using diagrammatic rules to obtain it. Than a RCVNN version of direct control schemes are derived. First, an inverse model control scheme is designed. Second, an extension of the first scheme with an integral term is done. Third a RCVNN for plant identification is added and the obtained state estimation is used for feedback control in order to perform a composite feedback-feed-forward control with I-term. Finally, comparative simulation results of flexible-joint robot model using the three schemes of direct complex value control are obtained. The obtained comparative simulation results confirmed the good quality of the proposed control methodology.

Keywords—Direct adaptive feedforward/feedback neural control with integral term, diagrammatic rules, backpropagation learning algorithm, recurrent complex-valued neural network, systems identification and control

I. INTRODUCTION

IN last decade there are some applications using Recurrent Complex-Valued Neural Networks (RCVNN). Most of them deal with oscillatory systems which by their physical nature it is convenient to be treated in the complex domain, such as electromagnetic waves, light waves, images processing, electric power systems, evaporator system, mechanical systems etc. (see [1], [2], [3], [4]). In [2] the authors apply a special type of a RCVNN for modeling of power transformer, obtaining good results. Some other papers like [3], [4] proposed to use RCVNN for mechanical plants identification and control, obtaining good results. In [3] the authors applied a CVNN for an industrial evaporator system identification using an evolutionary algorithm to design the network. They use radial basis functions NN avoiding the gradient terms computation in the learning algorithm. Other papers like [4], [5] used CVNN for these kind of systems, obtaining satisfactory results.

In [6], Leung and Haykin derived a Complex Value Backpropagation (CVBP) algorithm used for pattern classification. However, this learning algorithm presented some problems

because of activation function singularity. For that reason some papers (see [7], [8], [9], [10], [11]) proposed different activation functions that avoid activation function singularity. The paper [11] considered two type of activation functions avoiding singularity, applied for RCVNN identification of nonlinear oscillatory mechanical plant.

The present paper is based on the obtained in [11] results and extends these results to direct control using complex value control algorithms. First the paper gives a short description of the used RCVNN topology and BP learning using diagrammatic rules to obtain it. Than a complex value versions of direct control algorithms are derived, using a complex valued neural network (NN) to model the inverse of the plant. Further an extension of the first control scheme with an integral term is proposed. Than the control scheme is extended using RCVNN for plant identification. Further the estimated states are used for feedback control in order to obtain a composite feedback-feedforward control. Finally, comparative simulation results of flexible-joint robot plant model using three control schemes of direct complex value control are given, obtaining good comparative results.

II. TOPOLOGY AND BACKPROPAGATION LEARNING OF RECURRENT COMPLEX-VALUED NEURAL NETWORK

The considered general Recurrent Complex Valued Neural Network topology, [11], has complex valued input, output, and state vectors, and complex A, B, C weight matrices. In [11], the authors consider a new approach based on diagrammatic rules to obtain the training algorithm. The performance index to be minimized is given by:

$$\zeta(k) = \frac{1}{2} \sum_j [E_j(k)][E_j^*(k)], \quad j \in \mathbb{C}, \quad \zeta = \frac{1}{N_e} \sum_j \zeta(k) \quad (1)$$

The function $\zeta(k)$ is a mapping of the form $f: \mathbb{C} \rightarrow \mathbb{R}$, so it is not analytic in the sense that it does not have derivative and also it does not satisfy the Cauchy-Riemann equations. This complicates the use of the gradient descent algorithm, because we have to use the so-called Wirtinger's calculus. Using diagrammatic rules, [11], we avoid this complicated problem. The activation function that we consider has separate real and imaginary parts so it does not have singular points. It is given by the next equation, [11]:

Ieroham S. Baruch is with the Department of Automatic Control, CINVESTAV-IPN, Mexico City, Mexico, e-mail: baruch@ctrl.cinvestav.mx
Victor Manuel Arellano-Quintana is MS student in the Department of Automatic Control, CINVESTAV-IPN, Mexico City, Mexico, e-mail: varellano@ctrl.cinvestav.mx

$$f(z) = \tanh \operatorname{Re}(z) + i \tanh \operatorname{Im}(z), \quad z \in \mathbb{C} \quad (2)$$

This type of activation function representation allows us to apply diagrammatic rules so to derive the adjointed RCVNN and use it for NN learning. The topology of the RCVNN is given on Fig.1.

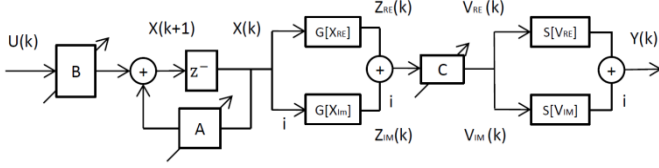


Fig.1 Topology of the RCVNN

The mathematical description of that topology is given by equations (3)-(6).

$$X(k+1) = AX(k) + BU(k) \quad (3)$$

$$A = \text{block-diag}(A_i); |A_i| < 1, i = 1, \dots, n$$

$$Z(k) = G[X_{Re}(k)] + iG[X_{Im}(k)] \quad (4)$$

$$V(k) = Z_{Re}C_{Re} + iZ_{Im}C_{Im} \quad (5)$$

$$Y(k) = S[V_{Re}(k)] + iS[V_{Im}(k)] \quad (6)$$

The vectors and matrices of the RCVNN topology are as follows:

- $A \in \mathbb{C}^{n \times n}$: Feedback Matrix;
- $B \in \mathbb{C}^{n \times m}$: Input matrix;
- $C \in \mathbb{C}^{p \times n}$: Output matrix;
- $X(k) \in \mathbb{C}^{n \times 1}$: State vector;
- $U(k) \in \mathbb{C}^{m \times 1}$: Network input;
- $Y(k) \in \mathbb{C}^{p \times 1}$: Network output;
- $G[\cdot], S[\cdot]$: Complex-valued vector-tanh-activation functions, given by(2);
- m : Number of inputs;

The Means Squared Error (MSE), (1), is minimized in real-time applications and the total MSE ζ is minimized for one epoch N_e in off-line applications. The general RCVNN real-time backpropagation learning algorithm with momentum term is given by the following vector-matricial equation:

$$W(k+1) = W(k) + \eta \Delta W(k) + \alpha \Delta W(k-1) \quad (7)$$

$$|W_{ij}| < W_o$$

Where: $W(\cdot)$ is a general weight matrix (in fact A, B, C); $\Delta W(\cdot)$ is the learning modification of $\Delta W(\cdot)$; η is a diagonal constant matrix of learning; α is a diagonal momentum term matrix; W_o is a restricted region for the common W_{ij} weight. Applying the complex valued diagrammatic rules we could obtain the adjointed RCVNN, given on Fig.2. Using the specified in Fig.2 errors and the obtained in the forward pass (3)-(6) intermediate vectors, we could obtain the following weight update algorithm for the matrices A, B, C .

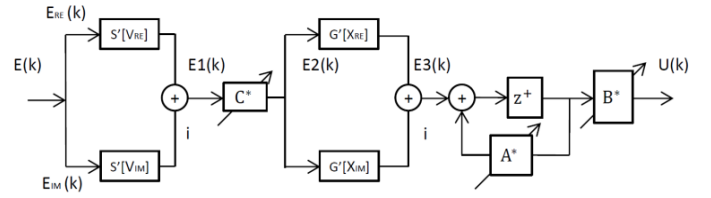


Fig. 2 Adjoined topology of the RCVNN

Now, the BP learning rule (7) could be defined in a complex domain using the adjointed RCVNN topology. The following weight update algorithm is defined as:

For the output layer:

$$\Delta C(k) = E_1(k)Z^*(k) \quad (8)$$

$$E_1(k) = E_{Re}S'[Y[V_{Re}(k)]] + iE_{Im}S'[Y[V_{Im}(k)]] \quad (9)$$

$$E(k) = T(k) - Y(k) \quad (10)$$

For the hidden layer:

$$\Delta A(k) = E_3(k)X^*(k-1) \quad (11)$$

$$E_3(k) = E_{2Re}G'[Z[X_{Re}(k)]] + iE_{2Im}G'[Z[X_{Im}(k)]] \quad (12)$$

$$E_2(k) = C^*(k)E_1(k) \quad (13)$$

$$\Delta vA(k) = E_3(k) \otimes X^*(k) \quad (14)$$

$$\Delta B(k) = E_3(k)U^*(k)$$

Where:

- $G'[\cdot], S'[\cdot]$: The derivatives of the activation functions;
- a^* : Transpose conjugate of the complex number a ;
- $T(k) \in \mathbb{C}^{p \times 1}$: Desired output vector;
- E_{Re} : Real part of $E(k)$;
- E_{Im} : Imaginary part of $E(k)$.

As it could be seen, the application of the diagrammatic rules and the adjointed RCVNN topology simplified the learning with respect to the classical gradient descent learning in complex domain, [6].

III. ADAPTIVE NEURAL CONTROL SYSTEMS DESIGN

This part of the paper illustrates the application of the RCVNN for direct I-Term adaptive neural control scheme of a nonlinear oscillatory plant. The nonlinear oscillatory plant model under investigation is a flexible – joint robot of two degree of freedom (DOF) that actually is a system with four DOF due to the flexible-joints. The model, the output and the input of the plant are given in continuous time. In order to use a recurrent neural network to control, the output/input signals of the plant are discretized with a sampling time T_o .

All neural networks used for system identification and control follow the topology mentioned above. The dimensions of each NN will be defined for the three different control schemes. The first control scheme under consideration is the direct feedforward adaptive control scheme with I-term.

A. Direct Feedforward Adaptive Neural Control with I-Term

The control scheme is depicted in Fig.3. The control objective is that the complex weight parameters of the RCVNN are adjusted in such manner that the RCVNN converges to the inverse of the plant in order that the output of the plant follows de reference vector.

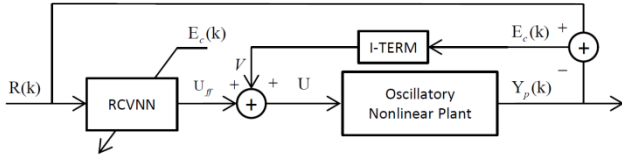


Fig.3 Block-diagram of the direct feedforward adaptive neural control system with I-Term

The RCVNN converges to the inverse model of the plant, trained by the control error: $E_c = Y_p - R$. Here output of the RCVNN is the vector control U so, if the RCVNN converges to the inverse model of the plant, the system output will follow the reference. In order to eliminate the steady-state error an I-Term is added to the control. The I-Term of the error is defined as:

$$V(k + 1) = V(k) + T_o k_i E_c \tag{15}$$

Where:

T_o : Sampling time.

k_i : Integral action gain.

E_c : Control error.

So, the total control is defined by the sum of the feed-forward and the I-Term parts, as it is:

$$U = U_{ff} + V \tag{16}$$

The stability of the whole system is assured by the boundedness of the activation function, and at the same time by the weight restricted condition for A, given in (3).

B. Direct Feedforward Adaptive Neural Control with State Feedback

The block-diagram of the control system is given in Fig.4. The control scheme contained three RCVNNs of the given up type: one RCVNN of plant identification and state estimation, one Feedforward control RCVNN, and one Feedback control RCVNN. The topologies of the three RCVNN are equal but they possessed different dimensions. For system identification, the desired complex target vector is the output of plant. The identification objective is that the complex weight parameters of the RCVNN-1 are adjusted in such manner that the RCVNN-1 output follows the plant output with minimum MSE.

The RCVNN-1 plant identifier and state estimator is learned by the identification error ($E_i = Y_p - Y$). The RCVNN-2 and RCVNN-3 are feedback and feedforward neural controllers, respectively, both learnt by the control error ($E_c = R - Y_p$).

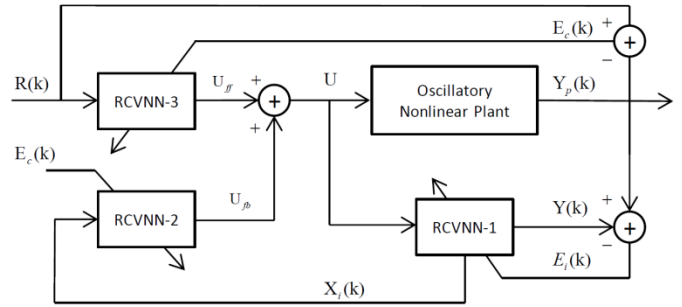


Fig.4 Block-diagram of the direct adaptive neural control system with state feedback

The control vector is sum of both control RCVNN tions U_{fb} , U_{ff} , generated by the corresponding RCVNN-2, 3 controllers.

C. Direct Feedforward Adaptive Neural Control with I-Term and State Feedback

The block-diagram of the control system is given on Fig.5. The control scheme contained three RCVNNs of the given up type: one RCVNN of plant identification and state estimation, one Feedforward control RCVNN, and one Feedback control RCVNN. To eliminate steady-state errors, an I-Term of the control error, (15), is added.

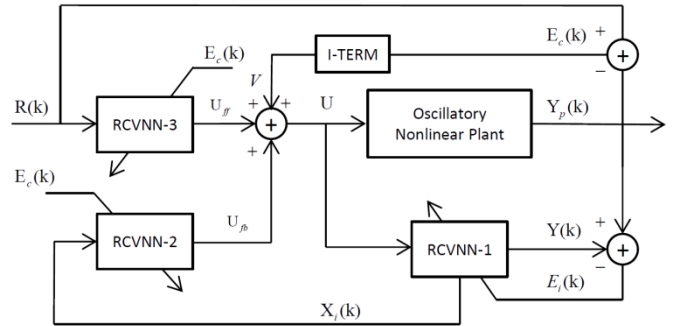


Fig. 5 Block-diagram of the direct adaptive neural control system with I-Term and state feedback

The control vector is sum of both control RCVNN tions (U_{fb} , U_{ff} – outputs of the corresponding RCVNN controllers) and V - the integral term, respectively.

D. Description of the Nonlinear Plant Model

The dynamic model of flexible-joint robot was developed due to the use of harmonic drives, which is a type of robot gear mechanism with high torque transmission, low backlash and compact size. The elastic coupling of the i -th joint is modeled as a linear torsional spring of constant stiffness K_i . The i -th elastic joint of a revolute robot is schematically shown in Fig.6.

The system is a robot of two DOF showed in Fig.7. It is considered that each joint is flexible of the type illustrated by Fig.6. The flexible joint robot model consists of an actuator

connected to a load through a torsional spring representing the joint flexibility.

To simplify, the model of the flexible joint robot, it is derived under the following assumptions, [12]:

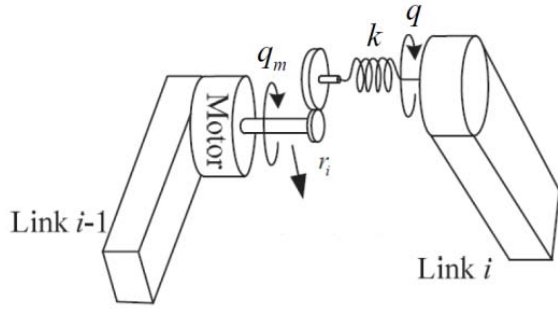


Fig. 6 Idealized model representing i -th elastic joint flexibility of a revolute robot

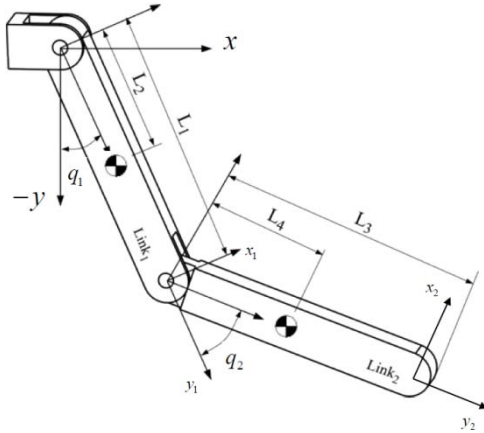


Fig. 7 Two- DOF- robot with flexible joints

- The Kinetic energy of the rotor is due to its own rotation. Equivalently, the motion of the rotor is a pure rotation with respect to an inertial frame.
- The rotor/gear inertia is symmetric about the rotor axis of rotation so that the gravitational potential of the system and the velocity of the rotor center of the mass are both independent of the rotor position.

Under these assumptions, the equations of motion of the flexible - joint robot are given as follows.

$$\begin{aligned} D(q)\ddot{q} + C(q, \dot{q})\dot{q} + G(q) + K(q - q_m) &= 0 \\ J\ddot{q}_m - K(q - q_m) &= u \end{aligned} \quad (17)$$

Where: q and $q_m \in \mathbb{R}^n$ denote the angular displacement of the links and the motor shaft, respectively; $D(q): \mathbb{R}^n \rightarrow \mathbb{R}^{n \times n}$ is the symmetric positive definite inertia matrix; $C(q, \dot{q}): \mathbb{R}^n \times \mathbb{R}^n \rightarrow \mathbb{R}^n$ represents the Coriolis and centrifugal forces; $G(q): \mathbb{R}^n \rightarrow \mathbb{R}^n$ is the gravitational force vector

of the rigid links; $K \in \mathbb{R}^{n \times n}$ is the diagonal positive definite spring constant matrix of the flexible joints; $J \in \mathbb{R}^{n \times n}$ is the moment of inertia matrix of the motor, and $u \in \mathbb{R}^n$ is the exogenous input torque vector.

If we define an extended vector $q_f = [q^T q_m^T]^T$ we can rewrite the two equations above in the following matrix form:

$$D_f(q)\ddot{q}_f + C_f(q, \dot{q})\dot{q}_f + G_f(q) + K_f q_f = u_f \quad (18)$$

Where:

$$\begin{aligned} D_f(q) &= \begin{bmatrix} D(q) & 0 \\ 0 & J \end{bmatrix}, & C_f(q, \dot{q}) &= \begin{bmatrix} C(q, \dot{q}) & 0 \\ 0 & 0 \end{bmatrix} \\ G_f(q) &= \begin{bmatrix} G(q) \\ 0 \end{bmatrix}, & K_f &= \begin{bmatrix} K & -K \\ -K & K \end{bmatrix}, & u_f &= \begin{bmatrix} 0 \\ u \end{bmatrix} \end{aligned}$$

The properties of this model are mentioned in [12]. As we can see, the plant is an oscillatory system, described by four second order differential equations, representing a system with four degrees of freedom but only two inputs which makes the system sub-actuated.

E. Simulation Results

This section described the simulation results, obtained using the given up three schemes of adaptive neural control. As a measure of comparison we use the final MSE of the output variables for the two schemes of adaptive neural control.

Direct Feedforward Adaptive Neural Control with I-Term.

The simulation was executed with the following RCVNN configuration: $m = 2, n = 6, p = 2$. The dimension of the hidden RCVNN layer was chosen by trial and error, based on the step response of the system. The same was done for the gain of the I-Term. The graphical results of the first neural control scheme outputs are given on Fig.8 for the first link and in Fig.9 for the second link. The output of the plant is compared with a constant stepwise reference. The reference signal is different for each of the links. It can see that the step response presented oscillations at the beginning, and then converge to the reference.

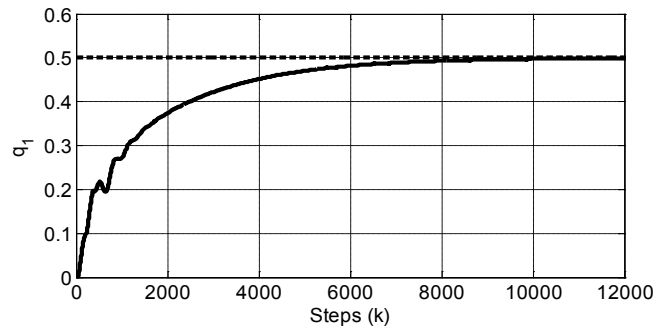


Fig. 8 Graphical simulation results for the plant output q_1 , controlled by the first control scheme; plant output (continued line); system reference (dashed line)

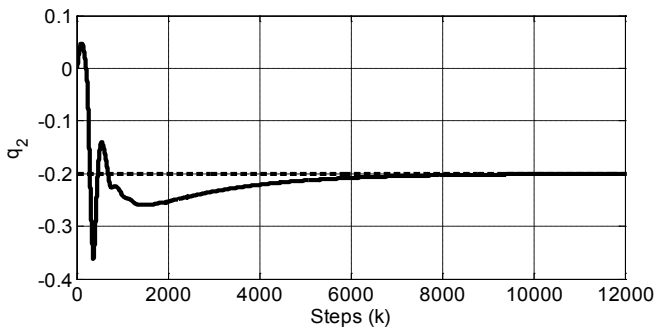


Fig. 9 Simulation results of q_2 , controlled by the first control scheme; plant output (continue line); system reference (dashed line)

Direct Feedforward Adaptive Neural Control with State Feedback. This scheme does not implement I-Term. The simulation was executed with the following NN configurations: RCVNN-1 has dimensions: $m = 2, n = 6, p = 2$; the dimension of the hidden layer of RCVNN-1 was chosen by trial and error, using the fact that the whole system has order eight; RCVNN-2 has dimensions: $m = 2, n = 4, p = 2$; the dimension of the hidden layer of RCVNN-2 was chosen by trial and error; RCVNN-3 has dimensions: $m = 2, n = 6, p = 2$; the dimension of the hidden layer of RCVNN-3 was chosen by trial and error.

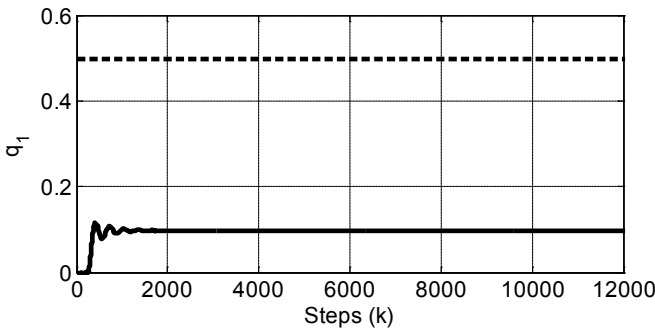


Fig. 10 Simulation results of q_1 , controlled by the second control scheme; plant output (continue line); system reference (dashed line)

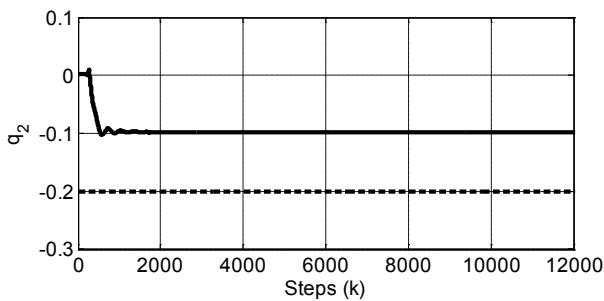


Fig. 11 Simulation results of q_2 , controlled by the second control scheme; plant output (continue line); system reference (dashed line)

The graphical results of the second neural control scheme plant outputs are given on Fig.10 for the first link and in

Fig.11 for the second link. Each output of the plant is compared with a constant reference. The reference is different for each of the links. It could be seen that the responses of the plant outputs presented oscillations at the beginning and generate static errors; which is due to the control signal behavior and the lack of I-term.

Direct Feedforward Adaptive Neural Control with I-Term and State Feedback. The simulation was executed with the following RCVNN configurations: RCVNN-1 has dimensions $m = 2, n = 6, p = 2$. The number of the hidden neurons was chosen by trial and error, based on the step response of the system and using the fact that the whole system has order eight; RCVNN-2 has dimensions $m = 2, n = 4, p = 2$. The number of the hidden neurons was chosen by trial and error based on the step response of the system; RCVNN-3 has dimensions $m = 2, n = 6, p = 2$. The number of the hidden neurons was chosen by trial and error, based on the step response of the system, also the gains of the I-term. The graphical results of the third neural control scheme are given on Fig.12 for the first link output and in Fig.13 for the second link output. The respective output of the plant is compared with a constant reference. The reference is different for each one of the links. It could be seen that each response does not present oscillation at the beginning which is achieved applying a state feedback control.

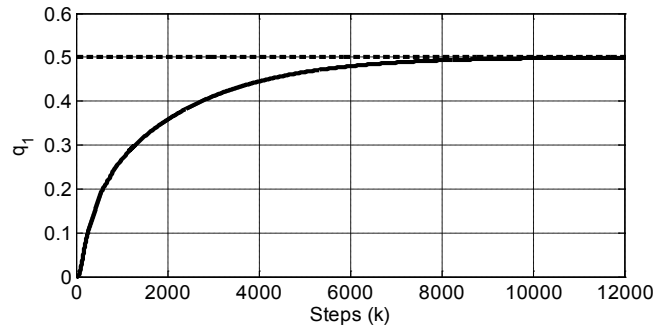


Fig. 12 Simulation results of q_1 , controlled by the third control scheme; plant output (continue line); system reference (dashed line)

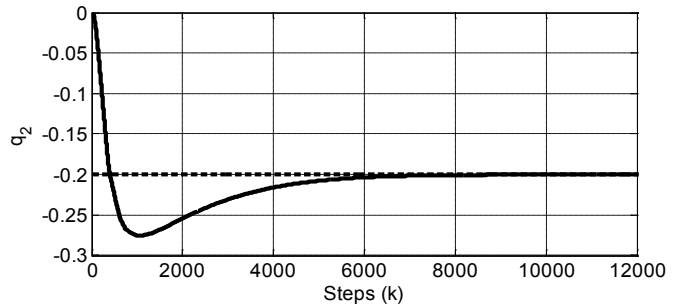


Fig.13 Simulation results of q_2 , controlled by the third control scheme, plant output (continue line); system reference (dashed line)

Comparative final MSE simulation results, obtained by the three adaptive control schemes. The MSE values obtained at

the final of the simulation (12000 iteration steps) with the three adaptive neural control schemes are shown on Table I. It could be seen that the use of the state feedback affects the step response of the system, decreasing the oscillations of the plant output step responses. Also the MSE decreases more quickly and converges to a small final value.

Table I. Final MSE of adaptive neural control schemes

DO F	Direct Feedforward Adaptive Neural Control with I-Term	Direct Feedforward Adaptive Neural Control with State Feedback.	Direct Feedforward Adaptive Neural Control with I-Term and State Feedback.
q_1	0.0088	0.1629	0.0090
q_2	0.0010	0.0109	0.0007

In Table I, we can see that the first control scheme and the last control scheme have smaller MSE with respect to the second control scheme, but the suppression of the oscillations is greater using the state feedback. So we could conclude that the third control scheme containing state feedback and I-term have better behavior. Also the I-Term reduces the error in steady state.

IV. CONCLUSIONS

In the present paper we purposed three schemes for direct adaptive control using RCVNNs. We applied diagrammatic rules for the complex value case in order to derive the backpropagation training algorithm of the RCVNN topology. Comparative simulation results of flexible-joint robot model using the three schemes of direct complex value control, are obtained. These results lead us to the conclusion that the presence of the state feedback decreases the oscillations in the output step response, and the I-Term reduces the error in steady state. As we can see in the Table I, the MSE is almost equal between the scheme one and the scheme three, but the suppression of oscillations for the third control scheme is considerable. The obtained results confirmed the good quality of the proposed control methodology.

REFERENCES

- [1] A. Hirose, *Complex-Valued Neural Networks*, 2nd ed., S. i. C. Intelligence, Springer Verlag, 2012, vol. 400.
- [2] A. Minin, Y. Chistyakov, E. Kholodova, H. G. Zimmermann, and A. Knoll, "Complex Valued Open Recurrent Neural Network for Power Transformer Modeling," *International Journal of Applied Mathematics and Informatics*, vol. 6, no. 1, pp. 41-48, 2012.
- [3] L. Ferariu, "Nonlinear System Identification Based on Evolutionary Dynamic Neural," in *Proc. of European Control Conference*, Cambridge, UK, 2003.
- [4] K. Kawashima and T. Ogawa, "Complex-Valued Neural Network for Group-Movement Control of Mobile Robots," in *Proc. SICE Annual Conference 2012*, Japan, 2012.
- [5] A. Hirose, "Motion Controls Using Complex-Valued Neural Networks with Feedback Loops," in *Proc. IEEE International Conference on Neural Networks*, vol. 1, San Francisco, CA, 1993, pp. 156-161.
- [6] H. Leung and S. Haykin, "The Complex Backpropagation Algorithm," *IEEE Transactions on Signal Processing*, vol. 39, no. 9, pp. 2101-2104, 1991.
- [7] T. Nitta, *Complex-Valued Neural Networks: Utilizing High-Dimensional Parameters*. IGI Global, 2009.
- [8] C. Woo and D. S. Hong, "Adaptive Equalization Using the Complex Backpropagation Algorithm," in *Proc. of IEEE International Conference on Neural Networks*, vol. 4, Washington, DC, 1996, pp. 2136-2141.
- [9] N. Miklos and B. Salik, "Neural Networks with Complex Activations and Connection Weights," *Complex Systems*, vol. 8, pp. 115-126, 1994.
- [10] G. Georgiou and C. Koutsougeras, "Complex Domain Backpropagation," *IEEE Transactions on Circuits and Systems-II: Analog and Digital Signal Processing*, vol. 39, no. 5, pp. 330-334, 1992.
- [11] V. M. Arellano-Quintana and I. S. Baruch, "Identification of Dynamical Systems Using Recurrent Complex-Valued Neural Networks," in *18th International Conference on Circuits, Systems, Communications and Computers*, Santorini, Greece, 2014 (accepted for presentation).
- [12] S. S. Ge, T. H. Lee, and C. J. Harris, *Adaptive Neural Network Control of Robotic Manipulators*, C. J. Harris, Ed. UK: World Scientific Publishing Co. Pte. Ltd., 1998, vol. 19.

Implementation of fuzzy MPC on embedded system

Jakub Novak and Petr Chalupa

Abstract—The paper describes an implementation of a fuzzy logic predictive controller on an ARM-Cortex microcontroller. The implementation issues of the fuzzy MPC controller on embedded systems are examined and the performance is evaluated. To find the solution of the resulting optimization problem arising from the model predictive control an online Fast Gradient method is used. As a case study the simulated nonlinear process of pH neutralization is considered.

Keywords— Embedded Systems, Fast Gradient Method, Model Predictive Control, Multiple Models

I. INTRODUCTION

MODEL predictive control (MPC) has gained a lot of interest of both academia and industry in the recent years. The main reason for the wide-scale adoption of MPC is its ability to handle constraints on inputs and states that arise in most applications. Moreover, MPC problem formulation enables direct inclusion of predictive information, allowing the controller to react to future changes in reference signal. MPC naturally handles processes with multiple inputs or outputs and its concept can be used with dynamic models of any dimension. MPC technology can now be found in a wide variety of application areas including chemicals, food processing, automotive, and aerospace applications [1]. With each new measurement the input to plant is determined by solving a finite horizon optimal control problem [2]. The problem is often in the form of a quadratic cost criterion with input constraints. Since the solution of the optimization problem is required every sample time the MPC was initially restricted to slow dynamics processes.

To avoid online optimization the solution of the control problem for different states can be pre-computed off-line. This explicit solution represent a piece-wise affine map over a partition of the state-space and can be stored efficiently in the form of a look-up table [3]. The explicit MPC offers reduction in online evaluation time but the primary limitation is that the complexity can grow quickly with the problem size, thus limiting the applicability of explicit MPC to small and medium-sized control problems.

Jakub Novak is with Faculty of Applied Informatics, Tomas Bata University in Zlin, nam. T.G. Masaryka 5555, 76001 Zlin, Czech Republic (email: jnovak@fai.utb.cz)

Petr Chalupa is with Faculty of Applied Informatics Tomas Bata University in Zlin, nam. T.G. Masaryka 5555, 76001 Zlin, Czech Republic (email: chalupa@fai.utb.cz).

The research was supported by the European Regional Development Fund under the project CEBIA-Tech No. CZ.1.05/2.1.00/03.0089. This assistance is very gratefully acknowledged.

The increase in computational power and advances in optimization algorithms has opened possibilities to use model predictive control for faster processes with online optimization. Interior point method (IPM) and active set method (ASM) appear to be the most efficient approaches for online solving of quadratic programming problem. A fast implementation of Interior point method is reported in [4] and its applicability is demonstrated in simulation studies. The method exploits the particular structure of the MPC problem and considerably reduces the computation time of control action. The comparison of both methods for implementation of MPC is presented in [5]. Richter et al. [6] reported an online-optimization for systems with input constraints using Fast Gradient Method (FGM) developed by Nesterov [7]. The strategy to compute an upper bound for the maximum number of iterations needed to ensure a predefined accuracy is provided in [8]. Kogel and Findeisen [9] developed a method for computation of the gradient in Fast Gradient method exploiting the problem structure, which requires less memory and is faster than the standard method for large horizons. In [10] the problem of input quantization and how it can be exploited in order to determine a suboptimality level is shown. The authors also present a real application with Segway-like robot controlled using a hard real-time operating system and a low-cost microcontroller. There are several reports of implementations of the MPC on a chip with reduced computational power and memory. Bleris and Kothare present a real-time implementation of the MPC on a microcontroller for Glucose regulation in [11] and [12], where they used logarithmic number system and Newton method for optimization of the objective function. Due *et al.* demonstrated in [13] applications of Multi-parametric model based control on a chip for a slow industrial system but also for fast sampled active valve train engine. MATLAB framework for generating fast model predictive controllers for embedded targets such as ARM processors has been developed and tested on inverted pendulum in [14]. The optimization algorithm is based on the work by Stephen Wright [16].

In this work we focus on the implementation aspects of fuzzy-based MPC on embedded systems where the quadratic programming problem is solved with FGM. Criteria for stability and robustness guarantees are beyond the scope of this paper. The paper is structured as follows Section 2 briefly repeats the MPC formulation. Section 3 describes the fast gradient algorithm. A description of the experimental setup can be found in Section 4. Section 5 contains the results for implementation of the fuzzy MPC on embedded system. The requirements in terms of computation time as well as in terms

of memory demand are discussed. Finally, the main conclusions are summarized in Section 6.

II. PROBLEM STATEMENT

In the MPC the control actions which optimize the forecasted process behavior are recalculated each sampling interval. The forecasted process behavior is based on a dynamic model of the process to be controlled. Thus, at each sampling instant an optimal control problem must be solved. Afterwards, the optimized control action is applied to the process until the next sampling instant when new states are available. Hence, MPC is sometimes also referred to as receding horizon control. To design an MPC controller for nonlinear process, the nonlinear process is modeled by a Takagi-Sugeno fuzzy system with linear functional consequents in the fuzzy rules and local linear models [15]. Different predictive controllers are designed for different rules (local sub-systems) and the global controller output is the fuzzy weighted integration of local ones. The models to be used in the control system design are taken to be discrete state-space models. By using a state-space model, the current information required for predicting ahead is represented by the state variable at the current time. The optimization problem is based on a time-invariant discrete process model, linear constraints and a convex quadratic objective function:

$$\min_{\Delta u(k), \Delta u(k+1), \dots, \Delta u(k+N_c)} J(k) \quad (1)$$

$$J(k) = \sum_{i=1}^{N_p} (\hat{y}(k+i) - y^r(k+i))^2 + \lambda \sum_{i=1}^{N_c} \Delta u(k+i-1)^2 \quad (2)$$

where $\hat{y}(k+i)$ is the i th step output prediction, $y^r(k+i)$ is the i th step reference trajectory, $\Delta u(k)$ is difference between $u(k)$ and $u(k-1)$, λ is the weighting factor and N_p and N_c are the prediction and control horizons, respectively. The control policy $\Delta u(k+i), i = 0, 1, 2, \dots, N_u$ can be developed by first generating m sets of local control policies, where m is the total number of local models. The weighted sum of the local control policies gives the overall control policy:

$$\Delta u(k+i) = \sum_{j=1}^m \omega^j \Delta u^j(k+i) \quad (3)$$

where ω^j is the validity of j th model. Apparently, the validities of local models are normalized to unity:

$$\sum_{j=1}^m \omega^j = 1 \quad (4)$$

The criterion (1) can be rewritten into a condensed quadratic problem

$$\min_{\Delta u(k), \Delta u(k+1), \dots, \Delta u(k+N_c)} \left(\frac{1}{2} \Delta \mathbf{u}^T \mathbf{H} \Delta \mathbf{u} + \mathbf{f}(\mathbf{x}) \Delta \mathbf{u} \right) \quad (5)$$

$u(k) \in U$

with input $u(k)$ constrained in each step to a closed set U . The Hessian matrix \mathbf{H} and vector $\mathbf{f}(\mathbf{x})$ depend on the cost criterion and system dynamics. Only input constraints are

considered so the condensed problem has $2N_p$ inequality constraints, but only N_p optimization variables. As usual in receding control strategy only the first input obtained by minimization of the quadratic criterion and satisfying the constraints is applied to system. The discrete linearized model is assumed in the form:

$$\begin{aligned} \mathbf{x}(k+1) &= \mathbf{A}\mathbf{x}(k) + \mathbf{B}\mathbf{u}(k) \\ \mathbf{y}(k) &= \mathbf{C}\mathbf{x}(k) \end{aligned} \quad (6)$$

where $\mathbf{u}(k)$ is the vector of manipulated variables or input variables; $\mathbf{y}(k)$ is the vector of the process outputs and $\mathbf{x}(k)$ is the state variable vector. Using the linear model the model predictive controller would exhibit steady - state offset in the presence of plant/model mismatch or unmeasured disturbance due to lack of integral action. In order to introduce integral behavior, a new state variable vector is chosen to be:

$$\mathbf{x} = [\Delta \mathbf{x}(k)^T \ \mathbf{y}(k)^T]^T \quad (7)$$

Combining (6) and (7) leads to the following state-space model:

$$\begin{aligned} \begin{bmatrix} \Delta \mathbf{x}(k+1) \\ \mathbf{y}(k+1) \end{bmatrix} &= \begin{bmatrix} \mathbf{A} & \mathbf{0} \\ \mathbf{C}\mathbf{A} & \mathbf{I} \end{bmatrix} \begin{bmatrix} \Delta \mathbf{x}(k) \\ \mathbf{y}(k) \end{bmatrix} + \begin{bmatrix} \mathbf{B} \\ \mathbf{C}\mathbf{B} \end{bmatrix} \Delta \mathbf{u}(k) \\ \mathbf{y}(k) &= [0 \ \mathbf{1}] \begin{bmatrix} \Delta \mathbf{x}(k) \\ \mathbf{y}(k) \end{bmatrix} \end{aligned} \quad (8)$$

The predictor for new state vector $\mathbf{x}(k)$ and control increment sequence $\Delta \mathbf{u}(k)$ for given horizons can be formulated in terms of vectors as:

$$\mathbf{Y} = \mathbf{K}\mathbf{x} + \mathbf{L}\Delta \mathbf{U} \quad (9)$$

where

$$\mathbf{Y} = \begin{bmatrix} \mathbf{y}(k+1) \\ \vdots \\ \mathbf{y}(k+N_y) \end{bmatrix} \Delta \mathbf{U} = \begin{bmatrix} \Delta \mathbf{u}(k+1) \\ \vdots \\ \Delta \mathbf{u}(k+N_u) \end{bmatrix} \quad (10)$$

and the relations for matrices \mathbf{K} and \mathbf{L} are:

$$\mathbf{K} = \begin{bmatrix} \mathbf{C}\mathbf{A} \\ \mathbf{C}\mathbf{A}^2 \\ \vdots \\ \mathbf{C}\mathbf{A}^{N_p-1} \end{bmatrix} \quad (11)$$

$$\mathbf{L} = \begin{bmatrix} \mathbf{L}_1 \\ \mathbf{L}_2 \end{bmatrix}, \mathbf{L}_1 = \begin{bmatrix} \mathbf{C}\mathbf{B} & \mathbf{0} & \dots & \mathbf{0} \\ \mathbf{C}\mathbf{A}\mathbf{B} & \mathbf{C}\mathbf{B} & \dots & \mathbf{0} \\ \vdots & \vdots & \ddots & \mathbf{0} \\ \mathbf{C}\mathbf{A}^{N_c-1}\mathbf{B} & \mathbf{C}\mathbf{A}^{N_c-2}\mathbf{B} & \dots & \mathbf{C}\mathbf{B} \end{bmatrix} \quad (12)$$

$$\mathbf{L}_2 = \begin{bmatrix} \mathbf{C}\mathbf{A}^{N_c}\mathbf{B} & \dots & \mathbf{C}\mathbf{A}^2\mathbf{B} & \mathbf{C}(\sum_{j=0}^1 \mathbf{A}^j)\mathbf{B} \\ \vdots & \vdots & \vdots & \vdots \\ \mathbf{C}\mathbf{A}^{N_p-1}\mathbf{B} & \dots & \mathbf{C}\mathbf{A}^{N_p-N_c+1}\mathbf{B} & \mathbf{C}(\sum_{j=0}^{N_p-N_c} \mathbf{A}^j)\mathbf{B} \end{bmatrix} \quad (13)$$

The Hessian matrix H and vector $f(x)$ from criterion can then be formulated as:

$$H = L^T L + \lambda I, f(x) = -(Y_r - Kx(k))^T L \quad (14)$$

where Y_r represents the vector of reference signals on prediction horizon. Using the fuzzy approach the original nonlinear model is composed of m MIMO linear models with j th MIMO rule as an example,

$$R_j \text{ IF } \varphi \in Z^j \text{ THEN } Y_p^j(k) = K^j x(k) + L^j U^j(x) \quad (15)$$

where $j=1, \dots, m$. and φ is the scheduling vector. Since the consequent part of each rule is a linear equation, it is easy to design a linear controller for each rule. The global nonlinear controller is a fuzzy weighted integration of linear ones. The Fig. 1 shows the structure of multiple model predictive control.

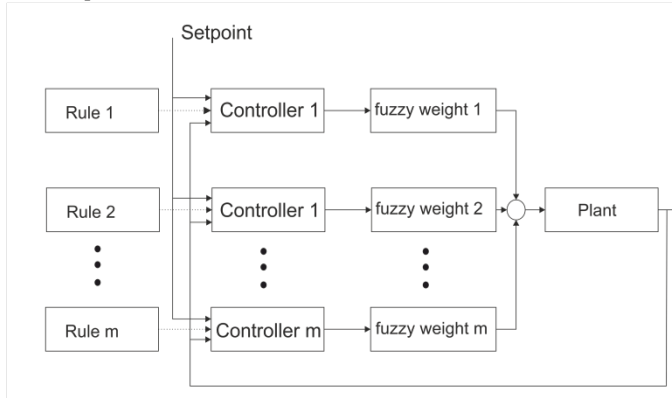


Fig. 1 Structure of multiple model control

III. FAST GRADIENT ALGORITHM

Efficient solution of the introduced quadratic programming problems with discrete-time linear model is a key feature for fast MPC control scheme. The optimization method utilized here to solve (1) is based on Nesterov's method also known as the Fast Gradient method, see [7]. The main benefit of the classical gradient schemes is that they do not rely on second order derivative information and take a damped steepest descent step in each iteration. Fast gradient method modifies this idea to yield faster convergence. Fast gradient method is easy to implement as it requires only to compute gradient and to perform projection operation into feasible set in each step. The optimization is started with an initial guess Δu^0 and stops after i_{max} iterations, such that

$$J(\Delta u^{i_{max}}) - J(\Delta u^*) \leq \epsilon \quad (16)$$

where $J(\Delta u^*)$ is the value of the optimal solution, $\epsilon > 0$ is the suboptimality level, and $\Delta u^{i_{max}}$ is called a suboptimal point. Theoretical bound for i_{max} can be found in [6]. We can describe the iterative scheme of fast gradient method by algorithm.

Fast Gradient method algorithm	
Requirements: Initial guess Δu^0 , number of iterations i_{max} , maximum and minimum eigenvalues of H : L, μ	
1.	Set $u_{old} = \Delta u^0, w = \Delta u^0$
2.	For $i=1$ to i_{max} Compute $u = P_U(w, 1/L)$ Compute $w = u + c(u - u_{old})$
3.	Return u

The constant c is defined as:

$$c > 0, c = \frac{\sqrt{L} - \sqrt{\mu}}{\sqrt{L} + \sqrt{\mu}} \quad (17)$$

Numbers L and μ are Lipschitz constant of the gradient and convexity parameter respectively. Both are computed from the eigenvalues of the Hessian matrix. L is the maximal eigenvalue and μ is the minimal eigenvalue. Note that, the projected gradient step $P_U(w, 1/L)$ is an Euclidean projection of w resulting from the gradient step

$$u = w - \frac{1}{L} \nabla J(w) \quad (18)$$

into the feasible set U . This projection is very easy for box constraints but for general constraints it gets more computationally demanding. The gradient of the cost function (5) is simply:

$$\nabla J(u) = H \Delta u + f(x) \quad (19)$$

The zero vector policy $\Delta u(k+i) = 0, i = 1, 2, \dots, N_u$ can be used as an initial feasible guess (*cold-starting*). However, using the solution of the previous optimal control problem, called *warm-starting* usually decreases computational effort.

IV. EXAMPLE

We consider the nonlinear process of neutralization as example. The simulated system consists of a continuous stirred tank reactor (CSTR) in which neutralization reaction between a strong acid (HA) and a strong base (BOH) takes place in the presence of a buffer (BX). The system has three states, single output and single input.

$$x_1 = [A^-], x_2 = [B^+], x_3 = [X^-], y = pH, u = q_B \quad (20)$$

where $[A^-], [B^+], [X^-]$ are acid, base and buffer concentrations, respectively. The term q_B represents the flow rate of the base. The scheme of the CSTR is depicted in Fig. 2. The process dynamics is given by the following set of differential equations:

$$\dot{x}_1 = \frac{q_A}{V}(x_{1,i} - x_1) - \frac{q_B}{V}x_1 \quad (21)$$

$$\dot{x}_2 = -\frac{q_A}{V}x_2 + \frac{q_B}{V}(x_{2,i} - x_2) \quad (22)$$

$$\dot{x}_3 = -\frac{q_A}{V}x_3 + \frac{q_B}{V}(x_{3,i} - x_3) \quad (23)$$

The pH value can be determined using the implicit equation:

$$[H^+] + x_2 + x_3 - x_1 - \frac{K_w}{[H^+]} - \frac{x_3}{1 + \frac{K_x[H^+]}{K_w}} = 0 \quad (24)$$

where $pH = \log_{10}[H^+]$ and K_w, K_x are the dissociation constants of water and buffer, respectively.

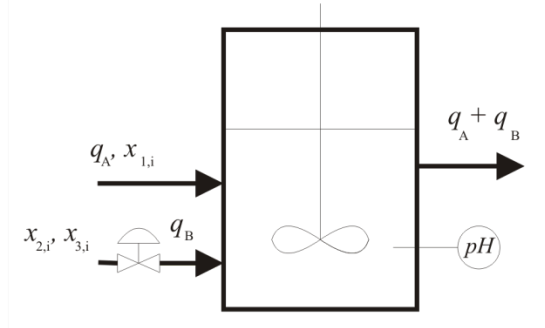


Fig. 2 pH neutralization process

Table I Model Parameters

symbol	parameter	value
$x_{1,i}$	acid inlet concentration	1.2×10^{-3} mol/L
$x_{2,i}$	base inlet concentration	2.0×10^{-3} mol/L
$x_{3,i}$	buffer inlet concentration	2.5×10^{-3} mol/L
K_x	buffer dissociation const.	10^{-7} mol/L
K_w	water dissociation const.	10^{-14} mol ² /L ²
V	reactor volume	2.5L

The system parameters used in this work were taken from [17] and are summarized in Table I.

The output equation is clearly strongly nonlinear. The titration curve and the gain variation that illustrate the nonlinearity of the pH neutralization process are depicted in Fig. 3.

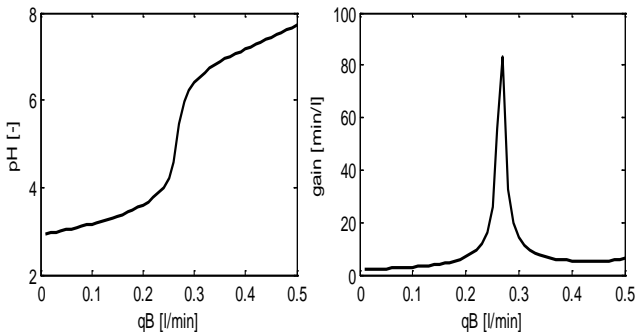


Fig. 3 Titration curve and gain variation of pH neutralization process

The sampling of the estimation and control schemes was set to 30s due to the dynamics of the process and constraints of the process input are assumed to be $0 \leq u(k) \leq 0.5$. The concentrations (states) are assumed to be measured. Six fuzzy sets with triangular membership functions were used for

approximation of the nonlinear process as shown in Fig. 4. The location of the models was obtained using C-means clustering. At these operation modes the nonlinear process was linearized to obtain parameters of local models. The fuzzy model is a good approximation of the process as presented in Fig. 4 which shows both steady-state characteristic of process and fuzzy membership functions. To account for high variation of gain of the process the weighting factor λ used in the predictive control cost function is also weighted using membership functions:

$$\lambda^j = \omega^j \text{gain}_j^2 \quad (25)$$

where the gain of the local model M_i is computed:

$$\text{gain}_j = C_j(I - A_j)^{-1}B_j \quad (26)$$

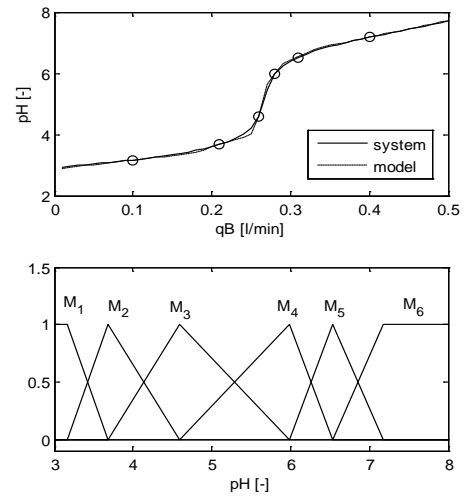


Fig. 4 Steady-state characteristic and distribution of membership functions

V. EMBEDDED SYSTEM IMPLEMENTATION

The proposed fuzzy logic predictive controller was implemented on The Stellaris® LM4F120 board which is a low-cost evaluation platform for 32-bit ARM® Cortex™-M4F-based microcontrollers from Texas Instruments. The microcontroller runs at 80 MHz. The board has 32KB of SRAM memory, 256KB of flash memory and 2KB EEPROM. The Fig. 5 shows the device. For implementation of MPC controller the requirements for memory and evaluation speed must be considered.

The board has only 32KB of RAM however model parameters can be pre-computed offline. The matrices from (14) $H \in R^{Np \times Np \times no \times no}$, $K \in R^{Np \times no \times ns}$, $L \in R^{Np \times Nc \times no \times ni}$, where no , ns , ni are number of outputs, states and inputs, respectively are stored in the flash memory while variables such as the vectors f and the internal variables must be stored in RAM. For given number of local models m the memory requirements in bytes are given by

$$m * n_b * N_p * n_o * (N_p * n_o + n_s + N_c * n_i) \quad (27)$$

where n_b is the number of bytes required to store a number. The 4 bytes are used in the example. The distribution of models in the operating space given by the centers of fuzzy sets is also stored in the flash memory.

The memory demands for online computation are given by the number of decision variables. The following vectors of size $N_u * n_i$ are needed for online computation: f, y, w, u, u_{old} and the auxiliary vector of the same dimension to store the values of gradient.

The fuzzy controller output is given by the weighted sum of local controllers. Thus the constrained optimization problem must be solved separately for each local controller. The online computation of the fast gradient algorithm only requires the computation of gradient which is for the case of MPC control a matrix-vector multiplication ($H\Delta u$). Another two matrix-vector multiplications are needed to compute $f(x)$. The Fast Gradient algorithm is rather simple to implement as it requires only simple linear algebra such as matrix-vector multiplications, vector additions and comparisons. The initial guess $\Delta u(k+i) = 0, i = 0, \dots, N_u$ is used in the example as it represents always a feasible solution to the optimization problem. The Fig. 6 shows the time of evaluation of control input in a single sampling interval which represents call of the Fast Gradient method for all the local models. The values are averages of 20 executions with different states. The control horizon N_c was set to the same value as prediction horizon. The MPC controller is implemented in plain C-code without the help of mathematical libraries BLAS/LAPACK.

The control courses and weights of each model during the example simulation are depicted in Fig. 7. Using multiple local models, the on-line nonlinear optimization can be avoided and simple quadratic programming problem is solved at each sampling interval. The control performance of the proposed fuzzy control scheme with MPC based on multiple models is comparable to the performance obtained when a computationally demanding nonlinear optimization procedure is used online at each sampling instant within a nonlinear MPC controller [18].

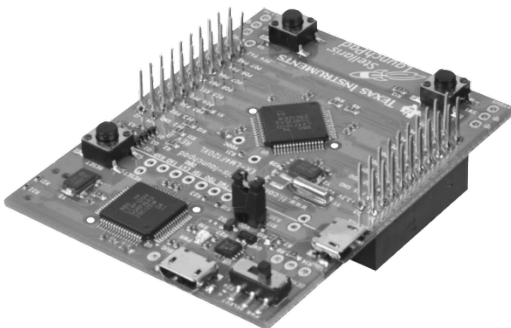


Fig. 5 Stellaris LM4F120 board

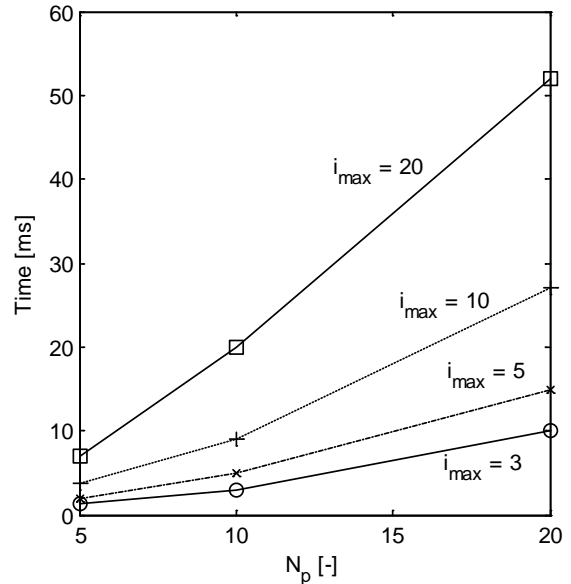


Fig. 6 Execution times for different values of i_{max}

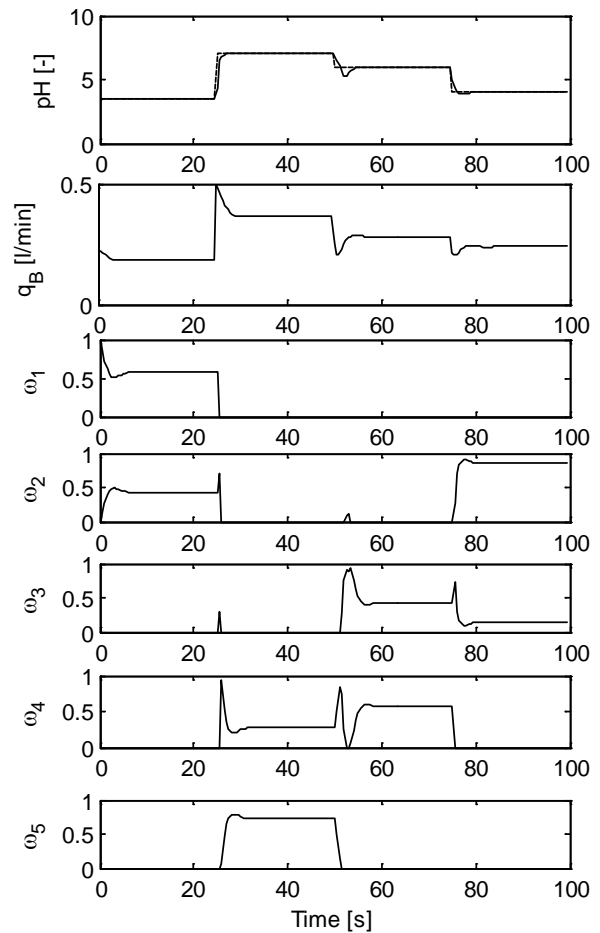


Fig. 7 Control courses for pH neutralization example

VI. CONCLUSION

In this work we consider fast online model predictive control with input constraints of nonlinear process represented by fuzzy model. The implementation aspects of the Fast Gradient algorithm and fuzzy MPC and its performance were illustrated by a benchmark example. Although the sampling frequency of the simulated process is in terms of second and the embedded system has much higher performance than required by the pH neutralization process, it allows to apply low-power techniques that would decrease the power consumption. The example also confirms that nonlinear process modeled as set of fuzzy linear models with the algorithmic and numerical simplicity of fast gradient methods allows fast online optimization for medium length of prediction horizon. With the development of cheap multi-core CPU in microcontrollers, the parallel computation might be the promising way for further decrease of computation time.

REFERENCES

- [1] S.J. Qin and B.J. Badgwell, "A survey of industrial model predictive control technology," in *Control Engineering Practice*, Vol. 11, 2003, pp. 733–764.
- [2] J.M. Maciejowski, *Predictive Control with Constraints*, Prentice Hall, 2000.
- [3] A. Alessio and A. Bemporad, "A Survey on Explicit Model Predictive Control," in *Nonlinear Model Predictive Control*, Vol. 384, 2009, pp.345-369.
- [4] Y. Wang and S. Boyd, "Fast Model Predictive Control Using Online Optimization," in *Proceedings of the 17th IFAC World Congress*, 2008.
- [5] M.S.K. Lau, S.P. Yue, K.V. Ling, and J.M. Maciejowski, "A comparison of interior point and active set methods for FPGA implementation of model predictive control" in *Proceeding of the European Control Conference*, 2009, pp. 156-161.
- [6] S. Richter, S. Mariethoz, and M. Morari, "High-speed online MPC based on a fast gradient method applied to power converter control" in *Proceedings of the 2010 American Control Conference*, 2010, pp. 4737–4743.
- [7] Y. Nesterov, "A method for solving a convex programming problem with convergence rate $1/k^2$," in *Soviet Math. Dokl.*, Vol. 27, no. 2, 1983, pp. 372–376.
- [8] S. Richter, C.N. Jones, and M. Morari, "Real-Time Input-Constrained MPC Using Fast Gradient Methods," in *Proceedings of the 48th IEEE Conference on Decision and Control*, 2009, pp. 7387-7393.
- [9] M. Kogel and R. Findeisen, "A fast gradient method for embedded linear predictive control," in *Proceedings of the 18th IFAC World Congress*, 2011, pp. 1362–1367.
- [10] P. Zometa, M. Kogel, T. Faulwasser, and R. Findeisen, "Implementation Aspects of Model Predictive Control for Embedded Systems," in *Proceeding of the American Control Conference*, 2012, pp. 1205-1210.
- [11] L.G. Bleris and M. V. Kothare, "Implementation of Model Predictive Control for Glucose Regulation on a General Purpose Microprocessor," in *Proceedings of the 44th IEEE Conference on Decision and Control*, 2005, pp. 5162-5168.
- [12] P.D. Vouzis, L.G. Bleris, M.G. Arnold, and M.V. Kothare, "A System-on-a-Chip Implementation for Embedded Real-Time Model Predictive Control," in *IEEE Transactions on Control Systems Technology*, Vol. 17, No. 5, 2009, pp. 1006-1017.
- [13] P. Dua, K. Kouramas, V. Dua, and E.N. Pistikopoulos, "MPC on a chip—Recent advances on the application of multi-parametric model-based control," in *Computers and Chemical Engineering*, Vol. 32, 2008, pp. 754-765.
- [14] J. Currie, A. Prince-Pike, and D.I. Wilson, "Auto-Code Generation for Fast Embedded Model Predictive Controllers," in *Proceedings of the International Conference on Mechatronics and Machine Vision in Practice*, Auckland, New Zealand, 2012, pp 122-128.
- [15] N. Li, S-Y. Li, and Y-G. Xi, "Multi-model predictive control based on the Takagi–Sugeno fuzzy models: a case study", in *Information Sciences*, Vol. 165 2004, pp. 247–263.
- [16] S.J. Wright, "Applying New Optimization Algorithms to Model Predictive Control", in *Chemical Process Control-V*, Vol. 93, 1997, pp. 147–155.
- [17] S.I. Biagiola and J.L. Figueroa, "State Estimation in Nonlinear Processes- Application to pH Process Control," in *Industrial & Engineering Chemical Research*, Vol. 41, 2003, pp. 4777-4785.
- [18] J. Novak and P. Chalupa, "Nonlinear State Estimation and Predictive Control of pH Neutralization Process," in *Advances in Intelligent Systems and Computing*, Vol. 210, 2013, pp 285-294.

Jakub Novak was born in Zlín, Czech Republic in 1978. He is a Researcher at Faculty of Applied Informatics of Tomas Bata University in Zlín, Czech Republic. He graduated from Faculty of Technology of the same university with an MSc in Automation and Control Engineering in 2002 and he received a PhD in Technical Cybernetics from Faculty of Applied Informatics in 2007. He is a researcher at the CEBIA-Tech research center at Tomas Bata University in Zlín. His research interests are modeling and predictive control of the nonlinear systems.

Petr Chalupa graduated in 1999 from Brno University of Technology and received the Ph.D. degree in Technical cybernetics from Tomas Bata University in Zlín in 2003.

He is a researcher at the CEBIA-Tech research center at Tomas Bata University in Zlín. His professional interests are adaptive and predictive control of real-time systems.

Analysis and web structures optimization

Zdenka Prokopova, Radek Silhavy, and Petr Silhavy

Abstract—The aim of the presented paper is to familiarize the reader with methods and techniques of web structures optimization. The main benefit of the work is description of analysis of existing non-optimized website, demonstration of the practical website optimization and testing and evaluation of optimized web structures. The work is focused on SEO search engine optimization. It is a method that helps online presentations and websites succeed in today's competitive world.

Keywords—Analysis, optimization, search engines, SEO, websites.

I. INTRODUCTION

NOWADAYS Nowadays it is very popular that every company or organization has its own websites. This trend has been developing for several years and therefore it is important to pay attention to it. With a number of websites increased a competition and a battle for first rungs in search results. It was necessary to begin to focus on the theme of how to optimize web structures. The main goal is to affect the placement of websites in search engines results. [1]

Generally, most visitors come to the websites just over search engines. For the reason that the search engines find our site, we have to inform them. One of relatively easy and fast way is to register our sites to the catalog link, which operates the most inland portals. Why register websites in some catalogs when they are separated from the search engines? A number of search robots as the first in its links hunt on the internet attending just these catalogs. The fact that most people coming to sites from search engines, we cannot generalize. More complex phrases are, however, less popular. Users prefer to search pages by scrolling through categories in the catalog. [2]

In contrast with full-text search engines in most catalogs we can buy display position. Search engines also offering the opportunity to visibility and display a link to your site, but for now there is a generally accepted custom that such paid sites are visually distinguished from the standard search results. Search engines are trying to present to its visitors especially

Z. Prokopova is with the Department of Computer and Communication Systems, Faculty of Applied Informatics, Tomas Bata University in Zlin, nam. T. G. Masaryka 5555, 760 01 Zlin, Czech Republic (corresponding author to provide phone: +420-57-6035011; e-mail: prokopova@fai.utb.cz).

R. Silhavy is with Department of Computer and Communication Systems, Faculty of Applied Informatics, Tomas Bata University in Zlin, nam. T. G. Masaryka 5555, 760 01 Zlin, Czech Republic (e-mail: rsilhavy@fai.utb.cz).

P. Silhavy is with Department of Computer and Communication Systems, Faculty of Applied Informatics, Tomas Bata University in Zlin, nam. T. G. Masaryka 5555, 760 01 Zlin, Czech Republic (e-mail: psilhavy@fai.utb.cz).

relevant results to their queries. On the contrary, catalog does not care about content of the site and de facto often does not know it. Catalog editors may sometimes go through the individual registrations, but often include references to its database automatically, without human control.

The goal of each website operator is to bring his own site to as many people as possible. Each visitor generates income. It is, for example, income from advertising or from sales of other services. Google (or Yahoo!) is trying to bring daily on their web-sites as many users as it is possible. And how this is accomplished? Just give users what they want - relevant search results. It is clear that on the problem of giving the most relevant answers, they are working "day and night". [3]

II. HOW SEARCH ENGINE WORKS

Let us focus, for example, on the very popular Google search engine. In the following overview you can find some of the many reasons, why Google is so popular. In addition, general facts about what Google offers with a brief list of the best known and most widely used services:

- Very fast and comprehensive full-text search engine – primarily are sites, that mediate responses to what we are looking for on the internet, divided into catalogs and search engines. There are two basic categories of search engines. Search engines from the first category are searching titles and descriptions of the sites and the content of the sites is not taken into account. The second category represents full-text search engines. They are searching the contents of websites and one of them is Google.
- Accuracy of results – despite the huge number of scanned pages Google will always return accurate results. There are results which contain the searched information. Google can be considered as one of the most successful search engine in terms of quality of results.
- No "annoying insect" (advertising) – in contrast with some of the other search engines Google does not offer paid links as a search results.

Google background consists of a server containing a list of URLs. Downloaded pages are sent to the storage server (warehouse). In the warehouse sites are compressed and stored in the depository. Each site receives a unique identification number, which is known as docId. The indexer and sorter take care about the inclusion in to the register (indexing). We could say that the indexer is the heart of search engines. Detailed description of its work can be found e.g. in [4].

A. Aspects affecting the location of website in search results

Search engines determine the placement of our website on the SERP (search engine result page) according to several criteria:

- The mutual positions of found words (searched for multiword phrases);
- Location of found words (position in the document);
- Location of a word or phrase in the page title, meta descriptions and titles;
- The page weight in the eyes of search engines (PageRank);
- The number of links on the sites, and the quality of those links.

1) Evaluation – PageRank (PR)

PageRank is an algorithm that shows authenticity of websites on a scale from 0-10. Display position in search results depends on the amount of PR. The authors of the original algorithm are former students at Stanford University, Lawrence Page and Sergey Brin the founders of Google. The algorithm is based on the Kandall-Wei evaluation theory from the fifties of the last century. The main idea of this theory is based on comparison of the importance of people and things based on their mutual influence. PageRank is the value of the credibility, i.e. how many pages simultaneously evaluated (using the same formula) refer to that page. PageRank is an important factor in determining the location of the site on the search engine result page (SERP). [1], [4]

2) SERP – search engine result page

SERP is an acronym, which we can sometimes meet on the pages dedicated to searching and search engine optimization. The main task of SEO is to get the best position in the SERP. The aim is to get the maximum number of relevant visitors - visitors who are interested in the information, products or services offered on our websites. [5]

III. SEO METHODS

SEO methods can be divided into two basic groups according ways of doing SEO. On-page SEO includes providing good content, good keyword selection etc. (on-page factors). Off-page SEO includes link building, link exchange etc. (off-page factors).

A. On-page SEO

On-page factors are factors that occur on one unique site. This means titles, headers, keywords, pure texts etc. The general rule in optimization is that every page on the optimized site must be unique. It is always important to keep in mind that search engines evaluate each page separately. So it is necessary to focus not only on the home page, it would be almost useless, but on all pages of the sites. [6]

1) Keywords

Keywords selection is the most important part of on-page SEO. If the site does not contain specific keyword, search engines cannot find it (except anchor text). If you are creating site from the beginning, just select the appropriate keywords

and distribute them well all over the site. Each page can be optimized for about 5-6 keywords. In the case of more competitive area is the number of keywords usually smaller (1-2). More detailed information we can find in [7].

2) Simplification of site navigation

Creation of file sitemap.xml is one of the way how to improve the position of site in the eyes of search engines. Using the sitemap we tell to the browser robot, which pages are on our site, and under what address there are.

The problem for a number of the authors is how to create a site map. Sitemap contains a list of pages in the form of XML structure. In addition, sitemaps contain their weight, date of last change and frequency of the page changes. Manual creation of such a list could be very frustrating or even impossible for very large sites. Curiously enough, a number of large sites do not have a sitemap for search engines. [8]

B. Off-page SEO

Off-page factors are connected with link building but not only that. Off-page SEO refers to activities outside the boundaries of the page e.g. social media (Facebook, twitter...), social bookmarking etc. It gives us a good indication on how other sites and users perceive our site.

Most popular off-page SEO method is link building. Links are like the streets between pages. Link building it's not only a matter of how many links are pointing to your site but it is more important from where these links are coming. [7]

IV. ANALYSIS OF THE EXISTING WEBSITE

The first step to good search engine optimization is the initial website analysis. It may be a current web presentation, which the company already has, but is not satisfied with it. We were asked for initial analysis of existing websites and their subsequent optimization by unnamed small manufacturing company. Initial analysis must be taken very seriously i.e. we cannot forget any important thing. The following sections briefly describe the shortcomings of the existing web server pages from the perspective of SEO optimization.

A. Analysis of index.html

When we look at the home page from the viewpoint of SEO optimization, we can find serious weaknesses on the very first and most important step. It can be found from the source code listing that missing basic meta tags as "descriptions" or "keywords". When we go on, we can find the most important tag <title>. The title tag in original source code of the index page is completely wrong. The main problem is the vague description which will not say the necessary information about the content of the website to the search robot.

B. Analysis of on-page factors

The next step will focus on analysis of the several on-page factors. For help we took application Seo Servis [9] that offers a very useful SEO tools such as source code analysis, keywords analysis, etc. The steps are divided into some subcategories.

1) Descriptive information and document header

The first point of analysis is descriptive information. This function lists all the important information such as title, description, keywords, robots info etc. We found that some items of the document header are filled, but the label of page (description) is not filled. As is written above, some search engines use the mentioned label in the search results, but it is not in all.

2) Source code

Clear and high-quality source code is also very important for good SEO optimization. Any text that appears on the page should be in paragraphs, headings and subheadings marked with the appropriate style. Images that are used must include an alternative description called "alt". If we write source code, we should avoid mixing semantic highlighting with physical formatting. All should be defined using CSS styles (avoid using labels). Very important is also to debug source code, to be free of errors and valid.

3) Content part

The last point in the analysis of on-page factors is part of the content. It is necessary to use keywords in headings and paragraphs of the text. Some search engines use tag , which is also good to use for each keyword.

C. Analysis using Google Analytics

Another very important step towards a good optimization is the analysis of the existing visitors of websites. Very powerful and useful tool is Google Analytics [10], which helped us determine e.g. how many visitors come to sites. After registration Google Analytics generates source code that must be inserted into each page that you want to monitor. In our case it was generated the following source code:

```
<script type="text/javascript">
var gaJsHost = (("https:" ==
document.location.protocol) ?
"https://ssl." : "http://www.");
document.write(unescape("%3Cscript src=' +
gaJsHost + "googleanalytics.
com/ga.js'
type='text/javascript'%3E%3C/script%3E"));
</script><script type="text/javascript">
try {var pageTracker = _gat._getTracker("UA-
10756895-2");
pageTracker._trackPageview();} catch(err) {}
</script>
```

Analysis by using Google Analytics started on 8th September 2013 and ended on 8th October 2013. During the analysis we found very interesting information about the existing websites which we have used in the preparation of new sites.

1) Analysis of access to web site

Analytics offers plenty of options to monitor a web-site. The most important factors are the total number of visitors and traffic sources overview. In the Table 1 (column "Before") you can find information received from the web server during the

measured time interval (30 days). The total number of websites visits for the test sample is 621 visitors. On average, there is about 15 visitors per day what is not very promising number. The bounce rate is about 57% what is on the other hand side a very high value. This number indicates that the visitor leaves the site from the main page. Average time on site (1:15 min) is sufficient, but the value should be larger. According to these indicators we can determine the poor quality of the website.

V. PRACTICAL WEBSITE OPTIMIZATION

Please note that the references at the end of this document are in the preferred referencing style. Give all authors' names; do not use "et al." unless there are six authors or more. Use a space after authors' initials. Papers that have not been published should be cited as "unpublished" [4]. Papers that have been submitted for publication should be cited as "submitted for publication" [5]. Papers that have been accepted for publication, but not yet specified for an issue should be cited as "to be published" [6]. Please give affiliations and addresses for private communications [7].

Capitalize only the first word in a paper title, except for proper nouns and element symbols. For papers published in translation journals, please give the English citation first, followed by the original foreign-language citation [8].

A. Index.php

The landing page is usually considered to be the most important page, because the user enters it mostly directly from search engines. Therefore, it is important to pay close attention to the landing page.

B. Meta tags

It is always better to use different descriptions and keywords on different pages. To search tips for new keywords we used a KeywordPlanner [11]. It is a tool which could help us with creating the best positioned websites.

C. Captions and headings

Title to be inserted into a website is very important. It should contain the keywords should not be overly long and mainly must be listed.

D. Optimization of subpages

It is important to stick to the strict rules for other pages and check for theirs SEO on-page factors. The most important factor is compliance with quality content and strict rules for optimization.

E. Structure of URL addresses

We assume that a well-structured and understandable address easily guide users to the page content. For users who want to refer to our website is a good idea to create a simpler URL address. The best way how to create a sitemap file is to download the special program (e.g. Sitemap Generator).

F. Quality content and useful services

The most important factor in terms of both users and search engines are high-quality content and provided services.

Appealing to users is the use of new useful services which no other comparable web offers. For users we created e.g. a service to compare indicators of price / performance ratio for the selected item.

G. Websites propagation

An important way to inform visitors about the new websites is to promote them on the appropriate fora. We decided to promote new websites on social networks (facebook, twitter...) and user’s blogs. The results of this promotion appeared later (after several months).

VI. TESTING AND EVALUATION OF OPTIMIZATION

To evaluate the optimization of pages, we again used the Google Analytics application (from 15th November 2013 to 15th December 2013). In addition, Google offers another tool called Website Optimizer [12] where you can experiment with your site and find what will work and what will not work. In Table I we can see the positive development of websites after optimization. It is noticeable increase in number of visits and greatly reduced bounce rate, which is very important. We must also note that increased average time on site and percentages of access from the search engines.

Table I Comparison of website development before and after optimization

	Before	After
Number of visits	621	964
Pages viewing	1548	5976
The bounce rate	59,63%	20,22%
Average time on site	1:15	2:39
Access from referring sites	46,17%	42,33%
Access from search engines	31,95%	45,70%
Direct visits	22,88%	10,55%

Since it takes several days or weeks until all search engines “reindex” theirs site content, it is clear that the keywords will have small representation yet. In the first case, indexes landing page index.php. Landing page is dominant and search engines take it as the highest authority.

On Fig. 1 we can see that the largest share of search engines has Seznam.cz (local search engine) – 71.35%. Right behind him is a search engine Google with 26.21%. There are also smaller full-text search engines like Bing and Search.

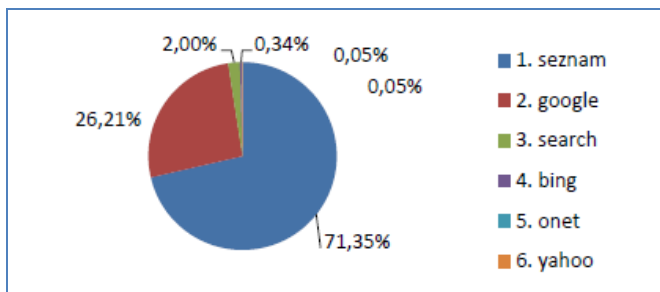


Fig. 1 Percentage distribution of various search engines

VII. CONCLUSION

The aim of the work was to propose a new structure of web sites in complying with the rules for SEO optimization. First, were analyzed all the websites factors which play a role in optimization. It was found that websites do not satisfy the basic conditions for a good search. Design of a new web sites structure was based on the per-formed analysis. The individual parts were optimized separately with the help of Website Optimizer. The aim was to reduce the bounce rate as low as possible, which succeeded. It was also necessary to increase the percentage representation of approach from search engines. Already the value increased from 31.95% to 45.70%. Individual sites were optimized by the most appropriate keywords and then tested in the search engines. Most of the results ranged from 1st to 10th places, what is the first page in the resulting search (users in most cases say that they are looking at the first maximum second page). From the test results it is apparent that e.g. optimization helped to reduce the bounce rate (the number of site exits) from 59.63% to 20.22%. When we look at the work from a global perspective, it is clear that the optimization was successful and the newly designed websites are more searchable.

REFERENCES

- [1] B. Croft, D. Metzler, T. Strohman, *Search Engines: Information Retrieval in Practice*, Addison-Wesley; pp. 552, (2009), ISBN: 978-0136072249.
- [2] J. Grappone, G. Couzin, *Search Engine Optimization: An Hour a Day*, Sybex, pp. 432, (2011), ISBN: 978-0470902592.
- [3] D. Dover, E.Dafforn, *Search Engine Optimization Secrets*, Wiley, pp. 141, (2011), ISBN: 978-0470554180.
- [4] P. Kent, *Search Engine Optimization For Dummies, For Dummies*, Wiley, pp. 456, (2012), ISBN: 978-1118336854.
- [5] M. H. Fleischner, *SEO Made Simple: Strategies for Dominating the World's Largest Search Engine*, CreateSpace Independent Publishing Platform, pp. 158, (2013), ISBN: 978-1481838061.
- [6] R. L. Adams, *SEO Simplified: Learn Search Engine Optimization Strategies and Principles for Beginners*, CreateSpace Independent Publishing Platform, pp. 100, (2013), ISBN: 978-1484831007.
- [7] R. L. Adams, *SEO White Book: The Organic Guide to Google Search Engine Optimization*, CreateSpace Independent Publishing Platform, pp. 114, (2013), ISBN: 978-1484815083.
- [8] R. L. Adams, *SEO Black Book: A Guide to the Search Engine Optimization Industry's Secrets*, CreateSpace Independent Publishing Platform, pp. 176, (2013), ISBN: 978-1482665161.
- [9] Seo Servis. Available : <http://seo-servis.cz>.
- [10] Google Analytics. Available : <https://www.google.com/analytics/web>
- [11] Keyword Planner Google AdWords. Available : <https://adwords.google.com/ko/KeywordPlanner>.
- [12] Google Website Optimizer. Available : <https://services.google.com/webstioptimizer>.

Zdenka Prokopova was born in Rimavska Sobota, Slovak Republic in 1965. She graduated from Slovak Technical University in 1988, with a master’s degree in automatic control theory. She has received in technical cybernetics doctor’s degree in 1993 from the same university. She worked as assistant at Slovak Technical University from 1988 to 1993. During years 1993-1995 she worked as programmer of database systems in Datalock business firm. From 1995 to 2000 she worked on position lecturer at Brno University of Technology. Since 2001 she has been at Tomas Bata University in Zlin, Faculty of Applied Informatics. She presently holds the position of associating professor at the Department of Computer and Communication Systems.

Her research activities include programming and application of database systems, mathematical modeling, computer simulation and control of technological systems.

Radek Silhavy was born in Vsetin in 1980. He received a B.Sc. (2004), M.Sc. (2006), and Ph.D. (2009) in engineering informatics from Faculty of Applied Informatics, Tomas Bata University in Zlin.

He is a senior lecturer and researcher at the Computer and Communication Systems Department.

His Ph.D. research was on the verification of the distributed schema for the electronic voting system. Major research interests are software engineering, empirical software engineering and system engineering.

Petr Silhavy was born in Vsetin in 1980. He received a B.Sc. (2004), M.Sc. (2006), and Ph.D. (2009) in engineering informatics from Faculty of Applied Informatics, Tomas Bata University in Zlin.

He is a senior lecturer and researcher at the Computer and Communication Systems Department.

His Ph.D. research was on the electronic communication and services in medical information systems. Major research interests are data mining, database systems and web-based services.

Artificial intelligence systems for knowledge management in e-health: the study of intelligent software agents.

M. Furmankiewicz, A. Sołtysik-Piorunkiewicz, and P. Ziuziański

Abstract— In this paper, authors describe the state of art of e-health artificial intelligence systems and describe and compare the features of the multi-agent systems in e-health. The study is based on theoretical models of multi-agent systems for knowledge management in organization: information allocation, the presence of authorities, organizational norms and culture, motivating. Authors divided the e-health multi-agent systems due to the areas of supported knowledge management in e-health.

Keywords— agent technology, artificial intelligence, e-health, expert systems

I. INTRODUCTION

Artificial intelligence, which is regarded as a scientific discipline, has emerged after the introduction of the first computers. Those were ascribed to the skills characteristic of intelligent beings, including proving hypotheses, concluding, and games playmaking [1]. Currently, the concept of the artificial intelligence is understood as a branch of IT, whose subject is the study of the rules governing the so-called intelligent human activities, and the creation of formal models of these behaviours, which in turn leads to the creation of computer programs that will simulate these behaviours. The above mentioned intelligent behaviours are [2]:

- 1) perception,
- 2) learning,
- 3) recognition,
- 4) usage of language,
- 5) symbol manipulation,
- 6) creativity,

This work was supported in part by the U.S. Department of Commerce under Grant BS123456 (sponsor and financial support acknowledgment goes here). Paper titles should be written in uppercase and lowercase letters, not all uppercase. Avoid writing long formulas with subscripts in the title; short formulas that identify the elements are fine (e.g., "Nd-Fe-B"). Do not write "(Invited)" in the title. Full names of authors are preferred in the author field, but are not required. Put a space between authors' initials.

F. A. Author is with the National Institute of Standards and Technology, Boulder, CO 80305 USA (corresponding author to provide phone: 303-555-5555; fax: 303-555-5555; e-mail: author@boulder.nist.gov).

S. B. Author, Jr., was with Rice University, Houston, TX 77005 USA. He is now with the Department of Physics, Colorado State University, Fort Collins, CO 80523 USA (e-mail: author@lamar.colostate.edu).

T. C. Author is with the Electrical Engineering Department, University of Colorado, Boulder, CO 80309 USA, on leave from the National Research Institute for Metals, Tsukuba, Japan (e-mail: author@nrim.go.jp).

- 7) solving problems.

Computer programs are used both for experimental and practical purposes, such as [2]:

- 1) sounds recognition (speech),
- 2) recognition of shapes (letters, drawings, photographs),
- 3) theorem proving,
- 4) running games (chess),
- 5) translation from one natural language to another,
- 6) music composition,
- 7) formulation of medical diagnoses,
- 8) expertise formulation.

II. ARTIFICIAL INTELLIGENCE

The notion "artificial intelligence" was suggested in 1956 by John McCarthy (Massachusetts Institute of Technology) as the subject of a conference in Dartmouth [3]. The aim of the conference was to summarize and intensify further research on "thinking machines". The conference was a success - after this event the work on projects that concern the field of artificial intelligence was greatly intensified. The concept of artificial intelligence cannot be precisely defined. One can find many definitions of artificial intelligence in the literature [5]. Nevertheless, it is worth mentioning the first definition of artificial intelligence, which was introduced by John McCarthy: "(...) the construction of the machines, which can be said to be similar to the human manifestations of intelligence" [4].

Definitions, which appeared later, can be divided into four categories, taking into account two main criteria. One group of the definitions refers to the process of thinking and reasoning, while others take into account the behavioural factor (called behaviour). The second distinction between the definition of artificial intelligence takes into account the category of success. The examples of the definitions referred to in the various categories were presented in Figure 1.

One can distinguish two different approaches to artificial intelligence. The first of these, referred to as weak AI (Artificial Intelligence) assume that the computer allows you to formulate and test specific hypotheses concerning the brain [2]. The second approach, named strong artificial intelligence extends much more radical claims about AI. Followers of strong AI believe that a properly programmed computer is not only a model of brain but a brain as such [5].

The history of artificial intelligence as a field of study is

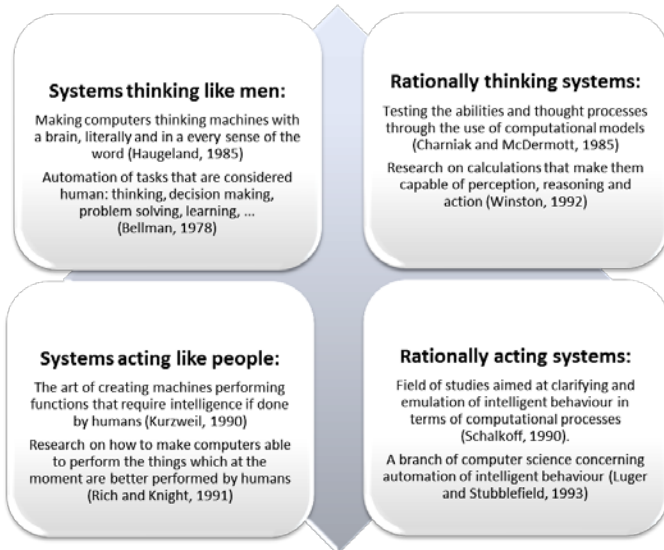


Fig. 1 Organization of the artificial intelligence definitions into four categories

very interesting. The origins of modern artificial intelligence can be traced to 1943, when McCulloch and Pitts proposed the neural network architecture to create intelligence. Seven years later, in 1950, A. Turing proposed the “intelligence test“ [4]. Another, important date in this field is year 1955, when Allen Newell and Herbert Simon developed “The Logic Theorist” to solve mathematical problems. For a lot of people just “The Logic Theorist” is considered to be the first program of AI. Another date remembered in a history of the development of artificial intelligence is the year 1958. In that year, John McCarthy developed a language that fulfils its role in tasks in the field of AI - LISP (LIST Processing). It is worth noting that LISP is still used today. In 1966, he created a program called ELIZA. The author of a computer system, which plays the role of a psychotherapist and that can lead the conversation with the “patient” is J. Weizenbaum. In the 70s, the works on artificial intelligence led to the creation of Expert Systems. However, before this, the language PROLOG had been created. It had a built-in mechanism of inference. This language was suitable for the creation of expert systems. The inventor of the PROLOG language is Colmerauer. In 1971, the work on the project DENDRAL was finished. This system was the prototype of all expert systems. The next system is MYCIN, whose creator is Edward Shortliffe. The purpose of the MYCIN system is a diagnosis of bacterial blood infections, as well as putting forward the proposition of a drug therapy. Both systems were created at Stanford. The 80s brought about a huge change, because corporations have recognized the possibility of using artificial intelligence. In the USA, in 1986 only, sales of software and hardware related to the artificial intelligence amounted to 425 million dollars. In the 80s, expert systems were created on request [6].

Works on artificial intelligence resulted in many significant results, which have already found practical applications.

Regardless of the purposes of a long-term field, which is artificial intelligence, specialists in this field deal with specific problems. Today, the key issues of artificial intelligence are presented in Figure 2.

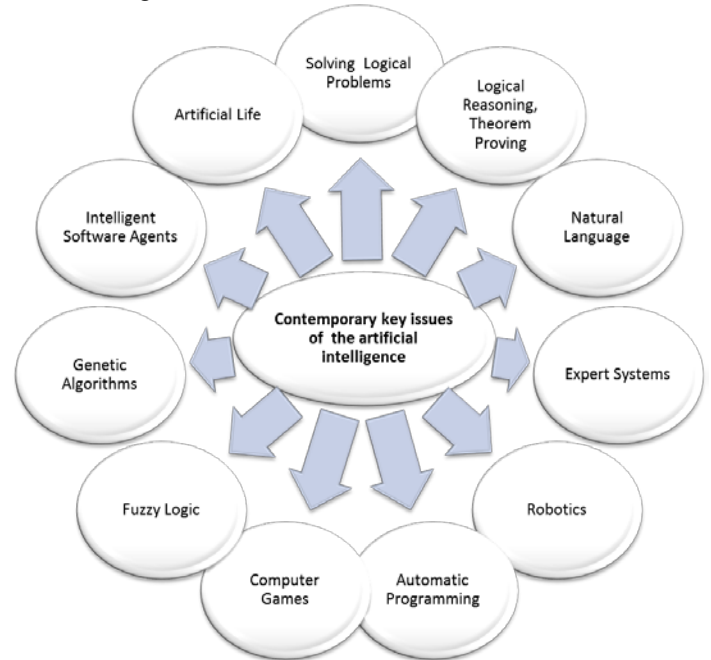


Fig. 2 Contemporary key issues of artificial intelligence

The types of logical problems addressed to the artificial intelligence include logic games and logic puzzles. They are a good area to test experimental methods of reasoning and problem solving. The techniques of planning and anticipation in properly defined situations that occur in board games are already well advanced. Computer programs achieve brilliant results in logical games. In 1994, a computer program defeated the world chess master [4].

In turn, logical reasoning and theorem proving are relatively easy type of reasoning. This is the reasoning, which the human mind is capable of [4].

In contrast, robotics, computer vision, recognition of shapes, images and characteristics of the individual subjects are associated with building robots. Computer programs that are designed to manipulate the robotic limbs must both solve optimization problems of movement and plan a sequence of actions that will enable to achieve the target [4].

Automatic programming allows to automatically generate computer programs (such as the description of the algorithm in natural language). However, to make this possible, automatic programming requires some elements of intelligent behaviour. These elements include: understanding the description, selection the guide, and actions planning [4].

Computer games can be considered as one of the first areas of artificial intelligence research. With a relatively easy evaluation of the results, computer games can be considered a great area to test new heuristics and strategies. The previously mentioned successful chess games are the best proof that confirms the tremendous growth in the field of artificial

intelligence. In addition to the described example of the use of artificial intelligence in logical games, artificial intelligence is used in video games (e.g. to control the movements and behaviour of the characters) [4].

The fuzzy logic means technology that is used for the processing of linguistic terms. It extends the binary notation of logic (true / false, yes / no) for a partial, even a continuous function of the truth. Technologies using fuzzy logic are used in expert systems that have their application in conditions of imprecise knowledge [4].

The creator of genetic algorithms is J.H. Holland. The name “genetic algorithms” is derived from the way the solutions are searched for. This method resembles the mixing and selection of genes during evolution [7]. Algorithms are looking for more and better results on the principle of natural selection and heredity. Genetic algorithms are thus a form of research, which is based on a process of natural selection and genetics [8].

Intelligent Software Agents are small software programs that perform certain tasks previously defined in an automated manner. A characteristic feature of Intelligent Software Agents is the fact that they operate in the background, monitoring the tested environment and reacting to the certain triggered conditions. One of the best examples of agents are anti-virus programs. They remain in the computer memory while scanning the incoming data. When they find a virus, they alert the user of the danger or automatically remove dangerous files [4].

Artificial Life (also called Alife) is a relatively new field of artificial intelligence, the aim of which is to study the “natural” life by attempting to recreate the biological phenomena by computer systems.

The most visible effects of research on artificial intelligence are expert systems. They contain a knowledge base and inference mechanisms that allow both to ask questions in natural language and receive a reply in the same language. Expert systems are created by the knowledge engineers, or experts in the specific fields of knowledge. Knowledge engineers are responsible both for the acquisition of knowledge from experts and gathering it in the knowledge base as well as for its verification. Expert systems solve problems in a narrow and well-defined area [4].

III. EXPERT SYSTEMS IN MEDICINE

Artificial intelligence is used in many areas in business and science. One of the first area where AI was applied was medical diagnosis. In this area the largest impact has got expert systems. Expert systems are AI tools which gained recognition both commercial and individual users. There are two expert systems classes [4]:

- 1) large one built by corporations for commercial or their own aims,
- 2) small one built to work on individual computers used to solve problems.

Expert system is a computer program which uses

“knowledge base“ to perform tasks in many categories (for example medical diagnosis) [9].

An exemplary expert system architecture includes: knowledge base, fact database, explanation system, knowledge base editor and user interface. Communication between mentioned elements is shown in Figure 3 [10].

There is special, separated area named expert system shell in expert system. Elements of this area do not contain specific information. Expert system shell therefore is general toolkit which can be used to build many different expert systems. Domain of this system is dependent on added knowledge base to the shell [10].

Knowledge base stores domain knowledge to resolve

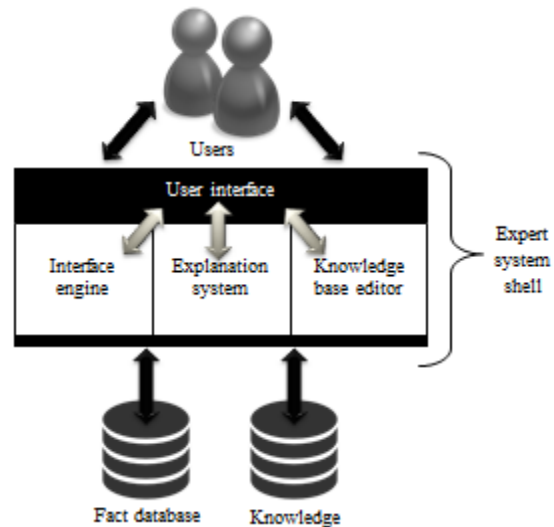


Fig. 3 Architecture of an expert system

problem and derive conclusion based on facts. This knowledge is represented in the form of number of rules. The fact database includes characteristic data for particular case used to derive a conclusion. For example medical experts system fact table could contain pieces of information obtained about the patient’s condition. Role of explanation system is delivering information for user how the inference engine found conclusion. It is relevant especially if expert system user should examine the data provided by the explanation system (for example medical issues) [10].

Communication between system and user takes place through user interface which supplies access to explanation system, inference engine and knowledge-base editor. Thanks to the last one expert knowledge engineer has the possibility to edit information in knowledge base. However the inference engine as a part of the system delivering conclusions based on rules and facts uses one of following methods (or combination of them) [12], [9]:

- 1) forward chaining (data-driven reasoning)– reasoning from set of facts and rules to the conclusion (goal),
- 2) backward chaining (goal-driven reasoning) – starts from the goal back to the starting premises.

As authors pointed earlier, medicine was one of the first area which expert systems were applied. Probably the most popular early expert system connected with medicine was MYCIN [11]. This project started in 1972 and its main aim was diagnosing infectious blood diseases thanks to about 450 implemented rules [12]. Figure 4 includes review of expert systems uses in the medicine. Most important growth of expert systems was in the last century 70's in United States of America [11], [13], [14].

Nowadays expert systems in medicine are used by doctors to support with hard to diagnose symptoms. Moreover experts systems are used to help prescribing treatments when even specialists have difficulties [10].

Simple expert systems using for self-treatment and auto

Name	Year(s)	Place	Description
AAPHHELP	1972	Leeds University (West Yorkshire, England)	Supporting the diagnosis of acute abdominal pain, based on analysis, and need for surgery; using naive Bayesian approach.
INTERNIST I	1974	University of Pittsburgh (Pennsylvania, United States)	Recognizing the complex diagnosis problems in general internal medicine.
MYCIN	1976	Stanford University (California, United States)	Diagnosing and recommend treatment for infectious blood diseases.
EMYCIN	1980	Stanford University (California, United States)	EMYCIN (Essential MYCIN) – Expert system shell, employing MYCIN's control structures.
CASNET/ GLAUCOMA	1960s	Rutgers University (New Jersey, United States)	CASNET (Causal ASsociational NETworks) – expert system building tool dedicated to diagnose and treat diseases; CASNET/Glaucoma – expert system based on CASNET for the glaucoma.
PIP	1970s	Massachusetts Institute of Technology in Cambridge (MIT) and Tufts-New England Medical Center in Boston (Massachusetts, United States)	PIP (Present Illness Program) – generating hypotheses based on gathered data from patients about renal disease.
ABEL	early 1980s	Laboratory for Computer Science, MIT	Causal reasoning, management of electrolyte and acid base derangements
ONCOCIN	1981	Stanford University (California, United States)	Helping physicians in treatment of cancer patients receiving chemotherapy
DXPLAIN	1984	Laboratory of Computer Science, Massachusetts General Hospital, Harvard Medical School in Boston (Massachusetts, United States)	DSS using clinical findings (for example symptoms, laboratory data) to perform ranked list of diagnoses which might be explained.
QMR (Quick Medical Reference)	1980	University of Pittsburgh (Pennsylvania, United States) and First Databank in San Francisco (California, United States)	DSS with knowledge base containing about 700 diseases and more than 5,000 symptoms, signs, and labs.

Fig. 4 Examples of medical expert systems and decision support systems

diagnosis are available on mobile devices and computer connected to Internet. For example there is an application on mobile devices called WebMD Symptom Checker for Android, iPhone and iPad. The application give their users the

opportunity to diagnose and treat themselves [15]. Figure 5 presents graphical user interface of this application.

Similar to WebMD Symptom Checker is for example



Fig. 5 WebMD Symptom Checker

website <http://www.dooktor.pl/diagnoza>. User entering symptoms has ability to find out possible disease [16].

IV. AGENT TECHNOLOGY IN E-HEALTH

Lately one of the most important area of research Artificial Intelligence became agent technology. At present applying it in healthcare is very interesting topic [17].

An agent is an entity capable of performing some tasks and help human user in that way. Agents can be biologic (for example people), computational (software agents) or robotic. Software agents could be defines as a computer program that aim is carrying out some task on behalf of a user. The most important properties of agents are: intelligence, autonomy, cooperation and ability to learn. [10]

Combined agents into one systems is named multiagent system and it could be very powerful tool. Characteristic in multiagent systems are those statements [10]:

- 1) each agent dispose not complete information that is why agent is not capable to solve entire problem on its own,
- 2) only combined agents can solve problem,
- 3) system do not use any centralized mechanism for solving problem .

Main aim of agents is observing knowledge base in current situation context and supporting in process of making decision on action by experts in their domain. The last step is executing that action on the environment [17].

Agents are often confused with expert systems. This results from the fact that those two entities have knowledge base. Basic difference between them is how they use knowledge base. Experts systems use logic in every situations, while agents act more like people: more important is to find result and accept some level of its probability than find perfect result [9].

V. STUDY OF KNOWLEDGE MANAGEMENT IN E-HEALTH MULTI-AGENT SYSTEMS

There is a diversity of areas in medical industry and health care systems that could benefit from systems based on agent technology (especially MAS) [17]:

- systems diagnosing diseases,
 - systems that recommend treatment,
 - patient history examination systems,
- the support of palliative care units.

One of the examples of agent using in e-health is HealthAgents. This support system is based on multi-agent technology and designed for diagnosing and forecasting brain tumors. Other example is SAPHIRE that is multi-agent system for monitoring remote healthcare through electronic clinical guidelines [17]. The examples using multi-agent systems in e-health is presented in figure 6 [17], [18], [19], [20], [21] in four areas:

1. Assistive living application,
2. Diagnosis,
3. Physical telemonitoring,
4. Smart-hospital, and smart-emergency application.

The study of knowledge management in e-health multi-agent systems is based on some criteria about knowledge that an agent should have:

- 1) knowledge about the user,
- 2) knowledge of the presented problem,
- 3) contextual knowledge about the course of the conversation,
- 4) knowledge of the organization

The study shows what kind of knowledge could be managed by the e-health system in the area of models of agent supported organizations [22]:

- information allocation,
- the presence of authorities,
- organizational norms and culture,
- motivating.

Information allocation in an agent model refers to the way information flows between the organization and its environment, and additionally the influence of the information on the organization, using a software agent, i.e. which agent and where is responsible for the information flow between the organization and the environment. The study shows that there are some examples of MAS:

- for knowledge management about the patient: K4CARE, U-R-SAFE, MyHeart,
- for knowledge of the presented medical problem: OHDS, HealthAgents,
- for contextual knowledge about the course of the conversation: CASIS, AID-N.

Area	Name	Description
Assistive Living Applications	CASIS Context-Aware Service Interaction System	Supplying context-aware healthcare services to the elderly resident in the intelligent space.
	K4CARE (2006)	Project combining healthcare and ICT experiences to develop, apply, and validate a knowledge-based healthcare model for assistance to patients living at home (elderly, the disabled persons, and the patients with chronic diseases).
Diagnosis	IHKA Intelligent Healthcare Knowledge Assistant	Healthcare knowledge procurement system based on six agent types for dynamic knowledge gathering, filtering, adaptation and acquisition from a healthcare enterprise memory.
	OHDS Ontology based Holonic Diagnostic System	System supporting doctors in the diagnostic and treatment, and overseeing processes of the evolution of new epidemics. System is based on the exploration of all data pertinent to each case and on the scientific data contained in various professional databases
	HealthAgents	Research project with the goal of improving the classification of brain tumours distributed network of local databases.
Physical Telemonitoring	MobiHealth	The main goal of it is telemonitoring of patients at home by monitoring, storage and transmission of vital signs data coming from the patient body are network (BAN).
	U-R-SAFE Universal Remote Signal Acquisition For hEalth	Research project with the goal of realizing a telemonitoring environment for elderly people and patients with chronic diseases.
	AID-N Advanced Health and Disaster Aid Network	Light-weight wireless medical system for efficiently gather and distribute information on the vital signs and locations of patients.
	MyHeart	Research project whose focus was on preventing cardiovascular diseases using sensors integrated in clothing to monitor heart activity.
	SAPHIRE	Research project whose goal was monitoring of chronic diseases both at hospital and at home using a semantic infrastructure.
Smart-Hospital, Smart-Emergency Applications	ERMA Emergency Medical Assistant	The main aim of ERMA was providing meaningful diagnoses and intervention suggestions to the healthcare team acting on behalf of the patient in the cases of emergency trauma with particular emphasis on types of shock and stabilization of arterial blood cases.
	Akogrimo	Research project whose main goal is the integration of the next generation Grids with the next generation networks.
	CASCOM Context-Aware Health-Care Service Coordination in Mobile Computing Environments	The main aim of project is to implement, validate, and trial a value-added supportive infrastructure for Semantic Web based business application services across mobile and fixed networks.

Fig. 6 Examples of multi-agent systems

The participation of agents as a authorities in a decision-making process relies on two features: modularity and decentralization. Modularity refers to a system-centric approach to management where a given process can be performed in several sub-processes, and these sub-processes can be performed by appropriate tasks, and as part of these

tasks certain operations can be conducted. Thus the problem that arises here is connected with the types of operations, tasks and sub-processes within a given process, what actions should be taken in a given module and possibilities of potential linkage of similar actions. The aspect of modularity is closely connected with decentralization, i.e. which agent is responsible at a given level for performing a given task. The research study shows that there are some examples of such a model of multi-agent systems:

- for knowledge of the presented medical problem: IHKA,
- for contextual knowledge about the course of the conversation: CASCOM,
- for knowledge of the health organization: ERMA

The third aspect of an agent-supported organization is connected with organizational culture. Referring to Sathe's definition of organizational culture we can assume that an agent's behavior depends on the organization's historical factors which are contained in the organization's norms and culture [24]. The study shows only two examples:

- for contextual knowledge about the course of the conversation: Akogrimo,
- for knowledge of the health organization: SAPHIRE.

The next aspect discussed in the literature is the sphere of motivation of the entity performing individual tasks within the framework of the processes run. In such a case, human factor can be subjected to various influences which in the case of the use of agent-based solutions come down to a certain decision imperative of an agent. In this aspect there is only one MAS:

- for knowledge management about the patient: MobiHealth.

The summary of study shows the table 1.

Table 1 Matrix of agent supported organizations models with the agent features in knowledge management e-health systems

Agent supported organizations model	Agent management functionality in e-health system			
	knowledge about the patient	knowledge of the presented medical problem	contextual knowledge about the course of the conversation	knowledge of the health organization
1. Information allocation	K4CARE U-R-SAFE MyHeart	OHDS HealthAgents	CASIS AID-N	-
2. The presence of authorities	-	IHKA	CASCOM	ERMA
3. Organizational norms and culture	-	-	Akogrimo	SAPHIRE
4. Motivating	MobiHealth	-	-	-

I. CONCLUSION

The features of the agent functionality in knowledge management e-health systems are divided in four areas. The results of the study shows the following groups e-health MAS: (1) knowledge about the patient: K4CARE, U-R-SAFE, MyHeart, MobiHealth, (2) knowledge of the presented medical problem: OHDS, HealthAgents, IHKA, (3) contextual knowledge about the course of the conversation: CASIS, AID-

N, CASCOM, Akogrimo and (4) knowledge of the health organization: ERMA, SAPHIRE. The future research will find the features of usability aspect of MAS for knowledge management in e-health organization.

REFERENCES

- [1] M. Białko, *Sztuczna inteligencja i elementy hybrydowych systemów ekspertowych*. Koszalin: Wydawnictwo Uczelniane Politechniki Koszalińskiej, 2005, p. 15.
- [2] H. Sroka, W. Wolny, Ed., *Inteligentne systemy wspomaganie decyzji*. Katowice: Wydawnictwo Akademii Ekonomicznej w Katowicach, 2009, pp.: 164, 166, 171 -173.
- [3] M. L. Owoc, "Pojęcie i struktura sztucznej inteligencji" in *Elementy systemów ekspertowych. Część I, Sztuczna inteligencja i systemy ekspertowe*, M.L. Owoc, Ed. Wrocław: Wydawnictwo Akademii Ekonomicznej im. Oskara Langego we Wrocławiu, 2006, p. 35.
- [4] H. Kwaśnicka, *Sztuczna inteligencja i systemy ekspertowe: rozwój, perspektywy*. Wrocław: Wydawnictwo Wyższej Szkoły Zarządzania i Finansów we Wrocławiu, 2005, pp.: 14, 45.
- [5] M. Flasiński, *Wstęp do sztucznej inteligencji*. Warszawa: Wydawnictwo Naukowe PWN, 2011, p. 242.
- [6] M. Furmankiewicz, *Zastosowanie sztucznej inteligencji w systemach ekspertowych*. Katowice, 2012, pp. 11-14.
- [7] Algorytmy genetyczne. [Online] Available: <http://www.algorytm.org/kurs-algorytmiki/algorytmy-genetyczne.html>
- [8] M. Kalita , J. Stasienko, "Algorytmy genetyczne" in *Sztuczna inteligencja i metody optymalizacji - od teorii do praktyki*, W. Wójcik, Ed. Lublin: Polskie Towarzystwo Informatyczne, 2008, p. 26.
- [9] H. Henderson, *Artificial Intelligence - Mirrors for the Mind*, New York: Chelsea House, 2007, pp.: 74, 108, 171.
- [10] B. Coppin, *Artificial Intelligence Illuminated*, Sudbury: Jones and Bartlett Publishers Inc., 2004, pp: 23, 73, 252-253, 543-546, 554.
- [11] V. S. Jadhav, A. A. Sattikar, "REVIEW of Application of Expert Systems in the Medicine," in *Proc. National Conference on Innovations in IT and Management* , Pune, 2014, pp. 122-124.
- [12] M. Negnevitsky, *Artificial Intelligence A Guide to Intelligent Systems*, Harlow: Addison-Wesley, 2005, pp. 8-10, 37-39.
- [13] E. H. Shortliffe, A. C. Scott, M. B. Bischoff, A. B. Campbell, W. Van Melle, C. D. Jacobs, "ONCOCIN: An expert system for oncology protocol management," in *Proc. 7th Int. Joint Conf. on Artificial Intelligence*, Vancouver, 1981, p. 876.
- [14] DXplain. [Online] Available: <http://lcs.mgh.harvard.edu/projects/dxplain.html>
- [15] WebMD for Android, iPhone & iPad. [Online] Available: <http://www.webmd.com/webmdapp3>
- [16] Diagnostyka On-line . [Online] Available: <http://www.dooktor.pl/diagnoza>
- [17] U. Cortés, R. Annicchiarico, C. Urdiales, "Agents and Healthcare: Usability and Acceptance," in *Agent Technology and e-Health*, R. Annicchiarico, U.C. Garcia, C. Urdiales, Ed. Basel: Birhauser Verlag, 2008, pp. 1-3.
- [18] F. Bergenti, A. Poggi (2009), "Multi-Agent Systems for E-health: Recent Projects and Initiatives," in *Proc. 10th International Workshop on Objects and Agents*, Rimini, 2009.
- [19] K4CARE. [Online] Available: <http://www.k4care.net/>
- [20] U-R-SAFE. [Online] Available: <http://ursafe.tesa.prd.fr/ursafe/new/description.html>
- [21] M. Peleg, T. Broens, A. González-Ferrer, E. Shalom (2013), *Architecture for a Ubiquitous Context-aware Clinical Guidance System for Patients and Care Providers, Knowledge Representation for Health Care and Process-oriented Information Systems in Healthcare*. KR4HC'13 / ProHealth'13, Murcia, Spain, 2013, <http://www.mobihealth.com/research/submission-KR4HC2013-final-2.pdf>.
- [22] A. Sołtysik-Piorunkiewicz, M. Żytniewski (2013), *Software agent societies for process management in knowledge-based organization*. ECKM 2013, ACPI, Edited by B. Janiūnaitė, A. Pundziene 2013.

Simulation of time-continuous chaotic systems for the generating of random numbers

Roman Senkerik, Michal Pluhacek, and Zuzana Kominkova Oplatkova

Abstract— This paper investigates the utilization of the time-continuous chaotic system as the chaotic pseudo random number generators. (CPRNGs) Several selected chaotic oscillators are simulated, statistically analyzed and compared within this initial research study.

Keywords—Evolutionary algorithms; Differential evolution; Chaos; Chaotic Oscillators, PRNG

I. INTRODUCTION

GENERALLY speaking, the term “chaos” can denote anything that cannot be predicted deterministically. In the case that the word “chaos” is combined with an attribute such as “deterministic”, then a specific type of chaotic phenomena is involved, having their specific laws, mathematical apparatus and a physical origin. The deterministic chaos is a phenomenon that - as its name suggests - is not based on the presence of a random or any stochastic effects. It is clear from the structure of the equations (see the section 4), that no mathematical term expressing randomness is present. The seeming randomness in deterministic chaos is related to the extreme sensitivity to the initial conditions [1].

Till now, the chaos has been observed in many of various systems (including evolutionary one). Systems exhibiting deterministic chaos include, for instance, weather, biological systems, many electronic circuits (Chua’s circuit), mechanical systems, such as double pendulum, magnetic pendulum, or so called billiard problem.

The idea of using chaotic systems instead of random processes (pseudo-number generators - PRNGs) has been presented in several research fields and in many applications with promising results [2], [3].

Another research joining deterministic chaos and pseudorandom number generator has been done for example in [4]. Possibility of generation of random or pseudorandom numbers by use of the ultra weak multidimensional coupling of p 1-dimensional dynamical systems is discussed there.

R.Senkerik, M. Pluhacek and Z. Kominkova Oplatkova are with the Department of Informatics and Artificial Intelligence, Faculty of Applied Informatics, Tomas Bata University in Zlin, Nam. T.G. Masaryka 5555, 760 01 Zlin, Czech Republic, (phone: +420576035189; fax: +420576035279; e-mail: senkerik@fai.utb.cz).

This work was supported by European Regional Development Fund under the project CEBIA-Tech No. CZ.1.05/2.1.00/03.0089; and by Internal Grant Agency of Tomas Bata University under the project No. IGA/FAI/2014/010.

Another paper [5] deeply investigate logistic map as a possible pseudorandom number generator and is compared with contemporary pseudo-random number generators. A comparison of logistic map results is made with conventional methods of generating pseudorandom numbers. The approach used to determine the number, delay, and period of the orbits of the logistic map at varying degrees of precision (3 to 23 bits). Another paper [6] proposed an algorithm of generating pseudorandom number generator, which is called (couple map lattice based on discrete chaotic iteration) and combine the couple map lattice and chaotic iteration. Authors also tested this algorithm in NIST 800-22 statistical test suits and for future utilization in image encryption. In [7] authors exploit interesting properties of chaotic systems to design a random bit generator, called CCCBG, in which two chaotic systems are cross-coupled with each other. A new binary stream-cipher algorithm based on dual one-dimensional chaotic maps is proposed in [8] with statistic proprieties showing that the sequence is of high randomness. Similar studies are also done in [9], [10] and [11].

II. MOTIVATION

Till now the chaos was observed in many of various systems (including evolutionary one) and in the last few years is also used to replace pseudo-number generators (PRNGs) in evolutionary algorithms (EAs).

Recent research in chaos driven heuristics has been fueled with the predisposition that unlike stochastic approaches, a chaotic approach is able to bypass local optima stagnation. This one clause is of deep importance to evolutionary algorithms. A chaotic approach generally uses the chaotic system in the place of a pseudo random number generator [12]. This causes the heuristic to map unique regions, since the chaotic system iterates to new regions. The task is then to select a very good chaotic system (either discrete or time-continuous) as the pseudo random number generator.

The initial concept of embedding chaotic dynamics into the evolutionary algorithms is given in [13]. Later, the initial study [14] was focused on the simple embedding of chaotic systems in the form of chaos pseudo random number generator (CPRNG) for DE (Differential Evolution) and SOMA [15] in the task of optimal PID tuning

Several papers have been recently focused on the connection of heuristic and chaotic dynamics either in the

form of hybridizing of DE with chaotic searching algorithm [16] or in the form of chaotic mutation factor and dynamically changing weighting and crossover factor in self-adaptive chaos differential evolution (SACDE) [17]. Also the PSO (Particle Swarm Optimization) algorithm with elements of chaos was introduced as CPSO [18] or CPSO combined with chaotic local search [19].

This idea was later extended with the successful experiments with chaos driven DE (ChaosDE) [20], [21] with both and complex simple test functions and in the task of chemical reactor geometry optimization [22].

The concept of Chaos DE has proved itself to be a powerful heuristic also in combinatorial problems domain [23].

At the same time the chaos embedded PSO with inertia weigh strategy was closely investigated [24], followed by the introduction of a PSO strategy driven alternately by two chaotic systems [25] and novel chaotic Multiple Choice PSO strategy (Chaos MC-PSO) [26].

The primary aim of this work is not to develop a new type of pseudo random number generator, which should pass many statistical tests, but to try to test, analyze and compare the implementation of different natural chaotic dynamics as the CPRNGs, thus to analyze and highlight the different influences to the system, which utilizes the selected CPRNG (including the evolutionary computational techniques).

III. THE CONCEPT OF CPRNG

The general idea of CPRNG is to replace the default PRNG with the chaotic system. As the chaotic system is a set of equations with a static start position, we created a random start position of the system, in order to have different start position for different experiments. This random position is initialized with the default PRNG, as a one-off randomizer. Once the start position of the chaotic system has been obtained, the system generates the next sequence using its current position.

Generally there exist many other approaches as to how to deal with the negative numbers as well as with the scaling of the wide range of the numbers given by the chaotic systems into the typical range 0 – 1:

- Finding of the maximum value of the pre-generated long discrete sequence and dividing of all the values in the sequence with such a maxval number.
- Shifting of all values to the positive numbers (avoiding of ABS command) and scaling.

IV. CHAOTIC SYSTEMS

This section contains the description of time-continuous chaotic system (flows or oscillators), which were used as the chaotic pseudo random generators. In this research, direct sampled output iterations of the chaotic systems were used for the generation of real numbers scaled into the typical range for random function: <0 - 1>. Following chaotic systems were used: unmodified UEDA oscillator (1) and Driven Van der Pol

Oscillator (2).

The x, y parametric plots of the chaotic systems are depicted in Fig. 1 (UEDA osc.) and Fig. 6 (Vander Pol osc.). The typical chaotic behavior of the utilized chaotic systems, represented by the examples of direct output for the variable x is depicted in Figures 2 and 7. Whereas Figures 3 and 8 represent the direct outputs of the systems sampled with the selected sampling rate of 0.5 seconds.

The illustrative histograms of the distribution of real numbers transferred into the range <0 - 1> generated by means of studied chaotic systems are in Figures 4 and 9.

Finally the Figures 5 and 10 show the example of dynamical sequencing during the generating of pseudo number numbers by means of both studied CPRNGs.

A. UEDA Oscillator

UEDA oscillator is the simple example of driven pendulums, which represent some of the most significant examples of chaos and regularity.

The UEDA system can be simply considered as a special case of intensively studied Duffing oscillator that has both a linear and cubic restoring force. Ueda oscillator represents the both biologically and physically important dynamical model exhibiting chaotic motion. It can be used to explore much physical behavior in biological systems. [27]

The UEDA chaotic system equations are given in (1). The parameters are: $a = 1.0$ $b = 0.05$, $c = 7.5$ and $\omega = 1.0$ as suggested in [28].

$$\begin{aligned} \frac{dx}{dt} &= y \\ \frac{dy}{dt} &= -ax^3 - by + c \sin \omega t \end{aligned} \tag{2}$$

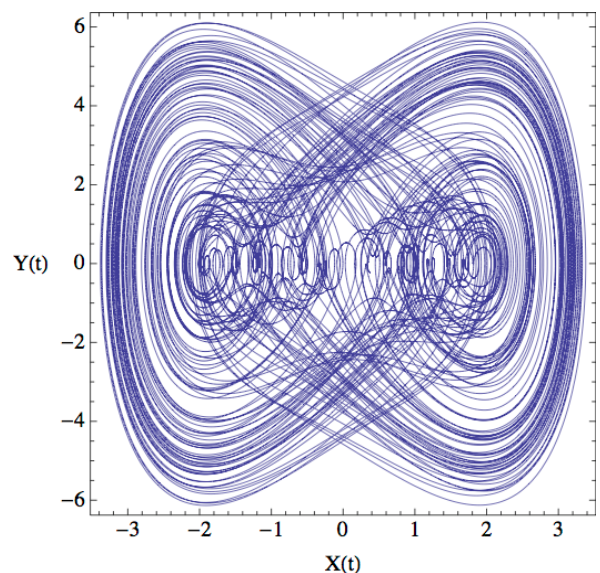


Fig. 1 x, y parametric plot of the UEDA oscillator

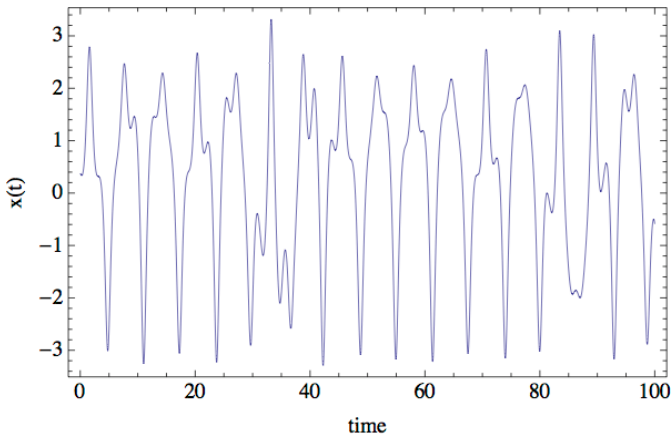


Fig. 2 Simulation of the UEDA oscillator (variable x – line-plot)

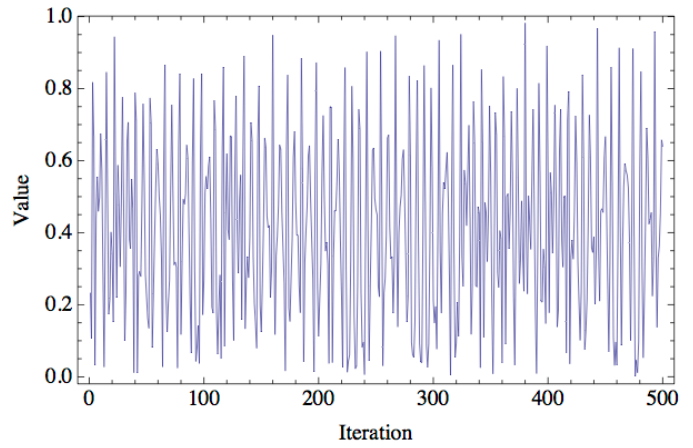


Fig. 5 Example of the chaotic dynamics: range $<0 - 1>$ generated by means of the UEDA chaotic oscillator

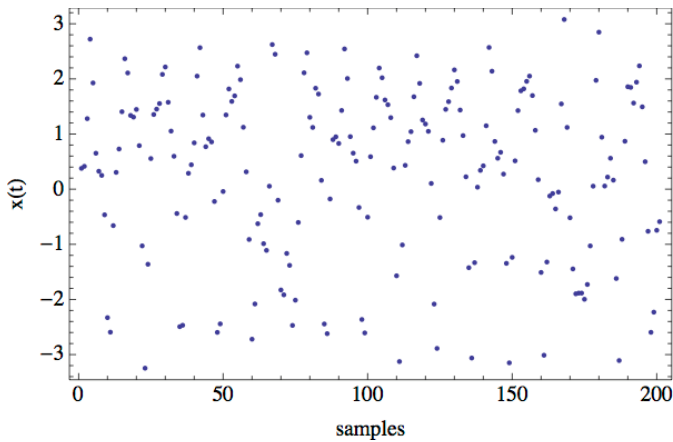


Fig. 3 Direct outputs of the UEDA oscillator chaotic system sampled with the selected sampling rate of 0.5 seconds – variable x

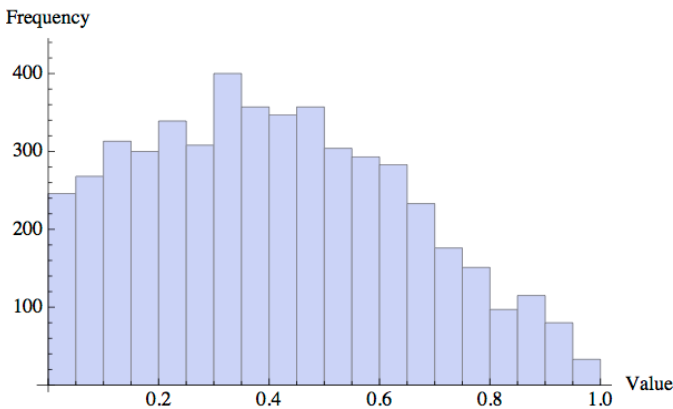


Fig. 4 Histogram of the distribution of real numbers transferred into the range $<0 - 1>$ generated by means of the chaotic UEDA oscillator – 5000 samples

B. Van der Pol Oscillator

Van der Pol oscillator is the simple example of the limit cycles and chaotic behavior in electrical circuits employing vacuum tubes. Similarly to the UEDA oscillator, it can be used to explore physical (unstable) behaviour in biological sciences. [29].

In this paper, the forced, or commonly known as driven, Van der Pol oscillator is investigated. This system consist of the original Van der Pol oscillator definition with the added driving function $a \sin(\omega t)$, thus the differential equations have the form (2). The parameters are: $\mu = 0.2$ $\gamma = 8.0$, $a = 0.35$ and $\omega = 1.02$ as suggested in [28].

$$\begin{aligned} \frac{dx}{dt} &= y \\ \frac{dy}{dt} &= \mu(1 - \gamma x^2)y - x^3 + a \sin \omega t \end{aligned} \tag{2}$$

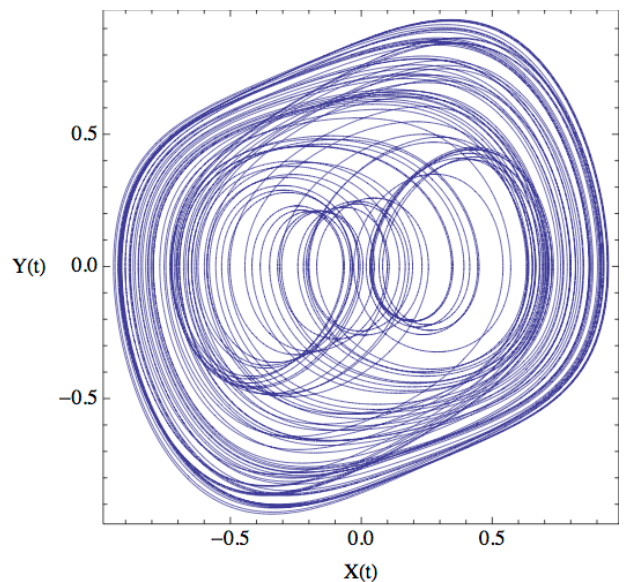


Fig.6 x, y parametric plot of the Van der Pol oscillator

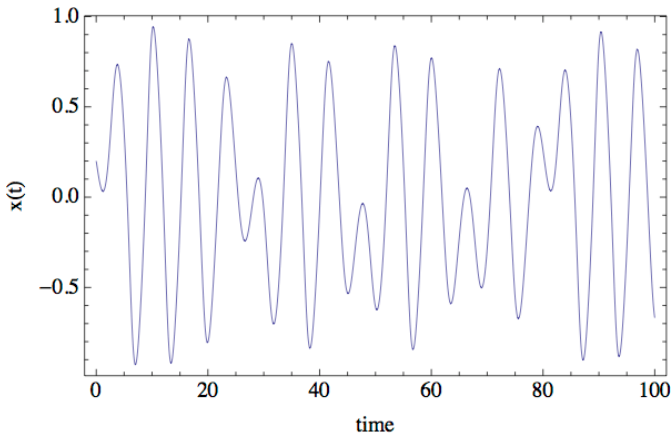


Fig. 7 Simulation of the Van der Pol oscillator (variable x – line-plot)

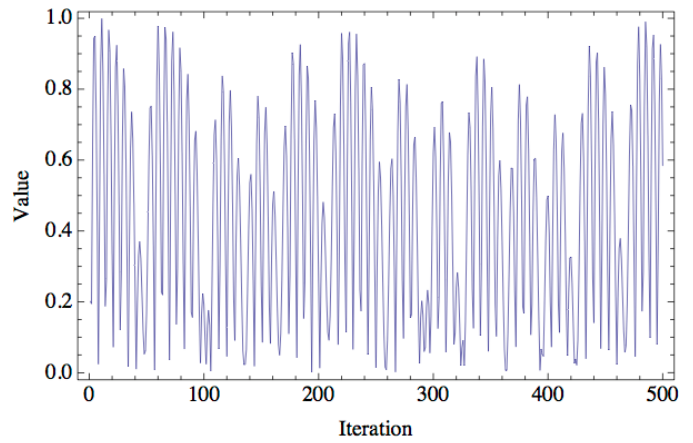


Fig. 10 Example of the chaotic dynamics: range $<0 - 1>$ generated by means of the Van der Pol chaotic oscillator

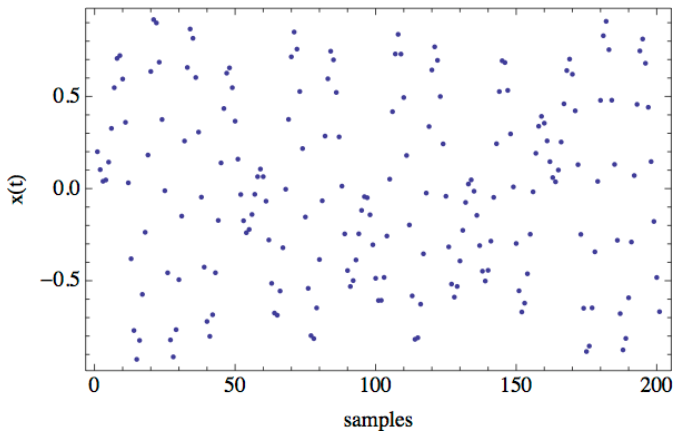


Fig. 8 Direct outputs of the Van der Pol oscillator chaotic system sampled with the selected sampling rate of 0.5 seconds – variable x

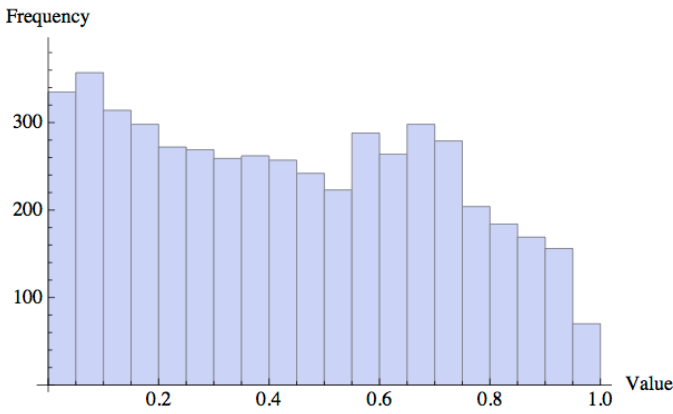


Fig. 9 Histogram of the distribution of real numbers transferred into the range $<0 - 1>$ generated by means of the chaotic Van der Pol oscillator – 5000 samples

V. CONCLUSIONS

This paper was investigating the utilization of the time-continuous chaotic system as the chaotic pseudo random number generators. (CPRNGs) Totally two different chaotic systems (oscillators) were simulated, statistically analyzed and compared within this initial research study.

From the graphical comparisons, it follows that through the utilization of different chaotic systems; entirely different statistical characteristics of CPRNGs can be achieved. Thus the different influence to the system, which utilizes the selected CPRNG, can be chosen through the implementation of particular inner chaotic dynamics given by the particular time-continuous chaotic system.

Furthermore chaotic systems have additional parameters, which can be tuned. This issue opens up the possibility of examining the impact of these parameters to generation of random numbers, and thus influence on the results obtained by means of either evolutionary techniques or different systems from the softcomputing/computational intelligence field.

REFERENCES

- [1] S. Celikovsky and I. Zelinka, "Chaos Theory for Evolutionary Algorithms Researchers," in *Evolutionary Algorithms and Chaotic Systems*. vol. 267, I. Zelinka, S. Celikovsky, H. Richter, and G. Chen, Eds., ed: Springer Berlin Heidelberg, 2010, pp. 89-143.
- [2] J. S. Lee and K. S. Chang, "Applications of chaos and fractals in process systems engineering," *Journal of Process Control*, vol. 6, pp. 71-87, 1996.
- [3] J. Wu, J. Lu, and J. Wang, "Application of chaos and fractal models to water quality time series prediction," *Environmental Modelling & Software*, vol. 24, pp. 632-636, 2009.
- [4] R. Lozi, "Emergence of Randomness from Chaos," *International Journal of Bifurcation and Chaos*, vol. 22, p. 1250021, 2012.
- [5] K. J. Persohn and R. J. Povinelli, "Analyzing logistic map pseudorandom number generators for periodicity induced by finite precision floating-point representation," *Chaos, Solitons & Fractals*, vol. 45, pp. 238-245, 2012.
- [6] X.-y. Wang and X. Qin, "A new pseudo-random number generator based on CML and chaotic iteration," *Nonlinear Dynamics*, vol. 70, pp. 1589-1592, 2012/10/01 2012.

- [7] K. P. Narendra, P. Vinod, and K. S. Krishan, "A Random Bit Generator Using Chaotic Maps," *International Journal of Network Security*, vol. 10, pp. 32 - 38, 2010.
- [8] L. Yang and X.-Y. Wang, "Design of Pseudo-random Bit Generator Based on Chaotic Maps," *International Journal of Modern Physics B*, vol. 26, p. 1250208, 2012.
- [9] M. Bucolo, R. Caponetto, L. Fortuna, M. Frasca, and A. Rizzo, "Does chaos work better than noise?," *Circuits and Systems Magazine, IEEE*, vol. 2, pp. 4-19, 2002.
- [10] H. Hu, L. Liu, and N. Ding, "Pseudorandom sequence generator based on the Chen chaotic system," *Computer Physics Communications*, vol. 184, pp. 765-768, 2013.
- [11] A. Pluchino, A. Rapisarda, and C. Tsallis, "Noise, synchrony, and correlations at the edge of chaos," *Physical Review E*, vol. 87, p. 022910, 2013.
- [12] I. Aydin, M. Karakose, and E. Akin, "Chaotic-based hybrid negative selection algorithm and its applications in fault and anomaly detection," *Expert Systems with Applications*, vol. 37, pp. 5285-5294, 2010.
- [13] R. Caponetto, L. Fortuna, S. Fazzino, and M. G. Xibilia, "Chaotic sequences to improve the performance of evolutionary algorithms," *IEEE Transactions on Evolutionary Computation*, vol. 7, pp. 289-304, 2003.
- [14] D. Davendra, I. Zelinka, and R. Senkerik, "Chaos driven evolutionary algorithms for the task of PID control," *Computers & Mathematics with Applications*, vol. 60, pp. 1088-1104, 2010.
- [15] I. Zelinka, "SOMA — Self-Organizing Migrating Algorithm," in *New Optimization Techniques in Engineering*. vol. 141, ed: Springer Berlin Heidelberg, 2004, pp. 167-217.
- [16] W. Liang, L. Zhang, and M. Wang, "The chaos differential evolution optimization algorithm and its application to support vector regression machine," *Journal of Software*, vol. 6, pp. 1297- 1304, 2011.
- [17] G. Zhenyu, C. Bo, Y. Min, and C. Binggang, "Self-Adaptive Chaos Differential Evolution," in *Advances in Natural Computation*. vol. 4221, L. Jiao, L. Wang, X.-b. Gao, J. Liu, and F. Wu, Eds., ed: Springer Berlin Heidelberg, 2006, pp. 972-975.
- [18] L. d. S. Coelho and V. C. Mariani, "A novel chaotic particle swarm optimization approach using Hénon map and implicit filtering local search for economic load dispatch," *Chaos, Solitons & Fractals*, vol. 39, pp. 510-518, 2009.
- [19] W.-C. Hong, "Chaotic particle swarm optimization algorithm in a support vector regression electric load forecasting model," *Energy Conversion and Management*, vol. 50, pp. 105-117, 2009.
- [20] R. Senkerik, M. Pluhacek, I. Zelinka, Z. Oplatkova, R. Vala, and R. Jasek, "Performance of Chaos Driven Differential Evolution on Shifted Benchmark Functions Set," in *Proc. International Joint Conference SOCO'13-CISIS'13-ICEUTE'13*. vol. 239, A. Herrero, B. Baruque, F. Klett, A. Abraham, V. Snášel, A. C. P. L. F. Carvalho, et al., Eds., ed: Springer International Publishing, 2014, pp. 41-50.
- [21] R. Senkerik, D. Davendra, I. Zelinka, M. Pluhacek, and Z. Kominkova Oplatkova, "On the Differential Evolution Driven by Selected Discrete Chaotic Systems: Extended Study," in *Proc. 19th International Conference on Soft Computing, MENDEL 2013*, 2013, pp. 137-144.
- [22] R. Senkerik, M. Pluhacek, Z. K. Oplatkova, D. Davendra, and I. Zelinka, "Investigation on the Differential Evolution driven by selected six chaotic systems in the task of reactor geometry optimization," in *Proc. 2013 IEEE Congress on Evolutionary Computation (CEC)*, 2013, pp. 3087-3094.
- [23] D. Davendra, M. Bialic-Davendra, and R. Senkerik, "Scheduling the Lot-Streaming Flowshop scheduling problem with setup time with the chaos-induced Enhanced Differential Evolution," in *Proc. 2013 IEEE Symposium on Differential Evolution (SDE)*, 2013, pp. 119-126.
- [24] M. Pluhacek, R. Senkerik, D. Davendra, Z. Kominkova Oplatkova, and I. Zelinka, "On the behavior and performance of chaos driven PSO algorithm with inertia weight," *Computers & Mathematics with Applications*, vol. 66, pp. 122-134, 2013.
- [25] M. Pluhacek, R. Senkerik, I. Zelinka, and D. Davendra, "Chaos PSO algorithm driven alternately by two different chaotic maps - An initial study," in *Proc. 2013 IEEE Congress on Evolutionary Computation (CEC)*, 2013, pp. 2444-2449.
- [26] M. Pluhacek, R. Senkerik, and I. Zelinka, "Multiple Choice Strategy Based PSO Algorithm with Chaotic Decision Making – A Preliminary Study," in *Proc. International Joint Conference SOCO'13-CISIS'13-ICEUTE'13*. vol. 239, A. Herrero, B. Baruque, F. Klett, A. Abraham, V. Snášel, A. C. P. L. F. Carvalho, et al., Eds., ed: Springer International Publishing, 2014, pp. 21-30.
- [27] L. Bharti and M. Yuasa. Energy Variability and Chaos in Ueda Oscillator.
Available: <http://www.rist.kindai.ac.jp/no.23/yuasa-EVCUO.pdf>
- [28] J. C. Sprott, *Chaos and Time-Series Analysis*: Oxford University Press, 2003.
- [29] T. Kanamaru, "Van der Pol oscillator," *Scholarpedia*, vol. 2, p. 2202, 2007.

Development of control system for rehabilitation device actuated by pneumatic artificial muscles

O. Líška and M. More

Abstract—Musculoskeletal rehabilitation is complicated and time consuming process. Therefore there is effort to use various automated devices for this task. In this paper we describe some aspects in design of rehabilitation device that is meant for rehabilitation of upper limbs. This device is meant for exercising shoulder and elbow joints at the same time and therefore it can perform simple, but also complex exercises. Main difference from similar rehabilitation devices is its drive - pneumatic artificial muscle. This type of actuation is relatively new in robotic devices, but it has few key features that make it suitable for use in devices that come to contact with humans. Because in control of these actuators there are several difficult challenges, there are used elements of artificial intelligence for enhancement of performance and quality of control.

Keywords—Artificial intelligence, control system, pneumatic muscles, rehabilitation device.

I. INTRODUCTION

MUSCULOSKELETAL rehabilitation is an important part of the healing process of patients who suffered an injury or illness that restrict range of motion. Main forms of limb rehabilitation include exercises involving joint motion and also positioning. Each of these exercises lasts for a few hours a day and depending on the diagnosis of the patient there may be need to perform them for several months. Usually are these exercises performed by physiotherapist, but because he can work only on one patient simultaneously, the whole process is demanding on time and money. Because of that, there is effort to at least partially automate this task with usage of robotic

The research work is supported by the Project of the Structural Funds of the EU, Operational Programme Research and Development, Measure 2.2 Transfer of knowledge and technology from research and development into practice. Title of the project: „Research and development of intelligent nonconventional actuators based on artificial muscles”, ITMS code: 26220220103.

This work has been supported by the Slovak Grant Agency VEGA contract Nb. 1/0911/14 "Implementation of wireless technologies into the design of new products and services to protect human health".

O. Líška, Technical University of Košice, Mechanical Engineering Faculty, Department of Automation, Control and Human Machine Interactions, Letná 9, 042 00 Košice, Slovak Republic (e-mail: ondrej.liska@tuke.sk).

M. More, Technical University of Košice, Mechanical Engineering Faculty, Department of Automation, Control and Human Machine Interactions, Letná 9, 042 00 Košice, Slovak Republic (e-mail: marcel.more@tuke.sk).

and mechatronic systems. The main advantage of these systems, especially those simpler is that they can be used in the patient's home, which is great advantage if daily exercise is necessary. In this case, patient can decide not only when, but also how long and how intense he will perform these exercises. Some studies show that the uses of such devices reduce the cost of rehabilitation up to 50%. Based on complexity, these devices can be simple mono-articular machines, designed particularly for one joint, or they may be complex robotic devices with several degrees of freedom capable of performing variety of exercises. Usually they can be connected to a computer that can be used for online monitoring and to make records of exercise. Such records are an important for the therapist, who can base on them appropriately choose next exercise methods. Currently manufactured rehabilitation devices usually use electric motors to drive them. This has resulted in their high price (in thousands euros) and also not entirely favorable dynamic characteristics. Alternative ways to drive these devices are pneumatic artificial muscles (PAM). Compared to a commonly used drives they are cheaper, have better weight to power ratio and thanks to their specific properties they are suitable for use in machines that interact with peoples.

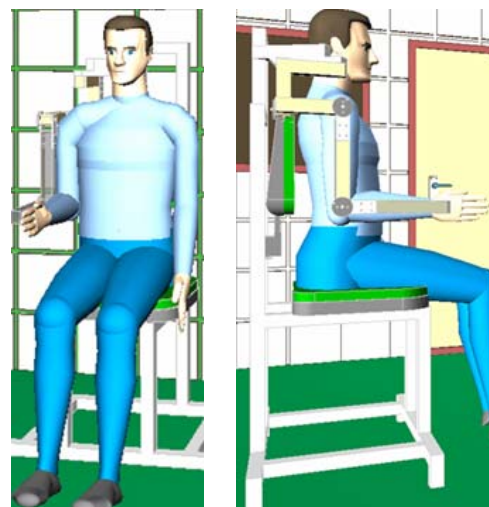


Fig. 1 Rehabilitation device in virtual reality [1]

II. REHABILITATION DEVICE WITH PAM

Specific requirements for this device arise from the fact that the rehabilitation robot, unlike industrial robots is intended for direct contact with humans and also because of the non-conventional drive - pneumatic muscles.

Compared to industrial robots, rehabilitation robot must have the following characteristics:

- kinematics, which allows him to copy human motions
- ergonomic design, allowing comfortable contact with the patient
- increased demands for safety and compliance with the required parameters of motion

Kinematics of the rehabilitation robot must reflect limb kinematics for which it is intended. Our robot is designed for exercising shoulder and elbow joints, which requires kinematics with 4 degrees of freedom. An important factor is ergonomic design. Robot must be designed so that it can be used by various peoples with different shape and size of figure and also with respect to their physical ailment. Necessity for robot that comes to contact with humans is safety. In this case this is even more important, because peoples that train with this device are generally weaker and are more prone to injury. Therefore the safety circuit of the rehabilitation robot must be designed for quick intervention so that potential error won't result in bodily harm.



Fig. 2 Rehabilitation device driven by PAM

Second particularity of this device is the drive. Pneumatic muscles have different attributes compared to conventionally used electrical drives. This leads to differences in design and also in control of this device. Pneumatic muscles even although they are bigger in size than electrical drives with equivalent power, have noticeably lower weight. This helps us to build lighter robots while maintaining their performance. In case of rehabilitation robot, the overall weight is important also because it easier to move it from place to place (e.g. to patients home if necessary). Another interesting feature of pneumatic muscles over other types of drives is compliance. Using different filling pressures in the muscles it is possible to achieve more or less rigid system. This makes the robots with this type of drive safer and more comfortable when working with people.

III. CONTROL SYSTEM COMPONENTS

The control system is a key component of the robot as it significantly influences the final properties of the device. In general, the control system consists of three parts: a sensor system, controller and actuating member. This is same for all automated devices, but each of these parts needs to reflect requirements that are specific to this type of device.

Sensor system

Sensors of rehabilitation robot are designed to collect data from the two areas. First there are data about the internal state of the robot (information on position, velocity and acceleration, state of pneumatic pressure, electrical energie, etc.), but also it should give some information about patient state or about the way how he interacts with device. The most important variable that is necessary to monitor is the load that is applied on patient during exercise. This is important for active rehabilitation exercises.

Controller

Currently, there are different systems that are able to acquire data from sensors, base on them control actuators and thus work as controllers. They may be embedded computers or handheld devices, personal computers but also industrial PCs and PLCs. When designing rehabilitation robot, we should keep in mind that it would be operated by non-technical personnel and therefore it is appropriate that the end point device is easy to operate for this people. Therefore the best solution appears to be use of a personal computer that interacts with embedded low-level control system of the device, or eventually even directly controlling it trough some input output equipment.

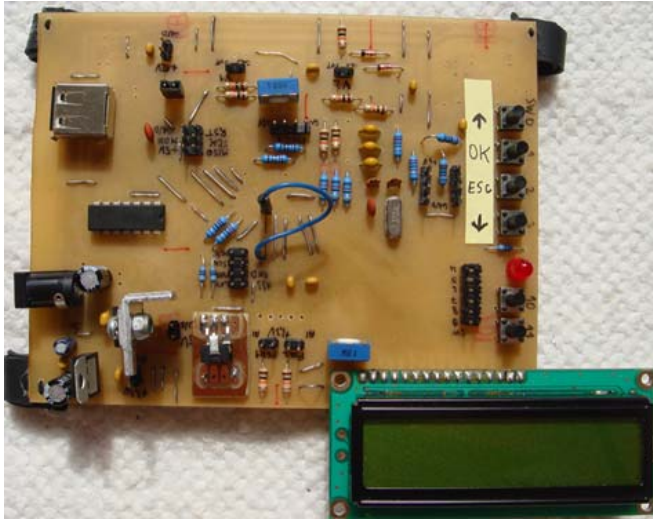


Fig. 3 Hardware of embedded control system

Actuating member

Because pneumatic muscles are significantly different from the drives commonly used in robotic devices, it is obvious that the biggest difference in the control system compared to other robots is in the actuating members used. In case of pneumatic systems there are mainly solenoid valves. Their job in control is to set desired pressure in muscles, which subsequently affect position of robots arm. For this task there are a number of appropriate solutions, from simple on-off valves controlled PWM, to the electronic pressure regulators or proportional valves.

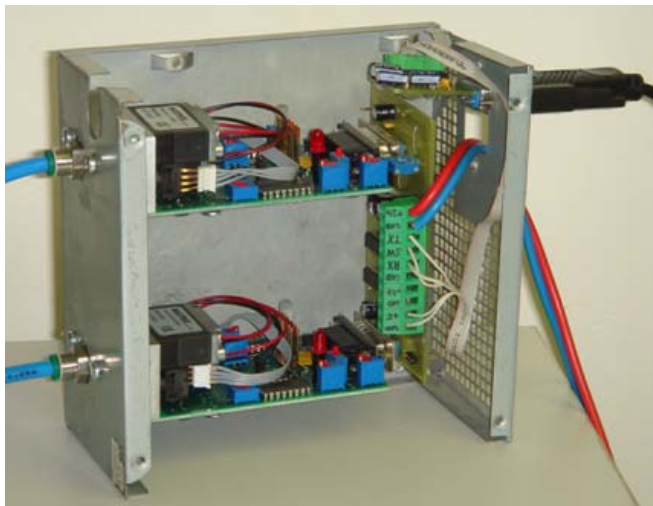


Fig. 4 Electronic pressure regulators EPR50

IV. HIGHER FORMS OF CONTROL

Since in the control of rehabilitation robot there are several non-trivial tasks, that are difficult to solve with conventional algorithms, there is opportunity to use artificial intelligence techniques. Appropriate tool to replace conventional algorithms respectively complicated mathematical functions is an artificial neural network (NN). This one can approximate the function based only on the sample cases, without need of knowing relationship between input and output variables. In control of the rehabilitation robot neural network can be used for following tasks:

- to build a model of controlled system
- to determine the optimal parameters of exercise during rehabilitation
- to recognize motion that the patient performs during exercise

Since pneumatic muscles have non-linear characteristics, actuator build from them also has non-linear properties. However, since some forms of control require model of controlled system, there is a problem how to simply and at the same time sufficiently accurately describe such a system. In this case, it is possible to use the neural network for this task, as it is described in [2].

Another application for the neural network may be using it directly to control the exercise. For rehabilitation to be most effective, it is necessary to determine the optimal parameters of exercise (e.g. speed and range of motion, load applied to individual joints, etc.). As these parameters change during exercise, the system must respond to these changes adaptively.

Of course neural networks can be used in other tasks where the dependency between variables is difficult to describe. The example of this can be inertial data processing in which neural network is used to determine type of motion which patient is performing during exercise. Because motions of different persons or even the same person in different situations are never identical, it is difficult to identify them by using standard mathematical functions and it may be better to use some form of artificial intelligence.

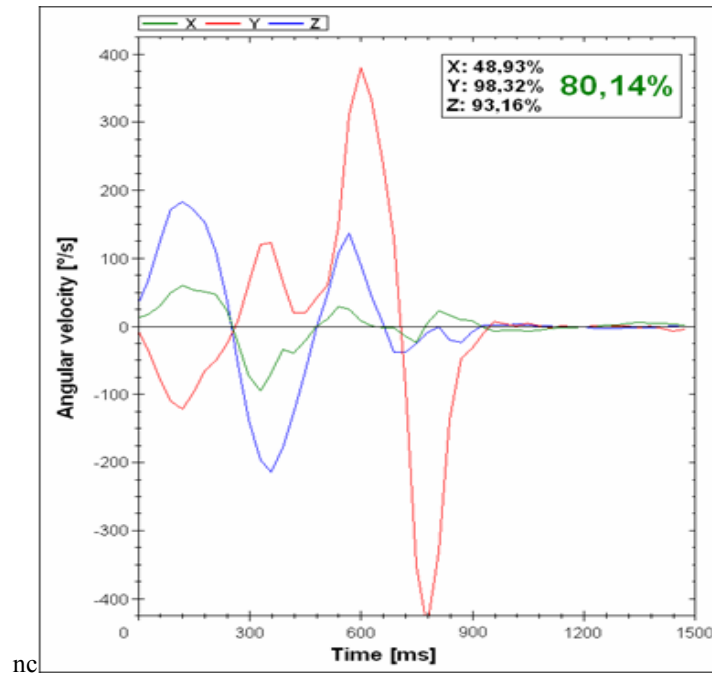


Fig. 5 Recognition of motion patterns with NN

V. CONCLUSION

Rehabilitation robot is a complex device and in his design it is necessary to combine knowledge from automation, robotics, biomedical engineering and also other fields. Device that we developing is pluri-articular exoskeleton with four degrees of freedom, designed to exercise muscles and joints of the shoulder and elbow. Its main difference compared to other similar devices is the use of unconventional source of force - pneumatic artificial muscle. This type of drive is suitable for use in such devices thanks to its low weight, high performance, low cost and also compliance. This is an important feature for machines that come in contact with people, because opposed to industrial applications in the rehabilitation it is not suitable for the device to be rigid.

Control of actuators based on pneumatic artificial muscles is nontrivial task. It is because PAMs themselves have nonlinear properties such as hysteresis, dead zones etc. For these reasons and also due to the complexity of some other control tasks, we decided to use elements of artificial intelligence to solve several tasks, mostly by artificial neural network.

REFERENCES

- [1] M. Fodor and O. Líška, "Virtuálny model rehabilitačného zariadenia s využitím umelých svalov", (in Slovak), in *ARTEP 2013*, Košice TU, Stará Lesná, SR, 2013.
- [2] Z. Assylova, "Comparison of Neural Network Models for Approximation of Pneumatic Muscle Actuator", Bachelor's thesis, Czech technical university in Prague, 2013.
- [3] D. Šimšík, et al., "Design of inertial module for rehabilitation device", in *SAMI 2013*, Budapest IEEE, Herľany, SR, 2013.
- [4] A. Hošovský, et al., "Model-based evolution of a fast hybrid fuzzy adaptive controller for a pneumatic muscle actuator," *International Journal of Advanced Robotic Systems*, vol. 9, 2012, pp. 1-11.
- [5] J. Piteľ and M. Balara, "Pneumatický umelý sval - perspektívny prvok mechatroniky," (in Slovak), *IAT&P Journal*, vol. 12, 2008.
- [6] A. Hošovský, "The control of the PAM-based position servosystem with acceleration loop," *Journal of applied science in the thermodynamics and fluid mechanics*, no. 2, no. 1, 2008.
- [7] K. Židek, A. Hošovský, and V. Maxim, "Real-time safety circuit based on combined MEMS sensor data for rehabilitation device", in *ICCC 2012*, Piscataway IEEE, Podbanské, SR, 2012.
- [8] B. Jobbágy, M. Fodor, and D. Šimšík, "Návrh konštrukcie rehabilitačného zariadenia s využitím umelých svalov", (in Slovak), in *ARTEP 2012*, Košice TU, Stará Lesná, SR.
- [9] J. Piteľ, M. Balara, and J. Boržiková, "Control of the Actuator with Pneumatic Artificial Muscles in Antagonistic Connection," *Collection of scientific works of the VŠB - Technical University of Ostrava, VŠB - TU of Ostrava*, vol. LIII, no. 2, 2007, pp. 101-106.
- [10] T. Deaconescu and A. Deaconescu, "Performance of a Pneumatic Muscle Actuated Rotation Module," in *Proceedings of the World Congress on Engineering*. London: 2009.
- [11] D. Janáčová, H. Charvátová, K. Kolomazník, and V. Vašek, *Creating software applications for solving diffusion problems in the MAPLE interface*. (in Czech), Zlín: Tomas Bata University in Zlín, 2012.
- [12] H. Charvátová, V. Vašek, R. Drga, and J. Křenek, "Software application for solving of non-stationary temperature fields", in *22nd International DAAAM Symposium*, Vienna, 2011.
- [13] D. Janáčová, "Řízení enzymové hydrolyzy," (in Czech), Habilitation lecture, VSB - Technical University of Ostrava, 2002.

Analysis of behavior of car stabilizer bushing

Jakub Javorik, David Samek, and Ondrej Bilek

Abstract—The goal of this work is to create numerical model, which will be used for design and optimization of a rubber bushing for stabilizer bar. Thanks this model we are able to predict the mechanical behavior of the bushing. To get material constants for the model, the material of bushing (rubber) was tested in special deformations modes. A hyperelastic material model was set and it was implemented into the numerical model of the bushing. Critical points in the construction of bushing were revealed by the analysis of the numerical model.

Keywords—bushing, hyperelasticity, numerical model, stabilizer bar.

I. INTRODUCTION

THE stabilizer bar is an important part of a car suspension. It is intended to force each side of the vehicle to lower, or rise, to similar heights, to reduce the sideways tilting of the vehicle on curves, sharp corners, or large bumps. One of the factors which influence the function and behavior of the stabilizer bar is a way in which it is connected with the car frame. This connection must be able to absorb quite large deformation of the stabilizer bar. Therefore the rubber bushings are commonly used to clamp stabilizer bar and to fasten it to the car frame. To design this bushing properly we need to predict the bushing behavior accurately. The numerical model of the bushing was created and the analysis of its behavior is described in this paper. Main goal of the work was to analyze the radial stiffness of the bushing.

II. MATERIAL AND METHODS

A. Geometry of Bushing

The scheme of half cut stabilizer bar bushing is shown in the Fig. 1. The bushing consists of three parts: two rubber parts (a) and (b), and steel clamp (c). Rubber parts are mounted on the stabilizer bar (d) and then together with the stabilizer bar they are fixed by the steel clamp (c) to the car frame. Both rubber parts of the bushing are reinforced by the aluminum core (e). There are eight holes in each core plate for better fixation of the core in the elastomer.

B. Material

We need to characterize two materials of bushing:

- material of elastomer: NR 60±3 Sh A
- material of bushing core: EN AW-ALMg3-H46

Material of the core (EN AW-ALMg3-H46) is standardized type of aluminum and we can get data from common material databases. Elastic modulus of this material is $E=70000$ MPa and Poisson ratio $\mu=0.3$. Contrary to the core, to characterize the rubber, from which the elastomer part of the bushing is made, we need to test the mechanical properties of this material. This material was tested in three basic deformation modes that are used to characterize a hyperelastic material. These tests are: uniaxial tension, equibiaxial tension and pure shear [1]-[4].

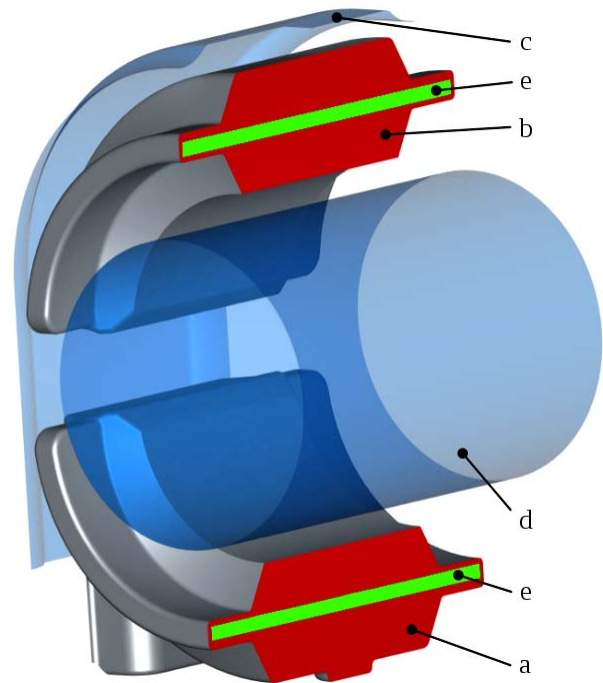


Fig. 1 half cut scheme of the stabilizer bar bushing

C. Numerical Model of the Bushing

An advanced nonlinear "Finite Element Method" (FEM) system was used for numerical model creation and analysis [5]. With regard to the symmetric shape of the bushing and to the symmetry of loads and boundary conditions (which will be described below) we can reduce the geometry of the numerical model to one quarter of original shape (Fig. 2). First plane of symmetry is normal to the axis of stabilizer bar and it

J. Javorik is with the Tomas Bata University in Zlin, nam. T. G. Masaryka 5555, 760 01 Zlin, Czech Republic (phone: +420 576 035 151; fax: +420 576 035 176; e-mail: javorik@ft.utb.cz).

D. Samek is with the Tomas Bata University in Zlin, nam. T. G. Masaryka 5555, 760 01 Zlin, Czech Republic (e-mail: samek@ft.utb.cz).

O. Bilek is with the Tomas Bata University in Zlin, nam. T. G. Masaryka 5555, 760 01 Zlin, Czech Republic (e-mail: bilek@ft.utb.cz).

is placed in the center of the bushing. Second symmetry plane coincides with the stabilizer bar axis and is perpendicular to the first plane (Fig. 2). Model has four parts: bottom bushing part, top bushing part, stabilizer bar and clamp. Aluminum cores are positioned inside the top and bottom bushing parts (they are not shown in the Fig. 2).

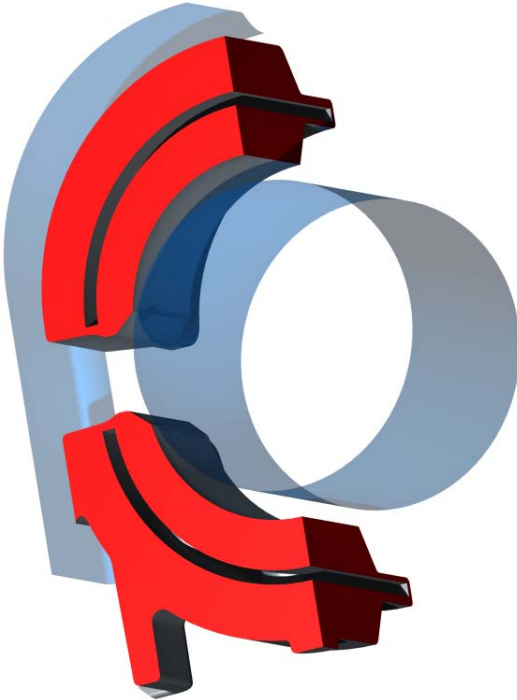


Fig. 2 geometry of the numerical model

In the model, the rubber parts and aluminum core were created of the "Four Node Tetrahedron FEM Elements" [6]. The stabilizer bar and top clamp are created as rigid bodies. Elastomer and core share nodes on their boundaries and therefore they are fixed together.

Material constants of aluminum are given above. For elastomer an appropriate hyperelastic material model had to be set [7]-[12]. Using results from uniaxial tension, equibiaxial tension and pure shear tests of elastomer, material constants of some hyperelastic models were computed. The closest agreement with experimental data (i.e. minimal error) showed a "2nd Order Invariant" hyperelastic model [13]. The strain energy density function W [14] of this model is as follows:

$$W = c_{10}(J_1 - 3) + c_{01}(J_2 - 3) + c_{11}(J_1 - 3)(J_2 - 3) + c_{20}(J_1 - 3)^2 \quad (1)$$

where J_1 and J_2 are first and second invariants of right Cauchy-Green deformation tensor [15]. There is the comparison of this model and experiment in the Fig. 3. Material constants of this model are: $c_{10}=0.23264$ MPa, $c_{01}=0.16711$ MPa, $c_{11}=-0.0060978$ MPa and $c_{20}=0.01475$ Mpa.

To be as close as possible to reality, the loads are applied in two steps. The first step can be considered as a "Mounting of

bushing on the stabilizer bar". During this step some deformation and stress of the bushing occurs and the model is in the state of initial "preload" at the end of the first step. During the second step required load is applied to the stabilizer bar.

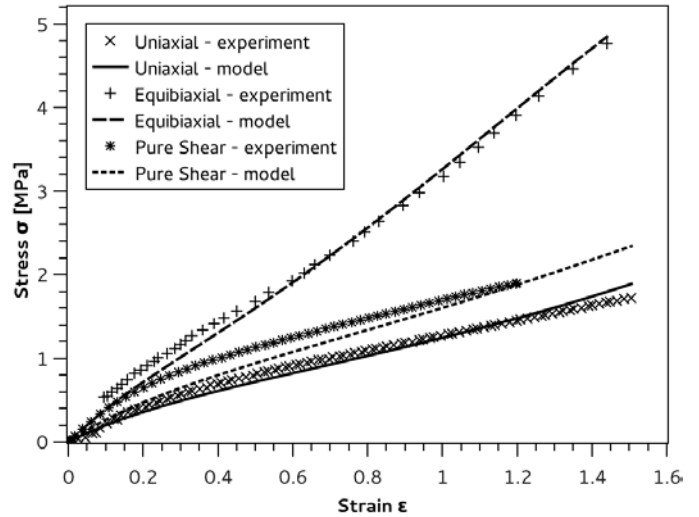


Fig. 3 comparison of experimental data and the 2nd Order Invariant hyperelastic model

First load step

All three degrees of freedom of displacement were constrained on surfaces of bottom part of elastomer, shown in Fig. 4, because these surfaces are fixed to the car frame. A symmetry conditions are set on symmetry planes (shown in Fig. 2) as a null displacement in planes normal directions. There is a contact defined between two rubber parts of bushing, between these parts and the stabilizer bar, and between these parts and clamp. No friction is defined between contact bodies.



Fig. 4 surfaces of bushing bottom part with null displacement

The bushing mounting is done by the displacement of the clamp. The Clamp is moved down against to bottom part of bushing (i.e. radial direction). During this motion the clamp touch the top part of bushing first, and then shift it to the

stabilizer bar. Stabilizer can move only vertically (other two displacements are not allowed), and thus it is pushed into the bottom part of bushing and is clamped from the top by other part of bushing and by clamp.

Second Load Step

At the beginning of this step, "glue" contact type is defined between rubber parts and the rigid stabilizer bar. It means that stabilizer bar is fixed on the surfaces of the bushing during whole second step. It should be in accordance with reality when bushing is fastened on stabilizer bar. Vertical radial force $F=2000\text{ N}$ is gradually applied on the stabilizer bar during second step. It should be remembered that this force is applied only to quarter model and thus the load of full model is four times larger (8000 N). Rigid clamp will remain in its final position from the first step and will not move during the second step.

III. RESULTS AND DISCUSSION

The main result is "Radial Stiffness" of the bushing. To compute this parameter the "loading radial force / radial displacement of stabilizer bar" relation was monitored (Fig. 5). The stiffness was determined in the range of loading from force $F=4000\text{ N}$ to $F=8000\text{ N}$ (as well as in the practical tests of a real bushing). Values of force above are given for the whole bushing (i.e. 1000 N and 2000 N for the quarter numerical model). The final value of the Radial Stiffness of the model is 11168 N/mm. Average value from the practical tests of a real bushing is 11190 N/mm.

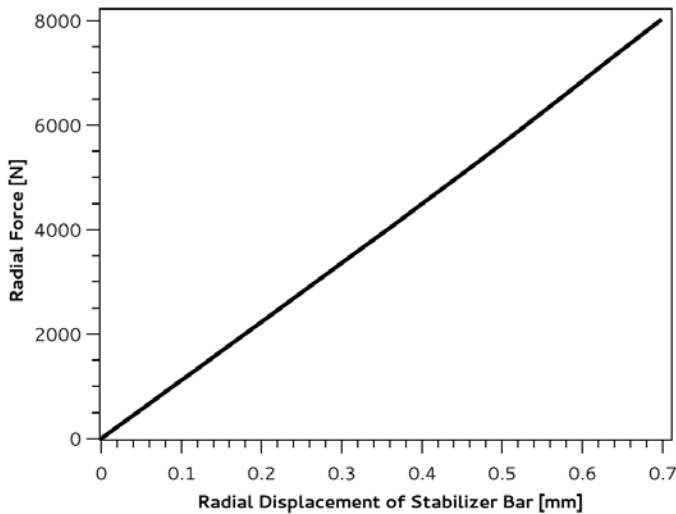


Fig. 5 Force/Displacement curve of numerical model analysis

In Fig. 6 there is a Von Mises equivalent of strain in the model shown. The deformation of the bushing at the end of the first load step (time=1.0) is shown in the first picture (a) and the deformation under the final radial loading of $F=8000\text{ N}$ at the end of the second load step (time=2.0) is shown in the second picture (b). We can see critical point with the maximum strain of $\epsilon=1.06$ at the end of second step (maximum

at the end of first step was $\epsilon=0.71$).

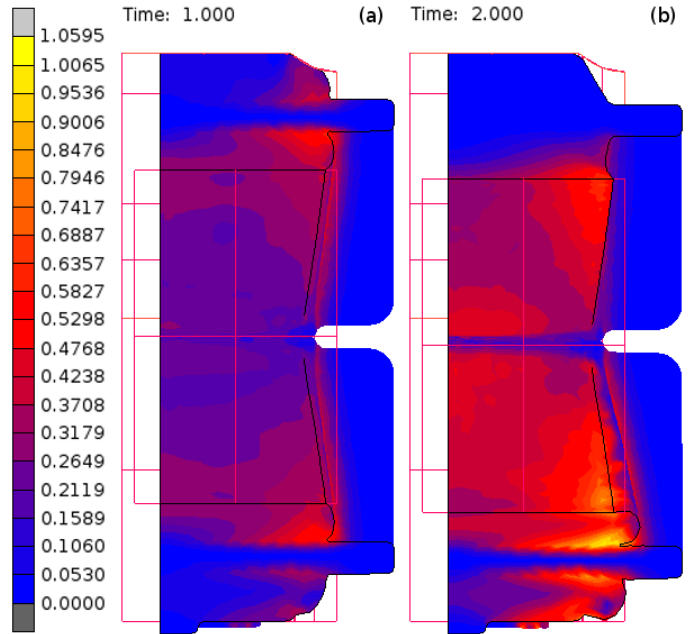


Fig. 6 Von Mises equivalent of strain in the model

Contrary the strain, the stress distribution is absolutely different. Stress is concentrated on the aluminum core and in its vicinity (Fig. 7). But because the stresses in the aluminum core do not reach the strength of the material, the core is excluded from the Fig. 7 and we can analyze the stress distribution in the elastomer only. Thus, we can see that the extreme stresses in the rubber part are located in the spaces of the core holes and that the stress values are very high here even at the end of first load step (time=1.0)

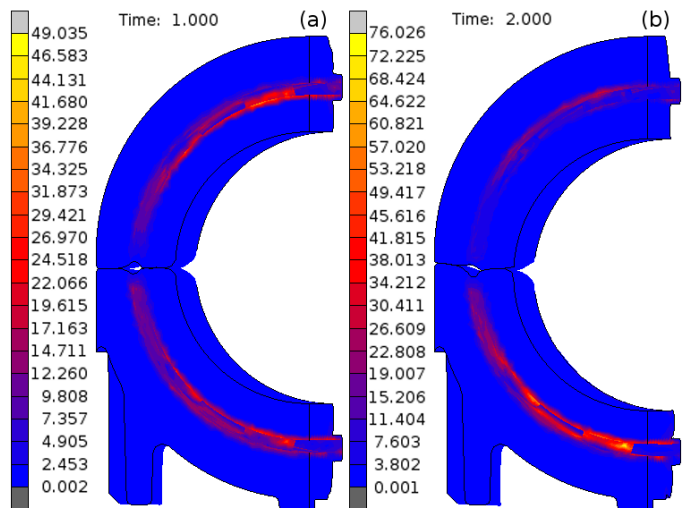


Fig. 7 Von Mises equivalent of stress [MPa] (only in elastomer)

The reason of this is that the elastomer has no space where to run out during the loading (it is closed in the core hole). Similar situation occurs on the core surfaces where the

deformation of the elastomer is constrained by the aluminum core. It means that the critical point of the bushing is the surface of the core (especially in the holes) where the stress is concentrated during the loading, and therefore there is a high risk of tearing off the rubber from the core. Next risk, resulting from this issue, is the fact that this defect of bushing is closed inside the device and can not be observed from outside. Thus we need special diagnostic methods to find such failings

IV. CONCLUSION

Based on the tests of material the appropriate hyperelastic model of elastomer was determined and the material constants were computed. Using this model, we are able to predict the behavior of the bushing under the radial loading. Even next modes of loading can be analyzed by this model and these analyses were carried out but they are outside the scope of this article and they will be published later. The suitability of the numerical model was approved by close agreement with the experiment of real bushing. Analysis of the model revealed the critical points of the bushing and its results will be used to future shape optimization of the product.

REFERENCES

- [1] R. W. Ogden, *Non-linear Elastic Deformations*. New York: Dover Publications, 1997.
- [2] L. R. G. Treloar, *The Physics of Rubber Elasticity*. Oxford: Clarendon Press, 1975.
- [3] J. Javorik and Z. Dvorak, "Equibiaxial test of elastomers," *KGK-Kautsch. Gummi Kunstst.*, vol. 60, pp. 608-610, 2007.
- [4] J. Javorik and Z. Dvorak, "The testing of hyperelastic properties of the rubber materials," *Chem. Listy*, vol. 105, pp. 273-274, 2011.
- [5] M. Bercovier, E. Jankovich, F. Leblanc and M. A. Durand, "A finite element method for the analysis of rubber parts: Experimental and analytical assessment," *Comput. Struct.*, vol. 14, pp. 384-391, 1981.
- [6] A. F. Bower, *Applied Mechanics of Solids*. New York: CRC Press, 2009.
- [7] A. Boukamel, L. Laiarinandrasana, S. Méo and E. Verron, *Constitutive Models for Rubber V*. London: Taylor & Francis, 2008.
- [8] E. M. Arruda and M.C. Boyce, "A three-dimensional constitutive model for the large stretch behavior of rubber elastic materials," *J. Mech. Phys. Solids*, vol. 41, pp. 389-412, 1993.
- [9] A. N. Gent, "A new constitutive relation for rubber," *Rubber Chem. Technol.*, vol. 69, pp. 781-785, 1996.
- [10] J. Javorik and M. Stanek, "The shape optimization of the pneumatic valve diaphragms," *Int. J. Math. Comput. Simul.*, vol. 5, pp. 361-369, 2011.
- [11] R. S. Rivlin and K. N. Sawyers, "Strain-energy function for elastomers," *Trans. Soc. Rheol.*, vol. 20, pp. 545-557, 1976.
- [12] O. H. YEOH, "Some forms of the strain energy function for rubber," *Rubber Chem. Technol.*, vol. 66, p. 754-771, 1993.
- [13] S. Cescotto and G. Fonder, "A finite element approach for large strains of nearly incompressible rubber-like materials," *Int. J. Solids Struct.*, vol. 15, pp. 589-605, 1979.
- [14] J. E. Mark, "Rubber elasticity," *Rubber Chem. Technol.*, vol. 55, pp. 1123-1136, 1982.
- [15] P. C. Chou and N. J. Pagano, *Elasticity: Tensor, Dyadic, and Engineering Approaches*. New York: Dover, 1992.

Traffic Management Solutions in Large Cities – the Integrated Centre of Urban Mobility (CIMU) in São Paulo

Dariusz Swiatek, Melissa S. Pokorny, Jilmar A. Tatto, José E. Gonçalo, Vidal A. Z. C. Melo,
Eduardo M. Dias

Abstract— The paper aims at presenting solutions which may tackle one of the major problems of contemporary big cities all over the world – traffic management. It brings into reader’s attention the example of São Paulo. Learning from examples of global cities as London and Chicago where traffic is managed with the use of open protocol solutions such as UTMC and NTCIP– here it is suggested that such a way of facilitating traffic management may also be successful in São Paulo. An answer for contemporary problems may be the Integrated Centre of Urban Mobility (CIMU), which with the use of open protocol communication will help to manage traffic problems of the city.

Keywords—Traffic management, São Paulo, Integrated Centre of Urban Mobility (CIMU), open protocol.

I. INTRODUCTION

An unrestrained development of global urbanization that can be witness all over the world brings numerous challenges which requires joint effort of experts from various disciplines to help develop new ways of dealing with city problems. An array of areas such as demography, infrastructure, climate issues, economy, ecology, social, legal and countless further need to be merged to enable working out solutions for complex and multifaceted challenges which appears on a day-to-day basis in global metropolises.

An effective transport system is a vital element facilitating life in modern cities, its influence on various levels of public life is undeniable (from moving goods and passengers, though

Dariusz Swiatek is a researcher of GAESI (swiatek@pea.usp.br)

Melissa Seriana Pokorny is a MSc student of Polytechnic School, University of São Paulo – USP and a researcher of GAESI (melissapokorny@pea.usp.br)

Jilmar Augustinho Tatto is a MSc student of Polytechnic School, University of São Paulo – USP and a researcher of GAESI (jtatto@prefeitura.sp.gov.br)

José Evaldo Gonçalo is a PhD student of Polytechnic School, University of São Paulo – USP and a researcher of GAESI (jevaldo@prefeitura.sp.gov.br)

Vidal Augusto Zapparoli Castro Melo is a PhD student of Polytechnic School, University of São Paulo – USP and a researcher of GAESI (vidal_melo@pea.usp.br)

E. M. Dias is full professor of the Escola Politécnica of the Universidade de São Paulo and coordinator of GAESI - Grupo de Automação Elétrica em Sistemas Industriais, a research group of the Electrical Energy and Automation Department,

Escola Politécnica, Universidade de São Paulo, Av. Prof. Luciano Gualberto, trav. 3, n. 158, São Paulo/SP, Brazil, CEP 05508-970 (emdias@pea.usp.br).

improving daily mobility and access to various services and labour market, up to improving social inclusion). The evidence for an existing connection between well-functioning transport and economic development, competitiveness, quality of life in urban areas were provided in number of studies: Wegener [1]; EUNOIA [2]; Llewelyn-Davies, Banister and May [3]; Portugali [4]; Le Gales [5], Leven [6], OECD [7], CEC [8].

Since the challenges of modern transport systems were enlisted in number of studies, where the authors presented also a number of thematic solutions that help addressing the most vivid issues. Each of the areas presented above has a number of both theoretical and practical solutions that has been developed in various academic and applied studies. The major challenges of transport systems can be organize into six thematic groups: organizational issues, infrastructure, technological (Intelligent Transport System - ITS), environmental, social and spatial issues.

The organizational area covers all issues connected to the traffic management [2], [9], [10] which include inter-modality of transport (use and connection of various transport modes like buses, metro, trains, private cars and others; including means like bikes, carpooling, electric vehicles etc.). Other group of answers to modern problems include the use of various tools for organization of traffic within the city such as control and monitoring centres, emergency monitoring, maintenance of traffic management tools, etc. [11]. One of the most important areas here is the creation of new traffic management regulations and holistic solutions [12], [13].

Within the infrastructural area the common problems can be tackled by the improvement of the quality of physical infrastructure such as parking spaces, roads, railways [14], [15] but also pedestrian areas and other type of urban infrastructure like bus stops, traffic controls and other tools for traffic measurement etc. [16]. Besides upgrade and development of traditional infrastructure, it is equally important to develop ITS infrastructure, which will not only facilitate traffic flow on daily basis [17], [18] but also allow to collect data about the traffic to support areas as urban modelling and planning, decision making and other processes [19].

The technological issues are interconnected with the infrastructure, however it covers not only the physical presence of equipment for traffic control and management but also provides structural and software solutions that allows to tackle such issues as automatic collection of traffic data, bulk data (storage and use), spatial and temporal movement of data, achieving transparency and efficiency [2], [18], [19].

Another area of transport challenges which importance is growing in recent years is undoubtedly environmental protection. It is also associated with economic, social and security issues (like shrinking energy resources, alternative/removable energy, contamination, etc.). An increasing air pollution to which transport is one of the major contributors in urban areas, requires far-reaching solutions which are present in our daily life like reduction of private transport use [1], [22], [23] (like plate based rotation scheme for private cars in São Paulo [20], reduction of traffic of heavy utility vehicles [21]). The answers for the environmental issues are sought in alternative transport (both on infrastructural and organizational level), renewable energy resources, sustainable mobility, etc. [24].

The area of social issues connected to traffic problems require highlighting of issues of participation and social inclusion, which influence quality of living but also other aspects of public sphere like safety or accessibility. Changes of mobility of urban population is interconnected with job relocation and settlement patterns.

In this paper, we formulate the basis for building an integrated centre for control of urban traffic in São Paulo city based on the experience of large world metropolises, presenting possible architecture solutions for various traffic management equipment, as well as for communication between existing traffic management centres.

II. SPECIFICITIES OF TRAFFIC IN SÃO PAULO

São Paulo, the largest city of South America, and one of the fifth largest cities of the world, face the same type of problems regarding transportation management as the majority of large world metropolises. With over 11.8 million inhabitants and almost half of this number in cars (see table 1), allow us to expect that solutions used within other cities will be effective in São Paulo as well.

Table 1: Population, area and number of cars in some large cities.

Cities	Population (in million)	Area (thus km ²)	Number of cars (in million)
London	8.3	1572	2.5
Chicago	2.7	606	1.5
São Paulo	11.8	1521	5.0

Source: IBGE, DENATRAN, US Census Bureau, UK National Statistics.

Currently there are already in São Paulo – and metropolitan area – systems and equipment using ITS (Intelligent Transport System) for traffic management, such as: (a) Traffic Signal Control System; (b) Traveller Information Services; (c) Freeway Management; Electronic Toll Payment; (d)

Emergency Management Services; (e) Transit Management; (f) Incident Management Systems; and (g) Railroad Grade Crossing Safety, among others.

These systems and equipment are spread around the city and aim to manage and provide specific services to the population or decision-makers. The above mentioned elements of traffic management architecture are shown on Fig. 1.

Since the majority of traffic infrastructure is already present in São Paulo, one may question: is it really necessary to change? There is currently a lack of integration in the systems used in São Paulo. The systems using ITS in São Paulo as well as city general traffic management can profit from complex information from various sources.

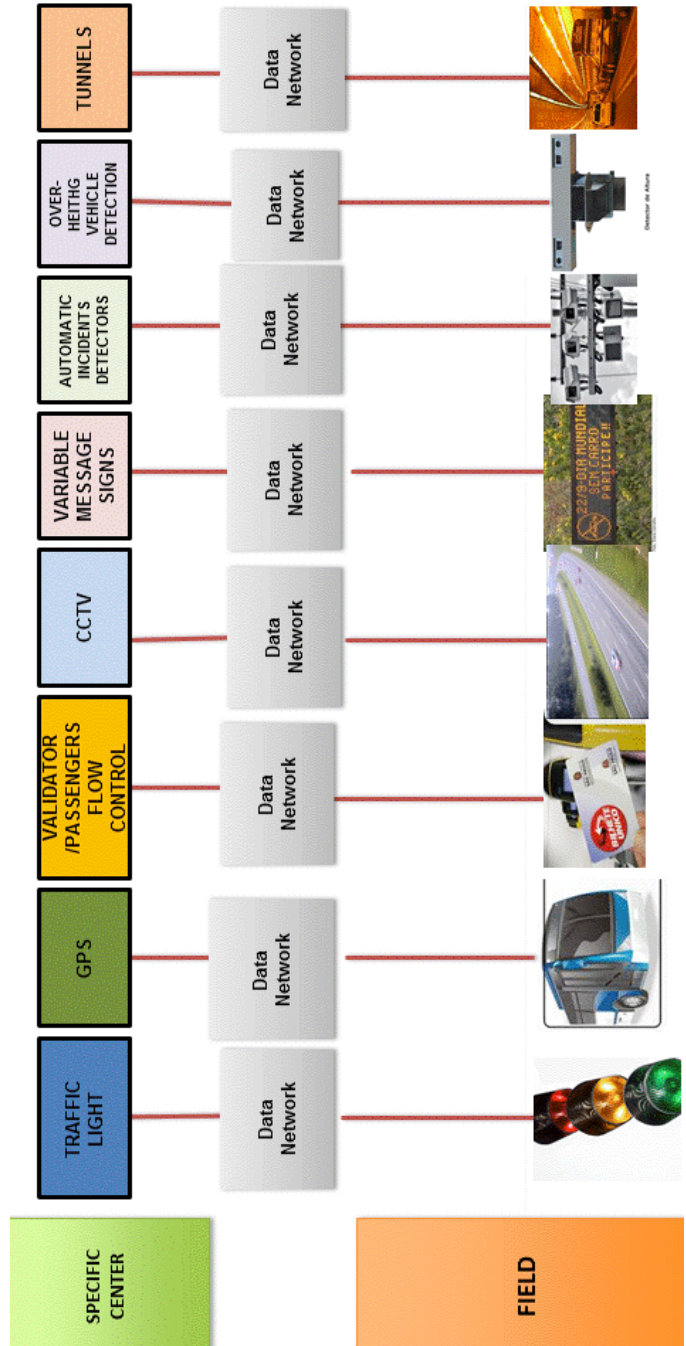


Fig. 1: Contemporary traffic management architecture in São Paulo.

Source: Authors' elaboration.

The major reason for lack of integration of existing ITS systems can be found in the manner that traffic equipment was built in the city. The majority of traffic infrastructure was built up as a response for growing demands and main problems of the time. In fact, the existing structures for traffic management very often function as isolated and independent systems, including the operational units of two major public companies dealing with mobility in São Paulo: the one responsible for traffic management (Companhia de Engenharia de Tráfego - CET) and the one managing public transport (São Paulo Transporte - SPTRANS).

The first, CET, is not only responsible for management of the transit in the city but also for setting up, maintenance and use of the majority of existing equipment for facilitating traffic. The second public company (SPTRANS) regulates and manages city's bus operators and the infrastructure of public transport connected to bus transport (such as bus corridors, terminals, bus-stops). Both companies has been traditionally acting independently in the provision of transportation services for the city.

As an attempt to answer to existing problems regarding transport, São Paulo authorities have adopted a few measures to minimize negative impacts on traffic and congestion of roads:

- in 1997 a license-plate-based car rotation scheme, by which 20% of the car fleet is kept off the streets during peak hours on central areas of the city on working days;
- restrictions at certain times of the day to truck traffic were implemented within the geographic area of the expanded CBD (2008);
- maximum speed limit was reduced in a number of city's streets and avenues, mainly in the centre (2012);
- since 2013 bus-only lanes were intensively created (over 300 km within the city borders), giving clear priority for public transport .

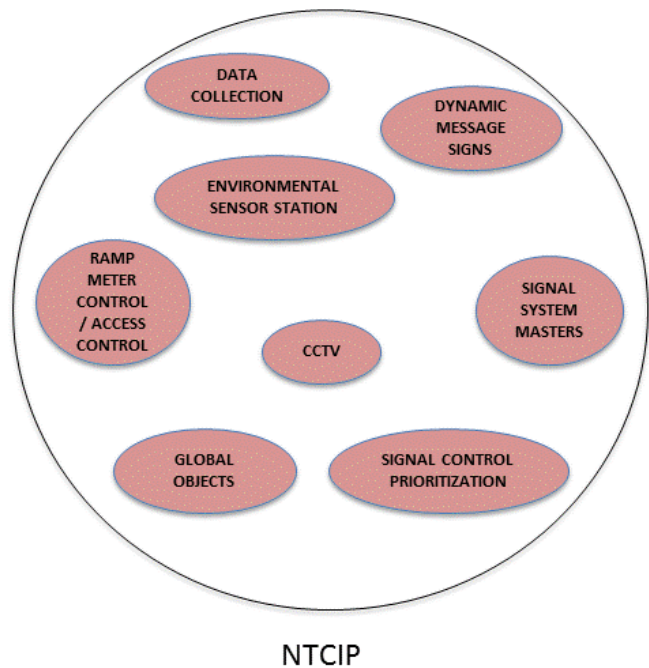
However, despite implementing the measures above and the various types of traffic infrastructures exiting within the city, unforeseen events (such as natural phenomena) and the excessive use of private cars still cause enormous traffic problems in the city, which remain highly jammed. For example, on 21st of March 2014, a normal working day with no special event or holiday eve, the city traffic management service observed the longest traffic jam of the year so far, with a length of 239 km [25]. There was no particular explanation for such a traffic to occur, apart from the excessive use of cars by the city inhabitants. This record was beaten two months later on 23rd of May, a Friday when a traffic jam of length of 344 km was registered; it was the longest traffic jam that São Paulo has ever suffered from [26]. This time, the explanations of the phenomena included such events like: the extreme rain fall that the city had for a period of a few hours; travels of city inhabitants for the weekend; accumulation of personal errands due to two days of strike of public transportation, and remaining strikes in public transport in ten cities of the metropolitan area. Individual accidents worsen traffic

conditions, specially due to the relatively long time of reaction of rescue services. This thus increase the disturbance of traffic, like the accident involving a heavy utility vehicle which blocked the crucial Rodovia Castelo Branco for about 5 hours causing traffic jam of 17 km on February 18th 2014 [27].

III. GLOBAL SOLUTIONS

Since various types of equipment are already located in São Paulo, the ideal solution for the city is that which bridges different system and technologies and allows for cooperation and communication between several sorts of traffic equipment. It would accommodate traffic in the city and facilitate movement of its inhabitants.

The National Transport Communication for ITS Protocol (NTCIP) is a group of standards for electronic communication protocols used for transportation (by traffic management agencies, producers, etc.). The protocols aim at providing solutions for communication between various tools and organizational units, and does not covers areas of functionality of the products. It covers communication between such groups of actors as: traffic operational centres (centre-to-centre communication C2C) and centre-to-field equipment communication (C2F). It , however, also provide information for various other participants of traffic activity as: vehicles users, travellers (by use of remote traveller support, personal information access), emergency services, payment administration, maintenance and construction services, fleet and freight management, emissions management, information service provides, archive data management, etc. [28].



NTCIP
Fig. 2. Architecture of NTCIP
Source: Authors' elaboration

The C2F covers the exchange of information between such areas as (see Fig. 2):
o Actuated Signal Controllers

- Dynamic Message Signs
- Environmental Sensor Station
- CCTV
- Data Collection
- Ramp Meter Control/Access Control
- Signal System Masters
- Signal Control Prioritization
- Global Objects (common objects across devices; time, scheduling, logging)

Apart from offering specific communication solutions between various types of equipment, the NTCIP provides the possibility of global solutions such as time adjustment, scheduling of various events between different elements of the system, etc.

The Urban Traffic Management and Control (UTMC) initiative was developed at the end of 1990's in the United Kingdom, initially aiming to point out, multiply and spread good practises and effective solutions among the many authorities involved in public transport. Since that time open standard protocols were the core activity of the initiative, as it was observed that interoperability between various elements of transport control systems were difficult due to the diverse standards of operation which resulted in a lack of a common platform between the many producers and specifications of equipment functioning both in the field and operational centres [13].

The works around UTMC open framework focus on developing the set of specifications for interfaces which allow communication between various systems, especially in manner of problems anticipation. The UTMC covers the interaction of various tools of traffic management such as: Closed Circuit Television (CCTV) which monitors roads, parking areas and highways; traffic signal management (such as Split Cycle Offset Optimization Technique – SCOOT used mainly in urban areas); car park management and guidance; air quality control (including wide range of vehicle emission data); access control (such as automatic number plate recognition or Vessel Monitoring System); travel info services (covering information channels on motorways, public transport and urban areas); infrastructure for Urban Traffic Control (UTC) and provides inputs of for planning and strategy making on various spatial level (starting from municipal, inter-municipal, regional or national) [29]. The scheme of UTMC coverage areas can be seen on Fig. 3.

The use of open protocols such as NTCIP and UTMC offers a wide array of advantages. Among the examples of what open protocols can help with, they allow systems of several different producers to interoperate, while reducing the danger of depending of solutions that are 'locked into' one specific supplier; therefore fostering competition, economic efficiency and quality assurance. This is a basic important condition to enable connecting diverse systems and expanding existing solutions.

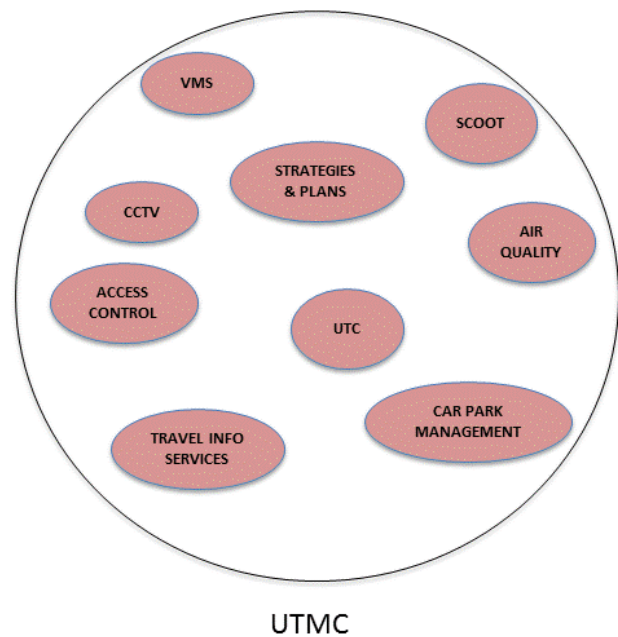


Fig. 3. Architecture of UTMC

Source: Authors' elaboration based on

<http://www.posse-openits.eu/en/Partners/UTMC-UK/> (last access 25.05.2014)

Deepening the relation between improvement of mobility and socio-economic issues, the use of open protocols creates an environment for innovation, fostering competition between producers and enabling equality of access to the market. Open protocols also permit evolutionary upgrades of hardware and software. Additionally, they support the creation of common data models which facilitate more effective delivery of multimodal real time travel information. To sum up, open protocols can provide a choice of vendors and phased procurement and deployment, enable interagency coordination, share communication channels and give a framework for specifying communications.

IV. CIMU

Since the beginning of 2013 a new direction was given to traffic management in São Paulo by the new mandate of city administration. It was emphasizing the integration of the agencies for traffic management (CET) and public transport by bus (SPTrans); innovation and the use of open protocols.

A solution that was thought to solve several traffic and transport problems was to create a unique database that integrates all the information about traffic and transport through a system based on open standards and open protocols, allowing different systems to benefit from the diverse gross data that up to now remained disperse and very much underused.

Therefore, the concept of the CIMU Centro Integrado de Mobilidade Urbana (Integrated Centre for Urban Mobility) was elaborated to address the government emphasis above cited.

The major purposes of CIMU are: (a) to visualize, in a complete and whole way, the information of all different components and sources to support strategic decision-making; (b) automate processes; (c) implement new functionalities; (d) provide information to users; e) share resources; shrink costs.

The architecture of CIMU is described in Fig. 4. As it is possible to see at the Fig., all data will be collected at field. Data from different sources is integrated in a data network of open protocols which enables control centres to use any information from the field. The data will be then transmitted

by network though specific control and coordination centres provided that all data from the specific centres will be replicated in CIMU.

By this design, field data is integrated and support many specific centres, and also, all the centres are integrated themselves, enabling decision-makers to get a whole picture of the city situation regarding mobility at a certain point and interfere in specific cases in real time.

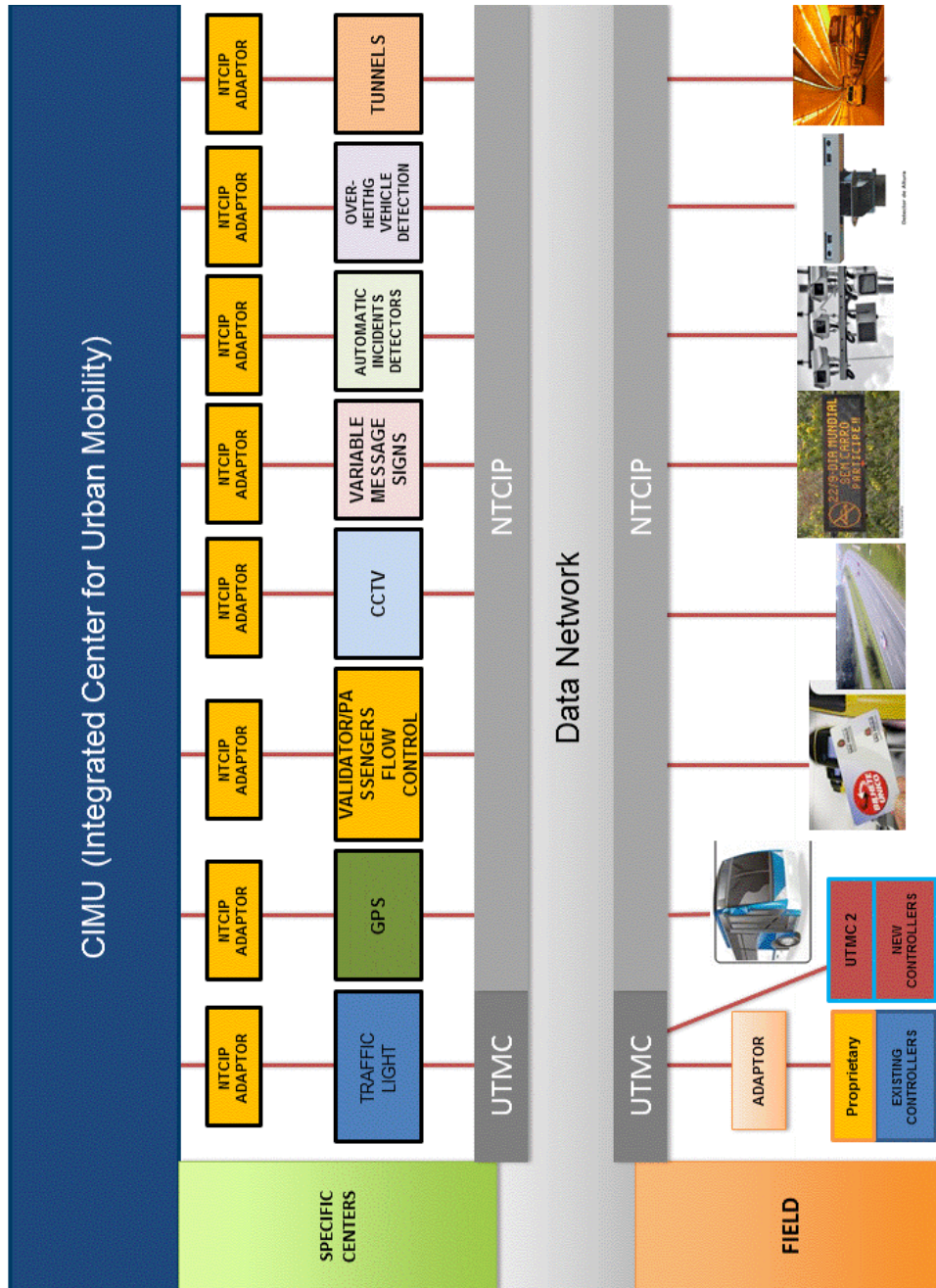


Fig. 4. Architecture of CIMU
Source: Authors' elaboration

V. CONCLUSION

Although it is well known that the simple fact of integrating technologies with open protocols will not be, just by itself, the solution for all mobility problems of São Paulo, one can assume that if such a centre as CIMU is accordingly associated with a proper infrastructure and organization, it can give more safety to users, allow more control, reduce time of journey, give accuracy, allow users to program their journey, reduce the damages to environment, give more information and predictability.

UTMC and NTCIP are not complete solutions, in the sense that they do not cover all systems and technologies, but they allow the incorporation of systems already existing in the city for traffic management and control. They can be considered as a starting point, a valuable one, indeed. Using open protocols to build the concept of CIMU is the way to combine and put together various solutions without the need of creating everything from scratch. It provides the framework that allows integrating the diversity of field data found in a diverse city as São Paulo, with a modern technology that eventually will permit city authorities to respond to mobility problems with the speed of the challenges that the city faces.

REFERENCES

- [1] M., Wegener, *The future of mobility in cities: challenges for urban modelling*. Proceedings of 12th World Conference on Transport Research, 2010.
- [2] EUNOIA, *Urban models for transportation and spatial planning, State-of-the-art and future challenges*, EUNOIA Consortium, Zurich, 2012.
- [3] Llewelyn-Davies, Banister and May, *Transport and City Competitiveness – Literature Review*, Department for Transport, United Kingdom, 2004.
- [4] J., Portugali, Complexity theories of cities: achievements, criticism and potentials. In: Portugali, J., Meyer, H., Stolk, E., Tan, E. (eds.) *Complexity Theories of Cities Have Come of Age: An Overview with Implications to Urban Planning and Design*, pp. 47–62. Springer, Berlin 2012.
- [5] Le Galès, *European Cities, social conflicts and governance*, Oxford University press, Oxford, 2002.
- [6] C.L. Leven, 1979, *The Mature Metropolis*, Boston, Lexington Books, Alvin Toffler, 1979.
- [7] OECD, Cities, Climate Change and Multilevel Governance, *Environment Working Papers*, OECD, Paris, 2009.
- [8] CEC, *Commission of the European Communities. Green Paper 'Towards a new culture for urban mobility'*. Communication COM(2007) 551 Final, September 2007.
- [9] E. Taniguchi, R.G. Thompson, *Intermodal Transport and City Logistics Policies*, *Recent Advances in City Logistics*, Elsevier, 2005.
- [10] B.S. Hoyle, R.D. Knowles, *Modern transport geography*, Belhaven Press, London, 1992.
- [11] B. Moore, K. Larkins, *Traffic control open systems: a working national system*, 9th International Conference on Road Transport Information and Control, 1998, p. 119-124.
- [12] Taiwan NTCIP Study and Traffic Control System Demonstration Project (Phase 4), Taiwan Government publication, 2006.
- [13] B., Radia, Integrating the Traffic Management Applications of ITS: an overview of the UTMC programme in the UK, *ITS Journal*, 2000, Vol. 6, pp. 83-90.
- [14] T. Komornicki, P. Korcelli, *Alternative Scenarios of Transportation Network Development for EU Accession Countries*, IASON Technical Note, IGiPZ PAN, 5, Polish Academy of Sciences, Warsaw, 2003.
- [15] G.M. Boarnet, *Transportation Infrastructure and Sustainable Development, New Planning Approaches for Urban Growth*, ACCESS No 33, Fall 2008, p. 27-33.
- [16] L.E.S. Brettas, V.A.Z.C. Melo, E.M. Dias, *Automation of the control of street furniture using mobile technologies*, (in-printing).
- [17] K.W., Axhausen, (2011). *Computational challenges for integrated micro-simulation models*. Arbeitsbericht Verkehrs- und Raumplanung, 719, IVT, ETH Zürich, Zurich.
- [18] G., Misuraca, D., Broster, C., Centeno, Y., Punie, F., Lampathaki, Y., Charalabidis, D., Askounis, D., Osimo, K., Szkuta, and M., Bicking, *Envisioning Digital Europe 2030: Scenarios for ICT in Future Governance and Policy Modelling*, European Commission JRC-IPTS, 2010.
- [19] J.L. Schofer, *Information Assets to Support Transportation Decision Making, Report of a Peer Exchange of State Transportation Organizations*, Transportation Research Board, Kansas City, 2007. <http://onlinepubs.trb.org/onlinepubs/circulars/ec121.pdf> (last accessed April 2014).
- [20] Municipal Decree N° 37.085 of 3rd of October 1997 - Regulations Law No. 12,490 authorizing the executives to implement the restriction program of motor vehicles in the city. (in Portuguese)
- [21] Official Gazette of the City of São Paulo, No. 87 (13/05/2008) - Decree No. 49,487 of May 12, 2008 - Regulates the truck traffic in the Top Zone Restriction of Movement - ZMRC (in Portuguese).

- [22] A. Kimms, K. Maassen, *Optimization and simulation of traffic flows in the case of evacuating urban areas*. OR Spectrum 33, 2011, 571–593
- [23] S. Kuhn, R. Schultz, *Risk neutral and risk averse power optimization in electricity networks with dispersed generation*. Math. Methods Oper. Res. 69, 2009, 353–367
- [24] Achieving Greater Safety and Environmental Protection in Road Transport, On the Road to Sustainable Mobility, Japan Automobile Manufacturers Association Inc., http://www.jama-english.jp/publications/sustainable_mobility_2011.pdf (last access: May 2014).
- [25] L. Formenti, “Com 239km de lentidão, SP bate recorde do ano. *O Estado de S. Paulo*, 22/03/2014, p. E7.
- [26] M. Reolom, R. Italiani, “SP tem maior lentidão da história: 344km” . *O Estado de S. Paulo*, 24/05/2014, p.E4.
- [27] F. Cambricoli, J.M.Tomazela, “Acidente com carga tóxica mata um e fecha Castelo”. *O Estado de S. Paulo*, 19/02/2014, p. A13.
- [28] Vanada D., NTCIP and overview (ppt presentation) <http://www.itsga.org/assets/1-ntcip.pdf> (last accessed: May 2014)
- [29] <http://www.utmc.uk.com/background/index.php> (last accessed: May 2014)

Treatment of chromium wastewater using membrane separation processes

Pavel Kocurek, Karel Kolomazník and Michaela Bařinová

Abstract—This paper deals with the application of membrane separation processes for chromium wastewater treatment. It describes the rejection of trivalent chromium using a commercial membrane for reverse osmosis (RO98pHt). Separation experiments were performed with model solutions of chromium. The effects of feed pH, chromium concentration and temperature were investigated. The results showed that pH of the feed solution has influence on the stability of dissolved particles with negative impact on membrane fouling. Prepared feed solutions were stable till pH=6, over this value floccules sedimentation occurred. RO98pHt rejected almost 100% Cr(III) at various pH values using 100 mg.L⁻¹ concentration level, operating pressure 1.5 MPa and at temperature 20°C. Similar results showed separation experiments using various Cr(III) concentration from 10 till 560 mg.L⁻¹ and pH=5±0.2. Increase of operating temperature causes higher permeate flux and has no significant influence on the rejection level of Cr(III). Obtained results show application possibility of reverse osmosis for chromium removal in wastewaters.

Keywords—chromium, membrane separation, reverse osmosis, wastewater treatment, leather industry.

I. INTRODUCTION

WIDE spectrum of physical-chemical and biological treatment methods and their combination is commonly used for treatment of various wastewater. With development of new methods and with focus on higher environmental protection, some technologies no longer meet current requirements. For this purpose, membrane separation processes, especially pressure-driven membrane separation processes, have found wide use abroad [1]. Membrane separation provides many advantages and versatility of usage. These processes have enforced in these areas of human activity where the other technologies dominate nowadays. We can regard them like clean, environmentally-friendly and efficient alternative to traditional processes.

This work was supported in part by the European Social Fund and by Czech Republic's state budget under Grant OP VK CZ.1.07/2.3.00/30.0035.

P. Kocurek is with the Tomas Bata University in Zlín, Faculty of Applied Informatics, Department of Automation and Control Technologies, Zlín, 76005, Czech Republic (phone: +420576035628; e-mail: kocurek@fai.utb.cz).

K. Kolomazník is with the Tomas Bata University in Zlín, Faculty of Applied Informatics, Department of Automation and Control Technologies, Zlín, 76005, Czech Republic (e-mail: kolomaznik@fai.utb.cz).

M. Bařinová is with the Tomas Bata University in Zlín, Faculty of Applied Informatics, Department of Automation and Control Technologies, Zlín, 76005, Czech Republic (e-mail: barinova@fai.utb.cz).

Chromium wastewaters occur in various industries and there is need of their treatment or of recycling of reagents. Leather industry belongs given to its size and the amount of produced waste to these industries with large negative impact on the environment. It produces big volume of wastewaters with different composition and some of them contain chromium. Many studies have been performed focusing on the recycling of reagents [2] and waste utilization [3]. From 1 tone of wet-salted hide is manufactured approximately 200 kg of leather. Concurrently is generated more than 600 kg of solid waste during tanning process and the volume 30-35 m³ of wastewater is discharged into environment in leather industry [4]. In these wastewaters we can expect several concentrations of chromium - basic chromium sulphate is the most popular tanning reagent. Besides high concentrations of chromium, sulphates, chlorides and organic substances wastewaters from chromium tanning are characterized by low pH value and high temperature. But according to these facts, membrane separation can find its place in treatment schema [5], for example to improve the quality of the recycled chromium. Metals, lipidic substances and other impurities could presence in recovered chromium using traditional method combining alkaline precipitation of chromium and dissolution of Cr(OH)₃ in sulphuric acid [6].

II. MEMBRANE SEPARATION

Membrane processes are used in general to separate homogeneous or heterogeneous liquid solutions and mixtures, gaseous mixtures, and suspensions of solid particles of microscopic dimensions (less than ca. 1x10⁻⁵ m) in liquids. A common feature of membrane separation is high separation efficiency. The separation selectivity depends on the particular membrane process and on the membrane type. Because membrane separations take place at ambient temperatures, there is no damage to thermo-labile substances. The membrane units may be operated remotely using modern control systems that reduce the cost of labour. Membrane processes are relatively extended abroad. The technique may be applied in low-volume batch equipment or in a continuous large capacity treatment plant.

Membrane processes are based on the separation of the solution into two different streams using a semipermeable membrane. Permeate contains solvent and the particles which passed through the membrane. The remaining particles which were captured by membrane form the concentrate. The

difference across the membrane of pressure, concentration, electrical potential, or temperature serves as the driving force.

Focus of this work is usage of pressure-driven membrane separation processes for wastewater treatment. Operating conditions of these processes are mentioned in Table I.

Table I pressure-driven membrane separation processes

separation process	particle size	operating pressure
microfiltration	>0.1 μm	<500 kPa
ultrafiltration	10-100 nm	500-1000 kPa
nanofiltration	1-10 nm	1-4 MPa
reverse osmosis	0.1-1 nm	3-10 MPa

Microfiltration and ultrafiltration are most similar to the classical filtration. They are suitable for the removal of suspended particles, colloids, bacteria and viruses, high-molecular substances etc. The separation is based on the sieve-effect. These processes are commonly used like pre-treatment.

The principle of nanofiltration and reverse osmosis is the same. But the separation ability of nanofiltration is usually considerably lower. This separation technology can separate especially monovalent ions with lower efficiency than reverse osmosis, separation level of polyvalent ions is comparable. The mechanism is not based on the sieve-effect but on the diffusion.

In the case of reverse osmosis the separation proceeds on the ionic level. Mono- and polyvalent ions and low-molecular organic substances are separated. Reverse osmosis technology can be installed in industry for dissolved matter reduction, especially inorganic salts removal (chlorides, nitrates, sulphates, ammonia nitrogen). This is related to the need to use the relatively compact and non-porous membranes. The higher is the concentration of dissolved salts in feed, the higher is the osmotic pressure of feed and the higher operating pressure of device must be applied. Solvent pass through the membrane and dissolved matter is caught by membrane [7].

Nanofiltration and reverse osmosis are used like the main technologies for wastewater treatment. Pre-treatment is necessary in most installations, post-treatment could be included too, but in most cases is not needed. It depends on the type of wastewater, on the applied separation process and on the desired level permeate (actual need of operator). Both can remove common cations and anions, organic matter and heavy metals [8] with high efficiency, but not limited to.

Osmotic pressure plays significant role in the description of reverse osmosis. It is generated by a semipermeable membrane which separates ions and solvent passes therethrough.

Osmotic pressure π is described in osmotic equilibrium. The following formula is valid for electrolyte solutions.

$$\pi = RTc[1 + \alpha(v_C + v_A - 1)]$$

$$C_{v_C} A_{v_C} \leftrightarrow v_C C + v_A A \quad (1)$$

T is thermodynamic temperature, R is molar gas constant, c is concentration of solutes, α is the degree of dissociation, C and A mean cation and anion and v refers to quantity. So concentration of solutes and temperature have main influence on the osmotic pressure of feed solution, subsequently on the operating condition of separation process. However, that formula is only valid for very diluted and simple solutions.

Among other factors that affect reverse osmosis belong rejection R , volume reduction factor and permeate flux. Rejection indicates the separation efficiency of component or total. For calculation serve concentration values in feed c_F and in permeate c_P or conductivity values κ can be used.

$$R = \frac{c_F - c_P}{c_F} \cong \frac{\kappa_F - \kappa_P}{\kappa_F} \quad (2)$$

Volume reduction factor is defined like ratio between feed volume and concentrate volume. Permeate flux is hourly flux of permeate through the membrane with area 1 m². Its values are different for setup of operating conditions of separation process and can indicate membrane fouling. For final comparison of separation experiments its necessary to hold the same operating temperature because permeate flux is increasing with temperature.

III. CHROMIUM AND ITS OCCURRENCE

The anthropogenic sources of chromium are wastewaters from metallurgy, metal coatings, leather industry and textile industry. Wastewater from chromium tanning can contain up to 4100 mg.L⁻¹ of Cr(III) [6].

Chromium occurs in waters most often in two oxidation states Cr(III) and Cr(VI). Chromium can be bonded to organic matter. The most stable form of occurrence is Cr(III); Cr(VI) compounds are strong oxidative reagents. Under normal conditions is hexavalent chromium simply reduced into trivalent chromium. But under some conditions opposite reaction occurs and toxic hexavalent chromium is formed [9]. Hexavalent chromium is classified as a carcinogen. Technical legislation of chromium wastewater treatment is strict from this purpose and is based on the probability of presence hexavalent chromium.

IV. MATERIALS AND METHODS

Behaviour simulation of Cr(III) solution on membrane was performed under various conditions. The influence of pH, concentration and temperature was studied. For this experiments the membrane typed RO98pHt (Alfa Laval, Sweden) for reverse osmosis was chosen. The rejection of NaCl solution of this composite membrane is higher than 97% (NaCl 2 g.L⁻¹, 1.6 MPa, 25°C). Operation conditions: pH range 2-11, typical operating pressure range: 1.5-4.2 MPa, maximum operating pressure: 55 MPa, temperature 5-60°C [10]. Hexavalent chromium is oxidation reagent and can destroy the membrane, so this solution wasn't used.

For this purpose the feed solution was prepared using $\text{CrCl}_3 \cdot 6\text{H}_2\text{O}$ (Lach-Ner) and distilled water. Solution of NaOH (Roana) was used for the pH adjustment of feed.

Feed solution 100 mg.L^{-1} of Cr(III) was prepared under various pH values within 3-6. After that membrane separation was applied. Separation experiments were performed under these parameters: operation pressure 1.5 MPa, temperature 20°C and value of achieved volume reduction factor 4. After this group of experiments one pH value was chosen and other separation experiments were performed under the same operating conditions using feed solutions 10, 100 and 560 mg.L^{-1} of Cr(III) . Finally, the influence of temperature on the separation of Cr(III) was investigated. Stability of membrane process, Cr(III) rejection, pH values of streams and permeate flux were measured during every experiment.

After every separation experiment analysis of all streams were performed. Chromium concentration was measured on AAS SensAA (GBC Scientific Equipment, Australia), conductivity on conductivity-meter GMH3430 and pH values on pH-meter GMH3530 (Greisinger Electronic, Germany).

All separation experiments were performed on membrane separation unit LAB-M20 (Alfa Laval, Sweden) in laboratory scale. The equipment was customized for batch processing. The volume of the feed tank was ca. 12 L. The actual separation takes place on a plate-and-frame module DSS equipped with 36 membranes with total membrane area 0.63 m^2 . A Rannie piston pump with maximum operating pressure of 6.0 MPa was used. A separate water supply was used to maintain the pistons of the pump moist. A flow liquid-liquid heat exchanger cooled the membrane module. Water from the faucet served as the cooling agent.

V. RESULTS AND DISCUSSION

A. Influence of pH

pH of solution is important factor influencing the stability of prepared Cr(III) solution. Solutions with pH values within 3-6 were stable; increasing pH over 6 flocculation occurred and floccules fallen to the bottom of the vessel. For the membrane separation only Cr(III) solutions with pH values 3.3 (RUN1), 5 (RUN2) and 5.5 (RUN3) were used.

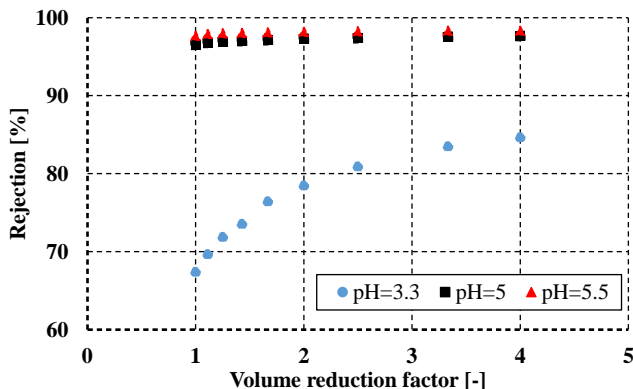


Fig. 1 dependence of rejection on volume reduction factor under different pH values (100 mg.L^{-1} Cr(III))

Fig. 1 describes rejection during the separation experiment based on streams conductivity measurement. According to obtained results - rejection and stability of separation process - pH=5 was chosen for experimental continuing. Separation at pH=3.3 (natural pH of CrCl_3 solution) brings cost with use of acid in higher amount in the case of "standard" wastewater treatment. For example carbonates decompose at pH=4.5 completely.

B. Influence of Concentration

Experiments using three different concentration of Cr(III) in wide range have been performed to evaluate the influence of concentration. They were concentrations 10, 100 and 560 mg.L^{-1} ; corresponding marking RUN4, RUN2 and RUN5. Feed pH value was adjusted in every separation experiment to 5. During separation experiments no significant change in rejection values was observed. Only in the case of experiment RUN4 it took a while to reach constant rejection similar to others. The course of separation experiments is described in Fig. 2 and Fig. 3.

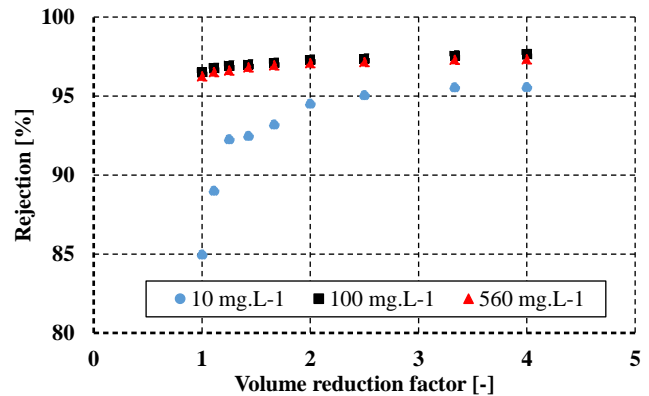


Fig. 2 dependence of rejection on volume reduction factor under different Cr(III) concentrations and pH=5

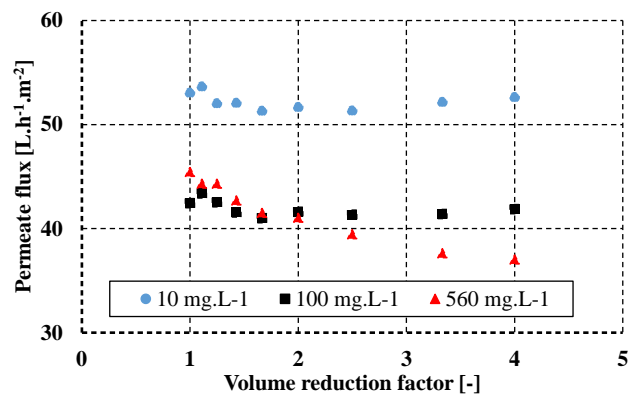


Fig. 3 dependence of permeate flux on volume reduction factor under different Cr(III) concentrations and pH=5

Using operating pressure 1.5 MPa we can observe changes of permeate flux comprising different feed concentrations. Permeate flux is the highest in experiment RUN4. Values for experiments RUN2 and RUN5 are comparable. There is no significant decrease of permeate flux in time but it could differ

using real wastewater sample. Only in the case of experiment RUN5 we can see a slight decrease of permeate flux because Cr(III) concentration of feed water was considerably higher.

C. Influence of Temperature

Temperature influences the following parameters of separation process - osmotic pressure and permeate flux. Feed solution was prepared under the same conditions like in the case of experiment RUN2. The operating temperature was increased in range 15-26°C and the influence of temperature on permeate flux and rejection was observed.

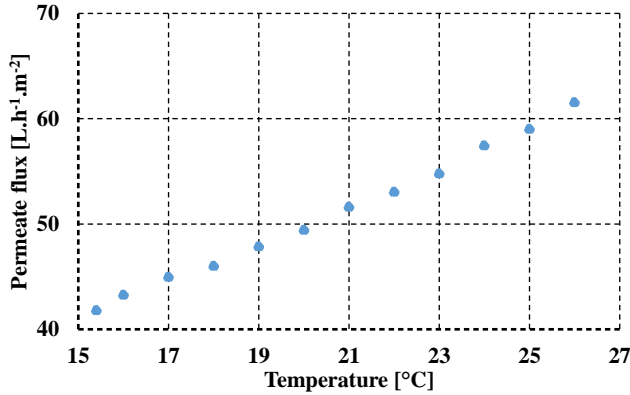


Fig. 4 dependence of permeate flux on temperature

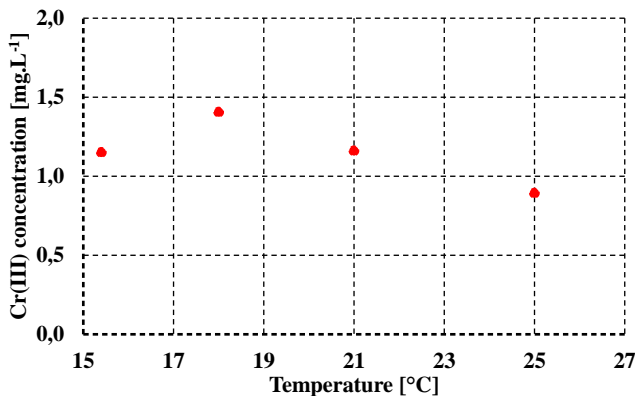


Fig. 5 dependence of Cr(III) concentration in permeate on temperature

In Fig. 4 we can see strictly linear trend of experimental values of permeate flux. Increasing the temperature by 1°C will increase the permeate flux of 3.6%. The effect of the chromium concentration in permeate is negligible. It is showed in Fig. 5. Concentration of chromium may be affected by small measurement error. These values are essentially comparable.

Table II feed and permeate composition in separation experiments

experiment		RUN1	RUN2	RUN3	RUN4	RUN5
pH [-]	feed	3.2	5	5.5	5.2	4.9
	permeate	1.6	0.62	0.07	0.13	3.3
Cr(III) [mg.L ⁻¹]	feed	108	96	84	10	562
rejection [%]		98.5	99.4	99.9	98.7	99.4

Table II comprises composition of the feed and permeate in all separation experiments. Rejection of Cr(III) achieves in all

cases high values near 100%. Due to the size of Cr³⁺ reverse osmosis provides sufficient reserve in rejection. Nanofiltration in general separates these ions with similar efficiency but rejection of monovalent ions could not be sufficient.

VI. CONCLUSION

In this study membrane separation of chromium by reverse osmosis using various operating conditions was performed. Separation experiments with Cr(III) solutions provided very good results given to high rejection values. The results showed that pH of feed solution has influence on the stability of dissolved particles with negative impact on membrane fouling. Prepared feed solutions were stable till pH=6, over this value floccules sedimentation occurred. RO98pHt rejected almost 100% Cr(III) at various pH values using 100 mg.L⁻¹ concentration level, operating pressure 1.5 MPa, volume reduction factor 4 and at temperature 20°C. Similar results showed separation experiments using various Cr(III) concentration from 10 till 560 mg.L⁻¹ and pH=5±0.2. Increase of operating temperature causes higher permeate flux and has no significant influence on the rejection.

These results have positive impact on the application of membrane separation processes in leather industry. But in the case of real wastewater from chromium tanning treatment, laboratory and pilot-plant experiments including appropriately pre-treatment for separation process optimization are needed.

REFERENCES

- [1] Z. Honzajková, M. Kubal, M. Podhola, T. Patočka, M. Šír, and Pavel Kocurek, "Membrane technologies and their use in treatment of groundwater and landfill leachate", Chem. Listy, vol. 105, 2011, pp. 245-250.
- [2] J. Kanagaraj, N. K. Chandra Babu, and A. B. Mandal, "Recovery and reuse of chromium from chrome tanning waste water aiming towards zero discharge of pollution", Journal of Cleaner Production, vol. 16, 2008, pp. 1807-1813.
- [3] K. Kolomaznik, M. Adamek, I. Andel, and M. Uhlírova, "Leather waste - Potential threat to human health, and a new technology of its treatment", Journal of Hazardous Materials, vol. 160, 2008, pp. 514-520.
- [4] H. Ozgunay, S. Colak, M. M. Mutlu, and F. Akyuz, "Characterization of leather industry wastes", Polish J. of Environ. Stud., vol. 16, 2007, pp. 867-873.
- [5] P. Religa, A. Kowalik, and P. Gierycz, "Effect of membrane properties on chromium(III) recirculation from concentrate salt mixture solution by nanofiltration", Desalination, vol. 274, 2011, pp. 164-170.
- [6] A. Cassano, R. Molinari, M. Romano, and E. Drioli, "Treatment of aqueous effluents of the leather industry by membrane processes: A review", Journal of Membrane Science, vol. 181, 2001, pp. 111-126.
- [7] H. Straathmann, "Membranes and membrane separation processes" [Online], 2005, Available: http://onlinelibrary.wiley.com/doi/10.1002/14356007.a16_187.pub2/full.
- [8] F. Fu, and Q. Wang, "Removal of heavy metal ions from wastewaters: A review", Journal of Environmental Management, vol. 92, 2011, pp. 407-418.
- [9] N. K. Chandra Babu, K. Asma, A. Raghupathi, R. Venba, R. Ramesh, and S. Sadulla, "Screening of leather auxiliaries for their role in toxic hexavalent chromium formation in leather - posing potential health hazard to the users, Journal of Cleaner Production, vol. 13, 2005, pp. 1189-1195..
- [10] Alfa Laval Flat Sheet Membranes: Reverse osmosis membrane RO98pHt.

Return on investment in photovoltaic panels and verification their effectiveness

P. Chrobak, M. Zalesak, M. Oplustil, S. Sehnalek, and J. Vincenec.

Abstract—This article deals with an economical evaluation of utilization of renewable energy sources and particularly of photovoltaic panels. In the introduction, the issue of conversion of the direction of the solar radiation flow on a horizontal surface of a solarimeter towards the direction normal to the plane surface of the photovoltaic panels is described. Based on these parameters, we can determine the total global radiation which is kept by the panels and accordingly calculate the theoretical production of electricity on the month base. These values are compared with the results of measurements and it is possible then to determine efficiency of the panels.

Keywords— photovoltaics, economical evaluation, photodiode, semiconductor, cell, solar radiation, azimuth, pollution, efficiency, inverter.

I. INTRODUCTION

Photovoltaics is a technology for the direct conversion of the solar radiation into DC current. The principle has been discovered more than 150 years ago by Alexander Edmond Becquerel. This technology is inexhaustible source of electricity but due to the rate of the solar radiation during the year it is not constant and even depends on weather conditions (clouds, rains, pollution etc.). In recent years, due to the technological development and mass production of the panels, the efficiency of photovoltaics conversion is getting higher and the price is dropping down what gets the photovoltaics utilization more favourable. The spread of photovoltaics thus depends mainly on the electricity price.

II. PHYSICAL PRINCIPLE OF PHOTOVOLTAIC CONVERSION

Photovoltaic is a method for the direct conversion of sunlight into electricity by using the photoelectric effect on large semiconductor photodiodes (photovoltaic cells). The individual photodiodes are called photovoltaic cells and are usually attached into larger units (photovoltaic panels).

The simplest photodiodes consists of two semiconductors with a different type of electrical conductivity. In one of the

layers the material of the type N predominate negatively charged electrons, while the second layer of material P predominate "holes" which are essentially blanks which readily accept electrons. At the point where these two layers meet with a P - N junction where there is a pair of electrons with holes, thereby creating an electric field that prevents other electrons move from the N - layer to the P - layer. Normally, the electrons in the semiconductor material are firmly bonded to the atoms of the crystal grid and the material is then nonconductive. By adding a very small amount of an element with a greater number of valence electrons to the crystal creates a region of conductivity of the type N, in which free electrons exist creates electrical charge. Conversely an impurity element with a reduced number of valence electrons creates a region with conductivity of the P type, in which the crystal grid range "hole are as" without electrons. If the semiconductor material capture of a photon of sufficient energy, it results in creation of one electron-hole pair [1]. If the circuit is closed, the wearer's hub starts to move in adverse directions to the negative electrode. A positive hole is shown in Figure 1.

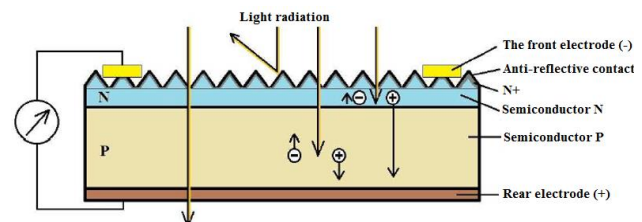


Fig. 1 The structure of the photovoltaic cell [2]

III. DIVISION OF PHOTOVOLTAIC CELLS

Photovoltaic cells can be divided accordingly to the type of photovoltaic cells into monocrystalline, polycrystalline and amorphous.

Monocrystalline cells are produced by chemical technologies by drawing molten base material in the form of rods which are then cut into slices of the substrate (most often is used material based on silicon). Cell consists of a single quartz crystal and its practical energy efficiency is in the range 13 - 17%. Production

This work was supported in frame of Internal Grant Agency of Tomas Bata University in Zlin, Faculty of Applied Informatics IGA/FAI/2014/047, IGA/FAI/2014/050, IGA/FAI/2014/015, IGA/FAI/2014/057 and under the project CEBIA-TECH NO. CZ.1.05/2.1.00/03.00089

P. Chrobak is with the Tomas Bata University in Zlin, Faculty of Applied Informatics, Department of Automation and Control Technologies, Zlin, 76005 Czech Republic (e-mail: chrobak@fai.utb.cz).

M. Zalesak, is with the Tomas Bata University in Zlin, Faculty of Applied Informatics, Department of Automation and Control Technologies, Zlin,

76005 Czech Republic (e-mail: zalesak@fai.utb.cz).

S. Sehnalek is with the Tomas Bata University in Zlin, Faculty of Applied Informatics, Department of Automation and Control Technologies, Zlin, 76005 Czech Republic (e-mail: sehnalek@fai.utb.cz).

J. Vincenec is with the Tomas Bata University in Zlin, Faculty of Applied Informatics, Department of Automation and Control Technologies, Zlin, 76005 Czech Republic (e-mail: vincenec@fai.utb.cz).

of monocrystalline solar cells is expensive as for the large consumption of silicon. However, monocrystalline cells are the largest stake of the market (around 85% of the world production) for the higher efficiency compared with other material of cells [3], [4].

Polycrystalline cells also include a silicon wafer, but unlike monocrystalline cells are formed by the crystal grid. The manufacture of these cells requires significantly less energy consumption than the production of monocrystalline cells, which is reflected in the price. The energy efficiency of these cells is in the range of 12-16 %. These cells use more effectively the diffuse part of the solar radiation than the monocrystalline, and thereby the efficiency of the both types is equivalent. [3], [4].

The type of amorphous cells consist of a thin silicon layer, which is applied to a material base formed of glass, plastic or fabric. The energy efficiency of these cells is significantly lower than that on previous mentioned cells and it is in the range of 7-9 %. These cells are suitable to be integrated in building structure surfaces. These type of the cells do not require excessive cooling as the previous mentioned types. [3], [4].

IV. DESCRIPTION OF THE SYSTEM

System described in this chapter is applied in the laboratory of environmental engineering at the FAI UTB in Zlín. The system consists of 9 photovoltaic panels with a total area of 11.25 square meters. The panels used, are of the type of polycrystalline photovoltaic cells. The producer of these panels declared an energy efficiency of 15% (the angle of panels surface inclined from the horizontal one of 45 ° with the southeast azimuth of the normal direction to the panel surface). Installed panels are shown in Figure 2.



Fig. 2 System under consideration

Surface reaches 750 Wm^{-2} , the electric power produced by the panels should be $P = 1265 \text{ W}$, based on the declared efficiency by the producer. The output DC voltage of the panels is converted by the AC voltage inverter in one phase AC current with the 230 V AC. This inverter also displays information

about the amount of energy produced by the various operating states of the system (fault, instantaneous power, voltage, total produced energy by the system, etc.) [5].



Fig. 3 Inverter Sunny Boy

Figure 3 shows the inverter Sunny Boy 1700 with defined efficiency by the European standards $\eta_{\text{euro}} = 91.8\%$. This value has been measured under varying climatic conditions where maximum efficiency were reached $\eta_{\text{max}} = 93.5\%$ with the optimal measuring conditions (stable temperature conditions, nominal DC voltage and medium values of AC power). The rest of the converted energy is lost by the electrical conversion in the form of heat [6], [7].

V. METHODOLOGY VALIDATION PARAMETERS

To determine the economical evaluation of the investment in photovoltaic systems, which is created by the panels and the electrical conversion facilities, it is crucial to verify energy efficiency of the whole system in the operation conditions. In order to verify the efficiency of the electrical energy production system, it is necessary to compare the total amount of energy produced by photovoltaic panels and total amount of solar radiation energy falling on the surface of the panels in the longer term.

The total amount of solar radiation falling on the photovoltaic panel surfaces can be measured directly by using a solarimeter device, which is inclined in the same angle as the panel surface. In this case, the energy of falling solar radiation to the surface which includes both direct and diffusion parts of the radiation, is compared with the energy produced by the system.

The second option of the evaluation is to measure solar energy by the solarimeter which is installed horizontally (the particular case). The measured values of solar radiation by the solarimeter has to be then converted to the radiation falling on the normal direction of the panels. This equation is given below according to CSN 73 0548 [9]. Solar declination is determined for 21st day of each month according to the formulas (1) to (9):

$$\delta = -23.5 \cos \cdot (30 \cdot M) \quad (1)$$

where δ is solar declination [°],

M number of the month in the year (1–12).

The solar declination δ are listed in Table I.

Table I Solar declination for each month

Month	III	IV	V	VI	VII	VIII	IX	X
δ [°]	0	12	20	24	20	12	0	-12

The height of the sun above the horizon, h , for ϑ north latitude is given by the following equation: (2)

$$\sin h = 0.766 \sin \delta - 0.643 \cos \delta \cdot \cos(15\tau) \quad (2)$$

where h is the height of the sun above the horizon [°],
 τ solar time [h].

Solar azimuth, a , determine the north in a clockwise direction by the relation: (3)

$$\sin a = \frac{\sin(15\tau) \cdot \cos \delta}{\cos h} \quad (3)$$

where a is solar azimuth [°].

The angle between the normal of surface and the direction of the rays, θ , is determined by the relationship: (4)

$$\cos \theta = \sin \cos h \cdot \cos a + \cos h \cdot \sin a \cdot \cos(a - \gamma) \quad (4)$$

where θ is the angle between the normal illuminated surface of sun and beam direction [°],
 α wall angle with the horizontal plane, taken on the side facing away from the sun [°],
 γ azimuth angle of the normal wall, taken as solar azimuth [°].

For the vertical surface is given by (5),

$$\cos \theta = \cos h \cdot \cos(a - \gamma) \quad (5)$$

for the horizontal surface given by (6),

$$\cos \theta = \sin h \quad (6)$$

The intensity of direct solar radiation is determined as follows, (7)

$$\dot{I}_D = 1350 \exp \left[-0.1z \left(\frac{16-H}{16+H} / \sin h \right)^{0.8} \right] \quad (7)$$

where \dot{I}_D is intensity of direct solar radiation [$W m^{-2}$],
 z coefficient of air pollution,
 H attitude [km].

For each month is recommended to use these levels of pollution that are listed in Table II.

Table II Values of pollution by month

Month	III	IV	V	VI	VII	VIII	IX	X
z [-]	3.0	4.0	4.0	5.0	5.0	4.0	4.0	3.0

The intensity of diffuse solar radiation is determined as follows, (8)

$$\dot{I}_d = \left[1350 - I_D - (1080 - 1.4 I_D) \sin^2 \frac{\alpha}{2} \right] \frac{\sin h}{3} \quad (8)$$

where \dot{I}_d is intensity of diffuse solar radiation [$W m^{-2}$],
 h mentioned in (2).

The total intensity of solar radiation I_C is calculated as (9),

$$I_C = \dot{I}_D + \dot{I}_d \quad (9)$$

where \dot{I}_D is shown in (7),
 \dot{I}_d shown in (8).

Using these relations, for every individual day and hour of a year the theoretical intensity of solar radiation falling on both horizontal surface and the panel surfaces is calculated. Based on these calculation, data obtained from the horizontally placed solarimeter are converted to the normal direction of the panel surfaces and in this manner the total energy falling on the panels during evaluated period of year could be achieved. The energy efficiency of a photovoltaic system is calculated according to an equation (10) [9]:

$$\eta = \frac{P_m}{P_{rad}} = \frac{P_m}{E \cdot A_C} \quad (10)$$

Where P_m is performance of a photovoltaic panel [W],
 P_{rad} power of the incident radiation, [W],
 E total intensity of solar radiation [$W m^{-2}$],
 A_C surface of the photovoltaic cell [$W m^2$].

VI. MEASUREMENT

In the evaluated period from July to December 2013 was recorded data of generated electricity from photovoltaic panels and the total solar radiation energy measured by the solarimeter.

Measured data of the evaluated period has been summarized in a database and the data of fallen energy measured by the solarimeter in horizontal level were converted from the horizontal surface to the inclined surface of the panels according to (9) in 0.5 h intervals. From the obtained values of total solar irradiance I_S was subtracted part of diffuse radiation.

Theoretical calculation:

$$q_{s\ skut\ pr} = q_{s\ skut} - q_{s\ skut.\ dif} \quad (11)$$

where $q_{s\ skut.\ pr}$ is direct radiation incident on solarimeter [W m⁻²],
 $q_{s\ skut}$ performance of a photovoltaic panel [W m⁻²],
 $q_{s\ skut.\ dif}$ calculated diffuse radiation [W m⁻²].

$$q_{f\ pr} = q_{s\ skut\ pr} \frac{q_{s\ skut\ pr}}{\sin h} \quad (12)$$

where $q_{f\ pr}$ is direct radiation incident on a vertical surface [W m⁻²],
 $g_{s\ skut.\ pr}$ shown in (11),
 $\sin h$ shown in (2).

$$q_{n\ pr} = \frac{q_{f\ pr}}{\cos \gamma} \quad (13)$$

where $q_{n\ pr}$ is direct solar radiation incident on photovoltaic panel [W m⁻²],
 $q_{f\ pr}$ shown in (12),
 $\cos \gamma$ shown in (4).

$$q_{n\ celk} = q_{n\ dif} + q_{n\ pr} \quad (14)$$

where $q_{n\ celk}$ is solar radiation incident on the photovoltaic panels [W m⁻²],
 $q_{n\ dif}$ radiation diffusion in the direction orientation photovoltaic panels [W m⁻²],
 $q_{n\ pr}$ shown in (13).

This method of conversion, however is questionable during the occurrence of strong clouding. Water vapour density of the atmosphere does not correspond to the coefficient of air pollution in equation (9). Hence, for the conversion mentioned above, the percentual way of calculation for separation of diffusion radiation intensity from solarimeter data was used.

Theoretical calculation:

$$\frac{I_{d\ vod}}{I_{D\ vod}} = p \quad (15)$$

where $I_{d\ vod}$ is intensity of diffuse radiation incident on a horizontal surface [W m⁻²],
 $I_{D\ vod}$ intensity of direct solar radiation horizontal surface [W m⁻²],
 p proportion of intensity.

$$\frac{I_{d\ sik}}{I_{D\ sik}} = p_1 \quad (16)$$

where $I_{d\ sik}$ is intensity of the diffuse radiation incident direction panel orientation [W m⁻²],

$I_{D\ sik}$ intensity of direct solar radiation in the direction of orientation of the panels [W m⁻²],
 p_1 proportion of intensity.

$$I_d = I_c \cdot p \quad (17)$$

where I_d is intensity of diffuse radiation incident on solarimeter in [W m⁻²],
 I_c measured data solarimeter [W m⁻²],
 p proportion of intensity.

$$I_D = I_c - I_d \quad (18)$$

where I_D is intensity of direct solar radiation incident solarimeter [W m⁻²],
 I_c measured data solarimeter [W m⁻²],
 I_d diffuse radiation incident on solarimetr [W m⁻²].

Conversion to the orientation angle of photovoltaic panels is given by formulas (19) (20),

$$I_c = I_d + p_1 \cdot I_c \quad (19)$$

$$I_c = \frac{I_D}{1 - p_1} \quad (20)$$

where I_c is total intensity of solar radiation incident panel [W m⁻²],
 I_d shown in (18),
 p_1 shown in (16).

The measured values were calculated for every individual month for an average intensity of solar radiation per hour and then were multiplied by the daily lighting time and the number of days in the month. Panel lighting time was different for individual months, which are reflected in the calculations. In the following example is presented a sample calculation for the September 2013 (21):

$$\eta = \frac{P_m}{P_{rad}} = \frac{P_m}{E \cdot A_C} = \left(\frac{143267}{((378.98 \cdot 11.25) \cdot 12) \cdot 30} \right) \cdot 100 = 9.34\% \quad (21)$$

where the values are used:

P_m = 143267 [W]
 E = 378.98 [W m⁻²]
 A_C = 11.25 [m²]
 Time = 12 [h]
 Days = 30

Similarly, the calculations for the other months were performed, following table.

Table III Calculated values

Month	Total global solar radiation[kW]	Power PV panel[kW]	Efficiency [%]
July	1096.9	105.2	9.59
August	2159.1	213.7	9.90
September	1532.8	143.3	9.35
October	761.7	142.4	9.68
November	317.3	52.8	9.58
December	237.6	39.9	9.56

Values in the Table III comprises even energy loss due to electrical conversion. Net efficiency of the panels is then evaluated to 10.5%.

VII. MEASURED VALUES

Table IV compares theoretical and measured values of the supply of electricity by photovoltaic panels on the first day of the month of September.

Figure 4 shows the comparison of the actual panel performance with data given by the producer of the panels.

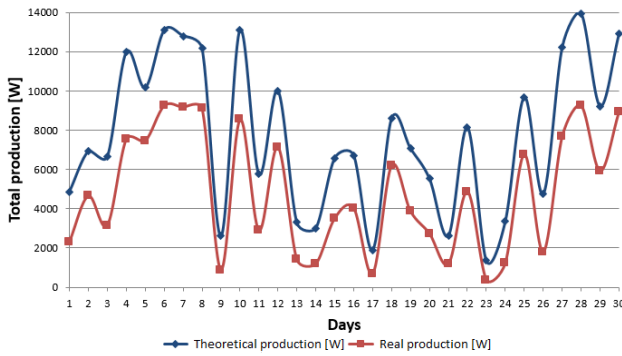


Fig. 4 Comparison of theoretical and real efficiency panels

Table IV Measured values September

Day	Theoretical production [kW]	Theoretical production PV [kW]	Real production [kW]
1	32.4	4.9	2.3
2	46.2	6.9	4.6
3	44.3	6.6	3.1
4	79.8	11.9	7.5
5	67.8	10.1	7.4
6	87.3	13.0	9.2
7	85.3	12.8	9.2
8	81.1	12.1	9.1
9	17.4	2.6	0.8
10	87.3	13.1	8.5
11	38.4	5.6	2.8
12	66.7	10.0	7.1

Table IV Measured values September - continuation

Day	Theoretical production [kW]	Theoretical production PV [kW]	Real production [kW]
13	21.9	3.3	1.4
14	20.0	3.0	1.1
15	43.9	6.6	3.5
16	44.8	6.7	4.0
17	12.6	1.9	0.6
18	57.3	8.6	6.2
19	47.1	7.0	3.8
20	36.9	5.5	2.7
21	17.6	2.6	1.2
22	54.2	8.1	4.9
23	9.0	1.3	0.4
24	22.4	3.3	1.2
25	64.6	9.7	6.8
26	31.6	4.7	1.8
27	81.4	12.2	7.7
28	92.9	13.9	9.2
29	61.4	9.2	5.9
30	86.0	12.9	8.9

Based on these parameters (measured efficiency of a photovoltaic panel, panel purchase price, guaranteed purchase price of electric energy) the economical evaluation can be determined. The following Figure 5 shows the profit from the production of electricity done by 1 m sq. per year, expected and actual return on 1 m² photovoltaic panel during one year, based on the conditions in the Table V.

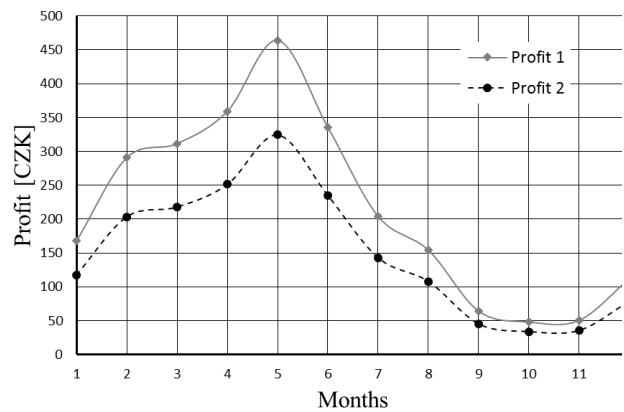


Fig. 5 Comparison of return 1m² photovoltaic panel

Table V shows, at which time it returns 1 m² of photovoltaic panels.

Table V Time of return of photovoltaic panel

		Year profit [CZK]	Return of investment [years]
Date of commissioning PV power plant	1.1.2008 – 31.12.2008	-	-
The redemption [CZK/kWh]	15180	-	-
The average amount of solar radiation [kWh/m ² year]	950 - 1250	-	-
The price of PV modules [CZK/1m ²]	18102.4	-	-
The efficiency of PV panels	15%	2563	7
The actual efficiency	10.50%	1794	10

The price of photovoltaic power systems is not only containing the panel itself but also the other components. Among which include cabling, inverter, control devices work professional firms and maintenance over their lifetime. All of these costs are therefore necessary to consider before deciding to invest funds into such a volatile renewable energy sources such as photovoltaic panels. The calculation can be carried out in accordance with act no. 318/2012 call [12]. Energy audits and energy assessment.

Calculation of economic evaluation is given by equation (22) to (25):

The simple payback period of the investment is given by the following equation: (22)

$$T_s = \frac{IN}{CF}, \tag{22}$$

where **IN** is capital expenditure of the project, **CF** annual benefits of the project.

The real payback period T_{sd} including the discount rate, r is given by the following equation: (23)

$$\sum_{t=1}^{T_z} CF_t \cdot (1+r)^{-t} - IN = 0, \tag{23}$$

where **CF_t** is annual cash flow of the project, **r** discount, **(1+r)^{-t}** discount factor.

Net present value **NPV** is given by the following equation: (24)

$$NPV = \sum_{t=1}^{T_z} CF_t \cdot (1+r)^{-t} - IN = 0, \tag{24}$$

where **T_z** is lifetime (evaluation) project, **CF_t** annual benefits of the project, **r** discount, **(1+r)^{-t}** discount factor, **t** number of returns.

Internal return rate **IRR** is calculated from the condition according to the following equation: (25)

$$\sum_{t=1}^{T_z} CF_t \cdot (1+IRR)^{-t} - IN = 0. \tag{25}$$

The following Table VI shows the time after which the entire investment in photovoltaic power returns.

Table VI Time of return of photovoltaic panel

Measure/variant		Efficiency [15%]	Efficiency [10.5%]
The investment cost of the project	[CZK]	447748	447748
Investments cost for the life of the project	[CZK]	490161	490161
Change in energy costs	[CZK/year]	28833	20182
Change in other operating expenses			
Change in personnel costs	[CZK/year]	0	0
Change in other operating expenses	[CZK/year]	0	0
Change in sales	[CZK/year]	0	0
The benefits of the projects total	[CZK/year]	28833	20182
Measure/variant	[CZK]	447748	447748
Economic evaluation			
Investment costs for the life of the project	N [CZK]	490161	490161
The benefits of the projects total	P [CZK/year]	28833	20182
Evaluation period	z [year]	25	25
Discount	r [-]	0.03	0.03
Inflation	p [-]	0.02	0.02
The simple payback period	T _s [year]	17.00	24.29
Disc. payback period	T _s [year]	19.10	28.52
NPV	[CZK]	144833	-45000
IRR	[-]	0.052	0.022

The following Figure 6 shows the return on investment in photovoltaic panels depending on their effectiveness.

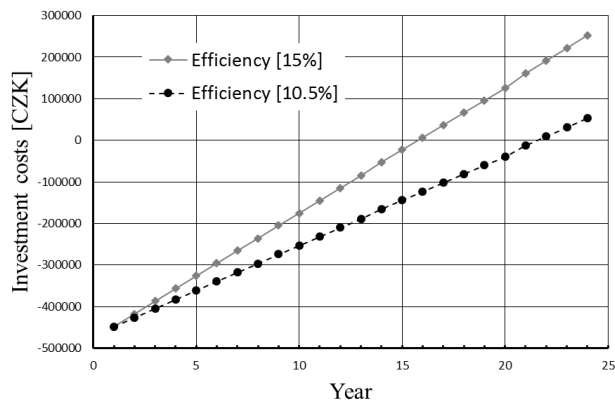


Fig. 6 Simple payback period

From the Figure 6 it follows that the entire investment in a photovoltaic power plant at 15% efficiency photovoltaic panels throughout their lifetime (25 years) should return for 17 years. Measurements showed that the investment will return at least in 24 years.

VIII. CONCLUSION

The aim of this experiment is to economical evaluation in photovoltaic panels for educational purposes. The panels are designed to power the experimental heating and cooling equipment in the laboratory of environmental engineering FAI UTB in Zlin. From the economical evaluation results the fact that based on the conditions of panels efficiency of electrical conversion of 15 % and conditions given by Table IV is the investment in photovoltaics system on edge of the economical effectiveness. For efficiency in level about 10 % is the system of photovoltaics in effective.

The subject of our further research will deal to determine real efficiency of the photovoltaics system including real weather conditions and its influence on the effectiveness and utilization of produced energy by the panels for direct cooling and heating via thermal accumulative panels installed in the laboratory of environmental engineering.

REFERENCES

- [1] PETERA, J and HERMAN J. "Photovoltaics," 2010. [Online]. Available: www.rescompass.org/IMG/pdf/Fotovoltaika.pdf
- [2] KOPUNEC, V. "Analytic methods of photovoltaic panels and systems" Brno, 2011. [Online]. Available: https://dspace.vutbr.cz/bitstream/handle/11012/1344/DIPLOMOVA%20prace_V%C3%ADt_Kopunec.pdf?sequence=1. MSc. thesis. VUT Brno.
- [3] Aldebaran Bulletin. *The present state and trends in the development of photovoltaic panels* 2010. [Online]. Available: http://www.aldebaran.cz/bulletin/2010_37_fot.php
- [4] Complet Energy. "Photovoltaic plants," [Online]. Available: <http://www.completenergy.cz/modules.php?name=News&file=article&sid=15>.
- [5] HABROVANSKY, T. "Control and monitoring of heating and cooling units in laboratory of building control systems," Zlin, 2008. [Online]. Available: <http://dspace.k.utb.cz/handle/10563/6910>. Msc. thesis. UTB Zlin.
- [6] Czech RE Agency. "Photovoltaic inverter," [Online]. Available: <http://www.czrea.org/cs/druhy-oze/fotovoltaika/fv-stridac>
- [7] SMA Solar Technology. "Photovoltaic inverter Sunny Boy 1100/1700". 2012. [Online]. Available: <http://www.sma-czech.com/cs/produkty/stridace-pro-zapojeni-do-rozvodne-site/sunny-boy.html>
- [8] CSN 73 0548. *Calculation of thermal load of air-conditioned spaces*. Prague 2: The Office for Standards, Metrology and Testing, 11.1.1985
- [9] STANEK, K. "Effectiveness of the building photovoltaic systems," Brno, 2011 Available: http://www.fce.vutbr.cz/veda/JUNIORSTAV2007/pdf/Sekce_1.4/Stanek_Kamil_CL.pdf
- [10] Solar Liglass. "Photovoltaic panels," 2009. Available: <http://www.solar-liglass.cz/fotovoltaicke-dotazy-a-odpovedi/47-jaka-je-zivotnost-fotovoltaiky>.
- [11] Department of Energy Regulation. *Energetic regulation bulletin*. Available: http://www.eru.cz/user_data/files/cenova%20rozhodnuti/CR%20elektro/2013/ERV7_2013titul_konec_fi.pdf
- [12] Law no. 318/2012 Sb. Energy Management. In: *no. 117/2012*. 2012. Available: <http://www.tzb-info.cz/pravni-predpisy/zakon-c-318-2012-sb-kterym-se-meni-zakon-c-406-2000-sb-o-hospodareni-energie-zneni-pozdejsich-predpisu>

Big Data Processing for E-Health Applications using a Decentralized Cloud M2M System

George Suciu, Victor Suciu and Octavian Fratu

Abstract— In this paper we study the way how to process big data gathered by a decentralized cloud system, based on general systems and Remote Telemetry Units (RTUs), for tele-monitoring of E-Health environmental parameters. Also, we analyze a proposed cloud M2M system, where each RTU communicates by radio with a telemetry data gateway connected to a cloud computing infrastructure equipped with appropriate software that delivers processed data.

Furthermore, we present how we use a search based application built on Exalead CloudView to search for weak signals in big data. In particular, given the E-Health application, we propose to leverage trivial and non-trivial connections between different sensor signals and data from other online environmental wireless sensor networks, in order to find patterns that are likely to provide innovative solutions to existing problems. The aggregation of such weak signals will provide evidence of connections between renewable energies and environmental related issues faster and better than trivial mining of sensor data. As a consequence, the software has a significant potential for matching environmental applications and challenges that are related in non-obvious ways in Internet of Things (IoT) scenarios.

Finally, we discuss the applicability for other information sources and use case scenarios.

Keywords—Big Data, Cloud computig, E-Health, IoT, M2M.

I. INTRODUCTION

CLOUD computing and Internet of Things (IoT) are nowadays two of the most prominent and popular ICT paradigms that are expected to shape the next era of computing.

The IoT paradigm relies on the identification and use of a large number of heterogeneous physical and virtual objects (i.e. both physical and virtual representations), which are connected to the internet [1]. IoT enables the communication between different objects, as well as the in-context invocation of their capabilities (services) towards added-value

This work was supported in part by the eWALL project and has been funded by the Sectoral Operational Programme Human Resources Development 2007-2013 of the Ministry of European Funds through the Financial Agreement POSDRU/159/1.5/S/134398.

G. Suciu is with the Faculty of Electronics, Telecommunications and IT, Telecommunication Department, University POLITEHNICA of Bucharest, Romania (phone: +40213323006; fax: +40213323005; e-mail: george.suciu@radio.pub.ro).

V. Suciu is with the Faculty of Electronics, Telecommunications and IT, Telecommunication Department, University POLITEHNICA of Bucharest, Romania (e-mail: victor.suciu@beia.ro).

O. Fratu is with the Faculty of Electronics, Telecommunications and IT, Telecommunication Department, University POLITEHNICA of Bucharest, Romania (e-mail: ofratu@elcom.pub.ro).

applications. Early IoT applications are based on RFID (Radio Frequency Identification) and Wireless Sensor Network (WSN) technologies and deliver tangible benefits in several areas including manufacturing, logistics, trade, retail, green/sustainable applications, as well as other sectors. Furthermore, the European Commission has already co-funded a number of FP7 projects (e.g., IOT-A, iCore, BUTLER) [2], which have researched the main building blocks of IoT systems (including reference architectures) and have built innovative added-value applications.

At the same time, the cloud computing paradigm [3] realizes and promotes the delivery of hardware and software resources over the Internet and according to an on-demand utility based model. Depending on the type of computing resources delivered via the cloud, cloud services take different forms such as Network as a Service (NaaS), Infrastructure as a service (IaaS), Platform as a service (PaaS), Software as a service (SaaS), Storage as a service (STaaS) and more. These services hold to promise to deliver increased reliability, security, high availability and improved QoS at an overall lower total cost of ownership (TCO). Similarly to the case of cloud computing, the EC has already co-funded a number of projects (e.g., RESERVOIR, VISION- CLOUD, OPTIMIS, CONTRAIL) [2], which have developed pan-European prototypical cloud infrastructures, while they have also built relevant cloud technologies (e.g., resource management, security) and applications.

Another common aspect of IoT applications is that many of them of practical interest involve control and monitoring functions, where human-in-the-loop actions are not required. As a matter of fact, the only reason for having many of these applications is to remove human intervention for improved efficiency, security, and safety. We focus specifically on these applications, which we call Ma-chine-to-Machine (M2M), which will create a bridge between the real world (made of sensors, actuators, tags that are pervasive in our lives) and the virtual world (the Internet and its associated services).

In the case of M2M, important research initiatives are proposing new reference models, defining standards and new communication architectures, with different approaches for solving security, reliability and energy-efficiency problems. However, many efforts are focused on largely distributed critical infrastructures and just a few initiatives are dedicated to the definition of platforms for deployment and execution of new M2M applications, based on new generations of WSN

and innovative sensor mining methods that can be deployed according to a cloud computing model.

Indeed, M2M applications are envisioned to be hosted within cloud computing systems and contribute to the converge of interactions between the real and virtual world, thus accomplishing improvements in industrial productivity and quality of life for citizens, based on secure and dependable automation of sensing and actuating tasks.

However, we argue that this kind of approach is sub-optimal for M2M because of its inherent paradigms: M2M applications are highly autonomous, implement simple and repetitive interactions in highly constrained environments, with limited scope in time and space, and must respond in a reliable manner to mission critical QoS needs, whereas usual cloud applications require that big volumes of data are redundantly stored and provided through content delivery networks, to be available for very long periods and accessible as ubiquitously as possible for the use by human beings.

The paper is organized as follows. Section 2 presents an overview of the state of the art in Cloud computing, IoT and M2M. Section 3 presents a Cloud computing architecture for E-Health applications, while Section 4 presents Big Data processing involved in the previously mentioned architecture. Finally, Section 5 draws the conclusions.

II. RELATED WORK

A. Convergence between Cloud computing and IoT

Since the early instantiations/implementations of both technologies, it has become apparent that their convergence could lead to a range of multiplicative benefits. Most IoT applications entail a large number of heterogeneous geographically distributed sensors. As a result, they need to handle many hundreds (sometimes thousands) of sensor streams, and could directly benefit from the immense distributed storage capacities of cloud computing infrastructures. Furthermore, cloud infrastructures could boost the computational capacities of IoT applications, given that several multi-sensor applications need to perform complex processing that is subject to timing (and other QoS constraints). Also, several IoT services (e.g., large scale sensing experiments, smart city applications) could benefit from a utility-based delivery paradigm, which emphasizes the on-demand establishment and delivery of IoT applications over a cloud-based infrastructure.

The proclaimed benefits of the IoT/cloud convergence have (early on) given rise to research efforts that attempted to integrate multi-sensory services into cloud computing infrastructures [4]. The most prominent of these efforts are the so-called sensor-clouds, which blend sensors into the data centre of the cloud and accordingly provide service oriented access to sensor data and resources [5]. Several recent research initiatives are focusing on real-life implementation of sensor clouds, including open source implementations [6]. Note that such initiatives are in progress both in the US and in the EU [7], aiming at developing middleware infrastructures for

sensor-clouds, which will enable the on-demand delivery of IoT services.

In addition to research efforts towards open source sensor-clouds, there are also a large number of commercial on-line cloud-like infrastructures, which enable end-users to attach their devices on the cloud, while also enabling the development of applications that use those devices and the relevant sensor streams. Such commercial systems include COSM [8], ThingsSpeak [9], and Sensor-Cloud [10]. These systems provide tools for application development, but they offer very poor semantics and no readily available capabilities for utility based delivery. There is also a number of other projects which have been using cloud infrastructures as a medium for Machine-to-Machine (M2M) interactions (e.g., [11]), without however adapting the cloud infrastructure to the needs of the IoT delivery.

In the area of IoT applications (e.g., for smart cities), we are also witnessing cases of IoT/cloud convergence. For example, in the scope of ICT-PSP project RADICAL [12], the partners will be deploying sensor streams over the BONFIRE cloud infrastructure, as means to benefitting from the cloud's storage capacity and applications hosting capabilities. A similar approach is followed in the scope of the FP7 SmartSantander project [13]. We note that smart cities is a privileged domain for exploring and realizing the IoT/cloud convergence, given that such applications need to manage and exploit a large number of distributed heterogeneous sensor streams and actuating devices.

B. Big Data

The European Union has declared Big Data as a priority for Horizon 2020, the EU's next European research framework. This is confirmed by the theme and budget of the last FP7 ICT call for projects to be started in 2014 [14,15].

The plethora of data types and formats (structured, unstructured, semistructured or multistructured) as well as the diversity of generating sources (sensors, devices, social networks, web content, mobile phones, etc.) generates a large variety of data. According to Tech Target [16], multistructured data already represents 80% of the volume of data that is available in an organization.

The economic potential of Big Data represents the greatest challenge and it consists of finding value in the large volume of unstructured data in (near) real time. The tendency to use this information for business analytics is becoming a worldwide management practice.

Fruitful sources of data, recently come to attention (IoT, sensor networks, social networks) have given an unprecedented growth rate of the volume of available microeconomic and macroeconomic data. It is estimated that in the year 2012 alone, 2.5 ExaBytes of data have been generated daily [17].

Big Data and their management (generating, storing, indexing, and searching) is a worldwide challenge because multiple factors, of which we mention:

- The need for highly skilled labourers: A Gartner study

[18] from 2012 estimates the creation of 4.4 million new jobs globally in relation to Big Data.

- Environment problem monitoring: warping dams, proactive maintenance and repair, using satellite imaging to monitor changes in the Earth's crust (earthquakes, erosion, floods, and landslides).
- Smart City management: this is based on gathering, managing and analysing large volumes of data regarding car and passenger traffic, the evolution of environmental factors, energy consumption dynamics, high risk situation monitoring etc. [2].

Variable prices and rising costs of production are forcing energy producers to optimize production costs. Therefore "precision energy production", the optimized use of natural energy resources such as water, sun or wind is now indispensable. The growing environmental awareness of consumers further accelerates this process and promotes the usage of remote automatic monitoring system for field information such as the one we propose. By running the M2M software over virtual machines it is possible to optimize the network performance and improve the energy consumption for the devices that are powered by batteries [19].

In previous approaches RTUs (Remote Telemetry Units) were implemented in most cases on a local server and no company could aggregate enough sensor data to consider automating the production process and providing the required resilience [20]. Furthermore, by using low power sensors and data aggregation the energy consumption of the M2M network can be optimized [21].

Some studies show that Cloud computing can actually make traditional data-centres more energy efficient by using technologies such as resource virtualization and workload consolidation [22]. Contrary to the above opinion, other studies, for example Greenpeace [23], observe that the Cloud phenomenon may aggravate the problem of carbon emissions and global warming.

C. M2M Communications in Wireless Networks

M2M communications (or Machine Type Communications - MTC) can use either wireless or fixed networks, gaining in recent years a considerable interest among mobile network operators. M2M communication solutions that use mobile networks can prove to be easier to deploy and can support a large number of de-vices, most importantly those with mobility features. The ubiquitous connectivity nature of mobile networks (especially from 3GPP Rel. 8 onwards) will enable M2M services that require reliable and immediate data delivery to distant M2M servers.

The different behaviour of M2M devices, compared to plain mobile network terminals poses a need for optimizing networking solutions, in order to specifically tailor them for M2M communications in mobile networks. Therefore, 3GPP, the Open Mobile Alliance (OMA), IEEE, ETSI and a number of other standardization bodies have launched standardization activities on M2M communications [24].

Regarding 3GPP, the focus is on system optimizations that

prevent M2M signalling congestion and network overload. These are the main important issues that prevent the mass-market adoption of M2M services.

Different models are foreseen by 3GPP for M2M traffic in regards to communication between the M2M Application and the 3GPP network. In a so called Direct Model, the M2M Application communicates with the UE directly as an over-the-top application on 3GPP network. This is shown as Fig. 1.

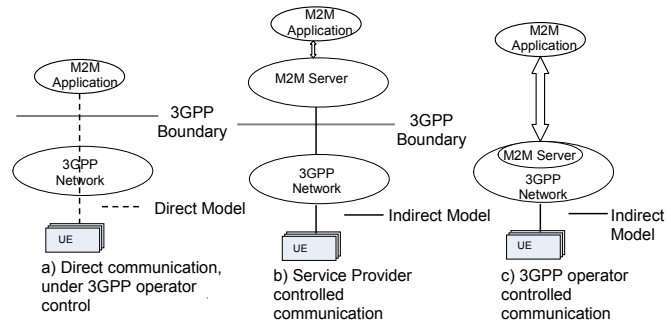


Fig. 1 M2M Application to UE for M2M Communication Models [24]

In short, the communication between the M2M server and 3GPP network is, within the scope of 3GPP, including when that communication becomes internal to the network. The communication between the M2M Application and the M2M Server is out of the scope of 3GPP.

III. COMPONENTS OF THE CLOUD E-HEALTH ARCHITECTURE

To illustrate the need for interconnecting extremely heterogeneous sensors and gateways we consider the following example scenarios, which show short-term realistic applications of smart things enabled by M2M communication:

- Continuous care: Citizens affected by chronic diseases can be provided with sensors continuously monitoring relevant health parameters, which produce data that are conveyed through a smart phone to a remote centre for real-time analysis. In case a potentially dangerous situation is detected an alarm can be fed back to the smart phone.
- Ambient assisted living: Activity detection sensors installed in houses where senior or disabled citizens live send data to a remote centre, so as to generate alarms in case anomalies are detected with respect to a typical pattern (e.g., prolonged lack of movement during daytime).
- Smart grid: The Distribution System Operator (DSO) provides the smart meter of a house with information on the next-house cost of electricity. Based on this piece of information, possibly combined with other sources (e.g., power currently generated by solar panels), a remote control system can switch on/off smart electric appliances.
- Traffic management: Road-side units (RSU) are placed along roadways to monitor the flow of vehicles. Based on the information collected from a given area, a remote centre can identify congestions and provider drivers with real-time feedback to reduce travel times, hence CO2 emissions.
- Fleet management: Vehicles provide the intelligent

transportation infrastructures with information on their location and health status, by allowing a remote control system to optimize logistics or track dangerous goods, for commercial vehicles only, and provide all drivers with improved safety or advanced services (e.g., pay-as-you-go insurance).

A. Cloud Architecture

We will introduce SlapOS [20], a decentralized cloud system based on a Master and Slave design, as shown in Fig. 2. In this section we are going to provide an overview of SlapOS architecture and are going in particular to explain the role of Master node and Slave nodes, as well as the software components which they rely on to operate a distributed cloud for E-Health applications. Slave nodes request to Master nodes which software they should install, which software they should run and report to Master node how much resources each running software has been using for a certain period of time. Master nodes keep track of available slave node capacity and available software. Master node also acts as Web portals and Web service so that end users and software bots can request software instances which are instantiated and run on Slave nodes.

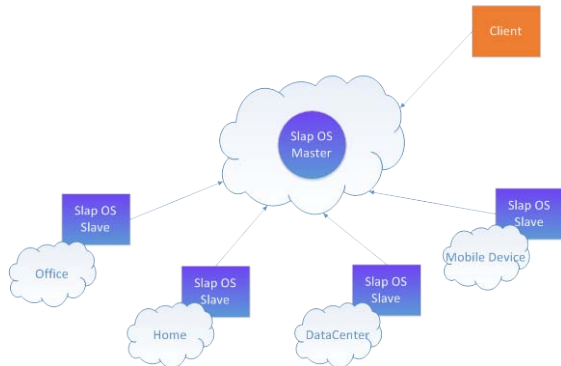


Fig. 2 SlapOS Master – Slave Cloud Architecture

Master nodes are stateful. Slave nodes are stateless. More precisely, all information required to rebuild a Slave node is stored in the Master node. This may include the URL of a backup service which keeps an online copy of data so that in case of failure of a Slave node, a replacement Slave node can be rebuilt with the same data.

It is thus very important to make sure that the state data present in Master node is well protected. This could be implemented by hosting Master node on a trusted IaaS infrastructure with redundant resource. Or - better - by hosting multiple Master nodes on many Slave nodes located in different regions of the world thanks to appropriate data redundancy heuristic. We are touching here the first reflexive nature of SlapOS. A SlapOS master is normally a running instance of SlapOS Master software instantiated on a collection of Slave nodes which, together, form a trusted hosting infrastructure. In other terms, SlapOS is self-hosted.

SlapOS Slave nodes are relatively simple compared to the Master node. Every slave node needs to run software requested by the Master node. It is thus on the Slave nodes that software is installed. To save disk space, Slave nodes only install the

software which they really need.

Each slave node is divided into a certain number of so-called computer partitions. One may view a computer partition as a lightweight secure container, based on UNIX users and directories rather than on virtualization. A typical barebone PC can easily provide 100 computer partitions and can thus run 100 RTU web portals or 100 sensors monitoring sites, each of which with its own independent database. A larger server can contain 200 to 500 computer partitions.

B. M2M Architecture for E-Health

In Fig. 3 we present the general structure of the system that we propose for the tele-monitoring of installation sites in hydro power stations.

At each of the monitored installation sites a system is set up composed mainly from distant RTUs, sensors and actuators. RTUs capable to communicate with the Gateway through GSM-GPRS and Internet will be used in standard configurations. For the installation sites which are situated in no GSM coverage areas, RTUs in the UHF band of 430-440 MHz will be used. These will communicate with the data concentrator through a bridge station (bridge) which will ensure the UHF-GPRS and GPRS-UHF conversion.

In the relatively few instances when this will be possible, the RTU-Gateway communication will be held by radio exclusively in the UHF band of 430-440 MHz. The system's key elements are:

- Gateway, which ensures the communication with the RTUs and available resource management;
- Presentation Server (PS) which is hosted on a computer with server features (for example, unattended operation 24/7), equipped with a software package focused mainly on data presentation in various forms, entirely available to users.
- Application Server (AS), focused on special tasks, which PS cannot perform.

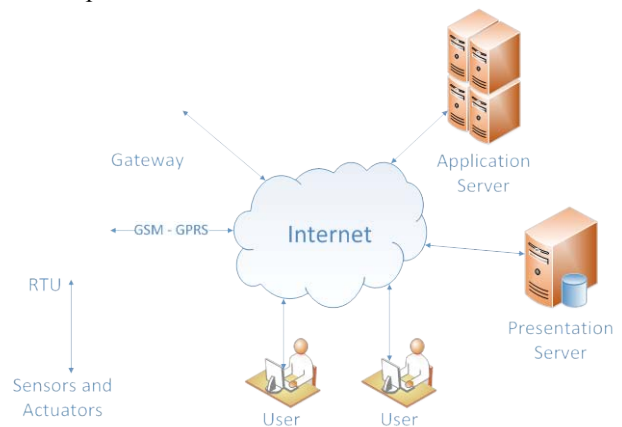


Fig. 3 General structure of the E-Health system

Practically, all system communication is done through the Internet and this gives the system investment and mostly operational advantages. It is mentioned that the users can access the processed data, offered by the PS and AS anywhere and anytime, from any terminal with Internet access (PC, tablet, mobile phone etc) [20].

The system's central elements are configured and scaled so that they would allow a system takeover of 100 RTUs.

IV. BIG DATA PROCESSING CHARACTERISTICS AND DISCUSSIONS

Currently there are many solutions on the market for search and analysis of large volumes of information. These solutions are focused on semantic technologies for aggregating and collating data, both structured and unstructured.

Since the well-known Google, which is used by all users, we have developed and are developing solutions for Enterprise Business Applications such as CRM (Customer Relationship Management), ERP (Enterprise Resource Planning) and BI (Business Intelligence) and web applications, such as applications B2B (Business to Business), B2C (Business to Customer), using data from various sources (databases, web content, user generated content, etc.).

In our approach we use CloudView Exalead [25], a search platform which offers wide access to information on infrastructure level and is used for both SBA (Search Business Application) for online and enterprise level. This application combines semantic technologies for developing applications such as drag-and-drop, as well as qualitative and quantitative analysis to provide information to the user.

Located at the intersection between search and Business Intelligence, Cloud-View is also a platform for the Exalead search engine, which was designed to implement semantic processing and selective navigation data volumes that are on the Web, making it easy for users searching and analysing information and enabling organizations to improve their knowledge and resources exploitation.

With the advent of cloud computing, the convergence of the cloud computing with WSN has been attempted, as an extension of the sensor grid concept in the scope of on-demand elastic cloud based environments. In particular, the convergence of cloud computing with WSN aims at compromising the radically differences and conflicting properties of the two technologies. In particular, sensor networks are location specific, resource constrained, expensive (in terms of development/deployment cost) and generally inflexible in terms of resource access and availability. On the contrary, cloud based infrastructures are location independent provide a wealth of inexpensive resources, as well as rapid elasticity

Fine-grained (raw) data have to be conveyed in a centralized manner over the Internet from sensors up to the remote centre, so as to give the latter the high-resolution information it needs to take decisions. Therefore, the things and gateways are effectively separated from the back-end, which has storage and computation functions, both physically, through the Internet, and logically via a set of abstraction layers. Such an approach has worked well in the past for similar technologies, like the Web, from which the initial IoT attempts inherit most of their design and characteristics. However, we argue that full and sustainable exploitation of M2M applications needs a tighter

integration between the real and virtual world. The following issues of what we can call "the current approach" can be identified: scalability, security, reliability, QoS, resource/energy efficiency and multi-domain implementation.

To overcome the limitations of the current systems for M2M applications, we propose a novel approach based on the following principles:

1. Storage and processing of data are as close as possible, in space and time, to where they are generated and consumed.

2. Important non-functional requirements, namely security, reliability and QoS, are supported by means of a tight integration of the high-level services provided with the physical resources of the peripheral devices, i.e., things and gateways.

3. Energy efficiency and scalability of the systems are achieved through the distribution of on-the-spot inferred content, rather than raw data.

4. Cross-domain applications using real-time data from multiple sources can be seamlessly implemented.

The current state of art of M2M platforms is quite fragmented and there isn't a single view toward an interoperable smart object world. The M2M commercial platforms are vertically focused on solving specific sector issues and are tightly integrated with applications. This approach, taken from the telemetry legacy applications, has created a bunch of sensor devices not interoperable one each other, with high boundaries and integration possible only at database or presentation layers.

For many years, M2M deployments were based on proprietary/custom applications and networking infrastructures, which were typically expensive to build, manage and maintain. Today's market for sensor devices is a hotbed of idea generation, as the prospect of embedding intelligence in the form of M2M (machine-to-machine) technology into mobile devices has everyone excited about the possibilities. The current market is already filled up with devices that can track everything from blood-glucose levels to traffic patterns.

In making the case for open-platform development in M2M, the sensor and communication device manufacturing community is only one part of the model, where the application and service side is pushing for enablers to seamlessly access to widely distributed, real-time data from the environment. Throughout the recent past years, the concept of open-platform development, management and monitoring has emerged, basically solving again problems mainly from the technological point only in specific sectors. For example, the medical device world faces regulatory and sensitive data issues when development is concerned. Embedded and mobile software provider emphasize this idea through the delivery of commercial off-the-shelf software solution. The emphasis with such a platform is to ensure companies optimize their software across the entire lifecycle of a product, starting with design, all the way through support of the deployed devices. This is merely one example in one specific market that demonstrates

how a technology platform can provide a jumpstart to the development process that, until now, has been lacking in the market.

The convergence between Telco, Media and Consumer Electronics leads ever more to the need to interpret as “network devices” items very different in themselves and detached from any form of connectivity. The Internet of Things is destined to become a fundamental sector for the distribution of new technologies, both within companies and in daily life.

V. CONCLUSION

The paper discussed a number of popular ICT paradigms, including Cloud computing, IoT and Big Data. It provided an extensive state of the art review of them and the convergence between them. Next, we proposed a M2M system based on a decentralized cloud architecture, general systems and Remote Telemetry Units (RTUs) for E-Health applications. The system was built for Big Data processing of sensors information in the way that data can be aggregated to generate “virtual” sensors, and some measurement results were presented.

With the advent of smart mobile devices, the Internet access has become ubiquitous, and has opened the way for new applications that use M2M communications. Indeed, the Internet of Things paradigm is an evolution of the traditional Internet for seamlessly integrating most things around us and collecting big data from sensors that track everything happening in our environment. IoT is already a reality and is growing, while the way we apply this new concept will drive new applications and may revolutionize life. Future research includes concepts such as flexible, open, and standardized service interfaces - Internet of Services (IoS), people becoming part of ubiquitous intelligent networks having the potential to seamlessly exchange information – Internet of People (IoP), and, finally, the ability to interconnect any web enabled device and provide natural Human-2-Machine (H2M) interaction interfaces - Internet of Everything (IoE).

REFERENCES

- [1] O. Vermesan, P. Friess, P. Guillemi, and S. Gusmeroli, “Internet of Things Strategic Research Agenda,” in *Internet of Things – Global Technological and Societal Trends*, River Publishers, 2011.
- [2] G. Suciu, S. Halunga, O. Fratu, A. Vasilescu, and V. Suciu, “Study for Renewable Energy Telemetry using a Decentralized Cloud M2M System,” in *Wireless Personal Multimedia Communications (WPMC), IEEE 15th International Symposium on*, 24-28 Jun. 2013, pp. 1-5.
- [3] P. McFedries, “The cloud is the computer”, *IEEE Spectrum*. Available: <http://spectrum.ieee.org/computing/hardware/the-cloud-is-the-computer>.
- [4] A. Basu, J. Vaidya, H. Kikuchi, and T. Dimitrakos, "Privacy-Preserving Collaborative Filtering on the Cloud and Practical Implementation Experiences," *Cloud Computing (CLOUD), 2013 IEEE Sixth International Conference on*, 2013, pp.406-413.
- [5] M. M. Hassan, B. Song, and E. N. Huh, “A framework of sensor-cloud integration opportunities and challenges,” in *Proceedings of International Conference Ubiquitous Information Management Communication*, 2009, pp. 618-626.
- [6] Open Source IoT Cloud. Available: <https://sites.google.com/site/opensourceiotcloud>.
- [7] Open Source Solution for the Internet of Things into the Cloud. Available: <http://www.openiot.eu>.
- [8] Xively – Public Cloud for the Internet of Things. Available: <https://www.xively.com>.
- [9] Internet of Things – ThingSpeak. Available: <https://www.thingspeak.com>.
- [10] Sensor Cloud. Available: <http://www.sensor-cloud.com>.
- [11] M. Kranz, P. Holleis, and A. Schmidt, “Embedded Interaction: Interacting with the Internet of Things” in *IEEE Internet Computing*, vol. 14, no. 2, 2010, pp. 46-53.
- [12] RADICAL: RAPid Deployment and adoption of sustainable socially-aware and intelligent sensing services for emerging smart cities. ICT-PSP project. Available: http://ec.europa.eu/information_society/apps/projects/factsheet/index.cfm?project_ref=325138.
- [13] SmartSantander. FP7 project. Available: <http://www.smartsantander.eu>.
- [14] FP7 Work Programme 2013. Cooperation Theme 3: ICT (2012). Available: http://ec.europa.eu/research/participants/portalplus/static/docs/calls/fp7/common/32767-annex_6_to_the_decision_ict_for_cap_en.pdf.
- [15] FP7 Work Programme 2013. Cooperation Theme 5: Energy (2012) Available: http://ec.europa.eu/research/participants/portalplus/static/docs/calls/fp7/common/32765-annex_8_to_the_decision_energy_for_cap_en.pdf.
- [16] Exploiting Big Data: Strategies for Integrating with Hadoop to Deliver Business Insights (2012). Available: http://media.techtarget.com/digitalguide/images/Misc/EA-Marketing/E-Zine/BAA%20assets/BigDataReport_final.pdf
- [17] A. McAfee, and E. Brynjolfsson, “Big Data: The Management Revolution”, Available: <http://hbr.org/2012/10/big-data-the-management-revolution>.
- [18] Gartner Says Worldwide Cloud Services Market to Surpass \$109 Billion in 2012, Available: <http://www.gartner.com/newsroom/id/2163616>.
- [19] S. H. Hung, C.H. Chen, and C.H. Tu, “Performance evaluation of machine-to-machine (M2M) systems with virtual machines.” In *International Symposium Wireless Personal Multimedia Communications*, IEEE, 2012, pp. 159-163.
- [20] G. Suciu, C. Cernat G. Todoran, V. Poenaru, T. Militaru, and S. Halunga, “A solution for implementing resilience in open source Cloud platforms,” in *International Conference on Communications*, IEEE, 2012, pp. 335-338.
- [21] S.Y. Tsai, S.I. Sou, and M.H Tsai, “Effect of data aggregation in M2M net-works,” in *International Symposium Wireless Personal Multimedia Communications*, 2012, pp. 95-99.
- [22] S.G. Kumar, and R. Buyya “Green Cloud computing and Environmental Sustainability,” in *Harnessing Green IT: Principles and Practices*, 2014, pp. 315-340.
- [23] Greenpeace International, “Make IT Green: Cloud computing and its contribution to climate change,” Available: <http://www.greenpeace.org/international/en/publications/reports/make-it-green-Cloudcomputing>.
- [24] 3GPP, TS 23.888 “System improvements for Machine-Type Communications (MTC),” Version 11.0.0 (Release 11), Sept. 2012
- [25] R. Eckstein, “Interactive search processes in complex work situations: a retrieval framework,” Vol. 10. University of Bamberg Press, 2011, pp. 62-67.

Modeling of protein sorption on chromium sludge as a tool for optimization of its deproteination

Michaela Bařinová, Jiří Pecha, and Karel Kolomazník

Abstract—Processing raw hides into leather is connected with production of large amount of chrome-tanned waste. Disposal of this waste in landfills is expensive and potentially hazardous from both public health and environmental point of view. Since this waste also represents a source of potentially valuable raw materials, it is advantageous to search for possibilities of its processing. Two-step enzyme hydrolysis seems the most attractive processing technology so far; however, it is not completely zero-waste due to its by-product, so-called chromium sludge (chromium cake). Relatively high protein content in the sludge represents technological obstruction and limits its further treatment and applications. The paper focuses on deproteination (removal of proteins) of chromium cake through a combination of mathematical and experimental methods. The deproteination level was studied via desorption of the protein fraction into the washing solution. A mathematical model of deproteination was proposed and its accuracy and suitability to predict the course of deproteination were verified experimentally. The model shows that appropriate choice of conditions can lead to practically total deproteination of chromium cake. The mathematical model also serves as a basis for optimization of the process.

Keywords—Chromium sludge, deproteination, mathematical modeling, sorption isotherm.

I. INTRODUCTION

Processing of solid chrome-tanned waste generated by the leather industry, the typical example of which are chromium shavings, represents a long-term technological challenge. The most promising approach so far seems to be a two-step enzyme hydrolysis [1, 2], particularly with respect to the economic aspects of the process. However, part of the waste (so-called chromium cake) is quite resistant to

degradation; the processing of chromium cake then remains the major problem in the hydrolytic treatment of chromium shavings. Intensive research has been carried out to find economically viable and environmentally friendly solutions, involving mainly chemical treatment, both direct and indirect [for example 1, 2, 3], or biotechnological methods [4]. Some of the cited solutions also include direct re-use of chromium cake in the manufacturing cycle.

Desorption of proteins into the washing bath after the second step of hydrolysis represents potentially suitable way of further reduction of the protein components in the chromium cake, with simultaneous desirable increase in the purity of chromium present in the cake. However, existing efforts dealing with this problem are limited either by very low efficiency of deproteination [5], or quite complex and energetically demanding reaction conditions, moreover connected with oxidation of part of trivalent chromium to its carcinogenic hexavalent form [6].

The aim of our contribution was to propose a mathematical model of desorption of protein fraction into the washing bath for various soaking numbers and decantation washing, to experimentally verify the reliability of the models for the prediction of the desorption progress and on the basis of the model to determine optimal conditions of the deproteination process.

II. MATHEMATICAL MODELING

A. Theory

Mathematical model of deproteination of chromium cake through its washing in water is based on the assumption that the protein part (collagen) is adsorbed onto chromium complex via coordination bonds with the glutamic and/or aspartic acids [5]. The modeling of desorption proceeds from the mass balance of the process. Not all the protein fraction is involved in the coordination bonds (this part is called unbound). This part passes into the washing bath by diffusion. However, part of the bound protein is also washed out into the bath through desorption – the level of desorption predicted by the model is closely dependent on the selected adsorption isotherm. Deproteination can be performed repeatedly, with lower amount of water in each step than in one-step washing; the process is then called decantation washing. This leads to

The work was supported by the European Regional Development Fund under the project CEBIA-Tech No. CZ.1.05/2.1.00/03.0089., and the project No. CZ.1.07/2.3.00/30.0035.

Michaela Barinova is with the Faculty of Applied Informatics, Tomas Bata University in Zlin, nám. T. G. Masaryka 5555, 760 01 Zlín, Czech Republic (phone: +420 57-603-5275, fax: +420 57-603-2716, e-mail: barinova@fai.utb.cz).

Jiri Pecha is with the Faculty of Applied Informatics, Tomas Bata University in Zlin, nám. T. G. Masaryka 5555, 760 01 Zlín, Czech Republic (e-mail: pecha@fai.utb.cz).

Karel Kolomaznik is with the Faculty of Applied Informatics, Tomas Bata University in Zlin, nám. T. G. Masaryka 5555, 760 01 Zlín, Czech Republic (e-mail: kolomaznik@fai.utb.cz).

reduction in the consumption of washing water, or higher efficiency of deproteination at the same water consumption [7].

B. Adsorption isotherm

Modeling of adsorption is often based “merely” in the selection of suitable isotherm, which most accurately reflects the experimental data. For the case of deproteination of chromium cake we used Langmuir isotherm that is based on the idea that the adsorbed substance forms only monomolecular layer on the adsorbent, the probability of adsorption is equal anywhere on the surface and there are no interactions between adsorbed molecules [8]. Langmuir isotherm can be expressed as:

$$c_A = \frac{A \cdot c}{1 + B \cdot c} \tag{1}$$

Where c_A is concentration of bound protein, A stands for bond strength, B is for sorption capacity, and c is equilibrium concentration of unbound protein. For determination of the course of deproteination it is useful to find out in which part of the isotherm the system is. In the area where c_A reaches its maximal value of a_m , only unbound component is washed out; then (1) can be simplified as ($Bc \gg 1$):

$$c_A = \frac{A}{B} = a_m \tag{2}$$

For very low concentrations we can assume linear dependence of c_A on c ($Bc \ll 1$):

$$c_A = A \cdot c \tag{3}$$

C. Mathematical model of deproteination using Langmuir isotherm

Mathematical description of deproteination is based on mass balance, in our case:

$$c_s V = c_A V + cV + c_0 V_0 \tag{4}$$

Where c_s is the total concentration of protein in chromium cake, c is concentration of unbound protein c_A stands for concentration of bound protein in the cake, c_0 is concentration of protein in the bath, V stands for the chromium cake volume and V_0 is the volume of the bath. By further arrangement we get:

$$c_s = c_A + c + c_0 Na \tag{5}$$

Where Na is soaking number for which it holds:

$$Na = \frac{V_0}{V} \tag{6}$$

It can be assumed for the amount of unbound protein present in the chromium cake that:

$$cV = c_0 V_f \rightarrow c = c_0 \frac{V_f}{V} = c_0 \varepsilon \tag{7}$$

By expressing c from (7) and c_A from (1) in (5), we get:

$$c_s = \varepsilon c_0 + \frac{A \varepsilon c_0}{1 + B \varepsilon c_0} + c_0 Na \tag{8}$$

Concentration of protein in the washing bath is then:

$$c_0 = \frac{-(\varepsilon + Na + A\varepsilon - c_s B\varepsilon) + \sqrt{(\varepsilon + Na + A\varepsilon - c_s B\varepsilon)^2 + 4(B\varepsilon^2 + NaB\varepsilon)c_s}}{2(B\varepsilon^2 + NaB\varepsilon)} \tag{9}$$

The efficiency y of the deproteination can be expressed as:

$$y = \frac{c_0 V_0}{c_s V} = \frac{c_0}{c_s} Na \tag{10}$$

After rearrangement, we get:

$$y = \left(\frac{-(\varepsilon + Na + A\varepsilon - c_s B\varepsilon) + \sqrt{(\varepsilon + Na + A\varepsilon - c_s B\varepsilon)^2 + 4(B\varepsilon^2 + NaB\varepsilon)c_s}}{2(B\varepsilon^2 + NaB\varepsilon)} \right) \cdot \frac{Na}{c_s} \tag{11}$$

For more comfortable calculation of the bond strength and sorption capacity from experimental data, the following rearrangement of (8) was made:

$$\frac{c_0}{c_s - c_0(\varepsilon + Na)} = \frac{1}{A\varepsilon} + c_0 \frac{B}{A} \tag{12}$$

Where V_f is volume of the pores in the cake and ε stands for porosity. Deproteination can be easily alternated by the change of soaking number. The range of efficiency at the porosity $\varepsilon = 0.5$, sorption capacity $B = 1$ g/l and initial concentration $c_s = 20$ g/l is depicted in Fig. 1.

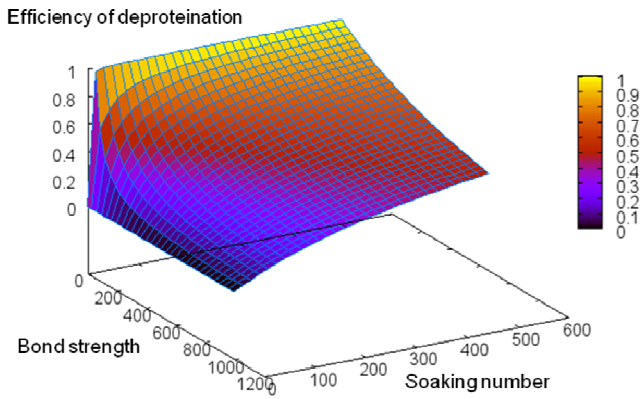


Fig. 1 Dependence of washing efficiency on soaking number and bond strength at $\epsilon = 0.5$; $B = 1$ g/l and $c_s = 20$ g/l

D. Mathematical model of deproteinization in linear area

By integration of (3) into (5), we get the relation describing the system in linear area for low concentration of protein in the bath:

$$c_s = c_0\epsilon + c_0A\epsilon + c_0Na \tag{13}$$

The concentration of protein in the bath is then:

$$c_0 = \frac{c_s}{Na + \epsilon(A+1)} \tag{14}$$

Analogously for the deproteinization efficiency:

$$y = \frac{Na}{Na + \epsilon(A+1)} \tag{15}$$

E. Mathematical model of decantation washing

Mathematical model of decantation washing is from major part derived in publication [7]. It holds for the deproteinization efficiency in the n -th step of decantation (y_n):

$$y_n = \frac{Na}{Na + \epsilon(A+1)} \frac{[\epsilon(A+1)]^n - 1}{[Na + \epsilon(A+1)]^n - 1} \tag{16}$$

The rearrangement of (16) gives:

$$y_n = 1 - \left[\frac{\epsilon(A+1)}{Na + \epsilon(A+1)} \right]^n \tag{17}$$

The bond strength A can be expressed as:

$$A = \frac{(1 - y_n)^{\frac{1}{n}}(Na + \epsilon) - \epsilon}{\epsilon \left[1 - \left((1 - y_n)^{\frac{1}{n}} \right) \right]} \tag{18}$$

III. EXPERIMENTAL

A. Preparation of the chromium cake

The chromium cake was prepared in the same way as described in [9]. The results of analyses of the input chrome-tanned shavings, as well as of the output chromium sludge and protein hydrolysate, are given in the following Table I:

Table I Analyses of chromium the input shavings and the obtained filtrate and filter cake, respectively.

	Chromium shavings	Filter cake (chromium sludge)
Dry matter	85.80 %	18.42 %
Ash*	9.58 %	26.83 %
Nitrogen*	14.04 %	10.63 %
Cr ₂ O ₃ *	4.19 %	7.18 %
Mg*	-	2.42 %

*related to the dry matter

All the per cent data mean w/w

B. Analytical methods

Standards analytical methods were used for analyses of the input materials and products. The content of protein is represented by the value of TNK (Total Kjeldahl Nitrogen). Higher protein concentrations in the washing bath were measured spectrophotometrically with the use of biuret reaction. Lower protein concentrations in the washing bath were determined through the Kjeldahl method (TNK) with subsequent determination of ammonium ions via coulometric titration. Dry matter content was determined by 12-hour drying of the samples at 103 °C. The ash content was measured by combustion of the sample for 0.5 hour and subsequent annealing of the ash in muffle furnace at 800 °C. The amount of chromium in the ash was measured iodometrically as content of Cr₂O₃. Magnesium content was determined via atomic absorption spectrometer GBC 933AA, GBC Scientific Equipment Pty Ltd.

C. Washing of the chromium cake at various soaking numbers

Chromium cake was placed in wash-bottles and proportional amount of water was added to achieve the required soaking number of 1, 10, 100, 250 and 500. The samples were washed for 7.5 hours in nitrogen atmosphere, and then left overnight in the wash-bottles. After that the samples were washed another 1 hours; the total time of washing was 8.5 hours. The suspension was then filtered under mild pressure through Buchner funnel equipped with filtration paper with fast rate of filtration. The protein content was measured as described in the previous sub-chapter.

D. Decantation washing of the chromium cake

Chromium cake and water in the volume ratio of 1:1 (i.e. $Na = 1$) were placed in a beaker. Deproteination was carried out for 1 hour under intensive stirring. The suspension was then filtered under mild pressure through Buchner funnel equipped with filtration paper with fast rate of filtration. The protein content in the filtrate was determined by biuret reaction. The filtration cake was again mixed with water to the ratio of 1:1 and the washing process was repeated in the same way. Five decantation cycles were carried out in total.

IV. RESULTS AND DISCUSSION

A. Washing of the chromium cake at various soaking numbers

The results are shown in Table II.

Table II The results of washing of chromium cake at various soaking numbers.

Na	c_0 [g/l]	y_i	$\frac{c_0}{c_s - c_0(\epsilon + Na)}$
1	3.638	0.19	0.258
10	0.578	0.30	0.043
100	0.138	0.70	0.024
250	0.056	0.72	0.010
500	0.033	0.85	0.012

The table shows the concentrations of protein in the washing baths at various soaking numbers, efficiencies of washing and the data necessary for calculations of the bond strength A and sorption capacity B from (17). It can be seen that there is significant increase in washing efficiency up to the soaking number of approximately 100; then the efficiency rises more slowly.

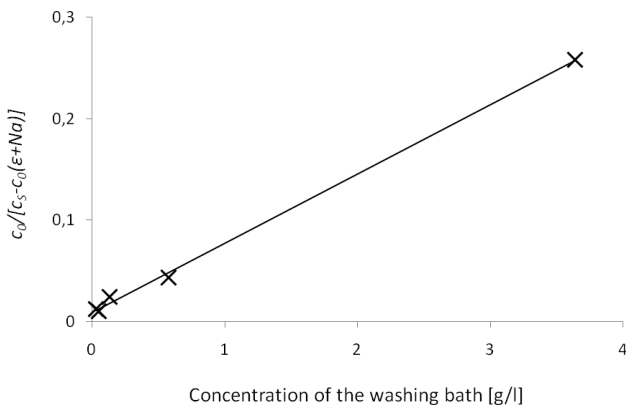


Fig. 2 Linearized deproteination model, Pearson correlation coefficient $r^2 = 0.998$.

B. Decantation washing

The results after decantation washing of the chromium cake are shown in Table III.

Table III Decantation washing of the chromium cake.

Decantation cycle	c_0 [g/l]	y_i	$\sum y_i$
1	7.72	0.394	0.394
2	2.55	0.130	0.524
3	0.78	0.040	0.564
4	0.62	0.032	0.596
5	0.14	0.007	0.603

The table shows protein concentrations in the washing baths in individual steps of decantation, deproteination efficiencies and also the sums of efficiencies in individual steps of decantation. It is apparent from the results that from the efficiency point of view it is reasonable to perform two, maximally three decantation steps at the given soaking number ($Na = 1$).

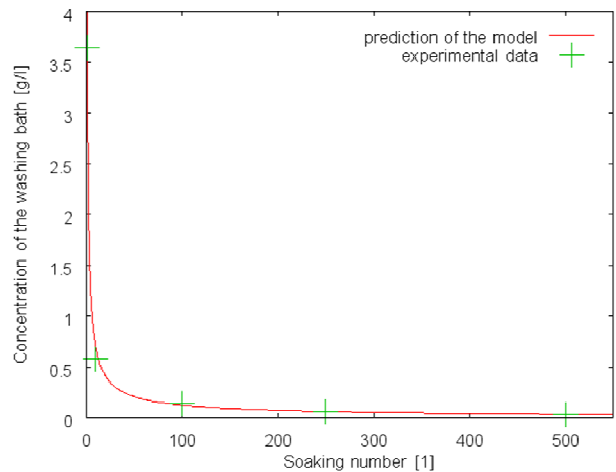


Fig. 3 Concentration of the washing bath predicted by the model in comparison with experimental data.

The graph of linearized deproteination model (Fig. 2) confirms the assumed linear dependence of the left side of (12) on the concentration of washing bath. The value of Pearson correlation coefficient suggests very good prediction of the concentration of protein in the washing bath for a wide range of soaking numbers. The graph of the prediction of the bath concentration (Fig. 3) further affirms this conclusion. The values of bond strength of $A = 231.5$ and sorption capacity $B = 15.8$ g/l were calculated from the linear regression of experimental data (Fig. 2) and from (12).

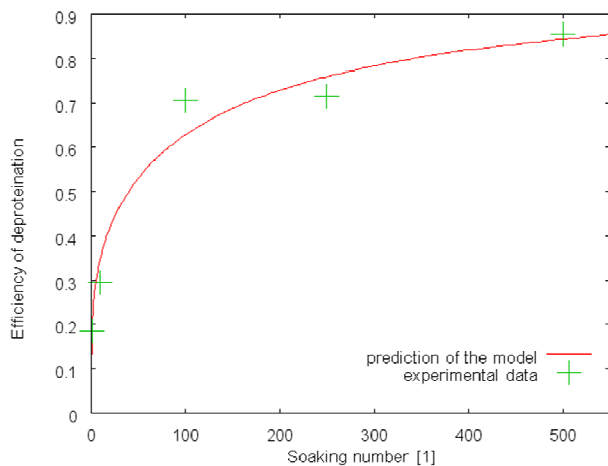


Fig. 4 Efficiency of deproteination predicted by the model for various soaking numbers in comparison with experimental data.

Closer examination of the prediction of deproteination efficiency (Fig. 4) leads to the conclusion that the model quite accurately reflects the course of deproteination efficiency; nevertheless it slightly differs from the experimental data. This is caused by high soaking numbers, at which even very small change of concentration in the washing bath leads to significant change in the entire process efficiency. For the prediction of the decantation washing we used (17); however, this relationship was derived for the linear area of deproteination. The average bond strength A calculated from (18) is 8.85.

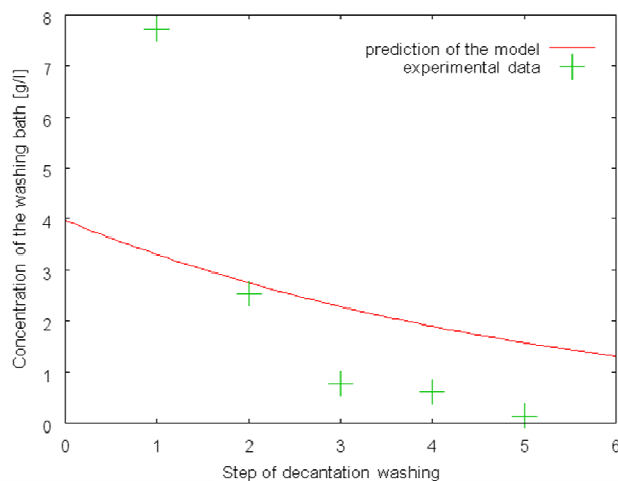


Fig. 5 Concentration of the washing bath predicted by the model in comparison with experimental data.

The prediction of the protein concentration in the washing bath during decantation washing shown in Fig. 5 suggests that the prediction is a very rough reflection of the actually measured data. That implies that deproteination does not take place in the linear area for which the model was derived.

V. CONCLUSION

Deproteination of chromium sludge by washing can be considered a perspective way of the processing of this kind of waste. The experiments showed that the efficiency of deproteination could reach up to 85 % at soaking number of 500. The most suitable technical design of deproteination in particular cases depends mainly on economic conditions and can be selected through optimization of the entire process. It can be concluded from the comparison of the predictions given by the proposed mathematical model with experimentally measured data that the model describes with good accuracy the real course of deproteination. Therefore it can be used for simulation of the process within wide range of soaking numbers. For reliable prediction it is necessary to know the values of the bond strength (A) and sorption capacity (B), which can be determined experimentally.

Simplified mathematical model applicable for the linear part of the isotherm was used for deproteination by decantation washing. The experiment showed that the model did not reflect to acceptable extent the real process. This could probably be caused by carrying out the experiment outside the range of the simplified linear model applicability. Practical utilization of the full model also in non-linear area encounters mathematical limitations coming from the fact that the series describing the sum of individual efficiencies is a general function series for which the sum of n first members is more complicated than in the case of the geometric series of the simplified model.

REFERENCES

- [1] L. F. Cabeza, M. M. Taylor, G. L. DiMaio, E. M. Brown, W. N. Marmer, R. Carrió, P. J. Celma, and J. Cot, "Processing of leather waste: pilot scale studies on chrome shavings. Isolation of potentially valuable protein products and chromium," *Waste Manage.*, vol. 18, no. 3, pp. 211-218, 1998.
- [2] K. Kolomaznik, M. Mladek, F. Langmaier, D. Janacova, and M. M. Taylor, "Experience in industrial practice of enzymatic dechromation of chrome shavings," *JALCA*, vol. 94, no. 2, pp. 55-63, 1999.
- [3] K. Kolomaznik, M. Mladek, F. Langmaier, D. C. Shelly, and M. M. Taylor, "Closed Loop for Chromium in Tannery Operation," *JALCA*, vol. 98, no. 12, pp. 487-490, 2003.
- [4] N. Saha, M. Křesálková, L. Sába, and K. Kolomazník, "The effect of anaerobic digestion on chrome sludge - a by-product of tanned leather waste," *JALCA*, vol. 98, no. 7, pp. 256-262, 2003.
- [5] J. Kupec, M. Dvořáčková, S. Rudlová, J. Růžička, and K. Kolomazník, "Deproteination of Chrome Waste by Washing and Enzymatic Hydrolysis," *JALCA*, vol. 97, no. 9, pp. 349-354, 2002.
- [6] M. Dvořáčková, M. Rienerová, M. Prostředníková, and J. Kupec, "Contribution to deproteination of residual chrome sludge after enzymatic hydrolysis of shavings with additional removal of magnesium," in *Technologies and Processes for Sustainable Development nad Pollution Reduction/Prevention. ICS UNIDO*, Trieste, 2002, pp. 243-250.
- [7] K. Kolomaznik, *Modeling of manufacturing processes* (Textbook style) [in Czech]. Brno University of Technology, Brno, Czech Republic, 1990.
- [8] L. Bartovská and M. Šišková, *Physical Chemistry of Surfaces and Colloid Systems, 5th ed.*, (Textbook style) [in Czech]. Institute of Chemical technology Prague, Czech Republic, 2005.
- [9] M. Barinova and K. Kolomaznik, "Mathematical Description of Magnesium Oxide Extraction from Chrome-Tanned Leather Waste," (Unpublished work style), Unpublished.

Real time monitoring of public transit passenger flows through Radio Frequency Identification - RFID technology embedded in fare smart cards

Maurício L. Ferreira, José A. M. de Gouveia, Eduardo Facchini, Melissa S. Pokorny, Eduardo M. Dias

Abstract—This paper discusses the advantages of using radio frequency identification (RFID) technology embedded in fare smart cards as a transit management and planning aid. It is shown how RFID can be used for systematic collection and analysis of passenger flows, thus providing useful information for transit operations management and short term planning. Additionally, in combination with intelligent transport systems (ITS) technology, RFID can also provide support for infrastructure and fleet management activities, as well as real time information for transit user.

Keywords— Radio frequency identification (RFID), passengers, public transportation, services management, smart cards and control of infrastructure.

I. INTRODUCTION

FOR several decades, urban growth has contributed to saturation of the structures which support citizens' everyday lives [1], with direct impact on the ability of many cities to warrant a healthy life for their population and to secure adequate supply support structures. Such situation leads away from the ideal conditions to sustain a good urban life quality [2].

It should be noted that as a result of this, some cities display an increase in the rate of traffic accidents and fatalities, increasing problems related to air pollution, an increasingly insecure environment, rising cost of living and rising rates of unemployment, poverty and social exclusion [3].

Aware of this condition, rulers, administrators and organized urban communities are seeking for solutions that support the construction of public policies to address current

M. Lima is project coordinator of São Paulo Transporte - SPTrans, R. Boa Vista n.236, São Paulo/SP, Brazil, CEP 01014-000, and a PhD student at Escola Politécnica of the Universidade de São Paulo (Polytechnic School of the University of São Paulo) (mauriciolima7@usp.br).

J. A. de Gouveia is systems analyst of São Paulo Transporte - SPTrans (jose.gouveia@gmail.com).

E. Facchini is a member of the technical advisor to the planning board of SPTrans (eduardo.facchini@sptrans.com.br).

M. S. Pokorny is a PhD student of Polytechnic School, University of São Paulo - USP and a researcher of GAESI (melissapokorny@pea.usp.br)

E. M. Dias is full professor of the Escola Politécnica da Universidade de São Paulo (Polytechnic School of the University of São Paulo) and coordinator of GAESI - Grupo de Automação Elétrica em Sistemas Industriais, a research group of the Electrical Energy and Automation Department, Escola Politécnica, Universidade de São Paulo, Av. Prof. Luciano Gualberto, trav. 3, n. 158, São Paulo/SP, Brazil, CEP 05508-970 (emdias@pea.usp.br).

and future challenges in cities [4].

The issues related to urban mobility of people, goods and services are among the priorities and, like other cities, São Paulo, Brazil, has adopted restrictive measures to minimize negative impacts on traffic and congestion of roads: (a) in 1997 a license-plate-based car rotation scheme, by which 20% of the car fleet is excluded from expanded CBD traffic on work days [5]; (b) 2007 marked the beginning of the metro rail network expansion plan which, when implemented, by 2018, will have increased the metro network to 200 km, tripling the current extension [6]; (c) in 2008 restrictions to truck traffic were implemented at certain times of the day within a geographic area in the expanded CBD [7]; (d) in 2011 an extensive program of pedestrian priorities was adopted [8]; (e) 2012 saw an increase in the number of streets and avenues with reduced maximum speed limit [9]; and (f) between 2013 and 2014 over 300 km of bus lanes were dedicated, giving priority to this mode of transport over individual motorized transport [10].

Actions such as those aim at cutting congestion and reducing the impacts of emissions and deaths from traffic accidents, attracting drivers and passengers from private cars to mass transit, and stopping the trend towards saturation of important roads, thereby improving urban mobility.

Many traffic experts agree that besides improving the mobility of people living in the cities, accessibility gains are also vitally important. Accessibility is characterized by many authors as "the ease (or difficulty) for people and goods to reach parts of the city, as measured by the time and cost involved" [11][12].

On the other hand, Brazilian cities witnessed growing migration of economic activities to business complexes and shopping malls, and also increasing concentrations of multistory residential buildings, as well as other high-rise developments including universities, supermarkets, convention centers, etc.

Additionally, while there is no compromise in land use development, the upsurge of new business, services and industry concentrations open up new working and shopping opportunities, generate additional travel needs which have to be satisfied. All of these are categorized as "traffic generation poles", as they bring up increasing traffic problems and additional restrictions to the displacement of people, goods and services [13].

Monitoring and understanding travel patterns of individuals becomes an important field of knowledge to promote proposals towards improving urban mobility and accessibility, especially provided by public transportation systems.

II. APPLICATIONS OF ITS

The city of Sao Paulo has a network of public transport (metro, trains and buses) which has been consolidated over the years. Bus services, which are managed by the Municipality, include 1,300 lines which are operated by a fleet of 15,000 buses over a 4,500 km street network. These buses run 190,000 daily vehicle trips, serving a patronage of 3.7 million which perform a total of 9.5 million daily person trips.

Since 2004, the city has benefited from Intelligent Transportation Systems - ITS resources to support the management of bus transportation services. All transit buses are equipped with Automatic Vehicle Location (AVL) and Global Positioning System (GPS) devices, as well as with electronic fare validation devices – AFC. Bus stops in exclusive bus corridors are interconnected by optic fiber networks and are equipped with Closed Circuit Television (CCTV) cameras and Variable Message Signs (VMS). Bus terminals are monitored by CCTV cameras and information is conveyed to users via multimedia devices, PA systems and VMS panels that inform the departure and arrival time of vehicles [14].

Electronic ticketing has also been in use since 2004. The vast majority of passengers pay for their trips using city-issued smart cards trademarked "Bilhete Único" (Single Ticket), of which roughly seven million are in current and frequent use (at least once a week). Only 5% of all bus transit users pay the fare value in cash [15].

The digital data collected from transactions with smart cards, are used exclusively to support the fare revenue clearing process involving the city bus management agency and the rail operators and to establish the payment due to each private bus operator company (all city buses are run by private companies through municipal concession contracts).

III. DEFICIENCIES

Even though much of the Intelligent Transport System devices collect data continuously, and processing systems make information available online, such information is basically used for monitoring purposes, the most often not leading to effective correction of operational activities.

IV. RFID

The use of automatic identification (Auto-ID) in public transport services has been evaluated by Information Technology and Communication (ICT) specialists as a possible add-on to ITS (Intelligent Transport System), as shown in Fig. 1.

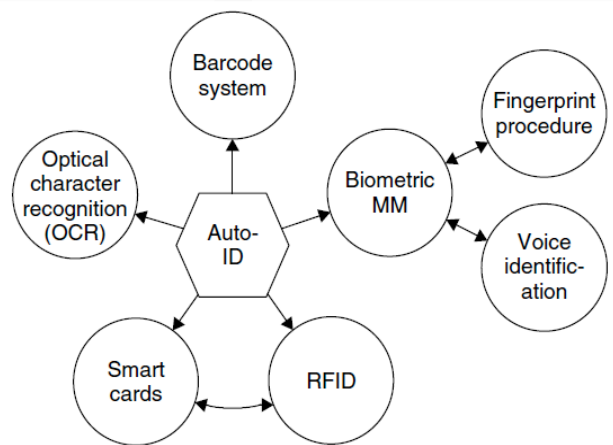


Fig. 1 – Overview of the most important procedures Auto-ID

Source: Handbook Fundamentals and Applications in Contactless Smart Cards and Identification (2003)

RFID technology has been widely discussed by companies, the technical community and specialists, and an extensive amount of existing literature, regarding its description and applications. Used by the military since World War II, is now considered as an alternative to bar code technology, RFID has the advantages of streamline processes and is able to store relevant information as well as transmit wirelessly to compatible interrogators without physical contact.

The barcode, used since 1940, is currently very popular for product identification. However, RFID had been in commercial use since the 1970s, is gaining momentum and becoming relevant for industry, business, services and government agencies, is also being used in a variety of applications such as: supply chain control (logistics), product tracking (agenda control), authentication (quality control), property access control (security), anti-theft systems (security), individual documentation and identification (passports and hospital patients data), electronic payment (smart cards and tolls) and smartphones (NFC - *Near Field Communication*).

Radio frequency identification (RFID) technologies are based on devices assembled from miniaturized components consisting of:

- 1) Receiver called “TAG” or “TAG-RFID” which includes a coil antenna and a microcircuit;
- 2) Read/Write equipment (transceiver) and their antennas;
- 3) Middleware modules to integrate field equipment to data processing systems.

The use of this technology allows the tag (in objects, products or people) to be recognized and identified at a distance by means of electromagnetic wave emissions. As to the way of being energized, receivers can be classify as active, passive or quasi-active (or quasi-passive).

In this paper we deal specifically with low cost passive power receivers, which only require electromagnetic waves emitted by dedicated antennas to be activated. Once activated, the receiver will be able to start transmitting data to the

reading equipment. The frequency bands used are LF - low frequency of 125kHz and HF - high frequency of 13.56 MHz, both also used in smart cards for connection with on-board fare readers and UHF - Ultra High Frequency (860MHz - 960MHz), also used in EPC (*Electronic Product Code*) systems. Microwave systems (2.45 GHz) are also used in some applications.

V. METHODOGY

This article discusses the use of low-cost RFID technology associated to infrastructure (vehicles, bus stops, transfer terminals, checkpoints on the route of the lines, etc.), and in combination with the technologies used in smart cards [17].

The first part of methodology is based on the installation of receivers and / or readers in public transport infrastructure components, such as buses, bus terminals and passenger boarding and alighting points along bus routes, as follows:

- In Buses: installation of labels and reader equipment;
- In Terminals: installation of labels at passenger boarding and alighting locations, and installation of readers with antennas near vehicle exit or entrance areas;
- At Bus Stops: installation of labels (tags).

The second part deal of the coexistence of smart card radio frequency technology as used by the “Bilhete Único” (NXP MIFARE® Classic) with RFID technology.

For the development, the SPTrans -the São Paulo Public Transit Management Agency -, had the company NXP Semiconductors perform a test and evaluate the recognition by reader devices installed in buses of a RFID tag embedded into a “Bilhete Único” fare payment smart card.

According to this methodology, a single sequential number is stored into the microchip tag (N-Bits transponder Read-Only system).

The stored number will be associated to the individual identification number of the smart card to which the tag is attached, allowing the tag, when activated, to transmit it as identification information to the reading device (reader). Thus, the records obtained correspond exclusively to the smart card to which the tag is attached. The proposed card structure is shown in Fig. 2.

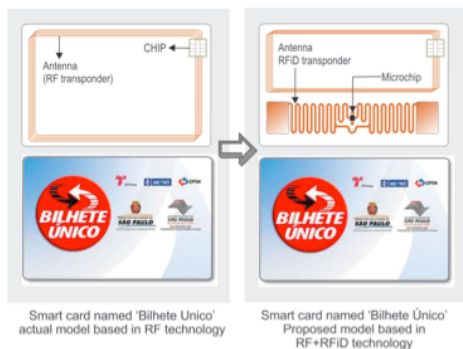


Fig. 2 - Example of smart card with RF technology and smart card with embedded RFID technology. Source: Ferreira 2013

VI. OPERATION OF THE PROPOSED SOLUTION

Through the antennas, an RFID reader can transmit electromagnetic waves and perform more than 100 readings per second from transmitters up to seven meters distant from the antennas in free area. Thus, a prospective passenger bearing a smart card which has RFID devices attached to it will be promptly recognized and identified as he approaches the bus. Fig. 3 shows a schematic diagram of passenger card tag reading as done by the bus equipment and by the bus stop equipment.

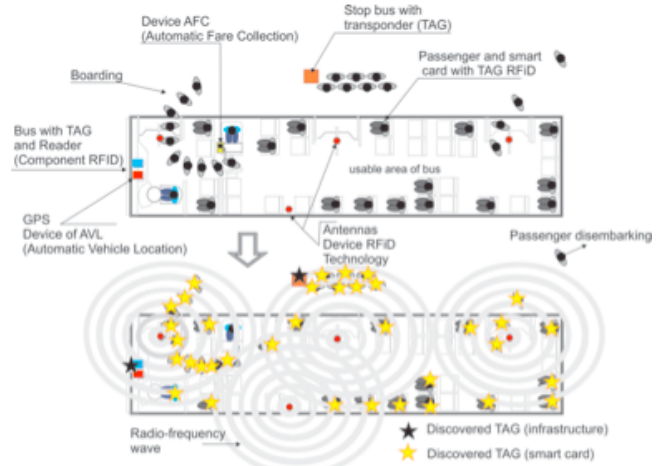


Fig. 3 – Schematic view of automatic identification through RFID technology. Source: Source: Ferreira 2013

This process will continue until the passenger's card is carried beyond the reading range of the bus interrogator antennas. When the passenger gets off the bus and moves away from it, and consequently carries the smart card equipped with RFID TAG away from the reach of the bus antennas the records in the card will no longer be transmitted. If the bus stop also equipped with RFID tags, then the smart cards carried by the passengers waiting for the bus, may have their tags activated and recognized by bus RFID devices.

To avoid receiving and processing an excess of repeated information from the same cards, while they remain within the range of the bus RFID readers, it is proposed that bus readers will be activated only while vehicle doors are open for passenger boarding and alighting. Thus, there will be no data collection while the vehicle is moving.

The data processing system (middleware) will identify the number associated with the RFID tag embedded into a specific smart card and compare it with the identification number of that smart card, as identified during the process of fare validation. Only if the two numbers are compatible will the system process the information received from that specific tag.

At terminals, a reader equipped with antennas installed near the bus entrance and exit gates will recognize and identify the vehicles as they enter or leave the terminal premises, and each event will be registered together with the respective date and time information.

VII. THE EXPERIMENT

There were some initial doubts as to the compatibility of bundling RF identification technology with smart card technology. The main concern was about the efficiency and reach of electromagnetic waves for tag reading, considering that the bus environment is essentially metallic, that its space is mostly occupied by a variable number of passengers, and that 70% of the human body is liquid content.

These difficulties are enhanced by the fact that, unlike artifacts a production line that have their tags affixed to the outside, generally respecting certain fixed patterns, and within an environment that is free from major constraints for the propagation of electromagnetic waves, persons behavior is random and independent, as they constantly and rapidly move about, even in restricted spaces. The fact that passengers normally keep their smart cards protected (hidden) in purses or wallets until the time comes to present them before a validator interface to pay the fare and unlock the turnstile does not help either.

The experiment was prepared with the purpose of checking the efficiency of inside-bus tag readers, and evaluating the capacity for reading smart-card-embedded tags carried in bags, packets, shirt pockets, trousers pockets, bundled with books, in wallets and with cell phones, simulating commonly encountered situations.

A bus was then equipped with a reader and two antennas which were positioned inside the vehicle and near the entrance door (Fig. 4).

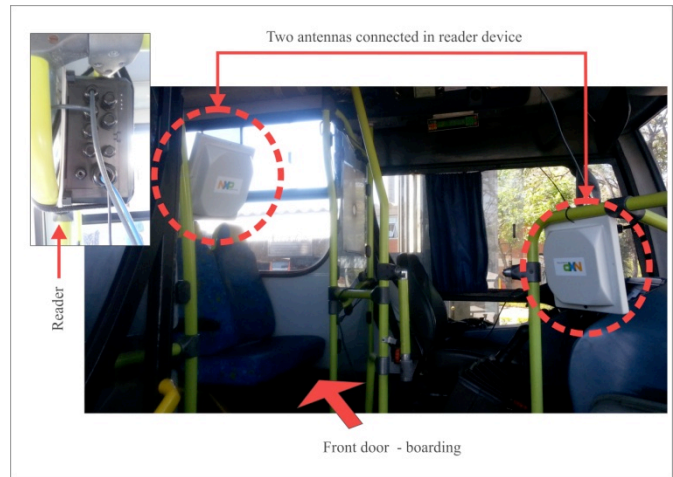


Fig. 4 - Buses equipped with equipment of radio frequency identification technology. Source: Experiment.

In the course of the experiment five volunteers boarded the bus, one after another, each carrying a different tag in hidden locations (in objects or clothing). This experiment evaluated products from four manufacturers and different designs, which were tested one after another to compare their performances, while the volunteers kept their tags hidden in the same position. Volunteers approached the bus, proceeded to the gate, boarded (passing between the antennas), walked down the vehicle aisle to the validator and then got off. The observations and findings were presented in Table 1.

Table 1 – Results of the experiment.

Round 4 - Tests in the Bus					+30dBm - 2 Antennas			Antenna 2 near the wind glass
	Volunteer	5 Digit Final EPC	Tag Local in the body	# of Readings / Time	Total Records	Antennas	Method	Observation
UCODE7 AD235	1	22201	Shirt Pocket	09 Records / 15 Seconds	25	Both	Enter, go to validator - return	
	2	22202	Left front trousers pocket	06 Records / 15 Seconds		Both	Enter, go to validator - return	
	3	22203	cell phone in front of it	06 Records / 22 Seconds		Both	Enter, go to validator - return	
	4	22204	pocket, cell phone in	02 Records / 15 Seconds		1	Enter, go to validator - return	
	5	22205	Left back trousers pocket	05 Records / 13 Seconds		Both	Enter, go to validator - return	Only 1 reading from antenna 1
UCODE7 AD370	1	33301	Shirt Pocket	04 Records / 02 Seconds	14	Both	Enter, go to validator - return	Only 1 reading from antenna 2
	2	33302	Left front trousers pocket	02 Records / 01 Seconds		Both	Enter, go to validator - return	Only getting in the bus
	3	33303	cell phone in front of it	02 Records / 15 Seconds		Both	Enter, go to validator - return	
	4	33304	pocket, cell phone in	No records at all		0	Enter, go to validator - return	
	5	33305	Left back trousers pocket	06 Records / 12 Seconds		Both	Enter, go to validator - return	Only 1 reading getting in the bus
Sirt - RS1654	1	55501	Shirt Pocket	08 Records / 16 Seconds	39	Both	Enter, go to validator - return	
	2	55502	Left front trousers pocket	07 Records / 13 Seconds		Both	Enter, go to validator - return	
	3	55503	cell phone in front of it	14 Records / 16 Seconds		Both	Enter, go to validator - return	
	4	55504	pocket, cell phone in	07 Records / 15 Seconds		Both	Enter, go to validator - return	
	5	55505	Left back trousers pocket	03 Records / 11 Seconds		Both	Enter, go to validator - return	
UCODE7 - Proto	1	77701	Shirt Pocket	11 Records / 15 Seconds	47	Both	Enter, go to validator - return	
	2	77702	Left front trousers pocket	08 Records / 13 Seconds		Both	Enter, go to validator - return	
	3	77703	cell phone in front of it	14 Records / 16 Seconds		Both	Enter, go to validator - return	Read 5 m from door out the bus
	4	77704	pocket, cell phone in	05 Records / 03 Seconds		Both	Enter, go to validator - return	Read only getting in the bus
	5	77705	Left back trousers pocket	09 Records / 13 Seconds		Both	Enter, go to validator - return	6 reading when leaving the bus

Source: Experiment performed by NXP Semiconductors

All tags tested were successfully energized and returned information, but variations were observed as to the time required and the number of readings which were transmitted in each collection cycle.

VIII. POTENTIAL OF OBTAINING DATA

The RFID technology can be used for data acquisition and processing of important information for the management of public transport. In this project the following information is obtained:

- 1) Punctuality and frequency of transport services at checkpoints;
- 2) The quantity of vehicles that are in operation, their ID's and real time positions;
- 3) Travel time averages of passengers;
- 4) Vehicle delays at intersections, bottlenecks and other relevant locations;

Radio frequency technology, as used for communication between buses and their infrastructure, makes it possible to constantly confirm the bus actual position, as related to established check points, thereby allowing real time scheduling control and adjustments.

It can also provide tools for updating infrastructure and

vehicle inventory information. On-board equipment allows following groups of “tagged” fare smart cards since the moment their bearers approach the bus for boarding, and continue following them while they are aboard, until the moment when they get off and the bus moves away.

Thereby, passengers boarding and alighting at each stop can be counted, and each of the boarding and alighting stops can be identified by association with fare card ID number. Such information will also allow us to confirm data obtained by GPS giving conditions to retrieve monitoring in cases of system breakdowns. Thus qualifies Operational Control Centers perform online actions to correct the chain of services every time.

Once in regular operation, the system shall routinely yield information which, once available, may widen the regulatory scope of Operation Control Centers, providing adjustment inputs to the system network and allowing short-term planning, and improvements in information to passenger. Fig. 6 shows an overview of the data processing subsystem (middleware) and respective connections.

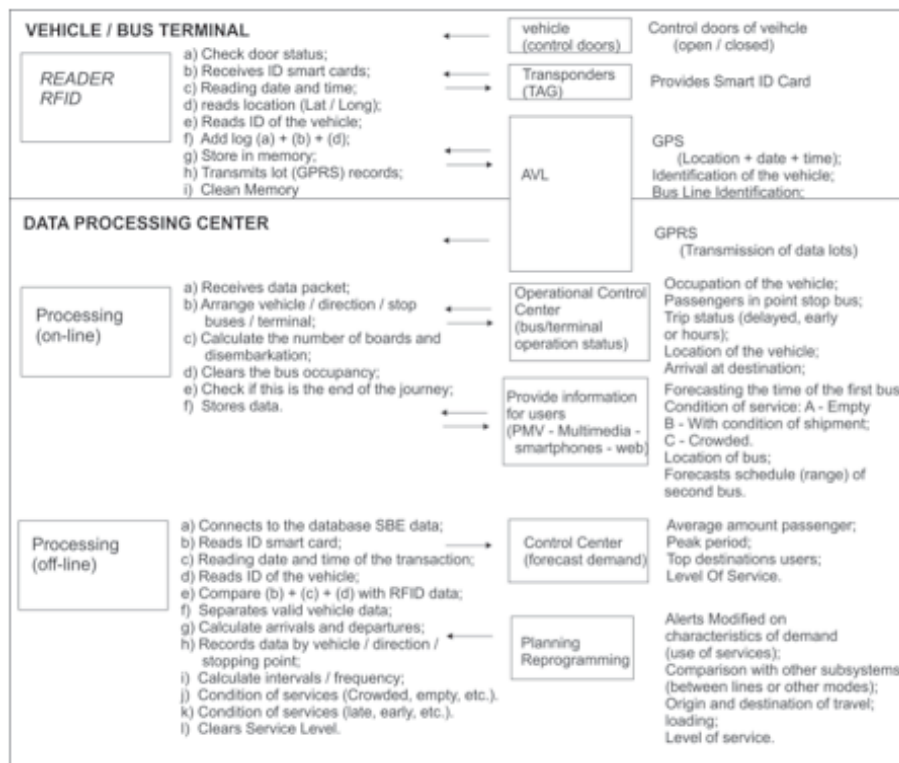


Fig. 6 - Overview of the data processing subsystem (middleware) including tasks and connections. Source: Author.

While managing demand of passengers, the system gives access to passenger displacement patterns and brings forth additional possibilities, including:

- 1) Counting the number of passengers which remains on the bus between each stop, allowing the identification of the highest load section along the bus route.

- 2) Number of passengers getting on and off the bus at each bus stop;
- 3) Number of passengers on board of the bus between each pair of subsequent bus stops;
- 4) Passengers travel time on board of the bus;
- 5) Total passengers public transportation travel time

- (excluding trip end walking times);
- 6) Plan new services in response to variations in passenger origin and destination survey information;

This information expands the conditions for efficient management of urban public transport and improve quality of services. Such information will lead to urban mobility and accessibility improvement and support appropriate public policies towards efficient transport system. Some benefits may include:

- 1) Savings financial resources with a perspectives for expanding infrastructure use management;
- 2) Better performance and efficiency of public transportation services;
- 3) Ensuring a better public transport by providing higher quality systems with improved service levels;
- 4) Development of urban mobility plans more compatible with the growth and functionality of cities;
- 5) Provision of relevant information supporting users' decisions on how and when to use public transport services;
- 6) Lowering transit management costs through a increase efficiency of use of human, financial and time resources in the development and implementation of passenger behavior or transport system operation surveys systems or research about characteristics of passenger demand;
- 7) Impart on proactivity of Transit Operations Control units;
- 8) Synchronization of bus services in order to minimize transfer waiting times of passengers;
- 9) Implementation of fraud detection routines to curb undue smart card usage practices;
- 10) Contribution to a technological innovation-friendly transit environment (V2I, V2V, I2C, IOT, etc.);
- 11) Development of plans for increment traffic attraction zones and attain balanced and sustainable land use patterns supported by efficient urban transport systems;
- 12) improvement of the quality of life of urban population by creating facilities that are appropriate to their daily needs;
- 13) Expanding tourist infrastructure;
- 14) Establishing comprehensive and dedicated transport system connections between public services facilities;
- 15) Creating tailored services dedicated to specific public transport user categories, like: students, senior citizens, disabled and others;
- 16) Providing updated information on passenger displacement patterns, which can be used for calibrating future transport network models;

However there are still difficulties to be overcome in order to consolidate the applicability of the RFID, such as:

- 1) Improvement of functionality of transponders so they become better suited for operation in areas with high density of passengers;
- 2) The cost-effectiveness analysis (considering time and money) of replacing current smart cards by cards with radio frequency identification technology;
- 3) Evaluation of the costs of acquiring, installation and maintenance of the tag readers, in buses and terminals, and compare them to expected benefits;

- 4) Evaluation of logistic efforts and costs associated with the installation of TAGS onto current bus stops;
- 5) Integration of data communication between the new devices and electronic equipment already installed in buses;
- 6) Development of the computational architecture and communication infrastructure that support the operation of the technology;
- 7) Development of data processing and producing information in user's interfaces (internal and external) systems;
- 8) Development of procedures to ensure efficient use of the information through actions, incorporating them in training.

IX. CONCLUSIONS

This article presents possible solutions for obtaining information arising from the use of radio frequency technology identification - RFID in urban public passenger transport systems and indicates the way for future discussions on the use of transit fare payment smart cards as a physical support for RFID devices.

The wide applicability of such resource is related to the ever growing adoption of smart electronic ticketing and vehicle monitoring systems, which have already been implemented and are in use in many cities worldwide, Sao Paulo being one of them. Since smart cards are commonly carried along by the public transportation systems users, they appear as potential providers of information concerning transit services.

The radio frequency identification components fulfill their role in monitoring the displacements of user's due to use of smart cards in their travels and thus appear as potential supplier of information. Moreover, adding it to travelers cards does not affect the current use of smart cards for electronic fare payment and does not require any specific action from the user in its daily card's maintenance.

However, recognition of the smart card identification data will provide information and control of time and place both users and vehicles.

Thus, the use of RFID and smart card infrastructure and public transport vehicles, justifies necessity for the creation of indicators and control of time, places, and consumption of services by users conditions, as well as collecting additional information on resources and infrastructure buses.

This paper discussed benefits of use of the RFID technology devices embedded into fare payment smart cards to public transport. Experiment results indicate that the efficient use of such technology does not require any change in the use of public transport fare payment smart card by passengers.

The use of RFID has the advantage of complementary information obtained by existing ITS systems and produces new information for the management of bus infrastructure and support users in real time. Allows to develop control systems for the passenger demand and systematizes and updates matrices of origin and destination (O/D) about the travel of passengers in bus systems and get their volumes. This

information is important supplement to implement improvements in urban public transport network.

Although with challenges, the use of RFID technology enables promising information about the characteristics of patterns of passenger's displacement and efficient use of infrastructure and resources of public transport. The use of RFID technology for providing of demand-related information about public transport system to its operators. The system can be effectively developed in the coming years, bringing number of benefits to passengers and contributing to the organization of sustainable cities. That is way it deserves attention and should be further development.

REFERENCES

- [1] GUPTA, J. Global Sustainable Development Governance: Institutional Challenges from a Theoretical Perspective. *International Environmental Agreements: Politics, Law and Economics*, v. 2, n. 4, p. 361-361, 2002.
- [2] TOPPETA, D. The smart city vision: how innovation and ICT can build smart, "livable", sustainable cities. The Innovation Knowledge Foundation, 2010.
- [3] BATAGAN, L. Smart Cities and Sustainability Models– *Informática Economica*, vol. 15, p. 81, nº3/2011.
- [4] INFOSYS - Innovation and the City - Rapid urbanization is creating opportunities for new technologies to make a new difference. Girish Khanzode, Shekhar Potnis. In: *Insights - Building Tomorrow's Enterprise*, p. 1, 2012.
- [5] Decreto Municipal Nº 37.085 de 3 de outubro de 1997 - Regulamentação da Lei nº 12.490 que autoriza o Executivo a implantar o Programa de Restrição ao Trânsito de Veículos Automotores.
- [6] Folha de São Paulo – Caderno Cotidiano – Alkimin promete mais 126 km de metrô em São Paulo até 2018, em 19/04/2012, em – <http://www1.folha.uol.com.br/cotidiano/2012/04/1078302-alkmin-promete-mais-126-km-de-metro-em-sao-paulo-ate-2018.shtml>. (Acesso em 05/03/2014).
- [7] Diário Oficial da Cidade de São Paulo, Nº 87 (13/05/2008) - Decreto Nº 49.487 de 12 de maio de 2008 - Regulamenta o trânsito de caminhões na Zona de Máxima Restrição de Circulação - ZMRC.
- [8] Programa "Dê Preferência à Vida" - Zona de Máxima Proteção ao Pedestre - ZMPP - disponível em <http://www.cetesp.com.br/consultas/zona-de-maxima-protecao-ao-pedestre.aspx> (Acesso em 01/03/2014).
- [9] Premissas para um plano de mobilidade urbana – Associação Nacional dos Transportes Públicos - ANTP/Secretária Municipal dos Transportes – SMT / São Paulo Transporte S.A. - Sptrans, 2013.
- [10] Programa "Dá Licença para o Ônibus" - A cidade que a gente quer é aquela que dá prioridade ao transporte público - disponível em <http://www.cetesp.com.br/consultas/da-licenca-para-o-onibus/o-programa.aspx> (Acesso em 01/03/2014).
- [11] VASCONCELLOS, E. A. - O que é o trânsito. São Paulo: Brasiliense. P. 26., 1985.
- [12] GOMIDE, A. A. Mobilidade urbana, iniquidade e políticas sociais. *Políticas sociais: acompanhamento e análise*, 12, p. 242-250, 2006.
- [13] Departamento Nacional de Trânsito – DENATRAN - Manual de procedimentos para o tratamento de polos geradores de tráfego. DENATRAN/FGV, Cap. I, p. 7-8. Brasília, 2001.
- [14] São Paulo boosts bus reliability by 30 percent, ups innovation with outside help - Microsoft Case Studies - http://www.microsoft.com/casestudies/Case_Study_Detail.aspx?CaseStudyID=710000001378. (Acesso em 01/03/2014).
- [15] Smarter e-ticketing for Sao Paulo – NXP – Global Press Release - <http://www.nxp.com/news/press-releases/2013/07/smarter-e-ticketing-for-sao-paulo.html> - (Acesso em 08/03/2014).
- [16] Handbook Fundamentals and Applications in Contactless Smart Cards and Identification, Overview of the most important procedures self-ID – RfID, Second Edition - John Wiley & Sons 2003.
- [17] FERREIRA, M. L. - RFID for Real Time Passenger Monitoring – WSEAS – World Scientific and Engineering Academy and Society: Recent Researches in Telecommunications, Electronics and Signal Processing, 2013.

Families of spherical polynomials: Description and robust stability analysis

Radek Matusů

Abstract—The main goal of this contribution is to present not so common and frequently used approach to definition of uncertainty bounding set for systems with parametric uncertainty. More specifically, the work is focused on spherical polynomial families, on their description and related robust stability analysis. The illustrative example demonstrates an easy-to-use graphical method of robust stability testing by means of the Polynomial Toolbox for Matlab.

Keywords—Spherical Uncertainty, Weighted Euclidean Norm, Robust Stability Analysis, Value Set Concept, Zero Exclusion Condition.

I. INTRODUCTION

PARAMETRIC uncertainty is commonly used tool for description of real plants as it allows using relatively simple and natural mathematical models for processes which behaviour can be much more complicated. The structure (i.e. order) of the models with parametric uncertainty is considered to be fixed, but its parameters can lie within given bounds. Within this contribution, these bounds are going to be assumed in not so frequently applied way.

The typical, mostly used and naturally comprehensible approach assumes the bounds in the shape of a box. Here, the alternative approach, which uses the bounds in the shape of a sphere (ellipsoid), is going to be studied. The scientific literature contains much more works related to the classical “box” uncertainties than to the spherical ones. However, some basic information as well as possible extensions and various applications can be found e.g. in [1] – [5].

This contribution is focused on polynomials with parametric uncertainty and spherical uncertainty bounding set. More specifically it deals with description of a spherical polynomial family and with tools for analysis of its robust stability. Special attention is paid to very universal graphical tool based on the combination of the value set concept and the zero exclusion condition [1]. The described ideas are followed by an illustrative example supported by plots from the Polynomial Toolbox for Matlab [6], [5].

The work was supported by the European Regional Development Fund under the project CEBIA-Tech No. CZ.1.05/2.1.00/03.0089. This assistance is very gratefully acknowledged.

Radek Matusů is with the Centre for Security, Information and Advanced Technologies (CEBIA – Tech), Faculty of Applied Informatics, Tomas Bata University in Zlín, nám. T. G. Masaryka 5555, 760 01 Zlín, Czech Republic. The email contact is: rmatusu@fai.utb.cz.

II. PARAMETRIC UNCERTAINTY AND UNCERTAINTY BOUNDING SET

Generally, the systems with parametric uncertainty can be described though a vector of real uncertain parameters (often called just uncertainty) q . The continuous-time uncertain polynomial, which is a typical object of researchers’ or engineers’ interest, can be written in the form:

$$p(s, q) = \sum_{i=0}^n \rho_i(q) s^i \quad (1)$$

where ρ_i are coefficient functions.

Then, so-called family of polynomials combines together the structure of uncertain polynomial given by (1) with the uncertainty bounding set Q . Therefore, the family of polynomials can be denoted as:

$$P = \{p(\cdot, q) : q \in Q\} \quad (2)$$

The uncertainty bounding set Q is usually given in advance, typically by user requirements. It is supposed as a ball in an appropriate norm. The mostly used case utilizes L_∞ norm:

$$\|q\|_\infty = \max_i |q_i| \quad (3)$$

which means that a ball in this norm is a box. Practically, the box is defined by the components, i.e. by the real intervals which can the uncertain parameters lie within.

Another approach employs L_2 (Euclidean) norm:

$$\|q\|_2 = \sqrt{\sum_{i=1}^n q_i^2} \quad (4)$$

or more generally the weighted Euclidean norm:

$$\|q\|_{2,W} = \sqrt{q^T W q} \quad (5)$$

where $q \in \mathbf{R}^k$ and W is positive definite symmetric matrix (weighting matrix) of size $k \times k$. Such definition of Q means that a ball in the norm can be referred as a sphere, or more generally as an ellipsoid. Under assumption of $r \geq 0$ and

$q^0 \in \mathbf{R}^k$, the ellipsoid (in \mathbf{R}^k) which is centered at q^0 can be expressed by means of:

$$(q - q^0)^T W (q - q^0) \leq r^2 \quad (6)$$

or equivalently by:

$$\|q - q^0\|_{2,W} \leq r \quad (7)$$

The ellipsoid can be easily visualized in two-dimensional space ($k = 2$) for:

$$W = \begin{bmatrix} w_1^2 & 0 \\ 0 & w_2^2 \end{bmatrix} \quad (8)$$

as it is shown in Fig. 1 [1].

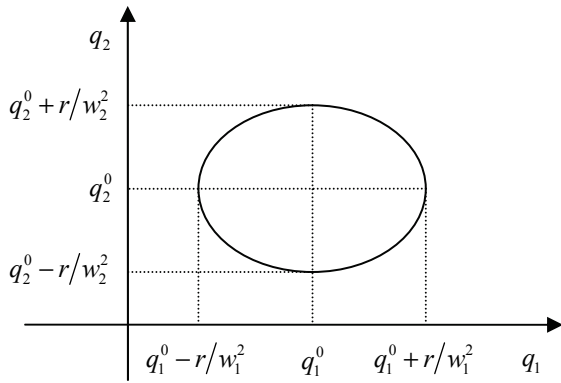


Fig. 1 Ellipsoid defined by weighted Euclidean norm

Decision on what type of norm should be used for uncertainty bounding set Q depends on several factors. In many engineering problems, the real uncertain physical parameters are independent on each other and thus Q should be a box naturally. However, according to [1], the ellipsoids could be useful and justifiable under “imprecise description” of the uncertainty bounds, i.e. if actual Q is located between some minimum and maximum and a suitable ellipsoid can interpolate them. The choice should respect also available tools for solving the specific problem. Besides, the mathematical models obtained on the basis of physical laws usually have Q in the shape of box, but the identification methods mostly lead to the ellipsoids [7].

III. SPHERICAL POLYNOMIAL FAMILY

The family of polynomials given by (2) is called spherical one [1] if $p(s, q)$ has an independent uncertainty structure (all coefficients of the polynomial are independent on each other) and Q is an ellipsoid.

In fact, one can work with two basic representations of spherical polynomial families.

The first type assumes that polynomial is centered at zero:

$$p(s, q) = \sum_{i=0}^n q_i s^i \quad (9)$$

$$\|q - q^0\|_{2,W} \leq r$$

where W is a positive definite symmetric matrix, q_0 is the nominal and $r \geq 0$ means the radius of uncertainty.

In the second representation, Q is considered to be centered at zero:

$$p(s, q) = p_0(s) + \sum_{i=1}^n q_i s^i \quad (10)$$

$$\|q\|_{2,W} \leq r$$

where moreover $p_0(s) = p(s, q^0)$.

As an example, suppose a spherical polynomial family:

$$p(s, q) = (0.5 + q_0) + (1.5 + q_1)s + (2.5 + q_2)s^2 \quad (11)$$

$$\|q\|_{2,W} \leq 1$$

$$W = \begin{bmatrix} 1 & 0 & 0 \\ 0 & 2 & 0 \\ 0 & 0 & 3 \end{bmatrix}$$

which can be centered on the vector:

$$\tilde{q}^0 = (0.5, 1.5, 2.5) \quad (12)$$

Then, the resulting spherical polynomial family, equivalent to (11) can be written as:

$$p(s, q) = \tilde{q}_0 + \tilde{q}_1 s + \tilde{q}_2 s^2 \quad (13)$$

$$\|\tilde{q} - \tilde{q}^0\|_{2,W} \leq 1$$

$$W = \begin{bmatrix} 1 & 0 & 0 \\ 0 & 2 & 0 \\ 0 & 0 & 3 \end{bmatrix}$$

IV. ROBUST STABILITY ANALYSIS

Obviously, the most important feature of all control circuits is their stability. Under conditions of parametric uncertainty, this term can be expanded to robust stability, which means that the whole family of closed-loop control systems must remain stable for all possible allowed perturbations of system parameters.

From the practical testing point of view, we are interested in the robust stability of the family of closed-loop characteristic polynomials in the form (2). This family is robustly stable if and only if $p(s, q)$ is stable for all $q \in Q$, i.e. all roots of $p(s, q)$ must be located in the strict left half of the complex plane for all $q \in Q$.

There are many results for robust stability analysis of

systems with parametric uncertainty for Q in a shape of box. Their choice depends mainly on the complexity of the structure of investigated polynomial (or system). Doubtless, the most famous tool is the Kharitonov theorem [8] which is suitable for investigation of robust stability of interval polynomials (with independent uncertainty structure). Moreover, several modifications and generalizations of classical Kharitonov theorem are also available in literature [1], [9]. Among other known tools it belong e.g. the edge theorem, the thirty-two edge theorem, the sixteen plant theorem, the mapping theorem, etc. [1]. Furthermore, it exists a graphical method which is applicable for wide range of robust stability analysis problems (from the simplest to the very complicated uncertainty structures, for various stability regions, etc.). This technique combines the value set concept with the zero exclusion condition [1], [10].

Robust stability analysis for systems affected by parametric uncertainty for the case of Q in a shape of ellipsoid is also relatively well developed and there are several methods available. The Soh-Barger-Dabke theorem [11], [1] represents analogical tool to Kharitonov theorem for spherical polynomial families. Furthermore, extensions are provided by the theorem of Barmish and Tempo [12], [1] based on the idea of the spectral set and the theorem of Biernacki, Hwang and Bhattacharyya [13], [1] which solves the robust stability for closed-loop system with affine linear uncertainty structure (e.g. a spherical plant family in feedback connection with a fixed controller).

Nevertheless, the very universal technique based on the value set concept and the zero exclusion condition, which is described in [1], is applicable also to the spherical polynomial families.

The value set at each frequency ω for a spherical polynomial family (2) supposed in the form:

$$\begin{aligned}
 p(s, q) &= p_0(s) + \sum_{i=0}^n q_i s^i \\
 p_0(s) &= p(s, q^0) = \sum_{i=0}^n a_i s^i \\
 \|q\|_{2,W} &\leq r \\
 \deg p(s) &\geq 1
 \end{aligned} \tag{14}$$

is given [1], [14] by an ellipse centered at nominal $p_0(j\omega)$, with major axis (in the real direction) having length:

$$R = 2r \left(\sum_{i \text{ even}} w_i^2 \omega^{2i} \right)^{1/2} \tag{15}$$

and with minor axis (in the imaginary direction) having length:

$$I = 2r \left(\sum_{i \text{ odd}} w_i^2 \omega^{2i} \right)^{1/2} \tag{16}$$

where W is a weighting matrix:

$$W = \text{diag} (w_1^2, w_2^2, \dots, w_n^2) \tag{17}$$

Moreover, for the special degenerate case of $\omega=0$, the value set is just the real interval:

$$p(j0, Q) = \langle a_0 - r, a_0 + r \rangle \tag{18}$$

The practical visualization of the ellipsoidal value sets can be conveniently performed by means of the Polynomial Toolbox 2.5 [6], [14], [5] by using the “spherplot” command.

Then, the zero exclusion condition can be applied for testing robust stability in the following way: The spherical polynomial family (2) with invariant degree and at least one stable member (e.g. nominal polynomial) is robustly stable if and only if the complex plane origin is excluded from the value set $p(j\omega, Q)$ at all frequencies $\omega \geq 0$, i.e. the spherical polynomial family is robustly stable if and only if:

$$0 \notin p(j\omega, Q) \quad \forall \omega \geq 0 \tag{19}$$

Generally, the detailed description, proofs and examples of the zero exclusion principle applications can be found in [1] or for instance in [7], [10].

V. ILLUSTRATIVE EXAMPLE

Suppose the spherical polynomial family defined by the uncertain polynomial:

$$\begin{aligned}
 p(s, q) &= (1 + q_4) s^4 + (3.5 + q_3) s^3 + (2.5 + q_2) s^2 + \dots \\
 &+ (1.5 + q_1) s + (0.5 + q_0)
 \end{aligned} \tag{20}$$

and by the uncertainty bounding set:

$$\begin{aligned}
 \|q\|_{2,W} &\leq 0.5 \\
 W &= \text{diag} (5, 4, 3, 2, 1)
 \end{aligned} \tag{21}$$

i.e.:

$$5q_0^2 + 4q_1^2 + 3q_2^2 + 2q_3^2 + q_4^2 \leq 0.5 \tag{22}$$

The polynomial (20) can be easily expressed in the form (14) as:

$$\begin{aligned}
 p(s, q) &= s^4 + 3.5s^3 + 2.5s^2 + 1.5s + 0.5 + \dots \\
 &+ q_4 s^4 + q_3 s^3 + q_2 s^2 + q_1 s + q_0
 \end{aligned} \tag{23}$$

The nominal polynomial is stable and so the family fulfills the condition of at least one stable member. The value sets for the range of frequencies from 0 to 3 with step 0.01 was obtained with the assistance of the Polynomial Toolbox 2.5

for Matlab and its routine “spherplot” [6], [14]. They are plotted in Fig. 2.

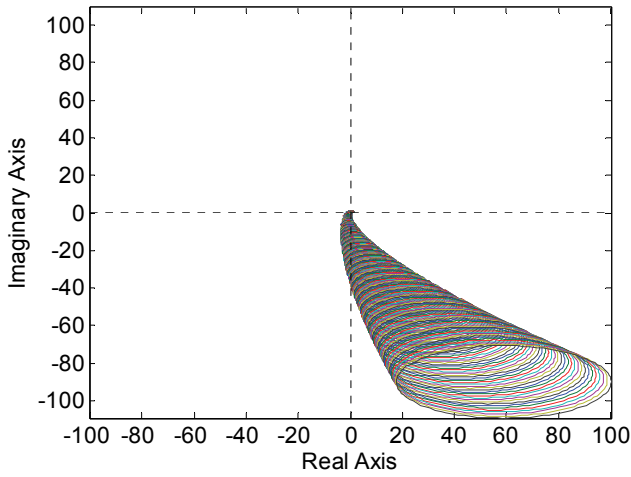


Fig. 2 The value sets for the family (20) + (21)

The zoomed version of the same value sets, visualized in Fig. 3, provides better view of the neighborhood of the complex plane origin.

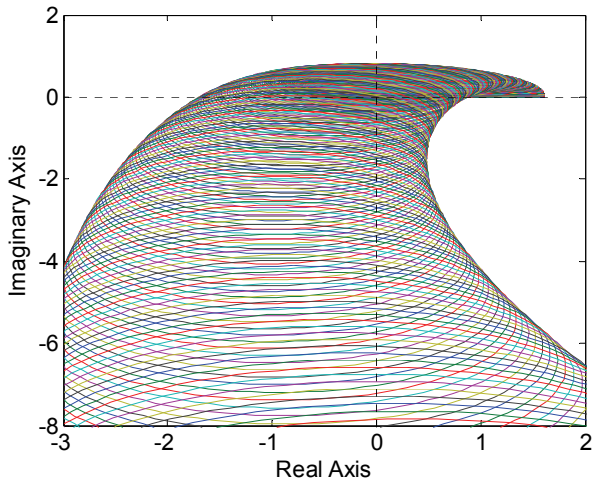


Fig. 3 The value sets for the family (20), (21) – detailed view near the point [0, 0j]

As can be observed the zero point is included in the value sets which means that the spherical polynomial family (20), (21) is not robustly stable. In other words, not all members of the prescribed family are stable.

The example of robustly stable case can be illustrated e.g. just by using the “narrower” uncertainty bounding set:

$$\|q\|_{2,W} \leq 0.1 \tag{24}$$

$$W = \text{diag}(5, 4, 3, 2, 1)$$

The full overview of the value sets for the same range of frequencies as in the previous plots can be seen in Fig. 4 and

the zoomed version in Fig. 5. Obviously, the family has a stable member and the value sets do not include the origin of the complex plane and consequently the family (20), (24) is robustly stable.

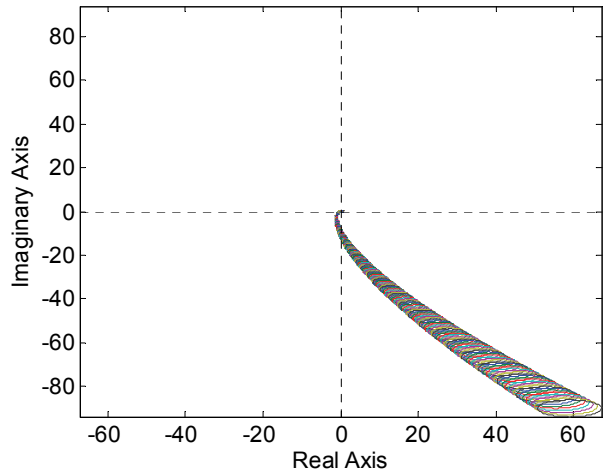


Fig. 4 The value sets for the family (20) + (24)

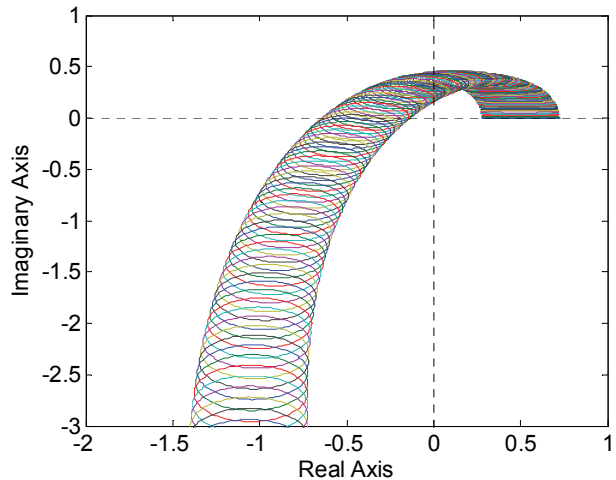


Fig. 5 The value sets for the family (20), (24) – detailed view near the point [0, 0j]

VI. CONCLUSION

The contribution has been aimed to an alternative bounding of uncertain parameters in systems with parametric uncertainty, i.e. the main object of interest has been the spherical polynomial family and its robust stability analysis. The basic theoretical descriptions have been accompanied by a simple illustrative example supported by the Polynomial Toolbox for Matlab.

REFERENCES

- [1] B. R. Barmish, *New Tools for Robustness of Linear Systems*, Macmillan, New York, USA, 1994.
- [2] A. Tesi, A. Vicino, F. Villoresi, “Robust Stability of Spherical Plants with Unstructured Uncertainty”, in *Proceedings of the American Control Conference*, Seattle, Washington, USA, 1995.

- [3] B. T. Polyak, P. S. Shcherbakov, "Random Spherical Uncertainty in Estimation and Robustness", in *Proceedings of the 39th IEEE Conference on Decision and Control*, Sydney, Australia, 2000.
- [4] J. Chen, S.-I. Niculescu, P. Fu, "Robust Stability of Quasi-Polynomials: Frequency-Sweeping Conditions and Vertex Tests", *IEEE Transactions on Automatic Control*, Vol. 53, No. 5, 2008, pp. 1219-1234.
- [5] Z. Hurák, M. Šebek, "New Tools for Spherical Uncertain Systems in Polynomial Toolbox for Matlab", in *Proceedings of the Technical Computing Prague 2000*, Prague, Czech Republic, 2000.
- [6] PolyX: The Polynomial Toolbox, [online], Available from URL: <http://www.polyx.com/>.
- [7] M. Šebek, Robustní řízení, PDF slides for course "Robust Control", ČVUT Prague, Available from URL: http://dce.felk.cvut.cz/ror/prednasky_sebek.html or http://www.polyx.com/_robust/. (In Czech).
- [8] V. L. Kharitonov, "Asymptotic stability of an equilibrium position of a family of systems of linear differential equations", *Differentsial'nye Uravneniya*, Vol. 14, 1978, pp. 2086-2088.
- [9] S. P. Bhattacharyya, H. Chapellat, L. H. Keel, *Robust control: The parametric approach*, Prentice Hall, Englewood Cliffs, New Jersey, USA, 1995.
- [10] R. Matuš, R. Prokop, "Graphical analysis of robust stability for systems with parametric uncertainty: an overview", *Transactions of the Institute of Measurement and Control*, Vol. 33, No. 2, 2011, pp. 274-290.
- [11] C. B. Soh, C. S. Berger, K. P. Dabke, "On the stability properties of polynomials with perturbed coefficients", *IEEE Transactions on Automatic Control*, Vol. 30, No. 10, 1985, pp. 1033-1036.
- [12] B. R. Barmish, R. Tempo, "On the spectral set for a family of polynomials", *IEEE Transactions on Automatic Control*, Vol. 36, No. 1, 1991, pp. 111-115.
- [13] R. M. Biernacki, H. Hwang, S. P. Bhattacharyya, "Robust stability with structured real parameter perturbations", *IEEE Transactions on Automatic Control*, Vol. 32, No. 6, 1987, pp. 495-506.
- [14] PolyX: The Polynomial Toolbox for Matlab – Upgrade Information for Version 2.5, 2001 Available from URL: <http://www.polyx.com/download/OnLineUpgradeInfo25.pdf.gz>.

Radek Matuš was born in Zlín, Czech Republic in 1978. He is a Researcher at Faculty of Applied Informatics of Tomas Bata University in Zlín, Czech Republic. He graduated from Faculty of Technology of the same university with an MSc in Automation and Control Engineering in 2002 and he received a PhD in Technical Cybernetics from Faculty of Applied Informatics in 2007. He worked as a Lecturer from 2004 to 2006. The main fields of his professional interest include robust systems and application of algebraic methods to control design.

Mathematical description of magnesium oxide extraction from chrome-tanned leather waste

Michaela Bařinová and Karel Kolomazník

Abstract—The contribution deals with the problems of optimization of the extraction of magnesium oxide (MgO) from chromium cake obtained by the filtration after alkaline hydrolysis of chromium shavings. The shavings represent potentially hazardous waste the processing of which is desirable not only from the economic, but particularly from the environmental point of view. After alkaline hydrolysis, it is necessary to subsequently remove some of the input chemicals to obtain products with the required properties. The most important compound from this aspect is magnesium oxide. The most perspective method so far – extraction with diluted sulfuric acid – does not lead to total removal of MgO from the chromium cake. We have studied in detail the conditions that could affect this technological procedure. The mechanism of the MgO extraction was studied through potentiometric titration and the kinetics data of the reaction of MgO with sulfuric acid within the given range of pH were obtained. Based on the experimental data, a mathematical model was proposed describing the extraction of MgO from chromium cake.

Keywords—Alkaline hydrolysis, chrome-tanned leather waste, magnesium oxide, mathematical modeling, optimization.

I. INTRODUCTION

CONVERSION of raw hides into leather is a complex procedure that involves a series of operations (soaking, liming, tanning, etc.) connected with addition of components necessary for the appropriate technological performance (technological water, electric power, chemicals). The entire manufacturing process leads to the production of large quantities of waste. Generally, waste generated by leather industry can be divided as non-tanned, generated before the tanning takes place, and tanned, generated during further processing of hides after tanning. Typical and far most abundant representative of the latter are chromium shavings, generated during shaving, an operation carried out to level out the thickness of the skin and to bring the material to a precise figure. Approximately 80% of global leather production is

The work was supported by the European Regional Development Fund under the project CEBIA-Tech No. CZ.1.05/2.1.00/03.0089., and the project No. CZ.1.07/2.3.00/30.0035.

Michaela Barinova is with the Faculty of Applied Informatics, Tomas Bata University in Zlín, nám. T. G. Masaryka 5555, 760 01 Zlín, Czech Republic (phone: +420 57-603-5275, fax: +420 57-603-2716, e-mail: barinova@fai.utb.cz).

Karel Kolomaznik is with the Faculty of Applied Informatics, Tomas Bata University in Zlín, nám. T. G. Masaryka 5555, 760 01 Zlín, Czech Republic (e-mail: kolomaznik@fai.utb.cz).

tanned with salts of trivalent chromium (Cr III). Chromium III itself is not toxic, but acid rains and other extrinsic conditions may lead to its oxidation into hexavalent form (Cr VI) [1], the compounds of which are highly toxic and reported carcinogens [2]. Therefore chrome-tanned waste is classified as hazardous and its disposal in landfills is disputable not only from environmental, but mainly from health protection point of view.

There are various possibilities of environmentally favorable ways of dealing with chrome-tanned wastes, but relatively few have been transferred into industrial practice. The most successful technologies so far are based on two-step alkaline-enzymatic hydrolysis, which is beneficial from both economic and environmental point of view [3]. The procedure gives quality products that can be further processed for applications in various industries. To achieve the required quality it is crucial to remove some of the chemicals used during hydrolysis, particularly magnesium oxide (MgO), which acts as promoter of the alkaline part of two-step alkaline-enzymatic hydrolysis.

So far, the most efficient methods of MgO removal are based on extraction with diluted sulfuric acid (H_2SO_4) (for example [4]). The efficiency of the operation ranges from 80 to 90 %. The fact that the extraction is not complete implies either formation of undesirable intermediate products, or/and the effect of other mechanisms such as transport phenomena.

Our contribution deals with preparation of chromium filtration cake by alkaline-enzymatic hydrolysis and subsequent kinetic measurements of MgO extraction with diluted H_2SO_4 to determine the reaction mechanism and conditions and propose suitable mathematical model for optimization of the process.

II. KINETICS OF THE REACTION OF MAGNESIUM OXIDE WITH SULFURIC ACID

Let us assume that the reaction of MgO with H_2SO_4 follows kinetic principles according to the mathematical model presented below. To determinate the velocity constants, we monitored the time during which the pH of the reaction mixture raised from the value of 4.5 to 5 after addition of sulfuric acid (see “Experimental”). Should the reaction actually run in accordance with kinetic principle, the velocity constants in all measurements will not significantly differ from each other. General equation is as follows:

$$\frac{dc}{d\tau} = k(c_0 - c) \quad (1)$$

Since we monitored not the change in concentration, but pH, (1) was adapted to:

$$\frac{dpH}{d\tau} = k[pH_R - pH(\tau)] \quad (2)$$

$$\int_{pH1}^{pH2} \frac{dpH}{pH_R - pH(\tau)} = \int_0^{\tau} k \cdot d\tau \quad (3)$$

After processing and integration of (3) we get:

$$k = \frac{\ln \frac{pH_R - pH1}{pH_R - pH2}}{\tau} \quad (4)$$

Where k stands for the velocity constant [s^{-1}], pH_R is the equilibrium pH (see "Experimental"), $pH1$ is the initial pH of 4.5, $pH2$ is the end pH of 5 and τ stands for time [s].

III. EXPERIMENTAL

The experiments comprised the following steps:

- 1) Preparation of the chromium cake via alkaline-enzymatic hydrolysis.
- 2) Potentiometric titrations of individual components of chromium cake with special focus on the titration curve of MgO, MgCO₃, and MgO in mixture with Cr₂O₃, respectively.
- 3) Measurement of the kinetics of MgO extraction from the chromium cake.

Preparation of the chromium cake

Input material

3 kg of chrome-tanned shavings

17 liters of water

90 g MgO

220 g Na₂CO₃ (added to adjust pH)

100 ml of alcalase (1 %)

3 kg of chrome-tanned shavings and 17 liters of waster were added into laboratory reactor (designed on a washing machine principle) equipped with thermostat. 90 g MgO (prepared by mashing in a small amount of water) and 60 g Na₂CO₃ were added into the reaction mixture. pH before heating was around 11. The mixture was subsequently heated to 70 °C. Due to constant reduction of pH during heating, the pH was adjusted by repeated adding of Na₂CO₃, 160 g in total. After that, the pH remained at the required value of 9-10 and the enzyme (100 ml of 1 % alcalase) could be added. The reaction was terminated after 6 hours from the start of the experiment. The content of the reactor was filtered through dense cloth. The total weight of filtration cake (chromium sludge) was 7 013 g and of filtrate (protein hydrolysate) 10 300 ml.

The results of analyses of the input chrome-tanned

shavings, as well as of the output chromium sludge and protein hydrolysate, are given in the following Table I:

Table I Analyses of chromium the input shavings and the obtained filtrate and filter cake, respectively.

	Chromium shavings	Filtrate (protein hydrolysate)	Filter cake (chromium sludge)
Dry matter	85.80 %	14.00 %	18.42 %
Ash*	9.58 %	5.01 %	26.83 %
Nitrogen*	14.04 %	13.98 %	10.63 %
Chromium*	2.85 %	23 ppm	4.88 %
MgO*	-	1 900 ppm	4.02 %

*related to the dry matter

All the per cent data mean w/w

Determination of titration curves

The titrations were carried out with the standard solution of 0.1N H₂SO₄, on titration apparatus with a 25 ml burette. The reaction blend was stirred with magnetic stirrer. pH of the solution was measured with Portable pH meter CPH 52 equipped with a measuring probe.

The kinetics of MgO extraction from the chromium cake

500 ml of a H₂SO₄ solution of pH 4.5 was placed in a beaker and 100 g of the filtration cake obtained in the previous experiment was added. The mixture was stirred intensively during the whole experiment. After stabilization of pH, additional H₂SO₄ was added to reduce the pH to the original level of 4.5. The time during which the pH raised from 4.5 to 5 was recorded, as well as the amount of H₂SO₄ necessary to reduce the pH to the value of 4.5.

After the addition of filtration cake (i.e. after the first pH stabilization) the pH of the mixture raised to 9.1. This pH will be referred to as the equilibrium pH_R in further calculations.

IV. RESULTS

The example of a titration curve of MgO titrated with 0.1N H₂SO₄ standard solution is shown in Fig. 1.

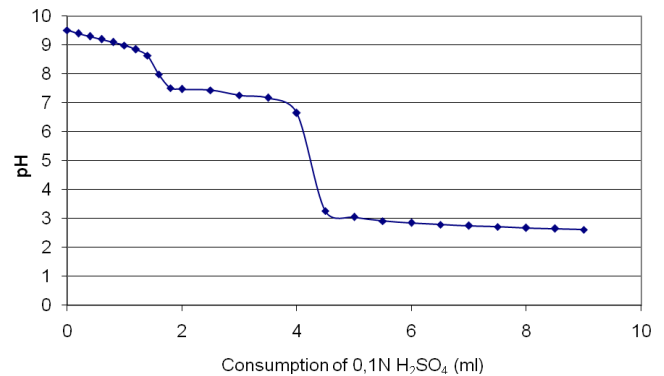


Fig. 1 Titration of MgO with 0.1N H₂SO₄.

The example of a titration curve of MgCO₃ titrated with 0.1N H₂SO₄ standard solution is shown in Fig. 2.

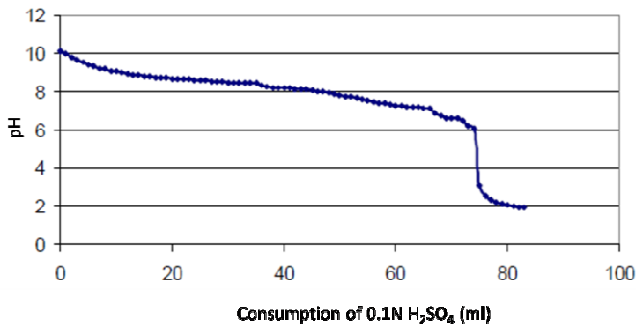


Fig. 2 Titration of MgCO₃ with 0.1N H₂SO₄.

The example of a titration curve of a mixture of MgO and Cr₂O₃ titrated with 0.1N H₂SO₄ standard solution is shown in Fig. 3.

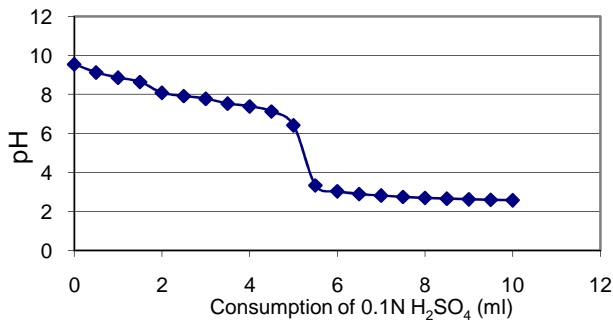


Fig. 3 Titration of MgO + Cr₂O₃ with 0.1N H₂SO₄.

The results of the kinetics of the extraction of MgO from the chromium cake with 0.1N H₂SO₄ are shown in the following Table II.

Table II Results of the kinetic measurement of the extraction of MgO with 0.1N H₂SO₄, as well as the velocity constants of the reaction of MgO with H₂SO₄ calculated according to (4).

Measr. No.	Consumption of 0.1N H ₂ SO ₄ [ml]	Time τ [s]	Velocity constant [s ⁻¹]
1	44.6	53	2.2·10 ⁻³
2	50.6	184	6.4·10 ⁻⁴
3	54.1	531	2.2·10 ⁻⁴
4	56.8	1982	5.9·10 ⁻⁵
5	59.0	10080	1.2·10 ⁻⁵

It is apparent from Table II that the velocity constants differ within two orders of magnitude. Together with the courses of titration of MgO and MgCO₃ (both reactions ran very slowly

and it took a long time for the pH after addition of H₂SO₄ to stabilize), the results imply that the reaction does not follow the kinetic model presented in Chapter II. Therefore it was necessary to search for mechanisms that could possibly affect the reaction to propose more accurate mathematical description. The most probable phenomenon is diffusion.

To verify whether diffusion can actually take place, we used the Nernst equation [5]:

$$D_0 = 8.931 \cdot 10^{-10} T \left(\frac{l_+^0 \cdot l_-^0}{l_+^0 + l_-^0} \right) \left(\frac{z_+ + z_-}{z_+ \cdot z_-} \right) \quad (5)$$

Where D_0 stands for diffusion coefficient of electrolyte at infinite dilution [cm³·s⁻¹], l_+^0 is cationic conductivity at infinite dilution [mhos/equivalent], l_-^0 is anionic conductivity at infinite dilution [mhos/equivalent], T is absolute temperature, z_+ is the valence of cation and z_- stands for the valence of anion.

By incorporation the table values for sulfuric acid [6] into (5) we get:

$$D_{0H_2SO_4} = 8.931 \cdot 10^{-10} \cdot 293 \left(\frac{349.8 \cdot 80.0}{349.8 + 80.0} \right) \left(\frac{2+1}{2 \cdot 1} \right) = 2.55 \cdot 10^{-9} m^2 s^{-1} \quad (6)$$

Now we need to find out the particle size at which diffusion of sulfuric acid takes place and to compare it with the approximate size of particles used in the experiments. We used Fourier equation [7] (the value of τ was taken from Table II, Measurement No.4, i.e. 1982 s):

$$Fo = \frac{D \cdot \tau}{a^2} \quad (7)$$

Where Fo stands for dimensionless time, D is the diffusion coefficient of a substance [cm³·s⁻¹], a is the size of the particle [m] and τ stands for time [s].

The calculated size of the particle was 2.26·10⁻³ m.

In real conditions, the size of the particles is usually by two orders of magnitude smaller (i.e. around 10⁻² mm), which according to [7] can be applied to our case.

V. MATHEMATICAL MODEL OF MAGNESIUM OXIDE EXTRACTION FROM CHROMIUM CAKE WITH SULFURIC ACID

According to the results described above it is highly probable that the extraction of MgO from filtration cake with H₂SO₄ is affected by diffusion. The diffusion for a spherical particle can be described according to [8]:

$$\frac{1}{D} \frac{\partial c(r, \tau)}{\partial \tau} = \frac{\partial^2 c(r, \tau)}{\partial r^2} + \frac{2}{r} \frac{\partial c(r, \tau)}{\partial r} \quad 0 < r < a, \tau < 0 \quad (8),$$

with the following initial and boundary conditions:

$$\frac{\partial c}{\partial r}(0, \tau) = 0 \quad (8a)$$

$$-SD \frac{\partial c}{\partial r}(a, \tau) = V_0 \frac{\partial c_0}{\partial \tau}(\tau) \quad (8b)$$

$$c(r, 0) = c_p \quad (8c)$$

$$c(a, \tau) = \varepsilon c_0(\tau) \quad (8d)$$

$$c_0(0) = 0 \quad (8e)$$

The following dimensionless quantities were introduced for further processing:

$$C = \frac{c}{c_p}; R = \frac{r}{a}; Fo = \frac{D \cdot \tau}{a^2}; C_0 = \frac{c_0}{c_p} \quad (9),$$

where Fo stands for dimensionless time (Fourier number), C is dimensionless concentration of the extracted component in the solid phase, C_0 is dimensionless concentration of the extracted component in the solution and R stands for dimensionless size of a spherical particle.

Through incorporation of the above stated dimensionless quantities in (8) we get the diffusion model in dimensionless form:

$$\frac{\partial C(R, Fo)}{\partial Fo} = \frac{\partial^2 C(R, Fo)}{\partial R^2} + \frac{2\partial C(R, Fo)}{R\partial R} \quad (10)$$

$$\frac{\partial C(0, Fo)}{\partial R} = 0 \quad (10a)$$

$$-\frac{\partial C(1, Fo)}{\partial R} = \frac{Na}{3\varepsilon} \cdot \frac{\partial C_0(Fo)}{\partial Fo} \quad (10b)$$

$$C(R, 0) = 1 \quad (10c)$$

$$C(1, Fo) = C_0(Fo) \quad (10d)$$

$$C_0(0) = 0 \quad (10e)$$

Analytical solution of (10-10b) was published in [9] for temperature field of a spherical body. After adjustment of the solution for concentration field of a spherical particle we get for the dimensionless concentration of the extracted component in the solid phase:

$$C = \frac{c}{c_p} = \frac{\varepsilon}{Na + \varepsilon} - \frac{2Na}{3\varepsilon R} \sum_{n=1}^{\infty} \frac{\left[\frac{Na^2}{\varepsilon^2} q_n^4 + 3 \left(2 \frac{Na}{\varepsilon} + 3 \right) q_n^2 + 9 \right] \sin(R \cdot q_n) \sin(q_n) \cdot e^{-Fo \cdot q_n^2}}{\frac{Na^2}{\varepsilon^2} q_n^4 + 9 \left(\frac{Na}{\varepsilon} + 1 \right) q_n^2} \quad (11),$$

where ε stands for porosity [dimensionless] and Na stands for dimensionless ratio of the volume of extraction solution to the volume of solid phase (V_0/V) (so-called soaking number).

Analogously, the dimensionless concentration field of the extracted component in the solution is given by (12):

$$C_0 = \frac{c_0}{c_p} = \frac{1}{Na + \varepsilon} - \frac{6Na}{\varepsilon} \sum_{n=1}^{\infty} \frac{e^{-Fo \cdot q_n^2}}{\frac{Na^2}{\varepsilon^2} q_n^2 + 9 \left(\frac{Na}{\varepsilon} + 1 \right)} \quad (12),$$

where q_n represent the roots of the following equation:

$$tg(g) = \frac{3q}{3 + \frac{Na}{\varepsilon} q^2} = 0 \quad (13)$$

VI. DISCUSSION

The extraction of magnesium oxide, MgO, from chromium sludge (chromium cake) was studied. The sludge was prepared by alkaline enzymatic hydrolysis, with MgO as promoter of the reaction. This compound has to be removed after the process to achieve the maximum quality of hydrolysis products. It emerges from few publications dealing with this problem (e.g. [4]), that the attempts to remove MgO from chromium cake were not completely successful. The most suitable method so far seems to be MgO extraction by diluted sulfuric acid, but the efficiency of MgO removal was not 100 % either. The possible mechanisms that might affect the technological method are discussed below.

The titration graphs of individual components of chromium cake were made with the use of potentiometric titrations. The graphs show the equivalence points of the components reaction with H_2SO_4 . We particularly focused on MgO and Cr_2O_3 titrations, because during MgO extraction it is necessary at the same time to prevent Cr_2O_3 from reaction with the acid. It follows from the graph for MgO (Fig. 1) that there are either further reactions of the products (e.g. $MgSO_4$) with H_2SO_4 , or the commercial MgO may contain $MgCO_3$.

Therefore, more details studies were carried out on the reactions of $MgCO_3$ and $MgSO_4$ with sulfuric acid. The balance calculations confirmed the possible participation of both compounds in the reaction, with prevalence of the reaction of $MgSO_4$ to $Mg(HSO_4)_2$. The occurrence of $MgCO_3$ cannot be excluded neither according to the balance calculations, nor to graphs.

One of possible explanations is that it coats the protein molecules and causes diffusion phenomena, particularly the

inner diffusion. The diffusion is signalized by:

- Calculation of diffusion coefficient for sulfuric acid, which shows that the real size of molecules in chrome cake would allow diffusion process.
- Calculation of the velocity constant for the reaction of MgO and H₂SO₄ in the given range of pH.

The kinetics of the reaction shows that the velocity constants differ significantly, which means that the reaction does not run in accordance with kinetics principles. Therefore, the mathematical model was selected for the situation when MgO extraction is hindered by the inner diffusion of H₂SO₄ into particles. The results can contribute to more efficient processing of chromium shavings. Suitability of this model for MgO extraction from chrome cake will be verified by further research.

REFERENCES

- [1] K. Kolomaznik, M. Adamek, and M. Uhlířová, "Potential danger of chromium tanned waste," in *Proceedings of the 5th IASME/WSEAS International Conference on Heat Transfer, Thermal Engineering and Environment*. Athens, 2007, pp. 137-141.
- [2] O. Kirk, *Encyclopedia of Chemical Technology*, 4th ed., John Wiley & Sons Inc., New York, 1992.
- [3] K. Kolomaznik, M. Mladek, F. Langmaier, D. Janacova, and M. M. Taylor, "Experience in industrial practice of enzymatic dechromation of chrome shavings," *JALCA*, vol. 94, no. 2, pp. 55-63, 1999.
- [4] P. Mokrejs, D. Janacova, K. Kolomaznik, M. Mladek, and F. Langmaier, "Bath washing of MgO from the chrome sludge using diluted sulfuric acid," in *Proceedings of CHISA 2006, 17 International Congress of Chemical and Process Engineering*, Prague, 2006, p. 454.
- [5] W. Nernst, "Zur Kinetik der in Lösung befindlichen Körper.-I. Theorie der Diffusion," *Zeitsch. f. Physik. Chem.*, vol. 2, pp. 613-637, 1888.
- [6] R. H. Perry and C. H. Chilton, *Chemical Engineer's Handbook*, 5th ed., McGraw-Hill, New York, 1973. 2640 pp.
- [7] K. Kolomaznik, *Modeling of manufacturing processes* (Textbook style) [in Czech]. Brno University of Technology, Brno, Czech Republic, 1990.
- [8] S. Paterson, "The heating or cooling of a solid sphere in a well-stirred fluid," *Proc. Phys. Soc.*, vol. 59, pp. 50-58, 1947.
- [9] H. S. Carslaw and J. C. Jaeger, *Conduction of Heat in Solids*. 2nd ed. Clarendon Press, Oxford, UK, 1959.

The ITS components in the optimization and control of people and vehicles circulation at the Brazilian Ports

Vander S. de Abreu, Luiz N. Rossi and Eduardo M. Dias

Abstract— This paper presents the current status of the use of ITS components in the optimization and control of movement of persons and vehicles at the Brazilian Ports, explaining the main characteristics, technologies used and how these components are assisting in the automation of a control processes existing and designed in compliance with local laws.

Keywords— Access Control, Ports, Port Authority.

I. INTRODUCTION

WITH the substantial increase of imports and exports as a consequence of development of Brazilian foreign trade, the need for processes and technological innovations for automating the entry and the exit of people and vehicles into and from the Brazilian ports is more and more clear.

In this article we will discuss the main components of the ITS that are being used today to deal with this challenge and allow Brazil to tackle those needs and continue to increase the ability of import and export cargo. To this end, the improvement of existing infrastructure, primarily, a reduction of procedural bureaucracy with intelligent use of support systems for decision making processes is required.

II. BACKGROUND

Brazil is the largest country of South America with geographical surface area of 8.5 million km², is ranking behind Russia, Canada, China and the USA. It borders every country of the South American continent except Ecuador and Chile. Brazil's current population is estimated to be approximately 190 million, making it the fifth most populated country in the world ranking behind China, India, the United

V. S. de Abreu is Master in Science (Electrical Engineering and IT Management / Automation at the University of São Paulo EPU SP), MBA in Technology Management from the Catholic University of Santos. BS in Computer Science from the Catholic University of Santos. Certified ITIL, COBIT, Scrum Master and Scrum Product Owner. Acts as IT Manager of the Association of Bonded Terminals and precincts (vandersa@gmail.com).

L. N. Rossi is Prof. Dr. of the Escola Politécnica da Universidade de São Paulo (Polytechnic School of the University of São Paulo) (natale@usp.br)

E. M. Dias is full professor of the Escola Politécnica of the Universidade de São Paulo and coordinator of GAESI - Grupo de Automação Elétrica em Sistemas Industriais, a research group of the Electrical Energy and Automation Department, Escola Politécnica, Universidade de São Paulo, Av. Prof. Luciano Gualberto, trav. 3, n. 158, São Paulo/SP, Brazil, CEP 05508-970 (emdias@pea.usp.br).

States and Indonesia [1]. Brazil's population has increased steadily at a rate of 1.2% per year since 2004 and is forecasted to continue to grow over the years 2013 and 2014 to reach level of approximately 205 million in 2013. The 1988 constitution grants broad powers to the federal government, made up of executive, legislative, and judicial branches, because the federal government is responsible for port operations, either directly or through delegation (authorization, concession or permission), legislation on ports is the exclusive responsibility of the federal government and port services may only be delegated through public bidding processes [12]. Brazil has 8.500 km of coastline for maritime ports and 44.000 km of potential navigable rivers as can be seen in Figure 1 [2].

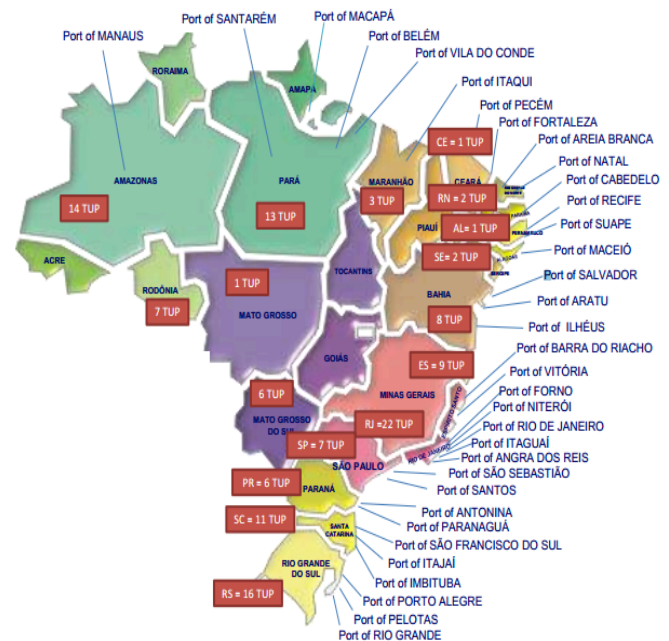


Fig. 1 Public ports in Brazil. Source: <http://www.portosdobrasil.gov.br/assuntos-1/sistema-portuario-nacional> - accessed on 26/03/2014.

III. ECONOMY AND LEGAL BACKGROUND

The global economy in recent years has been supported mainly by developing countries, eg. BRIC countries especially China and India. Brazil is an important player in this scenario, due to its territorial extension, population and market size.

Figure 2 shows that only Brazil, China, the United States and Russia have jointly greater than 4 thousand square kilometers, more than 100 million population and gross domestic product - GDP greater than four billion dollars.

	Business Environment	GDP	Business Environment	Logistic performance
	7 ^a	2,3	130 ^a	45 ^a
	9 ^a	1,8	112 ^a	95 ^a
	2 ^a	7,2	91 ^a	26 ^a
	1 ^a	15	4 ^a	9 ^a

Fig. 2 Positioning of Brazil against other countries.
Source: IBGE: PIB.

Ports are important instruments of economic and social development, requiring permanent measures to improve their logistics. With approximately 8,500 km of navigable coastline and its vast territory, Brazil needs to achieve integration of production, promote investment, create jobs and expand exports of goods and services. Thus, the strategic importance of the Port Sector should be recognized and entities involved in port activities should act to solve its most important problems, such as logistic bottlenecks.

Until the early 90's, the Brazilian Port sector was ruled by disparate and sparse legislation, and was subject to a centralized management system, which hindered the organization of the sector. In 1993, the Law No.8.630, known as the Port Law, was issued. Among other purposes, the document sought the decentralization of the Port management, the optimization of terminals and more efficient system of port-related fee rates.

The Law No. 8.630/1993 [3], however, was not enough to create a favorable environment for investments, and the sector was involved in intense judicial disputes. With the expansion of the Brazilian economy, new needs arose that were not met by the current legislation (actually, some players had a different opinion, believing that the mere regulation of the Law No. 8.630/1993 would be enough to fill the existing gaps). Thus, considering the need to eliminate bottlenecks in the Port sector, the Federal Government issued, late 2012, the Provisional Measure 595 (MP 595), revoking the Port Law and giving a new legal frame to the sector. The model introduced by the MP 595 is intended primarily for (i) the organization of the institutional arrangement of the Brazilian Port sector, with the modernization of terminals and, consequently, the reduction of logistics costs and the increase of the competitive conditions of the country, and (ii) the expansion of private investments in the sector.

The MP 595 was the object of intense discussions in the Brazilian Congress, given the competing interests at stake. In the House of Representatives, more than 600 amendments to the text of the MP 595 were presented.

According to the Brazilian Constitution, a provisional measure can be issued by the President of Brazil, and is valid for 60 days, a period that may be extended for an equal period.

It was just a few hours before the MP 595 would lose its validity that its text was approved by the Senate. On June 5, 2013, after President Dilma Rousseff had vetoed some points of the text approved by the Congress, a new Law of Ports – Law No.12.815/2013 – was approved, setting forth a new regulatory framework for the sector. On June 28, 2013, Decree No. 8033/2013 was issued with the purpose of regulating the Law No. 12.815/2013.

The ports perform costly complex and logistical operations involving millions of dollars. All this size and complexity create an enormous challenge for the optimization of existing infrastructure, besides the risk that needs to be mitigated due to increasing worldwide importance of Brazil on the eve of large events like FIFA World Cup (2014) and Olympics Games (2016). The ITS components represent the most effective solution for achieving those aims.

Table 1 below demonstrates, the Brazilian trade balance which grown 38% in 6 years. Some studies suggest that by 2024 the Brazilian ports will triple their current performance and thus the movement of people and vehicles in these areas will also be greatly expanded [4].

Table 1 - Brazilian Trade Balance.

YEAR	2008	2010	2011	2012	2013
EXPORT	US\$197,9 billions	US\$201,9 billions	US\$256,1 billions	US\$242,6 billions	US\$242,2 billions
IMPORT	US\$173,1 billions	US\$181,6 billions	US\$226,2 billions	US\$223,1 billions	US\$239,6 billions

Source: Alice System (MDIC).

IV. ACCESS CONTROL

Since majority of Brazilian ports were planned and built to meet the needs of the time, they did not had proper a spatial planning, and are currently located within large cities, making their areas difficult to access and causing the vehicles heading to the port to blend with the day+to+day traffic in the city and increasing further challenge for security in those areas.

The great spatial extent of most of ports also increase difficulties in controlling different port activities (storage, spawning, transport, etc.) and a large number of people and vehicles accessing the port facilities daily due to different purposes.

Nowadays, people and vehicles accessing the customs areas are controlled by different access control systems, working separately and do not respond to any control policy. Such situation makes it almost impossible to estimate quantity of both people and vehicles accessing the area, as well as the flow of the movement. However this information is essential for proper planning of the infrastructure, and provision of the necessary data for control and employment. Some initiatives are beginning to address these problems, as can be seen in section 5 "ITS Systems and Used Components" of the present article.

V. ITS SYSTEMS AND USED COMPONENTS

The Dock Company in Brazil is a mixed capital company, which is responsible for the certification process of the Brazilian Ports in the ISPS-Code. The project was initiated with the development of a the System of Public Port Security (Sistema de Segurança Público Portuária SSPP) [5] [6] which aims to provide port authorities with the automated control of access of individuals and vehicles passing through the port areas, more specifically, the public gates controlled by the Dock Company. Accesses to the port areas under their jurisdiction is allowed upon submission of an electronic badge, using RFID technology standardized by ISO/IEC 14443 and named MIFARE (trademark NXP - Philips). The gates of access to areas were refurbished and new equipment identification were installed with the following technologies:

- Readers - with equipment to read MIFARE cards so that the data of individuals or vehicles that are accessing the port area are recorded and checked electronically to prevent unauthorized access;
- Biometric equipment for identifications and verification of individuals depending on the chosen form of biometric technology (thumb, face, image, veins, etc.)
- Cameras for remote monitoring and recording of activities undertaken in the input and output ports of customs terminals (gates) streamlining the application processes for emergency personnel if necessary.

Due to limited scope, since it controls only the port authority gates that provide access to public and private zone, and some flaws in the process of using the system, since the SSPP reads only the ID badge. Service, specifically the Federal Revenue Customs of Port of Santos, began connect terminals and bonded to improve the control of all customs areas under their jurisdiction. Thus, a new project called The Database Joint Accreditation (*Banco de Dados Comum de Credenciamento BDCC*) [7] was developed with the similar goal, however being much more comprehensive.

The BDCC is a system developed by the Brazilian Association of Terminals and Customs (*Associação Brasileira de Terminais e Recintos Alfandegados ABTRA*) [8], under the guidance of teams of Customs Revenue Service of Brazil's Port of Santos, to establish an centralized data environment to confirm the identification of people and vehicles and for issuing electronic identification badge approved to be read in all locations and bonded warehouses of the Port of Santos and region. The BDCC was built in compliance with Ordinance No. 200 [9] Customs of the Internal Revenue Service of the Port of Santos, dated April 13, 2011. After the September 11 terrorist attacks in the U.S., the International Ship and Port Facility Security (ISPS) Code was created, establishing new security measures to be adopted by ships and port facilities to prevent terrorist activity. The ISPS Code classified all international ports according to predefined security levels, which the Brazilian government and other signatories undertook to implement by July 1, 2004.

The main concern was to prevent the access of unauthorized personnel to port facilities as well as passenger and cargo ships, and the transportation of weapons and objects that could be used for terrorist activity and sabotaging ships and port facilities. The ISPS Code establishes an international security structure and defines the roles and responsibilities of the signatory governments, government bodies, local administrations, ports, port terminals and shipping companies to ensure international maritime security. It also ensures the efficient exchange of security-related information, and also envisages a methodology for evaluating the safety targets and implementing the adequate safety measures [11] [13].

The main difference between the BDCC system of ABTRA on normative call and the RFB for the SSPP system of the Port Authority, is that the SSPP was created to meet the standards of the ISPS Code and then control vessels and primary zones Port Security (border areas) and the BDCC control all gates from various bonded sites, whether or not the border, as is the case of customs facilities for secondary zone, i.e. without access to the sea, and the dispatch terminal for export - REDEX. Furthermore, a the BDCC system is 100% digitally certified, and its only possible access to companies and individuals who hold the digital certificate be it legal or physical person.

VI. ADVANTAGES OF USING NEW SYSTEMS AND COMPONENTS OF ITS

The new ITS systems and components that are being used at the Port of Santos are helping to increase security, and facilitate the implementation of the defendants systems primarily of Federal Revenue through their ordinances and Brazil's Laws due to increase knowledge about the use of existing infrastructure. Companies that are already integrated into the BDCC to get pre - authorization from the RFB through the MIFARE cards, released by the office controlling access of individuals and vehicles entering and leaving the area without the need to submit any other documentation to the system. The only requirement is to register with the access control system of the company providing reason why person or vehicle has to enter the area.

Aiming to continue this process and maintain continuity of investment by tenants companies of the bonded terminals, the (Secretaria da Receita Federal do Brasil SRFB published in late 2011 Ordinance 3518 which requires that all companies, which remain bonded, have automated the processes to record entry truck and cargo [10].

The publication of ordinances 228, 229 and 230 by the Federal Revenue Office (FRO). They approve and publish a new port security, control and surveillance model at the Port of Santos, Latin America's largest. The instruments determine that all customs precincts must deliver at the customs headquarters building, located at the Santos (SP) Historical Center, real time images from their CCTV (closed-circuit television), OCR (Optical Character Recognition) and precision scanners. All of

them have to provide a data communication link, computer and video monitor for local supervision by part of Customs agents. The ordinances will come into effect in January 2014. In light of this, the terminals have autonomously begun to follow the norms, individually delivering their systems at the set locality. This has given rise to a new operational demand. What would ease the actions by part of federal agents, has actually presented a model that could compromise their activities. In the same room, there would be several systems running software's, computers and different screens, affecting the verification, control and speed of information. To solve such scenario, the Port of Santos Customs Operations and Surveillance Center (COV) was established, bringing together, in its initial phase, 20 customs precincts by means of integrated technology, where it is possible through a unique system, access more than 3,000 images from various centralized bonded terminals under the jurisdiction of a certain custom house.

VII. CONCLUSIONS

As shown in this article, the quantity of individuals and vehicles that travel daily through the port of Santos presents an immense challenge for management and therefore control of inputs and outputs could be made only through a technological process of electronic badges identification.

The ITS components and systems presented herein are part of the group of technologies that began to be employed at the Brazilian ports, and has proved to be very efficient in control and optimization of existing infrastructure.

Certainly the world was and never will be the same after the emergence of computers and after the revolution caused by the Internet. In today's globalized world, the Internet provides an important service, helping to further streamline this process of globalization.

Organizations, accustomed to this increasingly digital reality, come to depend on it for vital form. The information shall be considered an asset of enterprises, equity.

In this view, we realize how important and indispensable to Information Security for a company. The protection of your data at any cost lest great harm is a current topic. Following this trend, technologies that promise high level of security and protection arise, organizations and every day more and more become aware of the importance and need to protect their data.

In the case of local and then bonded warehouses, we can not forget they are areas of border control systems need to be regularly expanded and arrived continuously. To support organizations and professionals in the task of implementation of Information Security, the Standard ISO / IEC 27002:2005 as well as ISO 28000:2012 are shown as an important tool.

Through them, you can apply all controls relating to physical security thereby promoting desired protection. Such controls mentioned herein may carry a high investment cost initially, but considering the large losses that could be obtained with the absence of security, the investment is

justified.

As demonstrated in this dissertation, the sheer volume of people and vehicles that travel daily through the port of Santos represent an immeasurable challenge of management and control and therefore control of these inputs and outputs could be made only through a technological process of identification through Sourcing buttons. Systems and components presented here are part of the group of technologies that began to be employed at the Port of Santos, and that has proven very efficient in optimization and control of existing infrastructure. New projects begin to be realized in the Port of Santos using ITS components with different approaches such as identifying vehicle plates using OCR, cargo tracking using electronic seal, scanning cargo for purposes of supervision and control, etc. They all represent a new milestone in Brazilian logistics chain adding technology already used in many parts of the world, and allows increased productivity and mitigate increasingly larger and more difficult to detect risks in order to ensure that we have an increasingly Brazilian export growth safely, effectively and efficiently.

Finally, as presented, are many controls in the Port of Santos. And do not forget that there are not only the access of people and vehicles controls, there are also the control of cargo, whether containerized in liquid and solid bulk, vehicles or loose loads. So the lives of consenting bodies in monitoring these various processes and systems is quite complex.

Thinking about it, is the creation of a Single Window Port target presentation and my PhD project - JUP, this purely operational window, ready to be integrated with the port system without Role of the Federal Government. The model of this window follows the same pattern implemented in the ports of Hamburg in Germany, Rotterdam in Holland and Le Havre in France.

The JUP is nothing more than a system that focus the integration with all systems not only control access and control loads. Through a single portal you can access to all systems of enclosures and bonded local and government systems.

The project is divided into two phases. The first will be implemented exclusively in VOC through the PIX. The second phase can be accessed via the World Wide Web (Internet) of any computer as long as recorded via digital e- CPF accreditation and to replace the need to enter the various systems of government and enclosures and bonded locations to obtain information on compliance with the standards.

The new systems that are currently used in the Port of Santos are contributing to that security be increased, besides enabling the implementation of public policies, due to the fact of increasing knowledge about the use of existing infrastructure.

New projects are representing different approaches in use of ITS components at the Port of Santos such as: identification of vehicle license plates using OCR, cargo tracking using electronic seals, cargo scanning for surveillance and control, etc.

They all represent a new milestone in Brazilian logistics chain using technologies already used in various parts of the

world, and enable increase of productivity and mitigation of risks which ensures support for safety, efficiency and effectiveness of Brazilian ports.

REFERENCES

- [1] The world population and the top ten countries with the highest population. Available at: <http://www.internetworldstats.com/stats8.htm> (accessed 28.04.2014).
- [2] Secretariat of Ports (SEP) (material in Portuguese). Available at: <http://www.portosdobrasil.gov.br/assuntos-1/sistema-portuario-nacional> Accessed on May 20, 2014
- [3] BRAZIL. Presidency of the Republic. Civil House. Subchefia for Legal Affairs. Federal Law Port Modernization (Law No. 8630 of 25 February 1993) (material in Portuguese). Available at: http://www.planalto.gov.br/ccivil_03/LEIS/l8630.htm - published in [D.O.U. of 02.26.1993](#) Accessed on May 20, 2014
- [4] CODESP. Annual Report 2013 (material in Portuguese). Available at: <http://201.33.127.41/down/relatorio/Relatorio2013.pdf> Accessed at
- [5] Santos CONPORTOS certify as safe haven (material in Portuguese). Available at: <http://www.portodesantos.com.br/pressRelease.php?idRelease=470http://translate.google.com/translate?hl=pt-BR&prev=t&sl=pt&tl=en&u=> Accessed on May 20, 2014
- [6] Port Public Security System (SSPP) (material in Portuguese). Available at: http://www.portodesantos.com.br/isps_code.php Accessed on May 20, 2014
- [7] Database Joint Accreditation (BDCC). Available at: <http://www.bdcc.org.br> Accessed on May 20, 2014
- [8] Associação Brasileira de Terminais e Recintos Alfandegados (ABTRA) (material in Portuguese). Available at: <http://www.abtra.com.br/http://translate.google.com/translate?hl=pt-BR&prev=t&sl=pt&tl=en&u=http://www.abtra.com.br/> Accessed on May 20, 2014
- [9] Ordinance ALF / STS, 2011 n.200 (material in Portuguese). Available at: http://www.bdcc.org.br/bdccweb/faces/apresentacao_e_minuta_portaria.zip Accessed on May 20, 2014
- [10] Ordinance No SRF 3.518 2011 (material in Portuguese). Available at: <http://www.receita.fazenda.gov.br/legislacao/Portarias/2010/portrfb35182011.htm> Accessed on May 20, 2014
- [11] MORINI, C. – Logística internacional segura: Operador Econômico Autorizado (OEA) e a gestão de fronteiras no Século XXI, Atlas, 2011
- [12] RUSSO FILHO, A. - Comércio internacional, um modelo para segurança portuária e modernização da Aduana brasileira. 2006. 122 f. Dissertação (mestrado). Escola Politécnica. Universidade de São Paulo. São Paulo. 2006.
- [13] FONTANA, C. F. – Modelo de Automação de um sistema de Controle de Carga para a Aduana nos Portos Brasileiros; 2004. 129 p. Dissertação (Mestrado). Escola Politécnica. Universidade de São Paulo. São Paulo. 2005.

Computer application for determination of optimal economic costs of biomaterial waste treatment by enzymatic hydrolysis

H. Charvátová, D. Janáčková, V. Vašek, and K. Kolomazník

Abstract—The paper deals with the economic aspects of the enzymatic hydrolysis of tannery solid waste. It describes the software application created using Maple, which is focused on the calculation of operating costs in the processing of biomaterial waste to protein hydrolysates. The calculation is based on the solution of a mathematical model describing the dependence of the quantity of a protein hydrolysate on time of process. It is considered a diffusion mechanism of enzymatic hydrolysis. The application allows the user to compute cost functions for the required input conditions and can be used to determine the optimum process to the purpose of saving energy and raw materials.

Keywords—Biomaterial, cost curve determination, enzymatic hydrolysis, Maple, software application.

I. INTRODUCTION

PROCESSING of raw hides is a sequence of many operations, which produce a number of liquid and solid waste. As a result of using different chemicals may be those wastes often harmful. Therefore, it is necessary to find methods that lead to the minimization of waste and also find ways to remove unwanted substances from tanning waste for subsequent use [1], [2].

One of the possible methods of separation of undesirable substances from solid biomaterials is the use enzymatic hydrolysis [3]. To make this process economically feasible, it is necessary to minimize operating costs [4].

In the subsequent text will be described the calculation,

This work was supported by the European Regional Development Fund under the project CEBIA-Tech No. CZ.1.05/2.1.00/03.0089.

H. Charvátová, Tomas Bata University in Zlín, Faculty of Applied Informatics, Department of Automation and Control Engineering, nám. T. G. Masaryka 5555, 760 01 Zlín, Czech Republic; phone: +420 576 035 274; fax: +420 576 032 716; (e-mail: charvatova@fai.utb.cz)

D. Janáčková, Tomas Bata University in Zlín, Faculty of Applied Informatics, Department of Automation and Control Engineering, nám. T. G. Masaryka 5555, 760 01 Zlín, Czech Republic; phone: +420 576 035 241; fax: +420 576 032 716; (e-mail: janacova@fai.utb.cz)

V. Vašek, Tomas Bata University in Zlín, Faculty of Applied Informatics, Department of Automation and Control Engineering, nám. T. G. Masaryka 5555, 760 01 Zlín, Czech Republic (e-mail: vasek@fai.utb.cz)

K. Kolomazník, Tomas Bata University in Zlín, Faculty of Applied Informatics, Department of Automation and Control Engineering, nám. T. G. Masaryka 5555, 760 01 Zlín, Czech Republic (e-mail: kolomaznik@fai.utb.cz)

which we proposed to calculate the main operating costs during enzymatic hydrolysis by using Maple software interface. The calculation is based on the solution of a mathematical model describing the dependence of the quantity of a protein hydrolysate on time of process. The application allows the user to compute cost functions for the required input conditions and can be used to determine the optimum process for purpose of saving energy and raw materials.

II. MATHEMATICAL DESCRIPTION OF ENZYMATIC HYDROLYSIS

By enzymatic hydrolysis of biomaterials, solid phase reacts with liquid phase in the reactor. The reaction is catalyzed by protheolytic enzymes. Products of reaction are other solid and liquid phases.

In the following model we consider that hydrolyzed biomaterial particle is in a form of “infinite plate” of larger thickness. Therefore the rate of hydrolysis depends on the diffusion of alkali to the internal volume of hydrolyzed particles. Under these assumptions, the process takes a very long time.

To determine the dependence of the total process time on costs (cost function) is needed to determine the concentration of soluble protein product $c_{s,D}$ on the time of hydrolysis. Diffusion of alkali in biomaterial can be described by Fick's second law (1). The initial and boundary conditions of process are described by equations (2) – (5)

$$\frac{\partial c}{\partial \tau}(x, \tau) = \frac{D}{(1+K)} \cdot \frac{\partial^2 c}{\partial x^2}(x, \tau), \quad 0 \leq x \leq b, \quad \tau > 0. \quad (1)$$

We suppose symmetrical effect of alkali in biomaterials is given by equation (2):

$$\frac{\partial c}{\partial x}(0, \tau) = 0. \quad (2)$$

The initial concentration of alkali in biomaterial is described equation by (3):

$$c(x,0) = 0. \quad (3)$$

Perfectly mixing of liquid phase in reactor describes condition (4):

$$c(b,0) = \varepsilon \cdot c_{s,D}. \quad (4)$$

Equality of the diffusion flux at the boundary between the solid and the liquid phases with the speed of accumulation of the diffusing element in the surroundings is given by balance equation (5):

$$-DS \frac{\partial c}{\partial x}(b, \tau) = V_0 \frac{\partial c_0}{\partial \tau}. \quad (5)$$

The analytical solution of model (1) – (5) we obtained by Laplace transformation. Then concentration of soluble protein product $c_{s,D}$ on the time of hydrolysis is given by equation (6):

$$c_{s,D} = \frac{\varepsilon c_{s,C}}{\varepsilon + Na} - 2 \frac{Na \cdot c_{s,OP}}{\varepsilon} \sum_{n=1}^{\infty} \frac{e^{-Fo q_n^2}}{\varepsilon + Na + \frac{q_n^2 Na^2}{\varepsilon}}, \quad (6)$$

where Na is ratio of volume of liquid phase V_0 in reactor to volume of hydrolysed biomaterial V_B (7):

$$Na = \frac{V_0}{V_B}, \quad (7)$$

Fo is Fourier number (dimensionless time of hydrolysis) (8):

$$Fo = \frac{D\tau}{b^2}. \quad (8)$$

Roots q are computed from transcendental equations (9):

$$-\frac{Naq}{\varepsilon} = \tan(q). \quad (9)$$

III. DETERMINATION OF OPERATING COSTS FOR ENZYMATIC HYDROLYSIS

For the calculation of the major operating costs we used the manufacturing scheme given in Fig. 1.

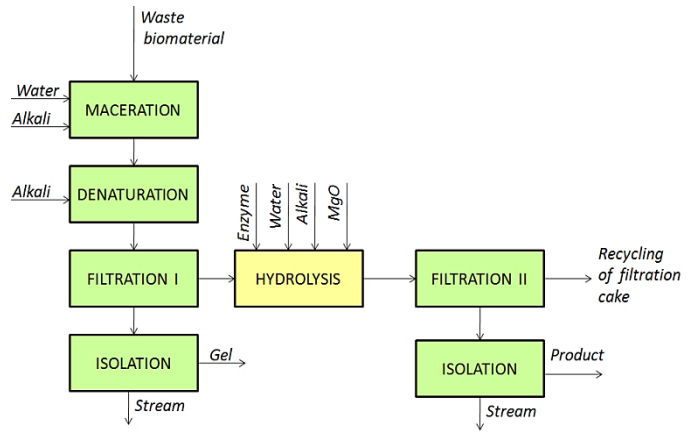


Fig. 1 Enzymatic hydrolysis - manufacturing scheme

The total unit operating costs N_T mainly include the unit costs of hydrolysis N_H and the unit costs of concentration of protein hydrolysates after separation of the heterogeneous reaction mixture N_C . Other unit costs include the price of chemicals, water and heat loss from the reactor into the environment N_O . Then it holds:

$$N_T = N_H + N_C + N_O, \quad (10)$$

where unit price of hydrolysis depends on energy consumption for propulsion of reactor, time of hydrolysis to weight of the product:

$$N_H = \frac{P \cdot K_E \cdot \tau}{m_p}, \quad (11)$$

Unit price of protein hydrolysate concentration is given by consumption on heat energy for evaporation of water:

$$N_C = \frac{m_{EW} \cdot K_S \cdot r}{m_p}, \quad (12)$$

where weight of evaporated water m_{EW} and weight of product m_p are computed from mass balance of the process (13), (14):

$$m_{EW} = \frac{m_p c_{s,P}}{c_{s,D}} - 1, \quad (13)$$

$$m_p = \frac{c_{s,D} \left[m_B (c_{s,C} - c_{s,FK}) - c_{s,FK} (m_A + m_{WR}) + m_{MgO} \right]}{c_{s,P} (c_{s,D} - c_{s,FK})}. \quad (14)$$

The other unit operating costs can be computed according to equation (15):

$$N_0 = \frac{c_{s,P}(c_{s,D} - c_{s,FK}) \left[m_B (c_C \cdot K_{MgO} + c_{s,B} \cdot K_{SB} + c_V \cdot K_V) + k_p \cdot \Delta t \cdot S \tau \cdot K_S + n \cdot K_L \cdot \tau \right]}{c_{s,D} \left[m_B (c_{s,C} - c_{s,FK}) - (m_A + m_{VR}) c_{s,FK} + m_{MgO} \right]} \quad (15)$$

The symbols mean:

- $c_{s,P}$ weight ratio of dry matter in product, [1]
- $c_{s,D}$ weight ratio of dry matter in diluted filtrate, [1]
- $c_{s,OP}$ weight ratio of dry matter in macerated mixture, [1]
- $c_{s,FK}$ weight ratio of dry matter in filter cake, [1]
- $c_{s,c}$ weight ratio of dry matter in hydrolyzed chromic waste, [1]
- c_C weight ratio of MgO to weight of hydrolysed biomaterial, [1]
- c_{sB} weight ratio of alkali to weight of hydrolysed biomaterial, [1]
- c_V weight ratio of water to weight of hydrolysed biomaterial, [1]
- b half thickness of hydrolysed biomaterial, [m]
- D effective diffusion coefficient, [m².s⁻¹]
- F_0 dimensionless time, [1]
- K sorption capacity of hydrolysed biomaterial, [1]
- K_A alkali price, [Euro.kg⁻¹]
- K_E unit price of the absorbed electrical power, [Euro.kg⁻¹]
- K_{MgO} price of MgO, [Euro.kg⁻¹]
- k_p heat passage coefficient, [W.m⁻².K⁻¹]
- K_V price of water, [Euro.kg⁻¹]
- K_L time rate, [Euro.h⁻¹]
- K_S heat energy price, [Euro.J⁻¹]
- N_T total processing costs, [Euro.kg⁻¹]
- N_H costs of hydrolysis, [Euro.kg⁻¹]
- N_C costs of the protein solution concentrate, [Euro.kg⁻¹]
- N_0 other costs, [Euro.kg⁻¹]
- P power requirement of the pump electrical engine, [kW]
- r vaporization heat of water, [J.kg⁻¹]
- m_A weight of alkaline mixture, [kg]
- m_{WR} weight of water dosed into reactor, [kg]
- m_{VR} weight of evaporated water, [kg]
- m_B weight of hydrolysed biomaterial, [kg]
- m_p weight of product, [kg]
- m_{MgO} weight of MgO, [kg]
- t temperature, [°C]
- V_0 volume of liquid reactive mixture, [m³]
- V_B volume of dry matter of hydrolysed biomaterial, [m³]
- ε porosity of biomaterial, [1]
- τ time, [s]

IV. COMPUTER CALCULATION OF COST CURVES WITH MAPLE

For automation and process control of enzymatic hydrolysis is necessary to create an algorithm for calculating the cost function, from which one can determine the optimal time of hydrolysis. The source code with the appropriate algorithm, we have created in a mathematical software MAPLE. The source code consists of the following main parts.

First, all the necessary mathematical relationships described in section II are defined:

```
> NT := NH + NC + NO;
```

$$NT := NH + NC + NO$$

```
> NH := (P * KE * tau) / mp;
```

$$NH := \frac{P \cdot KE \cdot \tau}{mp}$$

```
> NC := (mEW * r * KS) / mp;
```

$$NC := \frac{mEW \cdot r \cdot KS}{mp}$$

```
> NO := csP * (mB * (cC * KMgO + csB * KsB + cV *
KV + kp * 3600 * deltat * S * tau * KS + n * KL *
tau) * (csD - csFK) / ((mB * (csC - csFK) -
(mA + mVR) * csFK + mMgO) * csD) );
```

$$NO := (csP (mB (cC KMgO + csB KsB + cV KV + 3600 kp deltat S \tau KS + n KL \tau) (csD - csFK)) / ((mB (csC - csFK) - (mA + mVR) csFK + mMgO) csD))$$

⋮

Next roots of the transcendental equation (9) are calculated:

```
> for i from 1 to 100 do
> q[i] := fsolve (tan (q) + Na * q / (epsilon) = 0, q =
(i - 0.5) * Pi .. i * Pi) :
> od;
```

$$q_1 := 1.601997238$$

$$q_2 := 4.722975132$$

⋮

Then dependency of weight ratio of dry matter in diluted filtrate on time is calculated and displayed:

```
> plot (csD, tau = taumin .. taumax,
axes = box, labels = ["tau (h)", "csD (1)"]);
```

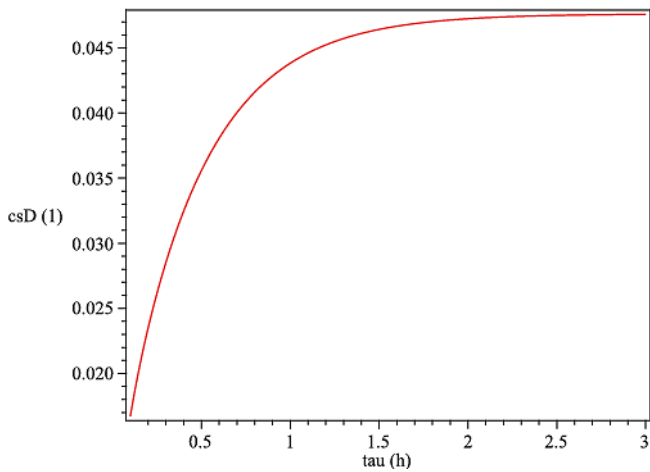


Fig. 2 Dependence of weight ratio of dry matter in diluted filtrate on time of hydrolysis computed by MAPLE.

Parameters: $b = 2 \text{ mm}$, $\varepsilon = 0.5$, $D = 3.6 \cdot 10^{-6} \text{ m}^2 \cdot \text{h}^{-1}$, $V_B = 1 \text{ m}^3$, $V_0 = 10 \text{ m}^3$, $c_{s,FK} = 0.17$, $c_{s,c} = 0.5$, $c_C = 0.02$, $c_v = 5$, $c_{sB} = 0.03$, $c_{s,OP} = 0.05$, $m_B = 800 \text{ kg}$, $\Delta t = 48 \text{ }^\circ\text{C}$, $K_L = 50 \text{ Euro} \cdot \text{h}^{-1}$, $r = 2260 \text{ kJ} \cdot \text{kg}^{-1}$, $P = 10 \text{ kW}$, $k_p = 60 \text{ W} \cdot \text{m}^{-2} \cdot \text{K}^{-1}$, $K_S = 1.8 \cdot 10^{-7} \text{ Euro} \cdot \text{J}^{-1}$, $K_E = 4 \text{ Euro} \cdot \text{kWh}^{-1}$, $K_V = 0.05 \text{ Euro} \cdot \text{kg}^{-1}$, $KMgO = 0.76 \text{ Euro} \cdot \text{kg}^{-1}$.

Finally, it is calculated and displayed the cost function:

```
> plot(NT, tau=0.1..8, axes=box,
labels=["tau (h)", "NT (Euro/kg)"]);
```

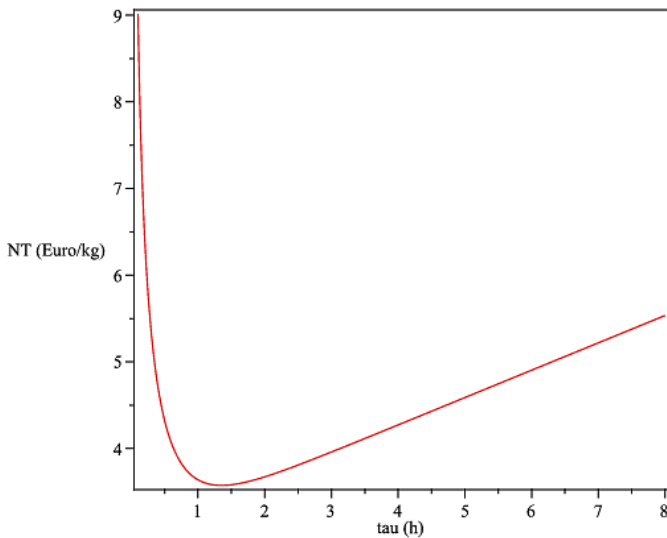


Fig. 3 Cost function computed by MAPLE

The computed data are displayed in the table, as is shown in Fig. 4.

Computed costs					
	A	B	C	D	E
1	"Time (h)"	"NT (Euro/kg)"			
2	0.1000	9.0148			
3	0.8900	3.6994			
4	1.6800	3.6060			
5	2.4700	3.8008			

Fig. 4 Table with computed data

V. CONCLUSION

The formulated mathematical model describing the dependence of the quantity of a protein hydrolysate on time of hydrolysis enabled us to programme application for computing of operating costs by the processing of biomaterial waste to protein hydrolysates. The application allows user to compute cost functions for the required input conditions and can be used to determine the optimum process to the purpose of saving energy and raw materials.

The above described application assumes the diffusion mechanism of studied process. We will also prepare application for computing of operating costs by kinematic mechanism. For this purpose, calculation of the ratio of weight of dry matter in diluted filtrate has to be modified.

REFERENCES

- [1] P. Mokrejš, et al., "Removal of MgO from the chrome cake produced by enzymatic hydrolysis of chrome shavings," *Asian Journal of Chemistry*, vol. 1, 2008.
- [2] P. Mokrejš, et al., "Processing of solid leather by-products from shoe-making," *Leather Science and Engineering*, vol. 17, 2007.
- [3] K. Kolomazník, et al., "Experience in Industrial Practice of Enzymatic Dechromation of Chrome Shavings," *JALCA*, 95,(2), 2000.
- [4] D. Janáčová, "Řízení enzymové hydrolyzy," (in Czech), Habilitation lecture, VSB - Technical University of Ostrava, 2002.
- [5] O. Liška and J. Mihalíková, "Modelovanie, programovanie a simulácia virtuálnej fabriky: modelovanie v programe Cosimir Professional/2008," (in Slovak), *Ai Magazine*, vol. 3, 2008.
- [6] D. Janáčová, H. Charvátová, K. Kolomazník, and V. Vašek, *Creating software applications for solving diffusion problems in the MAPLE interface*. (in Czech), Zlín: Tomas Bata University in Zlín, 2012.
- [7] M. Feriančík, O. Liška, and M. More, "Navigation of industrial manipulator based on computer vision," *Transfer inovácií*, vol. 28, 2013, pp. 140-142.
- [8] D. Janačová, et al., "Washing Processes Optimization," *Proceedings of International Union of Material Technologists and Chemists Societies*, London, 1997.
- [9] R. Drga, "Nepřesnosti při měření teploty zdroje IR záření termovizní kamerou," (in Czech), in *ARTEP*. Košice, pp. 19.1 - 19.8. 2012.
- [10] P. Mokrejš, F. Langmaier, and M. Mládek, "Acid treatment of Chromed Material Waste from Footwear and Garment Production," *Indian Chemical Engineer*, vol. 4, 2003, , č. 4, pp. 259-263.
- [11] P. Mokrejš, F. Langmaier, and M. Mládek, "Thermal properties of hydrolysates of chrome-tanned material waste," in *3rd Freiberg Collagen Symposium*, Freiberg, 2004, pp. 1-12.

Automatic Recognition and Synthesis System of Arabic Digit

H.TEBBI *, M. HAMADOUCHE** and H. Azzoune***

* LRIA, USTHB, Algiers (Algeria). E-mail: tebbi_hanane@yahoo.fr, htebbi@usthb.dz

** University SAAD DAHLEB of Blida (Algeria). E-mail: hamadouchemaamar@yahoo.fr

*** LRIA, USTHB, Algiers (Algeria). Email: azzoune@yahoo.fr, Hazzoune@usthb.dz

Abstract—In this work we cohabite the automatic recognition process with the automatic synthesis process applied on the first ten Arabic digits in one system that we called ARSSAD (Automatic Recognition and Synthesis System of Arabic Digits). The system is then composed of two sub-systems; a recognizer and a synthesizer. The main task of the recognizer is the automatic recognition of the pronounced digit, so it transforms the input sound wave into a text representing the appropriate digit, the second sub-system perform the opposite process of the first sub-system; in another word, it transforms the text (digit) produced by the recognizer to a speech generated by the synthesizer. The methodology used for the system design is based on three essential stages: the creation of the acoustic database (corpus development), the recognition of the read signal and the generation of the synthetic speech. We explain the basics modules that compose it, starting from the signal acquisition and finishing to the decision taken. For the recognition sub-system we make the choice to use the Dynamic Time Warping (DTW) method for the comparison task. ARSSAD contains a Front-End and a back-end module, the front-end module convert the input sound into feature vectors that are based on Mel Frequency Cepstral Coefficients (MFCCs), to be used in the DTW method. The back-end module uses the concatenative method to perform the synthesis of the recognized digit, for this end we create a sound database that contained diphones of the Arabic alphabets.

The obtained results show that the system presents a success rate of 94.85% on the three corpuses which we recorded in a noised environment.

Keywords: analysis techniques, speech recognition, speech synthesis, synthesis by diphones, synthesis by phonemes, PRAAT, MFCC, DTW, Standard Arabic.

I. INTRODUCTION

The automatic speech processing (ASP) is an area of research for which a significant effort has been undertaken over the past three decades. The challenges are considerable and have fundamental nature. They are also multidisciplinary: signal processing, pattern recognition, artificial intelligence, computer science, phonetics, linguistics, ergonomics and neurosciences; which behave at varying degrees in the solutions found.

These long-standing works nevertheless give birth at the present time to intermediate products which find their place in practical applications in the context of the Man-machine communication, as shown in [1], [2] and [3]. However, Automatic Speech Recognition/Synthesis (ASRS) systems dedicated to the Arabic language are at the moment still very modest. In

this article, we will introduce our ASRS system of the first ten digits of the Standards Arabic language (SA) in mono mode speaker. We are interested exclusively to the step of analysis of the speech signal which allows us to extract the acoustic vectors characterizing it. This step is very important and primordial in the process of automatic recognition, since it produces in output a set of parameters considered pertinent and efficient for the high-quality operation of the speech signal, on this same set we will apply the algorithms of recognition and comparison.

In speech recognition, the step of feature extraction, commonly known as the step of analysis, can be achieved in several ways. Indeed, the acoustic vectors are usually extracted using methods such as temporal encoding predictive linear (Linear Predictive Coding LPC) or Cepstral methods as the MFCC encoding (Mel Frequency Cepstral Coding), as well as the encoding PLP (Perceptual Linear Predictive coding) which is an example of the application of knowledge of the auditory system in human speech recognition. The extraction of characteristics is a key element for the development of an ASR system. The other part of our system represent a Text To Speech (TTS) system, in which the main techniques used in it design are Articulator synthesis, Formant synthesis, and Concatenative synthesis [4].

- 1) Articulatory synthesis attempts to model the human speech production system directly.
- 2) Formant synthesis, which models the pole frequencies of speech signal or transfer function of vocal tract based on source-filter-model.
- 3) Concatenative synthesis, which uses different length pre-recorded samples derived from natural speech.

In our case, we have used the concatenation method for the synthesis implementation which represent, in our opinion, the method that produce a synthetic voice the most natural and intelligible compared to the others. This result came from the fact of using a set of recording units pronounced by a real speaker, priory collected and embedded within our sound database.

So, for the recognizer, we have to deal with two essential problems, the first one is the choice of the technique of analysis used, and the second one is the choice of parameters and their number to extract the relevant parameters of the voice signal. The purpose is

to determine which gives the best recognition rate.

Whereas, for the synthesizer, we have to face two other problems; the choice of the transcription method (rule-based method or lexicon-based method) in one hand, and the co-articulation problem to improve the quality of the generated speech, in the other hand.

II. SYSTEM DESIGN

When designing a system, two broad ways could be taken into account, the first one is to design the whole system using the known theories, and use it as it is designed, in the real conditions. An alternative way would be to subdivide the system into modules that can be independently created and tested, to eventually be used in other systems to perform several functionalities.

To facilitate the implementation and improvement of our system, we have used the modular approach; this concept makes the program understandable on one part and decreases the cost of development of each module in another part. We have also used the concept of the object-oriented programming which is particularly suitable with the modular technique. We must therefore make out different modules which structure the system as shown in the following diagram (Fig.1):

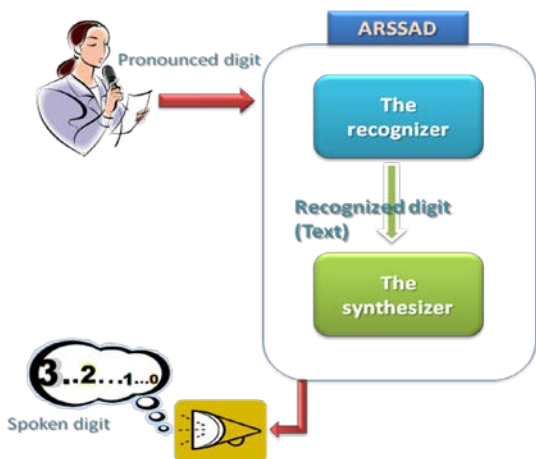


Figure 1 : General architecture of our system ARSSAD.

The objective here is to describe the role of each module, explaining in the same time the interest of links which provide the cooperation between them.

III. THE RECOGNIZER

This module represent the front-end of the whole system, it is also composed of a set of sub-modules that can be shown in the following diagram (Fig.2)

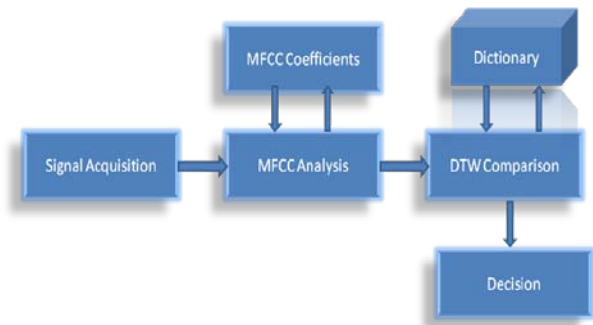


Fig. 2 general schema of the recognizer

We give now the principal functionalities of each sub-module one after another.

A. Signal Acquisition

This module carries out the acquisition of the acoustic signal recorded by a microphone and converts it into a digital form that can be used directly by a machine. There are many types of microphones but all of them provide the same function: transform the pressure fluctuations caused by the acoustic wave of speech into an electrical signal. This signal will be converted from the analogical form to the digital one, i.e. it will be discrete both in time (sampling) and value (quantification) [5]. As a result we obtain a digital signal in the form of a sequence of samples which measure the amplitude of the microphone's signal in regular spaced moments, and the amplitude of each sample is represented in its digital form. The choice of the sampling frequency is usually determined by the application and referred to the platform used [5]

B. Sampling Frequency

Some thoughts on the frequency of sampling are required in first. According to the theorem of Shannon [6]: « a bandlimited function can be perfectly reconstructed from a countable sequence of samples if the bandlimit, B , is no greater than half the sampling rate (samples per second)".

Sounds that are made by the human voice normally contain relatively insignificant frequency components at or above 10 kHz [6]. Sampling such an audio signal at 20k sam/sec, or more, provides an excellent approximation to ensure that the Shannon criterion is met. But often the sample-rate is pre-determined by other considerations, such as an industry standard format (e.g. 8k sam/sec). In this situation, the human voice should be filtered, to remove frequency components above 4 kHz, before being sampled. So we consider in our work that the acoustic signal is located mainly in the bandwidth (50 Hz -8 kHz), the frequency of sampling should therefore be at least equal to 16 kHz, according to the theorem of Shannon. For the case of our application, we have used a sampling frequency of the order of 22050Hz, the default value taken by the software used in this operation PRAAT [7].

C. *The corpus preparation*

Most of the works carried out in the field of Man-Machine communication often require the registration, and the manipulation of corpus of continuous speech, and this to carry out the studies on the contextual effects, on the phonetic indices, and on the variability intra and inter speakers. There were three recorded corpuses each one containing ten sounds of ten prime numbers of Standards Arabic (Wahid, Ithnane, Thalatha, Arbaa, Khamsa, Sita, Sabaa, Thamanian, Tisaa, Aachara) in a noisy environment and we have changed the speed of elocution from a corpus to another without changing the speaker. The step of analysis may therefore begin.

D. *The Cepstral Analysis (MFCC)*

The aim of the analysis of the voice signal is to extract the acoustic vectors which will be used in the stage of recognition follows. In this step the voice signal is transformed into a sequence of acoustic vectors on the way to decrease redundancy and the amount of data to be processed. And then a spectral analysis by the discrete Fourier transform is performed on a signal frame (typically of size 20 or 30 ms) [6]. In this frame, the voice signal is considered to be sufficiently stable and we extract a vector of parameters considered to be enough for the good operation of the voice signal, in our work we choose to use MFCCs coefficients resulting from a Cepstral analysis of the read signal.

The method of extraction of the MFCCs coefficients is one of most popular of calculation of the acoustic vectors in the field of automatic speech recognition. We have also decided to use it in our context of application and we chose a set of 12 coefficients. We expose the different steps leading to Cepstral analysis using the tool of speech analysis, PRAAT, we show the different parameters required for the analysis that we have chosen, and in the end the exploitation of the MFCCs coefficients resulting.

Step1: reading the file to analyze and the choice of MFCC method

- 1) Start PRAAT
- 2) Open the sound file:
- 3) Read > Read from file (open a sound file)
- 4) Edit (for the view)
- 5) File > Extract Selection (for "cut" the sound)
- 6) Write > Write to .wav file (to save a sound file)
- 7) Select the file to analyses
- 8) Choose the Cepstral method:
- 9) Formants&LPC > To MFCC

Step 2: determination of the parameters required for the analysis

- 1) Number of coefficients: 12
- 2) Duration of windows: 30 ms
- 3) Duration between the windows: 10 ms

Step 3: analysis Results

It remains now to save the results in a text file format with the extension .MFCC (Write > Write to txt file), to be used in the following stage.

E. *The use of DTW method*

Our speech recognition sub-system is based on the algorithm of DTW (Dynamic Time Warping), this method is based on an evaluation of the distance between an observation and a list of references (dictionary). As well the reference for which this distance is minimal allows us to decide what word is it. The evaluation of the distance between two signals is not performed with the signals themselves. This would lead to lot of calculations. It is therefore in a prime time to find a better representation of the signals. Here MFCC analysis shines.

So we have programmed the DTW method using, for the comparison, the MFCC coefficients. The training part concerns the recording of the sounds corpuses in order to design our dictionary which will be used as reference in the comparison of the signals tested. Problems of recognition may appear depending on the conditions in which the signal to test is recorded. If the word is pronounced more or less close to the microphone recognition rates can vary greatly. However if the user says the word always at the same distance and with the same intensity, the rate of recognition is very acceptable. We judge, however, that the representation using the MFCC coefficients provides better results, and it supports better the limitations related to the problem of the capture of the signal. The common skeleton of the DTW algorithm has three steps illustrated as follow:

- 1) Acquisition of the sound file to test
- 2) Extraction of the MFCC coefficients
- 3) Comparison with the dictionary of references

F. *The decision*

This last module of our recognizer plays two essential roles; it represents the interface in which the user interacts with the system. After the user has entered his voice signal, he starts the search and awaits the results. The system displays the recognized digit written in both Arabic and French language.

The second role is that this same decision (the displayed digit) represents the input (text) of the second module of our system, which is the synthesizer.

IV. THE SYNTHESIZER

It is based essentially on two principal parts; a front-end and a back-end. The front-end is composed of two modules, the first is for the sound database creation and the second is for the conversion text-to-phoneme or grapheme-to-phoneme.

The back-end part represents the speech generation module or in other words the synthesizer itself.

So the different modules that compose the system are as follow:

- 1) The sound database creation (segmentation): we have recorded a set of pieces of speech and store it in our database, this set is composed of phonemes and diphones which are the basic units utilized within the back-end module in order to generate voice using the concatenation method.
- 2) The grapheme/phoneme conversion: before achieving this process, a text normalization or preprocessing operation has to be done. After that the module assigns to each word in entry it phonetic transcription, and then divides and marks the text into prosodic units like syllables. This process of assigning phonetic transcription to words is called text-to-phoneme or grapheme-to-phoneme conversion. The output of the front-end module is a symbolic linguistic representation resulting from the phonetic transcription and prosody information together, which represents the input of the back-end module.
- 3) The synthesizer: the back-end module uses information provided by the front-end to converts the symbolic linguistic representation to speech using a specific method. In literature, there are two kind of synthesis method; rule-based method and concatenative corpus-based method.

Like we have mentioned before, we have used the concatenative method of phonemes and graphemes previously stored in our sound database.

The general architecture of this module could be shown in figure 1 as follow:

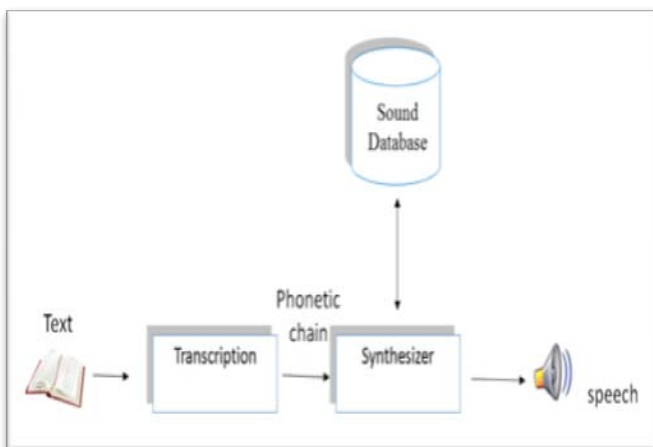


Fig. 3 the general architecture of the synthesizer.

A. The corpus description

We have created two corpuses; The first contains phonemes: It is composed of a set of basic sounds (which consists of the phonemes corresponding to the 28 consonants and 6 vowels, and other additional (corresponding to the three sounds of tanwiin ([an], [a], [in]), and the silence) character.

To improve the quality of the words synthesized by the method of concatenation of phonemes, and to reduce the effects of co-articulation, the solution is to record the transition that exists between phonemes instead of recording the phonemes themselves; we talk about diphones which are an adjacent pair of phones.

Indeed, the transition (diphones) is the bearer of a significant quantity of acoustic information in relation to the phoneme itself. Each transition or diphone also varies from the stable part of a phoneme up to the stable part of phoneme that follows.

B. The phonetic and orthographical transcription "POT":

Transcription provides a phonetic text from the alphabetic text. To accomplish this, it must apply to many pronunciation rules. French language has a few thousands of basic rules; English language has tens of thousands of rules. Therefore, during the passage from the written form to the spoken form two approaches can be used which are: the lexicon-based approach and the rule-based approach [8] [9];

- The use of rules

In this approach each grapheme is converted to phoneme depending on the context and this is thanks to the use of a set of rewriting rules [10]. The main advantage of this approach is the ability to model the linguistic knowledge of human beings by a set of rules that can be incorporated in expert systems. Each of these rules has the following form:

[Phoneme] = {LC (Left Context)} + {C (Character)} + {RC context}

Our transcription module grapheme-phoneme is based on a set of rules;

The rule of tanwin, al madd, etc... Prioritized, and organized in the form of a tree list. Each rule is written in the graphics context in which it is applied.

Here is a concrete example of transcription rule "The rule of Tanwin"

If (grapheme[char] == 'Tanwin')

{ If (API[position][0] == ' ')

Phoneme = phoneme + "an";

Else

{ If (API[position][0] == ' ')

Phoneme = phoneme + "in";

Else

Phoneme = phoneme + "a"; }

}

- The use of the lexicon
In this case we must assign to each word in entry the pronunciation which corresponds to it without taking into account its context. The speed, flexibility and simplicity are the main advantages of this approach.

C. The acoustic generation sub-module

This is the heartbeat of the synthesizer module, in fact the user after that he had pronounced the digit he will see the recognized digit displayed on the screen, and will hear the system spelling back the recognized digit. This is the task of the acoustic generation sub-module. To accomplish this work, we have implemented a reading function which is exposed below:

```

Position= seek (grapheme[ ig] ,API ) ;
If((grapheme[ig] == '٥') && (grapheme[ig+1] == '١'))
{
    MP2- >FileName= "C: \\son_hanane\\alif.wav";
    MP2- >Open( );
    MP2- >Wait=true;
    MP2- >Play( );
    IG=ig+2;
    Position=seek (grapheme[ig] ,PLC);
    If(API[position] [ 1] == ' ')
    {
        MP2- >FileName= "C: \\son_hanane\\l.wav";
        MP2- >Open( );
        MP2- >Wait=true;
        MP2- >Play( );
        MP2- >FileName=API[position] [ 2]);
        MP2- >Open( );
        MP2- >Wait=true;
        MP2- >Play( );
        IG++;
    }
}
Else
{
    If(API[position] [ 1] == 'S'
    {
        MP2- >FileName=API[position] [ 2]);
        MP2- >Open( );
        MP2- >Wait=true;
        MP2- >Play( );
        IG++;
    }
}
}
}

```

V. TESTS AND RESULTS

The main interface of our system, with an example of the recognition of the digit ten (AACHARA) is shown in the following figure (Fig.4):

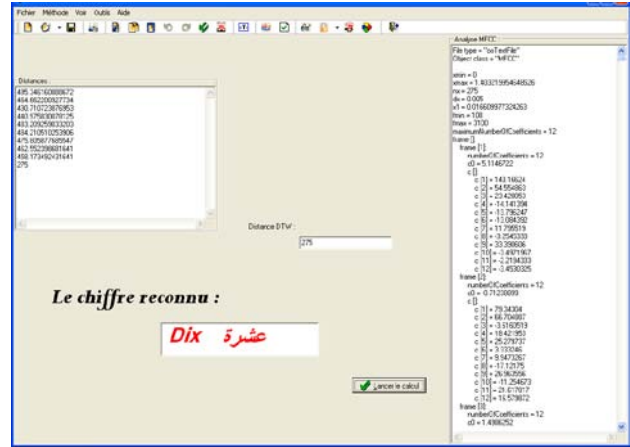


Fig 4 main interface of our system

We have applied the recognition on a corpus containing Arabic digits from one to ten pronounced by a male sex speaker in the Standard Arabic language.

To evaluate the performance of our system, we have illustrate two formula for each module; a recognition rate (RR) for the recognizer, and a success rate (SR) for the synthesizer.

We have fixed the number of tests performed to recognize a digit to twelve times. The recognition rate (RR) for each digit is calculated by the following formula:

$$RR = \frac{Nb_recognized_digit}{Nb_tested_digit(12)} * 100\%$$

In the other hand, to calculate the success rate (SR) associated with each digit tested; we got the following formula:

$$SR = \frac{Nb_well_pronounced_digit}{Nb_tested_digits} * 100\%$$

The results obtained for each digit are summarized in the following table:

Table 1 : Recognition/ Success rate for the ten digits

The word in Arabic	Transcript	The word in English	RR	SR
واحد	WAHID	ONE	85.7 %	100%
اثنان	ITHNAN	TWO	100%	100%
ثلاثة	THALATHA	THREE	100%	85%
أربعة	ARBAA	Oven	100%	100%
خمسة	KHAMSA	FIVE	100%	100%
ستة	SITTA	SIX	85.7 %	100%
سبعة	SABAA	SEVEN	100%	86%
ثمانية	THAMANIYA	EIGHT	100%	80%
تسعة	TISAA	NINE	100%	86%
عشرة	AACHARA	TEN	88.6 %	100%

When investigating across the natural language processing field, we haven't found a lot of works dealing with the automatic recognition and speech synthesis in a same work, especially for the Arabic language. Therefore, in the comparison with previous works, we take into account just the success accuracy of the automatic recognition. The comparison results obtained are summarized in the following table:

Table 2 : Comparison with previous work

ASR using CMUSphinx [7]	85.55 %
DTW-Based ArSR [8]	86%
DHMM-Based ArSR [8]	92%
Heuristic Method [9]	86.45 %
Heuristic Method with RNN [9]	95.82 %
Monophone-Based ArSR [10]	90.75 %
Triphone-Based ArSR [10]	92.24 %
Syllable-Based ArSR [10]	93.43 %
Word-Based ArSR [10]	91.64 %
VQ and HMM Rrna [11]	91%
MCCF-based Rrna [11]	61 %AP -92%
Wavelet-based Rrna [11]	76 %AP -92%
LBC-based FPGA Rrna [12]	91 % -96%
MCCF-based FPGA Rrna [12]	95 % -98%
ARSSAD	96%

The recognition sub-system achieved 96% correct digit recognition in the case of mono-speaker mode. On the other hand, the speech synthesis sub-system achieved 93.7% correct well synthesized digit. So the system present in general 94, 85 % of success rate.

VI. CONCLUSIONS

We set several objectives for this research: that of discover the definitional character of the human voice, to describe the various stages and components used in the production of the voice and to dissect an ASRS system in its main floors. To that end, we have detailed our system of recognition and synthesis of Arabic digit as well as the results obtained. The system presents, using isolated words and in the absence of noise, a success rate quite honorable and acceptable. The acoustic variability of the voice signal, and in particular that due to the effects of coarticulation, is better apprehended by the modeling of its production. In fact, the voice signal is not an ordinary acoustic signal and the Anatomical constraints may explain the effects of coarticulation, for example, in the framework of the articulatory phonology.

At the end of this rapid assessment on the voice recognition and synthesis, it has been noted that this area is particularly broad and that there is no miracle product capable of responding to all applications. The noise, for example, remains a brake to the generalization of recognition systems. The voice recognition is still a compromise between the size of the vocabulary, its possibilities multi-speaker, its rapidity, training time, etc... The power of the current calculating tools and the integration capabilities of systems have caused a resurgence of interest in the recent years among the industrials. In fact, they see in the voice recognition or synthesis, "the more commercial ", allowing making the difference with the competition. A quick tour of horizon on the very numerous publications allows us to set the ideas on the nature of the work in progress. Apart from the products dedicated to the voice recognition, the systems with analytical approach (HMM and ANN) give today the best results [11], and currently have the wind in their sails.

As regards the future prospects, the optimism is more measured than in the past. Without risk, we can say that the general problem of the automatic processing of the voice signal will probably not rule before the middle of the next century. We can as even quote a few perspectives to our work in the following points:

- 1) Enlargement of the vocabulary for all digits;
- 2) Recognition of continuous speech;
- 3) Recognition in speaker independent mode;
- 4) Use of the HMM, neural networks and hybrid methods.

REFERENCES

- [1] Halima Bahi , a NeuroExpert system for the recognition of the voice; NESSR: Neural Expert System for Speech Recognition, LRI Laboratory, Department of Computer Science, University of Annaba, Algeria, bahi@lri-annaba.net
- [2] Ali Sadiqui, Nouredine Chenfour, realization of a system of automatic speech recognition arabic based on CMU Sphinx, Anal. Computer Science Series. 8TH Volume 1st Parts, Faculty of Sciences Dhar El Mehraz, University Sidi Mhamed Ben Abdellah of Fez BP.1796- Fes- Morocco,. 2010.
- [3] H. Satori, N. Chenfour, MR. Harti, Introduction To Arabic speech recognition using CMU Sphinx System, International Journal Of Computer Science, 2007.
- [4] Othman. O. Khalifa, M.Z. Obaid, A.W. Naji and Jamal I. Daoud, "A Rule-Based Arabic Text-To-Speech System Based On Hybrid Synthesis Technique", Electrical and Computer Engineering Department, International Islamic, University Malaysia Gombak, P.O Box 10, 50728 Kuala Lumpur, Malaysia, Australian Journal of Basic and Applied Sciences, 5(6): 342-354, 2011.
- [5] S. Deketelaere, "automatic speech recognition", MULTITEL - Department automatic speech recognition, Park Initialis-Avenue Copernic, Mons Belgium, site: www.multitel.be
- [6] L. V. Tray, "automatic recognition of digits in English in noisy conditions", University Joseph Fourier, U .F .R Informatics & Applied Mathematics, June 20, 2002
- [7] Paul Boersma and David Weenink, "PRAAT: doing phonetics by computer" Phonetic Sciences, University of Amsterdam Spuistraat 210, 1012 VT Amsterdam The Netherlands.
- [8] Pierre DRAGICEVIC "a model of interaction in input for interactive systems multi-devices highly configurable ", Ph.d. thesis from the University of Nantes, the National College of Industrial Technology and Mines of Nantes, France, March 09, 2004
- [9] <http://www.crisco.unicaen.fr/description-des-differentes.html>, last access time : April 24th, 2014
- [10] P. Boula of Mareuil, "Synthesis of the floor from couriers and evaluation of conversion grapheme-phoneme ". LIMSI-CNRS [http://www.limsi.fr/ Individu/ mareuil/](http://www.limsi.fr/Individu/mareuil/)
- [11] F. A. Elmisery, A.H. Khalil, A. E. Salama, H. F. M'hammed, "A FPGA Based HMM for a discreet Arabic Speech Recognition System," Proceedings of the 15th International Conference on Microelectronics (ICM 2003), Cairo, Egypt, December 9-11, 2003.

On the usage of differential evolution for effort estimation

T. Urbanek, Z. Prokopova, and R. Silhavy

Abstract—This paper deals with effort estimation in software engineering. This task is very complex and very important in project management. Project managers have to do right decisions in early stages of project development. There are a large number of methods for effort estimation, however research in this field shows that there is no universal method for this task. Nevertheless there is a possibility to improve accuracy of these methods. Use Case Points method is one of these methods. This paper tries to explain how to use differential evolution and analytical programming for accuracy improvement of this method. Use Case Points method contains a mathematical equation for calculation of effort estimation. Differential evolution and analytical programming are used for synthesize new equation for Use Case Points method. The experimental results shows that this method improving accuracy of effort estimation from MMRE 62% to MMRE 21 %.

Keywords—Differential evolution, analytical programming, effort estimation, Use Case Points, DE, UCP, AP

I. INTRODUCTION

EFFORT estimation is the activity of predicting the amount of effort required to complete a software development project [1]. The reason for this research is to find effective method, which helps to project managers estimate effort more accurate. It is very important to predict effort estimation in the early stage of software development in the best case after requirement analysis [2]. Atkinson et al. [3] claims that regression analysis does not provide enough accuracy. Therefore, the use of artificial intelligence may be promising way to improvement of effort estimation. Accurate and consistent prediction of effort estimation is crucial point in project management for effective planning, monitoring and controlling of software projects. Project managers used these estimates for better management decisions. Software engineering is very complex process, because of a lot of factor, which inputs to prediction for example size of development team, requirements, programming language and other factors.

Attarzadeh et al. [4] claims that effort estimation in software engineering is divided into two categories. Algorithmic methods and non-algorithmic methods. Algorithmic methods carries mathematical formula, which is regression model of historical data. The most famous methods are COCOMO [5], FP [3] and UCP [2]. But there is a lot of algorithmic methods.

T. Urbanek is with the Department of Informatics and Communication Systems, Tomas Bata University in Zlin, Nad Stranemi 4511, Zlin, Czech Republic, e-mail: (turbanek@fai.utb.cz).

Z. Prokopova is with the Department of Informatics and Communication Systems, Tomas Bata University in Zlin, Nad Stranemi 4511, Zlin, Czech Republic, e-mail: (prokopova@fai.utb.cz).

R. Silhavy is with the Department of Informatics and Communication Systems, Tomas Bata University in Zlin, Nad Stranemi 4511, Zlin, Czech Republic, e-mail: (rsilhavy@fai.utb.cz).

To the second category belong methods like expert judgment and analogy based methods. The most famous methods are Delphi [6].

Underestimation of effort estimate can lead to reduction of quality of software. This software tend to be dysfunctional and then raise the cost for maintenance [7]. Software industry is very competitive and accurate effort estimation is key for companies to effectively manage software projects [8]. The management of software project could be less challenging with accurate prediction [2].

This paper is organized as follows. Section II gives an overview of datasets and define the problem. Section III builds the model for estimating the total effort for the development, and section IV gives results of new generated equation. Finally, section V presents the conclusion to the study.

A. Related work

Despite of a lot of effort of scientists, there is no optimal and effective method for every software project. Very promising way is a research of Kocuganeli et al. [9], this paper shows, that ensemble of effort estimation methods could provide better results then single estimator. Nonetheless, if we want to compose effort estimation method, we need building blocks. These blocks are effort estimation methods. There is a possibility, that better building blocks could create more accurate method. This research is aimed to develop a new method for effort estimation. This method uses artificial intelligence techniques for calibrating Use Case Points method.

The work of Kaushik et al. [8] and Attarzadeh et al. [4] uses neural networks and COCOMO [5] method for prediction. COCOMO method is widely used for testing and calibrating in cooperation with artificial intelligence. Neural networks in these cases searches parameters of regression function. Unlike presented method, which search for regression function. Differential evolution and analytical programming is used for this task. Because it is very difficulty obtain a reliable dataset in case of Use Case Points method, this paper shows results on dataset from Poznan University of Technology [10] and from this paper [11].

B. Differential evolution

Differential evolution is optimization algorithm introduced by Storn and Price 1995 [12]. Differential evolution is evolutionary algorithm based on population, mutation and recombination. Differential evolution is simple to implement and have only three parameters to set. These parameters are NP, F and Cr. Parameter NP is population size, parameter F is weighting factor and parameter CR is crossover probability.[13]

TABLE I
DATA USED FOR EFFORT ESTIMATION

ID	Act. Effort [h]	UCP * 20	MRE [%]
1	3037	2971	2
2	1917	1094	43
3	1173	1531	31
4	742	2103	183
5	614	1257	105
6	492	883	79
7	277	446	61
8	3593	6117	70
9	1681	1599	5
10	1344	1472	10
11	1220	1776	46
12	720	1011	40
13	514	627	22
14	397	1884	375
15	3684	6410	74
16	1980	2711	37
17	3950	6901	75
18	1925	2125	10
19	2175	2692	24
20	2226	2862	29
21	2640	3901	48
22	2568	3216	25
23	3042	5444	79
24	1696	2127	25
MMRE			62

C. Analytical programming

Analytical programming (AP) is a tool for symbolic regression. The core of analytical programming is set of functions and operands. These mathematical objects are used for synthesis a new function. Every function in the set of analytical programming core has various number of parameters. Functions are sorted by these parameter into general function sets (GFS). For example GFS_{1par} contains functions that have only 1 parameter like $sin()$, $cos()$ and other functions. AP must be used with any evolutionary algorithm that consists of a population of individuals for its run [14]. In this paper is used differential evolution (DE) as evolutionary algorithm for analytical programming [12]. The function of AP is following: A new individual is generated by evolutionary algorithm. Then this individual is remapped to new function by analytical programming. After that this new function is evaluated by cost function. Evolutionary algorithm decide either this new equation is suited or not for next evolution. This implies the fact, that the analytical programming is a method, which converts input set of numbers to the function.

II. PROBLEM DEFINITION

Dataset with Use Case Points method was obtained from Poznan University of Technology [10] and from this paper [11]. The Table III shows Use Case Points method data from 24 projects. Data of Use Case Points method with transitions is used in this paper in case of Poznan University of Technology dataset. There are 4 values for each software project UUCW, UAW, TCF and ECF.

Gustav Karner in his work [2] derived nominal value for calculation of man-hour from Use Case Points method. This value was set to 20. Thus, effort estimate in man-hours is calculated as $UCP * 20$.

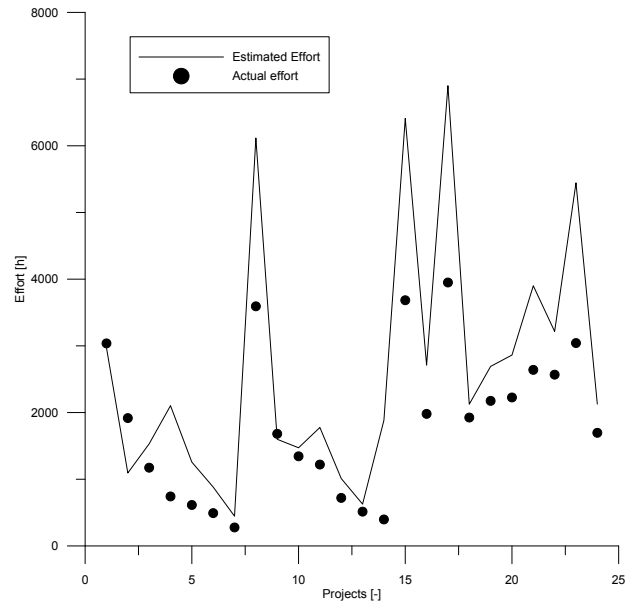


Fig. 1. Difference between estimated and real effort

Table I shows calculated differences. The equation for calculation of MRE is following:

$$MRE = \frac{|ActualEffort - (UCP * 20)|}{ActualEffort} \tag{1}$$

,where MRE is calculated error for each project in Table I. Results from MRE calculation and Equation 2 were used for calculation of MMRE.

$$MMRE = \frac{1}{n} \sum_{i=1}^n MRE \tag{2}$$

,where $MMRE$ is mean magnitude of relative error through all project in Table I.

$$MMRE = 62\%$$

The conclusion for problem definition is that, during estimation of 24 software projects was generated mean magnitude of relative error by Use Case Points method and this error had value 62 %. New equation, which is presented in this paper, tries to minimize this error. As shown in Figure 1, the Use Case Points method generate a significantly error in project 4,5 and 14.

III. METHOD

Dataset was obtained from Table III. Matrix A was constructed from this dataset and has size $M \times N$, where $M = 5$ and $N = 24$. Every row of this matrix A contains calculation of Use Case Points method and actual effort.

The columns from beginning to end are UUCW, UAW, TCF, ECF and actual effort. Whole dataset could not be optimized by evolutionary algorithm, because no data was remained for testing purposes. Because of this problem, the matrix A was

TABLE II
SET-UP OF DIFFERENTIAL EVOLUTION

Parameter	Value
NP	40
Generations	60
F	0.7
Cr	0.4

TABLE III
DATA USED FOR EFFORT ESTIMATION

ID	UUCW	UAW	TCF	ECF
1	195	12	0.780	0.780
2	80	10	0.750	0.810
3	75	6	0.900	1.050
4	130	9	0.850	0.890
5	85	12	0.820	0.790
6	50	9	0.850	0.880
7	50	6	0.780	0.510
8	305	14	0.940	1.020
9	85	12	1.030	0.800
10	130	12	0.710	0.730
11	80	9	1.050	0.950
12	70	12	0.780	0.790
13	30	4	0.960	0.960
14	100	15	0.900	0.910
15	355	15	1.125	0.770
16	145	18	1.080	0.770
17	325	12	1.095	0.935
18	90	6	1.085	1.085
19	125	9	1.025	0.980
20	120	9	1.115	0.995
21	200	12	1.000	0.920
22	175	9	0.950	0.920
23	245	12	0.890	1.190
24	140	6	0.965	0.755

divided into two matrices. Matrix B is training dataset and matrix C is testing dataset.

The Matrix B contains 12 rows of data for training purposes and the matrix C contains 12 rows for testing purposes. Therefore 50 % of dataset is used for training and the rest of dataset is used for testing. The matrix B was processed by analytical programming with differential evolution algorithm. Result of this process was a new equation. This equation contained variables and constants and these variables were UUCW, UAW, TCF and ECF. This new equation also describes relationships between variables in training dataset, moreover in testing dataset.

Table II shows the set-up of differential evolution. Parameters F and Cr were adjusted on standard values.

A. Cost function

The new equation that is generated by method of analytical programming contains these parameters UUCW, UAW, TCF and ECF. There is no force applied to analytical programming that equations generated by this method have to contain all of these parameters. Cost function that is used for this task is following:

$$CF = \sum_{i=1}^n |B_{n,5} - f(B_{n,1}, B_{n,2}, \dots, B_{n,4})| \quad (3)$$

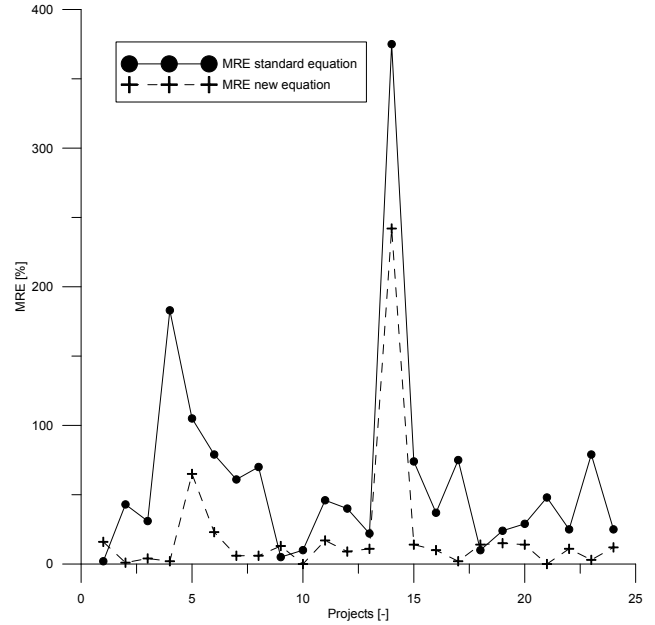


Fig. 2. Difference between MRE of estimated and real effort

,where n is equal to number of projects in dataset, $B_{n,5}$ is actual effort, $B_{n,1}$ is UUCW, $B_{n,2}$ is UAW, $B_{n,3}$ is TCF, $B_{n,4}$ is ECF.

IV. RESULTS

It was calculated 1000 equations. In this paper is presented only one the best estimation improving equation. Each calculation was generated in approximately 22 seconds. The best equation was synthesized in 192. iteration. Because of the length of new equation, this equation was split into three parts, p_1 , p_2 and p_3 . The complete equation is composition of these parts. The best equation is following:

$$p_1 = 9.53019 * (304.217 + t + e * t + a) \quad (4)$$

$$p_2 = \frac{53.4279 * (237.002 - t - u)}{(4.2228 + e) * t} \quad (5)$$

$$p_3 = \frac{(-1927.97 + a) * (-a - e)}{a * ((4.22196 + t) * (t - u) + \frac{5.29401 * t * u}{e})} \quad (6)$$

$$UCP = p_1 - p_2 - p_3 \quad (7)$$

,where u is UUCW, a is UAW, t is TCF and e is ECF.

The Table IV contains the results of MMRE calculation for new equation. It is very important that MMRE calculation was applied for both training data and testing data.

Figure 2 shows differences of MRE between standard equation and new equation. This new equation outperformed standard equation almost in every project in dataset. Nevertheless, standard equation was better in project ID 1, 9 and 18.

TABLE IV
CALCULATION OF MMRE FOR NEW EQUATION

ID	Act. Effort [h]	New equation	MRE [%]
1	3037	2543	16
2	1917	1899	1
3	1173	1218	4
4	742	757	2
5	614	1015	65
6	492	378	23
7	277	259	6
8	3593	3823	6
9	1681	1457	13
10	1344	1346	0
11	1220	1430	17
12	720	652	9
13	514	457	11
14	397	1358	242
15	3684	4192	14
16	1980	2182	10
17	3950	3870	2
18	1925	1659	14
19	2175	1841	15
20	2226	1914	14
21	2640	2639	0
22	2568	2297	11
23	3042	3138	3
24	1696	1895	12
MMRE			21

V. CONCLUSION

In this paper was presented method for effort estimation improvement. This method is combination of Use Case Points method and analytical programming with differential evolution. Presented approach is founded on generating new equations for Use Case Points method. From 1000 calculated equation was chosen only one the best equations. This equation improving estimation to MMRE 21 %. There will be necessary to find a proper set-up for differential evolution. There is also a problem in this method; the cost function minimization may not lead to minimization of error in estimation on data that is not subject of minimization. That means, the equations have to be checked by visual or some kind of algorithm. There is another disadvantage, this method still depend on human experience with Use Case Points method. The benefit of this solution is there are no weights in this method, because these weights are generated by analytical programming as constants in equations. The subject of further research will be that there is a possibility that this method can generate more accurate equations with larger datasets.

ACKNOWLEDGMENT

This study was supported by the internal grant of Tomas Bata University in Zlin No. IGA/FAI/2014/019 funded from the resources of specific university research.

REFERENCES

- [1] J. W. Keung, "Theoretical Maximum Prediction Accuracy for Analogy-Based Software Cost Estimation," *2008 15th Asia-Pacific Software Engineering Conference*, pp. 495–502, 2008.
- [2] G. Karner, "Resource estimation for objectory projects," *Objective Systems SF AB*, 1993.
- [3] K. Atkinson and M. Shepperd, "Using Function Points to Find Cost Analogies," *5th European Software Cost Modelling Meeting, Ivrea, Italy*, pp. 1–5, 1994.

- [4] I. Attarzadeh and S. Ow, "Software development cost and time forecasting using a high performance artificial neural network model," *Intelligent Computing and Information Science*, pp. 18–26, 2011.
- [5] B. W. Boehm, "Software Engineering Economics," *IEEE Transactions on Software Engineering*, vol. SE-10, no. 1, pp. 4–21, Jan. 1984.
- [6] G. Rowe and G. Wright, "The Delphi technique as a forecasting tool: issues and analysis," *International Journal of Forecasting*, vol. 15, no. 4, pp. 353–375, Oct. 1999.
- [7] Z. Jiang, P. Naudé, and B. Jiang, "The effects of software size on development effort and software quality," *Journal of Computer and Information Science* . . . , pp. 492–496, 2007.
- [8] A. Kaushik, a. K. Soni, and R. Soni, "An adaptive learning approach to software cost estimation," *2012 National Conference on Computing and Communication Systems*, pp. 1–6, Nov. 2012.
- [9] E. Kocaguneli, T. Menzies, and J. Keung, "On the value of ensemble effort estimation," *IEEE Transactions on Software Engineering*, vol. 38, no. 6, pp. 1403–1416, 2011.
- [10] M. Ochodek, J. Nawrocki, and K. Kwarciak, "Simplifying effort estimation based on Use Case Points," *Information and Software Technology*, vol. 53, no. 3, pp. 200–213, Mar. 2011.
- [11] A. P. Subriadi and P. A. Ningrum, "Critical review of the effort rate value in use case point method for estimating software development effort," *Journal of Theoretical and Applied Information Technology*, vol. 59, no. 3, pp. 735–744, 2014.
- [12] R. Storn and K. Price, *Differential evolution-a simple and efficient adaptive scheme for global optimization over continuous spaces*, 1995.
- [13] R. Storn, "On the usage of differential evolution for function optimization," *Fuzzy Information Processing Society, 1996. NAFIPS. . . .*, 1996.
- [14] Z. Kominkova Oplatkova, R. Senkerik, I. Zelinka, and M. Pluhacek, "Analytic programming in the task of evolutionary synthesis of a controller for high order oscillations stabilization of discrete chaotic systems," *Computers & Mathematics with Applications*, vol. 66, no. 2, pp. 177–189, Aug. 2013.

Tomas Urbanek was born in Zlin in 1987. He received a B.Sc. (2009), M.Sc. (2011) in information technology from Faculty of Applied Informatics, Tomas Bata University in Zlin. He is a doctoral student at the Computer and Communication Systems Department. Major research interests are software engineering, effort estimation in software engineering and artificial intelligence

Radek Silhavy was born in Vsetin in 1980. He received a B.Sc. (2004), M.Sc. (2006), and Ph.D. (2009) in Engineering Informatics from the Faculty of Applied Informatics, Tomas Bata University in Zlin. He is a Senior Lecturer and researcher in the Computer and Communication Systems Department. His Ph.D. research was on The Verification of the Distributed Schema for the Electronic Voting System. His major research interests are software engineering, empirical software engineering and system engineering.

Zdenka Prokopova was born in Rimavska Sobota, Slovak Republic in 1965. She graduated from the Slovak Technical University in 1988, with a Masters degree in Automatic Control Theory. She received her Technical Cybernetics Doctoral degree in 1993 from the same university. She worked as an Assistant at the Slovak Technical University from 1988 to 1993. During 1993-1995, she worked as a programmer of database systems in the Datalock business firm. From 1995 to 2000, she worked as a Lecturer at Brno University of Technology. Since 2001, she has been at Tomas Bata University in Zlin, in the Faculty of Applied Informatics. She presently holds the position of Associate Professor at the Department of Computer and Communication Systems. Her research activities include programming and applications of database systems, mathematical modeling, computer simulation and the control of technological systems.

Measurement and simulation of electromagnetic interference in low frequencies range

Jiří Otáhal, František Hruška, Stanislav Sehnálek

Abstract—Low voltage electrical installation with frequencies 50 or 60 Hz and voltages of 110 or 240 V are almost omnipresent in domestic homes, office spaces and industrial environments. These electrical installations are adjoined to electrical devices, other metallic cables, such as metallic data transmission cables and living organisms. Voltage and current in cables, which are commonly used for low voltage electrical installations, create an electromagnetic field around these cables. This intensity of electromagnetic field which electrical installation cables or especially single phase conductors create, depends on the magnitude of the current, magnitude of voltage, type of used cable and the distance between cable and the victim of influence of electromagnetic field. In this article, the electromagnetic field created by low voltage electrical installations is measured and simulated.

Keywords— electromagnetic field, electromagnetic wave, interference, influence interference, electric smog.

I. INTRODUCTION

ELECTROMAGNETIC interference (EMI) is the process of the emission and immission of electromagnetic field or electromagnetic radiation. This emission from electric devices or electrical lines generates electromagnetic field or radiation into free space. The immission is a state of environment, where a field is created, and depending upon specific conditions, this field affects other electrical equipment. The quality of the electrical arrangement is given by electromagnetic compatibility (EMC) – namely, the generation of the electromagnetic field, i.e. the electromagnetic interference and by immunity of electrical devices to this field, i.e. their electromagnetic susceptibility. [7,8,10] This immunity could be improved by the physical construction of an electrical device, i.e. the electrical device's shielding or the use of cables with shielding. Another method

This paper is supported by the Internal Grant Agency at Tomas Bata University in Zlín, project No. IGA/51/FAI/14/D and Internal Grant Agency of Tomas Bata University in Zlín, Faculty of Applied Informatics IGA/FAI/2014/015

Jiri Otahal is with the Department of Electronics and Measurement, Faculty of Applied Informatics, Tomas Bata University, Nad Stráněmi 4511, 760 01 Zlín, Czech Republic (e-mail: otahal@fai.utb.cz. www.fai.utb.cz).

Frantisek Hruska is with the Department of Electronics and Measurement, Faculty of Applied Informatics, Tomas Bata University, Nad Stráněmi 4511, 760 01 Zlín, Czech Republic (e-mail: hruska@fai.utb.cz. www.fai.utb.cz).

Stanislav Sehnalek is with the Department of Electronics and Measurement, Faculty of Applied Informatics, Tomas Bata University, Nad Stráněmi 4511, 760 01 Zlín, Czech Republic (e-mail: sehnalek@fai.utb.cz. www.fai.utb.cz).

is to use electronic filters on inputs and outputs. [8]. Economical aspects play an essential role in this aspect. The optimum costs to ensure the EMC immunity of an electrical device could be 2-10% of the development and manufacturing price. [8] The determination of the optimum balance between the technical solution for the immunity of electrical devices and the costs of these technical solutions is necessary.

One of the couplings between the EMI elements is realized by a cable - for instance a galvanic structure or an environment, such as a capacitive or an inductive structure. A general view of EMI is shown in Fig.1.

The problem of EMI can be universally displayed as a negative way of influencing the correct functioning of an electrical arrangement and instruments, if is not resolved well.[1]

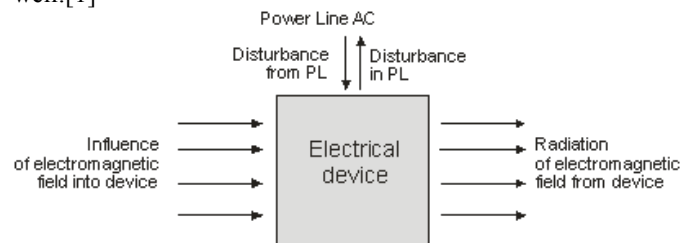


Fig. 1 Scheme of systems of intelligent buildings [1]

The primary focus of this paper is on the influence of electromagnetic field interference from two commonly used cables. The measured interfering electromagnetic fields around a 240V power line are described in this article. The magnitude of influence of electromagnetic field interference is dependent on the distance from cables and the type of cable, which is the source of interference.

II. BINDING BETWEEN ELECTRICAL DEVICES

Bindings between electrical devices cause EMI between the source and the receiver. Figure 2 shows the bindings.

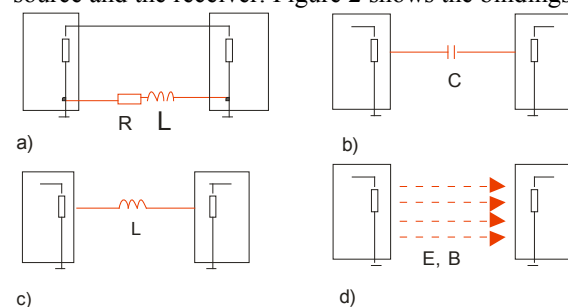


Fig. 2 Kinds of bindings: a) galvanic, b) capacitive, c) inductance, d) electrical (E) and magnetic fields (B). [1]

As seen in figure 2, electromagnetic field binding is the most important kind of these bindings.

Inductive bindings are found in magnetic fields. A magnetic field can be increased by the motion of the charge or by alternation of the electric field or by increasing magnetic inductance in the current flow through the line.

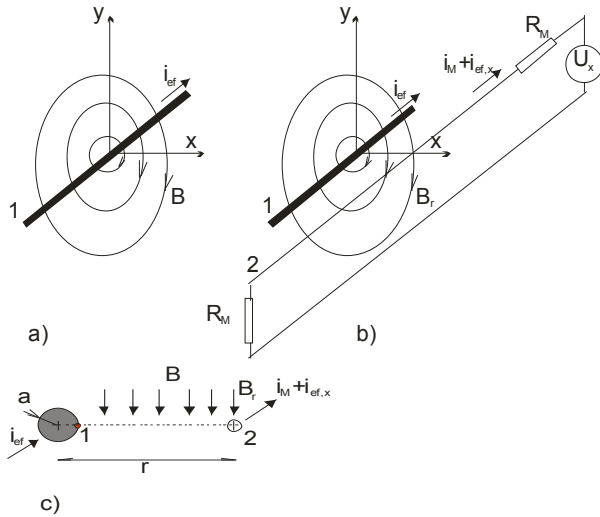


Fig. 3 Scheme of an inductive binding for evaluation of the calculation[1]

A magnetic field is defined by magnetic inductance B in accordance with the relationship for Distance x can be calculated for a conductor with current flow (with U_{rms} and with a 50 Hz frequency):

$$B_x = \frac{\mu \cdot i_{ef}}{2\pi \cdot x} \quad (1)$$

The quadratic equation below is valid for the description of Φ for an induction flux in a flat S, as follows:

$$\Phi = B \cdot S \cdot \cos \phi \quad (2)$$

Where B_{ef} is the effective value of the alternate magnetic inductance induced by a sine-wave frequency, e.g. 50 cps ($B \cdot \cos \phi$).

In close proximity of Conductor 1, there is a loop for measuring a circuit with Conductor 2. Changes in the magnetic field produce voltage U_2 :

$$U_2 = - \frac{d\Phi}{d\tau} = B_{ef,r} \cdot S_v \quad (3)$$

Where S_v is the area of line 2, and $B_{ef,r}$ is the magnetic induction.

This induced interferential voltage is added to the measuring voltage U_M and represents changes U_x . [14]

III. USED EQUIPMENT FOR MEASURING ELECTRIC AND MAGNETIC FIELD

Two kinds of equipment were used for measuring electric and magnetic field:

A. Low Frequency Analyzer ME3851A

The low frequency analyzer ME3851A has switchable frequency range from 5 Hz to 100 kHz with accuracy: $\pm 2\%$, ± 7 digits @ 50/60 Hz RMS. The measurement range for magnetic flux density is 0.1 - 1999 nT, and the measurement range for electric field strength is 0.1 - 1999 V/m. [3]

B. Gaussmeter LakeShore 421

The Hall effect devices used in gaussmeter probes produce a near linear response in the presence of a magnetic field. Gaussmeter LakeShore 421 has frequency range from 10 Hz to 100 kHz with accuracy: $\pm 2\%$ of reading (50 - 60 Hz.) RMS. AC Frequency Response is 0 to -3.5% of reading (10 - 400 Hz.) The measurement range for magnetic flux density is 30 G - 30kG. [4]

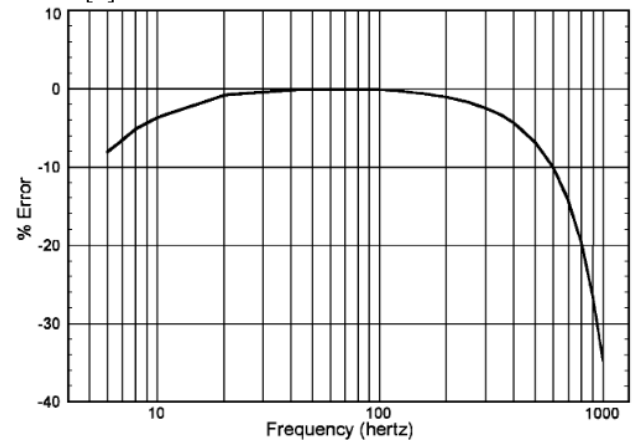


Fig. 4 The AC accuracy specs for sinusoidal input[5]

IV. THE EXPERIMENT ENVIRONMENT

The experiment was conducted on a wooden plate on a wooden table in anechoic shielded chamber. The anechoic shielded chamber has a 3-line low voltage power input power filter. The active length of phase conductor was 433 cm. The conductor had a "U" shape with dimensions 158, 118, 158 cm. The experiment overview can be seen in figure below. The measurements were done in axis between parallel phase conductors. The influence of magnetic fields interference was measured each 2 cm in the 20cm surroundings around cables and after that every 5 cm.

V. MULTIPHYSICS ENVIRONMENT SOFTWARE COMSOL

Comsol is the multiphysical environmental software which is used for simulation. For comparison with experiment could be used finite element method (FEM). For this purpose was used COMSOL Multiphysics 3.5, where domain was setup to 2 dimensional. Comsol used anisotropic mesh which can be seen in fig. 6.



Fig. 5 Experiment overview

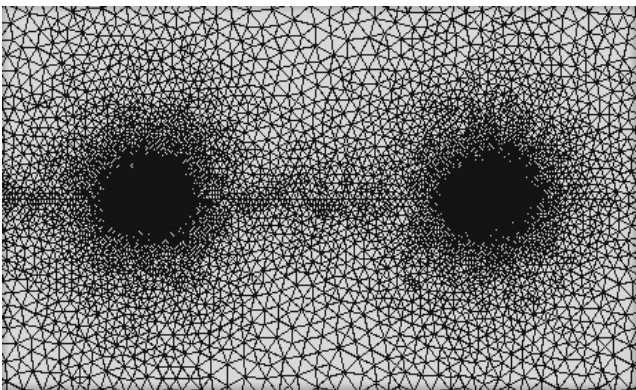


Fig. 6 The mesh for simulations

VI. MEASURING AND SIMULATION OF INFLUENCE INTERFERENCE FIELD

A. Measuring and simulation of influence interference field around single phase conductor

Interference influence magnetic field from single phase conductor was measured. As a source of the interference influence magnetic field was chosen conductor CYA 2,5mm².

The wire was a line with the voltage of 240V and frequency of 50Hz. The magnitude of current was 8.08 A. The electric field was measured by Low Frequency Analyzer ME3851A and the magnetic field was measured by Gaussmeter LakeShore 421. Simulation was done by software Comsol.

B. Measuring of interference influence field around cable CYKY 3x2,5

Interference influence magnetic field from cable 3G2,5 was measured. As a source of interference influence magnetic field, a 3 x 2,5mm² cable was chosen.

A typical connection of the cable was used. The first conductor in the cable was a line with the voltage of 240V and frequency 50Hz. The second was used like a neutral and the third was used like a ground. The magnitude of the current was 8.08 A. The electric and magnetic field was measured by Low Frequency Analyzer ME3851A.

VII. MEASURING AND SIMULATION OF INFLUENCE OF INTERFERENCE FIELD RESULTS

A. Measuring and simulation of the influence of field interference around a single phase conductor

The measurement was carried out and it was compared with data from simulation in software Comsol. As can be seen in fig. 7, simulation data strictly imitate measured values.

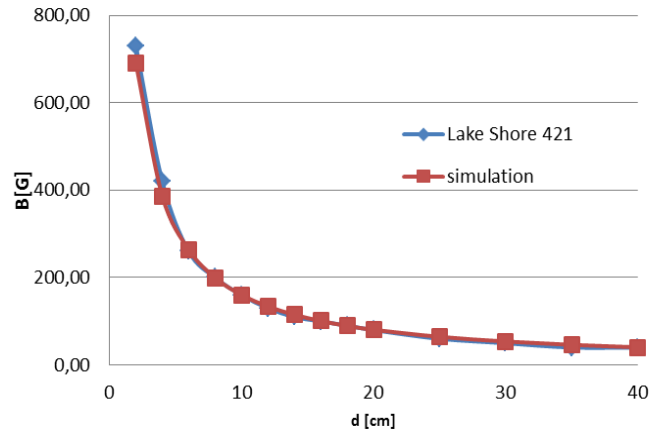


Fig. 7 Comparison between measurement of magnetic field around cable CYA 2.5 and simulation in software Comsol, U=240V and I= 8.08 A

Fig. 8 displays the magnetic field simulation around CYA 2.5 cable in software Comsol, U=240V and I= 8.08 A. A very large area with strong magnetic field can be seen.

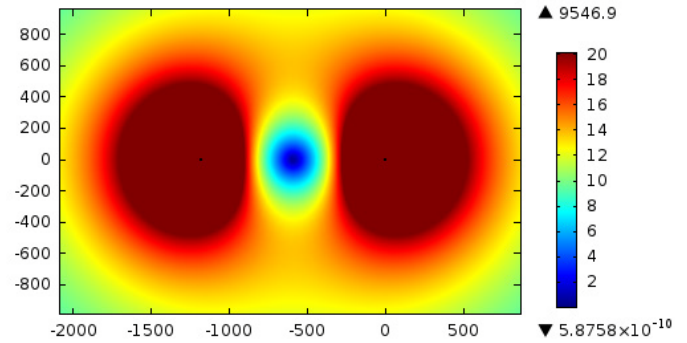


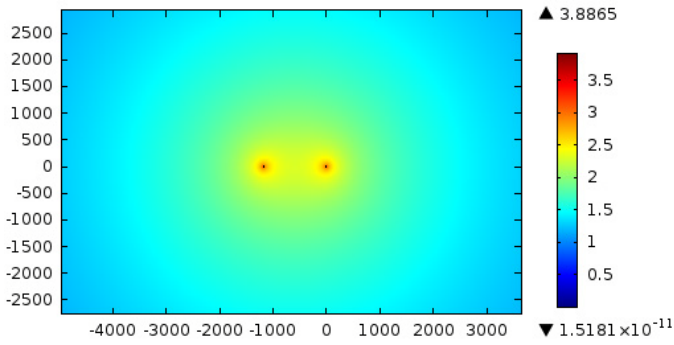
Fig. 8 Magnetic field simulation around CYA 2.5 cable in software Comsol, U=240V and I= 8.08 A

Fig. 9 displays the electric field simulation around CYA 2.5 cable in software Comsol, U=240V and I= 8.08 A. It should be noticed, the distance between cables is 118cm and the range of electric field is more than 2 m from the cable.

Measuring of interference influence field around cable CYKY 3G2,5

B. Measuring the influence of field interference around a CYKY 3G2,5 cable

The results from measurement of magnetic field can be seen in fig. 10 and fig.9 displays results from measurement of electric field.



IX. CONCLUSION

Electric and magnetic fields were measured around cables CYA 2.5 mm² and CYKY 3x2.5 mm². Results of measurement of fields around cables were compared and cable CYA 2.5 mm² had 1.9 times stronger electric field and 85 times stronger magnetic field than CYKY 3x2.5 mm². Electric and magnetic fields were simulated in Comsol software and simulations strictly imitate measured values.

Another part of the work in the next period will be the measurement and the simulation impact of electric and magnetic fields to unified signals used for transmission of measured values.

VIII. COMPARISON OF FIELDS WHICH CREATED CABLES USED FOR MEASUREMENT

A. Comparison of electric field which the cables used for measurement created.

Intensity of electric fields around selected cable were compared. Fig. 9 shows magnitudes of electric field in same places. The electric field around the cable CYA 2.5 is 1.9 times higher than around cable CYKY 3x2.5.

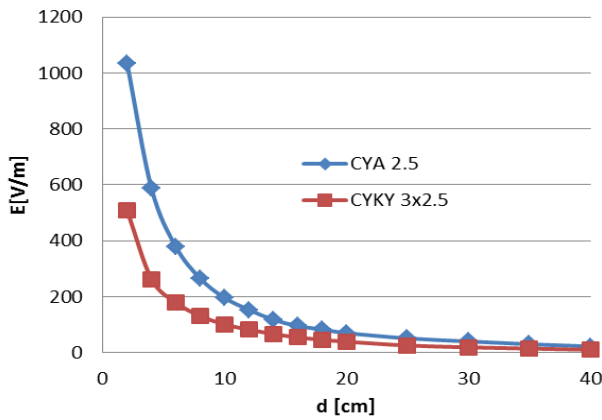


Fig. 9 Comparison of electric fields around cables

B. A. Comparison of electric field which the cables used for measurement created

Intensity of magnetic fields around selected cable were compared. Fig. 10 shows magnitudes of magnetic field in same places. The magnetic field around the cable CYKY 2.5 is 85 times higher than around cable CYKY 3x2.5.

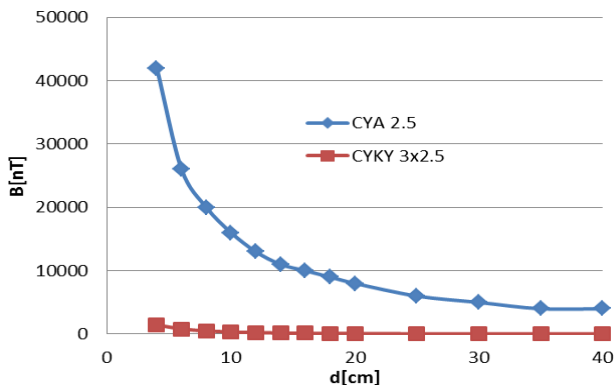


Fig. 10 Comparison of magnetic fields around cables

REFERENCES

- [1] F. Hruska, "Aspects of electromagnetic interference" , *Proceedings of the 4th International Conference on Circuits, Systems, Control, Signals (ICSCS'13)* , vol 1 , no 4, p.33 – 36
- [2] J. Otahal and F. Hruska, "Possible Protections of Embedded Systems Inputs" , *Annals of DAAAM for 2011 & Proceedings of the 22nd International DAAAM Symposium* , p.0813 – 0814
- [3] J. Otahal and F. Hruska, "Dynamic Identification of Circuit with Linear Optocoupler IL300" , *Annals of DAAAM for 2011 & Proceedings of the 22nd International DAAAM Symposium* , p.0817 - 0818
- [4] J. Otahal and F. Hruska, "Aspects of electromagnetic interference in low frequencies ranges (ICCC 2014 is part of the IEEE conferences — Submitted for publication)," Aspects of electromagnetic interference in low frequencies ranges. submitted for publication.
- [5] "User's Manual Model 421 Gaussmeter". Retrieved December , 2013 Available: <http://www.lakeshore.com>
- [6] "Low Frequency Analyser ME3851A". Retrieved December , 2013 Available: <http://www.gigahertz solutions.de>
- [7] J. Carr, *The Technician's EMI Handbook: Clues and Solutions*. Butterworth-Heinemann .2000.
- [8] F. S. Barnes and B. Greenebaum, *Biological and Medical Aspects of Electromagnetic Fields*. CRC Press Taylor & Francis Group ed , Vol . .2007.
- [9] S. Tumanski, *Principles of electrical measurement*. Taylor&Francis Group. 2006.
- [10] J. Svacina, *Elektromagnetická kompatibilita : Principy a metody*. Vysoké učení technické v Brně. 2001.
- [11] J. Balate, *Automatické řízení*. Praha. BEN. 2003.
- [12] J. Corriou, *Process control : Theory and applications*. Springer . 2004.
- [13] J. Otáhal, "Protections of embedded systems inputs", *Proceedings of 13th WSEAS International Conference on AUTOMATIC CONTROL, MODELLING & SIMULATION (ACMOS '11)*, p. 407-411
- [14] E. DARIE, "Signal Processing in measuring Electromagnetic Interference", *In Signal Processing in measuring Electromagnetic Interference*, s. 57-60.

Power Spectral Density in the RFID systems and its impacts in celular systems

Leandro R. Sergio, Maria L. R. P. Dias, Sergio L. Pereira and Eduardo M. Dias

Luciano Gualberto, trav. 3, n. 158, São Paulo/SP, Brazil, CEP 05508-970 (emdias@pea.usp.br).

Abstract— The use of wireless communication technologies is growing around the world. The need for mobility and the technological advances in this segment helps its dissemination. The RFID (Radio Frequency Identification) technology is another technology that also is growing in users number and applications. In Brazil, these technologies operate in a very close frequency range and the challenge of ensure an operation without interferences belong to the ANATEL (Brazilian Agency of Telecommunication). This paper presents the results of a study that analyzes the operating conditions of the RFID technology by the spectral power density focus, and evaluates its impacts in cellular communications systems. This paper presents the operational requirements for RFID, the problems in the homologation process and alternatives to allow the correct use of this technology in Brazil. The proposed alternatives can help the ANATEL in the improvement process of the existing requirements and can help other countries to solve similar operating problems.

Keywords— RFID (Radio Frequency IDentification), GSM, Spectral Power Density

I. INTRODUCTION

The RFID technology (Radio Frequency IDentification) has been consolidating in the last 10 years as the most applied in identification, traceability and intelligent transportation systems.

Results from a research carried out by the AUTO-ID LABS - a laboratory network that has headquarters in USA, Europe, Asia and Oceania - with 1247 companies pointing out that 47% of these companies are using RFID in its process and that other 37% are planning, testing or implementing solutions that consider the RFID use.

L. R. Ruzene is a system analyst of CNPq and a MSc student at Escola Politécnica da Universidade de São Paulo (Polytechnic School of the University of São Paulo) and (lsergio@cpqd.com.br).

M. L. R. P. Dias is a PhD student at Escola Politécnica da Universidade de São Paulo (Polytechnic School of the University of São Paulo) (lidiadias@pea.usp.br).

S. L. Pereira is associate professor of the Escola Politécnica of the Universidade de São Paulo. PhD in Electric Engineering from EPUSP; MSc in Robotics Systems and Applications from Coventry University (England) and Electric Engineer from Faculdade de Engenharia de São Paulo. He is a professor at the undergraduate and graduate courses and mentor of master's and doctor's degree programs of the Polytechnic School of USP. He is professor of the MBA programs of BSP (Business São Paulo School) and Pontificia Universidade Católica de São Paulo (PUC-SP). He is a consultant in Eco-Economics and Industrial Automation. (sergio@pea.usp.br)

E. M. Dias is full professor of the Escola Politécnica of the Universidade de São Paulo and coordinator of GAESI - Grupo de Automação Elétrica em Sistemas Industriais, a research group of the Electrical Energy and Automation Department, Escola Politécnica, Universidade de São Paulo, Av. Prof.

Fig. 1 shows the scenario of RFID utilization based on the AUTO-ID LABS' research

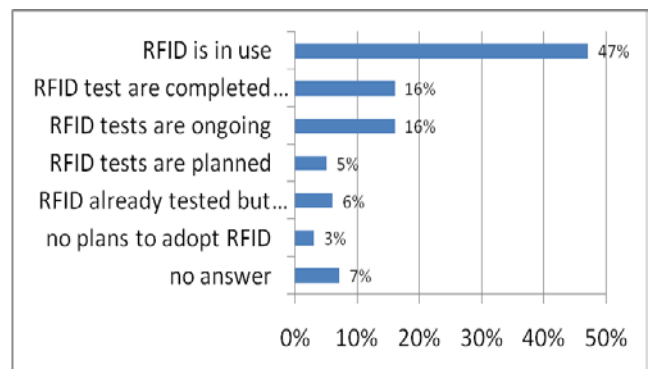


Fig. 1 – Status of RFID adoption.

Source: AUTO-ID LABS Status of RFID adoption – 2009.

In accordance to this research, more than half of applications are based in the UHF (Ultra High Frequency) solutions (Fig. 2).

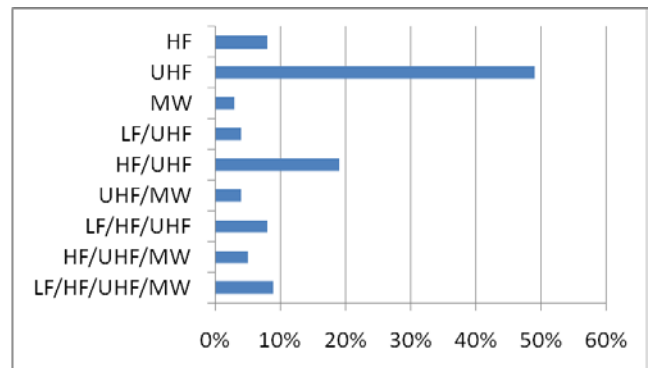


Fig. 2 – Frequency range applied in RFID applications.

Source: AUTO-ID LABS Status of RFID/EPC adoption – 2009.

The advantage of the UHF solutions relative to the other frequency bands is mainly due the existence of standardized protocols, for example, EPCglobal Class 1 Gen 2, technical characteristics (range, type of coupling and components dimensions) and due the availability of tags and readers.

This paper is limited to the analyze of 915 MHz frequency band, mainly because this is the most important frequency

range in RFID (in terms of adoption) and because this is the nearest frequency range of GSM systems.

In Brazil, ANATEL's data show the growth of RFID adoption. Information of the SGCH (System of Management of Homologation) shows that RFID systems occupied the 15th position in the homologated products ranking in 2011 and came to occupy the 9th position in 2012.

The RFID system need to be homologated to operate in Brazil. The establishment of the requirements is a responsibility of the ANATEL that defines it in the Resolution number 506/2008 that cover the Equipments for Restricted Radiation.

The regulation, defined the requirements that allows the operation of the Restricted Radiation systems, including RFID, without interference in primary or priority systems, for example cellular systems.

These requirements defines the frequency range and the limits for spurious or harmonics emissions for a large range of equipments and applications.

In the Section XII of Resolution 506 defines the requirements for RFID systems homologation. In accordance with this section the frequency range attributed to UHF RFID systems operation is from 902 to 907,5 MHz and from 915 to 928 MHz.

Differently of the frequency range attributed to RFID systems by FCC (Federal Communications Commission) range from 902 to 928 MHz, the brazilian frequency range is divided by a gap devoted to support the operation of the GSM 900 system.

Thus, considering the proximity between these technologies, the RFID equipment is more susceptible to produce and receive interference, when we compare it with the american (FCC) system.

Analyzing the ANATEL requirements is clear the similarity with the FCC requirements, once that the ANATEL's requirements clearly are based on the RFID requirements established by FCC..

This similarity just isn't true when are analyzed the requirements for three points: Transmission Power, Frequency Range and Power Spectral Density.

The imported equipment sold in Brazil has to be homologated by the ANATEL. However, they has to be adapted via firmware to set a new limit for power transmission (1W or 30 dBm) and adequated to allow the operation in the brazilian frequency range (902-907,5 and 915-928 MHz).

Considering the power spectral density level, both equipment, national and imported has some difficulty to be in conformance with the existent requirements. The problem is more complicated for equipment designated to operate in the SINIAV (brazilian system for automatic vehicle identification), because this system has a different frequency range, shorter than those of ANATEL and FCC.

In the next chapters, this paper presents test results to confirm the problem and give some alternatives to solve it. Additionally, the impacts of the behavior (in simultaneous operating) between both technologies, GSM and RFID, focusing the power spectral density level, will be analyzed.

II. POWER SPECTRAL DENSITY IN RFID SYSTEMS

A. Existing Requirements

Nowadays, the existing conformance requirements related to power spectral density are analyzed in the ANATEL Res. 506, in the section XII. The article N°53 says that: "The peak of power spectral density in any frequency range with 3KHz, during any time interval of continuous transmission, shall not be higher than 8 dBm". However, this requirement is not adherent with the RFID systems characteristics and it can't be obeyed.

This problem was confirmed in tests performed using RFID reader conFig.d to operate in the ANATEL frequency range.

Considering that RFID tags don't have a source, a continuous wave signal is transmitted by the reader with the modulated signal to provide the needed power to the tags, during all the process of communication between tag and reader.

This CW (Continuous Wave) signal is spread in the RFID dedicated frequency band using Frequency Hopping technique, with pseudo random sequence. The peak of this signal has spectral width equal Zero Hertz (Hz) and always passes thru the filter (RBW – Resolution Band Width), used in the spectral analyzer. Thus, the P.S.D (Power Spectral Density) measurement in a 3 kHz filter during any transmission time interval will extrapolate the +8 dBm limit, once that the ASK (Amplitude Shift Keying) modulation is applied and the P.S.D varies between +27 and +30 dBm, depending of the modulation index and of the power supply entropy (typically 50%). In this cases it is possible to consider that the P.S.D of a signal is equal of the transmitted power (usually +30 dBm).

Fig. 3 shows a typical RFID transmission signal, while Fig. 4 shows a measurement result that presents the conditions described in this section.

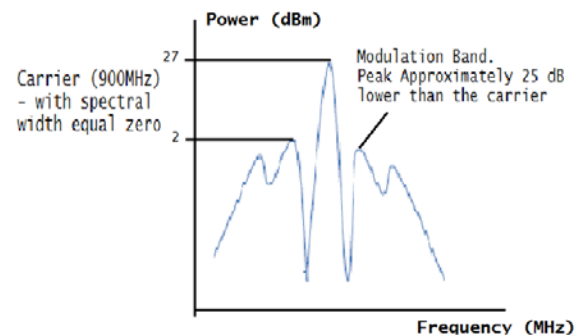


Fig. 3 – Spectrum of a RFID signal (PIE) modulated in DSB-ASK - Source: (C. Vieira e A. L. Xavier Jr., 2011)



Fig. 4 – Power spectral density measured with 3 kHz filter in 915,5 MHz.

Source: Experiment conducted by the authors

The measurement presented in the Fig. 4 was made using a device transmitting the maximum power allowed by the Brazilian national requirements, in frequency hopping mode and the device was connected in a spectral analyzer using a cable. All circuit losses were offset and are shown in the respective Fig..

As is shown in the Fig. 4, the measured P.S.D values based on the Res. 506 requirements reach values close to the transmitted power values. Thus, the need for a new approach to P.S.D in the Res. 506 becomes clear, which will be evaluated in the next section of this article.

B. New alternatives

1. FCC Techniques

Due the synergy between the American and Brazilian regulations. The first analyzed method is applied in the FCC homologation process.

The FCC publication CFR-2009-title47-vol1-part 15 47 (10-1-09 Edition) in the section 15.247 contains specifications and limits for RFID systems operating in a 902 to 928 MHz frequency range.

Differently of Res. 506, the FCC regulation does not analyze the P.S.D for the RFID equipment. For these systems, which operate in the Frequency Hopping mode, the American agency just analyzes the occupied band, the number of hops and the average channel occupation time. This way, the P.S.D is indirectly guaranteed.

For other systems that operates in frequency hopping, the Res. 506 has a section (section IX) that uses the occupation time technique, it is an equivalent technique if compared with the measure of P.S.D. However the occupation time established in section IX cannot be applied for RFID systems, because they are designed for systems that does not have high levels of spectral energy concentration, specially systems that uses a CW signal during all transmission, as happens with RFID technology.

The FCC's requirements specify that "For frequency hopping systems operating in the 902-928 MHz band: if the 20 dB bandwidth of the hopping channel is less than 250 kHz, the system shall use at least 50 hopping frequencies and the

average time of occupancy on any frequency shall not be greater than 0.4 seconds within a 20 second period; if the 20 dB bandwidth of the hopping channel is 250 kHz or greater, the system shall use at least 25 hopping frequencies and the average time of occupancy on any frequency shall not be greater than 0.4 seconds within a 10 second period.

The maximum allowed 20 dB bandwidth of the hopping channel is 500 kHz".[6]

However this requirement is not totally applied to Brazilian reality. It is necessary to fit the average time limits for channel occupation and the number of hops frequencies (not coincident), due the existent frequency gap from the 907,5 to 915 MHz in the Brazilian frequency plan, for RFID systems.

Below, this article presents a proposal for a new requirements, which fit to the Brazilian requirements for systems that operate in a 902 to 907,5 and 915 to 928 MHz frequency band.

If the 20 dB bandwidth of the hopping channel is less than 250 kHz, the system shall use at least 35 hopping (not coincident) frequencies and the average time of occupancy on any frequency shall not be greater than 0.58 seconds within a 20 second period; if the 20 dB bandwidth of the hopping channel is 250 kHz or greater, the system shall use at least 17 hopping frequencies and the average time of occupancy on any frequency shall not be greater than 0.58 seconds within a 10 second period.

These adaptations of the limits were validated in laboratory tests which results are shown in the Fig. 5 and 6.

The measurements of the occupation time were made with RFID system operating at frequency hopping mode, in the Res. 506 frequency band, and with the reader output connected to the spectrum analyzer using a radiofrequency cable.

To get the occupation time, initially is necessary to determine the pulse duration. Fig. 5 shows the results of pulse duration measurement.

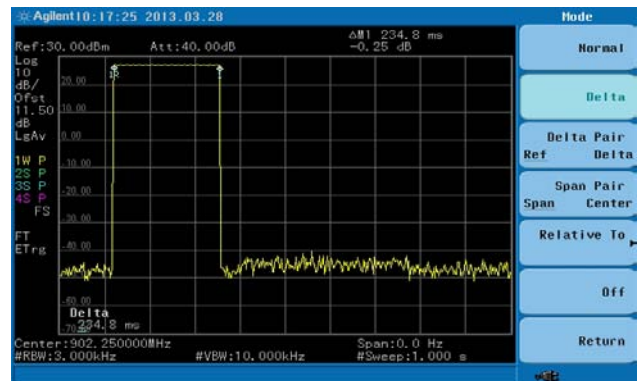


Fig. 5 – Measurement of the pulse duration. Source: Experiment conducted by the authors

The analyzed system presents the 20 dB bandwidth of the carrier level less than 250 kHz.

Thus, the number of events for the same channel was measured for an period of 20 seconds. (with zero span and sweep time of 20s), as shown in Fig. 6.

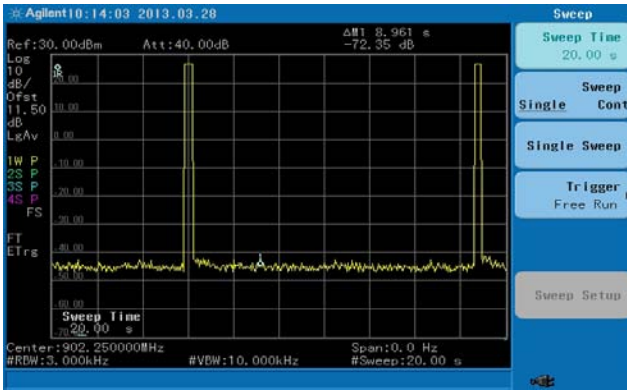


Fig. 6 – Occurrences in 20 seconds.

Source: Experiment conducted by the authors

As is shown in Fig. 8, were detected two occurrences in a 20s period. Multiplying the number of occurrences by the pulse duration (measured in Fig. 7), allows to acquire the channel occupation time. In this case 469,60 ms.

It can be drawn the conclusion that the suggested adaptation (of the FCC original requirements) and the applied technique are adherent with the Brazilian system characteristics, for ANATEL's frequency range.

However the situation is not the same for the SINIAV, due the difference in the frequency range, that is restricted to the interval between 915,25 to 927,75 MHz, the systems uses just 26 hopping frequency, different of ANATEL's frequency band that commonly uses 37. This way the carrier remains more time in the same channel, increasing the P.S.D level and the occupation time.

Fig. 7 shows the results of measurement of the P.S.D peak, using a spectrum analyzer with average peak detector, the average P.S.D peak for SINIAV frequency band were 12,70 dBm The extrapolation of the suggested time limit, due the reduced hopping frequency number, shown in Figs 8 and 9, indicates that value for the occupation time were 720,72 ms (pulse duration x number of events).

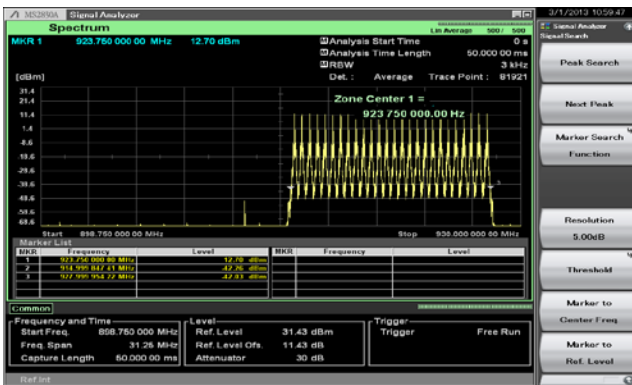


Fig. 7 – Power Spectral Density for a SINIAV systems.

Source: Experiment conducted by the authors

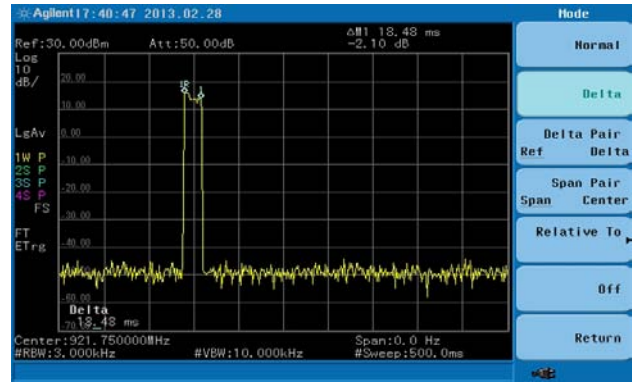


Fig. 8 – Power Spectral Density for a SINIAV systems.

Source: Experiment conducted by the authors

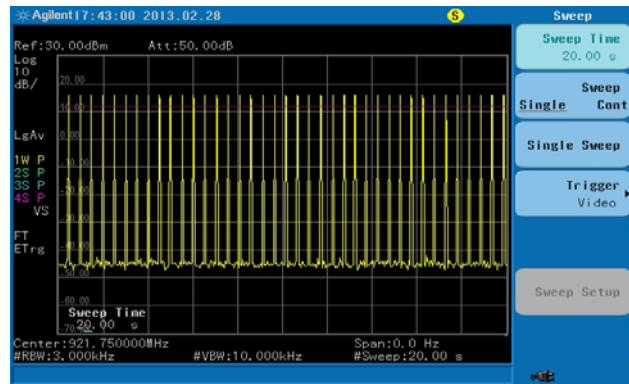


Fig. 9 – Number of events for SINIAV.

Source: Experiment conducted by the authors

To solve problem with the power limit and occupation time extrapolation for SINIAV, Vieira (2011) proposed the use of intercalated frequency hopping with distances less than the channel width.

2. Intercalated Frequency Hopping

In his Vieira (2011) analyzes the existing requirements for the measurement of P.S.D question and defines that the peak of the P.S.D does not depend on the frequency band but on the number of frequency hopping channels in to the same band.

The Vieira (2011) suggests the adaptation in the distance between the frequency hoppings which allow a "x" number of hoppings to get a P.S.D value adjusted to ANATEL requirements.

According to Vieira there are necessary 114 frequency hopping to reach the P.S.D level in conformance with ANATEL, for a limit of +8dBm.

Comparing both Figs 12 and 13 it is possible to verify the reduction in the P.S.D peak when more than 37 frequency hoppings are used.

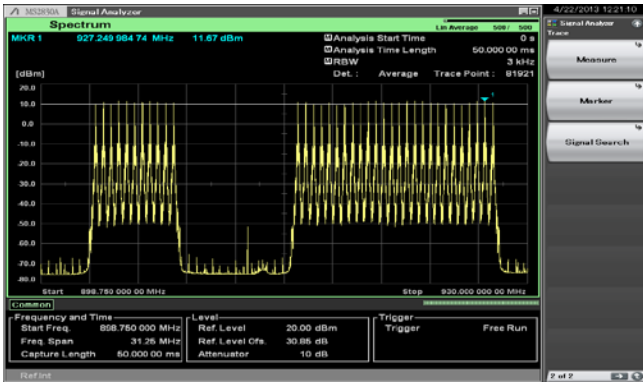


Fig. 10 – P.S.D for 37 frequency hops.
Source: Experiment conducted by the authors

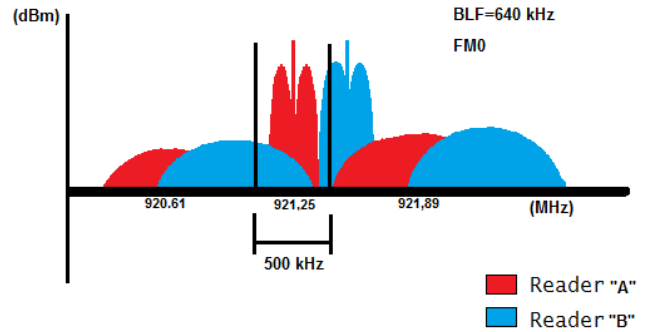


Fig. 12 – Channel superposition.
Source: Experiment conducted by the authors



Fig. 11 – P.S.D for 62 frequency hops.
Source: Experiment conducted by the authors

In order to verify this performance reduction, in cases where two or more readers are operating simultaneously in the SINIAV frequency band (in FM0 and BLF=640 kHz), some tests were performed inside a semi anechoic chamber (see Fig. 13) where two readers (separate by at least 20 dB) and the time to read 50 EPC C1 Gen2 tags were measured. The results (see Table 1) were compared with a reference measure that uses just one reader.

However, analyzing other characteristics of RFID system, based on the SINIAV specifications, it is possible to observe that the intercalated frequency hopping technique or any other that uses distances between frequency hoppings less than a width band of the channel, decrease the system performance, mainly in dense reader situations.

This occurs because the SINIAV's bandwidth is 500 kHz whilst the link frequency of the tag response (BLF) is 320 or 640 kHz, the response signal extrapolates the frequency limit of a transmission channel and occupies the eventual "space" of a next channel. Thus, when more than one reader is operating simultaneously the tag response signal that was sent for a reader "A" may extrapolate the limit of this transmission and be received by a reader "B", considering that both operate in frequency hopping mode with aleatory hops.

Fig. 12 shows the superposition condition and the channel extrapolation, that occurs when the frequency interval between the hops is less than a bandwidth.

Table 1 Results of channel superposition measurements

Baseline	
No of readings	Average time (ms)
50	36,67
SINIAV FHSS - portal A and B - ref. A	
No of readings	Average time (ms)
50	57

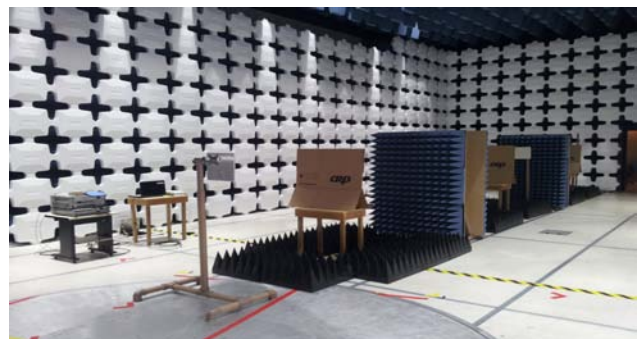


Fig. 13 – Test Setup.
Source: Experiment conducted by the authors

As is shown in Table 1, the reading performance based on the reading time of 50 tags decreased 55%. It proves that condition, that considers intercalated hops, although reduces the P.S.D peak, lowers the system performance in SINIAV

mode. Thus, it is possible to expect that it also occurs in systems that operates in other conventional systems (Tari 25µs, BLF 250 kHz and Miller 4), due to the increase of the number of hops within the same frequency band which also increases the probability of overlapping hops and channel extrapolation.

Additionally, it is very important to consider the performance interactions between RFID and GSM for establishing new limits for P.S.D. Since that these technologies operate in very close frequency bands, and that RFID does not have priority in case of interferences being a secondary operation technology.

The next section of this paper will explore the impacts of the interactions between RFID and GSM.

III. RFID VERSUS GSM ANALYSIS

A. Test Description

To evaluate the impacts of the performance loss caused by interferences, we used a setup that allowed the simultaneous operation between RFID and GSM, allowing the reproduction of a situation where the mobile phone was positioned near a RFID portal. (during an inventory operation).

The mobile phone was connected with a base station simulator (BSS) operating in GSM 900, in the channels 88 and 124, the nearest points from RFID frequency band. The analysis of the performance was based on the Bit Error Rate (BER).

The analysis of the RFID system performance was made based on the reading time of 50 EPC C1 Gen2 tags. Initially the RFID system was setup to operate in the ANATEL frequency band and after to operate in the SINIAV frequency band.

The mobile was positioned near the RFID tags reproducing a situation where the user is calling while passing thru the RFID portal (for example a SINIAV portal on a road).

The RFID system was setup with +30dBm (maximum output power level allowed by ANATEL) and the mobile phone was connected with the BSS using -15dBm.

The test setup inside the semi-anechoic chamber (Fig. 14).



Fig. 14 – RFID x GSM test setup.

Source: Experiment conducted by the authors

B. Impacts of RFID on GSM

Table 2 shows the performance loss caused in GSM system thru the BER increasing.

Table 2 - BER measurements results

Baseline – BER (channels 88 and 124)	
Index	Variation (%)
0	0,0 and 0,2%
ANATEL FHSS - portal A and B - ref. A	
Index	Variation (%)
Vary between 5 and 6	3,2 and 6,4 / 6,4 and 12,7
SINIAV FHSS - portal A and B - ref. A	
Index	Variation (%)
6	6,4 and 12,7

Source: Experiment conducted by the authors

The measured BER in a GSM link, with RFID system turned off, in a 1 minute period was "0" (in reception quality aspects). It means that the maximum degradation in the link was 0.2% (in a frame with 1.99 millions of bits)

When the RFID system is turned on, and operating in the ANATEL frequency band for 1 minute period, the BER variates between the indexes "5" (3,2 to 6,4 %) and "6" (up to 12,7%).

The same indexes were observed in the case of both GSM channels (88 and 124). These compatibility occurs due the similarity between the distances to the RFID frequency band for both channels.

According to ETSI rules [5] the indexes 0 to 5 are considered admissible and the indexes 6 and 7 represents a large probability of the call drop.

In a second phase the RFID system was setup to operate in the SINIAV frequency band. In this moment The measured BER was "fixed" index 6, it represents a 12,7% degradation probability.

C. Impacts of GSM on RFID

Using the same setup as previously, a reference measure was made with the RFID system operating without interferences from GSM. In this case the average time to read 50 tags was 380ms for ANATEL frequency band and 354ms for SINIAV band.

In a second phase of experiment, the GSM system was turned in a voice call mode and the time of reading of 50 tags was measured. It was not possible to analyze the performance loss in the RFID frequency based on the time reading of 50 tags because at the moment when the GSM system is operating the RFID system can not read the total number of tags (50).

D. Evaluation of the Guard Band

Considering the results presented in this paper, the distance needed to reduce the interference level in both cases was investigated.

An analysis with fixed frequency (without hops) was performed and the best achieved result where registered when both (ANATEL and SINIAV) systems had a minimum distance of two hop channel for each edge of the RFID system.

IV. CONCLUSION

Based on the performed analysis it is possible draw following conclusions about the methodologies and limits of measuring the P.S.D only the methodology that considers the occupation time (sub-chapter II - B) presented satisfactory results, in conformance with the requirements and keeping an adherence with the RFID systems characteristics. On the other hand, it is also possible to conclude that it was not possible to find a solution with performance and applicability adequate to the RFID frequency band in the other methodology.

Thus, based also on the analysis of the interference between the technologies, that resulted in a large performance loss for the GSM system, some adjustments in the RFID frequency band and also in the P.S.D limits or in the channel occupation time are necessary.

The final proposal of this paper are new limits for the RFID frequency band, preserving two channels hops of guard band in the lower part of the band and two channels hops in the upper part of the band. Thus, the new frequency band is: 902,25 to 906,25 MHz and 916,25 to 927,75 MHz to systems that does not operate in SINIAV and two channel hops in the lower part of the band to SINIAV systems (frequency range 916,25 to 927,75 MHz).

Additionally, due the changes in the number of hops it is suggested that:

- if the 20 dB bandwidth of the hopping channel is less than 250 kHz, the system shall use at least 33 hopping frequencies and the average time of occupancy on any frequency shall not be greater than 0.620 seconds within a 20 second period;
- if the 20 dB bandwidth of the hopping channel is 250 kHz or greater, the system shall use at least 15 hopping frequencies and the average time of occupancy on any frequency shall not be greater than 0.620 seconds within a 10 second period..

Specifically for SINIAV there are suggested two alternatives:

- adoption the range suggested in this article to other systems (ANATEL - 902,25 to 906,25 and 916,25 to 927,75 MHz), or ;increase of the time of occupancy of the channel to 0.840 seconds with at least 24 hops.

Through the experiments and its results described above, the Authors are hoping to contribute to the creation of new requirements for approval adherent to the characteristics of RFID technology in way that it can operate without causing interference in a system of primary importance in the operation of GSM.

REFERENCES

- [1] ANATEL - AGÊNCIA NACIONAL DE TELECOMUNICAÇÕES. R ESOLUÇÃO NÚMERO 506. Regulamento sobre Equipamentos de Radiocomunicação de Radiação Restrita - Brasília, 2008.
- [2] AUTO-ID LABS, *Status of RFID/EPC adoption*, 2009. Site<<http://www.autoidlabs.org/uploads/media/AUTOIDLABS-WP-BIZAPP-048.pdf>> accessed: 19/05/2013.
- [3] BRASIL. Site do projeto SINIAV. Disponível em: <<http://www.denatran.gov.br/siniav.htm>> accessed 08/10/2012.
- [4] DENATRAN – DEPARTAMENTO NACIONAL DE TRANSITO. *PORTARIA NÚMERO 570. ANEXO II. Especificação da Tecnologia SINIAV - Especificações Técnicas para Homologação do leitor SINIAV da Geração Zero (G0)*.
- [5] ETSI TS 100 911 V8.23.0 (2005-11): Digital cellular telecommunications system (Phase 2+); Radio subsystem link control; (3GPP TS 05.08 version 8.23.0 Release 1999)
- [6] FCC - *Federal Communications Commission - FCC CFR-2009-title47-vol1-part 15 47 - (10-1-09 Edition)*
- [7] Vieira, C.S. Cálculo e Medição da ‘DENSIDADE ESPECTRAL DE POTÊNCIA’ de um Sinal Modulado EM DSB-ASK, Espalhado por ‘SP -FREQUENCY HOPPING’ – Típico de Leitores de RFID. Março 2011.

Parameterization of module for testing of thermal stability in the room

H. Charvátová, M. Zálešák, and S. Sehnálek

Abstract—The paper deals with testing of the thermal stabilization of buildings by using COMSOL Multiphysics software. It describes the possibilities to parameterize the module for simulation the temperature distribution in a room heated by two heat sources. A parameterized model allows you to change the requirements of the geometric dimensions of all elements of the module and their spatial distribution, as well as a choice of physical properties and pasting real measured data needed to assess the distribution of temperature in the room depending on the ambient temperature and the heat input of the considered sources. Parameterization enables to insert all necessary data into COMSOL Multiphysics by using external txt files, which can be up to this end through a helper application in Microsoft Excel. Linking program COMSOL Multiphysics with applications created in Microsoft Excel allows comfortable loading parameters to external users via a web interface without knowledge of the work environment in COMSOL Multiphysics.

Keywords—COMSOL Multiphysics, parameterization of the room module, simulation the temperature distribution, thermal stabilization of building.

I. INTRODUCTION

AT present, the design of the intelligent building is in terms of optimization emphasis on minimizing energy consumption while minimizing investment and operating costs. In the design optimization is needed based on stationary parameters buildings, and also include non-stationary boundary and user conditions. In order to make a comprehensive assessment of all major factors, it is necessary to use a combination of experimental testing with modern computer technology that are continuously being developed for engineering and scientific calculations of stationary and non-stationary processes.

In order to use the available software tools for the simulation of the thermal behavior of systems with accumulation, we performed testing program COMSOL

This work was supported by the European Regional Development Fund under the project CEBIA-Tech No. CZ.1.05/2.1.00/03.0089.

H. Charvátová, Tomas Bata University in Zlín, Faculty of Applied Informatics, Department of Automation and Control Engineering, nám. T. G. Masaryka 5555, 760 01 Zlín, Czech Republic (e-mail: charvatova@fai.utb.cz)

M. Zálešák, Tomas Bata University in Zlín, Faculty of Applied Informatics, Department of Automation and Control Engineering, nám. T. G. Masaryka 5555, 760 01 Zlín, Czech Republic (e-mail: zalesak@fai.utb.cz)

S. Sehnálek, Tomas Bata University in Zlín, Faculty of Applied Informatics, Department of Automation and Control Engineering, nám. T. G. Masaryka 5555, 760 01 Zlín, Czech Republic (e-mail: sehnalek@fai.utb.cz).

Multiphysics using the comparative tests described in the job 34 [1], published within the IEA BESTEST methodology. The results confirmed the suitability of the program COMSOL Multiphysics [2], [3].

Now we want to use the program Comsol Multiphysics to create a complex software tool for the assessment of energy performance of selected models of building parts. Simultaneously, we would like to ensure the possibility of universal use of this tool not only for specialists who are trained to control the software, but also works for external users via a web interface.

For this purpose we are preparing a set of room modules in which users can specify both geometric and physical properties. In the subsequent sections we describe the chosen procedure of parameterization using the example of one of the modules, and also mentioned the possibilities of external loading of parameters required by the program Microsoft Excel.

II. DESCRIPTION OF THE TESTED MODULE

As a module we used the room heated by two heat sources, as you can see in Fig. 1.

For the simulation of unsteady heat transfer, the COMSOL Multiphysics uses the finite element method. The thermal analysis is based on solving partial differential equation under the defined initial and boundary conditions.

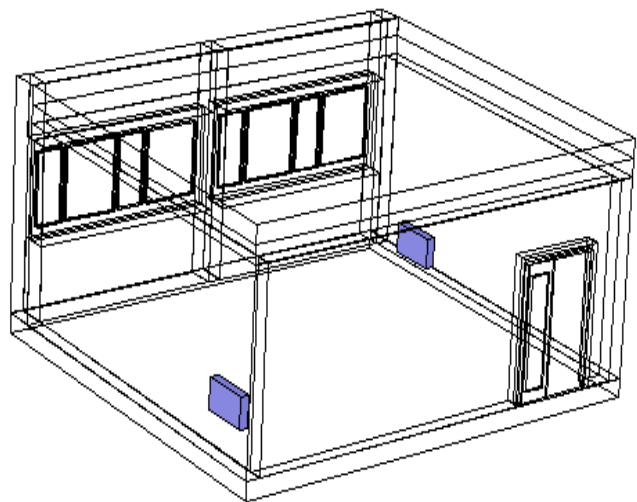


Fig. 1 Geometry sketch of the tested room module

The heat transfer in solids is computed by equation (1):

$$\rho \cdot c_p \frac{\partial T}{\partial t} - \nabla(k \cdot \nabla T) = Q \quad (1)$$

The non-stationary heat transfer in the air inside the room is computed according to balance equation (2):

$$\rho \cdot c_p \frac{\partial T}{\partial t} + \rho \cdot c_p \cdot u \cdot \nabla T = (k \cdot \nabla T) + Q \quad (2)$$

For the heat flux between walls of the room and air outside the room it holds

$$q_0 = h(T_{ext} - T) \quad (3)$$

where:

- ρ - density, [kg.m⁻³]
- c_p - heat capacity at constant pressure, [J.kg⁻¹.K⁻¹]
- k - thermal conductivity, [W.m⁻¹.K⁻¹]
- u - the fluid velocity, [m.s⁻¹]
- Q - the heat source (or sink), [W]
- T - temperature, [K]
- T_{ext} - external temperature, [K]
- h - heat transfer coefficient, [W.m⁻².K⁻¹]
- t - time, [s]
- q_0 - inward heat flux, [W.m⁻²].

The external temperature, temperature of the heat source surfaces and power of the heating sources were measured in dependence on time.

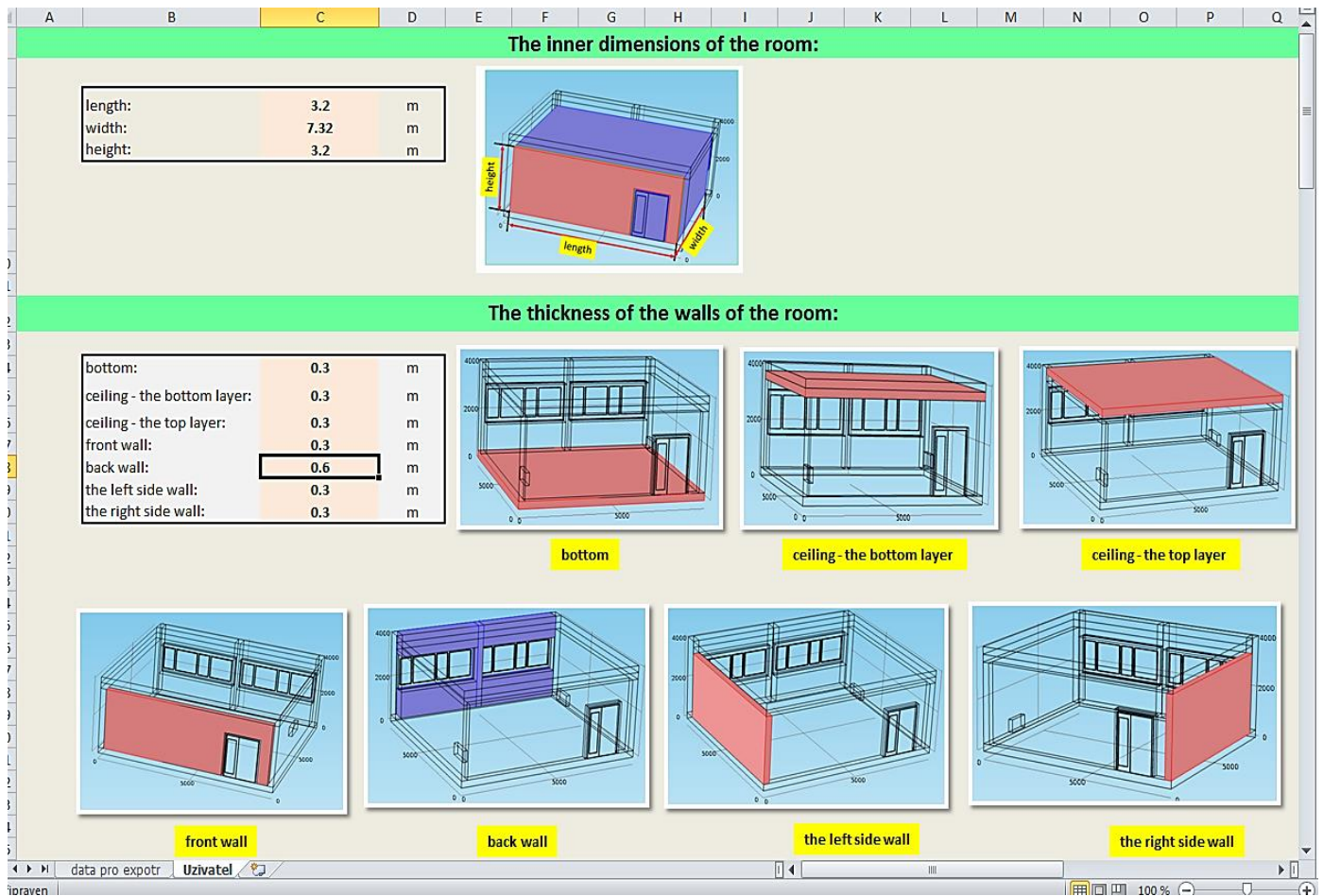


Fig.. 2 User form for insertion of module parameters

III. PARAMETERIZATION OF THE MODULE

In order to be provided to potential users of the module, with the option to change the geometrical dimensions of all elements of the module and also modify the physical

parameters without interfering with the source file in COMSOL Multiphysics, we proposed the possibility of external loading all the required parameters and their subsequent loading into the application itself in the form automatically generated txt files.

For comfortable inserting of the input parameters can be used the form that we have created in Microsoft Excel (Fig. 2). This form is for clarity when entering geometric dimensions accompanied by drawings, in which the required dimensions are marked in color. File with embedded data can be exported to txt file (Fig. 3). Created txt file is then imported into the table designed for definitions of parameters in COMSOL Multiphysics user interface (Fig. 4).

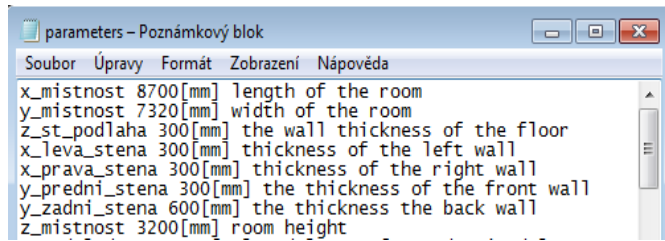


Fig. 3 The txt file with data exported from Microsoft Excel

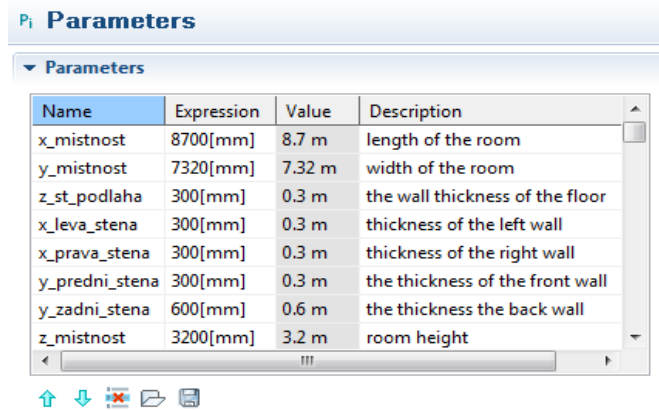


Fig. 4 Table with data imported from txt file into the COMSOL Multiphysics user interface

Also the measured dependences of temperature and power of the heating sources can be imported from txt files into the table for insertion of parameters in the COMSOL Multiphysics user interface (Fig. 5).

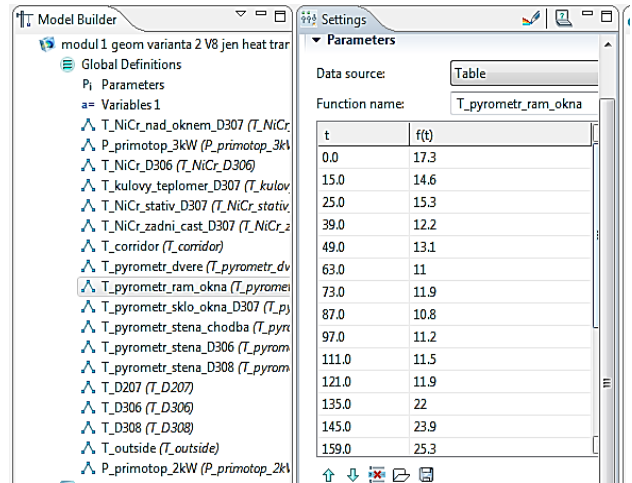


Fig. 5 Table with measured data imported from txt file into the COMSOL Multiphysics user interface

IV. DISPLAY THE RESULTS OF SIMULATION

The distribution of temperature in the room simulated by Comsol Multiphysics under the required input parameters can be displayed as 3D plot and as 2D plot.

The 3D temperature fields in form of slices are shown in Fig. 6. The 2D graph that represents temperature distribution in a required line through the room for a selected time. All computed plots can be exported as a graphic files (bmp, jpeg, png) or a txt files. The 3D plot can be also animated and exported to avi or gif files.

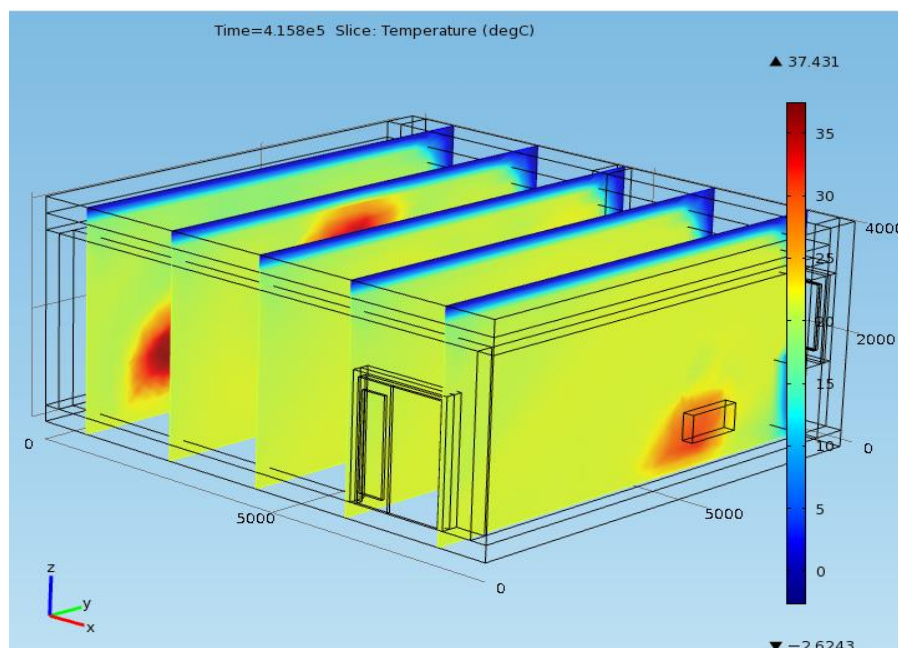


Fig. 6 3D temperature distribution in the room module

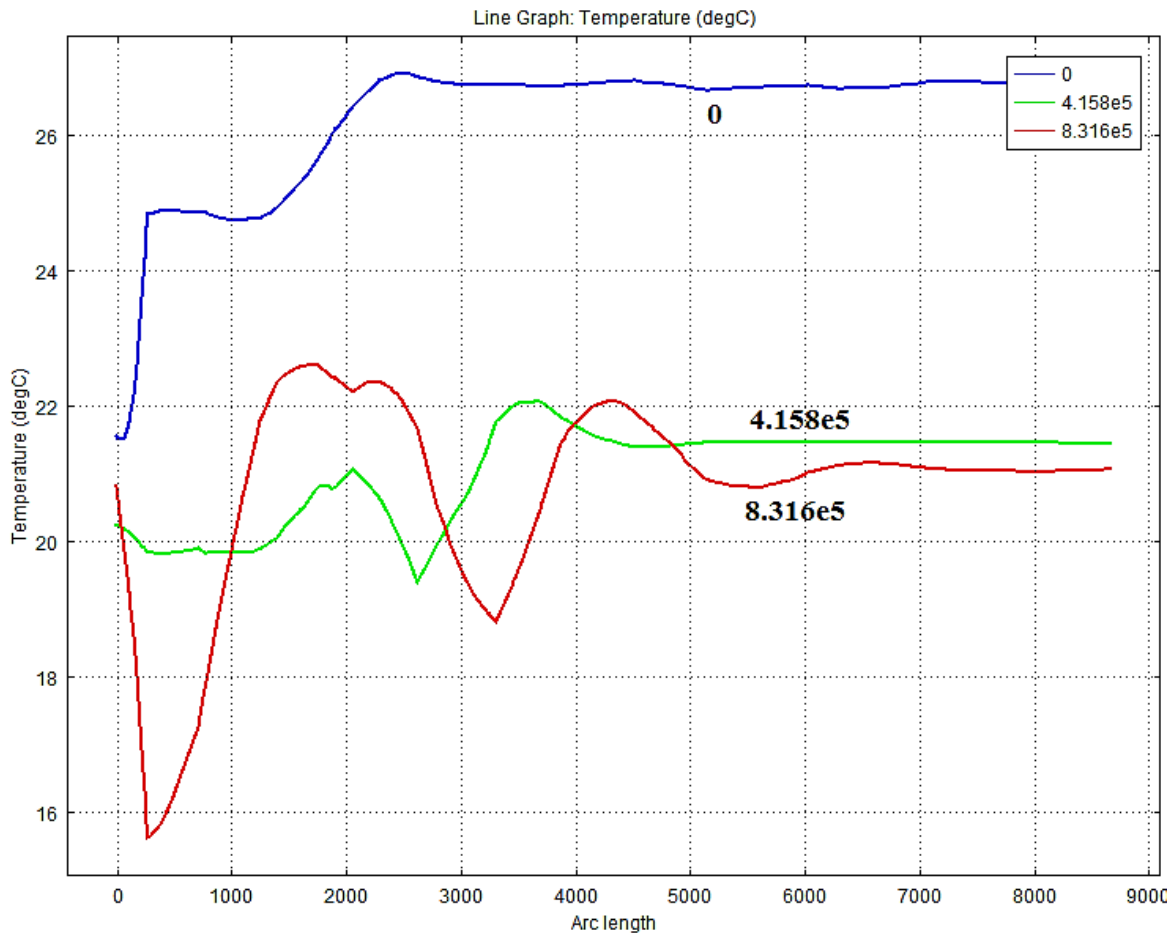


Fig. 7 2D temperature distribution in a required line through the room module

V. CONCLUSION

In the paper described parameterized module allows you to change the geometric dimensions of all elements of the module and their spatial distribution, as well as a choice of physical properties and pasting real measured data needed to assess the distribution of temperature in the room depending on the ambient temperature and the heat input of the considered sources. Parameterization also enables to insert all necessary data into COMSOL Multiphysics by using external txt files, which can be up to this end through a helper application in Microsoft Excel. Linking program COMSOL Multiphysics with applications created in Microsoft Excel allows comfortable loading parameters to external users via a web interface without knowledge of the work environment in COMSOL Multiphysics.

REFERENCES

- [1] J. Neymark and R. Judkoff. (2008). International Energy Agency Building Energy Simulation Test and Diagnostic Method (IEA BESTEST) In-Depth Diagnostic Cases for Ground Coupled Heat Transfer Related to Slab-On-Grade Construction. [Online]. *Technical Report NREL/TP-550-43388*. Available: http://www.ieashc.org/publications/downloads/task34Building_Energy_Simulation_Test.pdf.
- [2] V. Gerlich, "Verification of possibility of using COMSOL Multiphysics as simulation tool for heat transfer calculation in systems with accumulation," (in Czech), Ph.D. dissertation, Tomas Bata University in Zlín, 2012.
- [3] M. Zálešák and V. Gerlich, "Utilization of the Comsol Mutiphysics Programme as a Tool for Modelling of Thermal Behaviour of Building," in *Recent Advances in Automatic Control, Information and Communications*, WSEAS press, Valencia, Spain, 2013.
- [4] H. S. Carslav and J. C. Jaeger, *Conduction of Heat in Solids*. Oxford: Clarendon Press, 2008.
- [5] *Introduction to Heat Transfer Module* (2013), [Online], Comsol. Available: <http://www.comsol.com/model/download/173021/IntroductionToHeatTransferModule.pdf>
- [6] D. Janáčová, V. Vašek, P. Mokrejš, J. Křenek, and R. Drga, "Temperature Fields Solving in Two-Layer Plate with COMSOL Multiphysics Software," in *The 22nd International DAAAM Symposium*, Vienna, Austria, 2011.
- [7] R. Drga, "Nepřesnosti při měření teploty zdroje IR záření termovizní kamerou," (in Czech), in *ARTEP*, Košice, 1 - 19.8. 2012, p. 19.
- [8] R. Drga, "Teplné pozadí a PIR detektory," (in Czech), in *Bezpečnostní technologie, systémy a management 2013*, Zlín, 2013, p. 1-8.
- [9] M. Feriančík, O. Liška, and M. More, "Navigation of industrial manipulator based on computer vision", *Transfer inovací*, vol. 28, 2013, pp. 140-142.

Modelling and Analysis of Neural Network and Perturb and Observe MPPT Algorithm for PV Array Using Boost Converter

NAOUFEL KHALDI, HASSAN MAHMOUDI, MALIKA ZAZI, YOUSSEF BARRADI

Abstract— The maximum power point tracking (MPPT) system controls the voltage and the current output of the PV system to deliver maximum power to the load. Present work deals a comparative analysis of perturb observe, and neural network based MPPT techniques. Parameters values were extracted using Newton Raphson method from characteristics of Shell SP75 module. The simulations have been carried out on MATLAB/SIMULINK platform for solar photovoltaic system connected to boost dc-dc converter. For two MPPT algorithms, Performance assessment covers overshoot, time response, oscillation and stability as described further in this paper.

Keywords— Artificial neural network, dc-dc converter, MPPT, Newton Raphson, Photovoltaic systems.

I. INTRODUCTION

Demand for electrical energy has remarkably increased during the recent years with growing population and industrial progress. Since long time ago, fossil fuels have served as the major source of generating electrical energy. However the transfer of energy resulting from photovoltaic conversion remains relatively weak. Therefore, many tracking control strategies have been proposed in existing literatures, such as perturb and observe, incremental conductance, parasite capacitance, and fuzzy logic methods, etc [1],[2]. But for this work a novel BP neural networks MPPT algorithm has been used. These new control techniques feature advantages of simplicity, high flexibility and less fluctuation around the maximum power point which increase efficiency of the PV system [3]. In [4], Newton Raphson method is used due to the nonlinearity of I-V characteristics of PV module. Selection of appropriate converter is also very important for an efficient PV system. There are a few topologies can be used with PV system for load connectivity, among them boost converter has been selected here due to its available use in standalone and grid connected PV system and simultaneous step up capability [5],[6]. This paper results show that the proposed BP MPPT method can track maximum power point (MPP) in different temperature and irradiation, which has excellent output characteristic of high accuracy and good robustness as compare with traditional method PO. The sequential work flow of this paper is as follows: In section II, complete working procedure of the system has been described.

Section III covers mathematical modelling of PV using a Newton Raphson method, and followed by discussion on boost dc-dc converter and MPPT algorithms in Sections IV and V respectively. Simulation works and results are discussed in Section VI. Lastly, in section VII, a precise conclusion has been added to finalize the work.

II. COMPLETE SYSTEM OVERVIEW

A photovoltaic cell is basically a PN semiconductor junction diode and this cell converts solar light energy into electricity [7]. The complete system block diagram is shown in Fig. 1. After that this energy will be supplied to the load through the buck-boost converter and the converter will be controlled by a MPPT controller. Necessary programming for the PV module and MPPT algorithm has been imposed in Simulink.

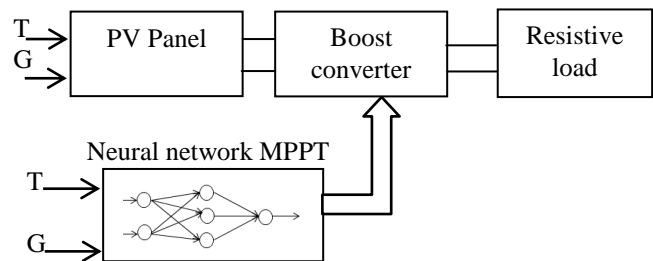


Fig. 1 Schematic arrangement for the complete system

III. PV MODELLING

A. Mathematical Modeling

There are various methods to perform modeling work on the PV module, and among of them is by using mathematical modeling [8-9]. The equivalent circuit of a photovoltaic (PV) array can be depicted in Fig. 2 where I_{ph} is current source of PV array, R_{sh} is an equivalent shunt resistance, R_s is an equivalent series resistance, i_{pv} and v_{pv} are the output current and output voltage of PV array, respectively. In general, for simplicity R_{sh} and R_s are assumed to be open circuit and short circuit, respectively. The simplified mathematical model of the output current is given as[10]:

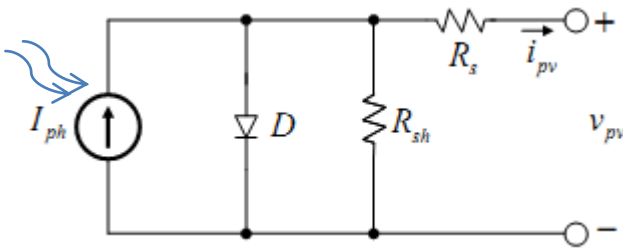


Fig. 2 The equivalent circuit of a photovoltaic array

$$i_{pv} = n_p I_{ph} - n_p I_{rs} \left[\exp\left(\frac{q}{pk n_s} \times \frac{v_{pv}}{T}\right) - 1 \right] \quad (1)$$

Where q is the electron charge, k the Boltzmann's constant (1.38×10^{-23} J/°K), p is the p-n junction ideality factor ($p=1\sim 5$), T is the cell temperature (°K) and I_{rs} is the cell reverse saturation current, n_s is the number of solar cells connected in series and n_p is the number of solar cells connected in parallel.

In addition, the mathematical model of the reverse saturation current is given below:

$$I_{rs} = I_r (T/T_{ref})^3 \exp\left\{\left(\frac{qE_g}{pk}\right)\left(\frac{1}{T} - \frac{1}{T_{ref}}\right)\right\} \quad (2)$$

With

$$I_r = \frac{I_{sc}}{\left[\exp\left(\frac{v_{oc} - v_{pv}}{p n_s v_{tr}} \times \frac{v_{pv}}{T}\right) - 1 \right]} \quad (3)$$

Where T_{ref} is the cell reference temperature, I_r is the reverse saturation current at T_{ref} , E_g is the band-gap energy of the semiconductor ($E_g \approx 1.1\text{eV}$) and V_{tr} is a thermal potential at T_{ref} .

The current source of PV array I_{ph} , varied according to solar irradiation and cell temperature, is given below:

$$I_{ph} = [I_{sc} + K(T - T_r)] \times \left(\frac{E}{E_r}\right) \quad (4)$$

Where I_{sc} is short-circuit current at reference temperature and radiation, E is the solar irradiance and K , the temperature coefficient for short-circuit current. Using the equations 1 to 4 the PV panel can be modelled. In this work the equation of solar module is solved with the help of Newton-Raphson method. A program of solar module is developed in MATLAB software and the different characteristics of solar module are obtained.

B. Newton Raphson Method

In determining the operational point of a nonlinear circuit, Newton Raphson method is commonly used. The method is based on linearizing the nonlinear equations and solving the resulting linear equations repeatedly [10-11]. For example, we will consider solving one variable equation $f(x) = (x \in R, f: R \rightarrow R)$. First, the initial value $x^{(0)}$ should be chosen to be close to the true solution \hat{x} . Considering a Taylor series expansion of $f(x)$ around $x^{(0)}$, $f(x)$ can be transformed to (5).

$$f(x) = f(x^{(0)}) + \frac{df}{dx}\bigg|_{x=x^{(0)}} (x - x^{(0)}) + \frac{1}{2} \frac{d^2f}{dx^2}\bigg|_{x=x^{(0)}} + \dots \quad (5)$$

The third term of (5) is expected to be very small due to the square. Therefore, the linearized model (6) can be formed.

$$f(x) = f(x^{(0)}) + \frac{df}{dx}\bigg|_{x=x^{(0)}} (x - x^{(0)}) \quad (6)$$

Solving $f(x) = 0$ for x leads to (7) on the assumption of $df(I^{(k)})/dI \neq 0$.

$$x^{(1)} = x^{(0)} - \left(\frac{df}{dx}\bigg|_{x=x^{(0)}}\right)^{-1} f(x^{(0)}) \quad (7)$$

If $x^{(1)}$ satisfies $f(x^{(1)}) < \delta$ which is the threshold value of the end condition, $x^{(1)}$ can be determined as the approximate solution of \hat{x} . Otherwise, the above procedure is calculated repeatedly until satisfying $|f(x^{(1)})| < \delta$. An iterative scheme of the method is described by the equation (8).

$$x^{(k+1)} = x^{(k)} - \left(\frac{df}{dx}\bigg|_{x=x^{(k)}}\right)^{-1} f(x^{(k)}) \quad (k = 0, 1, 2, \dots) \quad (8)$$

The graphical illustration of Newton-Raphson method in one dimension is depicted in Fig. 3. The process in Newton Raphson method corresponds to drawing the tangent lines to the curve of $f(x)$ repeatedly.

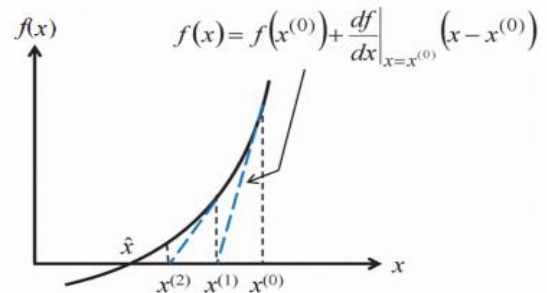


Fig. 3 The graphical illustration of Newton Raphson method in one dimension.

The proposed method using one variable Newton Raphson method, will allow us to calculate the current i_{pv} with the initial value $x^{(0)} = I_{ph}$ as shown in Fig. 4.

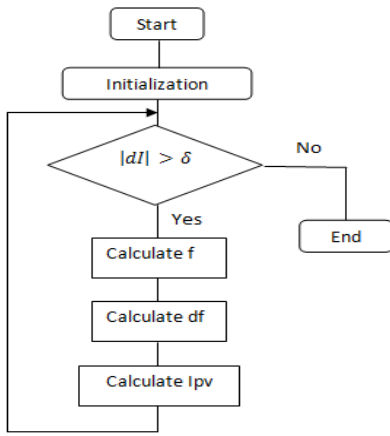


Fig. 4 A flow chart of the proposed method of calculating current i_{pv} of PV

C. Characteristic of solar panels

A complete Simulink block diagram of PV system is demonstrated below:

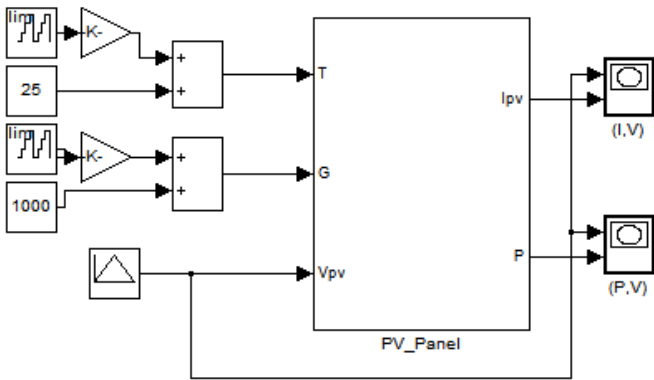


Fig. 5 External view of PV module in Simulink window using Newton Raphson method

Cell parameters are shown in Table I. PV module is made by Shell solar company and product name is SP75.

TABLE I. PARAMETRS OF SHELL SP75

Parameters	Values
Open Circuit Voltage(Voc)	21.7Volt
Short Circuit Current(Isc)	4.8Amp
Voltage at Pmax(Vmpp)	17Volt
Current at Pmax(Impp)	4.41Amp
Maximum Power (Pmpp)	75Watt
Number of Cell	36

With the increment in the temperature short circuit current increases but the open circuit voltage of cell decreases. So the I-V characteristics shift to the left to previous curve. Power output of cell is also decreased. Figs. 6 and 7 show the variation in the characteristics curves at different temperature when the irradiance is kept constant at $1000w/m^2$. Temperature varies from $0^{\circ}C$ to $75^{\circ}C$, where is in degree Celsius.

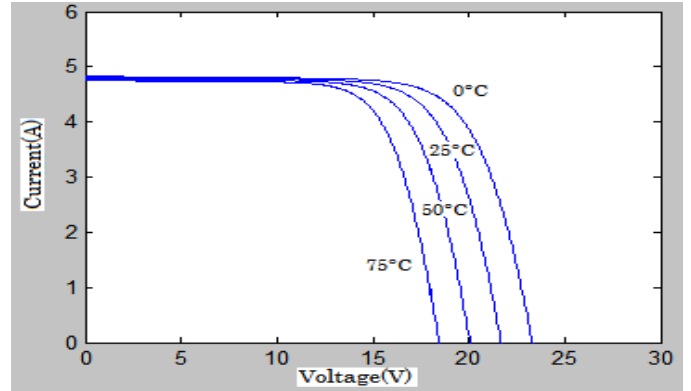


Fig. 6 I-V characteristics of solar module for different temperature

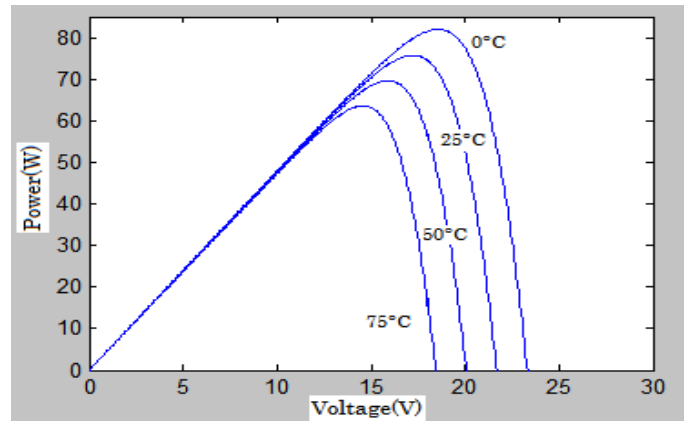


Fig. 7 P-V characteristics of solar module for different temperature

Fig. 8 and 9 show the variation in characteristics curve of the selected PV module by changing irradiance values from $400w/m^2$ to $1000w/m^2$ and $T=25^{\circ}C$. The maximum power is higher if the irradiance is getting higher and for the current, if the irradiance is kept increasing, it also increases.

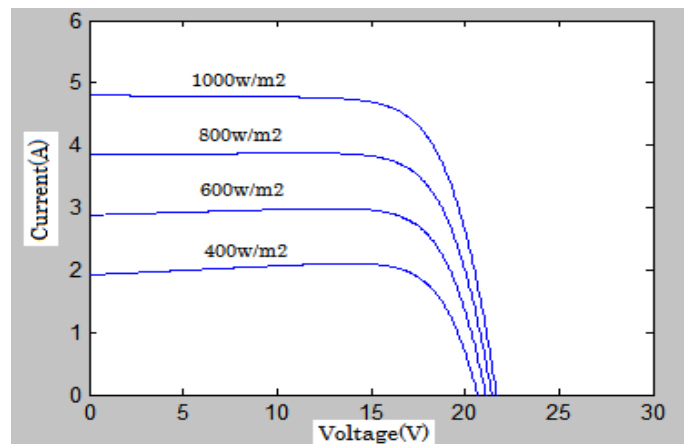


Fig. 8 I-V characteristics of solar module for different irradiance level

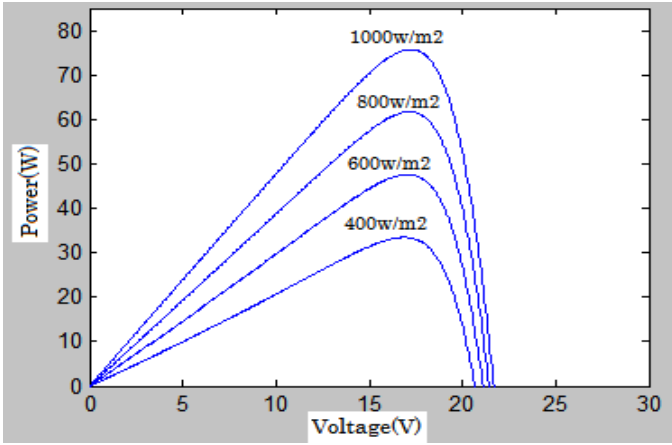


Fig. 9 P-V characteristics of solar module for different irradiance level

IV. DC-DC CONVERTER

DC-DC converters are used to transfer power of solar panel to load side ensuring that maximum power has been transferred [12]. The regulation is normally achieved by pulse width modulation (PWM) and the switching device is normally MOSFET or IGBT. Boost dc-dc converter's function is to step up dc voltage. Fig. 10 shows configuration of dc-dc boost converter with PV as input. Maximum power is reached when the MPPT algorithm changes and adjusts the duty cycle of the boost dc-dc converter.

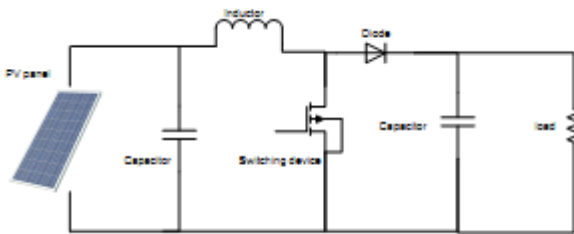


Fig. 10 Boost dc-dc converter with PV as input

V. THE PROPOSED MPPT SCHEME

Maximum power point tracking is a technique to extract maximum available power from PV module. This is done with the help of dc-dc converter which operate in such way that the output of converter is always give the maximum power that is produced by module in specific environment. At present, the most commonly used MPPT is PO method which is also has some shortcomings, such as the tracking speed is slow, and the output oscillation is big.

For this, this paper introduced a MPPT method based on back propagation neural network (BP NN). The trained neural networks can output the optimal voltage for the maximum power point under the various environment conditions. For training, gradient descent rule has been adopted. The two input (irradiance and temperature) and one output (duty cycle) is taken into consideration.

The training parameter of the network architecture is shown in Table II. The trainlm function is used to train the network, which has three hidden layer. The output of the function will give the output of the network. This algorithm

updates the network weights so as to minimize the SSE (sum square error) function.

TABLE II. NEURAL NETWORK PARAMETER FOR SIMULATION

Parameters	Values
Error Goal	0.000001
Epochs	10000

Fig. 11 shows the block diagram representation of neural network.

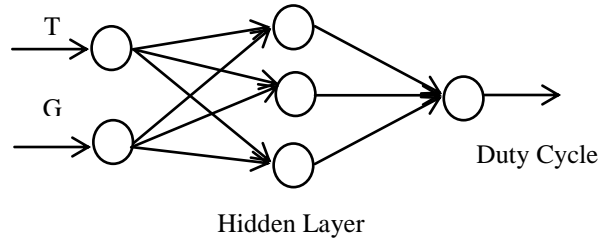


Fig. 11 Neural Network Block Diagram

VI. SIMULATION AND RESULTS

The results are obtained in MATLAB Simulink environment. The proposed PV module was connected to boost dc-dc converter to form a unit of PV system. Simulation works were carried out with conventional PO algorithm, and further with a neural network MPPT control algorithms respectively for evaluation and comparison analysis. The output of dc-dc converter was 24V, The inductor value was 82.5 mH, the input capacitor was 150 μF, the output capacitor was 320 μF, and the load was 10 ohm.

The main importance factor to analyze performance of each MPPT algorithm is time response, oscillation, overshoot and stability. In Fig. 12 the output current curve by using the BP NN method has more excellent output characteristic and smaller oscillation than the conventional PO method. Fig. 13 shows effect of each MPPT algorithm towards the maximum power point, the conventional PO did not work well, it contributes to the slowest time response, high oscillation and not that stable as compared with the BP NN.

Despite effect towards maximum power point, the algorithms should also affect the boost dc-dc converter. From Fig. 14, the PO produces high overshoot and oscillation as compared with BP NN method.

All simulations are done with a variation of temperature and irradiations. Fig. 11, Fig. 12.

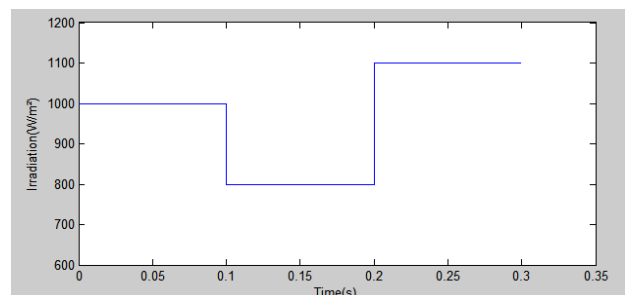


Fig. 11 Variable Irradiations with respect to time

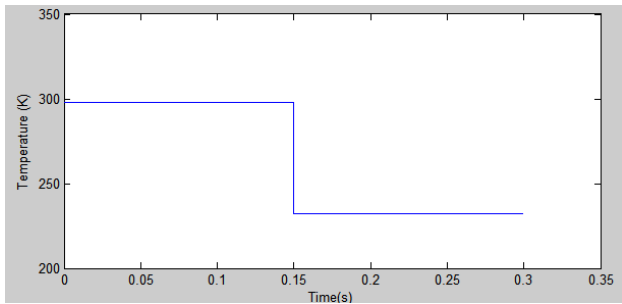


Fig. 12 Variable Temperature with respect to time

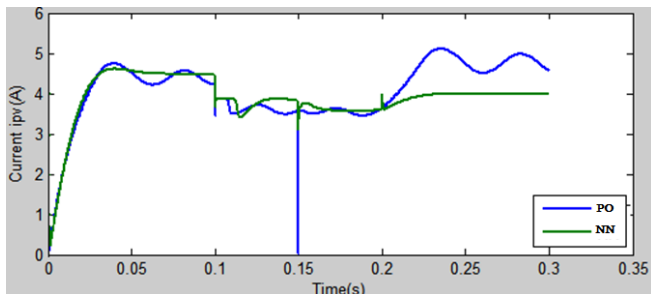


Fig. 13 PO method output current and BP NN method output current

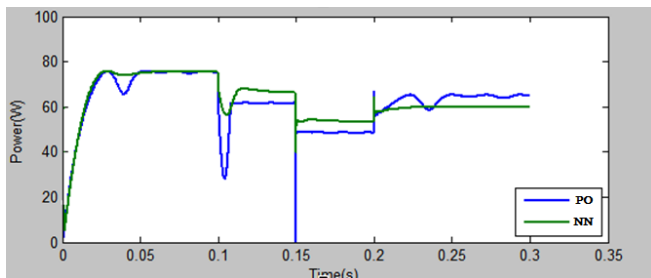


Fig. 14 PO method output power and BP NN method output power

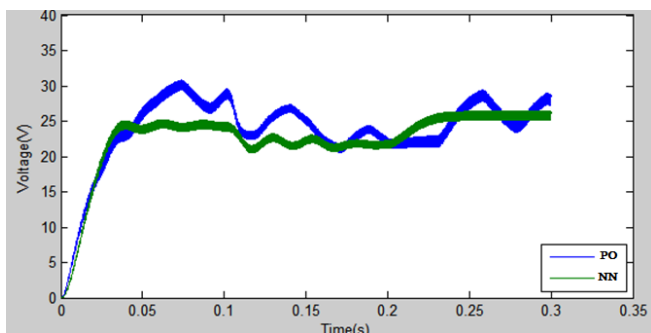


Fig. 15 Boost voltage effect with various algorithms MPPT

Sequentially all these figures coincide with theoretical prediction and company specified value which ensures the validity of the system.

VII. CONCLUSION

In this paper, a proposed neural network algorithm for MPPT control in boost dc-dc converter is presented. The output characteristic of PV system by using BP neural network MPPT method is compared with the conventional PO MPPT method, and the simulation result shows that the

proposed method gives very satisfactory results with a good efficiency.

REFERENCES

- [1] Hasan Mahamudul, Monirul Islam, Ahmad Shameem, Juel Rana and Dr. Henk Metselaar, "Modelling of PV Module with Incremental Conductance MPPT Controlled Buck-Boost Converter", 2nd International Conference on Advances in Electrical Engineering, pp. 197-202, march 2013.
- [2] M.A.A.Mohd Zainuri, M.A.Mohd Radzi, Azura Che Soh and N.Abdul Rahim, "Adaptive P&O-Fuzzy Control MPPT for PV Boost Dc-Dc Converter" IEEE International Conference on Power and Energy, pp. 524-529, 2012.
- [3] Whei-Min Lin; Chih-Ming Hong; Chiung-Hsing Chen, "Neural-Network-Based MPPT Control of a Stand-Alone Hybrid Power Generation System" IEEE Transactions on Power Electronics, Volume: 26 , pp.3571 – 3581, 2011.
- [4] N. Tat Luat and L. Kay-Soon, "A global maximum power point tracking scheme employing DIRECT search algorithm for photovoltaic systems" IEEE Trans. on Ind Electron., Vol 57, No. 10, pp. 3456-3467, Jan 2010.
- [5] S. Nema, R.K.Nema, and G.Agnihotri, "Matlab/Simulink based study of photovoltaic cells/modules/array and their experimental verification," International Journal of Energy and Environment, pp.487-500, Volume 1, Issue 3, 2010
- [6] Roberto Faranda, S.L., "Energy Comparison of MPPT Techniques for PV Systems". WSEAS Trans. on POWER SYSTEMS, vol. 3, No.6, 446-455.
- [7] Jee-Hoon Jung, and S. Ahmed, "Model Construction of Single Crystalline Photovoltaic Panels for Real-time Simulation" IEEE Energy Conversion Congress & Expo, September 12-16, 2010, Atlanta, USA.
- [8] Marcelo Gradella Villala, Jonas Rafael Gazoli, and Ernesto Ruppert Filho "Comprehensive Approach to modeling and simulation of photovoltaic arrays" IEEE Transactions on power electronics, vol.24, N0.5, May 2009.
- [9] A. Ghaffari, S. Seshagiri, and M. Krsti' c, "High-fidelity PV array modeling for advanced MPPT design" in Proc. of IEEE Canadian Conference on Electrical and Computer Engineering (CCECE), 2012.
- [10] Seyed Hossein Hosseinil, Amir Farakhor and Saeideh Khadem Haghighian, "Novel Algorithm of MPPT for PV Array Based on Variable Step Newton-Raphson Method Through Model Predictive Control" 13th International Conference on Control, Automation and Systems, pp 1577-1582, Oct. 20-23, 2013.
- [11] A. Ushida and M. Tanaka, Electronic Circuit Simulation. Japan: Corona ch. 5.1, pp. 148-158, 2002.
- [12] Long Jie, Chen Ziran, "Research on the MPPT Algorithms of Photovoltaic System Based on PV Neural Network" Chinese Control and Decision Conference, pp 1851-1854, 2011.

Computer simulation of the heating sensor PIR detector by radiation

R. Drga, D. Janáčková, and H. Charvátová

Abstract—The work is focused on testing the sensors of security systems in the infrared region and its application in the security industry. To determine the behaviour of PIR detector, it was necessary to design a mathematical model of heat sensor and sensor simulation of the thermal behaviour in the environment COMSOL Multiphysics, with subsequent verification of the proposed mathematical model. The theoretical conclusions of a mathematical description enabled the subsequent implementation of laboratory workplace of IR radiation for specific measurement properties of light sources and sensors, where it is also possible to measure the spatial characteristics of PIR detectors.

Keywords—PIR detector, pyroelement, radiation, mathematical model.

I. INTRODUCTION

THIS work deals with the testing of sensors of security systems in the field of infrared radiation and its use in the security industry, the output of work may also be used in courses technical means security industry, electronic security systems, which are the subjects of teaching at the Department of Security Engineering, Faculty of Applied Informatics, University of Tomas Bata University in Zlín. The work is focused mainly on the PIR detectors, which are used most widely in security technologies.

For thermal balance PIR detector and pyroelement was necessary to design a mathematical model described below and perform simulations of the thermal behavior of the sensors in the environment of COMSOL Multiphysics to verify the accuracy of the measurement pyroelement time close to zero at low density thermal radiation.

This work was supported by the European Regional Development Fund under the project CEBIA-Tech No. CZ.1.05/2.1.00/03.0089.

R. Drga, Tomas Bata University in Zlín, Faculty of Applied Informatics, Department of Security Engineering, nám. T. G. Masaryka 5555, 760 01 Zlín, Czech Republic (e-mail: rdraga@fai.utb.cz)

D. Janáčková, Tomas Bata University in Zlín, Faculty of Applied Informatics, Department of Automation and Control Engineering, nám. T. G. Masaryka 5555, 760 01 Zlín, Czech Republic (e-mail: janacova@fai.utb.cz)

H. Charvátová, Tomas Bata University in Zlín, Faculty of Applied Informatics, Department of Automation and Control Engineering, nám. T. G. Masaryka 5555, 760 01 Zlín, Czech Republic (e-mail: charvatova@fai.utb.cz)

II. MATHEMATICAL MODEL OF HEATING SENSOR BY RADIATION

As a module we used the room heated by two heat sources, as you can see in Fig1.

Thermal radiation incident on the sensor is partially reflected and some is absorbed by the sensor, thereby to ensure that the temperature measured at the beginning of the measurement does not fully effective temperature.

For the quantitative description of the temperature distribution in the heated pyroelement radiation we used the Stefan-Boltzmann law, according to which the density of heat flow between the source and the heated surface expressed as (1) [3]:

$$q(\tau) = \sigma \cdot C(T_2^4 - T_1^4) \quad (1)$$

where:

σ - Stefan-Boltzmann constant

C - emission surface and geometric properties, [1]

T_2 - source temperature, [K]

T_1 - temperature of heated surface, in this case the surface temperature, [K]

$$\frac{\partial T}{\partial \tau} = a \cdot \frac{\partial^2 T}{\partial x^2}, \quad (0 < x < b, 0 < \tau) \quad (2)$$

$$\left(\frac{\partial T}{\partial x} \right)_{x=0} = 0 \quad (3)$$

$$\lambda \left(\frac{\partial T}{\partial x} \right)_{x=b} = q \quad (4)$$

$$T = T_p \quad \text{for} \quad \tau = 0 \quad (5)$$

where:

b - half the thickness of the sensor, [m]

x - direction coordinates, [m]

Laplace transform of equation (1) with conditions (2) to (5) has been obtained analytical solution of unsteady temperature field for symmetrically heated by radiation sensor plate shape:

$$\frac{T - T_p}{T_c - T_p} = K_i \left[Fo + \frac{1}{2} \left(\frac{x}{b} \right)^2 - \frac{1}{6} - 2 \sum_{n=1}^{\infty} \frac{\cos \left(\frac{x}{b} p_n \right)}{p_n^2 \cos p_n} e^{(-Fop_n^2)} \right] \quad (6)$$

where K_i is Kirpičev criterion (7)

$$K_i = \frac{qb}{\lambda(T_c - T_p)} \quad (7)$$

where T_c is medium temperature of radiators. Fourier criterion Fo represents the dimensionless heating time is calculated by the equation:

$$Fo = \frac{a\tau}{b^2} \quad (8)$$

where:

τ - duration of heating, [s]

a - thermal conductivity sensor, [$m^2 \cdot s^{-1}$]:

$$a = \frac{\lambda}{\rho c_p} \quad (9)$$

where:

λ - the thermal conductivity sensor, [$W \cdot m^{-1} \cdot K^{-1}$]

ρ - the density of the sensor material, [$kg \cdot m^{-3}$]

c_p - the specific heat capacity of the sensor material, [$J \cdot kg^{-1} \cdot K^{-1}$].

Members p of the analytical solution of (6) are determined from equation (10):

$$p_n = n \cdot \pi \quad (10)$$

According to the form the solution (6) it is evident that with increasing time of heating effect element endless series decreases, i.e., we can also expect Fourier criterion Fo which influence endless series may be neglected and $Fo > Fok$ the temperature at any point in the wall almost linear function time and temperature profile across the plate (x -axis direction) is a parabola.

III. SOLUTION OF A MATHEMATICAL MODEL IN THE MAPLE ENVIRONMENT

Solution temperature distribution in pyroelement according to equation (6) was performed using the software applications created in Maple environment. To this purpose, the program created an application that performs automatic calculation of temperature fields for the specified input value. The source code is as follows:

Defining input values:

```
> q:=1;
> b:=0.005;
> lambda:=4.6;
> tc:=36;
> tp:=20;
> rho1:=7450;
```

```
> cp:=250;
> a:=lambda/(rho1*cp);
> Fo:=a*tau/b^2;
```

The calculation of the roots of p:

```
> for i from 1 to 300 do
p[i]:=evalf(Pi*i)
end do;
```

```
p1 := 3.141592654
p2 := 6.283185308
p3 := 9.424777962
⋮
```

Calculation of 3D temperature field based on the analytical solution (6):

```
> with(plots):
> grafreal:=plot3d((q/lambda*(a*tau/b+x^2/(2*b)-
(b/6))-2*q*b/lambda*Sum(cos(x/b*p[n])*exp(-
(a*tau/b^2)*p[n]^2)/(p[n]^2*cos(p[n])),n=1..300))+tp
,x=0..b,tau=0..60,axes=box,style=wireframe,color=red
,labels=["x (m)", "tau (s)", "t (degC)"]);
> display(grafreal);
```

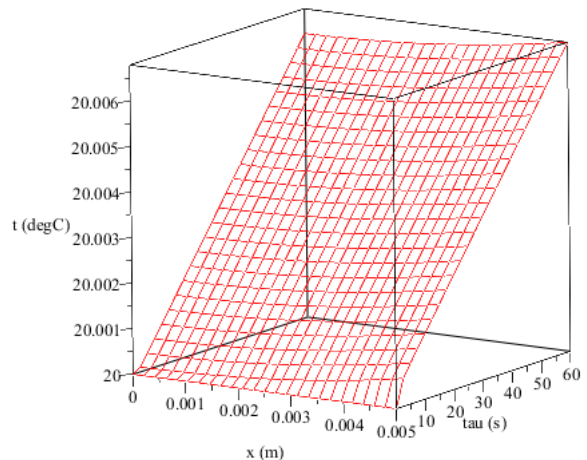


Fig. 1 3D temperature field in a heated sensor calculated in Maple

Calculation of temperature fields in 2D on the basis of analytical solutions (6):

```
> for j from 1 to 10 do
fce2D[j]:=q/lambda*(a*tau[j]/b+x^2/(2*b)-(b/6))-
2*b/lambda*Sum(cos(x/b*p[n])*exp(-
(a*tau[j]/b^2)*p[n]^2)/(p[n]^2*cos(p[n])),n=1..300)+tp
end do;
> for k from 1 to 10 do
tau[k]:=6*k
end do;
tau1 := 6
tau2 := 12
tau3 := 18
⋮
```

```
>graf1:=plot(fce2D[1],x=0..b,legend=tau[1],axes=box,color=
COLOR(HUE, .1));

>graf2:=plot(fce2D[2],x=0..b,legend=tau[2],axes=box,color=
COLOR(HUE, .2));

>graf3:=plot(fce2D[3],x=0..b,legend=tau[3],axes=box,color=
COLOR(HUE, .3));
:
:
>display(graf1,graf2,graf3,graf4,graf5,graf6,graf7,graf8,graf9,
graf10);
```

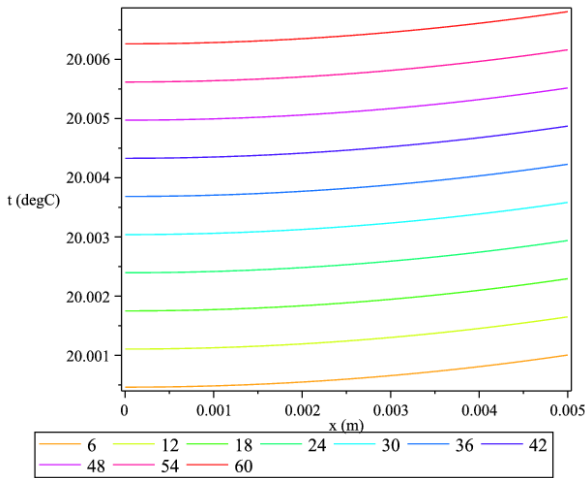


Fig. 2 3D temperature field in a heated sensor calculated in Maple

Calculation of the temperature sensor in the desired location and time:

```
> x[zvol]:=0.002;
    x_zvol := 0.002
> tau[zvol]:=550;
    tau_zvol := 550

>evalf((q/lambda*(a*tau[zvol]/b+x[zvol]^2/(2*b)-(b/6))-
2*b/lambda*Sum(cos(x[zvol]/b*p[n])*exp(-
(a*tau[zvol]/b^2)*p[n]^2)/(p[n]^2*cos(p[n])),n=1..300)+tp)
);
    20.05898920
```

The output of the program application is a plot showing the 3D and 2D real temperature field in a heated sensor to the desired input value. 3D temperature field shows the temperature distribution for a selected period of heating sensor (Fig. 1). 2D temperature field shows the temperature curve of the sensor at the desired times of heating (Fig. 2). The application also calculates the temperature of sensor in a given place and time, as shown in the last part of the above source file.

IV. SIMULATION AND VERIFICATION PROPOSED MODELS IN COMSOL MULTIPHYSICS

Because it was not possible to determine experimentally the necessary data, was used to assess the thermal behavior of the sensor software COMSOL Multiphysics, which is suitable for the simulation of physical processes and is intended primarily for developers, researchers and researchers. The aim of simulation is to determine the temperature distribution and the heat flow density in the surface of the pyroelectric element location depending on the distance from the intruder detector. The "Heat Transfer Module" was used for the simulation, for environment "Surface-to-Surface Radiation". Size intruder simulating the glowing area of 2 m x 0.5 m, the properties of the detector represents pyroelement of size 5 mm x 2.3 mm x 0.2 mm. The simulation was performed under the conditions:

- the surface temperature of an intruder 36 °C
- ambient air temperature 20 °C
- relative emissivity of the surface of a pyroelectric element 0.9
- relative emissivity of intruder 0.97
- thermal conductivity of the pyroelectric element $2,255 \cdot 10^{-6} \text{ m}^2/\text{s}$
- thermal conductivity intruder $1,484 \cdot 10^{-7} \text{ m}^2/\text{s}$
- thermal conductivity of air $2,14 \cdot 10^{-5} \text{ m}^2/\text{s}$

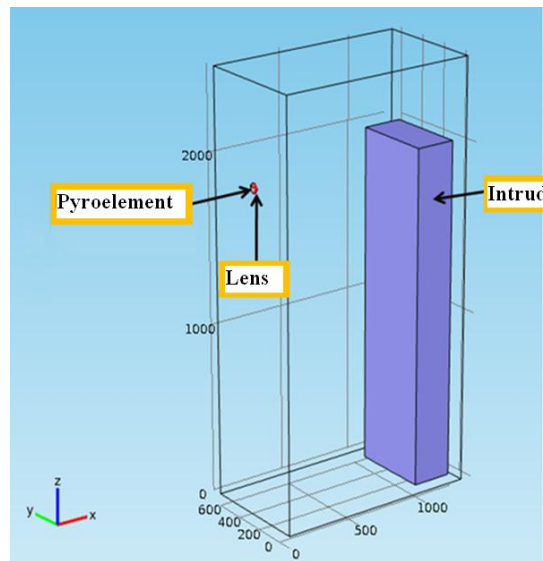


Fig. 3 The geometric layout of the situation

The following pictures show the simulation results, ie, temperature distribution and heat flow density at the surface of the pyroelectric element spot for intruder distance of 1 m from the detector. Similarly, simulations were performed for a distance of 3 and 5 m

According to Figure 5 it is apparent that near pyroelementu leads to increase in air temperature due to the temperature at a greater distance from the detector.

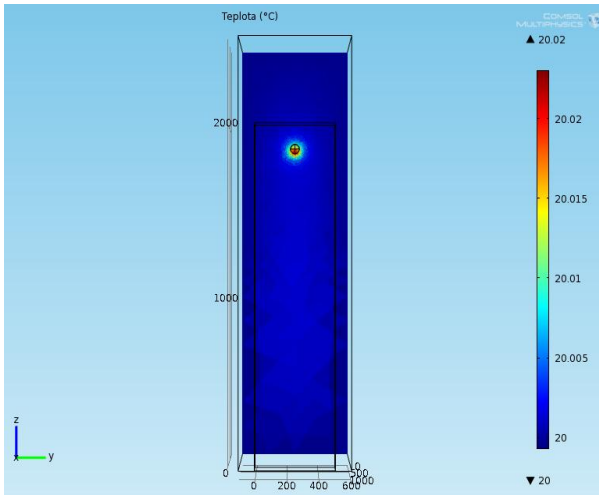


Fig. 4 The temperature distribution in the cross-sectional surface at the site of a pyroelectric element

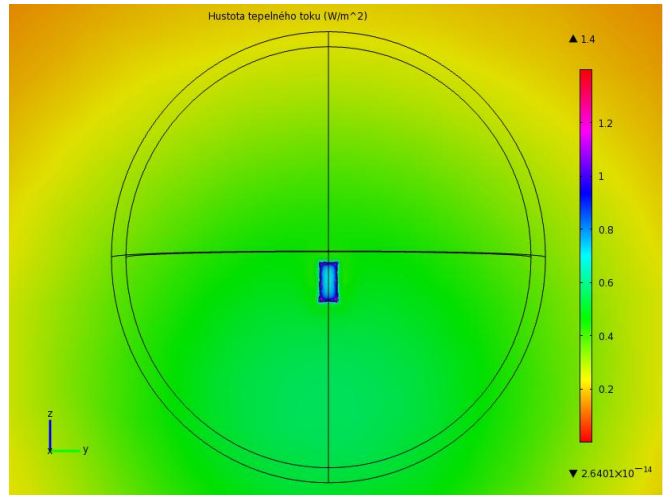


Fig. 7 The distribution density of the heat flow at the site of the cut surface of the pyroelectric element - detail in the place of the detector

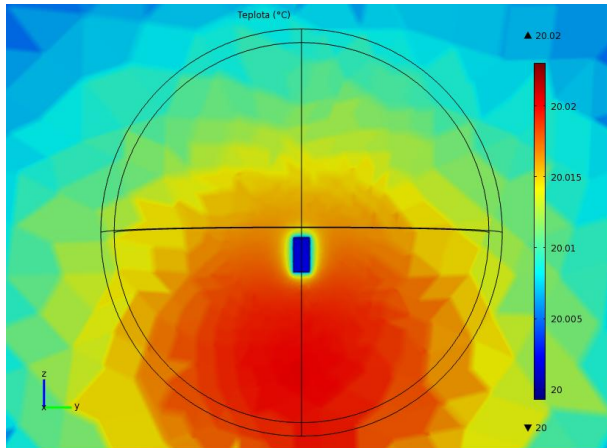


Fig. 5 The temperature distribution in the cut surface at the point a pyroelectric element - detail in location of the detector

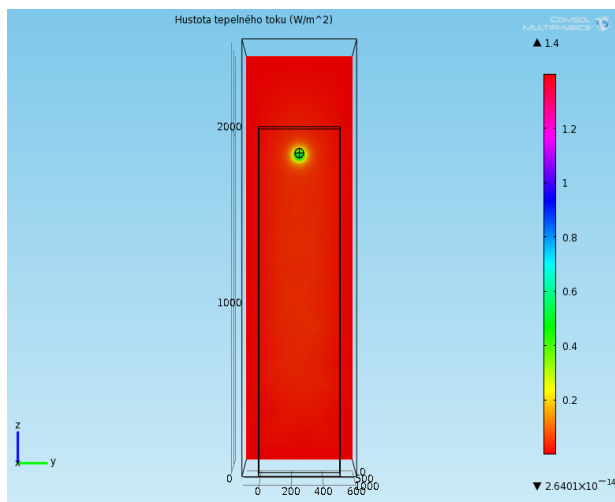


Fig. 6 The temperature distribution in the cut surface at the site of a pyroelektrick element - detail the location of the detector

Figure 7 is then detail the distribution of heat flow density in the vicinity pyroelementu. Near pyroelementu density of heat flow increases until it reaches about 0.5 W/m^2 higher relative to the surroundings.

In the case of an intruder detector distance 3 m decreased heat flow density to approximately 0.24 W/m^2 , while a further decrease of the surface temperature pyroelement.

Specified the value of the density of heat flow and temperature at the surface pyroelement according to the results of simulation in COMSOL Multiphysics is detailed in the following table. These values correspond to the mid-position of the element.

Table I Heat flux density on the surface of the pyroelectric element - the results of simulation in COMSOL Multiphysics

Distance detector from intruder [m]	Heat density [W/m ²]	Temperature [°C]
1	0,750	20,0230
2	0,380	20,0076
3	0,245	20,0012
4	0,035	20,0010
5	0,020	20,0004

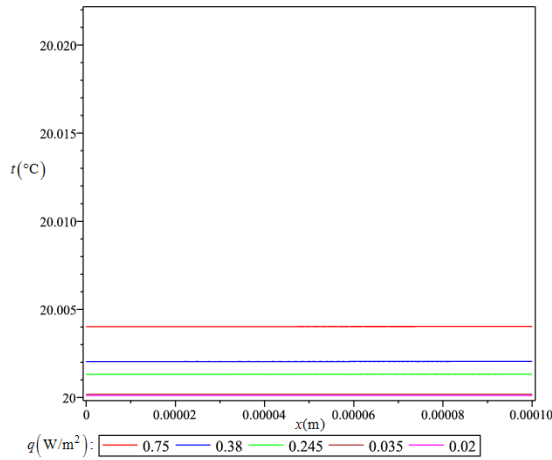
The table shows that with increasing distance decreases heat flow density on the surface of the original pyroelement 0.75 W/m^2 at 0.02 W/m^2 . It also reduces the surface temperature pyroelement value of 20.023 °C at 20.0004 °C .

V. CALCULATION OF TEMPERATURE FIELDS IN MAPLE

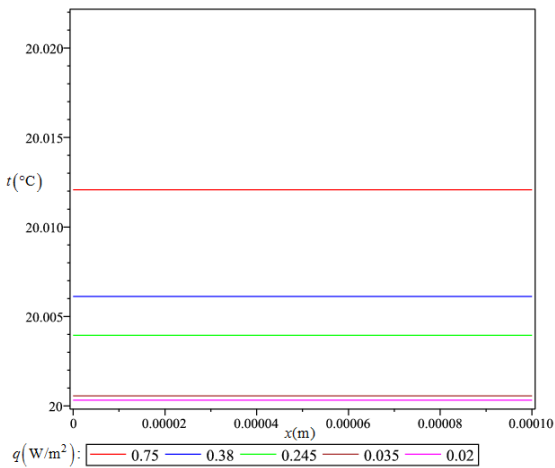
The density of heat flow, obtained by simulation in COMSOL Multiphysics is used for the calculation of unsteady temperature fields in pyroelement according to the analytical solution (6) model (2) - (5). For the calculation of temperature fields were used the following values:

element thickness 0.2 mm
 initial temperature of the pyroelectric element 20 °C
 surface temperature of the intruder (source) 36 °C

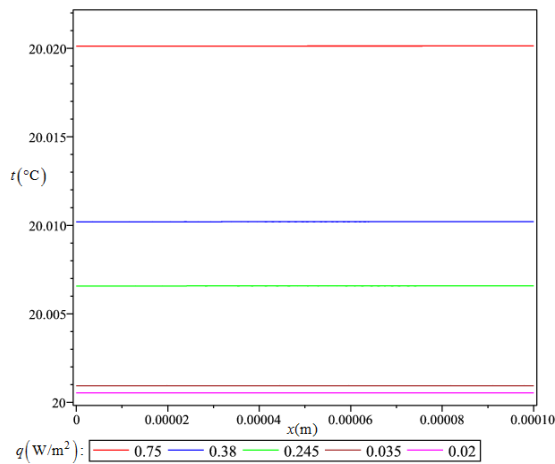
The following pictures show waveforms of temperature on the surface pyroelement in terms of heat flow density from 0.75 W/m² to 0.02 W/m², which corresponds to the distance from the intruder detector 1 m to 5 m.



The duration of heat exposure: 1 second



The duration of heat exposure: 3 seconds



The duration of heat exposure: 5 second

Fig. 8 The course of the temperature field in pyroelement depending on the density of heat flux at the surface of the element

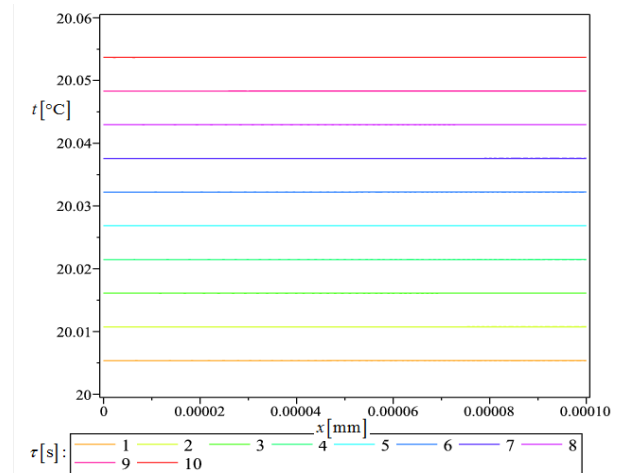
From the graphs it is evident that the heat treatment for 1-5 seconds for incident radiation having a density of 0.75 W/m² temperature pyroelement increased about 0.015 °C, while for incident radiation having a density of 0.02 W/m², the temperature hardly increased pyroelement. The calculations and simulations, the temperature distribution in the heated pyroelement also shows that even at low values of the density of heat flux at a given time, the surface temperature pyroelement nearly the same temperature throughout its thickness (no steep temperature field). This proves that pyroelement is flawed. It can be said that in the early stages of measurement evaluates pyroelement right temperature and laboratory measurements is therefore in the initial stages sufficiently accurate.

VI. COMPARISON OF THEORETICAL RESULTS WITH SIMULATIONS

Verification of the mathematical model was made by comparing the temperature fields in pyroelement calculated in the Maple on the basis of the analytical solution described by equation (6) with the results of the simulation of temperature field in COMSOL Multiphysics.

The Figure 9 shows the waveforms of temperature fields under the following conditions:

- secondary source temperature 30° C
- initial temperature pyroelement 20 °C
- the density of heat flux incident on a surface pyroelement 1 W/m²
- thermal conductivity pyroelement 2,255.10⁻⁶ m²/s,
- pyroelement thickness of 0.2 mm.



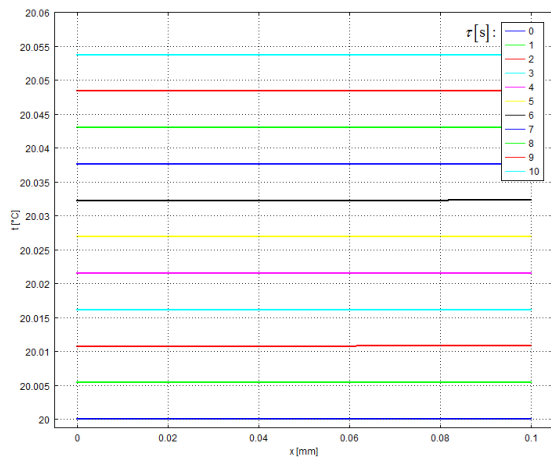


Fig. 9 Temperature field in pyroelement for the heat of the action 10 seconds calculated in Maple (up) and COMSOL Multiphysics (down)

It is evident that the curves of temperature fields calculated in Maple coincide with the courses of temperature fields obtained by simulation in COMSOL Multiphysics.

VII. CONCLUSION

Analytical solution of the proposed mathematical model describing heat radiation sensor was used to create applications for the calculation of temperature fields in pyroelement in the user interface of the program Maple. Because it was not possible to determine all the data needed for the calculation of temperature fields experimentation was conducted simulations to assess the thermal behavior pyroelement programming environment COMSOL Multiphysics. The simulations were designed waveforms temperature fields and heat flux density at the surface and under surface pyroelement for the selected distance from the intruder detector. The data obtained were then compared with the theoretical results obtained by the solution of the model through an application program created in Maple environment. The calculations and simulations, the temperature distribution in the heated pyroelement showed that even at low values of heat flow density in a given time the surface temperature pyroelement nearly the same temperature throughout its thickness, which confirmed that in the early stages of measurement evaluates pyroelement right temperature and laboratory measurements is therefore in the initial stages is sufficiently accurate.

Based on the theoretical results and the mathematical description was later realized laboratory workplace interior IR radiation, which was made specific measurements of the properties of radiation sources and detectors, and where it is also possible to measure the spatial characteristics PIR detectors.

REFERENCES

- [1] J. D. Vincent, *Fundamentals of infrared detector operation and testing*. USA, Texas: WILEY, 1990.
- [2] G. F. Knoll, *Radiation detection and measurement*. USA, Texas: WILEY, 2000.
- [3] B. Saleh, *Fundamentals of photonics*. USA, Texas: WILEY, 2007.
- [4] K. Kolomazník, *Teorie technologických procesů III*. (in Czech). University of Technology in Brno, Brno, 1978
- [5] A., R. Jha, . *Infrared technology*. USA – Texas: WILEY, 2006
- [6] C. Hotz, *Přenos tepla zářením* (in Czech), Prague: SNTL, 1979.
- [7] K. Kolomazník, *Modelování zpracovatelských procesů* (in Czech), Brno: University of Technology in Brno, 1990.
- [8] K. Židek and J. Píteř, "Smart 3D Pointing Device Based on MEMS Sensor and Bluetooth Low Energy," in *Proceedings of the 2013 IEEE Symposium on Computational Intelligence in Control and Automation (CICA)*, Singapore, April 16-19, 2013, pp. 165-168.
- [9] R. Makovník and O. Liška, "Contribution to experimental identification and simulation problems of dynamic systems", *Ovidius University Annual Scientific Journal*. vol. 9, No. 1, 2007.
- [10] O. Liška (2008). Monitorizačné systémy pre automatizovanú výrobu (in Slovak). *Transfer inovácií*. [Online]. 12. pp. 121-123. Available: <http://www.sjf.tuke.sk/>
- [11] M. Fodor, O. Liška (2010). Design and realization sensorial system on detection obstacle [CD-ROM].in *8th International Symposium on Applied Machine Intelligence and Informatics*, Herľany, Slovakia.

Electromagnetic field distribution within a semi anechoic chamber

Martin Pospisilik and Josef Soldan

Abstract— The paper deals with determination of a resonant frequency of a semi anechoic chamber with irregular shape. The authors also processed a set of measurements in the semi anechoic chamber installed at Tomas Bata University in Zlin in order to prove their expectations. Within the framework of this paper the results are discussed with regard to the contribution of the research to the improvement of accuracy of electromagnetic interferences measurements inside the chamber.

Keywords—Semianechoic Chamber, Electromagnetic Compatibility, Electrical Field Distribution, Dominant Modes

I. INTRODUCTION

THE semi anechoic chambers are often used to process measurements related to electromagnetic compatibility (EMC), especially for the measurement of emissions of the tested equipment or of the sensitivity of the measurement equipment to the external electric or magnetic field. The measurement processes are strictly defined by the appropriate standards which also allow a certain degree of uncertainty of the measurement, depending on technical possibilities. The authors of the paper are convinced that the uncertainties can be lowered by applying a correction that is based on the knowledge of the electric and magnetic field distribution within the semi anechoic chamber.

Because at Tomas Bata University in Zlin a semi anechoic chamber is used, its behaviour was studied by mapping of the electric field distribution within its space, especially at the frequencies that are expected to be close to the dominant modes of the chamber. The results of rough mapping of the spectrum inside the chamber are described in the framework of this paper.

The goal of the research consists in mapping of how the electromagnetic field inside the semi anechoic chamber is distributed and in analytical determining of corrections that could be applied to the measurement in order to improve its accuracy.

This work was supported in part by by the European Regional Development Fund under the project CEBIA-Tech No. CZ.1.05/2.1.00/03.0089. and by OPVK project CZ.1.07/2.3.00/30.0035.

Martin Pospisilik is with Tomas Bata University in Zlin, Faculty of Applied Informatics, Nad Stranemi 4511, 760 05 Zlin, Czech Republic. He is now at the department of Computer and Communication Systems (e-mail: pospisilik@fai.utb.cz)

Josef Soldan is with Tomas Bata University in Zlin, Faculty of Applied Informatics, Nad Stranemi 4511, 760 05, Zlin, Czech Republic. He is now a senior researcher at the Department of Electronics and Measurement. (e-mail: soldan@fai.utb.cz)

II. PROBLEM DESCRIPTION

It is expected that the chamber acts as an enclosed box with reflective surfaces in which several resonant modes occur, being partially, but not at all, attenuated by absorbers displaced around its walls. There are no absorbers on the floor (this is why the chamber is called Semi anechoic) in order to simulate conditions close to external measurement sites that are considered in relevant EMI measurement standards. According to [1], the resonant modes of the space inside the chamber can be calculated according to the following equation:

$$f_{ijk} = \frac{c}{2\pi\sqrt{\mu_r\epsilon_r}} \sqrt{\left(\frac{i\pi}{L}\right)^2 + \left(\frac{j\pi}{H}\right)^2 + \left(\frac{k\pi}{W}\right)^2} \quad (1)$$

Where:

c – field propagation velocity [m/s],

μ_r – relative permeability [-],

ϵ_r – relative permittivity [-],

i, j, k – wave indexes (case $i = j = k = 0$ is forbidden),

L – box length [m],

H – box height [m],

W – box width [m].

The semi anechoic chamber is equipped with flat ferrite and pyramidal absorbers that decrease the reflections of the electromagnetic waves inside the chamber. However, in practice the efficiency of the absorbers is limited by technical possibilities and small amounts of energy is reflected back to the space of the chamber, resulting in standing waves occurrence at various locations according to the wavelengths. The examples of reflection losses of the above mentioned absorbers are depicted in figures below. In technical standards, two main approaches are defined to eliminate this phenomenon:

- The minimum efficiency of the absorbers is defined.
- The mutual position of the tested equipment and the measuring antenna is changed during the testing process.

Usually, when the measurement is operated according to standards, measurement at different locations and mutual angles is quite time consuming. In addition, despite the above mentioned provisions, quite high uncertainty is allowed for such types of measurements. The knowledge of the chamber's response at different locations to various frequencies could be used to create a set of corrections that would lead to increasing

of the measurement accuracy or to acceleration of the measurement by decreasing of the number of the mutual positions of the equipment under test and the measuring antenna.

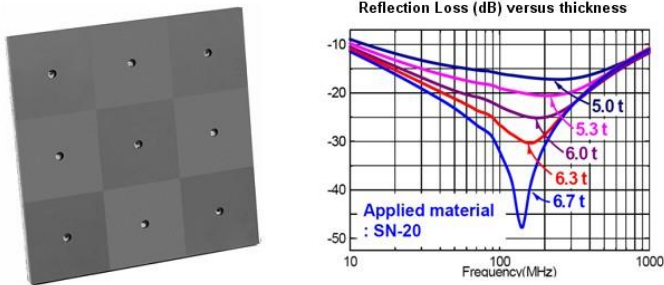


Fig. 1 Flat ferrite absorber and its performance (example) [2]

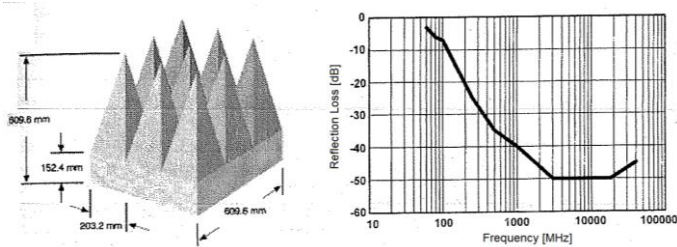


Fig. 2 Pyramidal absorbers and their performance (example) [3]

Examples on field distributions inside a resonant box are described in [1].

III. SEMI ANECHOIC CHAMBER DESCRIPTION

The experiment was held in a semi-anechoic chamber Frankonia SAC-3 plus, which is suitable for emissions measurements according to EN 55022 / CISPR 22 class B and immunity tests according to IEC/EN 61000-3-4. The construction of the chamber is specific for its cylindrically shaped ceiling. The manufacturer claims that the dome shaped roof as well as its optimized absorber layout, with ferrite and partial hybrid absorber lining, minimizes the reflections in between 26 MHz and 18 GHz [4]. The frequencies used at the experiment were set close to the lower frequency limit of the chamber as it was expected to drive the first dominant mode of electrical field in this spectrum. Generic configuration of the chamber is depicted at Fig. 3.

According to the documentation, the internal dimensions of the chamber are as enlisted in Table I.

Table I Dimensions of the chamber

Length	9 680 mm
Width	6 530 mm
Height – maximum	9 500 mm
Height – minimum	6 000 mm

The height of the chamber varies according to the position, as the ceiling is of cylindrical shape. The maximum height is in the longitudinal plane of the centre of the chamber, the minimum height is near the longer walls of the chamber. As

the chamber is equipped with cone absorbers, the internal area is effectively restricted to approximately 8 120 x 5 150 mm.

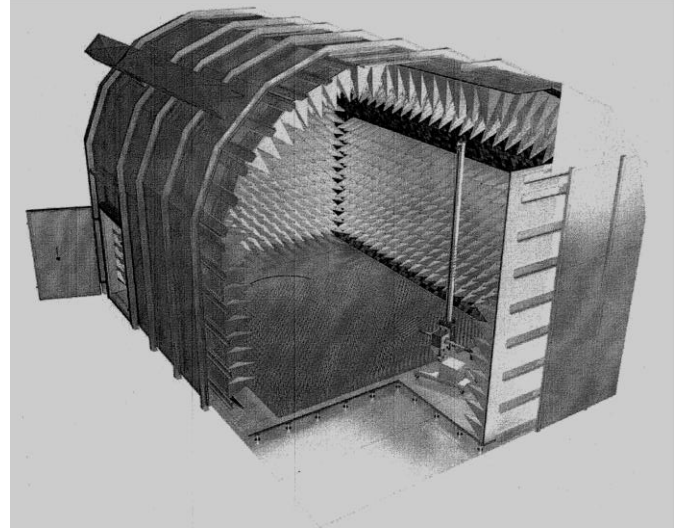


Fig. 3 Semi anechoic chamber Frankonia SAC 3 – plus [4]

IV. THE EXPERIMENT

15 points of measurement were indicated within the floor area as depicted in Fig. 4. The distance among the neighbouring points is 1 300 mm and the central point (H) is located in the middle of the chamber.

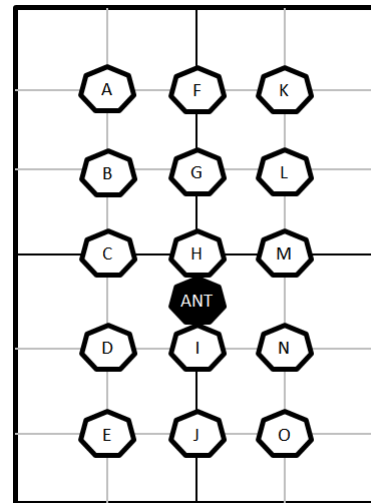


Fig. 4 Displacement of the measurement points in the chamber

Real environment was simulated inside the chamber. Behind the points (F) and (K) a passive semi-logarithmical antenna was left in the height of 4 000 mm. Between the points (I) and (J) there was a wooden table on which the Equipment under Test is placed where the tests are processed. Between points (H) and (I) an omnidirectional transmitting antenna (monopole) was placed (ANT). The antenna was fed with the power of 1 mW (0 dBm) in order to drive the electromagnetic field inside the chamber. The levels of electrical fields at the points (A) to (O) were measured with Rohde & Schwarz omnidirectional spherical field probe HZ-

11. The field probe was always placed in the height of 1 500 mm.

A. Expectations

Based on the below mentioned theory, the chamber was expected to resonate at the frequencies close to 30 MHz. Because the shape of the chamber combines two model cases – a cuboid and a cylinder, three cases were theoretically analysed:

- a) Cuboidal resonator with the height of 6 000 mm (minimum height)
- b) Cuboidal resonator with the height of 9 500 mm (maximum height)
- c) Cylindrical resonator

According to the above mentioned cases, two dominant modes were expected: TE₁₀₁ (for cuboidal resonator) and TE₁₁₁ (for cylindrical resonator). Because the height of the chamber is omitted for TE₁₀₁, for the cases a) and b) the resonant frequency can be calculated as follows:

$$\begin{aligned} \lambda_{01}^{TE_{101}} = \lambda_{02}^{TE_{101}} &= \frac{2\pi}{\sqrt{\left(\frac{i\pi}{a}\right)^2 + \left(\frac{j\pi}{b}\right)^2 + \left(\frac{k\pi}{c}\right)^2}} \\ &= \frac{2\pi}{\sqrt{\left(\frac{1 \cdot \pi}{6.53}\right)^2 + \left(\frac{0 \cdot \pi}{9.5}\right)^2 + \left(\frac{1 \cdot \pi}{9.68}\right)^2}} \quad (2) \\ &= 10.83 [m] \end{aligned}$$

$$f_{01} = f_{02} = \frac{c}{\lambda_{01}^{TE_{101}}} = \frac{3 \cdot 10^8}{10.83} = 27.7 [MHz] \quad (3)$$

Concerning the case c), in cylindrical resonator the first dominant mode is TE₁₁₁. The resonant frequency can be calculated as follows:

$$\begin{aligned} \lambda_{03}^{TE_{111}} &= \frac{2\pi}{\sqrt{\left(\frac{\alpha'_{11}}{r}\right)^2 + \left(\frac{\pi}{l}\right)^2}} = \frac{2\pi}{\sqrt{\left(\frac{1.84}{3.27}\right)^2 + \left(\frac{\pi}{9.68}\right)^2}} \quad (4) \\ &= 9.66 [m] \end{aligned}$$

$$f_{03} = \frac{c}{\lambda_{01}^{TE_{101}}} = \frac{3 \cdot 10^8}{9.66} = 31.05 [MHz] \quad (5)$$

The symbols used in equations (2) to (5) are as follows:

- λ – wavelength [m],
- i, j, k – wave indexes,
- a – width of the chamber [m],
- b – height of the chamber [m],
- c – length of the chamber (cuboidal shape) [m],
- l – length of the chamber (cylindrical shape) [m],
- r – cylinder radius (cylindrical resonator) [m],

α'_{11} – 1st derivation of appropriate Bessel's equation root.

According to the above mentioned calculations, the dominant resonance frequency of the chamber would occur between approximately 27 and 31.5 MHz. Based on this expectation, frequencies between 10 and 80 MHz were applied in the framework of the experiment.

B. Measurement

The transmitting antenna was fed with the constant power of 1 mW from a signal generator that was operating in a sweep mode. The transmitting frequency was periodically changed from 10 to 80 MHz with the step of 0.04 MHz. With the dwell time of 0.3 s this determined the measurement time to be 525 s per one measurement point. The frequency spectrum was scanned with Rohde & Schwarz spectrum analyzer ECU that was operated together with the data gathering software EMC32. The spectrum was scanned periodically with a period of 0.1 s, using the bandwidth of 120 kHz. With these settings at least two measurements were made for each frequency transmitted by the omnidirectional antenna. The resolution of the spectral analyzer, regarding to the scanning speed, was set to 625 points, resulting in a virtual frequency step of 112.179 kHz. For each point of measurement (see Fig. 4) the maximum measured values were recorded. After 525 seconds, spectrum of the electrical field for frequencies between 10 and 80 MHz was obtained for the pertinent measurement point, the field probe was moved to another measurement point and the measurement was repeated.

As stated above, the measurement was performed by anisotropic spherical probe HZ-11 [5], which is not sensitive to the orientation of the field. On the other hand, its antenna factor is quite poor, as depicted in Fig. 5. The corrections that were set for the probe and for the cables resulted in a noticeable increase in noise levels. Because there was no need to evaluate the absolute values of the electric field levels, but only differences among the points were recorded, the bias of the measured levels (y-axis drift in the diagrams) was not calibrated and the noise level was considered to be satisfactory.

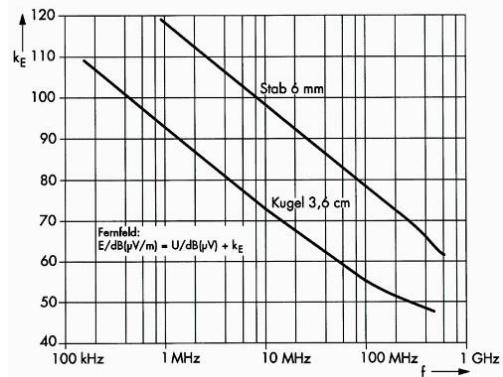


Fig. 5 Antenna factor of HZ-11 field probes (the relevant curve is “Kugel 3.6 cm”) [5]

Once the data were obtained, their analysis was made in MS Excell in order to visualize remarkable phenomena to be studied.

V. RESULTS

Due to quite large set of gathered results only the most important results can be presented within the framework of this paper. In the subchapters below several diagrams are presented with appropriate comments.

A. Longitudinal cuts

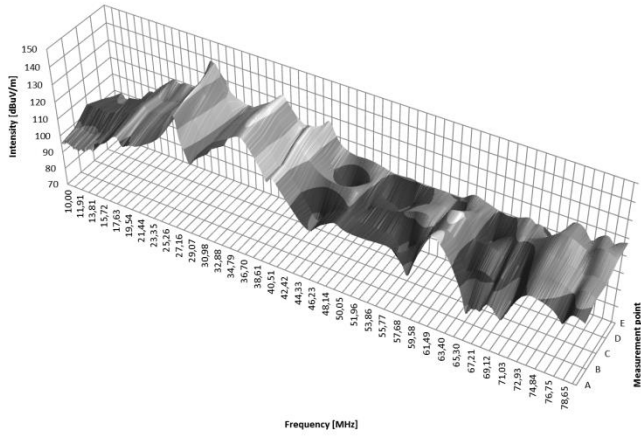


Fig. 5 Dependence of intensity on frequency and position (left part of the chamber)

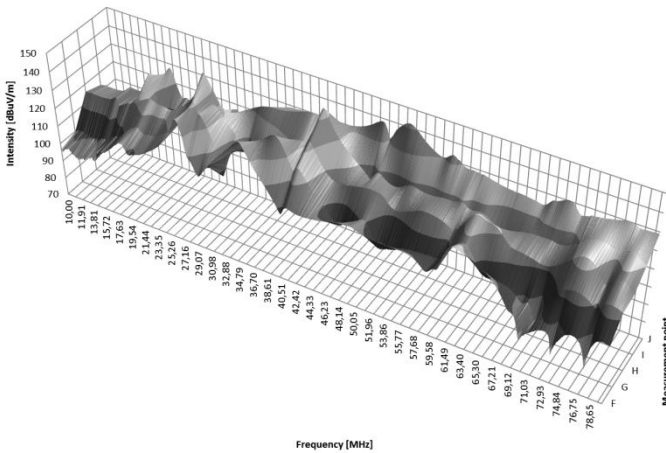


Fig. 6 Dependence of intensity on frequency and position (central part of the chamber)

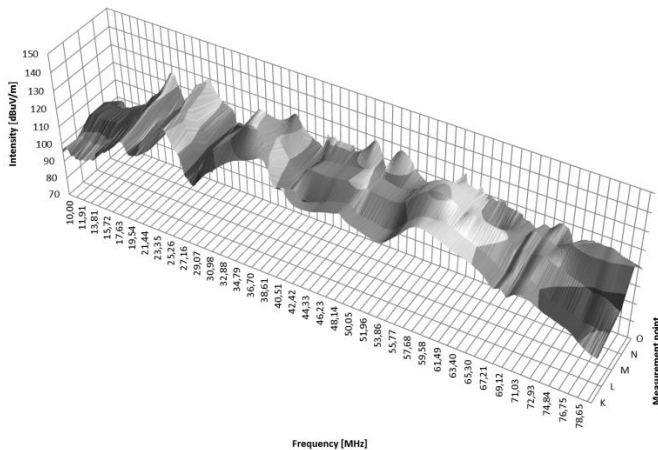


Fig. 7 Dependence of intensity on frequency and position (right part of the chamber)

The diagrams related to longitudinal cuts display how the intensity of the electrical field depends on frequency and position.

Each diagram consists of five measurements that were obtained in a longitudinal plane inside the chamber. The planes are, according to Fig. 4, defined by sets of points (A) to (E), (F) to (J) and (K) to (O).

According to Fig. 5, Fig. 6 and Fig. 7 it is obvious, that there are increased levels of intensity at the frequencies between 20 and 40 MHz, being probably related to the dominant modes. It is interesting that the frequencies at which there are maximum electrical field intensities are dependent on the position inside the chamber.

B. The most intensive frequencies

In Fig. 8 there is a diagram showing which at which frequencies the electrical field is most intensive depending on the location inside the chamber. It shows that in the central part of the chamber the maximum intensities can be observed at frequencies between 25 and 30 MHz while at the sides of the chamber the maximum intensities are achieved at frequencies between 35 and 40 MHz. In the right central part of the chamber (measurement point (J)) the frequencies with maximum intensity lie between 50 and 55 MHz.

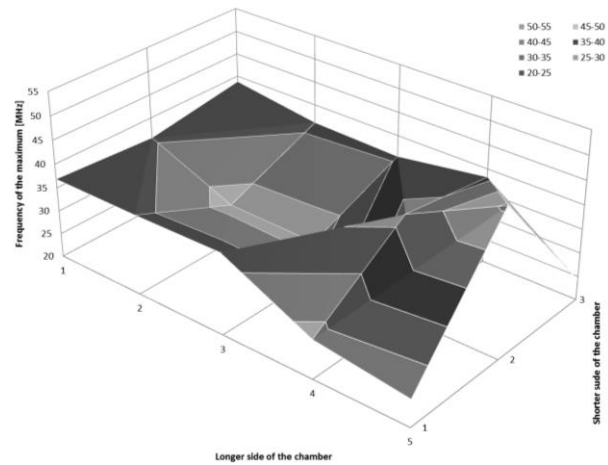


Fig. 8 Frequencies with maximum intensity in dependence on the location

C. Transversal cuts

From the gathered data, five transversal planes can be considered (AFK, BGL, ..., EJO). The values of all three points in each plane were averaged and all five averages were visualized in a 3D chart, showing the dependency of electrical field intensity on frequency and location (transversal plane). This diagram is depicted at Fig. 9.

For each of the transversal planes there were also 2D charts created. All these charts were merged into one in order the characteristic features could be observed. The merged chart is depicted in Fig. 10. It shows that at almost all points the resonant peaks can be observed in neighborhood of 25 and 35 MHz. The only exception is observed in the plane EJO that shows very poor resonance in the neighborhood of 35 MHz,

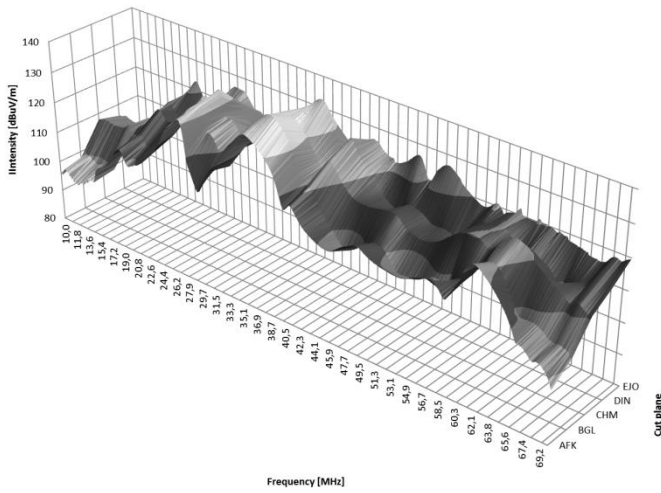


Fig. 9 Dependence of intensity on frequency and location (averages through transversal cuts)

transmitting antenna. The level at points (A), (F) and (K) is probably affected by the noise of the measuring system.

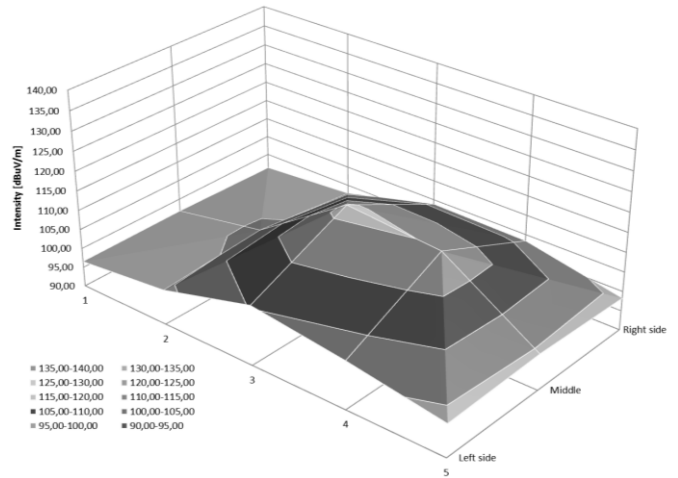


Fig. 11 Displacement of electrical field intensity for frequencies between 10 and 15 MHz

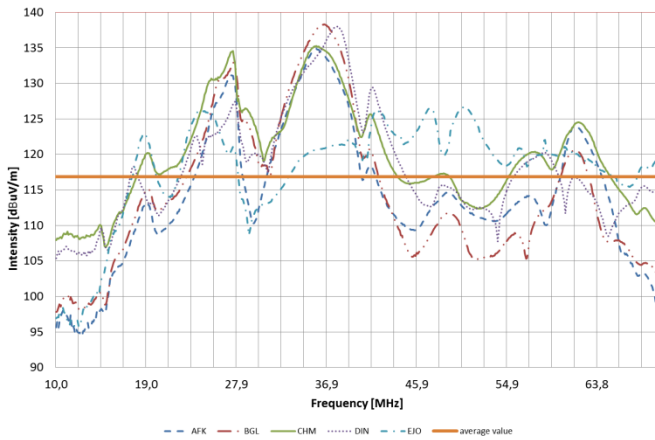


Fig. 10 2D expression of Fig. 9

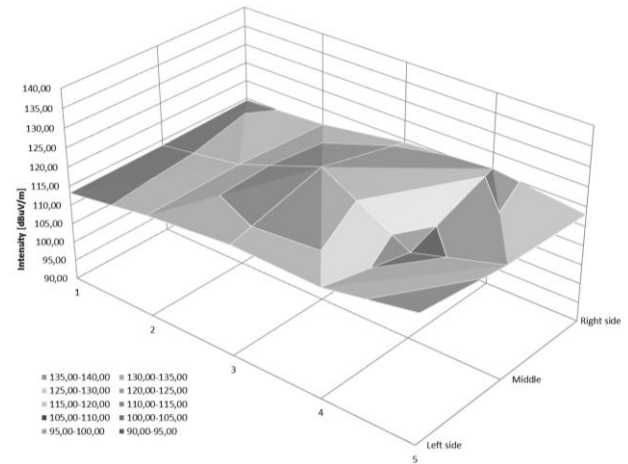


Fig. 12 Displacement of electrical field intensity for frequencies between 20 and 25 MHz

but higher intensities around 50 MHz. Generally it can be stated that the increase of intensity at the resonant frequencies is up to 20 dB compared to the average, which is quite considerable value.

D. Intensity displacement for certain frequency bands

In order to visualize the displacement of the intensities, the following charts were created, each for a frequency band of 5 MHz. Therefore, for each of the measurement points, relevant frequencies were averaged in order to achieve the state similar to the output of a spectral analyzer with a bandwidth of 5 MHz. The charts show how the displacement of the electrical field intensity differs for various frequency bands.

To make the interpretation of the measured data more clear, the authors show only the most illustrative charts.

In Fig. 11 the displacement of the field intensity at frequencies between 10 and 15 MHz is shown. As these frequencies are sub-critical (lower than ones at which dominant modes can occur), only a small peak can be observed in the middle of the chamber. Generally, it can be stated, that the energy is almost evenly distributed around the

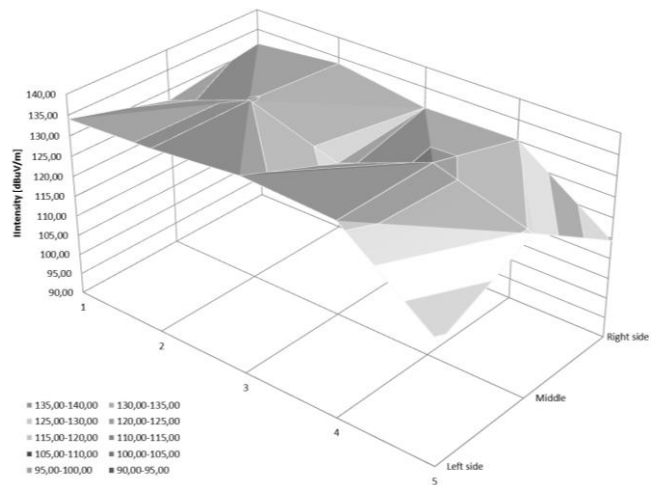


Fig. 13 Displacement of electrical field intensity for frequencies between 35 and 40 MHz

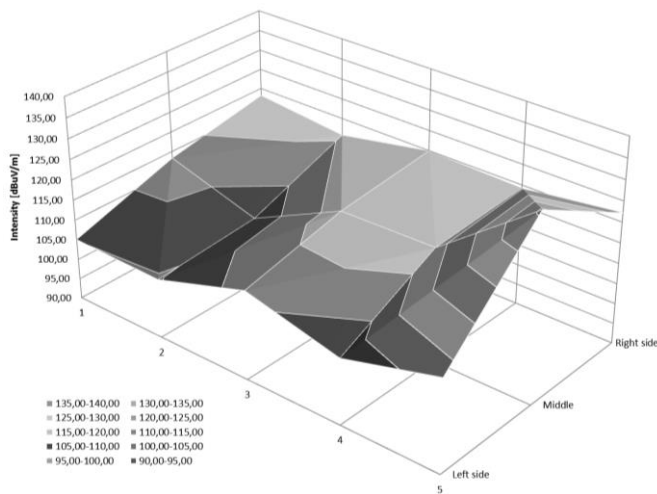


Fig. 14 Displacement of electrical field intensity for frequencies between 45 and 50 MHz

In Fig. 12 the displacement of the electrical field intensity for the frequency band from 20 to 25 MHz is displayed. One global maximum can be seen in the middle of the room (point (H)) as well as one local minimum in the same distance from the antenna (point (I)).

In Fig. 13 the same displacement is shown for the frequency band from 30 to 35 MHz. There is one global minimum in the center of the chamber while two almost identical maximums can be observed in the middle plane at the points (G) and (I). Different situation can be observed in Fig. 14 that shows the electrical field distribution for frequencies from 45 to 50 MHz. There are two minimums at the points (G) and (I) and one local maximum in the middle of the chamber. The global maximum can be observed at the point (J). From the figure it can also be read that these frequencies are better attenuated at the left side of the chamber although it has symmetrical shape.

For higher frequencies the field intensity graphs lose their explanatory power as it is obvious that the amount of 15 measurement points is not sufficient enough. The resolution of the displacement charts should be increased by increasing of measurement points.

VI. CONCLUSION

The paper deals with the problem of electrical field displacement within a semi anechoic chamber. It is expected that the semi anechoic chamber acts partly as a resonating box in which standing waves can occur at different modes, especially at those frequencies at which the absorbers mounted around the chamber's walls do not show their best performance due to quite large wavelengths.

Therefore an experiment was made in the semi anechoic chamber that is available at the Faculty of applied informatics at Tomas Bata University in Zlin in order to prove the expectations. The measurements were made by means of an anisotropic electrical field probe at 15 points inside the chamber. Although the amount of measurement points was

quite small, it was shown that the chamber behaves as expected. Minimums and maximums can be observed within the area of the chamber in dependence on frequency and location. This phenomenon is most evident between the calculated dominant mode frequencies and approximately 70 MHz, because below approximately 20 MHz no dominant modes can occur and above 70 MHz the attenuation of the reflections is quite effective due to combination of flat ferrite and pyramidal absorbers mounted across the walls of the chamber.

As it became clear that the expectations were valid, the authors decided to make new set of measurements with increased number of measurement points in order to increase the explanatory power of the data. Based on more accurate data, the correction methods can be proposed so the measurement of electromagnetic field radiations by tested equipment could be processed with higher accuracy.

REFERENCES

- [1] S. Radu., *Engineering Aspect of Electromagnetic Shielding*, Sun Microsystems
- [2] Compliance Engineering. Flat Ferrite RF Absorber: SFA version [online]. [cit. 2014-04-07].
- [3] J. Svačina. *Electromagnetic compatibility: Principles and notes* [Elektromagnetická kompatibilita: Principy a poznámky], 1st edition. Brno: Vysoké učení technické, 2001. ISBN 80-214-1873-7.
- [4] Frankonia: *Anechoic Chambers / RF-Shielded Rooms*, 2012
- [5] Rohde & Schwarz: *Probe Set HZ-11 for E and H near-field Measurements*, Probe set description
- [6] Z. Trnka, *Theory of Electrical Engineering* [Teoretická elektrotechnika], SNTL Alfa, Bratislava, 1972, Czechoslovakia

The role of traceability in the pharmaceutical safety supply chain

Jair Calixto, Maria L. R. P. Dias, Melissa S. Pokorny, Eduardo M. Dias

Abstract— The aim of this work is to demonstrate the need to trace pharmaceutical products and ensure their safety in the face of difficulties to operate the entire logistics in a country with continental dimensions devoid of infrastructure compatible with the needs of businesses and customers. This paper described the current pharmaceutical market and its business model, contextualizing the safety issue of the transport, counterfeiting, robberies and roads long distances that make it difficult to have control on the safety of medicines. In this context, this paper proposes alternatives, starting with greater control over the traceability of medicines. Secure tracking efficiency for medicines is one of the initial steps for solving some of the problems mentioned in the text.

Keywords— Traceability of medicines; counterfeiting of medicines; Safety supply chain; deviations; theft of medicines.

I. INTRODUCTION

THE product logistics developments led to the growing need to optimize the process and thereby deliver products in the shortest possible time in the markets. This result is sometimes hindered by a poor structure and devoid of the necessary safety.

Supply chain traceability assists in process control and, therefore, in the survey of metrics that provide data, which favor the quality of management and the product.

In this complex environment, the technologies are the tool with the possibility to assist companies, customers and Governments to control the process and to reduce the risks for patients.

Traceability, according to [1] Resolution RDC nr. 54/2013, is the set of procedures that allow to trace the history, application or location of medicines through information previously registered by unique identification system of products, service providers and users, to be applied in the control of any unit of medicine produced, released or sold on

J. Calixto is Pharmacist and Good Practices and Audits Pharmaceutical Manager in Sindusfarma -Pharmaceutical Association- (e-mail: jaircalixto@uol.com.br).

M. L. R. P. Dias is a PhD student at Escola Politécnica da Universidade de São Paulo (Polytechnic School of the University of São Paulo) (lidiad@pea.usp.br).

M. S. Pokorny is a PhD student of Polytechnic School, University of São Paulo – USP and a researcher of GAESI (melissapokorny@pea.usp.br)

E. M. Dias is full professor of the Escola Politécnica of the Universidade de São Paulo and coordinator of GAESI - Grupo de Automação Elétrica em Sistemas Industriais, a research group of the Electrical Energy and Automation Department, Escola Politécnica, Universidade de São Paulo, Av. Prof. Luciano Gualberto, trav. 3, n. 158, São Paulo/SP, Brazil, CEP 05508-970 (emdias@pea.usp.br).

national territory.

II. DEFINITION OF SUPPLY CHAIN IN THE CONTEXT OF THE PHARMACEUTICAL INDUSTRY

The pharmaceutical sector is composed of three main links in its supply chain, which are: production, distribution and dispensation. These steps are linked by product movement between one and another.

For the purposes of this study, the supply chain starts in the step of production, where the industry transforms inputs into pharmaceuticals, as provided by government regulations and business strategies.

The industry is responsible for the research and development processes well as the manufacturing of the medicines. It has a number of obligations and must follow the standards of quality and safety in its processes. Among these obligations, it has to maintain enough records of manufacturing, control and distribution of medicines, in order to ensure product traceability.

The distributor is part of the chain, purchasing the products for resale and, according to the requests received, realizes its shipment to your customer. The distributor delivers the shipment to a carrier, which will take the product to the customer, or in other cases, itself provides such delivery.

The dispensation is the point where the medicines are intended for end users and can be, for example, pharmacies, drugstores, hospitals, health centers or medical clinics.

The provisions of Law nr. 5.991/73, article 6, informs that the dispensation of medicines is exclusivity of pharmacy, drugstore and Health Unity and dispensary of medicines. In this same law, the definition of dispensation, says that is the act of providing to the consumer: drugs, medicines, medical devices, paid or not.

The carrier is responsible for carrying out the movement of medicines among the links in the supply chain. This step is very important to pay attention to the conditions of the movement. The temperature, for example, is a very important factor in maintaining the quality of the product and, therefore, of the properties which give it effectiveness.

The entire pharmaceutical chain is regulated and supervised by the National Agency of Sanitary Surveillance (ANVISA). ANVISA is the competent body to regulate and oversee the industry, established by the federal Government through the Law No. 9.782 from 01/26/1999. According to the article nr. 8, the Agency responsibilities, complied with the legislation in force, are to regulate, control and inspect the products and

services that involve risk to public health. Among other assignments, it sets rules and items to identify medicines label.

A. Research and development

The activities of the pharmaceutical industry are based in the sector of research and development (R & D), which seeks to identify substances (active ingredients) that may give rise to new medicines, either from synthesis or extraction processes of nature of the compound.

B. Production of pharmaceutical specialties

Production of pharmaceutical specialties is the production of medicines in a way that will be marketed and made available to patients, ready to be used. Medicines will be produced in their most varied forms, such as tablets (with or without coating), capsules, drops, syrups, suspensions, granular, injectables, etc.

C. Marketing and marketing of proprietary medicinal products

Marketing and marketing of proprietary medicinal products involves the entire commercial process for medicines, such as market studies, characterization of the consumer, distribution partnerships, development of marketing strategy, formatting of distribution channels, developing of the branding, strengthening the company or product brand, etc.

D. Possible Controls the supply chain of medicines

Appropriate controls of the medicine can be made through procedures and documents that ensure the quality of the process. Figure 1 presents a list of documents and procedures that aim to control each of the phases, either directly on the product, whether in the process. When these steps sequence are properly followed one have proper control over the process. Verification can point out the flaws and fix the problems. For example, when the documentation is not obeyed in its integrity, deviations are identified and eliminated

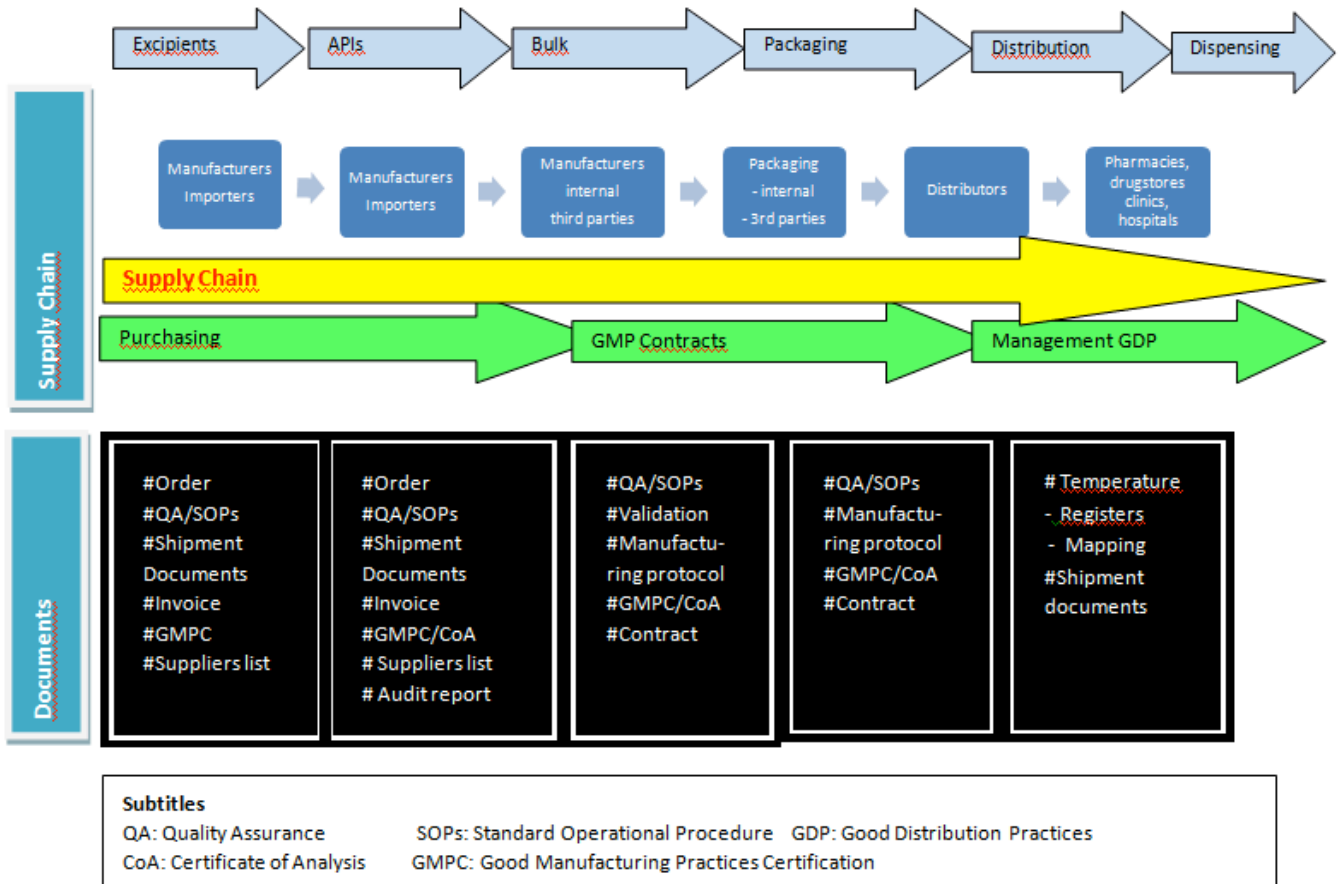


Fig. 1 – relevant Documents at every stage of pharmaceutical chain. As "Pharmaceutical finished products traceability" – Gilberto Rossi – Sindusfarma, SP. Nov, 2011

Although deployed controls, documents and certifications, there may be weaknesses in the supply chain, identified by entry points where can penetrate the illicit market actors. In a workshop conducted in São Paulo - Brazil, Dr Thomas

Zimmer, International Society for Pharmaceutical Engineering (ISPE) Vice President of European Operations, identified the following points as the most fragile of the supply chain: APIs, Excipients, packaging materials, third parties (repackers),

distribution, dispensation, and internet sales. The insertion of specific prevention and preventive mechanisms in these points will discourage the action and the penetration of illicit drug products in the pharmaceutical supply chain [2].

III. DEFINING THE PROBLEMS

Medicines have been the target of several illicit actions. Some of the main actions that affect the Brazilian pharmaceutical market are the theft, embezzlement and smuggling. These bad practices contribute heavily to insertion of the health risk to the patients.

On the other hand, for companies the risk can result in economic and financial loss, and high costs relative to the image and the brand of the product. Additionally, for Government they face taxes revenue subtraction and loss of credibility.

Intentional falsification occurs when products are produced with insufficient amount of active pharmaceutical ingredient (API) [3] [4]. These fakes are also known as substandard, meaning products containing asset amount below the regular or specifications containing no active ingredient.

Lots of products "substandard" contain defects of quality or do not comply with the Good Manufacturing Practices and Distribution [5].

Because of the technical difficulties to imitate or copy a pharmaceutical product, correctly and entirely, we can say the counterfeiting was more important than it currently is.

As a result of this technical difficulty, criminality focus in this field, instead of being production of fake medicine, is trucks thefts and deflections, which are much easier from the point of view of the product, but with much more risk from the point of view of criminal operation as a whole. Interest to notice that counterfeiting is more directly linked to high value-added products.

IV. TRACEABILITY

The main function of medicine traceability is to promote its recall from the market. This gathering aims to remove, from the pharmaceutical market, products suspected of causing health hazard due to defect or failure of quality, which would undermine its performance (quality, safety and efficacy) [6]. The recall is only possible if it is linked with a solid concept of traceability, making it possible to collect any unit of the pharmaceutical product in any pharmacy, clinic, distributor, hospital, health clinic or any other unit of dispensation of medicines, and bring it back to the industry.

In other words, traceability is the action that makes possible to identify the path followed by the product, from production to consumer. Internally, in the producer installations, it means making the reverse path of the documents involved in its manufacture. This route permits to identify the raw and packing materials used, process, operators who handled any of the products, as well the controls carried out. This information makes it possible to re-examine the process, the materials used and the final product collapsed, and, therefore, to identify causes of eventual problems.

In the year 2013, after the publication of ANVISA, Resolution RDC No. 54/2013, was presented the first definition of traceability for medicines in Brazil, that is "Tracking of medicines: a collection of procedures that allow a company to trace the history, application or location of medicines through information previously registered by unique identification system of products, service providers and users, to be applied in the control of any unit of medicine manufactured, released or sold on national territory".

A. History of medicine traceability in Brazil

The traceability of medicines has always been linked to the gathering of medicinal products, in the event of a failure or quality deviation that would compromise patient care, allowing their rapid return to the manufacturer and to eliminate the likely risk.

However, it did not happen so simply. It took major events to grow awareness before the deployment of the Good Manufacturing Practices (GMP) in the pharmaceutical industries. These occurrences accelerated the development of GMPs in the world.

The first publication mentioning gathering medicines was made by the Food and Drug Administration (FDA)-Federal Register, in 1963 [7], from where can be extracted the first notion of what would be later called traceability, which, as explained, is the need for records of distribution of medicines:

"§ 133,109 Distribution records. Complete records must be kept for each shipment in a manner that will facilitate the gathering, misuse or destruction of the product, if necessary. Such records must be retained for at least 6 months after the date of shipment and must include the name and address of the recipient, the date and the quantity shipped and manufacturing dates, tracking numbers or markings identifying the medicine shipped. If the medicine is handled under the control of the manufacturer, for following shipment to the establishments other than where it was produced, the records highlighted in this section must be maintained in these establishments." [7]

This first standard on GMP points the need to keep records of product distribution as mechanisms to withdraw from the market products improper for consumption. This practice, although already known and adopted by professionals in the pharmaceutical industries, can still be improved by the agents that operate in the market.

Other GMP documents were published by the World Health Organization (WHO), as the texts of 1969 [8], 1975 [9], 1992 [10]. In Brazil, in 1982, appeared one of the first documents, the GMP Manual SNVS's medicine of the Ministry of Health, [11], which said in its item 17.4. "For the eventual removal of a medicinal product be quickly arranged, there must be a distribution system that allows easy identification of your destiny".

We can, from these documents, extract the main objectives and reasons to track a product: facilitate product recall by removing those with suspected market failures; allow the trace of the product throughout the chain from manufacturing until the dispensation; assist in maintaining the safety of the use of

medicines and contribute to reduce the entry of illicit products in the pharmaceutical chain.

V. TECHNOLOGIES

For the most illicit or illegal activities mentioned earlier, the primary and immediate solution is fighting against crime, via supervision and police performance. However, for several reasons, it's not what happens in practice. Among the reasons can be listed the lack of police equipment, the absence of specific technologies to combat crime, the lack of material and human resources, among others. This is a problem involving the economic and social sectors, and that demand joint actions of public authorities and private initiative. [12]

Thus, it is important to know the appropriate existing technologies and their various applications, to enable effective control over the goods transported. Among the many solutions available today, different mechanisms, active in various stages of the process, can be related.

The applications of a system to unique identify an object, to capture, storage and transmit data, gives better control over the supply chain, therefore to its safety. As examples, it allows a recall and to prevent fake medicines to run into the regular market (v.g. the system identifies and detects products from cargo theft [3]).

Having an electronic system, with exchange of electronic information, represents gain of quality, therefore, security (for example, it prevents human errors and crosses available information from different sources in a short time).

A. Available tracing technologies

Several technologies are available that allow the tracking of products. According to Portugal e Paulino [13], a number of technological solutions can be applied to the sector: the printing of 2D codes (like Datamatrix) on packages, the use of forensic inks packs, the cryptographic signature, the security seals, the RFID labels, the packaging with special materials, the laser surface or the combination of multiple technologies.

Linear barcodes (1D): has low density of information unavailable for Mass Serialization. Low cost, infrastructure available. Is the code printed on the product packaging we consume daily, like cookies, milk, beverages, etc. Most products contains a barcode to identify it.

The code GTIN (Global Trade Item Number/Global Trade Item Number) is an identifier for trade items developed and managed by GS1, formerly EAN/UCC. The GTINs, formerly called EAN codes, are assigned to any item (product or service) that may be priced, ordered, or invoiced at any point in the supply chain. [14]



Fig. 2 – Representative image of a linear GTIN barcode 13

Bi-dimensional barcode (2D): between the bi-dimensional models available, there is the Datamatrix, nowadays elected

by the pharmaceutical market technology as part of the solution to several problems in the supply chain. It is available for bulk Serialization, has low cost, though some adaptation of infrastructure is needed.



Fig. 3 – Representative image of a datamatrix code

B. Difficulties of traceability

The use of the bi-dimensional barcode in the production, storage, shipping or receiving is considered advantageous to, between others, low cost (in relation with RFID tags), record of batch numbers and dates; record of the numbers of batches used; connection between the production batch number and the raw materials used, management of physical inputs of goods and shipments using the SSCC, managing separation and release of consignments, record of movement of merchandises, physical inventory, creation of logistical units, assignment and remarking of SSCC, tracking inventory movements, connecting the SSCC, lot number, product and destination of delivery, receive control through efficient coordination with boarding warnings, co-ordination of orders and deliveries, sending acknowledgments of receipt, entering data of the products in inventory records and transmission of information for efficient management of orders and invoices [14], [25].

The application of traceability is also useful in the hospital environment, to ensure the unit dose and protection of the patient. Barcode technology is also an important tool to ensure the traceability of medicines used in the hospital environment, enabling 100% traceability of medicines delivered by the dispensing pharmacy [15]. Important to notice that to some authors [16] the traceability of the medicinal product in hospital is only possible if it is registered to whom, when and by whom was administered the medicine.

Although there are dozens of advantages, the difficulties inherent in this process are not negligible, as for example, the necessary reorganization of the manufacturing and distribution processes and operating procedures, vital to restructure the medicine supply chain [17].

C. What happens in the world market

Some models of traceability in deployment or already deployed can serve as a benchmark for other countries, including Brazil, which can absorb best practices in implementation in each of them. Short description of these models is given below.

- 1) Argentina: The Administración Nacional de Medicamentos, Alimentos y Tecnología Médica (ANMAT) has published in May 2011 the Disposición 3683/2011-Report 5/31/2011: "Traceability system of medicines that companies must implement. This reaches companies that has legal interference in the supply chain of marketing, distribution and dispensation of medicinal

specialties included in marketing Authorization for Specialities". The health authority of Argentina accepts the code GS1-128 and RFID for a transitional period, but preferably companies should adopt, in the future, the GS1 Datamatrix – 2D- barcode".

- 2) Germany: In Germany the tracing system is being implemented by the industry itself. The securPharma, according to the European Policy 2011/62/I of 6/8/2011 mending the policy 2001/83/EC (regulation concerning products medicinal for human use), includes additional measures to ensure the protection against counterfeit medicines. Each package is marked with a Datamatrix barcode containing a number of a unique product associated with a serial number. This requires an extension of the German reimbursement system (PZN8) to the Pharmacy Product Number (PPN) or National Trade Item Number (NTIN). The Datamatrix code contains the PPN or the NTIN both of which are incorporated into the PZN8. [18], [19], [20].
- 3) China: In April 9, 2008 China's State Food and Drug Administration (SFDA) reported that the serialization would be mandatory for 275 therapeutic classes of products from December 2011. In May of 2013 the list was extended from 307 to 502. The regulation requires all drugs sold in the Chinese market. The program was divided into phases:
 - Phase 1 – Serialize and track all class 1 substances (subsidiaries), as of October 2007.
 - Phase 2 – Serialize blood products, vaccines and controlled substances class 2 and injectable medications since October 2008.
 - Phase 3 – Serialize and track all medicines.
- 4) Italy: In Italy the objective of traceability is the prevention of fraud in the system of reimbursement of medicines of the Italian Government, through the Servizio Sanitario Nazionale (SSN). On the Decree of July 15, 2004 [21], the Ministry of health establishes a central database to monitor the manufacture of medicines for the reimbursement system. The database is managed by the Italian Ministry of Health. The central database will join, via internet, all data concerning the supply of label (bollini), numbered.
- 5) France: The French Agency for Health Safety (AFSSAPS) decided to extend the product code CIP-7 for CIP-13. The CIP code is managed and delivered by the Club Inter Pharmaceutique (CIP) which includes manufacturers, distributors, agents, organizations representing drugstores, pharmacists from hospitals and healthcare experts technical French [22]. From 1/1/2011 Datamatrix is mandatory for all pharmaceutical products. The code should contain the batch number, the expiration date and the product number (CIP13).
- 6) Turkey: In Turkey The process of tracking medicines started in October 2007 as the initiative of the Turkish Ministry of Health. In August 2008 the tracking system had its first demonstration for the sector, where were presented the objectives of the project. By September 2009 was running the pilot project for testing the

efficiency of the system and to prove the model. Already in January 2010 the system began to operate in its first phase [23].

- 7) USA: In the State of California, the discussions led to the postponement of the implementation of traceability for 2015.

VI. PROPOSAL

To control of the entire pharmaceutical supply chain, from the production step until the dispensation step, it is proposed to print a Datamatrix barcode in each unit of the product available for sale. These units, belonging to a batch, will be marked with a Datamatrix, which contains an individual and unique serial number that identifies that item.

The sequence insertion of codes in production lines can be given following, as descriptive by GS1 standards, Brazil [24]: 2D code printing on secondary packaging, barcode printing GS1-128 on secondary packaging, barcode printing GS1-128 on tertiary packaging and barcode printing GS1-128 on pallet.

By means of suitable equipment, the 2D code is printed on the secondary packaging of the medicinal product. Then, the checking the printing quality by cameras and capture the data containing in the barcode (batch number, serial number, expiration date and number of registration number of medicine) [1] and transfer to the database, unit by unit. Each movement of the product is registered in the database, stating its position and location.

VII. CONCLUSION

The application of bi-dimensional barcode, such as Datamatrix, can be very useful in the control of illegal activities in the logistics chain for medicines, contributing to reduce robberies, counterfeiting, fraud, smuggling and diversions.

Additionally, it collaborates with the maintenance of the integrity and authenticity of the product, since existing a strong commitment from all agents (industries, distributors and pharmacies) in adopting and, effectively, managing the system.

The use of 2D barcode will become an element of high reliability in the transit of goods, assisting on the transit control. Therefore, it is expected there will be reduction of deviations and crimes through the distribution and marketing of medicines.

On the other hand, the use of this application, points to the costs reduction in the control of stocks. Also, by quickly providing quality information, the systems benefits agility in decisions making.

In a nutshell, in medicine traceability, the use of bi-dimensional barcode technology will bring immediate benefits and will contribute, as one of the necessary elements, for the safety of the whole medicines supply chain.

REFERENCES

- [1] Resolução ANVISA RDC nr.54, December 10, 2013. Dispõe sobre a implantação do sistema nacional de controle de medicamentos e os mecanismos e procedimentos para rastreamento de medicamentos na

- cadeia dos produtos farmacêuticos e dá outras providências. Brasil, ANVISA, 2013.
- [2] Zimmer, Thomas. “Entrada de produtos ilícitos na cadeia de abastecimento de medicamentos”. Adapted from Thomas Zimmer – presentation “Workshop Rastreabilidade”. Brasil. Sindusfarma. April, 2008.
- [3] Nogueira, Ellen; Vecina Neto, Gonçalo. “Falsificação de medicamentos e a Lei nº 11.903/09: aspectos legais e principais implicações”. Revista de Direito sanitário, São Paulo v.12n.2, p.112-139 Jul/Oct. 2011.
- [4] Ames, Joseane; Souza, Daniele Zago. “Falsificação de medicamentos no Brasil”. Rev. Saúde Pública 2012; 46(1): 154-9 Faculdade de Farmácia. Pontifícia Universidade Católica do Rio Grande do Sul. Porto Alegre, RS, Brasil. Programa de Pós-Graduação em Química. Instituto de Química. Universidade Federal do Rio de Janeiro. Rio de Janeiro, RJ, Brasil. III Setor Técnico-Científico. Superintendência no Estado do Rio Grande do Sul. Departamento de Polícia Federal. Porto Alegre, RS, Brasil.2012.
- [5] “Facts/Activities/Documents” developed by the Assembly and the Working Groups of IMPACT- International Medical Products Anti-Counterfeiting Taskforce, 2006-2010.
- [6] Resolução ANVISA RDC nº 17 de 2010. Brasil, ANVISA, 2010.
- [7] Food and Drug Administration (FDA) - Federal Register, “Drugs; Current Good Manufacturing Practice in Manufacture, Processing, Packing or Holding,” Part 133, 28 FR 6385, § 133.109 Registers of distribution, June 20, 1963.
- [8] WHO Technical Report Series nr 418, 22th. Report, Geneva, 1969.
- [9] WHO Technical Report Series 25º Report, nr 567, 1975,
- [10] WHO Technical Report Series 32º Report, nr. 823, 1992.
- [11] “Manual de Boas Práticas de Fabricação de Medicamentos”. SNVS, Ministério da Saúde, 1982.
- [12] Carvalho, Arilson Coelho. “O impacto negativo da pirataria no cenário mercadológico e as dificuldades no combate à falsificação”. Revista do IBRAC, p.47-84, 2005.
- [13] Portugal, B.; Paulino, M.A. “Falsificação de Medicamentos e Vigilância Sanitária”. Pontifícia Universidade Católica de Goiás. Instituto de Estudos Farmacêuticos. Goiás, Brasil, 2009
- [14] “Padrões GS1 na cadeia de suprimentos do setor da saúde”. GS1 Brasil. www.gs1br.org.
- [15] Almeida, Silvia Helena Oliveira. “Incorporação de novas tecnologias de informação em um sistema de distribuição de medicamentos: avaliação quanto ao aumento da segurança dos pacientes”. Porto Alegre – UFRGS, 2010, 129p. Dissertação (mestrado profissional). UFRGS. Faculdade de farmácia. Programa de Pós-graduação em Ciências Farmacêuticas.
- [16] Pazin Filho, Antonio et all. “Beira de Leito: Rastreabilidade da Dispensação à Administração do Medicamento”. Hospital das Clínicas da Faculdade de Medicina de Ribeirão Preto da Universidade de São Paulo (HCFMRP-USP). Ribeirão Preto, São Paulo, Brasil, 2010.
- [17] Ernesto Júnior, J. H. “A cadeia de suprimentos do setor farmacêutico e os impactos da Lei de rastreabilidade em uma distribuidora de medicamentos”. Ribeirão Preto, 2011. Conclusão do curso – TCC Administração apresentado no Departamento de Administração FEAR-USP. Faculdade de Economia Administração e Contabilidade de Ribeirão Preto-USP.
- [18] “securPharm: Der deutsche Schutzschild gegen Arzneimittelfälschungen Aktueller Stand des Projekts”. Berlim, May 23, 2013. Accessed in January 10, 2014. Avalaiable in www.securpharm.de.
- [19] “Coding rules for medicines requiring verification for the German market”. Version: 1.01. Frankfurt, Germany, December 03, 2013. Accessed in January 10, 2014. Avalaiable in www.securpharm.de.
- [20] “BPI-Bundesverband der Pharmazeutischen Industrie e.V. Unterlagen securPharm-Pilotprojekt”. Accessed in April 26, 2014. Avalaiable in www.bpi.de
- [21] Ministero della Salute, Decreto 15 luglio 2004. “Istituzione, presso l’Agenzia italiana del farmaco, di una banca dati centrale finalizzata a monitorare le confezioni dei medicinali all’interno del sistema distributivo”.(G.U. Serie Generale, nr. 2, January, 2005).
- [22] Notices and Communications Miscellaneous Notices. Ministry of Health and Solidarity. “Notice to human-use medicinal product marketing authorization holders and head pharmacists of the pharmaceutical establishments cited in article R. 51242 of the French Public Health Code (CSP)” NOR: SANM0720920V. 21/02/2007. Accessed in January 02, 2014. Available in [http://ansm.sante.fr/Activites/Elaboration-de-bonnes-pratiques/Codification-et-tracabilite-des-medicaments/\(offset\)/7](http://ansm.sante.fr/Activites/Elaboration-de-bonnes-pratiques/Codification-et-tracabilite-des-medicaments/(offset)/7)
- [23] T2 software et all. “Rastreabilidade de medicamentos. Relatório sobre a visita da delegação brasileira à Turquia”. São Paulo, SP, Brasil, 2012.
- [24] GS1 Brasil. “Reunião GT Saúde”. March 12, 2013. GS1 Brasil. www.gs1br.org.
- [25] GS1 Brasil. “SSCC (Serial Shipping Container Code)”. Accessed in February 20, 2014. Avalaiable in <http://www.gs1.org/barcodes/technical/idkeys/sscc>.
- [26] Secretaria Nacional de Vigilância Sanitária. “Portaria nº 16 de 6 de março de 1995”. Brasil, SNVS, Ministério da Saúde, 1995.
- [27] Resolução ANVISA RDC nº 134 de 13/07/2001. Brasil, ANVISA, 2001.
- [28] Resolução ANVISA RDC nº 210 de 2003. Brasil, ANVISA, 2003.
- [29] Fernandez, Marcelo Luis Alves. “Avaliação da utilização de documentos fiscais eletrônicos na rastreabilidade de cargas”. Escola Politécnica da USP. Agosto 10, 2012. São Paulo, 2012.
- [30] Oliveira da Silva, Luiz Roberto; Lima Alves, Marcelo. “O sistema nacional de metrologia legal: ações para o desenvolvimento da rastreabilidade”. METROLOGIA-2003 – Metrologia para a Vida. Sociedade Brasileira de Metrologia (SBM). Recife, Pernambuco, Brasil, Setembro, 2003.

Testing the properties of materials used for the measurement of the PIR detector in the infrared range

R. Drga, D. Janáčková, and H. Charvátová

Abstract - The work deals with the testing of emission and reflection properties of materials that are necessary for the workplace to measure the spatial characteristics of PIR detectors in the infrared region. The aim is to reduce the influence of parasitic radiation environment shading measuring sensors and detectors to define the characteristics of the source of radiation and the reflective properties of the surrounding area, eliminate the influence of thermal radiation operator.

Keywords - PIR detector, IR radiation, conductivity, mathematical model, shielding material

I. INTRODUCTION

WHEN measuring the workplace for measuring IR-radiation in the far field measurement PIR detectors were often influence parasitic radiation from various heat sources. The basic configuration is workplace in Fig. 1.

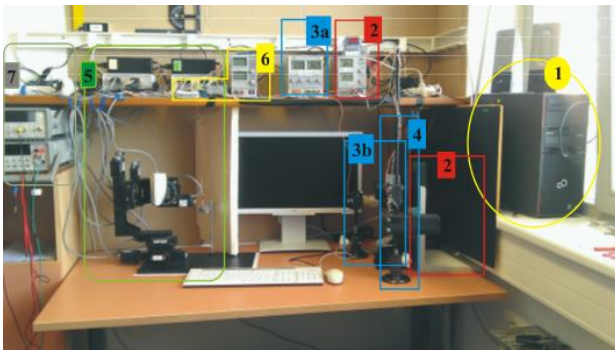


Fig. 1 Workplace for measuring IR radiation in the far field measurement PIR detectors

This work was supported by the European Regional Development Fund under the project CEBIA-Tech No. CZ.1.05/2.1.00/03.0089.

R. Drga, Tomas Bata University in Zlín, Faculty of Applied Informatics, Department of Security Engineering, nám. T. G. Masaryka 5555, 760 01 Zlín, Czech Republic (e-mail: rdraga@fai.utb.cz)

D. Janáčková, Tomas Bata University in Zlín, Faculty of Applied Informatics, Department of Automation and Control Engineering, nám. T. G. Masaryka 5555, 760 01 Zlín, Czech Republic (e-mail: janacova@fai.utb.cz)

H. Charvátová, Tomas Bata University in Zlín, Faculty of Applied Informatics, Department of Automation and Control Engineering, nám. T. G. Masaryka 5555, 760 01 Zlín, Czech Republic (e-mail: charvatova@fai.utb.cz)

On the right side you can see the control one computer on which the operating system Microsoft Windows 7, run applications created with NI LabView environment. This is connected via USB bus with two controllers for motion control positioner, the picture is a group of five devices, which are seen two sources, two control units and each unit go from 3 cables to individual drives the positioner, the unit left is for straight drive movements and rotational movements to the right, for a total of 6 drives.

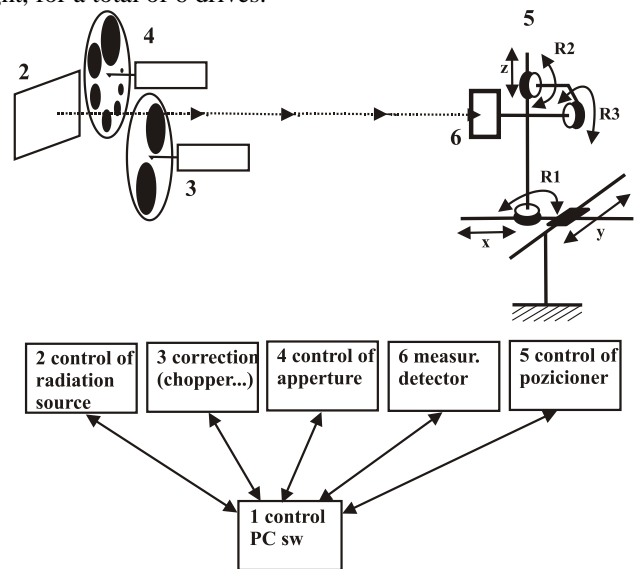


Fig. 2 Hardware concept of workplace

On the positioner is placed detector, whose output goes to the input-output units USB6008, which is on the image located in area 6. With this unit, you can then also control the function of aperture, focus the laser beam scanning and other features. Source 3 is used to control the speed of the chopper, which includes the drive is physically located on a pedestal on the table - the area 3b. In area 4 is located aperture - drive, disc aperture and optical adjusting the position. Area 2 represents the temperature control radiation source 2 (top) and its own Peltier element located down.

The whole workplace can be thought of as illustrated in Fig. 2, which is an important source of useful 2 simulating an intruder, then parasitic - unwanted sources of radiation from

the chopper drives 3, aperture 5 and positioner 5, as will be mentioned.

II. METHODS FOR THE DETECTION OF SPURIOUS RADIATION SOURCES

Any material having a temperature greater than absolute zero (- 273 ° C) emits infrared radiation whose intensity corresponds to the temperature. The diagram in Fig. 3 shows the emission characteristics of the body at different temperatures. It is apparent that the body at high temperatures emits a small amount of visible radiation.

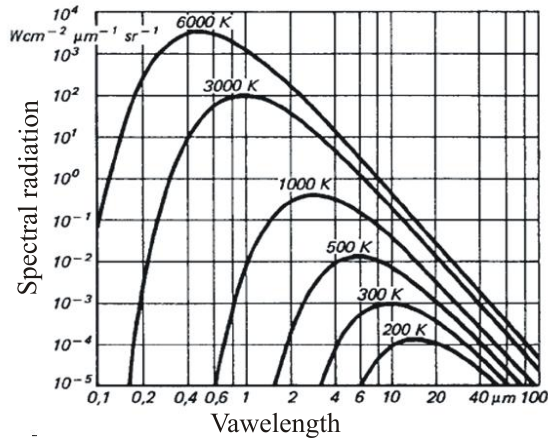


Fig. 3 Blackbody radiation characteristics depending on its temperature

Emitted energy over the full spectral range (area under each curve) increases with the fourth power of the temperature according to the Stefan-Boltzmann law (1) and it is clear that the peak wavelength of radiated energy can be determined by temperature.

$$Q_0 = H_0 \cdot S_1 = \delta_0 \cdot T_1^4 \cdot S_1 \tag{1}$$

where:

- Q_0 - total radiant flux [W]
- H_0 - total intensity of radiation [W/m²]
- S_1 - area of a black body [m²]
- T_1 - absolute temperature of the body [K]
- δ_0 - Stefan-Boltzmann constant 5,67.10⁻⁸ [Wm⁻²K⁻⁴]

Characteristics expresses the dependence of the shift, where the maximum value of spectral power densities shifted to shorter wavelengths with increasing temperature emitters - equation (2) which is known as Wien's law.

$$\lambda_{max} = \frac{b_w}{T_1} \tag{2}$$

- where: λ_{max} - wavelength of max.emission [m]
- T_1 - temperature of the body [K]
- b_w - Wien constant, $b_w = 2.898$ mmK

The spectral density of radiation in this maximum is proportionately fifth power of temperature,

$$W_1 = konst \cdot T_1^5 \tag{3}$$

For the area of IR radiation, wherein the simulated movement of an intruder, a person whose temperature is about 36 °C according to the characteristics set forth in Figure 3 can be deduced that the peak in the region of 10 micron wavelength.

To measure the surface temperature can be two measurement methods:

1. Contact measurement of surface temperatures - useful to define the source of radiation
2. Contactless measurement - suitable for parasitic difficult to define in advance the radiation source using pyrometer using IR cameras

III. SPURIOUS RADIATION SOURCES WORKPLACE

Primary sources of workplace transmitting IR radiation, which negatively affect the results of measurements include imaging and display devices, drives the moving parts, elements of design workplace and radiation physical operator workplace. Each of these elements has a direct effect on the response PIR detector, because using the positioner to move parallel to the detector relative to the environment and even static object with a higher temperature can change the radiation incident through the optics to pyroelement.

A. Imaging and indicating equipment

The first device is a display monitor, in which case the LCD screen type. As is shown in Fig. 4, the temperature reaches the top of the screen to 37 °C, it is the base temperature intruders.

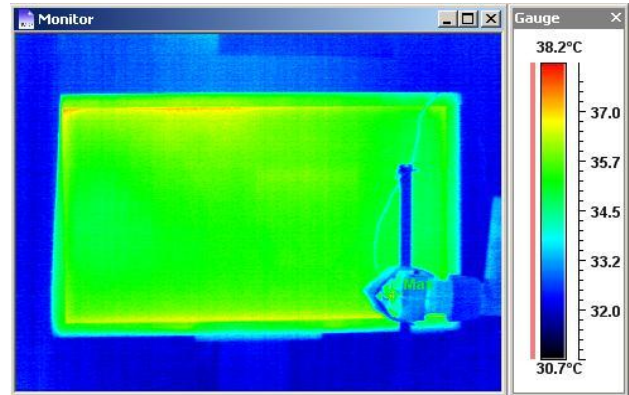


Fig. 4 IR image LCD monitor

B. Drives moving parts workplace

The first version was used to drive the chopper DC motor with gearbox. In Figure 5 it is seen that the temperature in the actuator reaches 34 °C.

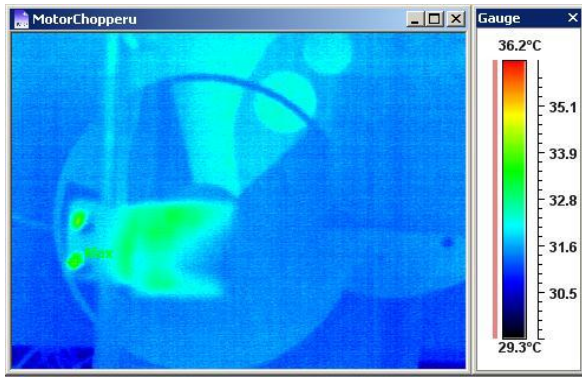


Fig. 5 IR image of the chopper drive

Figure 6 shows the IR image drives the positioner. This situation is worst of all, because the positioner is placed directly own detector and the radiation source is very close to its own sensor, thus pyroelement.

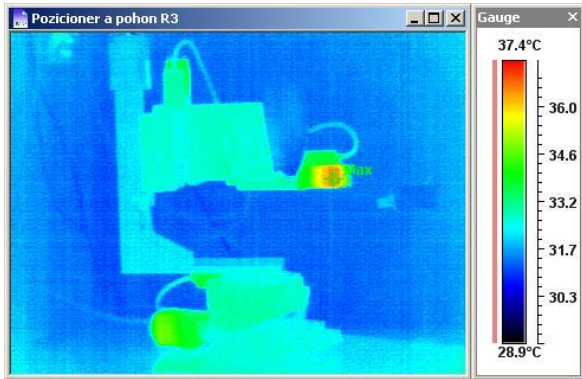


Fig. 6 IR image of the chopper drive

C. Components design workplace

In the defined area around the radiation source - the Peltier element leads to flow of heated air that accumulates in the upper part of the workplace and so heats the design of this source. Here, the temperature reaches 29.4 °C, as shown in Figure 7.

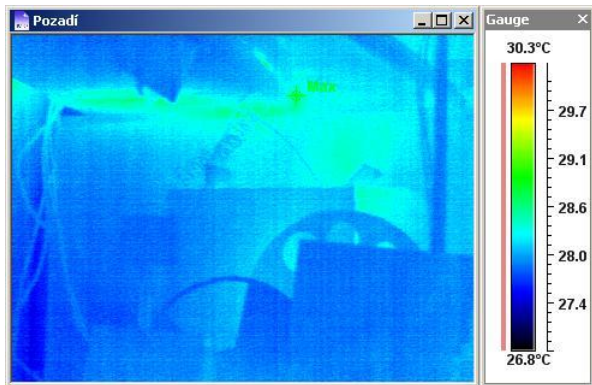


Fig. 7 IR image of construction workplace

IV. PROBLEM SOLVING OF SPURIOUS RADIATION SOURCES

For removal of spurious radiation sources can be used several basic methods:

- relocation of radiation sources outside the workplace
- reduce power consumption of drives
- reduce shielding of radiation sources
- the closure of roads radiation into heat tunnel

A. Moving sources of radiation outside workplace

For drive of the chopper was reduced power consumption own drive using a different type of drive and shading toward the detector. For drives of positioner is not possible to reduce the power consumption, because these drives are realized using stepper motors and they are fed well in the rest position when the shaft does not rotate because they have to ensure the stability and accuracy of the set position, as seen from the structure, presented in Figure 8. Longitudinal drives are marked blue color and red rotary drives.

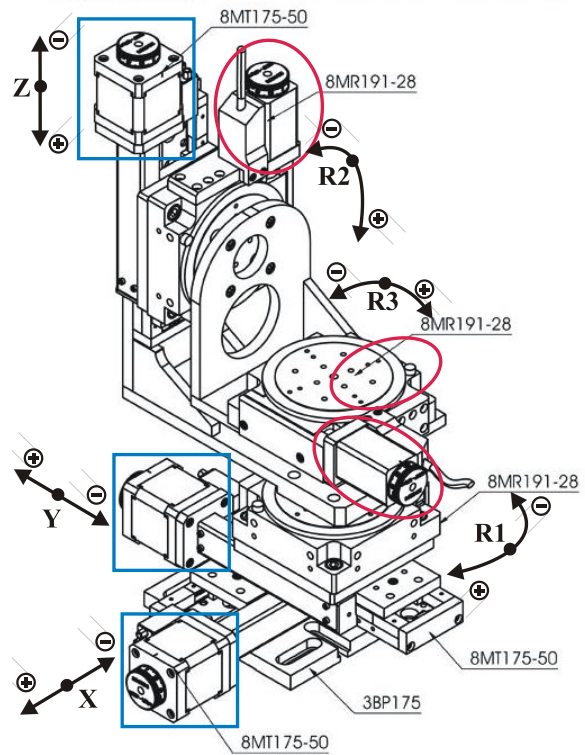


Fig. 8 Construction of positioner

B. Separation operators area and the workplace

For the separation space and operators workplace was used plexiglass, as shown in Figure 9. This material acts as a filter which suppresses IR radiation operators in far area.



Fig. 9 Separation workplace and operator

C. Separation of space temperature beams

For the separation of the useful heat radiation from the surroundings proved insulating material Tubex shaped stepped tube, as shown in Figure 10



Fig. 10 Separation workplace and operator

D. Shading radiation sources

For shading can be preferably used a few basic materials according to the required functions:

- cardboard
- galvanized iron sheet
- aluminum sheet

These materials are shown in Figure 11 and can be further adjusted by using a surface coating, matte black, thus increasing the coefficient of emissivity.

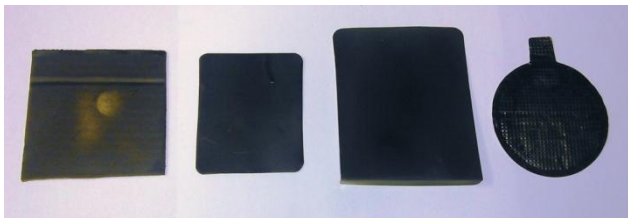


Fig. 11 Materials for shielding radiation sources

To describe the material temperature after the impact of heat radiation come out from equation (4), which defines the intensity of the radiation heat flux q incident on the shielding material:

$$q(\tau) = \delta_0 \cdot C(T_2^4 - T_1^4) \tag{4}$$

where: δ_0 - Stefan-Boltzmann constant

C - constant represents emission surface and geometric properties, [1]

T_2 - source temperature, [K]

T_1 - temperature of the heated surface, in our case the surface temperature of the shielding plate, [K].

The equation is then a modification of the relationship that is used to heat radiation.

The heat that hit the surface of the material to spread further conduction, as described in equation (5)

$$\frac{\partial T}{\partial \tau} = a \cdot \frac{\partial^2 T}{\partial x^2} \tag{5}$$

Apply the boundary condition (6):

$$\lambda \left(\frac{\partial T}{\partial x} \right)_{x=b} = q \tag{6}$$

and the initial condition (7):

$$T = T_p \quad \text{for} \quad \tau = 0 \tag{7}$$

where: b - half the thickness of the sensor, [m]

x - direction coordinate, [m]

This model can be solved in various ways, such as the Laplace transform. The result is equation (8), which represents the final solution of unsteady temperature field of slabs heated by radiation

$$\frac{T - T_p}{T_c - T_p} = K_i \left[Fo + \frac{1}{2} \left(\frac{x}{b} \right)^2 - \frac{1}{6} - 2 \sum_{n=1}^{\infty} \frac{\cos \left(\frac{x}{b} p_n \right)^{(-Fop_n^2)}}{p_n^2 \cos p_n} \right] \tag{8}$$

where: K_i - Kirpitch criterion, [1]

Fo - the Fourier criterion, [1]

p - roots of the equation (9)

$$p_n = \pi n \tag{9}$$

V. CONCLUSION

By measuring the temperature of the actuator R3 as shown in Fig. 12, wherein the front shading reached maximum temperature 37 °C, after shading the temperature decreased to 28 °C. It was possible to calculate the amount of heat absorbed partially shielding material. Based on measurements of surface temperatures was possible to compare these values with the calculated temperature of the solved mathematical model.

Results varied approximately 2%. It can be said that the mathematical model for the above case is valid.

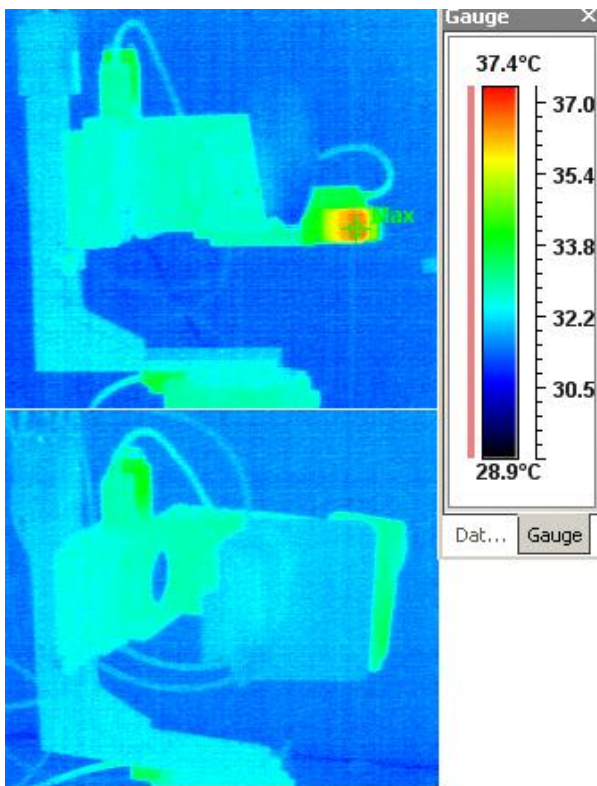


Fig. 12 Comparison of temperatures drive without shielding and with shielding

Using the described methods and materials were implemented to workplace, where it was possible successfully to measure the spatial characteristics of the PIR detector. Without the use of these materials and methods of measurement would not be feasible.

REFERENCES

- [1] J. D. Vincent, *Fundamentals of infrared detector operation and testing*. USA, Texas: WILEY, 1990.
- [2] G. F. Knoll, *Radiation detection and measurement*. USA, Texas: WILEY, 2000.
- [3] B. Saleh, *Fundamentals of photonics*. USA, Texas: WILEY, 2007.
- [4] K. Kolomazník, *Teorie technologických procesů III.* (in Czech). University of Technology in Brno, Brno, 1978
- [5] A., R. Jha, . *Infrared technology*. USA – Texas: WILEY, 2006
- [6] C. Hotz, *Přenos tepla zářením* (in Czech), Prague: SNTL, 1979.
- [7] K. Kolomazník, *Modelování zpracovatelských procesů* (in Czech), Brno: University of Technology in Brno, 1990.
- [8] K. Židek and J. Pítel, "Smart 3D Pointing Device Based on MEMS Sensor and Bluetooth Low Energy," in *Proceedings of the 2013 IEEE Symposium on Computational Intelligence in Control and Automation (CICA)*, Singapore, April 16-19, 2013, pp. 165-168.
- [9] R. Makovník and O. Liška, "Contribution to experimental identification and simulation problems of dynamic systems", *Ovidius University Annual Scientific Journal*. vol. 9, No. 1, 2007.
- [10] O. Liška (2008). Monitorizačné systémy pre automatizovanú výrobu (in Slovak). *Transfer inovácií*. [Online]. 12. pp. 121-123. Available: <http://www.sjf.tuke.sk/>
- [11] M. Fodor, O. Liška (2010). Design and realization sensorial system on detection obstacle [CD-ROM], in *8th International Symposium on Applied Machine Intelligence and Informatics*, Herľany, Slovakia.

Vehicle Inspection & Maintenance Program in São Paulo - Results and Environmental Benefits

Marcelo C. Branco, Fábio C. Branco, Gabriel M. Branco, Eduardo M. Dias; Alfred Szwarc

Abstract — The São Paulo City In-Use Vehicle Inspection and Maintenance Program – I/M-SP has resulted in increasing environmental benefits from the 30% to 50% reduction of excess exhaust emissions. The yearly averages of progressive emissions reduction indicate a new culture of vehicle maintenance, better services and greater awareness of society. The results also show that in-use vehicles need to be inspected from the first year of use, because the advanced technologies that equip modern vehicles are susceptible to high rise of emissions – from ten to over thirty times of normal levels – in case of problems leading to an increase of emission. Due to the impressive increase of new vehicles in the existing fleet the impacts of emissions growth are comparable to those of older vehicles. Therefore, the annual inspection requirements established by CONAMA (National Environmental Council) are strongly supported by technical reasons and proven to be needed. Also, it has been shown that the centralized program concept, as defined by CONAMA, is fundamental to the inspection quality control process and fraud detection. Results from the I/M-SP, after being thoroughly verified and certified by statistical analysis and technical studies also have been used by CONAMA for regulatory updates. They also have been used by the motor industry and repair network as a field feedback. All this facts allow the authors to state that the I/M-SP Program has reached significant results, comparable to the ones reached by the best international programs of its kind.

Keywords—air pollution, emissions, environmental impact, vehicle inspection.

1. INTRODUCTION

The In-Use Vehicle Inspection and Maintenance Program – I/M-SP started to be implemented in the city of São Paulo in

Marcelo C. Branco is a PhD student at Escola Politécnica of the Universidade de São Paulo (Polytechnic School of the University of São Paulo) (marcelobranco@uol.com.br)

Fábio C. Branco is Associate and Project Manager of EnvironMentality – Tecnologia com Conceitos Ambientais Ltda – Rua Michigan 177, CEP 04566-000-São Paulo/SP, Brasil (fabio.tcl@uol.com.br)

Gabriel M. Branco is Associate and Director of EnvironMentality – Tecnologia com Conceitos Ambientais Ltda – Rua Michigan 177, CEP 04566-000-São Paulo/SP, Brasil(gabriel.tcl@uol.com.br)

Eduardo M. Dias is full professor of the Escola Politécnica of the Universidade de São Paulo and coordinator of GAESI - Grupo de Automação Elétrica em Sistemas Industriais, a research group of the Electrical Energy and Automation Department, Escola Politécnica, Universidade de São Paulo, Av. Prof. Luciano Gualberto, trav. 3, n. 158, São Paulo/SP, Brazil, CEP 05508-970 (emdias@pea.usp.br)

Alfred Szwarc is Director of ADS – Tecnologia e Desenvolvimento Sustentável – Rua Albuquerque Lins, 848 / 11 CEP 01230-000 São Paulo/SP, Brasil (alfred.ads@terra.com.br)

2008 according the best practices (institutional design test-only, centralized, enforcement and compliance promotion, etc) [1], to curb excess vehicle emissions and noise and incentive social consciousness in the need of proper periodic vehicle maintenance. As a result, engine mistuning, parts wear and other causes that increase emissions could be minimized. The I/M-SP has inspected more than 3,5 million vehicles per year, and generated a huge and highly consistent emission database. This has allowed a precise knowledge of the status of vehicle maintenance in the city. It also allowed better understanding of the in-use fleet technical characteristics in terms of its potential to reduce emissions in real world conditions as the result of the technological improvements driven by the emission control programs implemented in progressive steps (shown in tables 1 and 2) for new vehicles and motorcycles in Brazil - PROCONVE and PROMOT. These new vehicle emission control programs started in 1986 and have been promoting the adoption of cleaner emission technologies such as electronic fuel injection and engine management, three-way catalytic converters, flex fuel engines, ethanol use etc.. The I/M-SP results provided means to easily compare the effectiveness and durability of these technologies along the vehicle useful life, among other parameters. These analyses led to a clear diagnose and comparisons between the well maintained and tampered/not properly maintained vehicles, which allowed designing the “avoidable emissions” to be controlled by the I/M-SP (see Fig. 1).

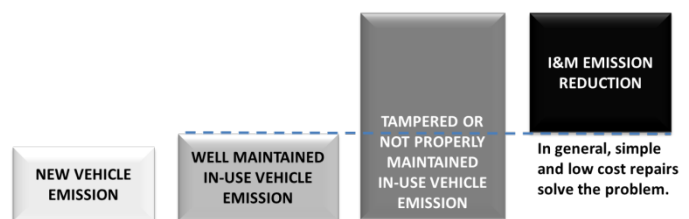


Fig. 1 - Technological vision of the vehicle emission control

2. GENERAL RESULTS OF THE VEHICLE INSPECTIONS

This paper shows the main benefits of the I&M Program in reducing the avoidable emission, which is estimated through the statistical analyses of inspections results.

The Brazilian Program of Vehicle Emission Control – PROCONVE has been in place since 1986 and promoted significant emission reductions through technological improvements. Carbon monoxide – CO, hydrocarbons – HC and oxides of nitrogen – NO_x decreased more than 95% in all new vehicles and, in addition, stringent particulate matter –

PM standards were implemented for the heavy duty (Diesel) vehicles. The age distribution of the in-use fleet concentrates higher numbers of newer vehicles, resulting from the natural fleet renewal. Therefore, the environmental impact of the in-use fleet is roughly distributed along all vehicle ages or PROCONVE's phases, since it comes from the product of fleet extension by the correspondent emission factors, as shown in Fig. 2.

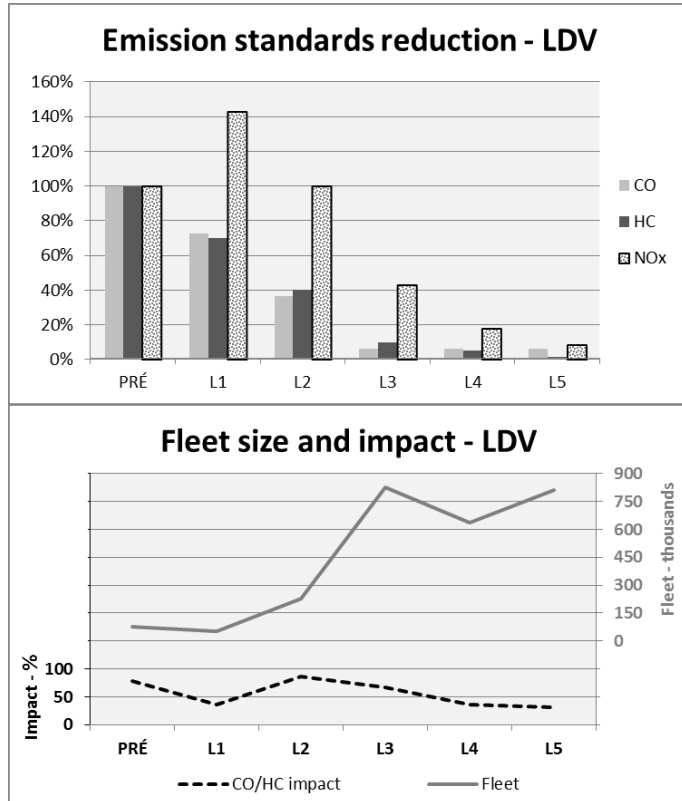


Fig. 2 – Technology x fleet size: equivalent environmental impact and emission standard reductions

2.1 The inspection process and vehicle evaluation

Vehicle inspection in the I/M_SP has three distinct phases: a pre-inspection to detect rough non conformities, such as visible blue smoke, oil and water leaks, loosen components etc. Non-qualified vehicles are “rejected”; the others are eligible to be inspected and have their emissions measured. A visual inspection verifies the presence of emission control systems, which should be in accordance to vehicle manufacturer specifications. Thirdly, the emissions are measured: CO and HC at idle for the vehicles equipped with Otto cycle engines, or smoke opacity at free acceleration for the Diesel engines. If high or unusual noise levels are observed, the vehicle is also submitted to a noise measurement at 2/3 of the engine maximum RPM. All measured results are compared to emission standards or the reference emission levels recommended and certified by vehicle manufacturer. In the average, 85% of Otto cycle, 75% of motorcycles and 60% of Diesel vehicles are approved in the first inspection. However older vehicles fail in higher rates and some 3% of

one year old vehicles also fail because of high emission levels due to tampering.

2.2 General statistics observed in the fleet

I/M-SP results indicate that each vehicle technological class shows a typical statistical distribution which demonstrates that the emission reduction remains along the vehicle useful life, except when tampering or mistuning occurs, as illustrated in Fig. 3. It is possible to observe that median values indicate reasonable levels of compliance, since the majority of the fleet demonstrate this possibility. The aim of the I/M-SP is the use of these statistics to design more stringent reference values, progressively, in line with the improvement of maintenance services.

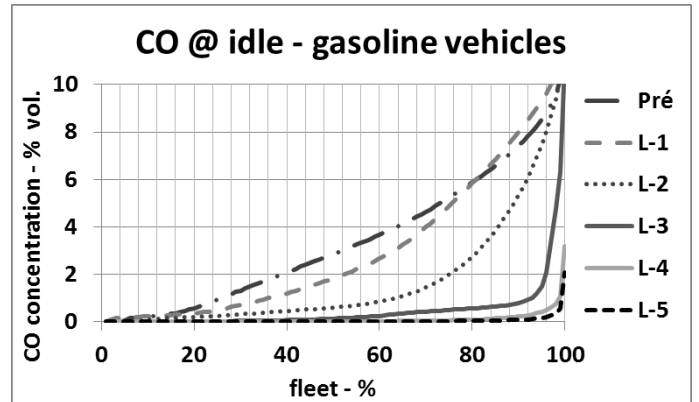


Fig. 3 – Statistical percentile distribution of CO emission according to technological level

The gasoline vehicles were taken as an example because these engines were always in the Brazilian market, but similar curves are observed for the other types.

Another important aspect to be observed is that visual inspection failure rates are close to the emission inspection ones. As presented in figure 4, some model years (1995 to 2002) show different rates, which suggests the possibility of establishing stricter reference values for those vehicles, as it was done in Kathmandu, Nepal [2], showing the potential use of I/M data.

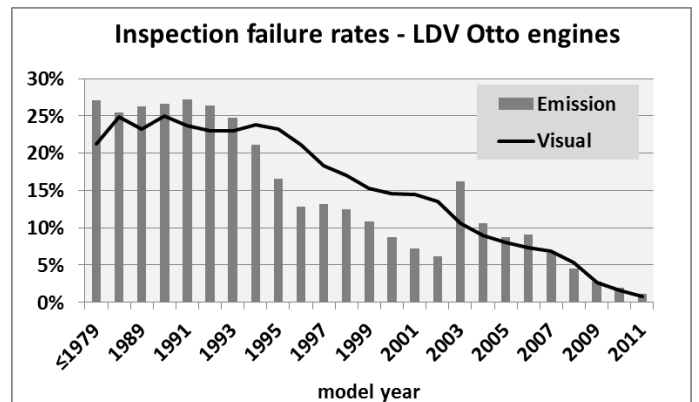


Fig. 4 – Consistency of visual and emission inspection

Another important analysis shows that failure rates at subsequent inspections decrease very fast, being less than 0,5% after the third inspection for cars and the 5th for trucks.

In all vehicle types, categories and model years, the emission averages of “failed” vehicles are many times higher than the ones “approved” in the first inspection. In addition, the “reinspected” vehicles, after proper maintenance, reduced emission to the same “approved” average, demonstrating the feasibility of environmental improvement in the maintenance procedures recommended by the vehicle manufacturer. Figure 5 presents the emission averages observed in the gasoline fleet, per vehicle technological level and the number of times the failed averages can be reduced. Gasoline cars are a good indicator of the statistical behavior, and similar figures apply to the other categories, and for HC and smoke opacity as well. It is worth of note that one year old low emission flex fuel vehicles showed increases up to 30 times when tampered.

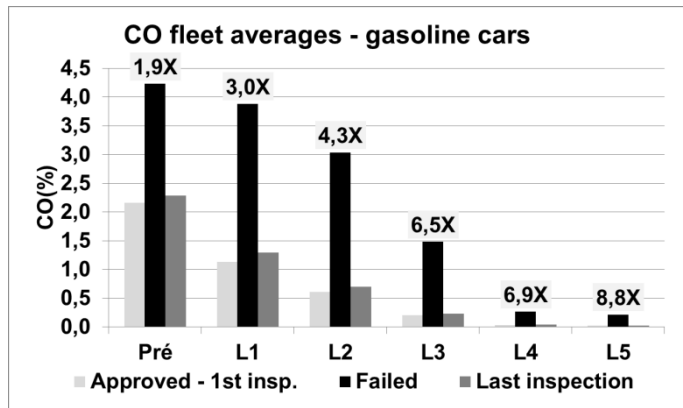


Fig. 5 – Average emission increase due to poor maintenance

The LDV statistics show a good dependence between the type approval emission certification and the I/M-SP reference conditions. However, for motorcycles this is not so evident up to the phase M3-second generation (produced after the economic crisis in 2009), when catalytic converter and fuel injection started to be applied in large scale. It was attempted to establish more stringent reference values for these 2-wheeled vehicles, but the I/M-SP results demonstrated that CO standards lower than 1,5% could induce, with Brazilian standard fuels, very lean mixtures and lead to misfire with significant increase of HC emission. Figure 6 presents the average and the ninth percentile (p90) of the hydrocarbon emission, corrected for exhaust dilution factor (HCc), as function of COc.

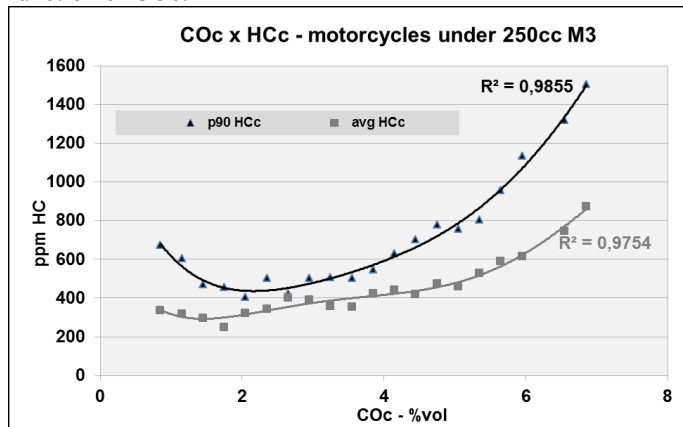


Fig. 6 – CO and HC emission of a carbureted motorcycle

2.3 Enhancing the traditional methods of inspection

I/M-SP statistics shows very high failure rates of vehicles converted to use natural gas (CNG), in a dual fuel mode. These vehicles were expected to be cleaner, however the conversion was done using “CNG kits”, whose application is generally made without proper attention to the original emission control functions, preexistent in the current engines. It is also common in these cases to inhibit the oxygen sensor using an “emulator” which produces the “right” signal for every condition, independently of air fuel ratio.

This fact led to tampering the test when using CNG (dual fuel vehicles are requested to test with both fuels, liquid and CNG). A statistical analysis of the dilution factor distribution results showed some biases of this parameter and proved occurrence of tampering practices. Normally (CO+CO₂) must be around 15% by volume when using ethanol or gasoline, and 12%vol. when using CNG.

On the other hand, the dilution factor, given by the quotient of these theoretical numbers and the respective measured (CO+CO₂) might result the same value, in a given vehicle, since the observed dilution provoked by any air intake in the exhaust might not vary with one or other fuel. Therefore, when the oxygen sensor maintains the stoichiometric mixture, the following equation must be satisfied:

$$\frac{(CO+CO_2)_{Liq.Fuel}}{(CO+CO_2)_{CNG}} = \frac{15}{12} = R \quad (Eq.1)$$

This parameter allows to identify three different conditions:

- R=1,25: constant air/fuel ratio; oxygen sensor OK;
- R=1,0: same fuel in both measurements; vehicle is not OK for testing;
- R<1,0: test is done in reverse fuel order; repeat testing.

Considering the measurement equipment tolerances, the parameter “R” may vary, and the statistics show very consistent distribution from 1,2 to 1,4 for the only vehicle model originally produced for multifuel use. However, most conversions of gasoline or flex fuel vehicles (designed for using ethanol, gasoline, and their blends) to use CNG lost their conformity with the parameter “R” for almost 70% of their fleet, indicating oxygen sensor tampering. Fig. 7 compares the statistical distribution of the oxygen sensor malfunction for the Fiat Siena Tetrafuel version (CNG designed by the car manufacturer) and converted vehicles. The figure also shows a non-controlled vehicle response as a reference of total absence electronic control of oxygen.

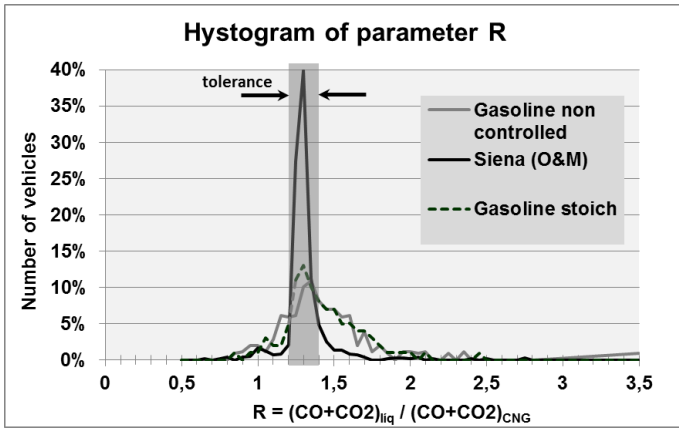


Fig. 7 – Oxygen sensor tampering in vehicles converted to CNG compared to the O&M model

This example shows how the data mining and statistical analyses may extract valuable information from simple test procedures, like the two-speed idle, and identify malfunction, electronic failures, and tampering, including hi-tech vehicles.

3. I/M-SP ENVIRONMENTAL BENEFITS

The environmental benefits are estimated by ratios between the “final and initial” fleet status in the considered calendar year, taking the averages of each emission concentration at the first and last inspection, and weighted by fleet category and model year. The Diesel smoke averages are shown in Fig. 8, considering two consecutive years.

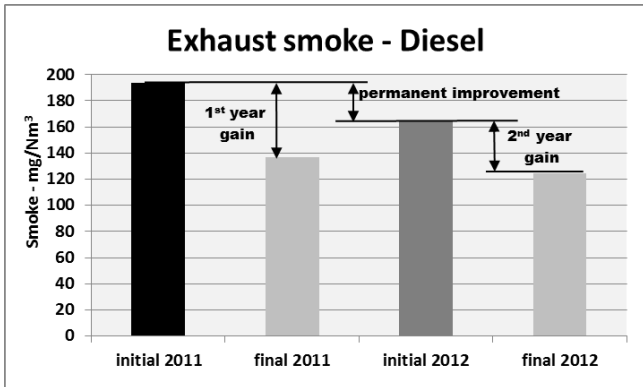


Fig. 8 – Diesel smoke averages compared annually

Similarly, CO and HC averages concentrations are presented for light duty vehicles in figure 9 and for motorcycles in figure 10, considering three consecutive years.

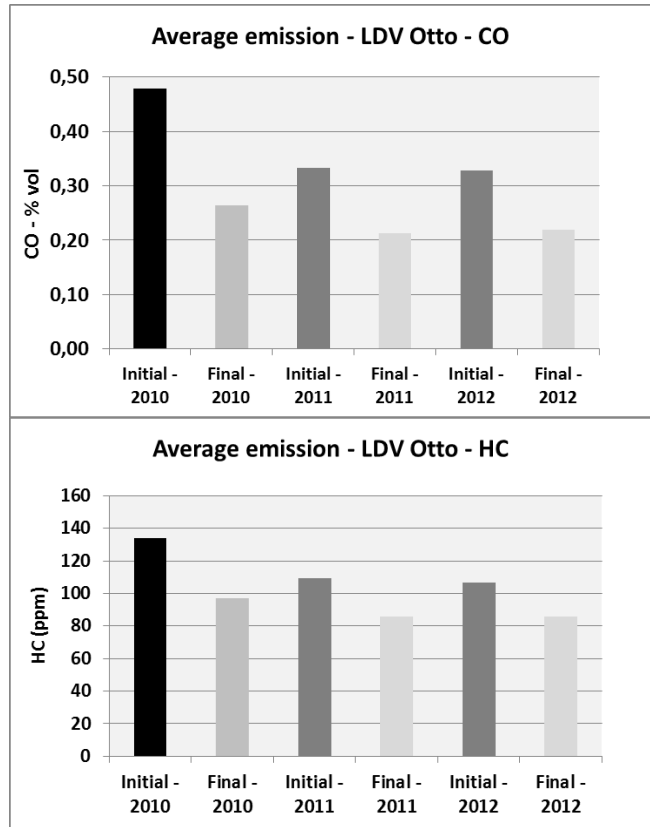


Fig. 9 – Otto LDV average concentrations of CO and HC compared annually

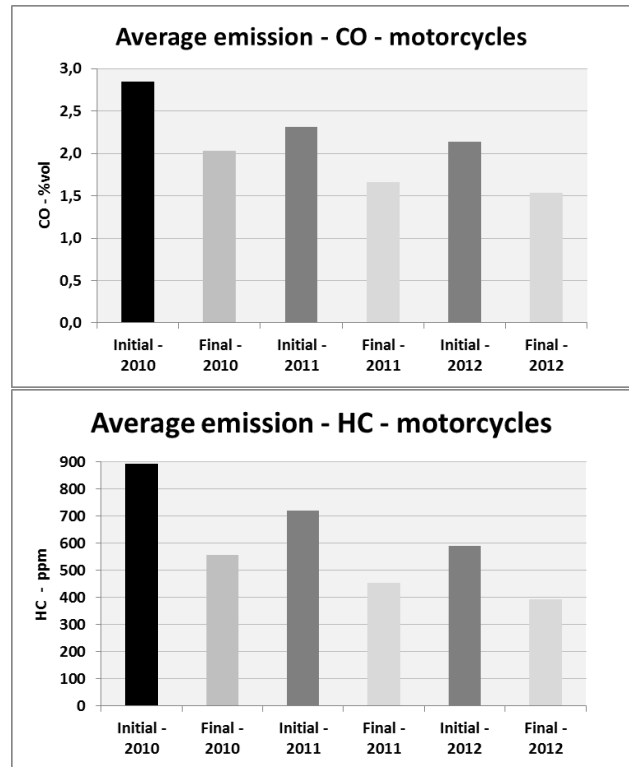


Fig. 10 – Motorcycle average concentrations of CO and HC compared annually

It is worth of note that it has been always observed lower initial averages after the first year, probably resulting from the services quality improvement and people consciousness about the Program objectives, representing medium/long term benefits. After the second year, the emission reductions become progressively more constant. Public acceptance of the I/M-SP also increased after the second inspection year in customer satisfaction surveys.

The net environmental benefits may be estimated by the relative gains shown above multiplied by the correspondent annual emissions calculated in the official inventory for each vehicle category[3]. It is worth of note that each vehicle class has it's a particular set of numerical parameters, such as annual mileage, emission standards in g/km, fleet size, deterioration factors, and is calculated separately. Table 1 presents environmental benefits related to Diesel vehicles per technological level of emission control, and a last row with the total benefit in the same class.

Table 1 – Environmental benefit from Diesel vehicles, in % of their respective annual PM emission in 2012

Diesel				
Tech phases	model year	Inspected vehicles	PM reduction in	
			in group	in class
Pre-control	≤ 1988	7.036	22%	5%
P1	1989 - 1993	3.573	24%	3%
P2	1994 - 1995	2.908	26%	2%
P3	1996 - 1999	8.662	25%	3%
P4	2000 - 2005	26.254	22%	3%
P5	≥2006	78.383	13%	4%
Total		126.816	20%	20%

Table 2 presents environmental benefits related to Otto cycle vehicles for each category, separately per technological level of emission control, and a last row with the total benefit in the same class.

Considering these estimations, where each vehicle category had its particular performance, the net benefit of the I/M-SP over the whole fleet is presented in Fig. 11. It can be observed the stronger influence of the cars on total emissions of CO and HC, regardless the other smaller fleets also have very high reduction rates, which justifies their inclusion in the inspection and maintenance program.

Table 2 – Environmental benefit from Otto engine vehicles, per class, in % of their respective annual emissions in 2012

Cars						
Tech phases	model year	inspected vehicles	reduction in group		reduction in class	
			CO	HC	CO	HC
Pre-control	≤ 1988	71.649	36%	44%	9%	11%
L1	1989 - 1991	47.644	53%	43%	8%	6%
L2	1992 - 1996	214.974	52%	38%	14%	9%
L3	1997 - 2005	807.488	51%	29%	7%	6%
L4	2006 - 2008	621.422	52%	29%	5%	3%
L5	≥2009	796.016	46%	10%	5%	1%
Total		2.559.193	47% ave	36% ave	total 47%	total 36%

Comercial LDV						
Tech phases	model year	inspected vehicles	reduction in group		reduction in class	
			CO	HC	CO	HC
Pre-control	≤ 1988	6.939	36%	53%	18%	26%
L1	1989 - 1991	2.541	43%	55%	5%	7%
L2	1992 - 1997	9.451	49%	54%	9%	10%
L3	1998 - 2005	20.134	57%	46%	5%	5%
L4	2006 - 2008	15.639	58%	34%	4%	2%
L5	≥2009	16.339	60%	26%	4%	1%
Total		71.043	44% ave	51% ave	total 44%	total 51%

Motorcycles						
Tech phases	model year	inspected vehicles	reduction in group		reduction in class	
			CO	HC	CO	HC
Pre-control	≤2002	45.930	31%	38%	8%	9%
M1	2003 - 2005	43.950	39%	41%	9%	9%
M2	2006 - 2008	146.176	36%	43%	13%	17%
M3	≥2009	100.553	31%	28%	5%	4%
Total		336.609	35% ave	39% ave	total 35%	total 39%

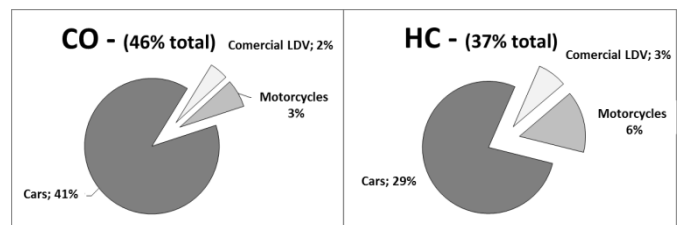


Fig. 11 – Net environmental benefit from Otto engine vehicles, in % of their respective annual emissions in 2012

4. COMPARISON OF CO NET BENEFIT AND AIR QUALITY DATA

The calculations described above, started from the statistical results obtained from the I/M-SP, and are referred to simple tests which are done under reference conditions, rather than according to expensive and time consuming loaded tests following driving cycles in dynamometers.

Despite these data are less representative of real driving conditions, they have the ability of identifying maintenance problems and establish the proportions of badly maintained vehicles in the fleet and the magnitude of their non-compliance to the emission limits. Therefore, these characteristics and the huge amount of data make the I/M-SP results an important tool to weight the inventory parameters and improve its power for planning the environmental strategies.

It has been long recognized for many years that carbon monoxide is the most appropriated pollutant to monitor traffic impact on air quality, since it is highly dependent on Otto cycle engines presence and responds very quickly to traffic hourly intensity, because its monitoring is made on the 8h moving average. Other pollutants monitored on the basis of the daily average are not sensitive to hourly variations.

The concepts presented in this paper may be validated experimentally through the comparison of these results and the air quality data, i.e. to the atmospheric concentration of CO and the number of days per year that this concentration exceeds the air quality standards. These data has been continuously monitored by CETESB - the São Paulo Environmental Agency – for some decades and show a very important decrease in the number of days with inadequate quality (concentrations above 9 ppm, or the AQS – Air Quality Standard) and the number of days of “regular” quality (between 50% and 100% of AQS), in the period from 1999 and 2003, when stabilized [4]. This is mainly due to the vehicle technology improvement, since 1986 (PROCONVE), despite the fleet grew three times in this period.

After this “first moment” the metropolitan region faced a “second one”, with an abrupt and additional improvement in air quality, probably resultant of some traffic modifications held in 2008/2009 and the I/M-SP implemented in 2009 for Otto cycle vehicles. It is worth of mention that the incidence of atmospheric stagnation (difficulty for pollutant dispersion) followed an opposite trend and, especially after 2008, the curve shapes became very compatible within each other.

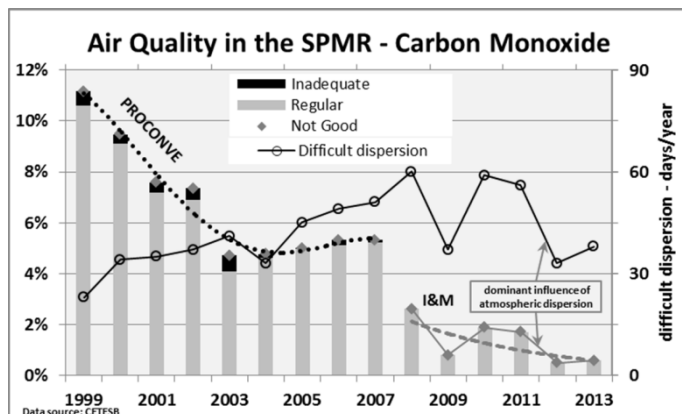


Fig. 12 – Air quality evolution in São Paulo

As a final conclusion, this comparison demonstrates that implementation of the I/M-SP showed a very strong correlation to the air quality improvement in the São Paulo Metropolitan Region - SPMR, whose extension is very similar to the calculated from the program statistics for carbon monoxide.

This validates the proposed methods for estimation of CO annual emission reduction and allows extending the same credibility in estimating the other measured pollutants, HC and PM.

An important achievement is that this credibility brought important knowledge on many aspects of the in-use fleet and valuable feedback to the technological development in Brazil

to comply with the emission control programs. One that may be worth highlighting is the possibility of estimating the rate of fleet deterioration of emissions, which is a key factor for inventory precision.

5. HEALTH EFFECTS AND ITS BENEFITS FROM PARTICLES EMISSION REDUCTION

The Medicine School of the São Paulo University used the calculated particles emission reduction resulting from the I/M-SP and estimated the resulted decrease of ambient PM and the correspondent reduction of the health impact of air pollution. Their statistical study is based in the correlation of 6% mortality decrease per 10micrograms per cubic meter of PM_{2,5} in the atmosphere, proposed by WHO – World Health Organization. Additionally, an economic valuation was based on the DALY method as recommended by the WHO, adapted to Brazilian conditions, and related to the increase in life expectancy attributed to air pollution reduction. It was considered that only 75% of São Paulo's diesel fleet was inspected, and no other city in the metropolitan region (SPMR) were included in the I&M program. Therefore, this program may be associated to a reduction of 1,18 µg/m³ in PM_{2,5} concentration in 2011 and avoided 584 deaths with an economic impact of US\$ 77,1 million. Assuming that the same results would be extensive for the whole SPMR, 1560 deaths could be avoided with an equivalent economic impact of US\$ 206 million annually [5].

This study was repeated for subsequent years and gave very similar results, as shown in table 3.

Table 3: Public health benefits from Diesel vehicles inspection in 2013, in the city (SPC) and in the metropolitan region (SPMR)

AIR BASIN CONTRIBUTION SCENARIO	REDUCTION MP _{2,5} µg/m ³	IMPACT (death/year)		ECONOMY (thousands US\$)	
		SPC	SPMR	MSP	RMSP
#1- Inspected fleet (75% real)	0,94	336	554	44.371	73.159
#2- Inspection of total fleet MSP	1,25	447	737	59.029	97.325
#3- Inspection of total fleet SPMR	2,5	894	1.474	118.058	194.650

The simplest way to evaluate these benefits in economic terms is dividing the total cost of diesel inspections by the number of avoided premature death, which results in less than US\$ 5000 per saved life!...the cheapest public health program in Brazil.

6. IMPORTANT ADDITIONAL ACHIEVEMENTS OF I&M PROGRAMS

As described above, the I/M-SP achieved significant reduction in vehicle emissions, which corresponded to a very important air quality and public health improvement. Besides these benefits, other important targets were achieved, especially as a better knowledge on the technical aspects of environmental strategy for vehicle impact abatement. This knowledge also contributed to the development of the Brazilian curve of Utility Factor to be used in the calculation of fuel consumption and emissions of plug-in hybrid vehicles according to the standard SAE J1711.

For the first time, the Brazilian technical community and environmental strategists have had the opportunity to access annual mileage real data of each vehicle category and model

year[6], emission deterioration rates, fleet noncompliance rates for different ages and technologies. A huge database of 17 million inspections provided the necessary information for better understanding the I/M-SP reference parameters, confirming most Federal requirements, and generated new proposals for future values [7], as well as lower characteristic levels of the same parameters for each vehicle model, to be used as targets during corrective maintenance [8].

The statistical distributions of measured emissions also allowed the identification of different trends in outlier vehicle models which generated specific maintenance instructions to improve preventative and corrective services.

The I/M-SP program also demonstrated that important contributions are possible to be extracted from simple measurements, as the two speed idle and the free acceleration tests. The key is to have the tests well conducted, the results well analyzed according to adequate statistical procedures and a comprehensive results interpretation.

Interpretation of statistics findings are a useful tool to explain certain engine and emission systems characteristics. To be successful, this requires a team with high expertise in automotive engineering, emission measurement and statistical analysis to work together, with a critical vision on technical details.

Many of these contributions were related to inspection procedures improvements, such as identification of bias and tampering, determination of key parameters to check consistencies during inspection process, monitoring equipment deviations, defining extra calibration when needed and permanent follow-up, of inspectors performance. Furthermore, the I/M-SP disseminated broadly the concept that correct maintenance practices not only reduces emissions but also saves fuel and extends the useful life of vehicles. As a result repair shops invested in training and equipment, and customers became more interested in using original and more durable parts instead of low quality products. More than four thousand repair shop technicians were trained in the last five years in São Paulo to identify and repair a wide range of problems that can cause avoidable excess emissions.

7. CONCLUSION

This paper shows key concepts and results from the I/M-SP program. They should part of a broad transport and mobility strategy and environmental policy. The São Paulo experience shows that a simple but well implemented, managed and audited in-use vehicle inspection and maintenance program can be a cost effective alternative and result in meaningful benefits to society.

With time, technical improvements may be implemented based on local statistics to reduce emission reference parameters, or even implement other tests procedures. Nevertheless it is paramount importance to communicate well the purpose, benefits and costs of the program in order to gain confidence and support of the public and stakeholders.

REFERENCES

- [1] USAID (2004) Vehicle Inspection and Maintenance Programs: International Experience and Best Practices
- [2] Ale BB, Nagarkoti RK (2003) Evaluation of Inspection and Maintenance Program on Vehicles in Kathmandu Valley. Kathmandu, Nepal. Report submitted to the World Bank
- [3] Branco, G.M.; Branco, F.C.; Branco, M.C.; Dias, E.M.; Napoleone, J.M.; Szwarc, A. - Criteria for Efficiency Determination of Inspection Maintenance Programs - 18th International Conference on Circuits, Systems, Communications and Computers, Santorini Island, Greece, July 17-21, 2014
- [4] CETESB – Air Quality Annual Reports for the State of São Paulo - <http://www.cetesb.sp.gov.br/ar/qualidade-do-ar/31-publicacoes-e-relatorios>
- [5] André, P.A. de; Miraglia, S.G.K.; Saldiva, P.H.N. - Impact of diesel vehicle inspection on health: the experience of São Paulo, Brazil - Abstracts of the 2013 Conference of the International Society of Environmental Epidemiology (ISEE), the International Society of Exposure Science (ISES), and the International Society of Indoor Air Quality and Climate (ISIAQ), August 19–23, 2013, Basel, Switzerland. 2013. Environ Health Perspect; <http://ehp.niehs.nih.gov/ehbasel13/p-2-02-12/> .
- [6] Bruni, A.C.; Bales, M.P. - Curvas de intensidade de uso por tipo de veículo automotor da frota da cidade de São Paulo – CETESB, Dec.2013 - ISBN 978-85-61405-61-8 - <http://www.ambiente.sp.gov.br>
- [7] Branco, F.C.; Branco, G.M.; Szwarc, A.; Napoleone, J.M. - Proposição de Novos Valores de Referência para Aprovação na Inspeção de Veículos Otto – to be presented in the International Symposium of Automotive Engineering – SIMEA, 2014
- [8] Branco, F.C.; Branco, G.M.; Szwarc, A.; Mello Filho, L.V.F.; Napoleone, J.M. - Valores Característicos dos Parâmetros de Referência de Emissões dos Veículos Brasileiros – presented in the International Symposium of Automotive Engineering – SIMEA, 2013

ABOUT AUTHORS

Branco, Marcelo Cardinale – born in São Paulo, in 1967, graduated in Administration, taking master of science degree in transportation, environment and energy conservation, Secretary of Transport in the city of São Paulo until 2012, member of the State Transportation Council 2011-13, and vice-president of ANTP – Public Transportation National Association since 2011.

Branco, Fábio Cardinale – born in São Paulo, in 1969, graduated in geology at the University of São Paulo, master of science in satellite images processing, consultant of the vehicle emission strategies and I&M Program at EnvironMentality since 1996.

Branco, Gabriel Murgel – born in São Paulo, in 1949, graduated in Mechanical Engineering at Polytechnic School of the University of São Paulo, worked at the State Environmental Agency for 20 years in the development and implementation the vehicle emission control program in Brazil, consultant for vehicle emission control at EnvironMentality since 1996.

Dias, Eduardo Mario – born in São Paulo, in 1951, is full professor of the Escola Politécnica of the Universidade de São Paulo (Polytechnic School of the University of São Paulo) and coordinator of GAESI - Grupo de Automação Elétrica em Sistemas Industriais, a research group of the Electrical Energy and Automation Department, Escola Politécnica, Universidade de São Paulo.

Szwarc, Alfred – born in Lodz, Poland, in 1952, graduated in mechanical engineering at Taubaté Engineering School, SP, worked at the State Environmental Agency for 20 years in the development and implementation of the vehicle emission control program in Brazil, presently consultant for vehicle emission control at ADS since 1998.

Communication requirements of laboratory management system

M. Krbeček, F. Schauer, and K. Vlček

Abstract— Remote laboratories start to be an important tool both in science and education. The massive spread of those modern technologies is hampered by the absence of the standardized solutions and difficulties with their implementation by the wide segment of scientists and educators.

The paper intends to contribute to the standardized solutions in communication schemes of remote experiments (REs), spread across the Internet at three levels: within the server of the remote experiment itself, outside the server of the remote experiment, establishing the working communication principle server-client and within so called Laboratory Management System (LMS), a new envisaged system for the management of many existing remote laboratories, at a nationwide or European scale.

The solutions are elaborated and presented by the scheme of the remote experiment based on the plug and play hardware of Internet School Experimental System (ISES). Besides the solutions for all three mentioned communication schemes, the last part of paper describes the creation of the data communication interface and the proposal of diagnostic interface for individual remote experiments as well.

Keywords—Remote laboratories, remote experiments, communication interface, RLMS, remote laboratory management system.

I. INTRODUCTION

THE contemporary society is characterized by sharing of resources and assets through the Internet and growing virtualization in ICT. This approach saves the cost of expensive shared devices, available through the network. This trend can be found in a wide range of sectors of human activities in general and in science and teaching processes in particular. Teaching of natural sciences is no exception. Next we intend to describe the situation typical for universities; in other fields the situation is similar. A great deal of attention worldwide at universities and teaching institutions have been devoted to e-laboratories offering access to various real world remote experiments (REs) [1-6]. The ultimate goal in the creation of teaching support for a teacher are global grids of remote laboratories (RLs) and their integration into a cloud-system with an easy data retrieving, processing and storing with sufficient security.

This work was supported by the Internal Grant Agency (IGA) of Tomas Bata University in Zlín.

M. Krbeček, F. Schauer and K. Vlček are with the Tomas Bata University in Zlín, Faculty of Applied Informatics, Nad Stráněmi 4511, Zlín, CZ- 76005, Czech Republic (krbecek@fai.utb.cz, fschauer@fai.utb.cz, vlcek@fai.utb.cz).

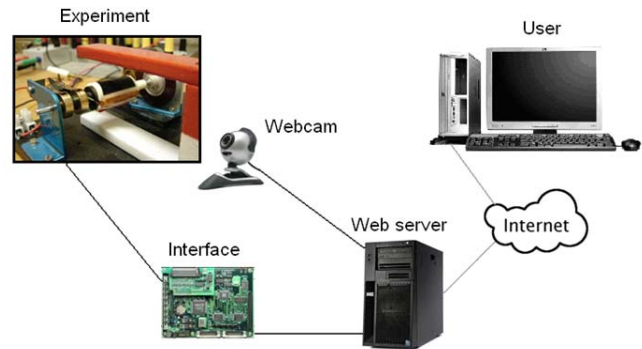


Fig. 1 Schematically arrangement of the remote experiment [7]

REs are mainly designed under the auspices of the universities for the purpose of education (teaching and learning). For this reason usage of some of them is only for students of the particular university in question and access is secured by the user name and password (especially at American universities). In Europe and Australia several projects exist supporting building of open remote laboratories - with free access, either with or without registration. Some labs offer to insert client's initials (name, country, e-mail) for voluntary statistical purposes. With the necessary exceptions (maintenance, modification, technical issues...) experiments are running on 24/7 scheme [8-14].

There are, rather unfortunately, plentiful and not compatible systems for creating of computer oriented physical experimental laboratories. But only a part of these systems allows remotely access and control of the devices via the Internet or internal network. From this group, we can select only certain systems that are suitable for the creation of remote experiments for educational and scientific purposes (iLab, Sahara, REMLABNET [15, 16 and 17]). On top of this, the first two mentioned systems are pioneering in the design and introduction of Laboratory management system (RLMS) both in USA and Australia, the last one - REMLABNET - for European use is under construction.

All described REs are based on ISES HW which is described in detail elsewhere [14].

II. COMMUNICATION SCHEME OF REMOTE EXPERIMENTS

As we can see in Figure 1, the remote experiment consists of several constituent blocks, which have to communicate with each other for the proper operation of the RE. This communication takes place at different level of complexity,

depending on the block of the experiment. It is clear that the communication among the physical hardware (measurement modules) and the D/A-A/D converters on the PCI transducer board will be completely different to control communication between the user and the server of experiment. In the same way the demands for reliability of each communication will be different accordingly. Demands vary depending on the importance of transmitted data and signals. Communication scheme of RE based on the ISES can be seen in the following Figure 2. According to the diagram, communication can be divided into two parts: communication of HW components (HW communication) and SW components (SW communication through the Internet).

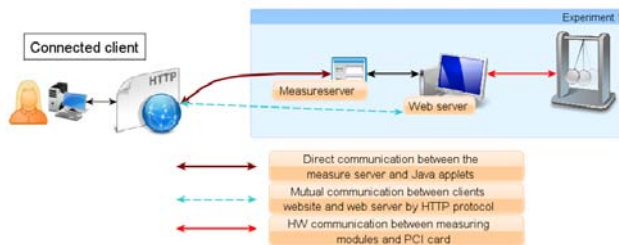


Fig. 2 Communication scheme of the present ISES RE

A. Hardware communication

As the HW communication we can denote all the signals and information transferred directly from the physical HW of the RE to PC. It comes mainly from individual measuring ISES modules via the ISES board into the PCI transducer board in case of the ISES system attached via the PCI bus. All this communication takes place via an analogue signal (0-5V). Since this communication takes place at very short distances, we don't have to take any precautions to maintain signal integrity. We are also limited directly by the hardware design and its possible disturbances and outages.

B. Software communication

To the SW communication group here we can include all data transmitted in the digital form. The majority of SW communication goes through the Internet towards the client. This route is mainly for bidirectional information exchange between the client and the server of the RE. This communication forms the basis of every RE and thus is very important, because it transfers not only the measurement data from the experiment to the client but also the control commands from the client according to which the experiment performs. Therefore there must be secured real-time communication with reasonable time-delay (in order of ms) and with superior reliability with respect to the bidirectional data transfer.

We can also include the communication of experiments with RLMS to the group of SW communication. RLMS is a new concept in the field of remote laboratories, which ensures their integration into larger grids. With this concept we can meet first in USA in the project iLab [13] and in Australia in the project LabShare [14]. The similar project is planned and is

under way at the European level. Here occurs another communication branch providing both the diagnostics of current working experiment, the transmission and storage of configurations of individual experiments and the measured data of individual clients for further use. Obviously even this communication must be very reliable and there mustn't be disturbance of transmission. In this case we can say that with proper implementation of socket connections on TCP protocol and sufficient bandwidth of internet connection we reach sufficient reliable data transmission for both control and information data.

III. COMMUNICATION NEEDS OF LABORATORY MANAGEMENT SYSTEM (RLMS)

Remote laboratories are usually not affordable to the outside world and confined to the use of their own university owing to the complexity of their interoperation. The inter-institutional sharing of remote laboratories is now more and more considered to be an important objective of their employment. Thus, creating remote laboratories able to be integrated in a generic and inter-institutional framework rather than limited to the individual academic institution is currently the trend in remote laboratories development. Exactly this task solve the RLMSs, giving answer to these needs by providing a common portal for the accessing and administrating a wide pool of heterogeneous but functioning remote laboratories that might be distributed among several universities in order to span their dissemination and inter-institutional cooperation. The pioneer RLMSs that have been adopted at many universities include the iLab Shared Architecture (ISA - USA) [13] and Sahara (Australia) [14].

Depending on the new trends in the field of remote experiments arises the need to create RLMS for European area. Since the two above mentioned systems provide interconnection of American and Australian laboratories and at present are not affordable for European participants. For this reason we decided to create such RLMS at our university first for the internal and testing purposes but subsequently expandable to the Czech Republic and later serving to the whole Europe. RLMS was primarily built on the ISES platform however it will allow the inclusion of any remote experiment. Such RLMS working in a cloud raises a number of new channels of communication which must be built. The scheme our proposed RLMS is shown at the Figure 3 below.

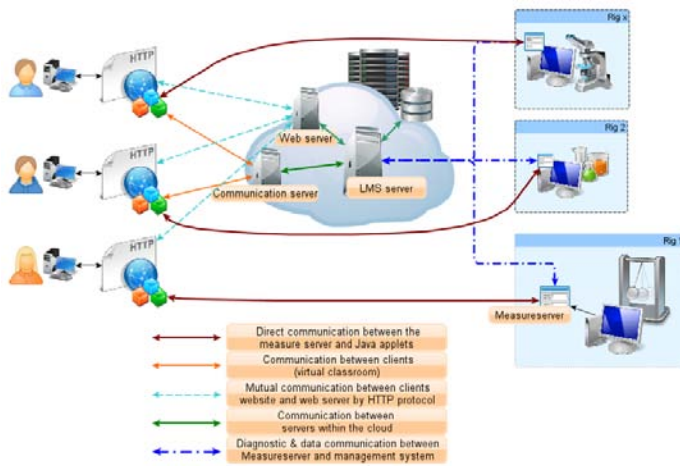


Fig. 3 Communication scheme of designed LMS

Compared to the original communication scheme of remote experiments, in RLMS there are three new types of communication. The first is the communication of the servers in the cloud (green line in Figure 3). This communication is ensured in the design of the cloud structure and takes place among the participating data centres. The second new channel of communication is communication among individual clients themselves via the communication server (orange line in Figure 3). On the client’s side will be used a simple messaging client most likely based on the Java language. Communication server will provide connection and transmission of video, audio and text messages between connected users. The last new channel of communication is the transfer of information between the “MeasuringServer” and the management server in the cloud (blue line in Figure 3). Transfer of measurement data and its storing for later use will take place there. This channel will also provide diagnostics of individual experiments and remote repair of their malfunctioning.

Next parts of the paper will be focused on creating of a communication interface for the data transmission and a communication between “MeasuringServer” and cloud.

IV. DESIGN AND CREATION OF COMMUNICATION INTERFACE

Let us focus on the transfer and storage of the measured data between the experiment-site (rig) and the management server of the RLMS. Data output from the “MeasuringServer” are implemented in the form of a text file. This text file is always compiled each time at measurements end. The first task is to transfer this file with measured data and store it in the RLMS storage. For this purpose communication interface was created. It consists of a part on the rig-side which controls data-file compiling and ensures its sending and the second part on the RLMS server that saves the file on the RLMS storage and possibly parses the received data into the database.

A. Creation of communication interface at the experiment-side

The experiment side communication interface is created in the Java programming language, primarily because of its

portability among platforms. The application starts at the same time as “MeasuringServer”. It allows the client to set the basic parameters of communication, later it runs as a background service. The parameters of the communication interface are pre-set according to the type of experiment and its installation.

Requirements for the communication service:

- The service repeatedly checks for a new data file,
- When the new file occurs the service checks if the file is readable (to avoid collision during creation of file),
- Service establishes socket connection with the opposite service running on the server,
- It sends the file in the byte form,
- After completion of dispatch service waits for confirmation of the correct reception of a file otherwise it sends the file again,
- It closes the connection,
- It deletes the uploaded file,
- Then service continues in cyclic checks of the newly created files.

Adjustable parameters of communication service:

- The communication address and port No,
- The interval of cyclic control of new file (depending on the time of measurement),
- The path to the new data files.

All these parameters will be present to correct values automatically.

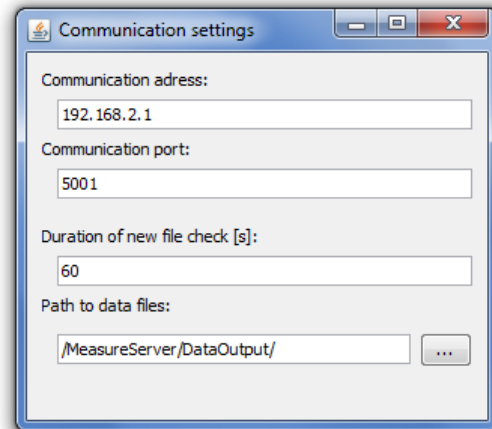


Fig. 4 Communication settings of experiment-side service

B. Creation of communication interface at the server-side

The server-side communication interface is created in the Java programming language, primarily because of its portability among platforms. It allows administrator to set the basic parameters of connection and saving of data at start. Then it runs as a background service. It is designed as stand-alone application but it can be easily included into management system.

Requirements for the communication service:

- Service listens on a particular port and waits for connection,

- Service establishes socket connections to the opposite service at the experiment-side,
- It receives a file in a byte form,
- After completion of reception service checks the integrity of the file and sends confirmation of correct reception of the file otherwise receiving will start again,
- Service ends the connection,
- It saves the received file to the selected directory / reads the received file and stores the data into the appropriate place of the database.

Adjustable parameters of communication service:

- The communication address and port No,
- The path to the directory for file storage / access settings to database.

All these parameters will be present to correct values automatically.

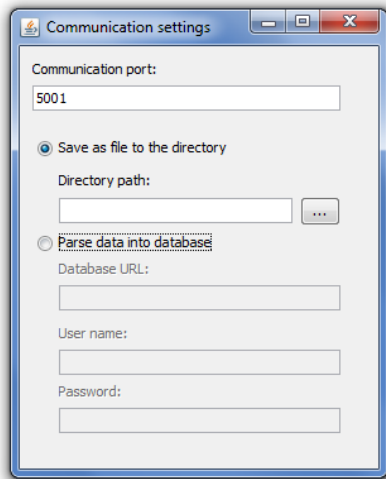


Fig. 5 Communication settings of server-side service

C. Design of diagnostic communication interface

Diagnostic services should ensure keeping track of the status of the experiments connected to the RLMS. Depending on the activity of the experiment, its breakdown or failure the status will be displayed at the access portal of RLMS. Diagnostic should also allow sending commands to the experiment in case of detected faults. From the description of the functionality it's clear that we need to communicate directly with "MeasuringServer" at the experiment-side because only there can be found the latest information about the availability and status of the experiment. It is necessary to intervene in the source code of "MeasuringServer" and to program diagnostic communication interface directly here. Depending on this is necessary to establish a communication interface on the server-side (cloud) which will communicate with "MeasuringServer". For this reason only a server part will be proposed and described, the "MeasuringServer" part will be subject of the following paper.

Because the RLMS will include many experiments, it is crucial that the interface will allow connection and supervision

of many experiments, and, on the other hand, will be able to identify the individual experiments and communicate with them individually. As there will be the IP address of each experiment stored in the server database, it will be appropriate to use these addresses for identification. For this purpose a service on the server-side will be created, which will allow connection of arbitrary number of experiments. Service will maintain a list of currently connected IP addresses and will allow communication with them.

The basic functionality of diagnostics is to determine whether the experiment is at present available or not. This is accomplished in several ways. The basic feature of the experiment's availability is the list of connected IP addresses. When you start the experiment the socket connection is created with the service on the server-side. This connection remains active until it is closed by one of the parties or one of them is disconnected. In case of malfunction occurring and experiment turning off, the service will be closed, connection will be lost which indicating experiment inaccessibility.

However an error may occur even with the experiment, which has not terminated the connection, but it is not proper for measurements. For this purpose another precaution is operative, as the server service will send a regular broadcast request for the status report to all connected experiments after a certain time frame. They will replay its current status or be considered as out of function. In this way not only fault of experiment will be detected, but its occupancy as well. Furthermore, the experiments themselves report their status change automatically. All these measures should ensure the availability of the actual table of experiments status at any time.

Besides, the diagnostic system allows so-called automatic self-repair of an experiment. In case of the experiment's failure and communication running (experiment answers on the broadcast by error) the server sends the instruction to perform a certain actions according to the type of error. One of them may be the restart of the experiment or the whole computer to which experiment is attached, which makes experiment operational in most cases.

If these or other measures don't bring the experiment back to operation, the system will contact the administrator of the experiment automatically. System will notify about found errors and will request the check of experiment. The system supports not only the diagnostics of the experiment as a whole but its parts as well to relieve the supervising load of the remote experiment administrator as much as possible. From the readings transmitted from the individual sensor, the system will be able to determine its malfunction easily giving the clue for its repair to administrator.

D. Future development of system

The first step in the future development will be the integration of the data and diagnostic interfaces into one unit, integrating the previous solutions into one without changes. The RLMS server, providing the experiments communication, will be built on the Apache Tomcat. Apache Tomcat (or

simply Tomcat, formerly Also Jakarta Tomcat) is an open source web server and servlet container developed by the Apache Software Foundation (ASF). Tomcat implements the Java Servlet and the Java Server Pages (JSP) specifications from Sun Microsystems, and provides a "pure Java" HTTP web server environment for Java code to run in [18]. Since the source code of the created communication interfaces are also written in Java, the implementation into this system will be very easy (just copied). We can say that created applications are a kind of preparation for allowing the development and testing of RLMS system but also part of the final solution of its communication interface.

The RLMS server will certainly undergo a series of changes and get many additional features, which will make its use even more attractive. Quite sure it will be on request data mining from the database with subsequent sending. The data flux will of course occur in the opposite direction as well concerning the experiment itself (physical theory, hardware design ...). RLMS server will also be ready for a possible extensions and communication with other RLMS using access to our experiments and vice versa.

V. CONCLUSIONS

RL as acute trend in education and science brought the need for further improvement in terms of integration of RL into large units by RLMS, which provide access to many experiments, provide their continuous availability and other services for teamwork and cooperation, while working with experiments. At the global level there are already several RLMS existing, but they are currently unavailable for general use. This was the reason to attempt at FAI UTB in creating and testing REMLABNET. Such an extensive project consists of many layers, which must seamless communicate, ensuring secure data transmission. Outside communication security of RLMS is to be achieved by using the TCP / IP protocol, which declares 100% transmission of transmitted data packets. Currently proposed inner RLMS communication system contains different types of communication, depending on the layers in where the communication takes place. The paper is focussing on the data communication between the experiment and the RLMS system, which ensures the transmission of the measured data and preserves them for later use. By the Java programming language the solution (service) was developed, which ensures the transmission of these data and their subsequent storage in a database. The service consists of a server-side and an experiment-side among them the transmission of data files takes place. Service was designed and created according to its functionality and adjustability, on the both sides of the communication channel.

The diagnostics communication interface was also designed providing information about the current status of the individual experiment allowing the management of any number of REs. It also brings a new feature of RL - auto repairing of experiment's defects. Diagnostics detects malfunction of measuring modules and immediately transmit this information

to the experiment manager, who will take the necessary steps.

All designed and created solutions will be implemented into a large robust system that will ensure transmission of all data in system and will be able to communicate with any number of experiments without performance loss. This compatibility is ensured by the selected programming language (Java) and Apache Tomcat application platform for building back-end part of the system.

REFERENCES

- [1] A. A. Humos, B. Alhalabi, M. Hamzal, E. Shufro, and W. Awada, "Remote labs environments (RLE): A constructivist online experimentation in science, engineering, and information technology". *31st Annual Conference of IEEE Industrial Electronics Society, 2005. IECON 2005*. IEEE, 2005, vol. 2, issue 4, pp. 6. DOI: 10.1109/IECON.2005.1569238.
- [2] C. Gravier, J. Fayolle, B. Bayard, M. Ates, and J. Lardon, "State of the art about remote laboratories paradigms - foundations of ongoing mutations". *International Journal of Online Engineering*, 2008, vol. 4, issue 1, p. 19-25. ISSN 1861-2121.
- [3] M.E. Auer and C. Gravier, "The many facets of remote laboratories in online engineering education". *IEEE Transactions on Learning Technologies*. 2009, vol. 2, issue 4, p. 260-262. DOI: 10.1109/TLT.2009.53.
- [4] M. A. Bochicchio and A. Longo, "eLabs for technology-enhanced universities". *International Conference on Remote Engineering and Virtual Instrumentation*, 29 June - 2 July, 2011, Brasov, Romania, p.372-379.
- [5] F., Schauer, F., Lustig, J., Dvorák, and M, Ožvoldová, "Easy to build remote laboratory with data transfer using ISES – Internet school experimental system". *European Journal of Physics*. 2008-07-01, vol. 29, issue 4, p. 753-765. DOI: 10.1088/0143-0807/29/4/010.
- [6] F. Schauer, F. Lustig, and M. Ožvoldová, "Internet natural science remote e-laboratory (INRe-L) for remote experiments". *Innovations 2011: World Innovations in Engineering Education and Research (USA)*, p.51-68.
- [7] M. Krbeček, "Creation of multimedia interactive teaching tool with utilisation of remote experiments. Zlín", 2011. 108 p. Diploma thesis. University of Tomas Baťa in Zlín.
- [8] M. Cooper, "Remote laboratories in teaching and learning – issues impinging on widespread adoption in science and engineering education". *International Journal of Online Engineering* 2005, vol.1 issue 1, ISSN 1861-2121.
- [9] S. Gröber, M. Vetter, B. Eckert and H. J. Jodl, "Experimenting from a distance – Remotely controlled laboratory (RCL)". *European Journal of Physics*. 2007-05-16, vol. 28, issue 3, p. 127-141. DOI: 10.1088/0143-0807/28/3/S12.
- [10] M. Krbeček, F. Schauer and R. Jašek. "Security aspects of remote e-laboratories". *International Journal of Online Engineering (iJOE)*. 2013-07-11, vol. 9, issue 3, p. 34-39. DOI: 10.3991/ijoe.v9i3.2586. Available from: <http://online-journals.org/i-joe/article/view/2586>.
- [11] Library of Labs. LiLa - Library of Labs [online]. [cited 2014-04-19]. Accessible from: <http://www.lila-project.org/home.html>.
- [12] Remote Farm. Remote Farm [online]. 2012 [cited 2014-04-19]. Available from: <http://remote.physik.tu-berlin.de/farm/>.
- [13] M. Krbeček, F. Schauer, and I. Zelinka. "Possible utilization of the artificial intelligence elements in the creation of remote experiments". *International Journal of Online Engineering (iJOE)*. 2014, vol. 10, issue 1, p. 46-52. DOI: 10.3991/ijoe.v10i1.3110. Available from: <http://online-journals.org/i-joe/article/view/3110>.
- [14] F. Schauer, I. Kuřitka, and F. Lustig, "Creative laboratory experiments for basic physics using computer data collection and evaluation exemplified on the intelligent school experimental system (ISES)". *World Innovations in Engineering Education and Research iNEER, USA, Special Volume*, 2006, p. 305-312.
- [15] V. J. Harward, J. A. del Alamo, S. R. Lerman, P. H. Bailey, J. Carpenter, K. DeLong, C. Felknor, J. Hardison, B. Harrison, I. Jabbour, P. D. Long, M. Tingting, L. Naamani, J. Northridge, M. Schulz, D. Talavera, C. Varadharajan, W. Shaomin, K. Yehia, R. Zbib, and D.

- Zych, "The iLab Shared Architecture: A web services infrastructure to build communities of internet accessible laboratories". *Proceedings of the IEEE*. IEEE, 2008, vol. 96, issue 6, p. 931-950. DOI: 10.1109/JPROC.2008.921607.
- [16] M. Tawfik, D. Lowe, S. Murray, M. de la Villefromoy, M. Diponio, E. Sancristobal, M. José Albert, G. Díaz, and M. Castro, "Grid remote laboratory management system - Sahara reaches Europe". *10th REV International Conference on Remote Engineering and Virtual Instrumentation*, Sydney, 2013. ISBN 978-1-4673-6345-7.
- [17] F. Schauer, M. Krbeček, P. Beňo, M. Gerža, L. Pálka, and P. Špilakova. "REMLABNET - open remote laboratory management system for e-experiments". *2014 11th International Conference on Remote Engineering and Virtual Instrumentation (REV)*. IEEE, 2014, vol. 2, issue 4, p. 268-273. DOI: 10.1109/REV.2014.6784273.
- [18] The Apache Software Foundation. Apache [online]. 2014 [cited 2014-04-18]. Accessible from: <http://www.apache.org/>.

ITS to monitor small vessels movements within port area - A study at Santos estuary

Aureo E. P. Figueiredo, Sérgio L. Hoeflich, Maria L. R. P. Dias, Sergio L. Pereira, Luiz N. Rossi and Eduardo M. Dias

Abstract— Ports connect the world through maritime transportation networks, promote international trade, and support global economic growth. In Brazil cargos are shipped in vessels and also several kinds of goods are shipped in all kinds of recreation boats and motorboats. In this paper, it was investigated the Santos estuary focusing on small vessels, considering only those endowed with some sort of mechanical propulsion, within specific requirements, where they are a great concern for port security. By using Intelligent Transportation Systems (ITS), we came to the feasible solution to deal with small vessels at the Santos estuary by monitoring its movements within that specific area.

Keywords— small vessels monitoring, port, ITS, RFID.

I. INTRODUCTION

PORTS installed near cities have to adapt their activities to the city routine. As examples, cargo transported to port terminal must consider its effects over the city traffic, and large proportion vessels must coexist with recreation boats and motorboats on the estuary. That necessity results in many conflicts of operational and social nature, since many of these small transportation boats carry a large number of passengers

A. E. P. Figueiredo, is professor at Universidade Santa Cecília (Santa Cecília University) and a PhD student at Escola Politécnica da Universidade de São Paulo (Polytechnic School of the University of São Paulo) (sureo@unisanta.br)

S. L. Hoeflich is invited professor of Fundação Getúlio Vargas (Getúlio Vargas Foundation) and a PhD student at Escola Politécnica da Universidade de São Paulo (Polytechnic School of the University of São Paulo) (shoeflich@ig.com.br)

M. L. R. P. Dias is a PhD student at Escola Politécnica da Universidade de São Paulo (Polytechnic School of the University of São Paulo) (lidiadias@pea.usp.br).

S. L. Pereira is associate professor of the Escola Politécnica of the Universidade de São Paulo. PhD in Electric Engineering from EPUSP; MSc in Robotics Systems and Applications from Coventry University (England) and Electric Engineer from Faculdade de Engenharia de São Paulo. He is a professor at the undergraduate and graduate courses and mentor of master's and doctor's degree programs of the Polytechnic School of USP. He is professor of the MBA programs of BSP (Business São Paulo School) and Pontifícia Universidade Católica de São Paulo (PUC-SP). He is a consultant in Eco-Economics and Industrial Automation. (sergio@pea.usp.br)

L. N. Rossi is Prof. Dr. of the Escola Politécnica da Universidade de São Paulo (Polytechnic School of the University of São Paulo) (natale@usp.br)

E. M. Dias is full professor of the Escola Politécnica da Universidade de São Paulo (Polytechnic School of the University of São Paulo) and coordinator of GAESI - Grupo de Automação Elétrica em Sistemas Industriais, a research group of the Electrical Energy and Automation Department, Escola Politécnica, Universidade de São Paulo, Av. Prof. Luciano Gualberto, trav. 3, n. 158, São Paulo/SP, Brazil, CEP 05508-970 (emdias@pea.usp.br).

susceptible of suffering hazardous consequences.

The control of the displacement of vessels allows one to check the vessel route and speed. Sized vessels at high-speed cause sea waves, which can contribute to sink small vessels. In other words, it can result in life and property losses. Another issue to be noted is motorized vessels distance from beaches for bathers safety.

Ports around the world still have very diversified practices and standards regarding “secure” [1]. In Brazilian estuary areas sized vessels speed cannot exceed the 6 knots and motorized vessels must be 200m distant from shore [2].

Brazil has many ports and Port of Santos is the main one, as the largest commercial harbor in Latin America and the most important metallurgical and petrochemical industrial center in Brazil, with more than 1100 industries, are also established in, and adjacent to, this estuary [Fig. 1].

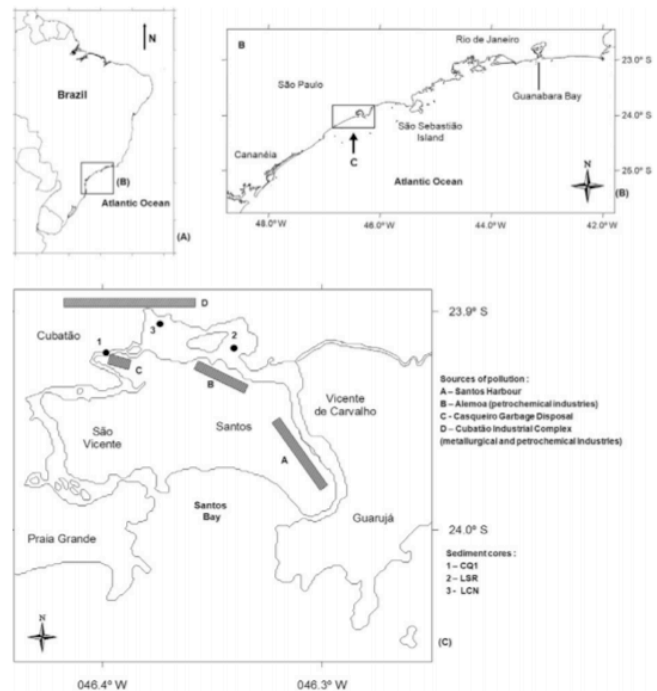


Fig. 1 - Map of the study area showing the sediment sampling sites (CQ1, LSR and LCN) in the Santos Estuary

Port of Santos is situated in the estuary of Santos, which is highly populated [3], therefore presenting many conflicts of operational and social nature.

The present article addresses monitoring small vessels movements within the port area by using Intelligent Transportation Systems (ITS), focusing on Port of Santos given his size and operational relevance to cargo distribution in Latin America.

This paper is divided in 6 sections. Section I presents an introduction and the article objective. Section II section presents aspects of vessels security and the necessity of effective vessel identification system at Port areas. Section III focuses on the dangers of small vessels not being monitored within the estuary area, exposing the objective of this study. Section IV presents the proposed approach using the Intelligent Transportation Systems (ITS), which is detailed over section V, that describes the proposed model. Section VI presents the conclusions.

II. ASPECTS OF VESSELS SECURITY

Being the sea/land interface and critical nodal points, ports security is crucial to ensure the smoothness and efficiency of supplies chains increasingly complex [4]. In this regard, vulnerabilities to potential threats are often high within such nodes due to the presence of numerous stakeholders and rather complex interactions among themselves) [5].

Unauthorized approach for criminal purposes may occur on high seas, in anchoring point or even in the ship dock. At Santos estuary, seaborne attacks occur with the use of small speedy boats operated by armed individuals seeking to steal transported goods and personal belongings of the crew. Table 1 presents the number of boats attacks in Brazil and in the world from 2008 until the first quarter of 2011.

Table 1 - Boats attacks in Brazil and in the world from 2008 until 1st quarter 2011 (Source: IMB/International Maritime Bureau)

YEAR	Attacks in Brazil	World
2008	1	293
2009	5	406
2010	9	445
2011	1*	439

*1st quarter 2011

In the case of merchant vessels, the guidelines are for the civilians (passengers and crews members) to report the occurrence immediately by radio and take refuge in their cabins, avoiding confrontation with the invaders, in order to prevent personal injury (or even death) and limit losses to material goods.

The event will be subject to investigation and verification by the competent authority and eventually by interested stakeholders, such as an insurance company, if the shipping company contracted it. In this case the cargo and eventually subtracted goods will be object of repair measures by insurance companies.

When anchored on the estuary, but not at the port, the vessel is more willing to suffer from such events, given its

relative distance from the mainland, therefore the difficulty to mobilize rescue at the sea. That is why air support near the coast is an important aid to combat and avoid it.

The estuarine area of the port of Santos has always been considered a risk, between other causes, because of boats attacks. In current times, the effective action of the Federal Police to combat this type of criminal act resulted in the rout of two local gangs. In the last two years there have not been reported robberies on board ships in the complex. Unfortunately, still occur attacks on fishing boats and land banking facilities near to shore, by leaking vessels.

The use of effective vessel identification systems that allow monitoring of its movement thus becomes an important element of control and identification of vessels, promoting increased security of persons and property, hindering the criminal actions. The annual report of the International Maritime Bureau of the International Chamber of Commerce informed that, in 2013, there was a 40% reduction in pirate attacks.

III. VESSELS AND ITS DANGERS ON THE ESTUARY AREA

Port operations emphasize the large vessels, with ever increasing gross weight allowing scale economy, with higher productivity and cost savings. These vessels are, in overwhelming majority, ships built and equipped to the various types of cargo, including containers, dry and liquid bulk, general cargo and special cargo.

However, the aquatic modal, besides the ships have a lot of types of vessels and boats that play auxiliary roles to port operations, moving in ports and adjacent estuarine areas. Besides these, other vessels/boats for people transport and/or recreation yachts also circulate by these water and harbor areas. Despite all the existing surveillance is easy to see the passage of boats and yachts in open exhibition, in flagrant disregard of legal restrictions.

The vessels also constitute an environmental issue, as "the use of motorized boats in estuarine and coastal areas can result in the emission and exhaust gases, loss of fuel and lubricant for the water environment, direct contact with propellers, generating ripples and turbulence for propulsion and noise emissions and odors, which in turn can have multiple effects on the environment and on the development of other recreational activities (windsurfing, kayaking, swimming, snorkeling, bird watching etc.) and commercial systems (fishing, aquaculture etc.).

Among these striking effects, we highlight the continuous suspension of sediments, contamination of air, water and sediment, and disturbance of fauna and aquatic flora associated with these systems, and the erosion of margins." [6]

Monitoring allows checking whether obliged conditions have been observed. In other words, the control of the displacement of vessels lets one check the routes and the speed of this displacement. Given that, it allows authorities to have a better control over vessels (large or small) movements, preventing hazardous situations for people, goods and environment.

This article addresses the monitoring of these smaller

vessels movements within the port area, considering only those endowed with some sort of mechanical propulsion, within specific requirements.

IV. PROPOSED SOLUTION

The focus of this study was to propose a new process using an electronic device based on RFID technology to identify the BOAT/BOARD/ETC and a smartphone application to track in real time - each 60 seconds - the position of the user.

The proposed solution uses the concept of issuing a RFID HF NFC compatible tag [Fig. 2], with a QR-CODE [fig.3] containing the same identification for each BOAT/BOARD/ETC. This tag can be bought in the market, allowing several suppliers, and the user is responsible for the identification.

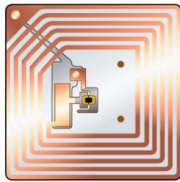


Fig. 2 - Example of a tag RFID
Source: <http://www2.ministries-online.org/biometrics/rfidchip2.html>



Fig. 3 - Example of QR CODE

Before starting the journey/use of the BOAT/BOARD/ETC, the user need to install a smartphone app thar will collect the RFID identification or capture the QR CODE using the camera.

The app will ask for user basic informations, such as social security number, sex, age and will start to collect the GPS data each 60 seconds and transmit the data to the cloud monitoring software, using 3G cellular networks.



Fig. 4 - Example of a mobile device that will be used in the field.

Some mobile devices [fig.4] need to be protected with special cases in order to have contact with water.

The whole process of communication between the mobile application and the backoffice is initiated by the mobile application.

Once stored in the backoffice, other players can monitor the position of the user and anticipate some potential risks.

Fig. 5 presents the proposed model.

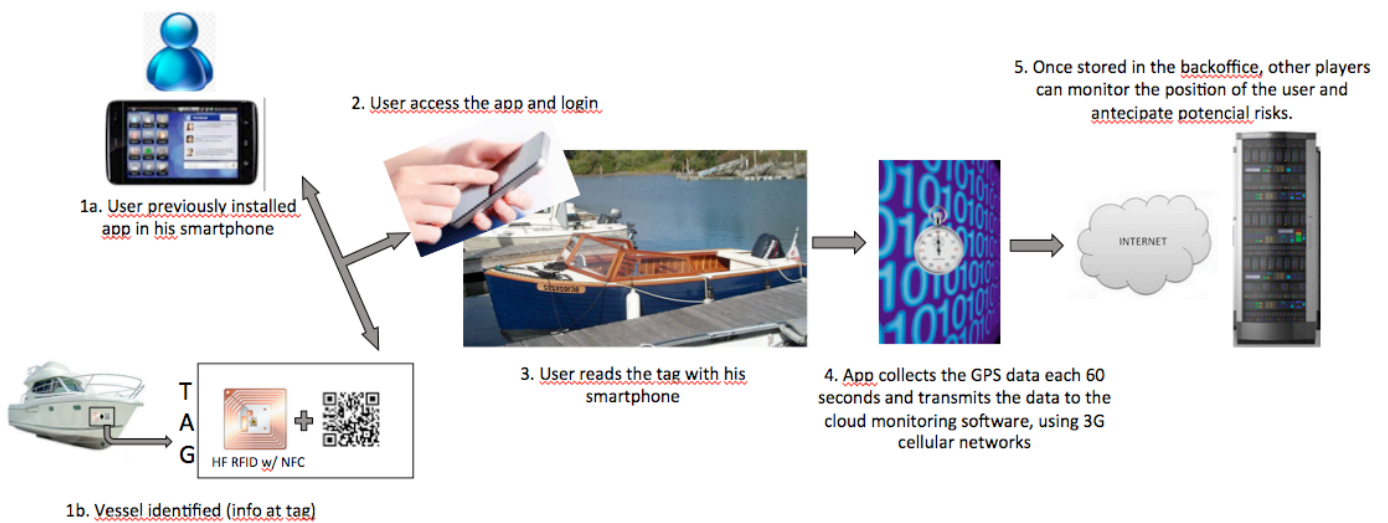


Fig. 5 - Proposed model

V. CONCLUSION

This work has a major operational and social interest, since many of these vessels carry large number of passengers, so they are susceptible of suffering hazardous consequences for failure to comply with relevant legislation.

It is important to monitor small vessel, specially the ones with some sort of mechanical propulsion, within specific requirements, when they share space with big vessels, such as the ones that transport containers and large amount of people (v.g. cruise ships). This sharing can cause major accidents, to people, cargos and, it must be consider, the environment.

Given this scenario, the present work presents a solution based on RFID technology to identify the vessel, in combination with a QR CODE, that will be readable by an app, installed in a smartphone. When the user uses his smartphone (with the app) to read the identification code (QR CODE or tag RFID), he will link the vessel to a user. By capturing the GPS data it will be possible to monitor the vessel, therefore, if the authorities have access to them they can have the necessary control to give effectiveness to the safety and security of the estuary.

It is necessary to make a pilot project of the app to analyze its real effects over this scenario and how the users and authorities will react to this reality.

REFERENCES

- [1] Yang, Zaili, Ng, A. K. Y., and Wang, Jim. 2014. A new risk quantification approach in port facility security assessment. *Transportation research Part A*. 59, pp.72-90.
- [2] BRAZIL. Law n.o 9537/1997. Brasília, 11 de dezembro de 1997, 176º da Independência e 109º da República.
- [3] Buruaem, L.M., de Castro, I. B. Hortellani, M. A., Taniguchi, S., Fillmann, G., Sasaki, S. T., Petti, M. A. V., Sarkis, J. E. de Souza, Bicego, M. C. Maranhão, L. A., Dowanso, M. B., Nonato, E. F., Cesar, A., Costa-Lotufo, L. V., Abessa, D. M. de Souza, 2013. Integrated quality assessment of sediments from harbour áreas in Santos-São Vicente estuarine system, Southern Brazil. *Estuarine, Coastal and Shelf Science*. 130, pp.179-189.
- [4] Robinson, R., 2002. Ports as elements in value-driven chain systems: the new paradigm. *Maritime Policy & Management*. 29 (3), pp.241–255.
- [5] Brooks, M.R., Pelot, R., 2008. Port security: a risk based perspective. In: Talley, W.K. (Ed.), *Maritime Safety. Security and Piracy*, LLP, London, pp.195–216.
- [6] LIMONGI, C. M. PROGRAMA DE ZONEAMENTO DO PERCURSO NO ESTUÁRIO E CONDIÇÕES DE NAVEGABILIDADE DAS EMBARCAÇÕES – Reserva do Paiva, 2007. Available: www.reservadopaiwa.com/pdf/pgazoneamento.pdf. Accessed at 20/04/2014.
- [7] Shaheen, S.A. and Finson, R. 2004. Intelligent Transportation Systems. *Energy Encyclopedia*, 3, pp.487-496.

Numerical model of behavior of pneumatic actuator

Jakub Javorik

Abstract—Goal of the work is to analyze the function of the pneumatic actuator. The dependence between the device construction and the hysteresis in the pressure/stroke relation was studied. A Numerical model of the actuator was created and its results were analyzed. Hyperelastic material properties of the rubber diaphragm were applied in the model and influence of friction between rubber and steel parts of the actuator was evaluated. Reasons of hysteresis were identified and some modifications of the actuator are suggested.

Keywords—hyperelasticity, hysteresis, numerical analysis, pneumatic actuator.

I. INTRODUCTION

THE paper deals with the numerical analysis of the mechanical behavior of the pneumatic actuator. High precision of control rod stroke is required for this important control and regulating device. Unfortunately, there is one negative effect, which affects the accuracy significantly. It is hysteresis in the stroke/pressure relation, i.e. difference in this relation during the pressure increase and decrease (Fig. 4). The work analyzes the possible causes of this hysteresis, and searches a way to reduce it to a minimum.

Analysis will reveal only the reasons caused by the shape and assembly of the actuator and its particular parts. Others reasons as a possible viscoelastic behavior of the elastomer parts are not included.

II. MATERIAL AND METHODS

A. Actuator Geometry

The geometric model of the actuator is shown in Fig. 1 and the scheme of the actuator parts can be seen in Fig. 2. The elastic (rubber) diaphragm (a) is fixed between two discs (b) in the closed case (c) and it is mounted on a metal core (d). This core is supported by the steel spring (e) on the one side. A control rod is connected with this assembly on the other side. The rubber diaphragm is reinforced by the textile on one side (f).

A pressure difference on the one and the second side of the diaphragm causes movement of the rod in the axial direction of the actuator.

B. Material Characterization

Basic element of the actuator is the rubber diaphragm (Fig. 2-a). Final position of the control rod depends on the mechanical properties of the diaphragm, on the spring stiffness (Fig. 2-e), and on the pressure.

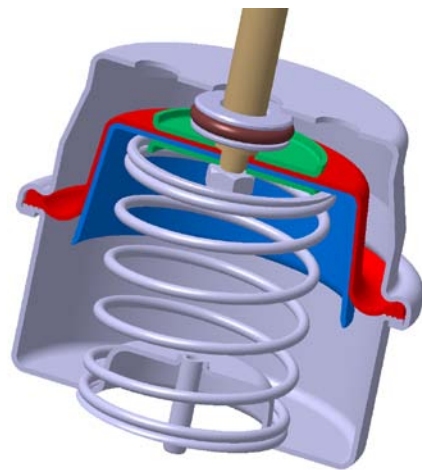


Fig. 1 partially cut model of the actuator

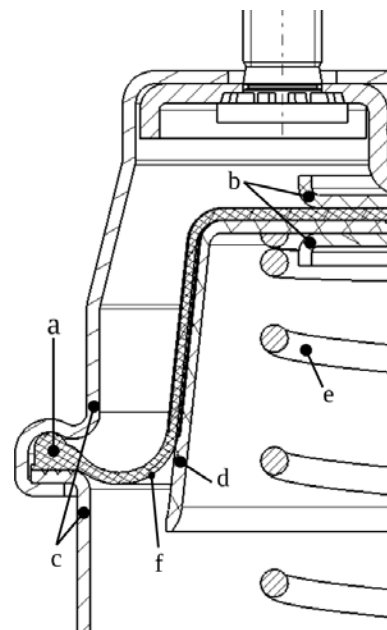


Fig. 2 scheme of the actuator structure

J. Javorik is with the Tomas Bata University in Zlin, nam. T. G. Masaryka 5555, 760 01 Zlin, Czech Republic (phone: +420 576 035 151; fax: +420 576 035 176; e-mail: javorik@ft.utb.cz).

Therefore we need to characterize the mechanics of the rubber diaphragm accurately. Due to these facts, the material of the diaphragm (elastomer) was tested in all three basic deformation modes (uniaxial tension, equibiaxial tension and pure shear) that are needed to set correct constants for hyperelastic material model [1]-[8]. The properties of textile were measured by the tension test in fiber directions.

C. Numerical (FEM) Model of the Actuator

Considering the geometry of actuator (Fig. 1 and 2), the finite element (FE) numerical model was created (Fig. 3) [9]-[11]. Thanks to the axial symmetry of the whole problem we could make 2D axisymmetric model with defined axis of symmetry. The model consists of planar surface which represents half section of the elastic diaphragm, then of three curves that represent rigid parts of the assembly, and of central element (lower straight line) that represents elastic support (spring) (Fig. 3). This element is located in the axis of symmetry of the actuator.

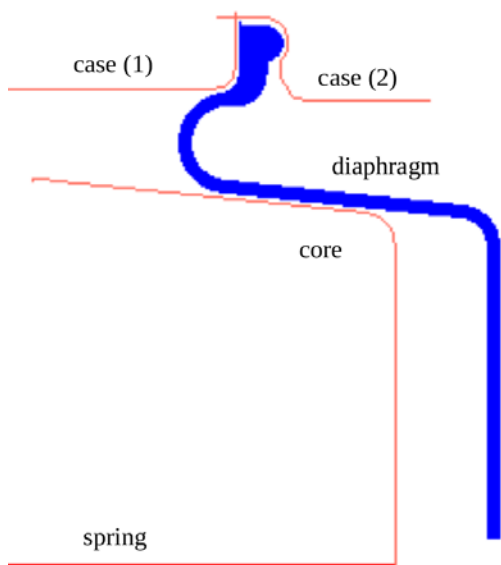


Fig. 3 numerical model of the actuator

The diaphragm consists of two materials: elastomer which is from one side joined with textile (Fig. 2-f). The textile is on the side where the diaphragm is in contact with the metal core of the actuator (Fig. 2). Material parameters of textile were measured in uniaxial tension test and they are: Young modulus $E=280$ MPa (and no bending stiffness, i.e. no rotation degrees of freedom are shared) and the Poisson ratio $\nu=0,3$ were set. From hyperelastic tests mentioned in the chapter II.B Arruda-Boyce hyperelastic model was set for elastomer with constants: $\mu=0.38793$ MPa and $\lambda_L=995567$ [12]-[14].

Curves of both parts of case and core (Fig. 3) are created as rigid bodies. Central spring stiffness is 3 N/mm. Next, a contact between rigid parts of the model and the elastic diaphragm was defined in the model.

D. Loads and Boundary Conditions

Whole analysis consists of four basic steps:

- clamping the rim of the diaphragm in the case of actuator
- mounting the diaphragm on the core
- pressure decreasing on the one side of the diaphragm
- returning the pressure to its initial value.

1) Clamping of the Diaphragm Rim in the Actuator Case

As we need to be as close to the reality as it is possible, the fixation of the diaphragm in the model is done by real clamping of the diaphragm rim between two parts of the actuator case. A contact between the case parts and the diaphragm is applied and the two parts of the case approach against each other.

2) Mounting the Diaphragm on the Core

The steel core (with the spring element) is pushed into the diaphragm during the second step. The contact between the core and the diaphragm occurs and the initial position of actuator parts, before the pressure application, is reached.

3) Pressure Application on One Side of the Diaphragm

Left end of the spring is fixed at the beginning of this step and the pressure decrease is applied on the inner side of the diaphragm (side with the textile). The spring is pressed by this condition and the core moves to left in the Fig. 3.

4) Returning the Pressure to Its Initial Value

The fourth step is opposite to the third step. The pressure increases to the initial value.

For the analysis of the influence of friction a number of friction coefficients were used. Computation were carried out with next friction coefficients (f_c): 0; 0.05; 0.07; 0.1; 0.15; 0.25; 0.35.

III. RESULTS AND DISCUSSION

Two main effects were evaluated. How could the friction influence the stroke/pressure hysteresis. And influence of diaphragm structure on its deformation and on the hysteresis.

A. Influence of Friction on the Hysteresis

The largest hysteresis occurred in the models with friction coefficient 0.05 and 0.07. The situation in these two cases is the same and the result is shown in the Fig. 4. The hysteresis is decreasing with a next increase or decrease of the value of friction coefficient (f_c) and it will vanish when the friction coefficient has value $f_c=0$ or its value is higher than 0.25 (Table 1 and Fig. 5).

During loading and movement of the diaphragm, it tends to slip over the surface of the core, and this fact causes a rising of the diaphragm edge from the core edge (Fig. 6). Then the hysteresis is caused by a difference between moments in which the slip occurs, because the moments of these slips can differ in case of pressure decreasing and pressure increasing. If the friction coefficient $f_c=0$, the slip should occur in the same moment without the influence of a previous history of loading

(decrease or increase of pressure) and thus no hysteresis should occur. This fact was also approved by the results of the model with $f_c=0$. This model was therefore used to approve initial hypothesis about the fact that the only the friction will be the reason of the hysteresis in the numerical model.

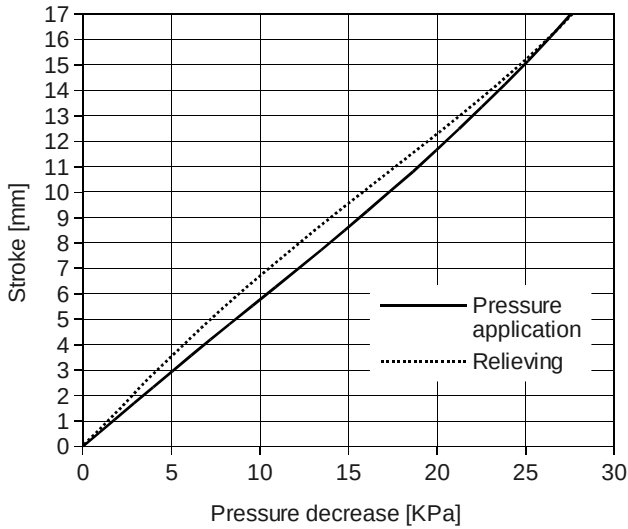


Fig. 4 hysteresis in the pressure/stroke relation with the friction coefficients 0.05 and 0.07

Table I Influence of the friction coefficient on the hysteresis

Friction coefficient f_c	Hysteresis [mm]
0	0
0,05	0,76
0,07	0,783
0,1	0,285
0,15	0,174
0,25	0,046
0,35	0

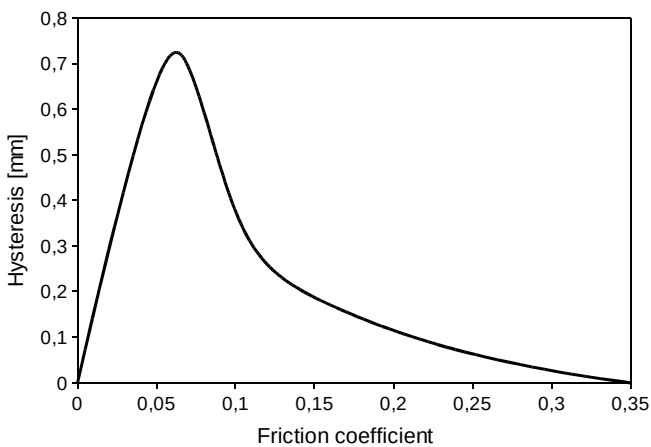


Fig. 5 relation between the friction and the hysteresis

Results, described above, shows that the pressure will not always be sufficient to fix the diaphragm to the core surface and then the slip of the diaphragm can occur. Thus some modification in shape and dimension of particular parts of actuator (for example large radius of the upper disc (b) in Fig. 2) could solve this problem.

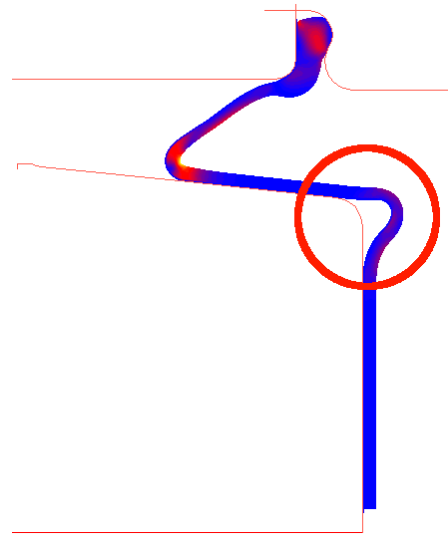


Fig. 6 the diaphragm edge raising during the pressure application and spring compression

B. Influence of Diaphragm Structure on Its Deformation

The bend of diaphragm, which occurs when the diaphragm is rolling on the surface of the core, is a next critical point. The maximum of stress and strain occurs here (Fig. 7).

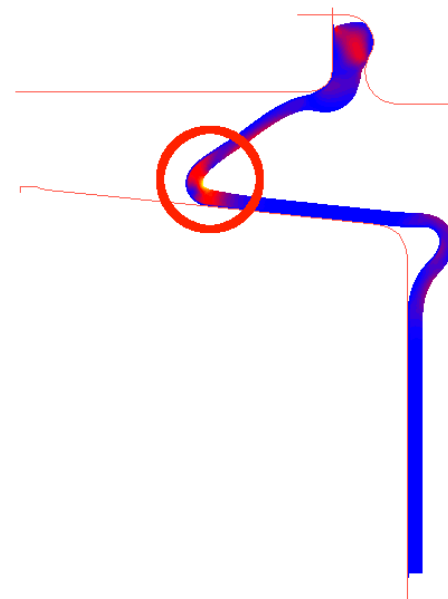


Fig. 7 critical point of model where the maximum of stress and strain occurs

The textile tension stiffness is significantly greater than the stiffness of the diaphragm elastomer. Thus, only the compression occurs in the entire thickness of the elastomer during the diaphragm bending shown in Fig. 8. Due to that fact a collapse of the diaphragm can occur at the end of stroke and a self contact of the diaphragm surface should occur (Fig. 8).

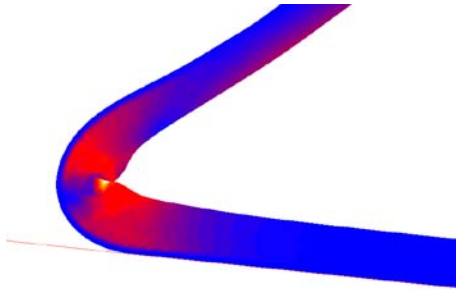


Fig. 8 the diaphragm collapse during its rolling on the core

Therefore, there is a contact between the two faces of the diaphragm. In this case, there would be a considerably greater friction than in the case of contact of the diaphragm (from the side with textile) with a steel core. That phenomenon could again strongly affect the hysteresis.

IV. CONCLUSION

Possible critical effects were revealed in the actuator analysis. They are: diaphragm slipping on the core surface and diaphragm collapse during the rolling along the core. These facts should be considered during future designs and modifications of actuators. Next possible effect as a viscoelastic character of elastomer (which is generally known and thus it is characterized in details in literature) were not the object of the analysis [15], [16].

REFERENCES

- [1] R. W. Ogden, *Non-linear Elastic Deformations*. New York: Dover Publications, 1997.
- [2] A. N. Gent, *Engineering with Rubber*. Munich: Hanser, 2001.
- [3] J. Javorik and Z. Dvorak, "Equibiaxial test of elastomers," *KGK-Kautsch. Gummi Kunstst.*, vol. 60, pp. 608-610, 2007.
- [4] W. D. Kim et al, "Some considerations on mechanical testing methods of rubbery materials using nonlinear finite element analysis," *Polym. Int.*, vol. 53, pp. 850-856, 2004.
- [5] L. Chevalier and Y. Marco, "Tools for multiaxial validation of behavior laws chosen for modeling hyperelasticity of rubber-like materials," *Polym. Eng. Sci.*, vol. 42, pp. 280-298, 2002.
- [6] L. P. Smith, *The Language of Rubber*. Oxford: Butterworth-Heinemann, 1993.
- [7] N. Reuge, F. M. Schmidt, Y. Le Maout, M. Rachik and F. Abbe, "Elastomer biaxial characterization using bubble inflation technique. I: Experimental investigations," *Polym. Eng. Sci.*, vol. 41, pp. 522-531, 2001.
- [8] J. Javorik and Z. Dvorak, "The testing of hyperelastic properties of the rubber materials," *Chem. Listy*, vol. 105, pp. 273-274, 2011.
- [9] A. F. Bower, *Applied Mechanics of Solids*. New York: CRC Press, 2009.
- [10] M. Bercovier, E. Jankovich, F. Leblanc and M. A. Durand, "A finite element method for the analysis of rubber parts: Experimental and analytical assessment," *Comput. Struct.*, vol. 14, pp. 384-391, 1981.

- [11] D. Samek and J. Javorik, "Numerical analysis of shape stability of rubber boot," *Int. J. Mech.*, vol. 7, pp. 293-301, 2013.
- [12] E. M. Arruda and M.C. Boyce, "A three-dimensional constitutive model for the large stretch behavior of rubber elastic materials," *J. Mech. Phys. Solids*, vol. 41, pp. 389-412, 1993.
- [13] M. C. Boyce, "Direct comparison of the Gent and the Arruda-Boyce constitutive models of the rubber elasticity," *Rubber Chem. Technol.*, vol. 69, pp. 781-785, 1996.
- [14] R. A. Brockman, "On the use of the Blatz-Ko constitutive model for nonlinear finite element analysis," *Comput. Struct.*, vol. 24, pp. 607-611, 1986.
- [15] A. Vandembroucke, H. Laurent, N. Ait Hocine, and G. Rio, "A hyperelasto-viscohysteresis model for an elastomeric behaviour: Experimental and numerical investigation," *Comput. Mater. Sci.*, vol. 48, pp. 495-503, 2010.
- [16] N. Huber and C. Tsakmakis, "Finite deformation viscoelasticity laws," *Mech. Mater.*, vol. 32, pp. 1-18, 2000.

Plasticity of the error monitoring and processing system

Menizibeya O. Welcome, Nikos E. Mastorakis, Vladimir A. Pereverzev

Abstract—An integral aspect of the domains of higher integrative brain functions is error commission, detection and correction, which are key indicators of cognition and behavior. The last decade was marked with substantial progress in mapping of the neural systems of error commission, detection and correction. Concurrently, significant development in neuroscience, sparked increased interest in plasticity of the neural systems responsible for various aspects of cognition and behavior. Error commission, detection and correction are the functions of the error monitoring and processing system (EMPS) located in diffuse brain regions. Almost a decade ago, it was not exactly clear whether the EMPS was tightly associated with neural systems of cognition and behavior. More recently, it is now becoming clearer that cognition, behavior and error monitoring and processing are closely related. Since neural systems of cognition and behavior exhibit plasticity, here we suggest that the EMPS also demonstrate plasticity. Owing to the tight coupling between neurons and astroglia, we propose that EMPS plasticity is largely due to neuro-astroglial cooperativity. In this mini-review, the mechanisms of this cooperativity are briefly discussed in relation to the EMPS activity

Keywords— Error monitoring and processing, neuroastroglial cooperativity, plasticity.

I. INTRODUCTION

THE error monitoring and processing system (EMPS) located in the substantia nigra of the midbrain, basal ganglia and cortex of the forebrain, plays a leading role in error commission, detection and correction [1-4]. According to electro-physiological studies, the function of the EMPS is reflected in the amplitude of the error related negativity, a negative deflection in the electroencephalogram with a maximum in the midline of the frontocentral region of the scalp having a latent period around 50-150ms [3,4]. A growing body of research data indicates that the error positivity that immediately follows error commission is also a useful component of the EMPS [5-7]. The positive component peaks approximately at 300ms after erroneous actions [4-6,8].

This work was supported in part by the World Scientific and Engineering Society and Academy (WSEAS).

M.O. Welcome is with the Belarusian State Medical University, Minsk, Pr., Dzerjinsky 83, Minsk 220116, Belarus (corresponding author phone: +375295647993; e-mail: menimed1@yahoo.com).

N.E. Mastorakis is with the World Scientific and Engineering Society and Academy, Athens, Greece (e-mail: mastor@tu-sofia.bg).

V. A. Pereverzev is with the Belarusian State Medical University, Minsk, Pr., Dzerjinsky 83, Minsk 220116, Belarus (e-mail: PereverzevVA@bsmu.by).

Research indicates the usefulness of this positive component in error awareness to be closely related to cognitive functions (behavioral components and executive functions [9,10]. Increased awareness of errors is related to the close engagement between cognitive functions and the brain EMPS [7]. For example, close engagement between memory/attention functions and EMPS might result in increased error awareness and reduced error commission [11-13].

Increased evidences about the inter-relationship between the EMPS and cognition probably came from studies on the importance of the error positivity in error awareness [5,9,10]. Endrass and colleagues (2012) have recently shown that error awareness mainly influences the error positivity, whereas the error negativity seems unaffected [6]. Some brain areas involved in cognitive functions are also known to participate in error monitoring and processing [14]. The major components of EMPS (dopaminergic system of the mediofrontal brain and anterior cingulate cortex) are also involved in cognitive functions [1,15]. Moreover, the plasticity and dynamics of the brain areas involved in error monitoring and processing are key factors that encourage the association between neural systems of cognition and error monitoring and processing [16-19].

In the past, researchers focused primarily on brain regions responsible for error monitoring and processing without giving adequate consideration to other systems that might otherwise be integrated with error monitoring and processing [3,4,20,21]. This led to a trend in the scientific community by viewing error monitoring and processing as the sole functions of neurons of those brain regions necessary for error monitoring and processing [3,15,19-22]. Probably, this was the reason why the error awareness effect remained elusive for several years and turned out to be the subject of a fierce debate in the scientific community [4,6].

In the last decade, imaging studies made substantial advancement in mapping the brain regions of EMPS [14,23]. Importantly, differences in error commission and detection were shown across different categories of people: normal healthy people in different age groups, patients with different cognitive and behavioral pathologies, substance users and abusers, people in different physiological states [1-3,24,25]. For example, gradual increase in brain regions involved in error monitoring processing was reported, and suggested being due to the maturation of the neural systems that identify different errors [22,26]. We suggest that neuro-astroglial

plasticity could account for a significant part of this variance.

Initial reports on error commission, detection and correction significantly shaped future studies. Error monitoring and processing were mostly attributed to the functions of neurons of the associated brain regions, whereas the contributions glia (especially astroglia) were entirely ignored. Lack of research data on the specific role of astroglia in cognition and behavior was probably a contributing factor. With increasing evidence about the role of astroglia in cognitive and behavioral pathologies, here we suggest that not only neural systems, but also glial networks are integral to EMPS activity. Since, glial cells (astroglia) significantly outnumber neuronal population [27], besides recent reports that astroglia are the powerhouse of neurons [28-33], here, we suggest that the functions of the EMPS are significantly dependent on neuro-astroglial cooperativity. Hence, this mini-review on the plasticity of EMPS is discussed in the light of neuro-astroglial cooperativity. Recent data on the mechanisms of this neuro-astroglial cooperativity in relation to the EMPS plasticity are briefly described.

II. PLASTICITY OF THE ERROR MONITORING AND PROCESSING SYSTEM: GENERAL VIEW, RELATIONSHIP TO NEUROASTROGLIAL COOPERATIVITY

Plasticity (neural, glial) is a term used to designate the changes that occur in the neuro-astroglial systems as a result of the impact of internal or external factors. Behavioral, cognitive, metabolic, environmental factors significantly modulate the neuro-astroglial plasticity (see figure 1) [34]. Here, we focused mostly on metabolic factors as regulators of plasticity of the neuro-astroglial system, which in our view is an integral component of the EMPS. Metabolic factors (glucose metabolic products) are the main factors linking astroglia to the neural systems of error monitoring and processing. Therefore, if there is a metabolic disorder in the neuro-astroglial system, the result is a disruption of error monitoring and processing. In fact, impairment of the neural systems associated with the EMPS is evident in brain pathologies such as Schizophrenia, Alzheimer's disease and other behavioral disorders, including substance abuse [24,25]. In our previous studies, impairments in metabolic regulation of glucose were identified as a necessary factor for increased error commission [1,2,35-37]. Adequate functioning of glucoregulatory systems is necessary in the maintenance of the EMPS activity. Glucose as the main energy substrate for neurons constantly enters into astroglia through glucose transporters [1,2]. In astrocytes, glucose is majorly metabolized to lactate or other intermediates or is converted to glycogen. The metabolic products of glucose in astroglia are transported into neurons. Functional and structural connections between astroglia and neurons ensure cooperativity in the neuro-astroglial system [38]. This cooperativity is pivotal in shaping the neural systems of error monitoring and processing. The molecular mechanisms linking this cooperativity to the EMPS are signaling pathways (mTOR, Notch, kinases

pathways), genetic, epigenetic (histone modifications and DNA methylation) [34,39,40].

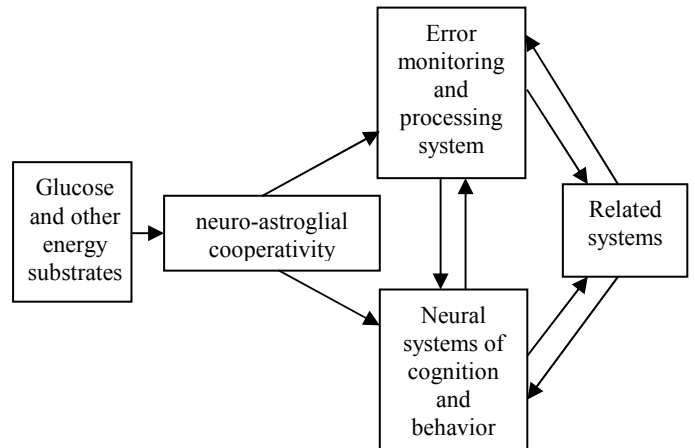


Figure 1. Association between neural systems of cognition/behavior and error monitoring and processing. Related systems through competing factors (internal or external) may modulate cognition, behavior and error monitoring and processing. Glucose and other energy substrates are the principal driving force for the functional cooperativity between neurons and astroglia. This functional cooperativity is integral in the regulation of neural systems of cognition, behavior and the EMPS [1-40]. Neuro-astroglial cooperativity and related systems influence the cognition, behavior and error monitoring and processing and regulate plasticity.

III. RECOMPOSITION OF THE NEURO-ASTROGLIAL COOPERATIVITY AS MAJOR FACTORS RESPONSIBLE FOR THE PLASTICITY OF THE EMPS: A GLIMPSE ON THE MECHANISMS OF NEUROASTROGLIAL COUPLING

With a gradual shift from neurocentric view of the nervous system functions in the last century to astrocentric view, scientists have begun extensive investigation into the role of these abundant glial cells in behavioral and cognitive disorders [41]. Many brain pathologies, initially perceived to be mainly due to neuronal dysfunctions, are now thought to be the result of impairment in astroglial functioning. For, instance, evidences are accumulating on astroglial dysfunction, precisely dysfunction of gap junctions in schizophrenia, resulting in a deficiency of d-serine and hypofunction of N-methyl-D-aspartic acid (NMDA) neurotransmission [42,43]. Importantly, several bodies of research data indicate impairment of error monitoring and processing in schizophrenia, including other behavioral and cognitive disorders [42-47]. Astroglial gap junction dysfunction has been reported in other brain pathologies [44-47], which are also reported to involving disorders of error monitoring and processing [24,25] The association between cognition and the EMPS suggests that impairment in cognitive processes will result in a disruption of EMPS activity [41].

The foremost contributing factor to the plasticity of EMPS is the neuro-astroglial cooperativity. Neuro-astroglial cooperativity is due to metabolic (glucose) regulatory systems, receptor cooperativity [48-50], peptides trafficking, regulation

of neurotransmitters release and activity, bidirectional signaling systems [27,51,52].

The cooperativity between astroglia and neurons is made possible through the regulation of ion concentration (potassium, calcium etc.), neurotransmitters (ATP, glutamate, aspartate etc.) and other signaling molecules [27,53,54]. Signals from adjacent neurons of brain regions traditionally involved in error monitoring and processing could trigger changes in astroglial ion dynamics. Astroglial ion dynamics will substantially affect the functions of both neurons and neighboring glial cells. Astroglial ion dynamics (for instance, calcium waves) may occur due to neurotransmitter release [54] Hoogland *et al.* (2009) showed that Bergmann glial calcium release could span numerous processes to modulate neuronal activity [54] Research has shown that an integral part of neurotransmitter cooperativity between astroglia and neurons is the glutamine–glutamate cycle [55]. Glutamine is necessary for the homeostasis of nitrogen and carbon, detoxification of ammonia and for the synthesis of glutamate and γ -aminobutyric acid (GABA) [56].

The neuro-astroglial cooperativity also involves receptor-receptor cooperativity [27] Research points to major role of ATP-sensitive (ligand-gated cationic channels and G protein-coupled receptors), NMDA, α -Amino-3-hydroxy-5-methyl-4-isoxazolepropionic acid (AMPA), adrenergic receptors in the modulation of the activity of the neuro-astroglial system [48,57,58].

Astroglial functional syncytia regulate the neuro-astroglial system – ensures regulated signaling of molecules [27,54]. This is made possible through the abundance of gap junctions. Gap junctions are special structures forming channels in brain cells that allow information integration. They are expressed in abundance not only in astroglia, but also in neurons [59-62]. Gap junctions are formed from connexins. Through oligomerization reaction, connexins form hexamers – connexons or hemichannels [63-65]. Evidences indicate a critical role of astroglial hemichannel conductivity in both normal and pathology [66]. Experimental data indicate the widespread expression of connexons (mostly of Cx43 and Cx30) and pannexons in astroglia and neurons – Cx36 among others [65,67,68]. These junctions allow the signaling of ions and second messengers (inositol-1,4,5-trisphosphate, cyclic AMP, calcium ions), amino acids (glutamate, aspartate, taurine), nucleotides (ADP, ATP, NAD), metabolites (glucose, glucose-6-phosphate, lactate), small peptides (glutathione) and RNA; however large molecules such as nucleic acids, proteins and lipids may not be transmitted [for details see ref. 41]. The presence of communicating hemichannels allows transmission of biomolecules between the cell and extracellular space. Glutamate, ATP, glucose and glutathione may be transmitted through hemichannels [41,66]. It is possible that other forms of gap junctions could be present in brain cells [65,69]. Functional hemichannels mediate auto-paracrine signaling of small molecules and neurotransmitters in the neuro-astroglial system [66,70,71]. One way in which the EMPS works is by

the astroglial information integration in different brain regions occurring through connexons, pannexons and hemichannels. Astroglial information integration may occur locally or in distributed pattern.

The cooperativity of astroglia with neighboring neuron or glial cell is term "local hub information integration" [41]. Pereira and Furlan (2010) proposed a "domino" and "carousel" effects for this pattern of cooperativity [41]. Astroglial cells release factors into glial cells and neurons to modulate their activities and plasticity. Information could spread to distance astroglial cells referred to as a "master hub", thus integrating results of distributed processing from glial cells and neurons. The functioning of this information integration pattern determines cognitive processes, including EMPS activity [41].

Physiological processes that modulate neuro-astroglial cooperativity had been outlined by Alfredo Pereira Jr, and Farbio Augusto Furlan (2010): short-term potentiation lasting for milliseconds, long-term potentiation lasting for hours or days; afterpotentiation – pre-synaptic reinforcement by means of retrograde messengers (nitric oxide, arachidonic acid) promoted by specific subunit activation of NMDA receptors, secondary activation of voltage-gated ion channels after initial activation of metabotropic receptor G-protein receptors; metapotentiation – series of events occurring in the neuro-astroglial system due to afterpotentiation of neurons; long-term depression – slowing of the activity in the neuro-astroglial system, which necessary to modulate nervous system functions [for details see 41].

A. Metabolic (glucose) regulation in the neuro-astroglial system is vital for cognitive/behavioral functions and error monitoring and processing

Adequate glycemic regulation is related to error commission, cognitive and behavioral functions. In our previous studies, we identified statistical relationships between these parameters of higher integrative brain functions and glycemic levels [1,2,36,37]. Regulation of glycemia is essential for brain glucose metabolism as a decrease in glycemia is associated with a corresponding decrease in neuronal/glial extracellular glucose levels; hence, a decrease in brain functions [71,72]. Both peripheral and central glucoregulatory processes are vital in the brain glucoregulation. However, this paper focuses on the central processes. The mechanisms by which hypoglycemia leads to lowering of cognitive functions is a complex one involving impairment of signaling pathways (e.g. mTOR), and decrease in long-term potentiation. Recently, it was reported that hypoglycemia results in impairments of gap junctions – a key communicating network in the neuro-astroglial cooperativity [55,58]. Key metabolic processes maintaining neuronal/astroglial glucose levels include glycolysis, glycogenolysis, and gluconeogenesis. Neuronal glycolysis is interrelated to the astroglial tricarboxylic acid (TCA) cycle via bidirectional signaling and exchange of metabolites. Astroglial TCA cycle forms a joining bridge with neurotransmitter synthesis. For example, neuronal glutamate is metabolized

through the astroglial TCA cycle, while astroglial glutamine is used by neurons as an energy substrate and glutamate precursor [55,58]. Elevated glutamate stimulates neuronal oxidative metabolism of astroglial-derived glycolytic products (lactate, pyruvate). Literature data indicate that this metabolic pathway represents a prime energy source for the neuro-astroglial system. Neuro-astroglial glucose homeostasis is also regulated by the functioning of adrenoreceptors [57,58]. Other neurotransmitters and their receptors could affect neuro-astroglial metabolic homeostasis [57,58].

Ion homeostasis also contributes to metabolic neuro-astroglial cooperativity [73,74]. Increase in potassium ions (resulting from glutamate release) had been shown to depolarize astroglial membrane, inducing intracellular calcium waves and hence, stimulating astroglial glycogenolysis and neuronal oxidative metabolism. These sequences of events are quantitatively related to cognitive processes, including motivation and learning [57,58]. Disruption in any phase of these events could impair learning, and hence, error monitoring and processing. Glucose metabolism (glycolysis) in other glia (oligodendroglia) by multiple mechanisms supports the integrity of axons, which is also crucial for information integration in the nervous system [72,74-77].

B. Regulation of neurotransmitter activity and receptor cooperativity in the neuro-astroglial system

Apart from metabolic regulation, receptor cooperativity remains a vital functioning of the neuro-astroglial system. In fact, the pattern of receptor cooperativity (astro-astroglial receptor cooperativity; astro-neuronal receptor cooperativity; neuro-neuronal receptor cooperativity) might significantly modulate brain functioning (cognitive, behavioral and EMPS functions) by enhancing or slowing down activities. Receptor cooperativity could be enhanced through receptor dimerization or polymerization [78-79]. Receptor cooperativity may be due to cross-talks between different intracellular signaling pathways, such as kinases pathways or other intermolecular forces. The interactions between different pathways in receptor cooperativity are essential in understanding the etiology of tumors of astroglial or neuronal origin [80,81]. This cooperativity between receptors may affect neurotransmitter activities (including gap junction mediated neuro-astroglial neurotransmitter release), hence modulating information integration in the cognitive, behavioral and EMPS domains. In addition, receptor cooperativity is closely related to metabolic regulation. Behar and Rothman (2001) reported that glutamate-GABA-glutamine cycling flux is linearly related to the rate of glucose oxidation, and linked to substrate cycling between astroglia and neurons [56]. Rouach *et al.* (2002) reported that costimulation of neuronal NMDA and muscarinic receptors modulate astroglial gap junctional communication, thereby leading to significant changes in exchange of biomolecules with the surrounding glial cells and neurons [82].

Regulation of neurotransmitters release and activity in the neuro-astroglial system is carried out mainly by astroglia through a three-component communicating medium [83].

Astroglial processes contact with neuronal synapse producing tripartite synapse – a major point of information integration – regulation of neurotransmitters release and activity. One astroglia can contact approximately 2 million synapses in the cortex of the human brain [41].

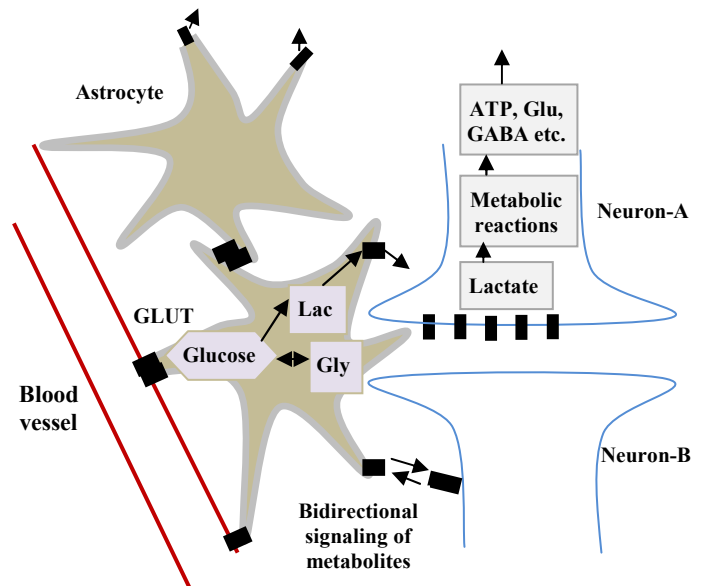


Figure 2. A simplified scheme of neuro-astroglial cooperativity (metabolites, especially of glucose; and other signaling molecules). Note: – Receptors, transporters or gap junctions; MCT – monocarboxylic transporter; GLUT – glucose transporter. Glucose and other nutrients may pass through blood vessels into astroglia, where they undergo a series of metabolic reactions to form intermediates of TCA cycle or could enter into other reactions. In astroglia, metabolites may be transported into neighboring astroglia or into neurons where they are utilized for production of biomolecules, including cellular components. Bidirectional signaling of different types of substrates and mediators occurs not only between astroglia and neurons, but also between neurons or astroglia [41,74-77]. Decrease in glycemia results in a corresponding decrease in glucose entrance into astroglia and hence TCA cycle intermediates entrance into neurons significantly reduces [72,74]. During mental tasks (especially demanding tasks), substrates supply cannot adequately meet the energy needs of actively working neurons due to reduced glucose level. Subsequently information is not adequately processed, thereby leading to increase in error commission; decrease in cognitive functions [1-4].

In the past decades, many hypotheses of the neuro-astroglial cooperativity were formulated. Apart from the classical understanding of information transmission (through electrical or chemical synapses), emerging evidences point to ephaptic (Greek "ephapsis" meaning "to touch") coupling of information between astroglia and neurons [84,85]. Ephaptic transmission is a non-synaptic exchange of information between adjacent nerve fibers caused by the exchange of ions between them, or as a result of local electric fields, thereby influencing the synchronization and timing of neuronal action potentials [85-87]. The induction of the firing of an adjacent neuron following initial excitation in the first neuron is referred to secondary excitation. This non-classical form of information transmission was noted in the pioneering works of du Bois-Reymond, Katz, Schmitt, and Arvanitaki [84,86,88]. More recently, works by Banaclocha (2007) [89] and Plankar *et al.* (2013) [90] suggest that ephaptic transmission of information

is pivotal in cognitive functions, mediating local and long-range communication and affecting plasticity in astroglia and neurons. Ephaptic coupling may be due to the matrix and binding proteins that structurally and functionally connect brain cells [90]. Kamermans and Fahrenfort (2004) reported that hemichannels support ephaptic coupling of information [91]. Pereira and Furlan (2010) proposed the “carousel effect” analogy to illustrate the effect of synchronized neuronal action potentials on an ensemble of interconnected astroglia. According to Pereira and Furlan (2010), this effect, in turn, is sustained by a reverse effect of astroglial activation on neuronal synchrony [41]. Pereira and Furlan (2010) presented a systemic view of neuro-astroglial information integration involving a synergy of glutamatergic, purinergic and other kinds of neurons co-activating a neighbor astroglia [41].

C. Bidirectional signaling

Bidirectional signaling, including peptide trafficking represents a key feature of the neuro-astroglial system. Several metabolites and neurotransmitters participate in this bidirectional signaling between glial cells and neurons (see figure 2) [41,74-77]. Functional plasticity as an important property of the neuro-astroglial system is aided by bidirectional signaling maintained between astroglia/neurons, neurons/neurons or astroglia/astroglia [41]. Bidirectional signaling is aided by gap junctions between these cells and through the exchange of signaling molecules. Signaling molecules released in one cell affect a neighboring one [73] or distanced cell according to the model earlier designed by Pereira and Furlan (2010) [41].

IV. MODULATORS OF THE EMPS: POSITIVE AND NEGATIVE REGULATIONS OF THE PLASTICITY OF ERROR MONITORING AND PROCESSING

Research has shown that certain factors affect error commission, correction and detection [1-4,23,92,93]. These factors might negatively or positively modulate the error commission rate or detection capacity of the neural systems of the error monitoring and processing [1-4,23,92-97]. Research on the neural systems of error monitoring and processing could provide new directions into drug development aimed at enhancing error detection and precision of performance for the necessary contingents of people including pilots.

A. Positive modulators

Positive modulators of EMPS that allow minimal error commission are adequate sleep, metabolic (glycemic) regulation, normal cognitive functioning [1,2,98,99]. In our previous studies, [2,35-37] we reported that adequate glycemic regulation was a necessary factor in error commission. Participants with proper functional glycemic control had minimal range of erroneous actions, whereas high erroneous actions were related to poor glycemic control [2,35-37]. Statistical analysis confirmed a strong negative relationship between error commission and glycemic control. A positive

relationship was noted between memory function and glucose control [2,36,37]. Studies report an inverted U-curve for the relation between glucose and memory function, [100,101] however further research is necessary. Adequate metabolic (glycemic) regulation and sleep may positively modulate the plasticity of EMPS.

B. Negative modulators

Several factors may negatively modulate EMPS activity [1-4,23,92-97]. Ridderinkhof and coworkers were the first to report that acute alcohol intake negatively modulate error monitoring and processing [3]. Holroyd and Yeung proposed possible pathways of alcohol action on error monitoring and processing: direct and indirect pathways through the disruption of the stimulus processing system upon which the EMPS depends [15]. We had discussed the indirect pathways in our previous works [1,37]. More recently, the direct pathways were partly discussed [2,96]. Additionally, we suggested that the disruption of EMPS might be possible in sober people who use alcohol episodically, even in moderate doses, especially under prolonged mental activities.

V. THE EMPS IN EVERYDAY LIFE: FUTURISTIC EXPECTATIONS IN RESEARCH INVOLVING THE NEURAL SYSTEM OF ERROR MONITORING AND PROCESSING

The everyday activities of humans are evaluated based on successfully completed tasks. Conversely, unsuccessful tasks do not contribute to performance quality. Unsuccessful execution of tasks due to error commission or inability to detect an error during task execution is the result of impairment in error monitoring and processing [1,2,95]. While a normal range of error commission, detection and correction had been suggested in our earlier report, research in this direction is scanty. In our previous study, approximately 5% error commission rate was identified as physiologically normal (it is suggested that the basal level of error commission for a normal physiological state is due to the automatic component of brain processing of information) [2]. However, further research in this direction in different categories of people is imminent. Why is research regarding the EMPS so valuable to humans? Reports show that several catastrophes experienced by humans were due to errors – often referred to the “human factor”. Such cases are experienced in aviation, etc. In medicine, errors (cognitive errors of omission or commission) had been reported to be the result of catastrophic situations for the patient [94].

Catastrophic cases due to the human factor have provided a means for people to believe that in those situations, there are no options. While this might be true in most cases, goal driven research in this direction could help solve those catastrophic cases due to human factor, not only by improving the technological bases, but also by improving the efficiency of the EMPS. For instance, drug research into effectiveness of engaging the neuro-astroglial system of the brain regions

involved in EMPS for high-level precision of tasks execution is necessary.

VI. CONCLUSION

The brain error monitoring and processing system is tightly associated with neural systems of cognitive and behavioral functions. Cognitive plasticity could shape the brain error monitoring and processing system. This plasticity is due to neuro-astroglial cooperativity and is related mainly to adequate metabolic (glucose) regulation. Adequate enhancement of cognitive plasticity will lead to improved capacity of the EMPS.

REFERENCES

- [1] M. O. Welcome, Y. E. Razvodovsky, E. V. Pereverzeva and V. A. Pereverzev, "The error monitoring and processing system in alcohol use", *IJCRIMPH*, vol. 2, no. 10, pp. 318-336, 2010.
- [2] M. O. Welcome, V. A. Pereverzev, "Basal Ganglia and the Error Monitoring and Processing System: How Alcohol Modulates the Error Monitoring and Processing Capacity of the Basal Ganglia", In: Barrios FA, Bauer C, Editors, *Basal Ganglia – An Integrative View*. Croatia: InTech, pp. 65-86, 2013.
- [3] K. R. Ridderinkhof, Y. de Vlugt, A. Bramlage, et al, "Alcohol consumption impairs detection of performance errors in mediofrontal cortex", *Science*, vol. 298, pp. 2209–2211, 2002.
- [4] M. Falkenstein, J. Hoormann, S. Christ, J. Hohnsbein, "ERP components on reaction errors and their functional significance: a tutorial", *Biol. Psychol.*, vol. 51, no. 2-3, pp. 87-107, 2000.
- [5] M. Dhar, J. R. Wiersema, G. Pourtois, "Cascade of Neural Events Leading from Error Commission to Subsequent Awareness Revealed Using EEG Source Imaging," *PLoS ONE*, vol. 6, no. 5, e19578, 2011.
- [6] T. Endrass, J. Klawohn, J. Preuss, N. Kathmann, "Temporospatial dissociation of Pe subcomponents for perceived and unperceived errors," *Front. Hum. Neurosci.*, no. 6 (Article178), pp. 1-10, 2012.
- [7] J. D. Charlesworth, T. L. Warren, M. S. Brainard, "Covert skill learning in a cortical-basal ganglia circuit," *Nature*, vol. 486, pp. 251–255, 2012.
- [8] R. Vocat, G. Pourtois, P. Vuilleumier, "Unavoidable errors: a spatio-temporal analysis of time-course and neural sources of evoked potentials associated with error processing in a speeded task," *Neuropsychologia*, vol. 46, no. 10, pp. 2545-55, 2008.
- [9] J. Marco-Pallarés, E. Camara, T. F. Münte, A. Rodríguez-Fornells, "Neural mechanisms underlying adaptive actions after slips," *J. Cogn. Neurosci.*, vol. 20, no. 9, pp. 1595-610, 2008.
- [10] H. Garavan, T. J. Ross, K. Murphy, R. A. Roche, E. A. Stein, "Dissociable executive functions in the dynamic control of behavior: inhibition, error detection, and correction," *Neuroimage*, vol. 17, no. 4, pp. 1820-1829, 2002.
- [11] E. R. A. De Bruijn, R. B. Mars, H. Bekkering, M. G. H. Coles, "Your mistake is my mistake . . . or is it? Behavioural adjustments following own and observed actions in cooperative and competitive contexts," *Quart. J. Exp. Psychol.*, vol. 65, no. 2, pp. 317-325, 2012.
- [12] R. P. Spunt, M. D. Lieberman, J. R. Cohen, N. I. Eisenberger, "The Phenomenology of Error Processing: The Dorsal ACC Response to Stop-signal Errors Tracks Reports of Negative Affect," *J. Cogn. Neurosci.*, vol. 24, no. 8, pp. 1753-1765, 2012.
- [13] A. L. Manuel, F. Bernasconi, M. M. Murray, L. Spierer, "Spatio-temporal Brain Dynamics Mediating Post-error Behavioral Adjustments," *J. Cogn. Neurosci.*, vol. 24, no. 6, pp. 1331-1343, 2012.
- [14] S. F. Taylor, E. R. Stern, W. J. Gehring, "Neural Systems for Error Monitoring: Recent Findings and Theoretical Perspectives," *Neuroscientist*, vol. 13, no. 2, pp. 160–172, 2007.
- [15] C. B. Holroyd, N. Yeung, "Alcohol and error processing," *Trends Neurosci.*, vol. 26, no. 8, pp. 402- 404, 2003.
- [16] B. Kolb, A. Muhammad, R. Gibb, "Searching for factors underlying cerebral plasticity in the normal and injured brain," *J Comm. Dis.*, vol. 44, no. 5, pp. 503–514, 2011.
- [17] J. Stiles, "Neural plasticity and cognitive development," *Dev. Neuropsychol.*, vol. 18, no. 2, pp. 237-72, 2000.
- [18] H. Neville, D. Bavelier, "Human brain plasticity: evidence from sensory deprivation and altered language experience," *Prog. Brain Res.*, vol. 138, pp. 177-88, 2002.
- [19] R. L. Bryck, P. A. Fisher, "Training the Brain: Practical Applications of Neural Plasticity From the Intersection of Cognitive Neuroscience, Developmental Psychology, and Prevention Science," *Am. Psychol.*, vol. 67, no. 2, pp. 87–100, 2012.
- [20] M. M. Botvinick, J. D. Cohen, C. S. Carter, "Conflict monitoring and anterior cingulate cortex: an update," *Trends Cogn. Sci.*, vol. 8, no. 12, pp. 539-546, 2004.
- [21] C. S. Carter, T. S. Braver, D. M. Barch, M. M. Botvinick, D. Noll, J. D. Cohen, "Anterior cingulate cortex, error detection, and the online monitoring of performance," *Science*, vol. 280, pp. 747-749, 1998.
- [22] M. C. Stevens, K. A. Kiehl, G. D. Pearson, V. D. Calhoun, "Brain Network Dynamics During Error Commission," *Hum. Brain Mapp.*, vol. 30, no. 1, pp. 24–37, 2009.
- [23] M. P. Paulus, N. Hozack, L. Frank, G. G. Brown, "Error Rate and Outcome Predictability Affect Neural Activation in Prefrontal Cortex and Anterior Cingulate during Decision-Making," *NeuroImage*, vol. 15, pp. 836–846, 2002.
- [24] D. M. Olvet, G. Hajcak, "The error-related negativity (ERN) and psychopathology: Toward an Endophenotype," *Clin. Psychol. Rev.*, vol. 28, no. 8, pp. 1343–1354, 2008.
- [25] D. S. Manoachand, Y. Agam, "Neural markers of errors as endophenotypes in neuropsychiatric disorders," *Front. Hum. Neurosci.*, vol. 7, no. 350, 2013.
- [26] M. B. Pontifex, M. R. Scudder, M. L. Brown, K. C. O’Leary, C.-T. Wu, J. R. Themanson, C. H. Hillman, "On the number of trials necessary for stabilization of error-related brain activity across the life span," *Psychophysiology*, vol. 47, pp. 767–773, 2010.
- [27] M. Bélanger, P. J. Magistretti, "The role of astroglia in neuroprotection," *Dialogues Clin. Neurosci.*, vol. 11, no. 3, pp. 281-295, 2009.
- [28] A. Taberero, J. M. Medina, C. Giaume, "Glucose metabolism and proliferation in glia: role of astrocytic gap junctions," *J. Neurochem.*, vol. 99, pp. 1049–1061, 2006.
- [29] L. H. Bergersen, A. Gjedde, "Is lactate a volume transmitter of metabolic states of the brain?," *Front. Neuroenerg.*, vol. 4, no. 5, 2012.
- [30] L. Pellerin, P. J. Magistretti, "Sweet sixteen for ANLS," *J. Cereb. Blood Flow Metab.*, vol. 32, pp. 1152–1166, 2012.
- [31] D. Sampol, E. Ostrofet, M.-L. Jobin, et al., "Glucose and lactate metabolism in the awake and stimulated rat: a 13C-NMR study," *Front. Neuroenerg.*, vol. 5, no. 5, 2013.
- [32] A. Suzuki, S. A. Stern, O. Bozdagi, et al., "Astrocyte-neuron lactate transport is required for long-term memory formation," *Cell*, vol. 144, pp. 810–823, 2011.
- [33] P. Bezzi, A. Volterra, "Astrocytes: Powering Memory," *Cell*, vol. 144, no. 5, pp. 644-645, 2011.
- [34] J. Feng, Y. Zhou, S. L. Campbell, et al., "Dnmt1 and Dnmt3a maintain DNA methylation and regulate synaptic function in adult forebrain neurons," *Nat. Neurosci.*, vol. 1, no. 4, pp. 423-30, 2010.
- [35] M. O. Welcome, V. A. Pereverzev, "Glycemic allostasis in the sober - what happens when the mental sphere is overloaded?," *Eur. Psychiatr.*, vol. 28, no. 1, p.1, 2013.
- [36] M. O. Welcome, E. V. Pereverzeva and V. A. Pereverzev, "Long-term disorders of cognitive functions in sober people who episodically use alcohol, role of functional hypoglycemia and insufficiency of gluconeogenesis," *Vest. Smolensk Med. Acad.*, no. 3, pp. 2-20, 2011.
- [37] M. O. Welcome, Y. E. Razvodovsky, E. V. Pereverzeva and V. A. Pereverzev, "The effect of blood glucose concentration on the error monitoring and processing system in alcohol users during intensive mental activities," *Port Harcourt Med. J.*, vol. 5, no. 3, pp. 293-306, 2011.
- [38] M. Caleo, G. M. Innocenti, M. Pfitz, "Physiology and Plasticity of Interhemispheric Connections, Neural Plasticity, Article 176183, 2013. <http://dx.doi.org/10.1155/2013/176183>.
- [39] W. B. Potter, K. J. O’Riordan, D. Barnett, et al., "Metabolic Regulation of Neuronal Plasticity by the Energy Sensor AMPK," *PLoS One*, vol. 5, no. 2, e8996, 2010.

- [40] C. A. Hoeffer, E. Klann, "mTOR Signaling: At the Crossroads of Plasticity, Memory, and Disease," *Trends Neurosci.*, vol. 33, no. 2, pp. 67–75, 2010.
- [41] A. J. Pereira, F. A. Furlan, "Astrocytes and human cognition: Modeling information integration and modulation of neuronal activity," *Prog. Neurobiol.*, vol. 92, pp. 405–420, 2010.
- [42] N. S. Kolomeets, N. Uranova, "Ultrastructural abnormalities of astrocytes in the hippocampus in schizophrenia and duration of illness: a postmortem morphometric study," *World J. Biol. Psychiatry*, vol. 11 (2 Pt 2), pp. 282–92, 2010.
- [43] Ma TM, Abazyan S, Abazyan B, et al. Pathogenic disruption of DISC1-serine racemase binding elicits schizophrenia-like behavior via D-serine depletion. *Mol Psychiatry* 2013;18(5):557-67.
- [44] Nemani VM, Binder DK. Emerging role of gap junctions in epilepsy. *Histol Histopathol* 2005; 20: 253-259.
- [45] Bargiotas P, Krenz A, Hormuzdi SG, et al. Pannexins in ischemia-induced neurodegeneration. *Proc Natl Acad Sci U S A* 2011;108(51):20772-7.
- [46] Penuela S, Laird DW. The cellular life of pannexins. *WIREs Membr Transp Signal* 2012; 1:621–632.
- [47] Santiago MF, Veliskova J, Patel NK, et al. Targeting pannexin1 improves seizure outcome. *PLoS ONE* 2011; 6: e25178.
- [48] Illes P, Ribeiro JA. Molecular physiology of P2 receptors in the central nervous system. *Eur J Pharmacol* 2004; 483: 5– 17.
- [49] Samarasinghe RA, Witchel SF, DeFranco DB. Cooperativity and complementarity: Synergies in non-classical and classical glucocorticoid signaling. *Cell Cycle* 2012;11:15, 2819-2827.
- [50] Marchetti B. Cross-talk signals in the CNS: role of neurotrophic and Hormonal factors, adhesion molecules and intercellular signaling agents in luteinizing hormone-releasing hormone (LHRH)-astroglial interactive network. *Front Biosci* 1997; 2 :d88-125.
- [51] Agrawal S, Archer C, Schaffer DV. Computational Models of the Notch Network Elucidate Mechanisms of Context-dependent Signaling. *PLoS Comput Biol* 2009; 5(5): e1000390.
- [52] El-Etr M, Cordier J, Glowinski J, Premont J. A Neuroglial Cooperativity Is Required for the Potentiation by 2Ghloroadenosine of the Muscarinic-Sensitive Phospholipase C in the Striatum. *J Neurosci* 1989; 9(5): 1473-1480.
- [53] Kaufman EE, Driscoll BF. Evidence for Cooperativity between Neurons and Astroglia in the Regulation of CO₂ Fixation in vitro. *Dev Neurosci* 1993;15:299–305.
- [54] Hoogland TM, Kuhn B, Göbel W, et al. Radially expanding transglial calcium waves in the intact cerebellum. *Proc Natl Acad Sci U S A* 2009;106(9):3496-501.
- [55] Zwingmann C, Leibfritz D. Glial–Neuronal Shuttle Systems. In: Editors Gibson GE, Dienel G. Vol. 5 Brain Energetics: Integration of Molecular and Cellular Processes in Handbook of Neurochemistry & Molecular Neurobiology 3rd Edition. New York: Springer; 2007. 197-238.
- [56] Behar KL, Rothman DL. In Vivo Nuclear Magnetic Resonance Studies of Glutamate-g-Aminobutyric Acid-Glutamine Cycling in Rodent and Human Cortex: the Central Role of Glutamine. *J Nutr* 2001; 131: 2498S–2504S.
- [57] Hertz L, Xu J, Song D, Du T, Yan E, Peng L. Brain Glycogenolysis, Adrenoceptors, Pyruvate Carboxylase, Na⁺,K⁺-ATPase and Marie E. Gibbs' Pioneering Learning Studies. *Front Integr Neurosci* 2013; 7:20.
- [58] Laming PR, Kimelberg H, Robinson S, et al. Neuronal-glia interactions and behaviour. *Neurosci Biobehav Rev* 2000;24(3):295-340.
- [59] Schools GP, Zhou M, Kimelberg HK. Development of gap junctions in hippocampal astrocytes: evidence that whole cell electrophysiological phenotype is an intrinsic property of the individual cell. *J Neurophysiol* 2006; 96: 1383–1392.
- [60] Söhl G, Maxeiner S, Willecke K. Expression and functions of neuronal gap junctions. *Nat Rev Neurosci* 2005;6(3):191-200.
- [61] Nagy JI, Rash JE. Connexins and gap junctions of astrocytes and oligodendrocytes in the CNS. *Brain Res Brain Res Rev* 2000;32(1):29-44.
- [62] Wang Y, Denisova JV, Kang KS, Fontes JD, Zhu BT, Belousov AB. Neuronal gap junctions are required for NMDA receptor-mediated excitotoxicity: implications in ischemic stroke. *J Neurophysiol* 2010;104(6):3551-6.
- [63] Ambrosi C, Gassmann O, Pranskevich JN, et al. Pannexin1 and Pannexin2 Channels Show Quaternary Similarities to Connexons and Different Oligomerization Numbers from Each Other. *J Biol Chem* 2010, 285:24420-24431.
- [64] Abascal F, Zardoya R. LRRC8 proteins share a common ancestor with pannexins, and may form hexameric channels involved in cell-cell communication. *Bioessays* 2012; 34: 551–560.
- [65] Samuels E, Lipitz JB, Dahl G, Muller KJ. Neuroglial ATP release through innexin channels controls microglial cell movement to a nerve injury. *JGP* 2010; 136 (4):425-442.
- [66] Sáez JC, Contreras JE, Bukauskas FF, Retamal MA, Bennett MV. Gap junction hemichannels in astrocytes of the CNS. *Acta Physiol Scand* 2003;179(1):9-22.
- [67] Yoon SY, Robinson CR, Zhang H, Dougherty PM. Spinal astrocyte gap junctions contribute to oxaliplatin-induced mechanical hypersensitivity. *J Pain* 2013;14(2):205-14.
- [68] Scemes E, Suardicani SO, Dahl G, Spray DC. Connexin and pannexin mediated cell–cell communication. *Neuron Glia Biol* 2007; 3(3): 199–208.
- [69] McCracken CB, Roberts DCS. Neuronal Gap Junctions: Expression, Function, And Implications For Behavior. *Int Rev Neurobiol* 2006; 73: 125-151.
- [70] Gomes FCA, Spohr TCLS, Martinez R, Neto VM. Cross-talk between neurons and glia: highlights on soluble factors. *Br J Med Biol Res* 2001; 34: 611-620.
- [71] Fukuda T, Kosaka T, Singer W, Galuske RAW. Gap Junctions among Dendrites of Cortical GABAergic Neurons Establish a Dense and Widespread Intercolumnar Network. *J Neurosci* 2006; 26(13):3434 – 3443.
- [72] Won SJ, Jang BG, Yoo BH, et al. Prevention of acute/severe hypoglycemia-induced neuron death by lactate administration *J Cereb Blood Flow Metab* 2012; 32: 1086–1096.
- [73] Ni Y, Malarkey EB, Parpura V. Vesicular release of glutamate mediates bidirectional signaling between astrocytes and neurons. *J Neurochem* 2007;103(4):1273-84.
- [74] Parpura V, Verkhratsky A. Homeostatic function of astrocytes: Ca²⁺ and Na⁺ signaling. *Trans Neurosci* 2012;3(4):334-344.
- [75] Fünfschilling U, Supplie LM, Mahad D, et al. Glycolytic oligodendrocytes maintain myelin and long-term axonal integrity. *Nature* 2012;485(7399):517-21.
- [76] Lee Y, Morrison BM, Li Y, et al. Oligodendroglia metabolically support axons and contribute to neurodegeneration. *Nature* 2012;487(7408):443-8.
- [77] Matsui T, Soya H. Brain Glycogen Decrease and Supercompensation with Prolonged Exhaustive Exercise. *Soc Neurosci Public Health* 2013: 253-264.
- [78] Danysz W, Parsons CG. Glycine and N-Methyl-D-Aspartate Receptors: Physiological Significance and Possible Therapeutic Applications. *Pharmacol Rev* 1998;50(4):597-664.
- [79] Kenakin T, Miller LJ. Seven Transmembrane Receptors as Shapeshifting Proteins: The Impact of Allosteric Modulation and Functional Selectivity on New Drug Discovery. *Pharmacol Rev* 2010;62:265–304.
- [80] Vitucci M, Kapinich NO, Bash RE, et al. Cooperativity between MAPK and PI3K signaling activation is required for glioblastoma pathogenesis. *Neuro Oncol* 2013. doi: 10.1093/neuonc/not084.
- [81] André C, Dos Santos G, Koulakoff A. Muscarinic Receptor Profiles of Mouse Brain Astrocytes in Culture Vary With Their Tissue Of Origin but Differ From Those of Neurons. *Eur J Neurosci* 1994; 6(11): 1702–1709.
- [82] Rouach N, Tence M, Glowinski J, Giaume C. Costimulation of N-methyl-D-aspartate and muscarinic neuronal receptors modulates gap junctional communication in striatal astrocytes. *PNAS* 2002; 99 (2):1023–1028.
- [83] Wiedemann C. Neuron–glia interactions: An intimate relationship. *Nat Rev Neurosci* 2009;10 (5): 318-318.
- [84] Arvanitaki A. Effects Evoked in an Axon by the Activity of a Contiguous One. *J Neurophysiol* 1942;5(2):89-108.
- [85] Su C, Menuz K, Reisert J, Carlson J. Non-Synaptic Inhibition Between Grouped Neurons in an Olfactory Circuit. *Nature* 2012; 492 (7427): 66-71.
- [86] Aur D, Jog MS. Neuroelectrodynamics: Understanding the brain language. Amsterdam, The Netherlands: IOS Press; 2010.
- [87] Wilhelm B. Electrophysiology. South Carolina, USA: Nabu Press; 2010.

- [88] Katz B, Schmitt OH. Electric Interaction Between Two Adjacent Nerve Fibers. *J Physiol* 1940;97(4):471-488.
- [89] Banaclocha MA. Neuromagnetic dialogue between neuronal minicolumns and astroglial network: a new approach for memory and cerebral computation. *Brain Res Bull* 2007;73(1-3):21-7.
- [90] M. Plankar, S. Brežan, I. Jerman, "The principle of coherence in multi-level brain information processing," *Prog. Biophys. Mol. Biol.*, vol. 111, no. 1, pp. 8-29, 2013.
- [91] M. Kamermans, I. Fahrenfort, "Ephaptic interactions within a chemical synapse: hemichannel-mediated ephaptic inhibition in the retina," *Curr. Opin. Neurobiol.*, vol. 14, no. 5, pp. 531-41, 2004.
- [92] Z. Susic-Vasic, M. Ulrich, M. Ruchsow, N. Vasic, G. Gron, "The Modulating Effect of Personality Traits on Neural Error Monitoring: Evidence from Event-Related fMRI," *PLoS ONE*, vol. 7, no. 8, e42930, 2012.
- [93] P. Thoma, C. Bellebaum, "Factors mediating performance monitoring in humans—from context to personality," *Front. Hum. Neurosci.*, vol. 7, no. 23, 2013.
- [94] J. W. Hurst, "Cognitive Errors (Can They Be Prevented?)," *Am. J. Cardiol.*, vol. 101, no. 10, pp. 1513- 1517, 2008.
- [95] T. Schulte, E. M. Müller-Oehring, H. Strasburger, H. Warzel, B. A. Sabel, "Acute effects of alcohol on divided and covert attention in men," *Psychopharmacology*, vol. 154, no. 1, pp. 61–69, 2001.
- [96] M. O. Welcome, V. A. Pereverzev, "The mistake system of the brain and ethanol: a direct pathway possible?," *Eur. Psychiatr.*, vol. 28, no. 1, p. 1, 2013.
- [97] M. O. Welcome, V. A. Pereverzev, "A classical view of the error processing effect", *Eur. Psychiatr.*, vol. 28, no. 1, p. 1, 2013.
- [98] M. M. Mitler, M. A. Carskadon, C. A. Czeisler, W. C. Dement, D. F. Dinges, R. C. Graeber, "Catastrophes, Sleep, and Public Policy: Consensus Report Sleep, vol. 11, no. 1, pp. 100–109, 1988.
- [99] M. Kramer, "Sleep loss in resident physicians: the cause of medical errors?," *Front. Neurol.*, vol. 1, no. 128, 2010.
- [100] M. W. Parsons, P. E. Gold, "Glucose enhancement of memory in elderly humans: an inverted-U dose-response curve," *Neurobiol. Aging*, vol. 13, pp. 401–4, 1992.
- [101] E. Baldi, C. Bucherelli, "The inverted "u-shaped" dose-effect relationships in learning and memory: Modulation of Arousal and Consolidation," *Nonlinear Biol. Toxicol. Med.*, vol. 3, pp. 9–21, 2005.

Conversion of the METCM into the METEO-11

Karel Šilinger

University of Defense
Department of fire support control
Brno, Czech Republic
karel.silinger@unob.cz

Ladislav Potužák

University of Defense
Department of fire support control
Brno, Czech Republic

Jiří Šotnar

University of Defense
Department of fire support control
Brno, Czech Republic

Abstract—This article deals with a proposed method of conversion of the METCM meteorological message into the METEO-11 format. This method is designed for artillery of these armies that are using the METEO-11 meteorological message during a spare (manual) method of firing data calculation. The proposed method is based on the simulation of temperature and wind sounding by radiosonde from the values of the METCM meteorological message. Then the values of the METEO-11 meteorological message are calculated with using carried out simulation of temperature and wind sounding by radiosonde. The conversion of the METCM meteorological message into the METEO-11 format consists of the recalculating of the meteorological message header, recalculation of meteorological data in the METCM meteorological message onto the units used in the METEO-11 meteorological message, conversion of the ground meteorological data, conversion of the meteorological data from the particular zones used in METCM meteorological message into the needed heights above an artillery meteorological station used in the METEO-11 meteorological message and the calculation of the meteorological data average values in the individual layers of the METEO-11 meteorological message.

Keywords—Artillery; METCM meteorological message; METEO-11 meteorological message; conversion of meteorological message

I. INTRODUCTION

Two standard types of meteorological messages are used in the North Atlantic Treaty Organisation (NATO) during the firing data calculation – METCM meteorological-computer message and the METBK meteorological-ballistic message [1, 2]. The METCM is used in automated artillery fire control systems and the METB3 during spare (manual) methods of firing data calculation.

Artilleries of NATO armies have to be able to provide meteorological messages to each other. The compatibility in using of the same meteorological messages is currently achieved only in the automated mode – in using of the METCM. Some artillery of NATO armies still use the non-standardized format of the METEO-11 meteorological message in case of the classic (spare, manual) mode is used. The transition to the exclusive use of standard meteorological messages is not often possible (because of implemented weapon systems and their firing tables, due to the implemented firing data calculation methods, for economic reasons, etc.) [3 - 5].

If the artillery, uses the METEO-11, could not realize own comprehensive meteorological sounding of atmosphere for

various reasons, some other artillery can provide the METCM for this artillery. If this artillery cannot carry out the firing data calculation with using of automated artillery fire control system, it has to be capable to transpose (convert) the METCM into the METEO-11 format. However, the algorithm of this conversion has not been defined yet [6 - 9].

The proposed method of conversion of the METCM into the METEO-11 format can be divided into three consecutive phases:

- 1.) header (baseline data) of the meteorological message recalculation;
- 2.) ground meteorological data conversion;
- 3.) meteorological data average values in the individual layers conversion.

II. HEADER OF THE METEOROLOGICAL MESSAGE RECALCULATION

The header of the METCM consists of the following symbols:

METCMQ L_AL_AL_AL₀L₀L₀YYG₀G₀G₀hhhP_dP_dP_d,

where: METCM is signification (type) for the meteorological message;

Q is the designation of the earth octant;
L_AL_AL_A is the latitude of centre of the valid area in tens, unit and tenths of degree;

L₀L₀L₀ is the longitude of centre of the valid area in tens, units and tenths of degree. The hundreds digits are leaving out for longitude 100-180° including.

YY is the day of that month in which the time validity starts beginning;

G₀G₀G₀ is the world time GMT of the time validity beginning in tens, units and tenths of hours. It is used the 24hours interval from 000 to 239;

G is the time of meteorological message validity in hours. The time validity is determining in the interval from 1 to 8 hours. The number 9 designates the time validity of 12 hours;

hhh is the altitude of the artillery meteorological station (AMS) in tens of meters;

P_dP_dP_d is the air pressure at the level of the AMS in

units of millibars. If the air pressure is more than 1000 millibars, thousands digits are leaving out [9].

The header of the METEO-11 consists of the following symbols (different countries can use different letters):

METEO-11CC-DDHHM-VVVV,

where: METEO-11 is signification (type) for the meteorological message;
 CC is meteorological unit number which compiled the meteorological message;
 DD is the day of the end of meteorological sounding;
 HH is the hour of the end of meteorological sounding;
 M are tens of time minutes of the end of meteorological sounding;
 VVVV is the altitude of the AMS in meters[9].

The recalculation of METCM header into the METEO-11 format will be carried out according to the following rules:

- a) the label of the METEO-11 is always the same – „METEO-11“;
- b) CC – this information is not possible to get from the METCM, as a result it must always be fill in manually;
- c) DD – it corresponds to the YY data in the METCM;
- d) HH – it corresponds to the first two symbols $G_0G_0G_0$ in the METCM;
- e) M – it corresponds to the third symbol $G_0G_0G_0$ in the METCM. Tenths of an hour will be converted to the tens of minutes as follow:

$$M = G_0 \cdot \frac{6}{10}, \quad (1)$$

- f) VVVV – it corresponds to the hhh in the METCM. The altitude of AMS (hhh) will be multiplied by 10 for getting the altitude in meters:

$$VVVV = hhh \cdot 10 \quad (2)$$

III. GROUND METEOROLOGICAL DATA CONVERSION

The ground meteorological data are listed in the METCM in the line (zone) 00, which consists of the following symbols:

00dddFFFTTTTPPPP,

where: 00 shows the line in the meteorological message (zone code 00);
 ddd is the wind direction – from which the wind vector is coming (from where the wind is blowing) – in tens of mils (in the METCM is usually used the division of the circle into the 6400 mils);
 FFF is the wind speed in units of knots;
 TTTT is the virtual air temperature in tenths of Kelvin degrees;

PPPP is the air pressure in units of millibars[9].

The ground meteorological data are shown in the METEO-11 by following symbols:

$B_0B_0B_0T_0T_0$,

where: $B_0B_0B_0$ is the change of the ground air pressure due to the tabular value in the altitude of AMS;
 T_0T_0 is the change of the virtual ground air temperature due to the tabular value in units of Celsius degrees[9].

The conversion of METCM ground meteorological data into the METEO-11 format will be carried out according to the following rules:

- a) $B_0B_0B_0$ will be converted from PPPP indication of the zone 00 at first by determining the value of auxiliary change of the ground air pressure due to tabular value ($B_0B_0B_0'$) as follows:

$$B_0B_0B_0' = 0,750064 \cdot PPPP_{00} - 750, \quad (3)$$

where: $PPPP_{00}$ is the air pressure in the 00 zone (in the AMS altitude).

Then the $B_0B_0B_0$ value will be determined by the follow relation:

$$B_0B_0B_0 = \begin{cases} (-1) \cdot B_0B_0B_0' + 500, & \text{pro } B_0B_0B_0' < -0,5 \\ B_0B_0B_0', & \text{pro } B_0B_0B_0' \geq -0,5 \end{cases} \quad (4)$$

- b) T_0T_0 will be converted from TTTT of zone 00 at first by determining the value of auxiliary change of the virtual ground air temperature due to tabular value (T_0T_0') as follows:

$$T_0T_0' = \left(\frac{TTTT_{00}}{10} - 273,15 \right) - 15,9, \quad (5)$$

where: $TTTT_{00}$ is the virtual air temperature in the 00 zone (in the AMS altitude).

Then the T_0T_0 value will be determined by the follow relation:

$$T_0T_0 = \begin{cases} (-1) \cdot T_0T_0' + 50, & \text{pro } T_0T_0' < -0,5 \\ T_0T_0', & \text{pro } T_0T_0' \geq -0,5 \end{cases} \quad (6)$$

IV. METEOROLOGICAL DATA AVERAGE VALUES IN THE INDIVIDUAL LAYERS CONVERSION

Meteorological data in the individual zones of the METCM are listed in the relevant lines of the meteorological message and they are expressed by the following symbols:

ZZdddFFFTTTTPPPP,

where: ZZ is the line number indicating the zone code (table I);
 ddd is the wind direction;
 FFF is the wind speed in units of knots;
 TTTT is the virtual air temperature in tenths of Kelvin degrees;
 PPPP is the air pressure in units of millibars[9].

Virtual air temperature, wind direction and wind speed are expressed as average values of the appropriate zone in the

METCM. Therefore it was established an assumption – these meteorological data average values correspond to the meteorological data in the medium height of particular zones (table I). Hence the courses of the virtual air temperature, wind direction and wind speed are linear in the interval from the bottom to the upper boundary of the appropriate zone.

The air pressure in the individual heights above AMS is not consider during the firing data calculation (its effect is included in the virtual air temperature)[10]. Therefore the air pressure in the individual heights above AMS is not converted.

TABLE I. HEIGHTS INTERVALS OF INDIVIDUAL METCM ZONES

Zone code	Zone height above AMS [m]	Medium height of zone [m]	Zone code	Zone height above AMS [m]	Medium height of zone [m]
01	0 - 200	100	14	14 000 - 16 000	15 000
02	200 - 500	350	15	16 000 - 18 000	17 000
03	500 - 1 000	750	16	18 000 - 20 000	19 000
04	1 000 - 1 500	1 250	17	20 000 - 22 000	21 000
05	1 500 - 2 000	1 750	18	22 000 - 24 000	23 000
06	2 000 - 3 000	2 500	19	24 000 - 26 000	25 000
07	3 000 - 4 000	3 500	20	26 000 - 28 000	27 000
08	4 000 - 5 000	4 500	21	28 000 - 30 000	29 000
09	5 000 - 6 000	5 500	22	30 000 - 32 000	31 000
10	6 000 - 8 000	7 000	23	32 000 - 34 000	33 000
11	8 000 - 10 000	9 000	24	34 000 - 36 000	35 000
12	10 000 - 12 000	11 000	25	36 000 - 38 000	37 000
13	12 000 - 14 000	13 000	26	38 000 - 40 000	39 000

Meteorological data in the individual layers of the METEO-11 are expressed by the following symbols:

hhTTSSRR,

where: hh is the layer code;
 TT is the average change of virtual air temperature due to tabular value;
 SS is the average wind direction in hundreds of mils (in the METEO-11 is usually used the division of the circle into the 6000 mils);

RR is the average wind speed in meters persecond[9].

The average change of virtual air temperature due to tabular value corresponds to the entire high interval from the AMS altitude up to the medium height of appropriate layer above AMS (table II).

The average wind direction and the average wind speed correspond to the entire high interval from the AMS altitude up to the upper boundary of appropriate layer above AMS (table II).

TABLE II. HEIGHTS INTERVALS OF INDIVIDUAL METEO-11 LAYERS

Zone code	Zone height above AMS [m]	Medium height of zone [m]	Zone code	Zone height above AMS [m]	Medium height of zone [m]
02	0 - 200	100	40	3 000 - 4 000	3 500
04	200 - 400	300	50	4 000 - 5 000	4 500
08	400 - 800	600	60	5 000 - 6 000	5 500
12	800 - 1 200	1 000	80	6 000 - 8 000	7 000
16	1 200 - 1 600	1 400	10	8 000 - 10 000	9 000
20	1 600 - 2 000	1 800	12	10 000 - 12 000	11 000
24	2 000 - 2 400	2 200	14	12 000 - 14 000	13 000
30	2 400 - 3 000	2 700	18	14 000 - 18 000	16 000

For each METEO-11 layer is need to calculate:

- a) the average change of virtual air temperature due to tabular value in Celsius degrees (TT);
- b) the average wind direction in hundreds of mils (SS);
- c) the wind speed in meters per second (RR).

and then it can be calculated the change of virtual air temperature in the height of 50 m above AMS due to tabular value in Celsius degree (ΔT_{50}):

$$\Delta T_{50} = T_{50} - (15,9 - 0,006328 \cdot v), \quad (9)$$

- for $v=100$ m:

$$T_{100} = T_{(^{\circ}C)_{01}}, \quad (10)$$

$$\Delta T_{100} = T_{100} - (15,9 - 0,006328 \cdot v), \quad (11)$$

- for $v=150$ m:

$$T_{150} = \left[T_{(^{\circ}C)_{02}} - T_{100} \right] \cdot \frac{50}{v_{02} - (v - 50)} + T_{100}, \quad (12)$$

where v_{02} is the medium height of the METCM 02 zone ($v_{02} = 350$ m) – table I, (7)

$$\Delta T_{150} = T_{150} - (15,9 - 0,006328 \cdot v), \quad (13)$$

Analogously it is needed to carry out the calculation of all changes of virtual air temperature in the heights after 50 m above AMS due to tabular value in Celsius degree – up to required height above AMS.

Then it will be calculated auxiliary average changes of virtual air temperature due to tabular value in the particular METEO-11 layers (TT'_{hh}) according to (14) to (16):

$$TT'_{02} = \frac{\sum_{n=1}^2 \Delta T_{50 \cdot n}}{2}, \quad (14)$$

where $50 \cdot n$ is the height (v) above AMS in meters,

$$TT'_{04} = \frac{\sum_{n=1}^6 \Delta T_{50 \cdot n}}{6}, \quad (15)$$

$$TT'_{08} = \frac{\sum_{n=1}^{12} \Delta T_{50 \cdot n}}{12}, \quad (16)$$

etc.

The average changes of virtual air temperature due to tabular value in the particular METEO-11 layers (TT_{hh}) will be determined according to the follow relation:

$$TT_{hh} = \begin{cases} (-1) \cdot TT'_{hh} + 50, & \text{pro } TT'_{hh} < -0,5 \\ TT'_{hh}, & \text{pro } TT'_{hh} \geq -0,5 \end{cases}, \quad (17)$$

where hh is the code of the METEO-11 layer.

B. The Everage Wind Direction (SS) Calculation

The average wind directions in the individual METCM zones (ddd_{ZZ}) correspond to the wind directions in the medium heights of appropriate zones. The average wind directions in the medium heights of appropriate zones (ddd_{ZZ}) is needed to convert to mil (usually used in the METEO-11 – 6000 mils for one circle) as follow:

$$\alpha'_{w(dc)_{ZZ}} = ddd_{ZZ} \cdot 10 \cdot \frac{15}{16}, \quad (18)$$

where $\alpha'_{w(dc)_{ZZ}}$ is the wind direction in the medium height of appropriate zone (ZZ) in mils;

ddd_{ZZ} is the average wind direction in the appropriate zone (ZZ) in tens of mils.

A. The Average Changes of Virtual Air Temperature due to Tabular Value (TT) Calculation

The average virtual air temperatures in the individual METCM zones ($TTTT_{ZZ}$) correspond to the virtual air temperature values in the medium heights of appropriate zones. The average virtual air temperatures in the individual METCM zones in tenths of Kelvin degrees ($TTTT_{ZZ}$) have to be converted to Celsius degrees as follow:

$$T_{(^{\circ}C)_{ZZ}} = \frac{TTTT_{ZZ}}{10} - 273,15, \quad (7)$$

where: $T_{(^{\circ}C)_{ZZ}}$ is the virtual air temperature in the medium height of appropriate zone (ZZ) in Celsius degrees.

It is necessary to carry out a simulation (budgeting) of temperature (and also wind) sounding in the particular heights above AMS from the values established according to the (7) relation for calculation of the average changes of virtual air temperature (and also the average wind directions and the average wind speeds) in the individual METEO-11 layers – as if they were actually measured by radiosonde. The radiosonde sends the measured meteorological data at specified intervals after approximately 25-50 meters (depending on the speed of meteorological balloon ascent and on the used meteorological sets). The simulation (budgeting) of temperature and wind soundings can be carried out on the basis of linear interpolations of particular meteorological data in the appropriate heights above AMS from the meteorological data mentioned in the METCM. For these simulations it is sufficient to calculate the meteorological data at intervals of 50 m (in heights above AMS)[11 - 13].

For each height (v) above AMS (after 50 meters) it necessary to calculate the appropriate changes of virtual air temperature due to tabular value (ΔT_v) according to (8) to (13):

- for $v=50$ m:

at first it is needed to determine the virtual air temperature at the height of 50 m above AMS in Celsius degrees:

$$T_{50} = \frac{T_{(^{\circ}C)_{00}} + T_{(^{\circ}C)_{01}}}{2}, \quad (8)$$

where: $T_{(^{\circ}C)_{00}}$ is the virtual air temperature in the height of 50 m above AMS and it corresponds to $T_0 T'_0$ value,
 $T_{(^{\circ}C)_{01}}$ is the virtual air temperature in the medium height of the 01 zone (100 m) determined according to (7)

Then it will be compared the course of the wind direction. If the wind direction crosses the kilometre north direction (from left or right) the particular wind direction values must be adjusted. If the wind direction crosses the kilometre north direction from the left during a movement from one layer to the next (higher), the 60-00 value must be added to the $\alpha'_{w(dc)ZZ}$ value. If the wind direction crosses the kilometre north direction from the right during a movement from one layer to the next (higher), the $\alpha'_{w(dc)ZZ}$ value must be deduced from the 60-00 value. By this way will be got all adjusted wind direction values in the individual METCM zones $\alpha_{w(dc)ZZ}$ in units of mils. If the wind direction does not cross the kilometre north direction with increasing height above AMS, then the wind direction will be:

$$\alpha_{w(dc)ZZ} = \alpha'_{w(dc)ZZ} \cdot (19)$$

For each height (v) above AMS it is necessary to calculate the wind directions (α_v) in hundreds of mils from the $\alpha_{w(dc)ZZ}$ values according to (20) to (22):

$$\alpha_{50} = \frac{\alpha_{w(dc)00} + \alpha_{w(dc)01}}{2} \cdot 0,01, \quad (20)$$

$$\alpha_{100} = \alpha_{w(dc)01} \cdot 0,01, \quad (21)$$

$$\alpha_{150} = \left\{ \left[\alpha_{w(dc)02} - \alpha_{100} \right] \cdot \frac{50}{v_{02} - (v-50)} + \alpha_{100} \right\} \cdot 0,01, \quad (22)$$

etc.

Then auxiliary average wind directions (in hundreds of mils) in the particular METEO-11 layers (SS'_{hh}) will be calculated according to (23) to (24):

$$SS'_{02} = \frac{\sum_{n=1}^4 \alpha_{50-n}}{4}, \quad (23)$$

$$SS'_{04} = \frac{\sum_{n=1}^8 \alpha_{50-n}}{8}, \quad (24)$$

etc.

The average wind directions in the particular METEO-11 layers (SS_{hh}) will be determined according to the follow relation:

$$SS_{hh} = \begin{cases} (-1) \cdot SS'_{hh} + 50, & \text{pro } SS'_{hh} < -0,5 \\ SS'_{hh}, & \text{pro } SS'_{hh} \geq -0,5 \end{cases} \quad (25)$$

C. The Average Wind Speeds (RR) Calculation

The average wind speeds in the individual METCM zones (FFF_{ZZ}) correspond to the wind speed values in the medium heights of appropriate zones. The wind speeds in the medium heights of appropriate zones in meters per second (FFF_{ZZ}) is needed to convert to meters per second as follow:

$$w_{(m \cdot s^{-1})_{ZZ}} = 0,51 \cdot FFF_{ZZ}, \quad (26)$$

where $w_{(m \cdot s^{-1})_{ZZ}}$ is the wind speed in the medium height of appropriate zone (ZZ) in meters per second.

For each height (v) above AMS it is necessary to calculate the wind speeds (w_v) in meters per second from the $w_{(m \cdot s^{-1})_{ZZ}}$ values according to (27) to (29):

$$w_{50} = \frac{w_{(m \cdot s^{-1})_{00}} + w_{(m \cdot s^{-1})_{01}}}{2}, \quad (27)$$

$$w_{100} = w_{(m \cdot s^{-1})_{01}}, \quad (28)$$

$$w_{150} = \left[w_{(m \cdot s^{-1})_{02}} - w_{100} \right] \cdot \frac{50}{v_{02} - (v-50)} + w_{100}, \quad (29)$$

etc.

Then the average wind speeds in the particular METEO-11 layers (RR_{hh}) (in meters per second) will be calculated according to (30) to (31):

$$RR_{02} = \frac{\sum_{n=1}^4 w_{50-n}}{4}, \quad (30)$$

$$RR_{04} = \frac{\sum_{n=1}^8 w_{50-n}}{8}, \quad (31)$$

etc.

V. CONCLUSION

The conversion of the METCM into the METEO-11 format is needed to be carried out by using the computer because the manual conversion is time-consuming and can leads to errors. It is advantageous to use the defined mathematical apparatus for the conversion in the own software application or to use it in some program – for example in the MS Excel.

Philosophy of the conversion of the METCM into the METEO-11 format can be also used to develop mathematical apparatuses for other conversions of meteorological messages (as METB3 into METEO-11 format or METCM into METB3 format) in the future.

REFERENCES

- [1] NATO Standardization Agency. AArtyP-1 (A) – Artillery Procedures. Brussels, Belgium, 2004. 102 p.
- [2] NATO Standardization Agency. AArtyP-5 (A) – NATO Indirect Fire Systems Tactical Doctrine. Brussels, Belgium, 2013. 121 p.
- [3] Mukhedkar, R. J. & Naik, S. D. Effects of different meteorological standards on projectile path. *Def. Sci. J.* 2013, **63** (1), 101-107.
- [4] Chusilp, P.; Charubhun, W. & Ridluan, A. Developing firing table software for artillery projectile using iterative search and 6-DOF trajectory model. *In the Second TSME International Conference on Mechanical Engineering*, Krabi, 19-21 October 2011.
- [5] Chusilp, P.; Charubhun, W. & Nuktumhang, N. Investigating and iterative method to compute firing angles for artillery projectiles. *In the 2012 IEEE/ASME International Conference on Advanced Intelligent Mechatronics*, Kaohsiung, Taiwan, 11-14, July 2012, pp 940-945.
- [6] Vondrák, J. A Complex utilization of artillery reconnaissance assets in a reconnaissance data acquisition for artillery requirements. University of Defence, Brno, Czech Republic, 2008. PhD Thesis.
- [7] Blaha, M. A complex utilization of artillery reconnaissance assets in a reconnaissance data acquisition for artillery requirements. University of Defence, Brno, Czech Republic, 2012. PhD Thesis.

- [8] 8. Blaha, M. & Sobarňa, M. Some Develop aspects of perspective fire support control system. In The 6th WSEAS International Conference on DYNAMICAL SYSTEMS & CONTROL (CONTROL '10): WSEAS Press, Tunisia, 2010. pp 179-183.
- [9] Preparation Department of ACR. Meteorological preparation of the Czech Artillery. ACR, Prague, Czech Republic, 1998. 112 p.
- [10] Jirsák, Č. & Kodym, P. External ballistics and theory of artillery fire. Prague, Czech Republic, 1984. 399 p.
- [11] Bartolucci, L.; Chang, M.; Anuta, P. & Graves, M. Atmospheric effects on Landsat TM thermal IR data. IEEE Trans. Geosci. Remote Sensing, 1988, **26** (2), 171-176.
- [12] Taeho, L.; Sangjin, L.; Seogbong, K. & Jongmoon, B. A distributed parallel simulation environment for interoperability and reusability of models in military applications. *Def. Sci. J.* 2012, **62** (6), 412-419.
- [13] Jameson, T. Computer met message accuracy studies relating to the met measuring set – profiler; ARL-Project report; U.S. Army Research Laboratory: White Sands Missile Range, NM, 2003.

Criteria for Efficiency Determination of Inspection Maintenance Programs

Gabriel M. Branco, Fábio C. Branco, Marcelo C. Branco, Eduardo M. Dias, José M. Napoleone, Alfred Szwarc

Abstract—This study estimates the emission reductions brought by the Vehicle Inspection and Maintenance Program in São Paulo City, and quantifies its benefits. The reference data for the present analysis were the results of the measurements carried out by CONTROLAR in 2011 to measure free acceleration exhaust gas opacity of Diesel vehicles and exhaust emission of carbon monoxide and hydrocarbons at idle from vehicles equipped with Otto cycle engines. These measurements are part of the inspection procedures conducted routinely to assess the state of vehicle maintenance. The calculation of emission reduction was done with the aid of a methodology that correlates the emission levels of type approval certification with the statistics relating to concentrations of pollutants, engine size, maximum RPM of the engine and the annual average mileage. Such correlations allow assessing the relative reduction of the inspected fleet annual emissions and are expressed as equivalent percentages of the fleet that would be withdrawn from circulation to produce the same effect. The purpose of this methodology is to translate the achieved benefits to a language easily understood by the general population.

Keywords—air pollution, emissions, environmental impact, vehicle inspection.

1. INTRODUCTION

One of the biggest air pollution sources in metropolitan areas is the vehicle fleet. Technology improvements are highly necessary to control this problem, but vehicle owners are also key for successful emission reduction. Therefore, annual In-Use Vehicle Inspection and Maintenance Programs - I&M are necessary to increase the effectiveness of emission control measures.

While type approval emission control certification requires sophisticated laboratories and complex tests procedures I&M tests must be simple, expedite and low cost. Therefore,

Gabriel M. Branco is Associate and Director of EnvironMentality – Tecnologia com Conceitos Ambientais Ltda – Rua Michigan 177, CEP 04566_000 -São Paulo/SP, Brasil (gabriel.tcl@uol.com.br)

Fábio C. Branco is Associate and Project Manager of EnvironMentality – Tecnologia com Conceitos Ambientais Ltda – Rua Michigan 177, CEP 04566-000 -São Paulo/SP, Brasil(fabio.tcl@uol.com.br)

Marcelo C. Branco is a PhD student at Escola Politécnica of the Universidade de São Paulo (Polytechnic School of the University of São Paulo) (marcelobranco@uol.com.br)

Eduardo M. Dias is full professor of the Escola Politécnica of the Universidade de São Paulo and coordinator of GAESI - Grupo de Automação Elétrica em Sistemas Industriais, a reseach group of the Electrical Energy and Automation Department, Escola Politécnica, Universidade de São Paulo, Av. Prof. Luciano Gualberto, trav. 3, n. 158, São Paulo/SP, Brazil, CEP 05508-970 (emdias@pea.usp.br)

José M. Napoleone is a technical consultant of CONTROLAR (I&M operator) (napoleone@terra.com.br)

Alfred Szwarc is Director of ADS – Tecnologia e Desenvolvimento Sustentável – Rua Albuquerque Lins, 848 / 11 CEP 01230-000 São Paulo/SP, Brasil (alfred.ads@terra.com.br)

emission measurement of pollutants in some key engine operating conditions must be sufficient to evaluate vital maintenance failures, mistuning and illegal modifications that result in emission degradation. This can be accomplished with the free acceleration smoke opacity measurement of Diesel vehicles and the carbon monoxide – CO and hydrocarbon – HC emission measurement at idle, in vehicles with Otto cycle engines. In order to have a meaningful inspection, vehicles are also submitted to a visual evaluation to check abnormal engine and muffler noise, water, fuel and oil leaks, and integrity of engine and emission control systems.

These tests should be regarded as indicative, since the test vehicles are under only one engine condition instead of following a full driving cycle, with forces and speeds representative of normal driving. However, although simple, these test procedures submit engines and emission control systems to operating conditions that are able to expose problems. To do so they have to be associated to representative emission inspection limits. The so-called “emission inspection limits” are, in fact, only reference parameters for relative comparisons between similar vehicles having new vehicles as the benchmark.

Despite not directly comparable to driving cycle results, the relative differences and variations showed by these measurements present very good statistical correlation of the fleet averages to the emissions determined in mass per kilometer for each model year. Therefore it can be said that they allow accurate determination of emission deterioration factors and annual emissions inventories calculations to quantify the overall benefits of the I&M program.

Therefore, based on the extensive data obtained during the period of 2008-2013 from the São Paulo I&M program (I/M-SP) it is safe to say that simple test procedures as those mentioned before provide valuable knowledge to control the emission of in-use vehicles.

2. FUNDAMENTALS OF VEHICLE EMISSION DETERMINATIONS

The emission certification of new vehicles (type approval) requires representative vehicles to run tests simulating “real world” driving conditions. Light duty vehicles are tested in chassis dynamometers following a speed time cycle, under inertia and friction forces determined on the road. Emission results are integrated and expressed as grams/km of the regulated pollutant of interest. The exhaust CO and HC concentrations are measured at idle, since this condition is the most susceptible to ignition failures and catalytic converter malfunction due to engine mistuning, and is a robust indicator of common emission problems.

Heavy duty vehicles have their engines tested in a dynamometer test bench in a sequence designed to cover the entire engine map of torque and angular speed. This is a standard representation of all possible combinations of both parameters in a given engine, as follows:

RPM is represented within zero (idle) and 100% (maximum allowed);

Torque is plotted within -5% (engine friction) and 100% (maximum possible in each RPM)

Fig. 1 presents the European Transient Driving Cycle – ETC plotted in the engine map of a typical truck. The triangles relate to a statistical distribution of city driving, the round dots are representative of rural road driving and crosses are correspond to highways. This test protocol is used to certify the engine’s technological ability to comply to emission limits, given in grams/kWh. These results may also be converted into grams/km using the specific fuel consumption averaged in the emission test and the fuel consumption measured in the vehicle in km/liter. This indirect parameter is the key to estimate the annual emissions in the inventory calculations [1].

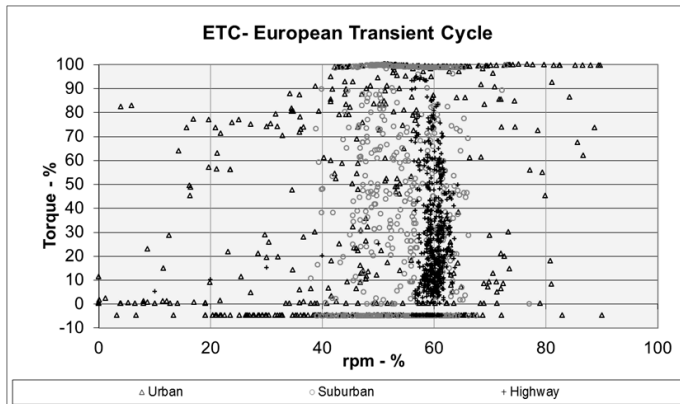


Fig. 1 – The ETC test cycle in a Diesel engine map

The emissions are measured in each point and weighted through the entire test, in grams/kWh. In this test, the upper points have the highest influence on the particulates emission. On the other hand, the free acceleration test uses the rotating parts inertia to produce torque under acceleration and identify the smoke opacity near these points. Therefore, these results are a good parameter to indicate particles emission - PM. Other protocols are possible and used in some countries, but the simple free acceleration test is adequate to characterize the most common engine maintenance failures.

2.1 Smoke and PM correlations

The highest mass constituent of Diesel smoke particles is unburned black carbon. Sulfates, hydrocarbons, metals and ashes are also contained in the particle mass. Smoke is the main target of Diesel vehicle inspection, because it greatly depends on engine tuning, fuel injection system and nozzles wear and air filters blockage.

Smoke opacity, measured in m-1, also correlates to Filter Smoke Number – FSN (Bacharach or Bosch gray scales to be used in a filtered sample of exhaust gases) [2] and may be

converted to mass concentration in the exhaust according to several studies, as illustrated in Fig. 2.

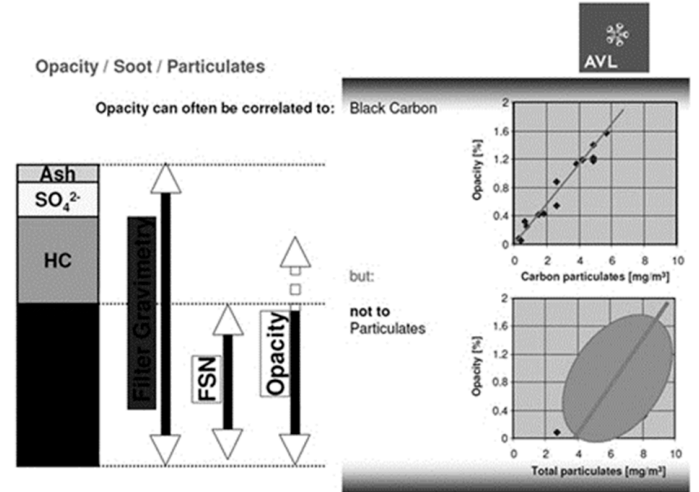


Fig. 2 – Interrelations of opacity, smoke and particulates mass (source AVL)

The numerical correlation of smoke opacity and FSN was observed experimentally by AVL in distinct Diesel technologies and engine sizes and presented in Fig. 3, showing very good repetitiveness. In general, opacity is the preferred protocol because it is easy and rapid to measure. Moreover, it is also valid for transient measurements 1.

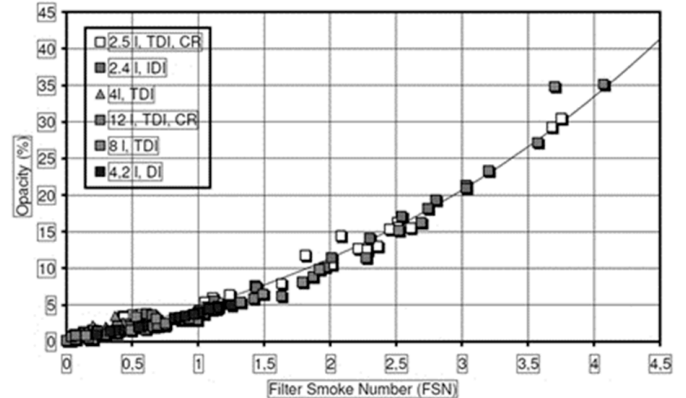


Fig. 3 – Smoke measurement FSN and opacity correlation (source AVL)

The equivalence of opacity and smoke was firstly established by The Motor Industry Research Association - MIRA and was adopted internationally [3]. The equivalence factors were transformed into a linear regression equation, valid for opacimeters with optical length of 43 cm, operating under 75°C, as established by the following equation:

$$\text{Concentration (mg/Nm}^3\text{)} = 147,509 * \text{opacity (m}^{-1}\text{)} \quad (\text{Eq.1})$$

Considering the ETC driving cycle, smoke opacity varies a lot, as showed in Fig. 4 for the same test in two time scales.

¹ The FSN measurement requires 30 seconds sampling, while opacimeters have 0,1 second to 90% total signal variation.

But when ordering all points from zero to maximum and integrating the smoke mass conversion it is possible to see that total particle mass is proportional to maximum allowed peak value. In other words, the maximum peak is a representative parameter of the particle emission of a given engine.

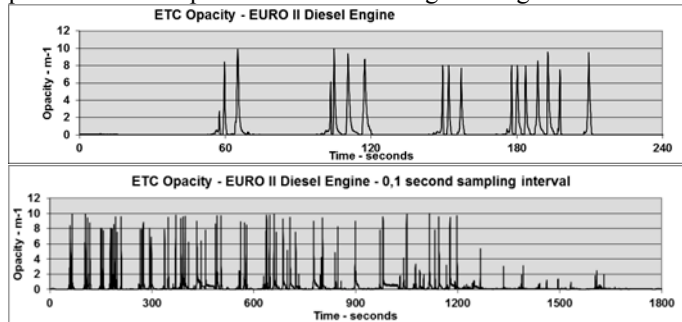


Fig. 4 – Diesel exhaust opacity curve during an ETC test

In this case, of an EURO II Diesel engine, the allowed limit is $2,0 \text{ m}^{-1}$ and was exceeded in 4,5% of test time, but these exceedances correspond to 53% of total emitted particle mass during the driving cycle. Therefore, reducing smoke peaks to the allowed limit, decreases its emission in the same order of magnitude in 95,5% of the running conditions.

Considering the linear correlations between smoke and particle emission, the average variation of smoke prompted by proper maintenance may also estimate its particle mass emission reduction for the same vehicle.

Comparing the particle mass emission according to the Brazilian emission certification procedure and its corresponding free acceleration tests, it is also possible to establish linear correlations between them for each technology level, as shown in Fig. 5.

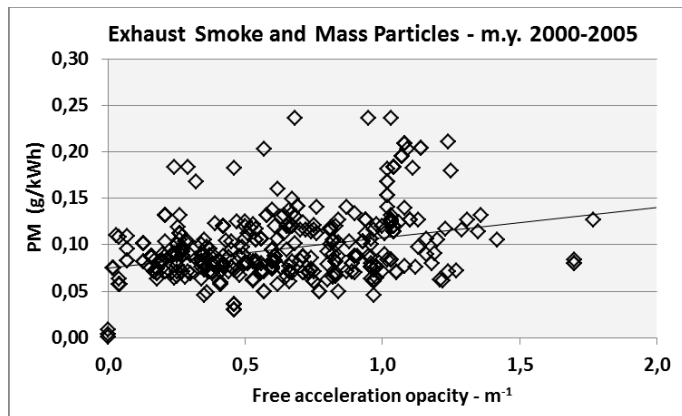


Fig. 5 – Observed correlations in certification tests in Brazil

In the I/M-SP, the opacity is averaged for each category (vehicle size) and model year (technology level 2) to characterize the proportional parameter of each one in the

² The Brazilian Vehicle Emission Control Program has established several technology stages in a long term chronogram. For heavy duty vehicles, these levels are identified as P1 to P7; for light duty vehicles L1 to L6; and for motorcycles M1 to M4, being the last ones in each group representative of current vehicles.

annual emission inventory. The smoke averages of approved vehicles are several times lower when compared to the averages of the vehicles failed in the same category. However, when properly maintained and reinspected, this average is reduced to near the same level of the approved ones, as shown in Fig. 6.

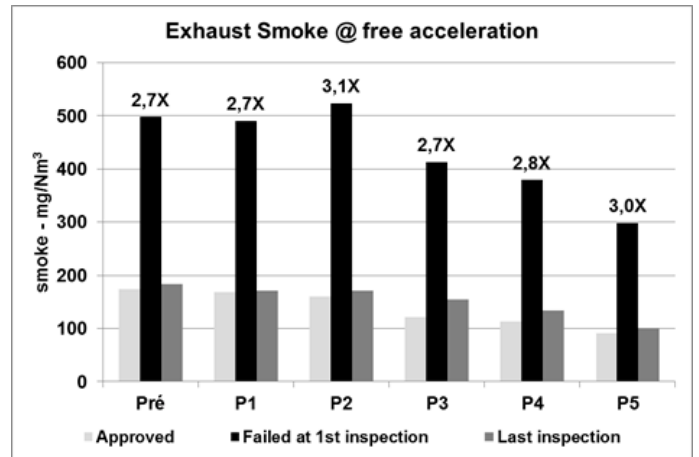


Fig. 6 – Smoke opacity levels compared for each technology level

Therefore, in an I&M Program, the average reduction of smoke opacity, converted to mass concentration in mg/m^3 for each vehicle category and technology can be calculated for two cases:

- “initial” status of the fleet, estimated by the first inspections of all vehicles (approved + failed), properly weighted according to the failure rate;
- “final” status” of the fleet, estimated by the initially approved and the last reinspection of the failed vehicles;

The emission reduction rate is calculated by the ratio of both final and initial status averages for each vehicle category and model year, and therefore can be used as tons per year in an annual emission inventory.

2.2 Correlations for carbon monoxide and hydrocarbons

The emission measurement of CO and HC in the Otto cycle is done at idle, which is an engine operating regime especially sensitive to engine failures.

Theoretically, the results at idle are not convertible into the emission measured in a driving cycle, since it is possible to tamper the idle tuning without changing the engine behavior under load. However, the comparison of thousands or millions of measurements in an I&M inspection shows a clear evidence of a statistical correlation between the concentrations of CO and HC idle and their respective emissions measured in the driving cycle, in g/km^3 , as shown in Fig. 7 for carbon monoxide measured in gasoline vehicles, in the 2012 calendar year. Similar curves were obtained for hydrocarbons, both for all vehicle categories, which are also used to determine the statistical trends of the emission deterioration factors in the “real word”. Usually I&M statistics identify two distinct

³ In Brazil, the adopted driving cycle for light duty vehicles is the US FTP-75

groups of vehicles: “normal maintenance”, defined by the average of the best 90% of the fleet; and “tampered” vehicles, defined by the average of the worst 10% of the fleet.

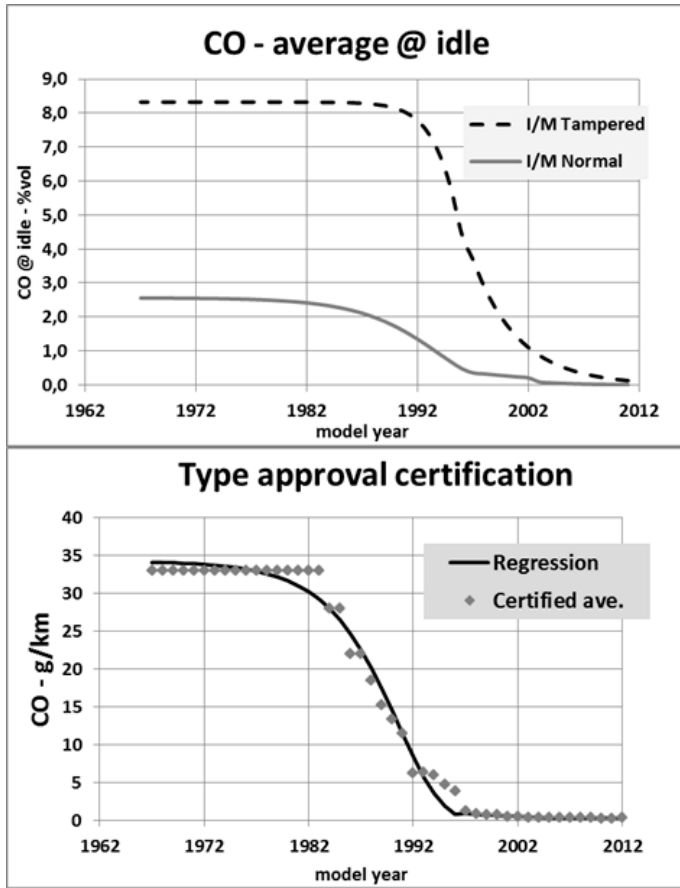


Fig.7 – Carbon monoxide levels for gasoline vehicles

Similarly to the smoke case, the averages of CO and HC also show a significant difference between the approved/reinspected and failed vehicles. Therefore, the emission reductions may be estimated through the same calculation concepts, based on the “initial” and “final” statuses of the fleet, outlined in 2.1.

3. FINAL CALCULATION TO ESTIMATE THE ENVIRONMENTAL BENEFITS OF AN I&M PROGRAM

Based on the “final and initial” pollutant concentration averages, the environmental benefits are given by ratios between them, multiplied to the correspondent annual emissions calculated in the official inventory for each vehicle category. The relative reduction of annual emissions are calculated based on the current (initial) emission basis, as follows:

$$R_{PM} (\%) = (PM_{initial} - PM_{final}) / PM_{initial} \quad (Eq.2)$$

$$R_{CO} (\%) = (CO_{initial} - CO_{final}) / CO_{initial} \quad (Eq.3)$$

$$R_{HC} (\%) = (HC_{initial} - HC_{final}) / HC_{initial} \quad (Eq.4)$$

where:

R = reduction of annual emission from the considered fleet;

$PM_{initial}$, $CO_{initial}$ and $HC_{initial}$ = PM, CO and HC average concentrations calculated for the initial inspection, for each vehicle category and model year

PM_{final} , CO_{final} e HC_{final} = PM, CO and HC average concentrations calculated for the final inspection, for each vehicle category and model year

The emission benefits are then determined in tons/year multiplying the inventory annual emissions by the relative reductions calculated above, and may be applied to estimate the relative decrease in atmospheric concentrations, as a comparative parameter.

$$ER_{annual,i} = \sum Ri(\%)*N * EF_{cert,i} * DF_{normal,i} * km_{annual} * 10^{-6} \quad (Eq.5)$$

where:

$ER_{annual,i}$ = reference average reduction annual emission of pollutant “i”, in ton/year;

N = number of considered vehicles in each category and model year

$EF_{cert,i}$ = average of certified emission factors of pollutant “i”, in g/km

$DF_{normal,i}$ = “normal” deterioration factors of pollutant “i” emission, $\geq 1,00$ (vehicles in good maintenance conditions)

km_{annual} = annual average mileage for each vehicle category and age, in km/yr

Once calculated according to the above criteria, the emission reduction of each part of the fleet may be added and compared under the same basis and independently of being different vehicles categories and technologies, i.e. proportionally to their final effect on the environment.

4. FINAL REMARKS

In order to achieve the adequate parameters for the environmental benefits estimate, some approaches might be assumed, if there are shortages in some inspections, as the absence of emission measurements in rejected vehicles earlier during visual inspection. Therefore, the estimation might consider:

- a) the “INITIAL” emission concentration averages calculations for each category and model year is based on all vehicles at the first inspection, no matter if they are approved, failed in the test or rejected in the visual inspection;
- b) in the rejection cases, when the appointed failure is related to emission increase, as loosen hoses, broken canister etc., it is assumed the emission is as high as the failed vehicles average. Other items that are not necessarily linked to exhaust emission increase, as lubricant leaks for example, it is assumed that this vehicle may be represented by the overall average taken from the first inspection of measured vehicles;
- c) the “FINAL” emission concentration averages calculations is based on the last inspection of all vehicles failed and the ones approved at the first inspection;

- d) The “normal” fleet annual emission shall be calculated for the certified emission factors (EF) and deterioration factors (DF) for each category and model year and summed up to estimate the total inventory benefit;
- e) The “final” fleet annual emission may consider the residual percentage of failed vehicles, per category and model year, or assumed as the normal fleet annual emission if this residue is negligible;
- f) The “initial” annual emission shall be calculated by multiplying the “final” fleet emission by the correspondent “% reduction” rate” calculated from equations 2 to 4, above, for each category and model year and summed up to estimate the total inventory benefit.

All these results can be grouped by technology level, or vehicle category, or the whole fleet, according to the purpose of the study and environmental control strategy.

Fig. 8 presents the particles control benefits from the diesel fleet in 2012, as an example, segregated by technology level according to the Brazilian Vehicle Emission Program to Control Air Pollution – PROCONVE, where the blanks represent the total reduction per group and the colored bars represent each vehicle category in the tech group.

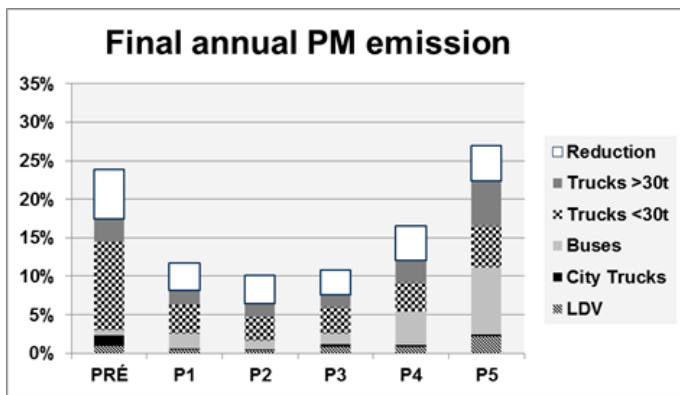


Fig. 8 – Particles reduction in diesel fleet in São Paulo - 2012

Considering each homogeneous group separately, it is also interesting to calculate the “number of equivalent vehicles”, which is the number of vehicles that would produce equivalent environmental effect if removed from the fleet. This is another parameter that may be useful to translate these abstract calculations into a more understandable Fig. to the general population, as shown in Fig. 9.

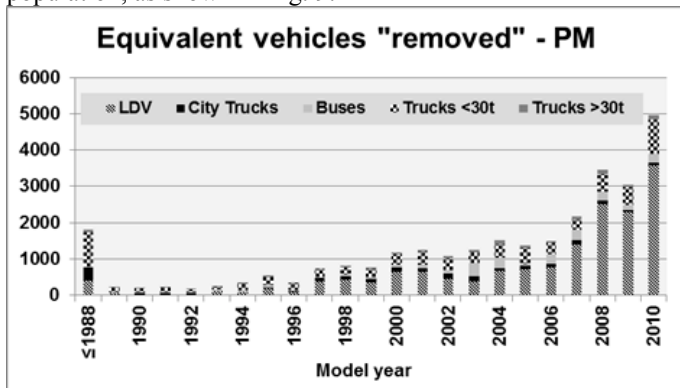


Fig. 9 – Particles reduction in diesel fleet in São Paulo expressed in “equivalent vehicles” - 2012

Integrating all different vehicle classes and ages, the above calculations result in two weighted estimates of the fleet *initial* and *final* annual emissions. Differences between them provide the annual “net” benefit and their series shows the evolution in subsequent years, the remanent benefit from the previous year to the next and the influence of other associated environmental strategies. Fig. 10 shows the diesel PM emission as an example. The reduced gain from one year to the other indicates an evolution of the I/M-SP program and this effect can be associated to the improvement of maintenance services being other factors equal.

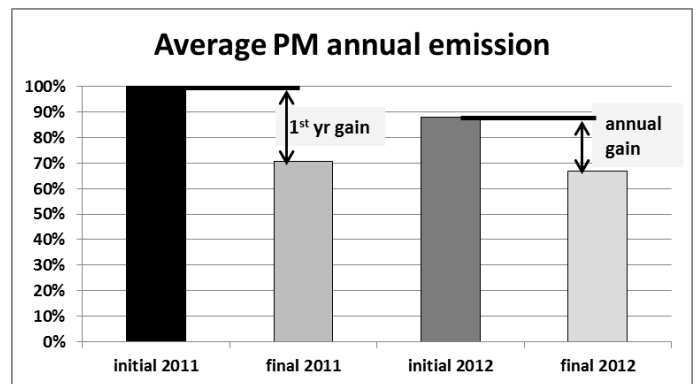


Fig. 10 – Diesel particles environmental benefits compared annually

The annual balance of I/M-SP environmental benefits is shown on table 1. Based on the particles (particulate matter – PM) emission reduction, it was estimated the annual PM reduction in the inventory and this indicated 10,5% reduction in PM atmospheric concentration. The Experimental Air Pollution Laboratory of the Medical School of the University of São Paulo (LPAE/FMUSP), used these results to estimate the public health benefits, and concluded that I/M-SP has potentially avoided 580 premature death per year [4]. Their study demonstrated that the costs of inspections distributed by the number of saved lives by the I/M-SP Program resulted extremely low when compared to other public health programs.

Table 1 – I&M emission reductions in São Paulo

	inspected vehicles	CO	HC	PM
LDV - Otto	2.700.000	49%	39%	
Motorcycles	268.000	34%	42%	
Diesel vehicles	128.000			28%

5. CONCLUSIONS

The methodology presented in this paper was developed to evaluate the I/M-SP effectiveness, not only in terms of

operational performance, generally given by the numbers of inspections, vehicle failures and other statistics, but also through the estimation of its main objective: the environmental benefits produced by the preventative and corrective vehicle maintenance.

The statistical correlation of the measured concentrations and true emission factors in real use was found as the best parameter to evaluate the environmental benefits. Despite there is no direct conversion from pollutant concentrations at idle or under free acceleration into its mass emission determination in a dynamic driving cycle, the variations of the average concentrations measured in the fleet does correlates to the variation of the true emission in grams per kilometer, and represents a very valuable tool for fleet management and transport strategies.

Planning and proposing solutions to problems that affect large cities in the world, both in the area of urban transport, health and environment, certainly would benefit from the concepts developed in this paper, since they provide a simple way to quantify the results of an I&M program and create valuable data that could help to compare different transport strategies and also quantify the associated environmental impacts.

group of the Electrical Energy and Automation Department, Escola Politécnica, Universidade de São Paulo.

Napoleone, José Mauro - born in Agudos – SP, in 1946, graduated in mechanical engineering at the Military Engineering Institute, worked in CONTROLAR (the I&M company) since 2007 until January 2014.

Szwarc, Alfred – born in Lodz, Poland, in 1952, graduated in mechanical engineering at Taubaté Engineering School, SP, worked at the State Environmental Agency for 20 years in the development and implementation of the vehicle emission control program in Brazil, presently consultant for vehicle emission control at ADS since 1998.

REFERENCES

- [1] Branco, G.M.; Ryan, J.J.; Branco, F.C. - IMPACTO AMBIENTAL DA FROTA DIESEL ATÉ 2030 - ESTUDO DE CASO: RMSP - XIII Congresso e Exposição Internacionais de Tecnologia da Mobilidade - SAE BRASIL 2004 - 16 de novembro de 2004 – São Paulo – Brasil.
- [2] Westlund, A. - Measuring and Predicting Transient Diesel Engine Emissions – Licentiate thesis; KTH CICERO; Department of Machine Design - Royal Institute of Technology – Stockholm – 2009..
- [3] DX250 SMOKEMETER PROGRAM UK MOT 2002 - Conversion chart for k, HSU, FSN and mg/m³, extracted from MIRA Report No. 1965/10, Nuneaton Warwickshire, UK - 1965, AG Dodd and Z. Holubecki.
- [4] Saldiva, P.H.N.; André, P.A. de; Miraglia, S.G.K. - Impact of diesel vehicle inspection on health: the experience of São Paulo, Brazil - ISEE - International Society for Environmental Epidemiology - <http://www.iseepi.org/About/history.htm> - Basel 2013.

ABOUT AUTHORS

Branco, Gabriel Murgel – born in São Paulo, in 1949, graduated in Mechanical Engineering at Polytechnic School of the University of São Paulo, worked at the State Environmental Agency for 20 years in the development and implementation the vehicle emission control program in Brazil, consultant for vehicle emission control at EnvironMentality since 1996.

Branco, Fábio Cardinale – born in São Paulo, in 1969, graduated in geology at the University of São Paulo, master of science in satellite images processing, consultant of the vehicle emission strategies and I&M Program at EnvironMentality since 1996.

Branco, Marcelo Cardinale – born in São Paulo, in 1967, graduated in Administration, taking master of science degree in transportation, environment and energy conservation, Secretary of Transport in the city of São Paulo until 2012, member of the State Transportation Council 2011-13, and vice-president of ANTP – Public Transportation National Association since 2011.

Dias, Eduardo Mario – born in São Paulo, in 1951, is full professor of the Escola Politécnica of the Universidade de São Paulo and coordinator of GAESI - Grupo de Automação Elétrica em Sistemas Industriais, a research

Electronic switch for accumulator connection in a backup power source

Martin Pospisilik and Tomas Dulik

Abstract— The paper describes an approach to design and construction of a switching module for accumulator connection that is to be used within backup power sources for devices that are powered by the technology called Power over Ethernet. Electromechanical relays are replaced by MOSFET transistors, as well as power diodes, in order to minimize the power losses and to increase the reliability of the appliance. Without active cooling, the module made of SMT devices can be loaded with a current up to 6 A. The switch enables switching the power output between the AC power source and the battery. It also enables recharging of the battery, switching the power off when the battery is deeply discharged and communication with the backup source's controller. In order to test the function of the battery, the automatic switching between the power sources can be overridden. Furthermore, monitoring of several states inside the module is supported. As the authors tried to minimize the risk of accidental malfunction, the switching of the power sources is processed on a hardware level and when no signals from the controller are received, the AC power mains priority is always kept.

Keywords—Power over Ethernet, Electronic Diode, Low Power Dissipation, Power Backup.

I. INTRODUCTION

ANY electrical appliance's performance is affected by the quality of the electrical power network from which the appliance is fed. This problem is crucial in case of those appliances that are expected to operate permanently, such as network devices. According to [2] the following power supply network malfunctions occur at most:

- total power network failure (blackout),
- short undervoltage (usually without negative consequences),
- long undervoltage showing the decrease of the power supply voltage by more than 15 %,
- overvoltage,
- short voltage spikes,

This work was supported in part by the European Regional Development Fund under the project CEBIA-Tech No. CZ.1.05/2.1.00/03.0089. and by OPVK project CZ.1.07/2.3.00/30.0035.

Martin Pospisilik is with Tomas Bata University in Zlin, Faculty of Applied Informatics, Nad Stranemi 4511, 760 05 Zlin, Czech Republic. He is now at the department of Computer and Communication Systems (e-mail: pospisilik@fai.utb.cz)

Tomas Dulik is with Tomas Bata University in Zlin, Faculty of Applied Informatics, Nad Stranemi 4511, 760 05, Zlin, Czech Republic. He is now a researcher at the Department of Informatics and Artificial Intelligence (e-mail: dulik@fai.utb.cz)

- waveform distortion,
- noise,
- electromagnetic interferences.

The statistics published in [2] shows that more than 90 % of power supply network failures are the total power network failure and long undervoltage, resulting in the lack of the supplied power and malfunctions of the powered appliances. This problem has been solved by employing the UPS (Uninterruptable Power Supply source) units that are capable of delivering the power from accumulators in case the power supply network failed. The more sophisticated systems are capable of the voltage spikes and noise on the power line elimination.

On the other hand, the power supply backups for Power over Ethernet applications deliver DC supply and therefore there is no need to control and restore the shape of the AC sinusoidal waveform.

In [6] the authors introduced a functional sample of a simple battery switch. Because the needs for extended functions have arisen, the former concept was fully revised.

II. CONCEPT REVISION

The complex revision of the concept introduced in [6] was necessitated mainly due to the following requirements:

- Communication with an independent controlling unit,
- Improved power factor correction (switched mode power supply unit must be involved),
- Monitoring of the mains power delivery,
- Decrease of power dissipation,
- Independent operation in case of controlling unit failure,

Due to the above mentioned requirements, the design was divided into several sub blocks the design of which can be individually fine-tuned, including the components placement on the printed circuit board.

The block diagram of the revised electronic switch is depicted in figure 1. Except of the $230 V_{AC}$ to $24 V_{DC}$ switched mode voltage converter, all components are placed on a single printed circuit board.

For better description of the design, several standardized signals were defined as well as some of the wires were named. Some of them are connected to the interface with the controlling unit. In that case their voltages are adjusted to 3.3V TTL logic signals. Their description is provided in Table I.

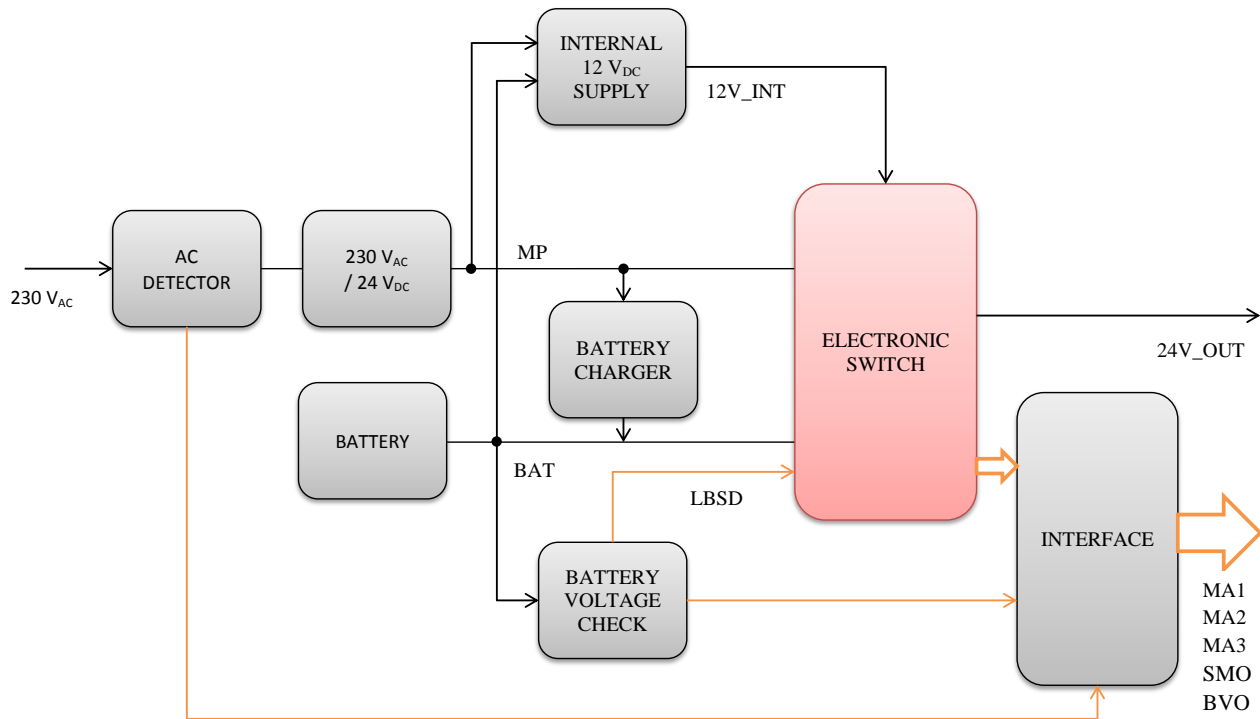


Fig.1 Electronic switch block diagram

Table I Controller interface signals

Abbreviation	Description
SMO	Switch Mains Off If a rectangular waveform with a frequency higher than 20 kHz is applied, the mains power supply is disconnected. This can be used to check the state of the battery by the controller. See text for more details.
MA1	Mains Active 1 Gives information about the presence of mains voltage. It is in HIGH state when the mains voltage is present.
MA2	Mains Active 2 Gives information about the operation of the AC/DC converter. It is in HIGH state when there is 24 V _{DC} present at the output of the converter. If MA1 = H and MA2 = L, the malfunction of the converter is indicated.
MA3	Mains Active 3 Gives feedback on SMO signal. If MA2 is in HIGH state and SMO signal is present, MA3 must be in LOW state. This indicates that although the mains supply is active, the output of the switch is fed from the battery.
BVO	Battery Voltage The voltage at this output is proportional to the voltage on the battery with a negative DC offset. The measurement range is from 21.5 V to 29 V, resulting in voltages from 0.54 to 2.8 V at this output.

The internal signals that are given names are described by Table II.

Table II Internal signals

Abbreviation	Description
V_REF	Reference voltage derived from the internal power supply, approximately 5 V.
12V_INT	Internal power supply stabilized to 12 V.
BAT	Positive pole of the battery (fuse protected).
MP	Mains power First node at the back end of the AC/DC converter
LBSD	Low Battery Shut Down If the output is fed from the battery and the battery goes too low, the LBSD signal is generated to switch off the whole system immediately. The operation of the system is restored once the mains power supply is active.
24V_OUT	Power output, max. 6 A

According to Fig. 1, the blocks of the electronic switch module are as follows. The mains power supply is monitored by AC detector. The only duty of the detector is to give the controller information on the presence of the AC power supply. Switching between the mains and the battery supply is operated at the hardware level, not using the AC detector. This solution increases the reliability of the system. The AC power supply is converted by the switched mode AC/DC power converter that incorporates power factor correction. This

component has been bought from an external supplier. Once the AC power supply is present, at the output of the AC/DC converter there is a voltage of 24 V in the MP node. This voltage feeds the Internal power supply block that is necessary to power the internal electronics, mainly the operational amplifiers. It also feeds the battery charger that keeps the battery in the charged state. Most of the energy is delivered to the power output through the electronic switch with low power dissipation. In case of AC power supply malfunction, the Internal power supply block is fed directly from the battery, the battery charger is out of order and the Electronic switch delivers the power from the battery to the output of the circuit. The state of the battery is monitored by the Battery voltage check module that can, in case of the deep discharge of the battery, generate the LBSD hibernating signal. If the AC power delivery is resumed sooner than the battery is discharged, the output is automatically switched to the AC power delivery and the battery is being recharged. In case the AC power deliver is out of order for a prolonged time and the battery is discharged, the whole system is switched off by the LBSD signal in order to protect the battery from its destruction by deep discharge. Once the AC power delivery is restored, the system is switched on, being fed from the AC power, and the battery is recharged again. The possible states of the circuit are indicated by the appropriate signals as described in Table III.

Table III Possible states of the system

Combination			State
MA1	MA2	MA3	
H	H	H	The AC power supply delivery is active, no errors detected.
H	H	L	The controller delivers the SMO signal in order to test the state of the battery by short time monitoring of its voltage drop. In this case the output is fed from the battery although the AC power is present. In case the SMO signal is not generated, this indicates malfunction of some of the electronic circuits.
H	L	L	This state indicates that the AC power supply delivery is present, but the output of the circuit is fed from the battery due to malfunction of the AC/DC converter. This is a state of emergency. The AC/DC converter must be replaced sooner than the battery is discharged.
L	L	L	The AC power supply delivery is not present and the output is fed from the battery.
L	H	H	A malfunction of the Electronic switch is indicated. This is a state of emergency. The whole module must be replaced until the battery runs low.
L	L	H	
L	H	L	

During all the possible states the voltage at the battery can be monitored by means of the BVO signal. The conversion table between the BVO voltage and the voltage of the battery is enlisted below.

Table IV Conversion table between BVO and battery voltage

BVO	Battery voltage
0.54 V	21.5 V (LBSD threshold)
1.0 V	23 V
1.45 V	24.5 V (nominal voltage)
1.9 V	26 V
2.37 V	27.5 V (fully charged)
2.8 V	29 V (overcharged)

As obvious from Table IV, the LBSD signal is generated when the battery voltage drops below approximately 21.5 V.

III. CONSTRUCTION

The complex description on construction of all of the circuits cannot be provided in the framework of this paper. However a brief description on the circuits is provided below.

A. Electronic switch

The most important of the circuits is the Electronic switch. This circuit switches the power delivery from the AC/DC converter and the battery. The switching is done on the hardware basis, using a simple comparator. This increases the robustness and the reliability of the solution and enables the system to operate without any controller, if needed. The electronic switch also supports LBSD and SMO signals and generates the MA2 and MA3 signals. It involves one low-voltage quadruple operating amplifier with non-symmetrical power supply of 12 V. The schema of the Electronic switch circuitry is depicted at Fig. 2. The power terminals are as described in Table V.

Table V Power terminals of the Electronic switch

Terminal	Description
X1	24 V _{DC} input from the AC/DC power converter
X2	Battery (fuse protected)
X3	Power output

At the X1-1 terminal, there is the MP node. The voltage at this node is monitored by a comparator that involves IC1C operating amplifier. The threshold is set to approximately 20 V. The reference voltage of the comparator is defined by the voltage at V_REF node. The output of this comparator delivers MA2 signal, which is adjusted by resistors R21 and R30 to LVTTTL levels. The power from the MP node can be switched on and off by means of Q1 low-drop MOSFET transistor. This transistor is controlled by IC1B operational amplifier and Q9 transistor respectively. Normally, the capacitor C2 is charged to the internal power supply voltage and the comparator involving IC1B is in H state (the reference is also taken from the V_REF node). The voltage at the gate of the Q1 transistor is low, keeping it in open state. The power is

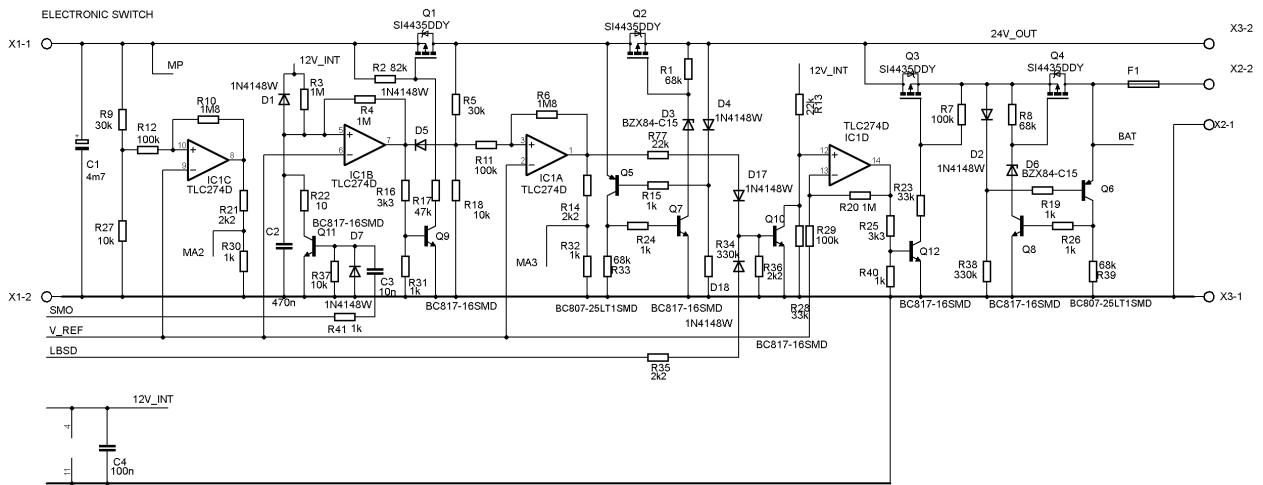


Fig. 2 Connection diagram of the Electronic switch

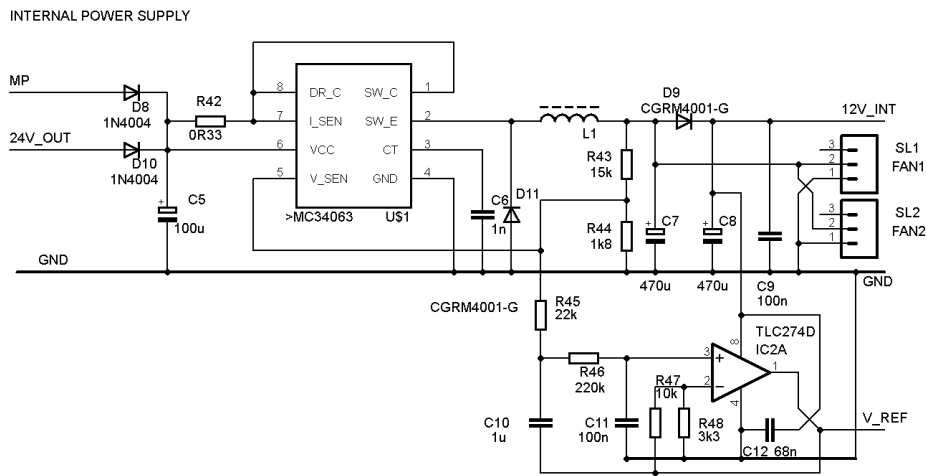


Fig. 3 Connection diagram of Internal power supply block

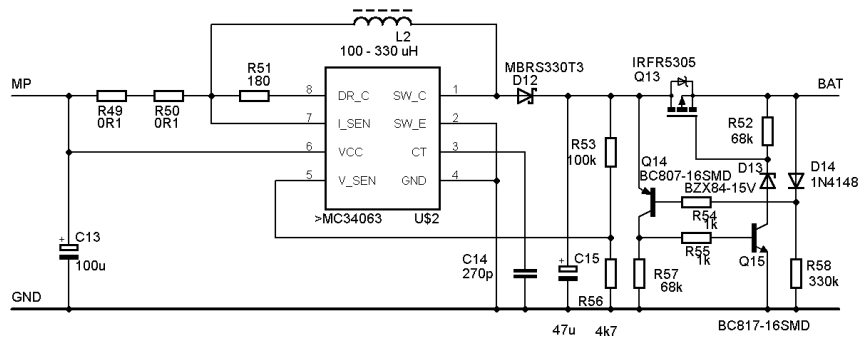


Fig. 4 Connection diagram of the battery charger

then delivered to the output via Q2 which is connected as a low-drop diode, involving also the transistors Q5, Q7 and the Zener diode D3. The voltage in the node between the

transistors Q1 and Q2 is monitored by another operational amplifier, IC1A. This amplifier is connected in the same way as IC1C and generates the MA3 signal. When the output of

reaches 28 V, only the refreshing current is delivered to the battery. The output of the converter is protected by an electronic diode involving the transistor Q13. The circuit diagram is depicted in Fig. 4.

D. AC Detector

This circuit generates MA1 signal, when the power in the AC mains is present. Its connection diagram is depicted in Fig. 5. When the AC voltage is present, the LED in OK1 optocoupler flashes rhythmically, discharging the capacitor C17. This keeps the comparator involving the operating amplifier IC2B in HIGH state. When more than 3 periods of the AC voltage are omitted, the capacitor C17 is charged and the IC2B goes to the LOW state.

E. Battery monitor

The battery monitoring circuit permanently measures the voltage of the battery and delivers the BVO signal, described by Table IV. The operating amplifier IC3A is connected as a comparator with a hysteresis of approximately 0.5 V. Once the voltage at the battery drops below the acceptable limit (approximately 21.5 V), the comparator goes to the HIGH state, generating LBSD signal.

IV. CURRENT STATE

Most of the circuits described in this paper were tested as separated functional samples in order to fine-tune their operation. On the basis of the practical experience the final version of the advanced switching circuit has been sent to production.

In figure 7 an example of a functional sample of the Electronic switch module with TO220 transistors is depicted.

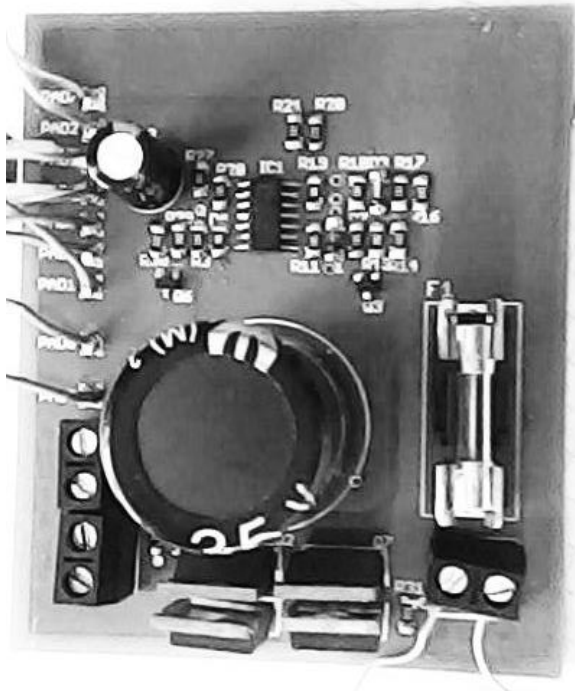


Fig. 7 Electronic switch functional sample

V. CONCLUSION

This paper describes the design and construction of electronic switch that is a part of uninterruptable power supply system for devices that utilize the Power over Ethernet technology. With low power dissipation, this module switches between the AC mains and the battery power supply. It is also capable of recharging the battery and of communication with an external controller, when involved in more complex system. The controller can obtain information about the state of the circuits and the battery. As there is a need to check the battery performance at certain intervals, the module supports overriding of the automatic switching, so the output can be fed from the battery although the AC power delivery is present.

The hereby described module is suitable for all Power over Ethernet backup sources that operate with the 24 V_{DC} voltage provided the power consumption of the connected devices is not higher than approximately 150 W.

Compared to conventional solutions, based usually on on-line backup sources [4], [2], this solution protects the battery from excessive voltage spikes, overcharging and deep discharging which results in its longer life.

REFERENCES

- [1] Z. Trnka, *Theory of Electrical Engineering* [Teoretická elektrotechnika], SNTL Alfa, Bratislava, 1972, Czechoslovakia
- [2] *Backup Power Sources (Záložní zdroje UPS)* [online]. ElektroTrh.cz, 2011 [cit. 2013-01-17]. Available at: <http://www.elektrotrh.cz/cs/elektricke-a-zalozni-zdroje-energie/zalozni-zdroje-ups>
- [3] J. Hammerbauer, *Electrical Power Sources and Accumulators* [Elektrické napájecí zdroje a akumulátory], pp. 41 – 60, University of West Bohemia, Czech Rep., 1996
- [4] N. Ramussen, *The Different Types of UPS Systems*, Schneider Electric, [online], 2011, [cit. 2013-01-17], Available at: http://www.apcmedia.com/salestools/SADE-5TNM3Y_R7_EN.pdf
- [5] M. W. Saslow, *Electricity, Magnetism, and Light*. Toronto: Thomson Learning, 2002, pp. 302–4. ISBN 0-12-619455-6.
- [6] M. Pospisilik, T. Dulik, P. Varacha, M. Adamek, “A novel approach to uninterruptable power supply unit for powering of network devices design.” In: *Recent Advances in Systems Science Proceedings of the 17th International Conference on Systems (part of CSCC'13)*. Rhodes : WSEAS Press (GR), 2013, s. 239 - 242. ISSN 1790-5117. ISBN 978-960-474-314-8

ITS Components in Risk Management in the Port of Santos

Alexsandro S. de Lima, Melissa S. Pokorny, Eduardo M. Dias

Abstract— This paper presents the current status of the use of ITS Components in Risk Management at the entrance and exit of cargo, explaining about the local characteristics, technologies used and how these components can help the inspections of cargo and speed of release of those in the Port of Santos.

Keywords— Port of Santos, Customs, Radio-Frequency Identification, Scanner, Optical Character Recognition

I. INTRODUCTION

BRAZIL ended the year 2012 as the seventh largest economy in the world with \$ 2.25 trillion [1] GDP, but only 140th in the volume of goods and services exported relative to the size of its economy [2] which puts it in a very weak position in relation to the current foreign trade. Even with these unfavorable indicators, the balance of imports and exports between 1994 and 2013 grew significantly and the balance of trade was consistently positive since 2001, as seen in Figure 1.

The government has continuously encouraged the increasingly intensive use of technology to optimize, control and monitor all this trade flow. This effort began with the Federal Law of the Port Modernization (Law No. 8.630/93 [3], Revoked by Law No. 12.815/13 [4]), the law which provoked significant changes in the old and admittedly precarious conditions of port logistics,

A. S. de Lima is with a PhD student at Escola Politécnica of the Universidade de São Paulo - EPUSP (e-mail: alexlima123@usp.br).

M. S. Pokorny is a PhD student of Polytechnic School, University of São Paulo – USP and a researcher of GAESI (melissapokorny@pea.usp.br)

E. M. Dias is full professor of the Escola Politécnica of the Universidade de São Paulo and coordinator of GAESI - Grupo de Automação Elétrica em Sistemas Industriais, a research group of the Electrical Energy and Automation Department, Escola Politécnica, Universidade de São Paulo, Av. Prof. Luciano Gualberto, trav. 3, n. 158, São Paulo/SP, Brazil, CEP 05508-970 (emdias@pea.usp.br).

opening operations to the private sector, regulating the activities with the creation of public use and private use terminals, and since then has intensified with regulations, declaratory acts and ordinances of the *Receita Federal do Brasil* - RFB [5] and the Secretaria de Portos - SEP [6], which process culminated in the Law 12.815/13.

The Port of Santos has a special focus in this analysis for being the largest port in the Southern Hemisphere, with 7,765,100 m² of port area [7] and more than 114 million tons of throughput in 2013 [8], and perform complex and logistics costly operations involving millions of dollars. All of this size and complexity represent a huge challenge for the optimization of existing infrastructure, and the risk that must be mitigated due to the increasing relevance of Brazil due to the increase in imports and exports, and before large events like World Cup (2014) and the Olympics (2016), and the components of ITS represent the most effective solution to achieve this goal. This article will report the major components of ITS which are currently being used to improve the port operations and to increase the ability to import and export cargo at the Port of Santos with efficiency, effectiveness and safety.

II. BACKGROUND

From 2012 to 2013 the increase in container handling at the Port of Santos was about 8.11% [8] over 114 million tons in over 2 million containers [8]. Fig. 1 present Brazilian Foreign Trade Balance (billions of US\$ per year), from 1994 to 2012. Fig. 2 present total containers handled in TEU in 2012. TEU is an abbreviation for 20 foot equivalent unit, a standard measure for a container for transporting goods, used to calculate how many containers a ship can carry, or a port can deal with.

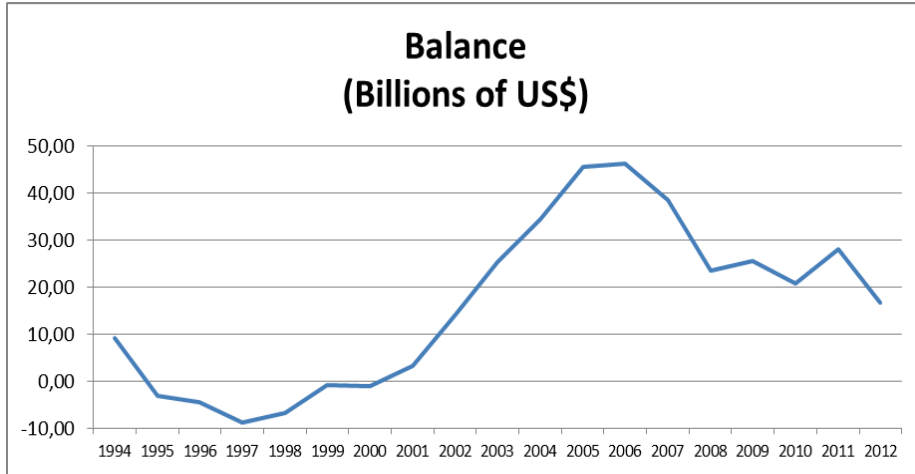


Fig. 1 - Brazilian Foreign Trade Balance - Source: MDIC [9].

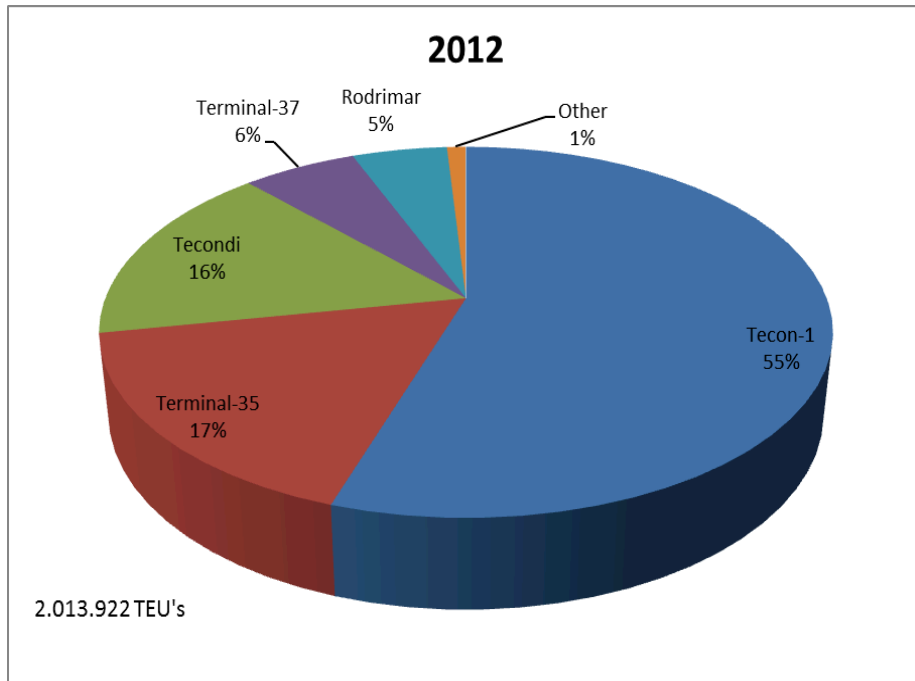


Fig. 2 - Total Containers handled in TEUs in 2012 - Source: CODESP.

Tecon-1, Terminal Santos Brazil located on the left bank of the port of Santos in the city of Guarujá, now represents about 55% of container handling at the Port of Santos, followed by Terminal Group-35 with 17% and Tecondi with 16% of both located the right bank.

It is true that compared to other ports, the increase in containers handled at the port of

Santos is still discrete, but because of the difficulties faced due to lack of investments for number of years, and geographic conditions of both Port and City, there is a need for immediate improvement and investments so that Brazil can be more competitive.

Fig. 3 present the volume of container handling in TEUs in the World.

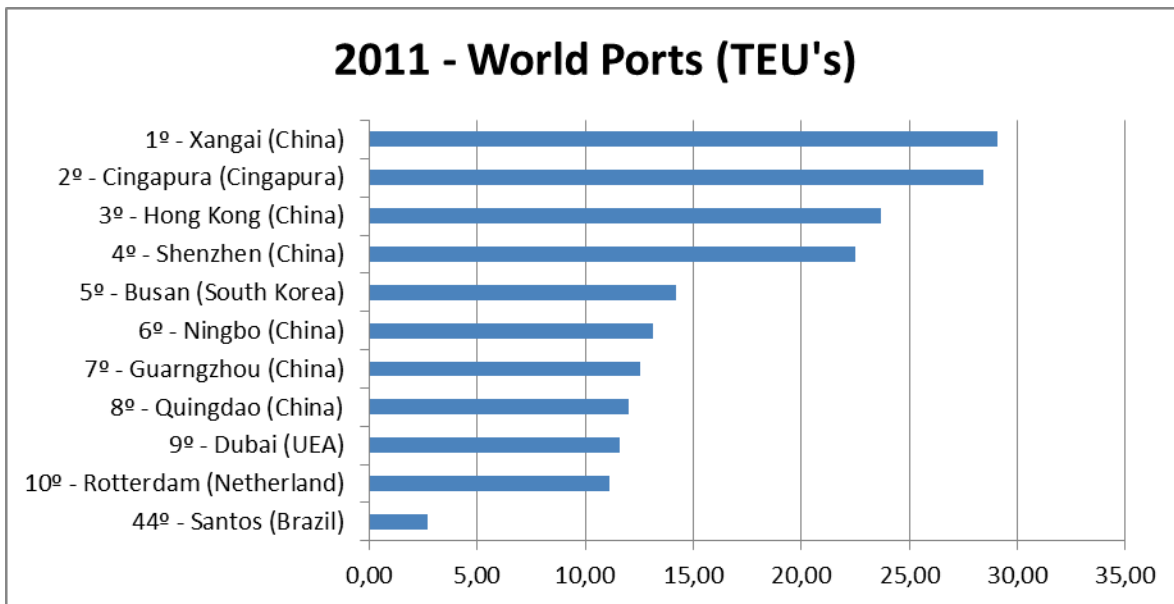


Fig.3 - Container Handling in TEUs in the World - Source: World Shipping Council (2011).

The increase of imports and exports is beneficial, but should be dealt with so that there is a no problems in processes of cargo inspection while maintaining security in the process of entry and departure of cargo at the Port of Santos, as there are many authorities responsible for freeing the entry and exit of cargo in port of Santos, making the agile process or not, depending on demand and facilities imposed by technology.

III. PROBLEMS FACED

Several agencies interact in the process of release of cargo, depending on the type of load or a particular non-compliance that is being sought.

The RFB is responsible for customs supervision, or to see if the container that actually contains the BL - Bill of Lading said to contain.

The Federal Police act, in conjunction with the RFB, when drugs or weapons are found, than monitor the surroundings of the vessels moored at the Port [10].

The *Agência Nacional de Vigilância Sanitária* - ANVISA is responsible for supervision of drugs, including the transport and storage of these [11].

The *Ministério da Agricultura, Pecuária e Abastecimento* - MAPA, is responsible for overseeing cargo of animal (meat) and vegetable (fruit, vegetables and other perishables) [12].

Many systems and procedures have been established at the port of Santos in view greater control and optimization of processes such as: planning routines arrival of trucks with scheduling systems for cargo deliveries and withdrawals;

installation of patios for parking of trucks along the highways in order to control and manage the flow of trucks and avoid overload and congestion in urban networks; addition to sharing information relating to cargo handling, access control individuals and vehicles and handling of cargo and goods.

Tax and organizational issues complement the Brazilian scenario. Brazil is among the 30 nations with the highest tax burdens in the world and stands as the last place of quality public services to the population, such as health, education, safety, transportation and other provider [14].

IV. ITS SYSTEMS AND USED COMPONENTS

The group Ecorodovias Infrastructure and Logistics since its inauguration in April 2006, (containing area of approximately 443,000 m²) has invested more than \$ 100 million in *Ecopátio* Cubatão. Initially, the *Ecopátio* was used only as a truck park, and with the regulation of courtyards screening, came to be used by trucks bound for the port that need to pass through a terminal for control and release of load in accordance orders release the port.

There are 11 gates to the terminal fully computerized. The input and output of trucks is controlled by a system which identifies characters on a plate of the vehicle or the transport unit (container), and streamlines the data about entry and exit of cargo without human interference, what gives greater security to the process as given load can only go on certain truck if it is released

for all systems of different organs besides having been previously scheduled (the input or output) by the scheduling system of the terminal [11].

Fig. 4 present automatic identification number of the container and the plate of the vehicle transporter (truck) via OCR.



Fig.4 - Automatic identification number of the container and the plate of the vehicle transporter (truck) via OCR. Source: Asia Visions

Besides automating the process of entry and exit of cargo, the terminal has a scanner to analyze the contents of a cargo container.

The scanner performs about 60 surveys per hour, or one every minute. The machine can identify any type of product. While doing the inspection, the truck moves underneath the metal

structure of the scanner, which emits X-ray. The image of the cargo is sent to a computer system connected to the Ecopátio network, and is available for 30 days for both customers and the RFB and other agencies [12]. Fig. 5 present scanning a container at Ecopátio Cubatão.



Fig.5 – Scanning a Container at Ecopátio Cubatão. Source: Ecopátio Cubatão e EBCO.

V. ADVANTAGES AND DISADVANTAGES OF USING NEW SYSTEMS AND ITS COMPONENTS

The new ITS systems and its components that are now being used at the Port of Santos are contributing to the safety and are increasing speed of cargo inspection.

The scanner can ease import and export process. In the case of import the main bottlenecks are: the need for identification of hazardous materials and drugs under ANVISA's, containers that transport wood that are so under supervision of the MAPA. In the case of exports, the main problem is requirement of scanning 100% of cargo which is exported to the United States of America.

As the use of scanner can identify the type of merchandise that contains container, so there is no need for its opening by consenting agencies to confirm the contents of the container, or to inspect and examine whether there are weapons, drugs, pharmaceuticals, etc., or if a container actually contains wood packaging to be opened and selected for inspection by the national correspondent consenting party.

Fig.6 and Fig. 7 present images of the contents of a container scanning

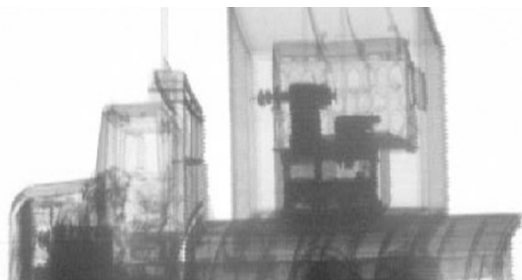


Fig. 6 - Image of the contents of a container scanning

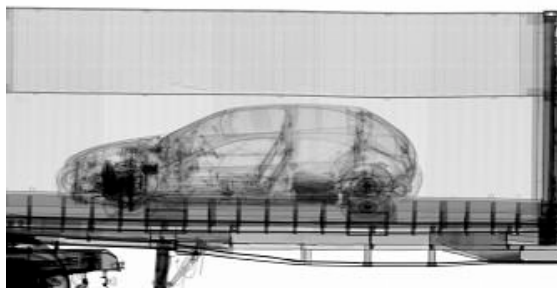


Fig. 7 - Image of the contents of a container scanning

The adoption of scanning cargo technology allows a much more thorough analysis of risk of its contents without opening the container. The time spent on unnecessary openings is best enjoyed by the authorizing agencies to enhance the checks and terminals have streamlined their operations, increasing the productivity of operations in the largest Brazilian port.

VI. CONCLUSION

As shown in this article, the large volume of cargo entering and leaving daily from the port of Santos represent a major challenge in risk management and analysis of these risks and

therefore it is necessary to automate the input and output of trucks and loads identifying characters, and the automatic analysis of images of the container with the use of a scanner. The ITS components and systems presented herein are part of the group of technologies that began to be employed at the Port of Santos, which has proved very effective in optimizing the audits of consenting agencies. The automatic generation of alerts by various control devices and existing analysis allow greater flexibility in operations. These alerts allow a performance in real time and ensure that the totality of cargo to be inspected. The authorizing agencies thus has important tools to increase the safety of operations and act more forcefully on contraband and counterfeit.

The automation of port processes require highly skilled professionals that are currently missing in Brazil. These projects will be made possible only with the importation of equipment and hand labor already experienced in technologically advanced environments. Unfortunately these actions have not happened as often as would be needed and what has driven them suspended major investment so needed to improve our infrastructure.

The implementation of ITS equipment represent an important step in the automation process of port, but it is possible go much further. Despite bringing significant gains in efficiency, the analysis of data collected by existing equipment will bring the possibility of a substantial deepening to predict and simulate how process changes will impact operations. Big data systems will have an increasingly frequent use and allow errors to be known in advance, and allow more alternative scenarios are simulated.

VII. REFERENCES

- [1] THE WORLD BANK. Gross Domestic Product 2012. Available: <http://databank.worldbank.org/data/download/GDP.pdf>
- [2] WORLD ECONOMIC FORUM. Global Competitiveness Report 2012-2013. Available: <http://reports.weforum.org/global-competitiveness-report-2012-2013/#>
- [3] Law No. 8.630/93. Available: http://www.planalto.gov.br/ccivil_03/leis/18630.htm
- [4] Law No. 12.815/13. Available: http://www.planalto.gov.br/ccivil_03/_ato2011-2014/2013/Lei/L12815.htm
- [5] RFB. Available: <http://www.receita.fazenda.gov.br/SRF/ConhecaRFB.htm>
- [6] SEP. Available: <http://www.portosdobrasil.gov.br/sobre-1/institucional/secretaria-de-portos>
- [7] Características Gerais do Porto de Santos. Available: <http://www.portodesantos.com.br/historia.php>
- [8] CODESP. Mensário Estatístico. December/2013. Available: http://201.33.127.41/DocPublico/estmen_CPT/2013/estmen-2013-12.pdf
- [9] MDIC. Available: http://www.desenvolvimento.gov.br/arquivos/dwnl_1386852310.xls
- [10] PF. Available: <http://www.dpf.gov.br/institucional/historia/historico>
- [11] ANVISA. Available: <http://portal.anvisa.gov.br/wps/portal/anvisa/anvisa/agencia>
- [12] MAPA. Available: <http://www.agricultura.gov.br/ministerio>
- [13] Ordinance No SRF 2438, 2010. Available: <http://www.receita.fazenda.gov.br/legislacao/Portarias/2010/portrfb24382010.htm> Accessed at
- [14] IBPT. Estudo sobre a Carga Tributária/PIB x IDH.. Available: https://www.ibpt.org.br/img/uploads/novelty/estudo/787/ESTUDOFI_NALSOBRECARGATRIBUTARIAPIBXIDHIRBESMARCO2013.pdf

Authors Index

Abed, N.	334	Chougule, S. V.	344	Giernacki, W.	57
Ahmad Khan, S. A.	378	Christova, N. G.	419	Goh, T.	104
Alberdi, M.	521	Chrobak, P.	226, 492, 581	Gombár, M.	168
Alexander, P.	86, 117	Coelho, J. P.	57	Gonçalo, J. E.	570
Alexandris, G. P.	408	Dahi, K.	109	González-Lee, M.	273
Amundarain, M.	521	De Abreu, V. S.	616	Guarnaccia, C.	443, 499
Aouf, N.	391	De Gouveia, J. A. M.	467, 599	Guedira, S.	109
Arellano-Quintana, V. M.	74, 534	De Lima, A. S.	726	Guillaume, D.	39
Aulenbacher, I. L.	206	Demidova, G. L.	157	Gurenko, B. V.	46
Ayumba, E. M.	382	Dias, E. M.	467, 570, 599	Hamadouche, M.	625
Azzoune, H.	625	Dias, E. M.	616, 640, 668	Hammadi, S.	482
Bardis, N. G.	179, 198, 408	Dias, E. M.	679, 692, 714	Hedjar, R.	334
Bařinová, M.	523, 577, 594	Dias, E. M.	726	Herman, G.	39
Bařinová, M.	611	Dias, M. L. R. P.	467, 640, 668	Hidaka, N.	127
Barradi, Y.	651	Dias, M. L. R. P.	692	Hlaváček, P.	234
Baruch, I. S.	74, 534	Dobrescu, R.	262, 296	Hoeflich, S. L.	692
Bednarik, M.	123, 243, 268	Dolinay, J.	488	Holik, Z.	243
Bekyarski, A.	153, 251	Dolinay, V.	474	Honig, R.	529
Beneš, M.	523	Dostálek, P.	310, 488	Hošovský, A.	306
Benkraouda, S.	326	Doukas, N.	179	Hrehová, S.	230
Bílek, O.	184, 193, 566	Drazan, L.	174	Hruška, F.	338, 462, 636
Boaventura-Cunha, J.	57	Drga, R.	656, 674	Huerta-Chua, J.	273
Bobál, V.	402	Dubják, J.	306	Hyniova, K.	161, 353
Boujemaa, H.	334	Dulik, T.	720	Iacovici, I.	374
Boussalis, H.	39	Elhani, S.	109	Ibarra-Manzano, O. G.	273
Bouziane, A.	326	Facchini, E.	599	Igaz, R.	234
Branco, F. C.	679, 714	Fechová, E.	230	Itina, M.	96
Branco, G. M.	679, 714	Fedorechko, O.	179	Itins, I.	96
Branco, M. C.	679, 714	Ferreira, M. L.	467, 599	Janáčková, D.	395, 621, 656
Branescu-Raspop, I.	262	Figueiredo, A. E. P.	692	Janáčková, D.	674
Buckova, M.	211	Florea, G.	296	Jančíková, Z.	234
Calixto, J.	668	Flores, E. R. C.	206	Jarnea, A. D.	296
Carrascal, E.	521	Fratu, O.	588	Javorik, J.	184, 193, 566
Cerón Bretón, J. G.	499	Freixas, J.	52	Javořík, J.	696
Cerón Bretón, R. M.	499	Furmankiewicz, M.	551	Jeon, Y.-J.	239, 315
Chalupa, P.	523, 540	Garcia, M.	39	Jurado, J. M. S.	206
Charvátová, H.	621, 647, 656	Garrido, A. J.	521	Karadimas, N. V.	285
Charvátová, H.	674	Garrido, I.	521	Kawasue, K.	127
Chavan, M. S.	344	Garzinová, R.	234	Khalidi, N.	651
Choi, D.-C.	239, 315	Ghelichkhani, M.	359	Khater, F.	455

Kim, D.	104	Manolova, A. H.	419	Piteř, J.	92
Kim, S. W.	104, 239, 315	Markovskiy, O. P.	179	Pleshkova, S.	153, 251
Kim, Se. Hu.	104	Martínek, T.	338	Plšek, S.	100, 147
Kim, Su. Hy.	399	Martinot, A.	482	Pluhacek, M.	516, 557
Kim, T.	399	Mastorakis, N. E.	443, 700	Pokorny, M. S.	467, 570, 599
Kmec, J.	168, 230	Matušů, R.	424, 450, 606	Pokorny, M. S.	668, 726
Kocurek, P.	577	Matveev, M.	189	Pons, M.	52
Koliskina, V.	62	Medvedev, M. Y.	46	Pospisilik, M.	529, 662, 720
Kolomaznik, K.	363, 395, 577	Melo, V. A. Z. C.	570	Potužák, L.	708
Kolomaznik, K.	594, 611, 621	Michal, P.	168	Poulos, M.	247
Kolouch, J.	385	Milanova, M.	189	Prokop, R.	321, 424, 438
Kolyshkin, A.	62, 96	Milshsteyn, A.	39	Prokop, R.	450
Korbel, J.	438, 450	Mittal, R. K.	378	Prokopova, Z.	478, 546, 632
Košťal, P.	234	Mizera, A.	123, 243, 268	Pshikhopov, V. K.	46
Kratky, P.	257, 279, 290	Morales-Mendoza, E.	273	Purcarea, V. L.	262
Krbeček, M.	686	Morales-Mendoza, L. J.	273	Quartieri, J.	443, 499
Kresalek, V.	134, 202, 338	More, M.	562	Quillot, A.	482
Krizan, R.	174	Mouats, T.	391	Rad, K.	39
Kropáčová, A.	385	Napoleone, J. M.	714	Rajagopal, K.	86, 117
Kubalčík, M.	402	Navrátil, J.	123, 243, 268	Renard, J.-M.	482
Kučerka, D.	168	Navrátil, J.	290, 302	Reznicek, M.	279
Kudělka, J.	338	Navrátil, M.	330, 338, 462	Rigopoulos, G.	285
Kujawa, D.	430	Neumann, P.	506, 529	Rossi, L. N.	616, 692
Kumar, A.	378	Novák, J.	523, 540	Rusnák, V.	234
Kyprianidis, I. M.	86, 117, 198	Novosad, D.	330	Ružiak, I.	234
Lee, S. J.	239, 315	Oborný, Z.	310	Sámek, D.	184, 193, 566
Lin, A.	39	Omar, A.	455	Šaur, D.	147
Líška, O.	562	Oplatkova, Z. K.	516, 557	Schauer, F.	686
Liu, C.	39	Opluřtil, M.	66, 226, 492	Scheibenreiter, P.	529
Liu, F.	367	Opluřtil, M.	581	Schmitter, E. D.	35
Lukichev, D. V.	157, 511	Otáhal, J.	462, 636	Sehnalek, S.	492, 581, 647
Macků, L.	330	Othman, S. B.	482	Sehnalek, S.	226, 636
Maevsky, A. M.	46	Ovsik, M.	257, 279, 290	Senkerik, R.	516, 557
Mahmoudi, H.	651	Parappat, P. B.	378	Senkerik, V.	257, 290, 302
Manas, D.	123, 243, 257	Pecha, J.	594	Sergio, L. R.	640
Manas, D.	268, 279, 290	Peeva, K.	251	Shaltout, A.	455
Manas, D.	302	Pekař, L.	310, 321	Shmaliy, Y. S.	273, 367
Manas, M.	123, 243, 257	Pereira, S. L.	640, 692	Silhavy, P.	478, 546
Manas, M.	268, 279, 290	Pereverzev, V. A.	700	Silhavy, R.	478, 546, 632
Manas, M.	302	Pérez-Cáceres, S.	273	Šilinger, K.	708

Sirbiladze, G.	71	Taranu, I.	374	Vaskova, H.	211, 363
Skrobak, A.	279, 302	Tatto, J. A.	570	Vázquez-Bautista, R. F.	273
Smirnov, N.	511	Tebbi, H.	625	Vincenec, J.	492, 581
Smitkova-Janku, L.	161	Tepedino, C.	499	Viček, K.	686
Sobota, J.	338	Tobolova, M.	134, 202	Volodko, I.	62
Soldan, J.	662	Tóthová, M.	92	Volos, Ch. K.	86, 117, 198
Sołtysik-Piorunkiewicz, A.	551	Touati, S.	334	Welcome, M. O.	700
Šotnar, J.	708	Triano-Carballo, G.	273	Yagoubi, B.	326
Spišák, E.	168	Tsamatsoulis, D. C.	138	Yoshida, K.	127
Stanek, M.	123, 243, 257	Tsenov, G. T.	419	Yun, J. P.	239, 315
Stanek, M.	268, 279, 290	Tsulaia, G.	71	Zalesak, M.	226, 414, 492
Stanek, M.	302	Urbanek, T.	632,	Zálešák, M.	581, 647
Stouboulos, I. N.	86, 117, 198	Úředníček, Z.	66, 80	Zanka, F.	506
Suciu, G.	588	Vachkov, G. L.	419	Zazi, M.	651
Suciu, V.	588	Vagaská, A.	168	Zhao, S.	367
Sumedrea, A. G.	216	Vaidyanathan, S.	86, 117, 198	Židek, K.	306
Swiatek, D.	570	Vasek, L.	474, 506	Ziuziański, P.	551
Sysala, T.	474, 506	Vašek, V.	100, 395, 488	Zoghiami, N.	482
Szwarc, A.	679, 714	Vašek, V.	621		